

GDANSK UNIVERSITY OF TECHNOLOGY  
FACULTY OF OCEAN ENGINEERING AND SHIP TECHNOLOGY  
SECTION OF TRANSPORT TECHNICAL MEANS  
OF TRANSPORT COMMITTEE OF POLISH ACADEMY OF SCIENCES  
UTILITY FOUNDATIONS SECTION  
OF MECHANICAL ENGINEERING COMMITTEE OF POLISH ACADEMY OF SCIENCE

ISSN 1231 – 3998  
ISBN 83 – 900666 – 2 – 9

# **Journal of POLISH CIMAC**

**SELECTED PROBLEMS  
OF DESIGNING  
AND OPERATING  
TECHNICAL SYSTEMS**

**Vol. 7**

**No. 3**

Gdansk, 2012

**Science publication of Editorial Advisory Board of POLISH CIMAC**



### Editorial Advisory Board

**J. Girtler** (President) - *Gdansk University of Technology*  
**L. Piaseczny** (Vice President) - *Naval Academy of Gdynia*  
**A. Adamkiewicz** - *Maritime Academy of Szczecin*  
**J. Adamczyk** - *University of Mining and Metallurgy of Krakow*  
**J. Blachnio** - *Air Force Institute of Technology*  
**C. Behrendt** - *Maritime Academy of Szczecin*  
**P. Bielawski** - *Maritime Academy of Szczecin*  
**T. Chmielniak** - *Silesian Technical University*  
**R. Cwilewicz** - *Maritime Academy of Gdynia*  
**T. Dąbrowski** - *WAT Military University of Technology*  
**Z. Domachowski** - *Gdansk University of Technology*  
**C. Dymarski** - *Gdansk University of Technology*  
**M. Dzida** - *Gdansk University of Technology*  
**J. Gardulski** - *Silesian University of Technology*  
**J. Gronowicz** - *Maritime University of Szczecin*  
**V. Hlavna** - *University of Žilina, Slovak Republic*  
**M. Idzior** - *Poznan University of Technology*  
**A. Iskra** - *Poznan University of Technology*  
**A. Jankowski** - *President of KONES*  
**J. Jaźwiński** - *Air Force Institute of Technology*  
**R. Jedliński** - *Bydgoszcz University of Technology and Agriculture*  
**J. Kiciński** - *President of SEF MEC PAS, member of MEC*  
**O. Klyus** - *Maritime Academy of Szczecin*  
**Z. Korczewski** - *Gdansk University of Technology*  
**K. Kosowski** - *Gdansk University of Technology*  
**L. Ignatiewicz Kowalczyk** - *Baltic State Maritime Academy in Kaliningrad*  
**J. Lewitowicz** - *Air Force Institute of Technology*  
**K. Lejda** - *Rzeszow University of Technology*

**J. Macek** - *Czech Technical University in Prague*  
**Z. Matuszak** - *Maritime Academy of Szczecin*  
**J. Merksiz** - *Poznan University of Technology*  
**R. Michalski** - *Olsztyn Warmia-Mazurian University*  
**A. Niewczas** - *Lublin University of Technology*  
**Y. Ohta** - *Nagoya Institute of Technology*  
**M. Orkisz** - *Rzeszow University of Technology*  
**S. Radkowski** - *President of the Board of PTDT*  
**Y. Sato** - *National Traffic Safety and Environment Laboratory, Japan*  
**M. Sobieszczanski** - *Bielsko-Biala Technology-Humanistic Academy*  
**A. Soudarev** - *Russian Academy of Engineering Sciences*  
**Z. Stelmasiak** - *Bielsko-Biala Technology-Humanistic Academy*  
**Z. Smalko** - *Warsaw University of Technology*  
**M. Ślęzak** - *Ministry of Scientific Research and Information Technology*  
**W. Tarelko** - *Maritime Academy of Gdynia*  
**W. Wasilewicz Szczagin** - *Kaliningrad State Technology Institute*  
**F. Tomaszewski** - *Poznan University of Technology*  
**J. Wajand** - *Lodz University of Technology*  
**W. Wawrzyński** - *Warsaw University of Technology*  
**E. Wiederuh** - *Fachhochschule Giessen Friedberg*  
**M. Wyszynski** - *The University of Birmingham, United Kingdom*  
**S. Żmudzki** - *West Pomeranian University of Technology in Szczecin*  
**B. Żółtowski** - *Bydgoszcz University of Technology and Life Sciences*  
**J. Żurek** - *Air Force Institute of Technology*

### Editorial Office:

GDANSK UNIVERSITY OF TECHNOLOGY  
Faculty of Ocean Engineering and Ship Technology  
Department of Ship Power Plants  
G. Narutowicza 11/12 80-233 GDANSK POLAND  
tel. +48 58 347 29 73, e – mail: sek4oce@pg.gda.pl

[www.polishcimag.pl](http://www.polishcimag.pl)

This journal is devoted to designing of diesel engines, gas turbines and ships' power transmission systems containing these engines and also machines and other appliances necessary to keep these engines in movement with special regard to their energetic and pro-ecological properties and also their durability, reliability, diagnostics and safety of their work and operation of diesel engines, gas turbines and also machines and other appliances necessary to keep these engines in movement with special regard to their energetic and pro-ecological properties, their durability, reliability, diagnostics and safety of their work, and, above all, rational (and optimal) control of the processes of their operation and specially rational service works (including control and diagnosing systems), analysing of properties and treatment of liquid fuels and lubricating oils, etc.

All papers have been reviewed

@Copyright by Faculty of Ocean Engineering and Ship Technology Gdansk University of Technology

All rights reserved

ISSN 1231 – 3998

ISBN 83 – 900666 – 2 – 9

Printed in Poland





## Introduction

In contemporary science we can observe more and more specialization in various scientific disciplines. This specialization makes that research is conducted with not proper consideration of the knowledge of other scientific disciplines even if they belong to the same field of knowledge. Thus, the specialists dealing with the theme that belongs to the „Machine Building and Operating” discipline, are reluctant to study achievements of the related disciplines such as: „Automation and Robotics”, „Electronics”, „Electrical Engineering”, „Energetics”, „Computer Science”, „Mechanics” or “Transport”. Much more unconcerned is the knowledge of such disciplines as: „Biocybernetics & Biomedical Engineering” and „Biotechnology”, although they are classified to the field of knowledge defined as „technical sciences”. The situation is understandable. It follows from the anxiety that study of developments in other scientific disciplines may cause falling behind with developments in the discipline practiced by the given scientist. In consequence, making a Doctoral Thesis can be admittedly easier but making a Habilitation Thesis – much more difficult. Habilitation can be achieved among others when a candidate in his/her research output can prove application for the first time the knowledge of any other discipline, e.g. „Mathematical Sciences”.

In each scientific discipline, independently which field of knowledge it belongs to, the science is being developed in result of applying proper scientific methods. However, regardless of application of the specific methods, in each scientific discipline there are also used deductive and inductive methods if the created knowledge is supposed to have essential cognitive properties. Deductive methods are used when it is necessary to prove a thesis statement (statements). When a hypothesis (hypotheses) is (are) to be verified then the inductive or deductive methods are applied. As a rule, underestimated is the method called analogy. The analogy, however, enables searching for a common *reason (rationale, cause)* characterizing different research objects (specific for particular scientific disciplines), while deduction consists in matching *consequence (result, conclusion)* to *reason*, and induction – *reason to consequence*.

For this reason it might be of interest to many scientists and also beneficial for development of technical sciences to present in the *Journal of POLISH CIMAC* designed for publication of articles concerning the knowledge enclosed in the „Machine Building and Operating” discipline, also these works which are classified to other mentioned scientific disciplines belonging to the field of knowledge - „technical sciences”, although they are not directly related to the theme being the mainstream of this journal. This volume contains precisely this kind of publications. I remain with the conviction that such an approach to the dissemination of knowledge comprising both cognitive properties (important for science) and utilitarian properties (important in practice of designing, manufacturing and operating technical equipment), will contribute to accelerating the development of the technical sciences.

Editor-in-Chief  
*prof. Jerzy Girtler*



## CONTENTS

|  |     |
|--|-----|
| Bochat A., Zastempowski M.: KINEMATICS OF DRUM MOVEMENT OF THE CUTTING UNIT OF A STRAW CUTTER .....  | 11  |
| Borowski B.: CONTROLLING RATE OF DELIVERY OF APPLICATORS AT THE HARVEST OF SUBSTRATES BIOGASWORKS - PRELIMINARY ISSUES .....                               | 17  |
| Borowski S., Dulcet E., Kaszkowiak J., Bujaczek R., Chojnacki J.: BALLERS FOR MOLDING BALES OF SHREDDED MATERIAL .....                                     | 23  |
| Cichański A., Burak M., Skibicki D., Stopel M.: NUMERICAL ANALYSIS OF FORAGE TRAILER SUPPORTING STRUCTURE .....  | 29  |
| Cichański A., Burak M., Skibicki D., Pejkowski Ł.: ANALYTICAL VERIFICATION OF NUMERICAL ANALYSIS OF FORAGE TRAILER SUPPORTING STRUCTURE .....              | 35  |
| Cichański A., Burak M., Skibicki D., Lis Z.: STRAIN GAUGE VERIFICATION OF NUMERICAL ANALYSIS OF FORAGE TRAILER SUPPORTING STRUCTURE .....                  | 41  |
| Ciechacki K., Szykowny T.: THE EFFECT OF A WELDING METHOD ON THE STRUCTURE OF A WELDED JOINT .....   | 47  |
| Domanowski P.: AUTOMATION OF PLASMA MACHINING IN A CONTINUOUS OPERATION LINE .....   | 53  |
| Flizikowski J., Tomporowski A.: MOTIONAL CHARACTERISTICS OF GRAINS IN THE MULTI-HOLE SPACE OF A MULTI-DISC GRINDER .....                                   | 59  |
| Holka T., Jarzyna T.: MACHINE VIBRATIONS ON A FLEXIBLE ROOF .....  | 69  |
| Kaczmarek A.: APPLICATION A LABORATORY STAND FOR MULTI-SYMPTOMS TESTS FOR HIGH CYCLIC FATIGUE OF CONSTRUCTIONAL MATERIAL .....                             | 75  |
| Kalwaj J.: NEW, ENERGY SAVING ROTOR SOLUTION OF BEATER GRINDER FOR CORN GRAIN ..   | 85  |
| Kolber P., Perczyński D., Landowski B.: ANALYSIS OF THE QUALITY OF ELECTRICITY ON THE BASIS OF THE RESULTS OF THE RESEARCH MODEL OF LOW VOLTAGE LINE ..... | 89  |
| Koralewski G.: OPTIMAL CONTROL ALGORITHMS FOR TRANSMISSIONS IN CITY BUSES .....  | 97  |
| Królikowski B., Zimniak J.: INVESTIGATION OF THERMAL PROPERTIES OF SELECTED POLYMER BLENDS .....   | 107 |
| Leppert T.: INFLUENCE OF COOLING AND LUBRICATION ON SELECTED FEATURES OF GEOMETRICAL STRUCTURE OF SURFACES TURNED AT HIGH CUTTING SPEEDS .....             | 113 |
| Leppert T.: SURFACE LAYER PROPERTIES IN DRY TURNING OF C45 STEEL .....   | 121 |
| Ligaj B.: INFLUENCE OF STRESS AND STRAIN CONTROL ON CYCLIC PROPERTIES OF AW-2017A ALUMINIUM ALLOY .....  | 127 |

|   |     |
|---|-----|
| Lipski A.: EVALUATION OF THE SELECTED FACTORS EFFECT ON THE FATIGUE LIFE OF SPECIMENS WITH SIZED AND RIVETED HOLE PART I. DESIGN OF EXPERIMENT AND TESTS RESULTS .....        | 135 |
| Lipski A.: EVALUATION OF THE SELECTED FACTORS EFFECT ON THE FATIGUE LIFE OF SPECIMENS WITH SIZED AND RIVETED HOLE PART II. STATISTICAL ANALYSES OF EXPERIMENTAL RESULTS ..... | 145 |
| Lis Z., Szczutkowski M.: DETERMINATION OF INPUT DATA FOR THE PROCESS OF VALIDATION OF OWN CALCULATION SOFTWARE FOR BASIC MATERIAL DATA IN STATIC STRENGTH TESTS .....         | 159 |
| Ławrynowicz Z.: CARBON PARTITIONING AND MECHANISM OF BAINITE REACTION IN EXPERIMENTAL FE-CR-MO-C STEEL .....  | 167 |
| Ławrynowicz Z.: BAINITE MORPHOLOGY IN EXPERIMENTAL FE-MO-CR-V-TI-C STEEL .....  | 175 |
| Marchewka A., Wocianiec R., Zdrojewski J.: PCB EXPOSURE AND DATA MATRIX BASED JOB VERIFICATION .....  | 183 |
| Matuszewski M., Łukasiewicz M., Musiał J.: APPLICATION OF SPECTRAL ANALYSES FOR SURFACE LAYERCHANGES ESTIMATION OF CO-OPERATING UNITS WITH CONFORMAL CONTACT .....            | 191 |
| Mikołajczyk T., Kamieniecki Ł.: PC CONTROLLED TURNING TOOL .....  | 199 |
| Mroziński S., Skocki R., Lis Z.: INFLUENCE OF TEMPERATURE ON MATERIAL DATA DETERMINED ON THE BASE OF LOW CYCLE FATIGUE TESTS .....  | 205 |
| Mroziński S., Włodarczyk S.: EXAMINATION OF CAST STEEL IN TERMS OF THERMO-MECHANICAL FATIGUE .....  | 211 |
| Pejkowski Ł., Skibicki D.: A PROPOSAL OF MODIFICATION OF THE ZENNER'S FATIGUE CRITERION FOR THE CASE OF NON-PROPORTIONAL LOADING .....  | 217 |
| Pepliński K., Kubielski A.: SIMULATION OF BLOWING PREFORM AND OPTIMIZATION THEIR THICKNESS DISTRIBUTION FOR FINAL TARGET SHAPE OF IN CONTAINER .....                          | 225 |
| Pepliński K., Mozer A.: COMPARISON OF BOTTLE WALL THICKNESS DISTRIBUTION OBTAIN IN REAL MANUFACTURING CONDITIONS AND IN ANSYS POLYFLOW SIMULATION ENVIRONMENT .....           | 231 |
| Pepliński K.: MICROCELLULAR MONOLAYER EXTRUSION BLOW MOLDING FOR HOLLOW OBJECT .....  | 237 |
| Piątkowski T., Sempruch J., Tomaszewski T.: SPATIAL APPROXIMATION OF IMPACT TEST RESULTS OF UNIT LOAD .....   | 243 |
| Sadowski J.: MINIMIZATION OF NOISE IN FOUNDRIES ON THE EXAMPLE OF THE IRON FOUNDRY IN BYDGOSZCZ .....   | 253 |
| Sawicki J., Paczkowski T.: COMPUTER AIDED ELECTROCHEMICAL SHAPING OF CURVILINEAR SURFACES .....   | 261 |
| Skibicki A.: FEM CALCULATION OF RESIDUAL STRESS AFTER PULSED CURRENT ARC WELDING OF ALUMINUM ALLOY .....  | 269 |

|   |     |
|---|-----|
| Starosta R.: THE INFLUENCE OF BURNISHING ON SURFACE TEXTURE OF REGENERATIVE NI-AL-15%AL <sub>2</sub> O <sub>3</sub> PLASMA SPRAYED COATINGS .....   | 275 |
| Strzelecki P., Sempruch J.: ANALYTICAL-EXPERIMENTAL METHOD OF DETERMINING FATIGUE CHARACTERISTICS FOR DESIGN ELEMENTS .....   | 285 |
| Styp-Rekowski M., Matuszewski M., Oborski I.L.: POSSIBILITIES OF SOME CONSTRUCTIONAL MATERIALS CUTTING BY MEANS OF WATER-ABRASIVE JET .....   | 293 |
| Sykutera D., Czyżewski P.: RECYCLING ABILITIES OF THERMOPLASTIC IONOMERS, AS EXAMPLIFIED BY SURLYN® .....   | 301 |
| Sykutera D.: POROUS POLYSTYRENE GRINDING REASERCH .....   | 309 |
| Szczutkowski M.: COMPUTER AIDED LABORATORY ACCREDITATION PROCESS - SERVICE TO THE CUSTOMER AS A REQUIREMENT OF ISO/IEC 17025 STANDARD – INITIAL DISCUSSION PAPER .....                    | 315 |
| Szczutkowski M.: ELABORATION OF THE WIND TURBINE CONSTANT DIAGNOSTIC SYSTEM AS A TESTING PROCEDURE IN AN ACCREDITED LABORATORY – THE PROCESS APPROACH TO WRITING THE DRAFT DOCUMENT ..... | 321 |
| Szykowny T., Ciechacki K.: THE INFLUENCE OF ISOTHERMAL QUENCHING ON THE EFFECTS OF THERMOMECHANICAL TREATMENT OF SPHEROIDAL CAST IRON .....   | 327 |
| Szymczak M.: RENEWABLE FUELS - ADDITIONAL SOURCE OF HEAT ENERGY .....   | 333 |
| Tomaszewski T., Sempruch J., Piątkowski T.: INVESTIGATING THE SIZE EFFECT FOR THE SMALL-DIMENSION SPECIMENS MADE FROM THE EN AW-6063 ALUMINUM ALLOY .....                                 | 339 |
| Trepczyńska-Łent M.: THE METASTABLE EUTECTIC GROWTH .....   | 347 |
| Wdzięczny A., Knopik L.: GRAPHICAL ANALYSIS OF BUS LIFETIME .....   | 353 |
| Wdzięczny A.: EVALUATION OF THE EFFECTIVENESS OF REPAIRS CARRIED OUT OF CENTRES OF THE ROAD TRANSPORT .....   | 361 |
| Wirwicki M., Topoliński T.: ZIRCONIUM DIOXIDE AS A BIOMATERIAL; THE MICROSTRUCTURE .....  | 369 |
| Zachwieja J., Gołębiowska I.: DAMPING BUIDLING VIBRATIONS EXCITED BY SURFACE WAVE PROPAGATING IN THE GROUND .....   | 373 |
| Zimniak J., Królikowski B.: CONSTITUTING OF COMPOSITE MATERIALS FROM RECYCLED PLASTICS SHOWING NOISE-SUPPRESSING PROPERTIES .....   | 383 |
| Zimniak J., Sadowski B.: SELECTED PROBLEMS OF TEMPERATURE CONTROL IN INJECTION MOULDS .....   | 391 |





## KINEMATICS OF DRUM MOVEMENT OF THE CUTTING UNIT OF A STRAW CUTTER

**Andrzej Bochat, Marcin Zastempowski**

*University of Technology and Life Sciences in Bydgoszcz  
Faculty of Mechanical Engineering  
ul. Kaliskiego 7, 85-796 Bydgoszcz, Poland  
e-mail: zastemp@utp.edu.pl*

### **Abstract**

*In the study there have been presented mathematical dependencies describing the kinematics of the drum movement of a straw cutter's cutting unit. Formulating of dependencies may be used at the stage of different types of analyses and simulation studies on new drum constructions of cutting units for cutting of a layer of vegetal material into chaff.*

**Key words:** straw cutter, drum cutting unit, kinematics of movement, vegetal material

### **1.Introduction**

The drum cutting unit constitutes the basic operating assembly of self-propelled, attached or stationary straw cutters. The task of the drum assembly is to cut the vegetal material (stalks or stems) into parts of a definite length – into chaff.

Application of this type of an assembly in straw cutters makes it possible to obtain the required degree of material's size-reduction [1, 3, 4, 7].

The rotational motion of a cutting drum results in relocating of cutting knives together with it. Knives moving in relation to the immovable counter cutting edge cause at the first stage squeeze – pressing of a layer of vegetal material and then its cutting.

Feeding of material between the knife's blade and the counter cutting blade takes place thanks to the rotary movement of pulling in-squeezing rollers, which pre-form and compact the material.

The essence of the process of feeding and cutting of vegetal material with the use of a cutting drum is presented in the Fig. 1.

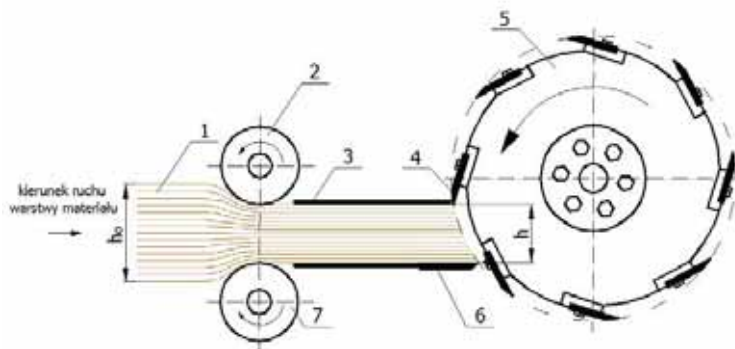


Fig. 1. Process of feeding and cutting of vegetal material with the use of a cutting drum:  
 1 – layer of material, 2 – upper pulling in- squeezing roller, 3 – pressure plate, 4 – cutting knife, 5 – cutting drum,  
 6 – counter cutting edge, 7 – lower pulling in-squeezing roller,  
 $h_0$  – height of the layer of material before compacting,  $h$  – height of the layer of material after compacting

One of the basic problems facing the design engineers of the straw cutter is the correct designing of their operating-drum cutting assembly. It shall be possible on condition of precise finding of dependencies between geometrical and kinematic parameters of construction of a given drum assembly and the location and thickness of the layer of the cut material.

It results from the literature studies, that the above issue [1, 2, 3, 4, 5, 6, 7] has not been precisely solved yet.

That is why in this study, the attempt of mathematical description of a cutting drum's movement has been assumed as the basic goal of the work particularly considering its knives at the stage of cutting of a material's layer.

## 2. Analysis of the issue

Analyzing a complex movement of a single cutting edge it may be noticed, that the cutting speed  $\mathcal{G}_c$  is a variable value and is strictly determined by the tangential velocity of knives  $\mathcal{G}_b$  and the speed of material feeding  $\mathcal{G}_m$  for cutting. The direction and value of the speed  $\mathcal{G}_c$ , vary together with the value of the drum's rotation angle  $\varphi$ . For any location of a knife's location, pursuant to Fig. 2, speed  $\mathcal{G}_c$  may be calculated from dependencies:

$$\mathcal{G}_c = \sqrt{\mathcal{G}_b^2 + \mathcal{G}_m^2 + 2\mathcal{G}_b\mathcal{G}_m\cos\psi} . \quad (1)$$

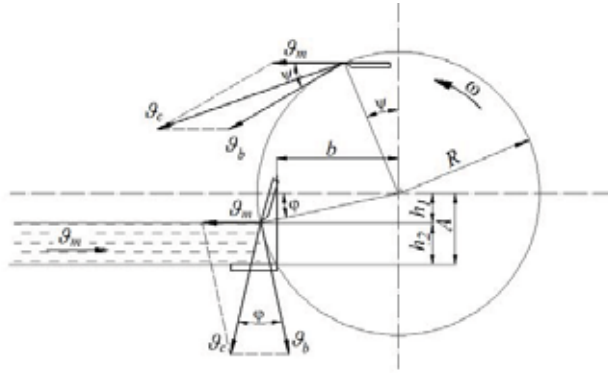


Fig.2. Location of the drum rotation's axis in relation to the counter cutting edge

In case of no specific location of the counter cutting edge in relation to the drum's axis, the knife shall cause pushing away of material what shall result in the increase of cutting resistances and the increase of unevenness of chaff's cutting.

Limiting location of the counter cutting edge at constant thickness of fed layer assuring correct cutting shall take place when the component horizontal linear velocity of a knife is equal to the material's feeding speed what takes place when :

$$\sin \varphi = \frac{g_m}{g_b}. \quad (2)$$

It results from the analysis of the Fig. 2, that:

$$h_1 = R \sin \varphi = R \frac{g_m}{g_b} = R \frac{1}{\lambda}, \quad (3)$$

where:

$R$  – radius of cutting drum,

$\lambda$  – kinematic ratio of a drum cutting assembly specified as a quotient of the tangential velocity  $g_b$  of cutting knife to feeding speed  $g_m$  of material to be cut.

So, the distance of the counter cutting edge from the drum's axis in the vertical plane may be calculated from the formula:

$$A = h_2 + \frac{R}{\lambda}. \quad (4)$$

While the distance of the drum rotation's axis from the counter cutting edge in the horizontal plane may be calculated from the dependence:

$$b = \sqrt{R^2 - A^2} = \sqrt{R^2 - \left(h_2 + \frac{R}{\lambda}\right)^2}. \quad (5)$$

From the analysis of equations (4) and (5) it results, that location of counter cutting edge in relation to the rotation's axis of a cutting drum depends on a drum's radius, thickness of cut laser of material and the kinematic index.

Due to the fact, that the cutting drum makes rotational motion and material moves with uniformly linear motion in its direction, the movement path of knives has the form of a trochoid which, pursuant to Fig. 3 is described by a parametric equation:

$$x_a = \mathcal{G}_m t + R \cos \omega t, \quad (6)$$

$$y_a = R(1 - \sin \omega t). \quad (7)$$

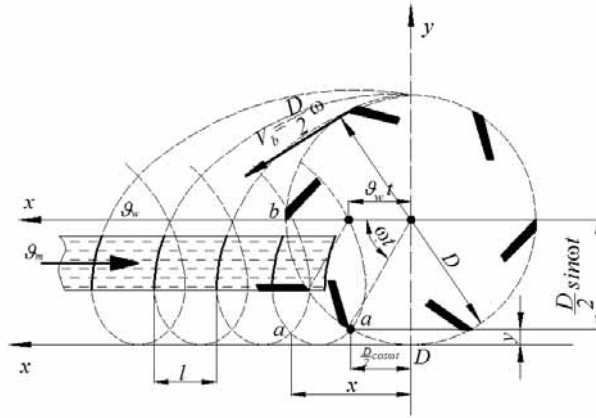


Fig.3. Path of drum's knives in relation to the cut layer of material

In order to determine resultant speed  $\mathcal{G}$  and acceleration  $a$  of a knife, one should appropriately differentiate equations (6) and (7) and to make appropriate mathematical operations.

Differentiating equations (6) and (7) once, the below was received:

$$\mathcal{G}_{xa} = \frac{dx_a}{dt} = \mathcal{G}_m - R\omega \sin \omega t, \quad (8)$$

$$\mathcal{G}_{ya} = \frac{dy_a}{dt} = -R\omega \cos \omega t. \quad (9)$$

Taking into account that the resultant speed of the knife is described by the dependence:

$$\mathcal{G} = \sqrt{\mathcal{G}_{xa}^2 + \mathcal{G}_{ya}^2}, \quad (10)$$

after conversions there has been received:

$$\mathcal{G} = \sqrt{\mathcal{G}_m^2 - 2\mathcal{G}_m R\omega \sin \omega t + R^2 \omega^2}. \quad (11)$$

However, differentiating twice the equations (6) and (7) there has been obtained:

$$a_{xa} = \frac{d\mathcal{G}_{xa}}{dt} = -R\omega^2 \cos \omega t, \quad (12)$$

$$a_{ya} = \frac{d\mathcal{G}_{ya}}{dt} = R\omega^2 \sin \omega t. \quad (13)$$

Taking into account that the resultant acceleration of the knife is described by the dependence:

$$a = \sqrt{a_{xa}^2 + a_{ya}^2}, \quad (14)$$

after conversion there has been received:

$$a = \sqrt{\left(-R\omega^2 \cos \omega t\right)^2 + \left(R\omega^2 \sin \omega t\right)^2} = R\omega^2. \quad (15)$$

Distances between the adjacent trochoid loops deposited on the layer of cut material are equal to each other and constitute the so-called computational cutting length corresponding to the length of chaff.

The theoretical length of chaff  $l$  with sufficient approximation may be calculated from the dependence:

$$l = \frac{\mathcal{G}_m}{n \cdot z} = \frac{\pi \mathcal{G}_m}{30\omega \cdot z}, \quad (16)$$

where:

$\mathcal{G}_m$  – speed of material feeding,

$n$  – rotational speed of cutting drum,

$\omega$  – angular velocity of cutting drum,

$z$  – number of knives.

### 3. Final conclusions

In the light of the conducted analysis of this issue, the following conclusions may be formed:

1. Mathematical dependencies presented in the study describing kinematics of drum movement of a cutting assembly of a straw cutter and in particular of its cutting knives, constitute the first attempt of comprehensive presentation of that issue.
2. Derived dependencies make it possible to establish relationships between the basic operational parameters of a cutting drum and its constructional and geometric features in the aspect of kinematics of the movement of knives cutting the layer of material.
3. Developing the dependencies may be used at the stage of simulation tests with new drum constructions of cutting assemblies of a straw cutter and in the process of automation of their operation's steering.

### References

- [1] Bochat A., Zastempowski M.: *Analiza badań cięcia źdźbeł roślin zbożowych i nowy bębnowy zespół tnący*. Inżynieria i Aparatura Chemiczna 1-2/2005, ss. 31-33.

- [2] Bochat A., Błaszczuk M., *Próba modelowania matematycznego odkształceń sprężystych źdźbeł*. Journal of Research and Applications in Agricultural Engineering 52(1)/2007, ss. 21-26.
- [3] Haffert A., Harms H.H., *Schnittvorgang im Fel dhäckslern*. Landtechnik 2/2002, pp.106 -107.
- [4] Kanafojski Cz., *Teoria i konstrukcja maszyn rolniczych*. Tom 2. PWRiL, Warszawa, 1980.
- [5] O'Dogherty M.J., Gale G., *Laboratory studies of the cutting of Grass stems*. Journal of Agricultural Engineering Research 35/1986, pp.115-129.
- [6] O'Dogherty M.J., Huber J.A., Dyson J., Marshall C.J., *A study of the physical and mechanical properties of wheat straw*. Journal of Agricultural Engineering Research 62/1995, pp.133-142.
- [7] Advertising material, catalogs and websites of companies: Claas, John Deere, Mengele, Taarup.



## CONTROLLING RATE OF DELIVERY OF APPLICATORS AT THE HARVEST OF SUBSTRATES BIOGASWORKS - PRELIMINARY ISSUES.

**Sylwester Borowski,**

University of Technology and Life Sciences in Bydgoszcz

al. Prof. S. Kaliskiego 7, 85-789 Bydgoszcz

tel.: +48 52 3408132 e-mail: sylwa@utp.edu.pl

*At the paper preliminary issues concerning applications of preparations preserving to silages were introduced. Such silages can be used as forage of animals and substrates of the bio-gasworks. During the harvest of green fodder to silages getting an end product of the better quality is one of more important problems. It is possible to obtain it using additions facilitating ensilage. Using them allows also for the improvement of the quality of the long preserved silage. One should aspire to it to get regular distributing preparation in the entire capacity of the silo. In the course of the application losses of preparation should be minimal.*

**Keywords:** additives, biogasworks, silage, substrates,

### 1. Introduction

Achievement of the best quality products and application of high preservation technology and methods for loss reduction in each phase of production are of top priority in plant production. In order to achieve this goal it is necessary to implement agricultural-technical procedures consistent with the philosophy of precise agriculture whose main element is mapping of crops. It stimulates the development of technological solutions connected with recording and processing of data concerning the crops. Collected and analyzed in this way information allows to synchronize local and temporary land-soil properties with intensity of agricultural -technical processes.

In case of harvesting machines, definition of temporary volume of plant stream can not only be used for elaboration of a harvest map for a given area but also for determination of a precise dose of supporting preservatives applied during the harvest. In both cases the development of this technology involves improving precision of detection of changes occurring in the used machines which can be associated with a nonlinear rate of the plant stream flow. For this, purpose there are used different types of sensors, which properly sited, enable generation of signals which make it possible to define the plant material stream volume in a real time.

Application of additives during silage preparation reduces losses of energy contained in the substrate which are connected with lactic fermentation and further storage in silos. Thanks to additives it is also possible to obtain a higher level of the biogas yield [3, 2].

Nowadays, additives are dosed during the harvest or during loading and placing the plants into containers. Although the methods of application of preservatives into fodder plants undergo constant modification each of them allows to adjust the preparation dose to: field conditions, kind of the harvested plant, type of the additive and model of the harvesting machine or the machine loading the material to containers (silos). Methods of the applicator rate control can be divided into three basic groups, including: manual, semi-manual and automatic.

## 2. Rate of applicators

The rate of applicators can be referred to as volume or mass of the preservative, which is being applied into the plant material, during a given time. This value can be characterized by the following formulas:

$$Q_1 = \frac{V}{t}, (\text{ml min}^{-1}) \quad (1)$$

$$Q_2 = \frac{m}{t}, (\text{g min}^{-1}) \quad (2)$$

where:

$Q_1$  – rate of applicators dosing preservatives in the form of fluid, ( $\text{ml min}^{-1}$ )

$Q_2$  – rate of applicators dosing solid preparations, ( $\text{g min}^{-1}$ )

$V$  – the preparation volume, (ml),

$m$  – the preparation mass, (g),

$t$  – time in which a given mass or volume is placed in the harvested material (min).

Control of the applicator rate enables to match the additive dose with the applied fodder preservation technology, species of plants and recommendations of the preservative producer. One of the simplest methods enabling to change the dose of fluid additives is application of a system of exchange nozzles. It is the most common solution as it does not affect significantly the costs connected with construction of the application installations.

Another manual solution involves using choking valves, by means of which, it is possible to control flow of the additive. This kind of control is used, among others, in a fluid applicator Junkkari HP5 of Finnish production, presented in figure 1. The rate is regulated by screw in the flow-meter.



Fig. 1. Picture of HP 100 dosing installation of Junkkari company: 1 – cords; 2 – membrane pump with a flow-meter; 3 – container with a preservative with an elastic conduit; 4 – controller; 5 – nozzle; 6 – leak protection valve

A popular solution is also a remote control of the rate by means of electronic controllers. This solution involves fixing a regulation device in the tractor cabin (self-propelled straw cutter) by means of which the machine operator can control the installation operation [10].

By means of a controller the operator can cut off the preservative inflow during manoeuvres. The controller has also an automatic summing meter of the flow, thanks to which, it is possible to read the actual amount of the pumped additive. Additionally, the system notifies of low amount of an additive in the container. If HP 1000 dosing system is equipped with a speed sensor it is possible to obtain a reading in the approximate area from which the plants have been harvested. Moreover, application of a the controller special mode of operation, after being preprogrammed, increases the amount of preservative in relation to the speed [10]. The operation principle of automatic dosing systems is based on defining temporary mass or volume of the harvested green crop. Distribution of the preservatives can also depend on the harvested fodder plant quality. Such an innovative solution is offered by Harvest Tec (USA) in the harvest technology of green fodder for hay by means of both roll and cube balers. It is the most efficient method as it provides not only effective distribution of the preparation measured dose but also improves the operator's comfort. Additionally, application of such systems reduces losses of additives which contributes to decreasing costs of fodder production. It also leads to elimination of the environment degradation threat connected with the use of chemical compounds and prolongation of lifetime of the machine elements being in direct contact with them [11].

Optimal adjustment of the applicator rate has an influence on the level of the additive losses. The best solution is to control the dose which is to be adjusted to the plant stream flow changes during the harvest machine operation. It has a positive influence not only on improving the preservative distribution efficiency but also increases the comfort of work as well as reduces the phenomenon of corrosion of elements which are in contact with the preservation solution.

An assessment of dosing devices operation is based mainly on the degree of mixing uniformity of precisely measured preservative doses with the plant material, with regard to its potential losses. Factors which determine the quality of this procedure include: distribution of nozzles applying the substance in harvesting or cutting machines and the degree of the plant material fragmentation. A uniform distribution of the preservative in the harvested material is the only way to achieve good results [4, 5, 6, 7, 16, 8, 9].

### 3. Experiment

In order to establish the site for green fodder application in a roll baler the material used for the analysis was a mixture of meadow grass with moisture content 56%. 5% water solution of sodium chloride was used as an additive. The preparation of green fodder was added to green fodder during its harvest by means of Junkkari HP5 applicator which was mounted in the front part of the round baler (fig.1). The applicator was equipped with two vortex nozzles of Hardi with the inlet opening diameter  $\varnothing$  0,025 mm, pressure was 0,5 MPa. The nozzles were placed in three different places (Fig. 2) in such a way that they could spray the additive on the whole width of the round baler.

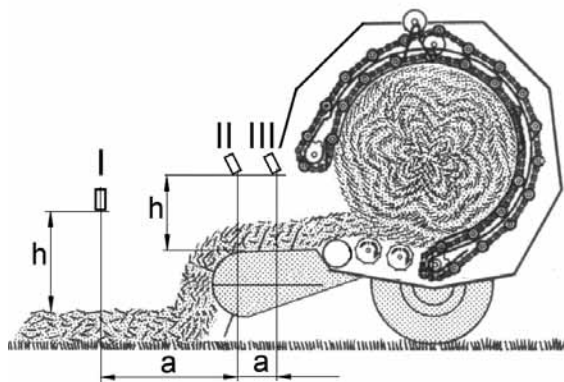


Fig. 2. Location of fastening the nozzle of applicator in round baler: I —ahead of the pick-up unit; II —over the pick-up; III —in the front part of the press chamber

The size of additive losses (water solution of NaCl) was determined basing on the marking of CL concentration of ions. The size of these losses is referred to as a ratio of the preparation amount left on measurement plates to the amount given according to dependence:

$$L = \frac{V_p}{V_z} \cdot 100\% \quad (3)$$

where:

L —losses of sodium chloride %

$V_p$ —amount of sodium on measurement plates,  $\text{dm}^3/\text{ton}$  of green fodder

$V_z$ —given amount of sodium chloride (control),  $\text{dm}^3/\text{ton}$  of green fodder

Measurement distances with length 100 m were determined by means of poles prior to the test. Rollers with plant material were manually arranged in such a way that they were characterized with equal height and width and uniform distribution of mass over the whole length.

The aggregate moved at the speed  $4.58 \text{ km h}^{-1}$  ( $1.27 \text{ m s}^{-1}$ ). Three plates with dimensions  $1.0 \text{ m} \cdot 2.5 \text{ m}$  were placed on the line of its pass under green fodder lying in the roller. The plates provided coverage of the aggregate whole working space. Plates were fixed to the ground by steel bolts in order to avoid pulling them up during the bale pass. Along the ride of the unit the plate was rinsed with the distilled water (100 ml).

The solution, obtained in result of rinsing the preparation which remained on the base (plate), was put into glass containers. Mrking of the concentration of CL ions was made by mercurymetric method [1].

Measurements of concentration of CL ions were made for all the locations of nozzles. Tests were performed three times. The obtained tests results were subjected to analysis of variance. Calculations were performed according to computer program ANAWAR 1.0. Significance of differences between experimental groups (different locations of nozzles) was examined by Tukey's range test.

### 3. Results

On the basis of the obtained results there was made a histogram of sodium chloride losses

distribution in dependence on its application to green fodder in roll baler which has been presented in figure 3. It shows that in relation to the quantity of the given amount ( $2.5 \text{ dm}^3 \text{ t}^{-1}$  of green fodder), losses of the preparation in the amount 35.6% occurred while dosing it to green fodder placed in the roller. It was 12.8%. The smallest losses, in the amount 2.0%, were found for dosing it to green fodder lying in the baler. A distinct losses reduction occurred for dosing the solution into green fodder placed in the baler pickup. It was 12.8%. the smallest losses, in the amount of 2.0%, were found for dosing green fodder in the front part of the rolling chamber.

The carried out statistical analysis of tests results show that losses of sodium chloride differ statistically significantly between application sites – ahead of the pickup (watered roller of green fodder) and application sites above the pickup and in the front part of the prees chamber. Statistically significant differences occurred between the application site above the pickup and application site in the front part of the rolling chamber (fig.3).

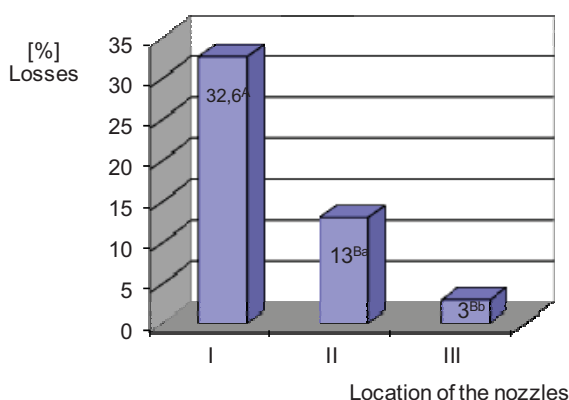


Fig. 3. Distribution histogram for the loss sodium chloride with respect to the location of the applicator in a forage harvester. Mounting locations for the applicator: I -ahead of the pick-up unit (the roll of crop sprinkled), II - over the pick-up unit, III - in the front part of the bale chamber. The values A and B (denoted by capital letters) are significantly different from one another ( $p \leq 0.01$ ), whereas the values a and b (denoted by lower-case letters) are statistically significant ( $p \leq 0.05$ ).

Results of markings of the number of lactic acid bacteria have been presented in table 1. It proves that the smallest amount of lactic acid bacteria was characteristic for green fodder of group I (without additives) with moisture content 81% ( $6.1\% \times 10^2$  of units making up cells per one gram of green fodder).

#### 4. Conclusions

The location of the applicator significantly affected the loss of additive. The smallest losses (about 2%) occurred of the applicators mounted in the front part of the bale chamber, whereas, the highest losses (up to 35.6%) occurred with the applications ahead of the pick-up unit.

For forage of moisture content up to 70% (wet and wilted forage), additive application produced silage of higher quality compared with forage without additive.

## References

- [1] AOAC, Official Methods of Analysis,. 15th., Assos. Offic. Anal. Chem., Darlington, Wirginia, USA, 1990.
- [2] AG-BAGS News, Magazyn informacyjny technologii AG-BAG,. Nr 9, 2009.
- [3] BOROWSKI, S., DULCET, E., Analiza kształtowania się temperatury w belach uzyskanych z siana, także z dodatkiem preparatu ciekłego, pp. 37-46, Technica Agraria, 2003.
- [4] BOROWSKI, S., DULCET, E., KASZKOWIAK, J., Analiza kształtowania się temperatury w belach siana z dodatkiem preparatu mikrobiologicznego INOCULANT 1155, Inżynieria Rolnicza, 12/2006.
- [5] BOROWSKI, S., Ocena jakości rozprowadzenia dodatków w paszach objętościowych., Technika Rolnicza, Ogrodnicza, Leśna, str.: 13-15, Nr 3., 2009.
- [6] DULCET, E., Badania nad równomiernością wymieszania konserwantu z zielonką w procesie zbioru na kiszonkę oraz nad wielkością jego strat, Wyd. I, Bydgoszcz, Wydawnictwo Uczelniane ATR, 1993,
- [7] DULCET, E., BOROWSKI, S., *Dokładna aplikacja.*, pp. 36-37, Rolniczy Przegląd Techniczny, Nr 5, maj 2008.
- [8] DULCET, E., Równomierność wymieszania ciekłego konserwantu z zielonką w procesie jej zbioru siewkarnią zbierającą., str. 109-120, Problemy Inżynierii Rolniczej, Nr 1, styczeń 1998.
- [9] DULCET, E., MIKOŁAJCZAK, J., OLSZEWSKI, T., *Technika zastosowania konserwantów przy zbiorze wilgotnego siana prasami zwijającymi.*, Wyd. I, Bydgoszcz, Wydawnictwo Uczelniane ATR, 2002,
- [10] DULCET, E., *Nowoczesne techniki zbioru zielonek i metody ich zakiszania.*, Wyd. I, Bydgoszcz, Wydawnictwo Uczelniane ATR, 2001,
- [11] Muck, R., Savoie, P., Holmes, B. Laboratory assessment of bunker silo density, Part I: Alfalfa and grass. Applied Engineering in Agriculture, 20(2), s. 157-164, 2004.



## BALLERS FOR MOLDING BALES OF SHREDDED MATERIAL

**Sylwester Borowski, Edmund Dulcet, Jerzy Kaszkowiak,**  
*University of Technology and Life Sciences in Bydgoszcz*  
*al. Prof. S. Kaliskiego 7, 85-789 Bydgoszcz*  
*tel.: +48 52 3408132 e-mail: sylwa@utp.edu.pl*

**Robert Bujaczek, Jerzy Chojnacki**  
*Koszalin University of Technology*  
*ul. Raclawicka 15-17, 75-620 Koszalin*  
*tel.: tel. +48 94 3478440*

*The article deals with the design and the operation principle of presses for forming cylindrical bales from shredded materials, there has been made an assessment of the quality of silage obtained from beet pulp prepared by a press manufactured by Norwegian company Orkel (model MP 2000 Compactor). It has been proved that quality of the obtained fodder does not differ from the quality of fodders formed in long foil sleeves. It has been found that on the domestic market machines of this type are not available for small and medium companies.*

**Keywords:** shredded materials, pulp, biogas power plant, silage

### 1. Introduction

Shredded materials include: pressed pulp, spent grain, sawdust, tree bark, short straw, and other production materials often referred to as production waste. Products of plant origin are often used as animal fodder for cattle. However, due to limited access to these materials during the whole year it can't be provided throughout it. In such a situation silage of these products seems to be a good solution. Silage of fragmented materials with minimum loss is possible only by maximum reduction of pollution and ensuring oxygen free conditions of storage throughout the whole period of their fermentation, storage and feeding [4,5,6,18]. Such possibilities are provided by the newest – currently offered technology of fodder silage in the form of cylindrical bales. This technology does not apply merely to fodders collected by a round baller (straw, hay, green crop) but also includes solutions basing on stationary machines whose task is to form bales from shredded material with simultaneous protecting it from access of air [5,10,15,19]. The silage quality obtained for the cylindrical bales depends largely on the material density degree and its protection from the air access.

The density degree is affected mostly by physical properties of the material used for silage, that is, dimensions, humidity, elasticity. These properties, apart from their distinct impact on the fermentation process course, also affect the use of consumables (net, foil) as well as the costs of transport and storage [1,8,13,16,20].

### 2. Review of designs of stationary round balers for shredded materials

In the small group of manufacturers of these machines there are two European companies: Norwegian company Orkel (MP2000 model Compactor) and Austrian (model LT-Master).

Presently, in Poland there are used only two presses by Orkel companies in sugar factories of groups: Pfeifer und Langen and Nordzucker. They are used for silage of beet pulp. The design of this machine (Fig. 1) is based on a uni-axial chassis. In the back part of the machine (Fig. 1b) there is a cutting basket 4, with a horizontal chain - strip conveyor to which the pulp is fed. The basket can be supplied directly from the production line or by means of different types of loaders (grip, head, telescopic loaders, etc.). The main operation system of the machine is an innovative box for rolling bale 2, consisting of powered smooth rollers and two structural rubber belts of length 1.2 m. The operation box is powered by a channel from the top by means of a inclined chain - strip conveyor.

Formation of the bales is based on the principle of hybrid baller. In the initial phase of its operation the rubber belts, run through a stationary rolling chamber and their positions in relation to each other is of 'V' shape (Fig. 2).

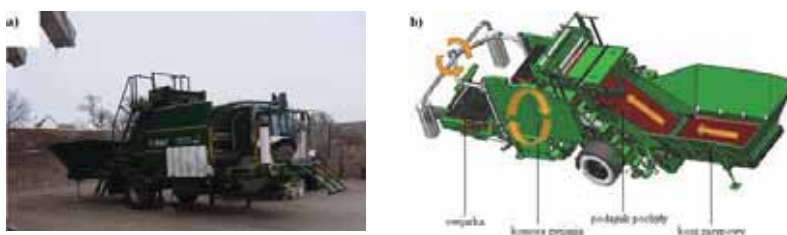


Fig. 1. Press Orkel MP 2000 Compactor: a - general view, b - construction schedule: 1 - wrapper, 2 - chamber collapse, 3 - inclined conveyor, 4 - receiving basket

Along with supplying the pulp, the chamber successively increases and the rubber belts are pressed down to steel rollers. A formed in this way ballot can be protected from falling apart by means of a net or polyurethane foil. This process is continued in the rolling chamber. The ballot after being wrapped by a net goes to the wrapper table where it is protected from the impact of atmospheric factors by 6 layers of standard tensile foil for silages of width 0.75 m. (fig.3).

After being wrapped by a foil the ballot falls freely on the ground along an inclined ramp. Ready ballots can be loaded onto transport means and carried directly to customers or stored in the sugar company. Operation of the machine MP 2000 Compactor is fully automatic and all functions of its subsystems are monitored, displayed and programmed by a controller. According to the manufacturer a demand for power is 90 kW and the capacity is within 40-60 bales per hour (to 60 t h<sup>-1</sup> for the bale dimensions 1.2 m x 1.2 m) depending on the pressed material. The source of power can be both an agricultural tractor and an electric motor [6].



Fig. 2. Folding chamber shape in the initial phase of work (top view): 1-wrapper, 2-coiled material, 3- lateral ventricle wall collapse



Fig. 3. Formed bale wrapping with stretch film

Göweil company offers a press marked with symbol LT-Master (Fig. 4). Its design and the operation principle of the main operating system, that is, the rolling chamber, is quite similar to the press MP 2000 Compactor. The main differences between presses Orkel and Göweil involve: the way of connection with the tractor, the place of drive transmission and the manner of supplying the formed bale on the wrapper table. Change of the transporting position into the operating one and the other way round does not require its disconnection with the tractor [6]. The design of the dumping basket is a big advantage because it can be loaded directly from the self-loading trailer.

Similar solutions are offered by a Japanese manufacturer Takakita Co, Ltd. This company offers presses designed for forming cylindrical bales from fragmented materials with symbol MR - 810 (Fig. 5), MW 1020 and MW 1220 (Fig. 6). In these machines there is a stationary rolling chamber which is an immovable front part 2 and a movable (lifted and lowered) back part 3. A distinctive feature of this Japanese manufacturer's presses is a dumping basket which rises after being filled, thus facilitating transport of the material to the pressing chamber [6].

Machines with symbols MW 1020 and MW 1220 combine a steady-chamber stationary press with a dumping basket 2 and wrapper 3 with two rotary arms (Fig. 6).



Fig. 4. Baler Göweil LT-Master: 1-unloading ramp, 2-wrapper, 3-chamber collapse, 4-inclined conveyor, 5-receiving basket



Fig. 5. Japanese business newspaper Takakita Co. Ltd model MR 810: 1-receiving basket, 2- the front part of the chamber collapse, 3-back, moving part of the chamber collapse



Fig. 6. Japanese business newspaper Takakita Co. Ltd model MW 1220: 1-chamber collapse, 2-hopper, 3-wrapper, with two rotating arms

### 3. Analysis of the fodder quality

An analysis of the quality of fodder prepared with the use of Orkel (model MP 2000 Compactor) has been made. Samples of silage from the pulp in a sugar factory in Opalenica near Poznań belonging to the Nordzucker Polska Group. Silage had been stored for 8 weeks in bales. Samples for assessment were taken from 15 different sites of the bale (7).

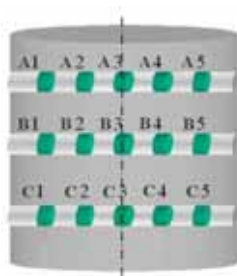


Fig. 7. Scheme of sampling sites

The range of chemical analysis covered marking of the dry mass and raw ash content (according to weedeńska method) and ammonium (by Conway method) as well as organic acids (Lepper's method): lactic, acetic and butyric acids [2]. Value of pH was marked by means of pH - meter N5172. The main parameters of chemical content and quality of silages prepared from beet pulp in bales have been presented in table 1.

Tab. 1. The chemical composition and quality of pulp silage

| Dry matter     | pH            | Raw ash                 | Ammonia       | Lactic acid     | Acetic acid   | Butyric acid | Flieg-Zimmer's quality |           |
|----------------|---------------|-------------------------|---------------|-----------------|---------------|--------------|------------------------|-----------|
| g              |               | g kg <sup>-1</sup> D.M. |               |                 |               |              | points                 | rating    |
| 279,4<br>±18,5 | 3,53<br>±0,03 | 55,03<br>±2,05          | 0,85<br>±0,22 | 68,55<br>±16,39 | 8,95<br>±1,40 | 0,00<br>0,00 | 100                    | very good |

D.M. – dry matter

Comparing quantity of the obtained parameters with literature data it should be remembered that the kind of material must be accounted for. Usually the data concerning good silages refer to fodders prepared from green crop or grass papilionaceous plants or corn.

The content of dry mass in the analyzed samples was characteristic for a good silage prepared from pressed beet pulp. Mc Donald at al. [7] claim that the share of dry mass in pressed pulps ranges from 180 to 250 g kg<sup>-1</sup>. Low concentration of raw ash indicates high purity of the obtained fodder. Wilkinson [17] says that the content of this component in an ideal fodder is below 80 g kg<sup>-1</sup> of dry mass.

The quality of silages is defined by numerous parameters connected with the process of fermentation, one of the most important being pH [3]. The value of this parameter was lower than the value referred to as the proper one for good silages 4,0 - 4,2 [17]. Fodders with low pH can be the cause of occurrence of acidosis in ruminants [12].

Content of ammonium as a product of protein decomposition is also an index of the silage quality. In the carried out tests the content of ammonium was at a low level. Silages of good quality contain less of this compound than those poor ones [7].

The content of lactic acid shows that the fermentation process during silage runs in a proper way. In fact, its content in good silages should reach the level 100 - 150 g kg<sup>-1</sup> of dry mass, however, the share of this acid in the sum of all the acids was 88.45%, which is considered to be a proper index.

In the tested silages the content of fungistatic, that is, acetic acid was 2.5 g in fresh mass which does not guarantee the fodder stability in oxygen conditions, after being taken out from the cylindrical bale. High concentration of lactic acid and lack of fungistatic volatile fatty acids inhibiting yeasts, can have a detrimental effect on the silage durability after being taken out from a

container. Only with the content of 8 g of un-dissociated acetic acid in a fresh mass inhibits a development of fungi and yeasts which are responsible for the silage heating [11]. According to Wilkinson [17] an ideal silage can contain from 20 to 30 g of acetic acid in its dry mass.

In the analyzed silages there was no butyric which can be considered as an ideal result [17]. Absence of butyric acid in cylindrical bales of beet pulp silages indicates no effects of *Clostridium* bacteria operation during fermentation and – apart from the content of raw ash, it is an indicator of their purity. However, low pH can also be considered to be the inhibitor as it limits a growth of these microorganisms [7, 14].

An appropriate ratio of butyric acid in the sum of the three acids has found reflection in a high assessment of quality. According to Flieg - Zimmer scale the analyzed silages reached the highest grade – very good.

#### 4. Conclusion

Balers forming cylindrical bales from fragmented materials are mainly stationary machines. They are usually powered by a power take off shaft and designed for formation of cylindrical bales from such materials as: beet pulp, spent grain, fragmented corn cobs, corn chaff. As compared to the classical presses instead of a net dipper they have a built-in dumping basket and the bale forming chamber usually consists of powered smooth shafts and two structural rubber belts whose width is equal to the width of the press. Formation of bales is performed according to the rule of hybrid press operation. The ballot, after being wrapped by a net, goes to the bottom of the wrapper where it is protected from atmospheric factors by a few layers of standard foil for silages. The carried out assessment of the obtained silages quality revealed that their quality was very high, though were characterized by low pH.

Due to small content of acetic acid they can't be durable in oxygen conditions. Lack of butyric acid indicates a good hygienic status of the silages from pressed beet pulps prepared in cylindrical bales. It can be stated that their quality is not lower than the quality of fodders formed in long foil sleeves.

The above presented machines are extremely useful for service units and food production companies whose by-products are a desirable fodder for farm cattle.

It can be expected that the technology for silage of different plant materials with the use of presses will be competitive for foil bags (sleeves) formed by a silo press.

It should be emphasized that on the domestic market machines of this type are not available for small and medium companies (maximal capacity up to 10 bales per hour). The concept of such a press has been developed in the Division of Agricultural Technology of the University of Technology and Life Sciences in Bydgoszcz and Department of Agricultural Engineering of the Technological University in Koszalin. Cylindrical bales of different fragmented fodders protected from the air access by a flexible foil, have already become an attractive product available on the market of many countries.

#### References

- [1] Amours, L. D., Savoie, P., *Density profile of corn silage in bunker silos*, Canadian Biosystems Engineering, 47, s. 221-228, 2005.
- [2] AOAC, *Official Methods of Analysis*. 15th., Assoc. Offic. Anal. Chem., Arlington, Virginia, USA, 1990.
- [3] Doroszewski, P.A., *Efektywność stosowania dodatków kiszonkarskich w konserwacji zielonek z mieszanki motylkowato-trawiastej oraz z całych roślin kukurydzy*, Rozprawy nr 136, Wyd. Ucz. UTP, Bydgoszcz 2009.

- [4] Dulcet, E., Kaszkowiak, J., Ledóchowski P., *Zakiszanie wysłodków buraczanych w belach cylindrycznych*, Inżynieria Rolnicza, 4(102), s. 241-248, 2008.
- [5] Dulcet, E., Ledóchowski, P., *Technologia zakiszania wysłodków buraczanych w postaci bel cylindrycznych owiniętych folią*, Journal of Research and Applications in Agricultural Engineering, 52(3), s. 37-39, 2007.
- [6] Magazyn informacyjny technologii Ag – Bag, 7, s. 10-11, 2007.
- [7] McDonald, P., Henderson, A. R., Heron, S. J. E., *The biochemistry of silage*, Chalcombe Publications, Bucks, 1991.
- [8] Muck, R., Savoie, P., Holmes, B., *Laboratory assessment of bunker silo density, Part I: Alfalfa and grass*, Applied Engineering in Agriculture, 20(2), s. 157-164, 2004.
- [9] Nowak, J., *Maszyny do formowania bel cylindrycznych z materiałów rozdrobnionych i sypkich*, Technika Rolnicza Ogrodnicza Leśna, 3 s. 10-12, 2010.
- [10] Nowak, J., Karaś, M., *Badania technologii zbioru słomy i siana*, Postępy Nauk Rolniczych, 1 s. 101-110, 2006.
- [11] Pahlow, G., *Erfahrungen mit Mikroorganismen in der Silierung. Mikrobiologie und Tierernährung*, 20. Hülsenberger Gespräche, Lübeck, s. 85-93, 2004.
- [12] Mikołajczak, J., *Praca zbiorowa, Żywnienie bydła*. Wyd. Ucz. ATR, Bydgoszcz, 2006.
- [13] Purwin, C., *Rozprawy i monografie, Jakość kiszonek z traw i mieszanek traw z roślinami motylkowymi produkowanych prasami zwijającymi*, Wydawnictwo Uniwersytetu Warmińsko-Mazurskiego, s. 11-15 Olsztyn, 2007.
- [14] Purwin, C., Łaniewska-Trokenheim, Ł., Warmińska-Radyko, I., Tywończuk, J., *Jakość kiszonek – aspekty mikrobiologiczne, zdrowotne i produkcyjne*, Medycyna Weterynaryjna 62(8), s.865-869, 2006.
- [15] Shito, H., Yamana, N., Shibuya, Y., Takahashi, K. *Review. Development of the roll baler for chopped material*, Japan Agricultural Research Quarterly, 40(3), s. 233-237, 2006.
- [16] Sun, Y., Buescher, W., Lin, J., Schulze, Lammers, P., Ross, F., Maack, C., Cheng, Q., Sun, W., *An improved penetrometer technique for determining bale density*, Biosystems Engineering, 105, s. 273-277, 2010.
- [17] Wilkinson, J. M., *Silage*, Chalcombe Publications, Lincoln, 2005.
- [18] Winnicki, S., Domagalski, Z., Pleskot, R., *Ekspertyza. Technika w zakresie konserwacji, przechowywania i zadawania pasz dla bydła*, IBMER, s. 4-8, Poznań 2009,.
- [19] Wyss, A., *Silierung von Apfel – und Birnentrester*. Agrarforschung 10(3), s. 104-109, 2003.
- [20] Żurawska, M., Kamieniarz, J., *Technologie zagospodarowania wysłodków prasowanych, Burak cukrowy 4*, s. 25-29, 2007.



## NUMERICAL ANALYSIS OF FORAGE TRAILER SUPPORTING STRUCTURE

**Artur Cichański, Michał Burak, Dariusz Skibicki, Michał Stopel**

*University of Technology and Life Sciences in Bydgoszcz  
ul. Kaliskiego 7, 85-789 Bydgoszcz, Poland  
tel.: +48 52 3408235, fax: +48 52 3408245  
e-mail: artur.cichanski@utp.edu.pl*

### **Abstract**

*The paper discusses issues of examination supporting structure of forage trailer. Tests were applied to supporting structure, lowered in order to adjust the height of mix feeding for younger cattle. Lowering obtained by spreading of supports caused increase of the structure effort and increase of stress exceeding acceptable values. The paper describes the manner of preparation of numerical model and results of tests performed with its application. Based upon the results modification of the structure in critical areas was proposed. Implementation of such modifications resulted in improvement of effort of forage trailer supporting structure..*

**Keywords:** agricultural machinery, forage trailer, structure tests, FEM, ANSYS

### **1. Introduction**

Forage trailer are widely used in particular on big farms which breed the cattle on large scale and intend to improve their stock efficiency through correct feeding of animals. Basic functions of forage trailer (Fig. 1) are: dosing correct feed dose, mixing and transportation to pasture.



*Fig. 1. Forage trailer EVO*

Special screw with knives is used for feed mixing and crushing. High and large capacity box allows for feed supply. Appropriately located gears transfer trailer supplied drive, move the screws and belt conveyors. Whole structure, additionally loaded by significant amount of feed is based on supporting frame. One of crucial parameters of forage trailer structure is the height at which animals take the mix – if its too high, shorter animals have difficulties with reaching the feed. The paper undertakes testing of lowered supporting frame structure. Such lowering was obtained by moving away of rear support which resulted in increase of deflecting moments acting on the frame. Numerical analyses were performed in order to set the structure strength and guidelines were specified for further modification of frame which was subsequently verified.

Tested object was supporting frame of low EVO forage trailer. Characteristic dimensions of the object are presented at Fig. 2. On rear and front holders (Fig. 2) there is a basket containing the screw for feed mixing. Main supporting beams are made of closed sections 80 x160. The frame is made of S235JR steel.

Fig. 2. Dimensional drawing of supporting frame of low EVO forage trailer

screw, 5 000 kg - feed, after summing up total mass - 8 300 kg. It was assumed for analyses that force of  $Q=81.5$  kN will be applied to the frame. The force was divided into components: rear loads  $R_T$  operating in rear holders and front loads  $R_P$  operating in front holder. The form of both components is defined by set dependencies (1) and (2).

$$R_P = Q \left( 1 - \frac{R}{H} \right) \quad (1)$$

$$R_T = Q \times \frac{R}{2H} \quad (2)$$

gdzie:

$R$  – radius of a circle defined on points setting centres of supports.

$H$  - distance between supports measured in direction  $OZ$  acc. to Fig. 2.

Based upon measurements performed with supplied documentation values of  $R = 976.5$  mm and  $H = 1672.5$  mm were set resulting in the fact that the frame is loaded with three forces: at front holder with force of 33.9kN and at rear holders with forces of 23.8 kN.

### 3. Conditions for performing of numerical analyses

Numerical examinations were performed according to method of complete elements [2] in ANSYS Workbench environment. Based upon geometrical models of EVO frame, layer division grid was prepared. Threshold conditions for analyses were selected in such manner that at rear supports translation degrees of freedom in direction  $OY$  (Fig. 3a) were achieved. In front support condition of *Remote displacement* [3] type was defined which is presented schematically at Fig. 3b. In holders forces of *Remote force* [3] type were introduced of values specified in point 2, operating in direction  $OY$  (Fig. 4).

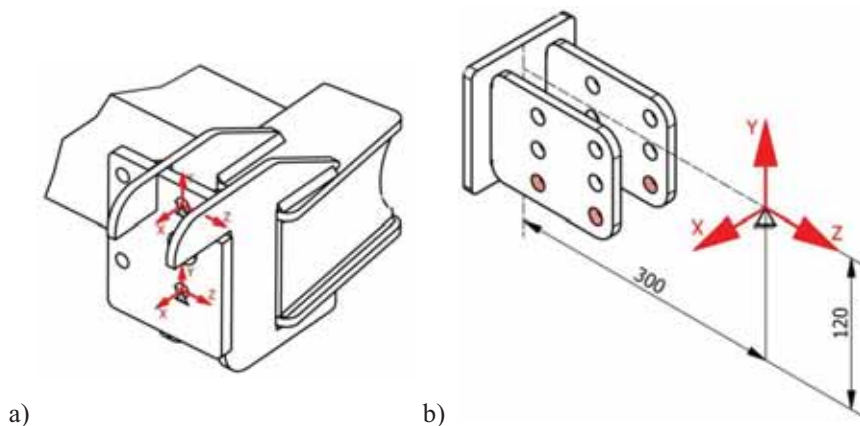


Fig. 3. Supports defining scheme: a) rear, b) front

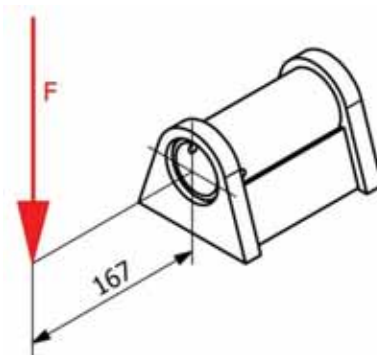


Fig. 4. Scheme of load application

#### 4. Numerical tests and modification of supporting frame

After preparation of division grid and defining of threshold conditions numerical solution of the problem was obtained. Calculation results were presented in the form of distribution of stresses in the frame at Fig. 5.

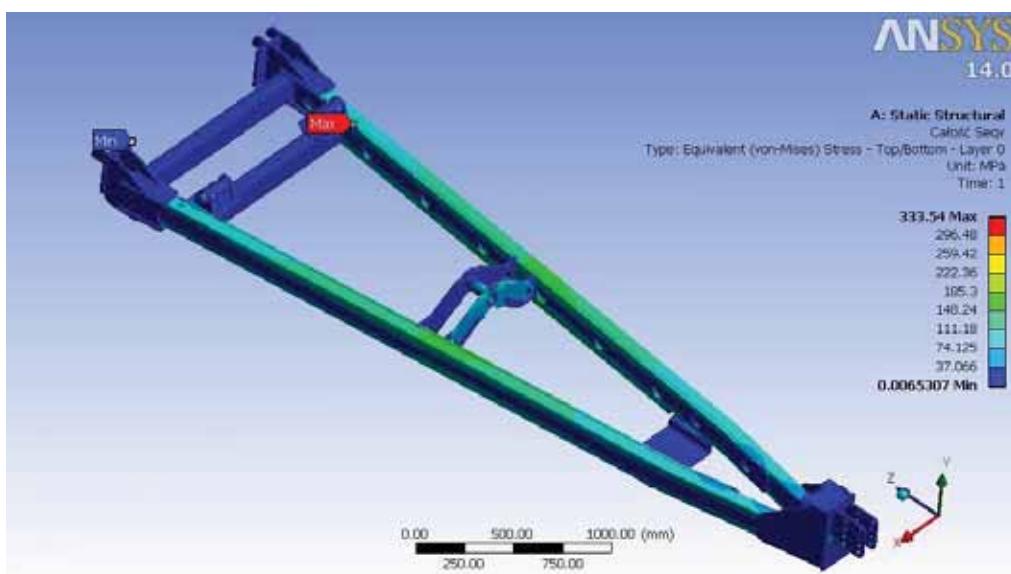
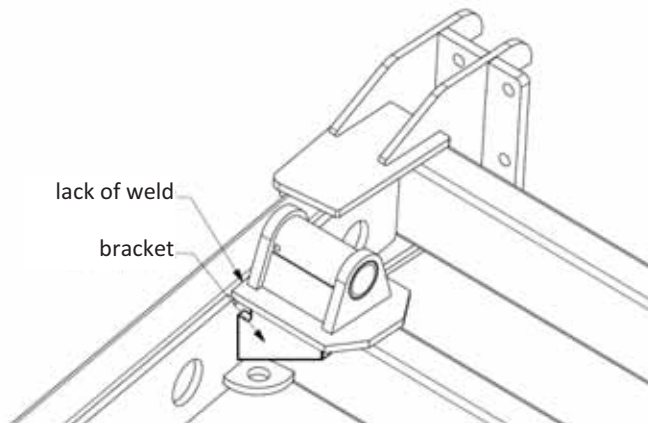


Fig. 5. Distribution of stresses reduced in EVO frame prior to modifications

It was stated that values of maximum stresses for the frame, identified with symbol Max at Fig. 5, which are present at the point of rear support fixing, significantly exceed acceptable stresses. In order to improve the state of frame effort in this area constructional changes were proposed. The changes would focus on introduction of ribs of 10mm thickness, supporting the support. Weld between rear support and main supporting beam was eliminated. The frame modified in this area is presented at Fig. 6.



*Fig. 6. Geometrical form of modified rear support*

Moreover, a number of fine modifications was proposed leading to reduction of stresses at selected frame nodes. First modification was based on lowering down to 4mm of thickness of platform for drive gears (Fig. 2). In case of front bridge radius R55 was changed to radius R65 and the bridge thickness was increased to 24mm. Also, front holder height was increased from 210 mm to 380 mm (Fig. 7b). Geometrical form of modified bridge is presented at Fig. 7a, and modified holder at Fig. 7b.

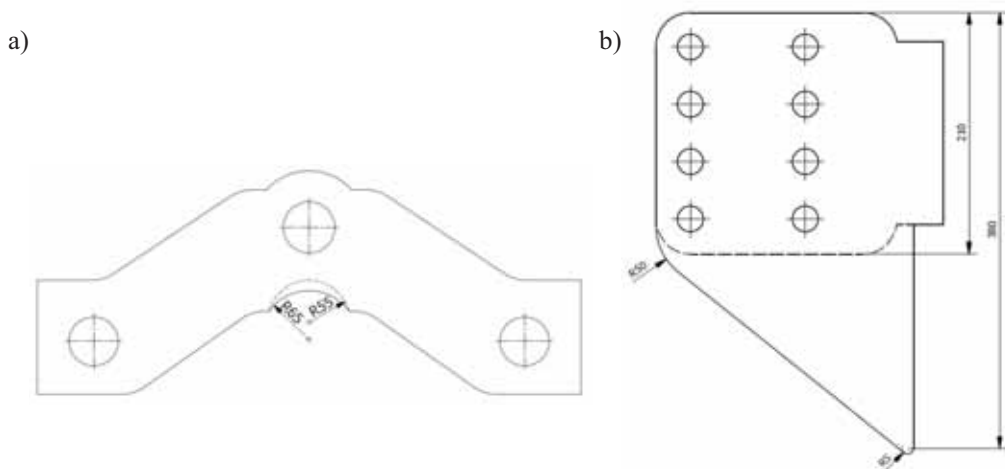


*Fig. 7. Geometrical form of modified: a) front bridge, b) holder*

After introduction of modifications of geometrical form for unchanged threshold conditions numerical solution to the problem was obtained. Calculation results are presented in the form of stress distribution in the frame at Fig. 8.

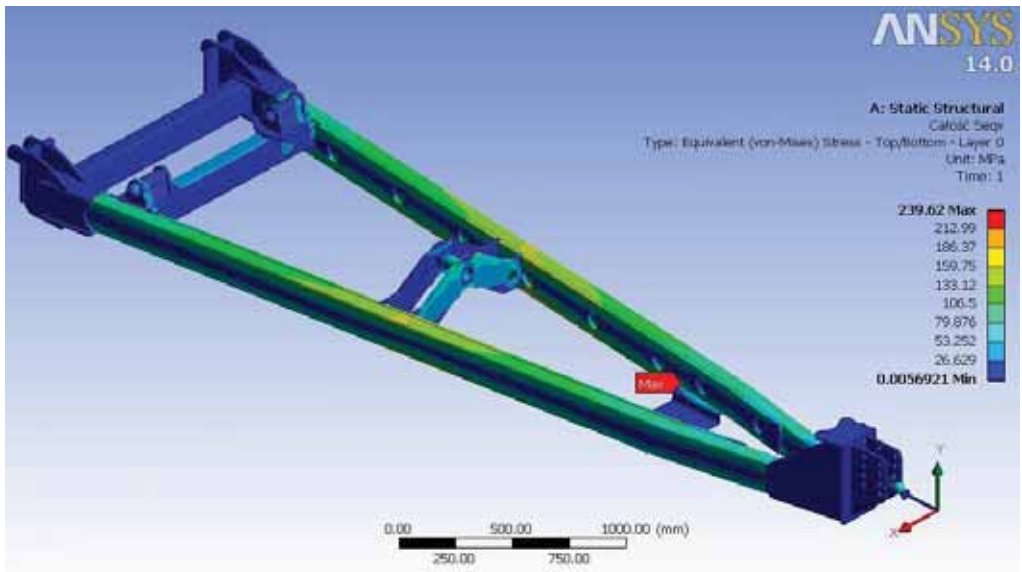


Fig. 8. Distribution of reduced stresses in EVO frame after modifications

## 5. Summary

The paper presents conditions for performance and results of numerical analyses of lowered supporting structure of forage trailer. After performing of calculations it was stated that values of acceptable stresses in the area of rear support were significantly exceeded. Moreover, it was stated that acceptable stresses were exceeded to a lesser degree in main supporting beam in the area of platform for drive gears and in holder and front bridge. In order to reduce stresses in critical nodes of the frame constructional changes were proposed. Their introduction led to improvement of the structure effort state.

In order to verify correctness of performance of numerical analyses one should compare their results with the results of analytical calculations performed for main supporting beams. Also, performance of experimental tests e.g. with strain gauge method at selected points of supporting structure, would allow for verification of assumptions applied for analyses.

## References

- [1] Sęk, P., *Wozy paszowe do żywienia krów w systemie TMR*, Journal of Research and Applications in Agricultural Engineering, Vol. 50, No. 4, 2005.
- [2] Rakowski G., Kacprzyk Z., W., *Metoda Elementów Skończonych w mechanice konstrukcji*, Oficyna Wydawnicza Politechniki Warszawskiej, Warszawa, 2005.
- [3] ANSYS Inc., *ANSYS Mechanical Application User's Guide*, ANSYS 14.0, 2011.



## ANALYTICAL VERIFICATION OF NUMERICAL ANALYSIS OF FORAGE TRAILER SUPPORTING STRUCTURE

Artur Cichański, Michał Burak, Dariusz Skibicki, Łukasz Pejkowski

*University of Technology and Life Sciences in Bydgoszcz*  
ul. Kaliskiego 7, 85-789 Bydgoszcz, Poland  
tel.: +48 52 3408235, fax: +48 52 3408245  
e-mail: artur.cichanski@utp.edu.pl

### *Abstract*

*The paper presents manner of analytical modelling of forage trailer supporting structure. Process of obtaining mathematical model from physical model was presented as well as final form of mathematical model in the form of equations describing deflections and stresses of the forage trailer construction. Results of analytical calculations were compared with results of numerical calculations with the method of complete elements. Good, 5%, compliance of the results of analytical and numerical calculations was achieved.*

**Keywords:** *agricultural machinery, mathematic modelling, Clebsch method,*

### 1. Introduction

The paper [1] presents results of calculations with MES method of forage trailer supporting structure. Basic functions of forage trailers are: dosing of correct feed dose, feed mixing and transportation to pasture. It is a complex object – contains large number of constructional elements and many constructional nodes of complicated manner of stress transmission. Construction of numerical model for such structure is very time consuming and can be burdened with many errors. Modelling errors can be avoided by using the possibility of verification of numerical model with analytical calculations.

The paper presents analytical mathematical model of forage trailer supporting frame. With model application, analytical calculations were performed in order to specify stresses and deflections in the function of wagon frame length. Results of analytical calculations were compared with results of numerical calculations, obtaining good, 5%, compliance.

### 2. Object and testing conditions

Based upon supplied constructional documentation of low forage trailer frame, simplification of its geometrical form was performed. Simplified form is presented at Fig.1. The figure presents dimensional scheme and locations of supports and application of external loads.

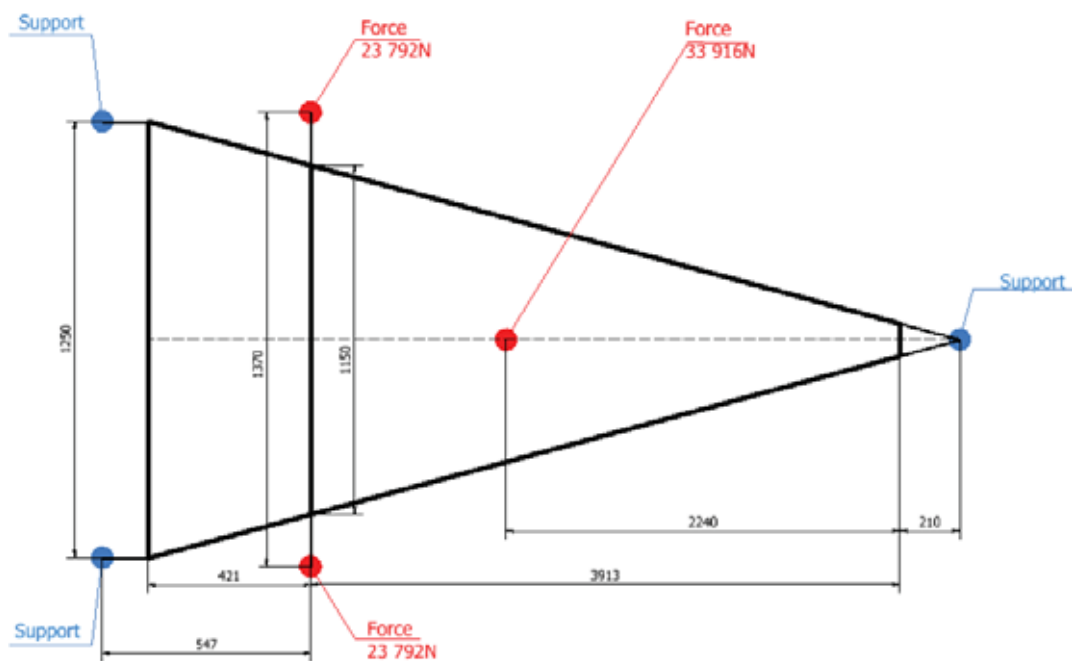


Fig. 1. Characteristic dimensions of EVO 12 frame

Based upon the scheme as of Figure 1, values of parameters present in analytical dependencies (1÷3) were specified. Based upon the scheme as of Figure 2 the form of dependency was set and value of moment of inertia of beams horizontal cross-section (4÷5) was calculated. Main supporting beams are made of closed sections 80x160mm and flat sections 180x14mm. Values of the aforementioned parameters are presented in Table 1.

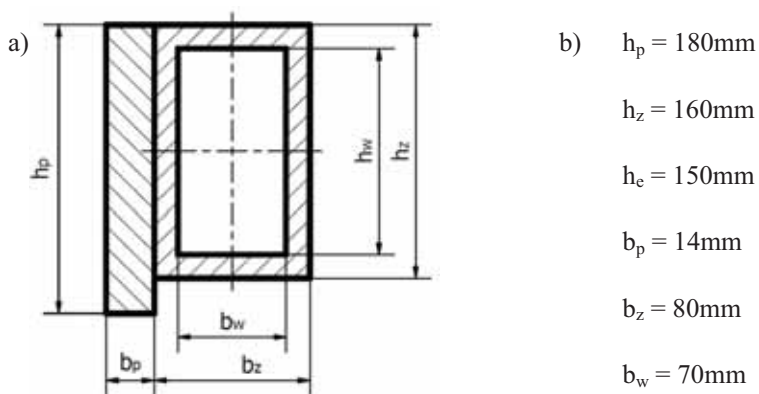


Fig. 2. Cross-section of main supporting beam a) scheme, b) values of parameters

### 3. Analytical calculations

Simplified geometry of forage trailer was modelled with beam supported on both sides (Fig. 3). After dismantling of knots and application of external loads mathematical model as on Figure 3 was obtained.

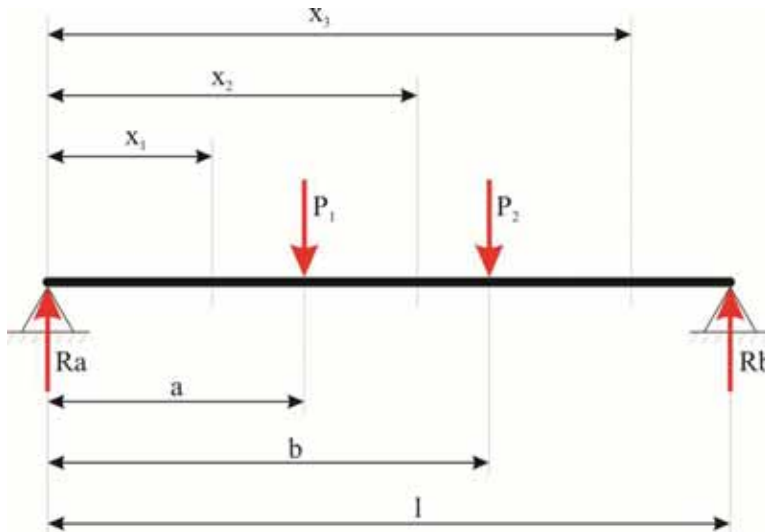


Fig. 3. Scheme of forces layout

Solving of layout presented at Figure 3 with Clebsch method [2] leads to setting the deflecting functions with dependency (1) and deflecting moments with dependency (2):

$$y = \frac{1}{EI} \left( \frac{R_A \cdot x^3}{6} \Big|_{x_1} - \frac{P_1 \cdot (x-a)^3}{6} \Big|_{x_2} - \frac{P_2 \cdot (x-b)^3}{6} \Big|_{x_3} + c_1 \cdot x + c_2 \right) \quad (1)$$

$$Mg = R_A \cdot x \Big|_{x_1} - P_1 \cdot (x-a) \Big|_{x_1} - P_2 \cdot (x-b) \Big|_{x_1} \quad (2)$$

Where integration constants and reaction values are described with dependencies (3):

$$c_1 = -\frac{R_A \cdot L^2}{6} + \frac{P_1 \cdot (L-a)^3}{6L} + \frac{P_2 \cdot (L-b)^3}{6L} \quad (3a)$$

$$c_2 = 0 \quad (3b)$$

$$R_A = \frac{P_1 \cdot (L-a)}{L} + \frac{P_2 \cdot (L-b)}{L} \quad (3c)$$

Crucial element of calculations of frame deflecting (1) is correct setting of inertia moments for supporting beam cross-section, presented as a scheme at Fig. 2.

After necessary transformations, location of gravity centre was described with dependency (4) and value of inertia moment with dependency (5):

$$y_c = \frac{b_p h_p \frac{h_p}{2} + b_z h_z \frac{h_z}{2} - b_w h_w \frac{h_w}{2}}{b_p h_p + b_z h_z - b_w h_w} \quad (4)$$

$$I_x = \frac{b_p h_p^3}{12} + b_p h_p \left( \frac{h_p}{2} - y_c \right)^2 + \frac{b_z h_z^3}{12} + b_z h_z \left( \frac{h_z}{2} - y_c \right)^2 - \frac{b_w h_w^3}{12} - b_w h_w \left( \frac{h_z}{2} - y_c \right)^2 \quad (5)$$

Thus, it was possible to specify value of stress in the most distant fibres from neutral axis (6):

$$\sigma = \frac{Mg \cdot y_c}{I_x} \quad (6)$$

#### 4. Results of analytical calculations

Based upon dependencies (1)÷(6) assuming values of individual parameters presented in Table 1, distributions of normal stresses and deflections of main beam, changing along wagon frame length, were set. Table of distributions specified by analytical and numerical means is presented for stresses as at Fig. 4 and for deflections as at Fig. 5. for such comparisons, in numerical models platform for drive gears fixing was skipped.

Table 1. Values of parameters specifying balance layout at Fig. 3

| Parameter      | Value                      |
|----------------|----------------------------|
| a              | 547 mm                     |
| b              | 2 220 mm                   |
| L              | 4 670 mm                   |
| P1             | 47 584 N                   |
| P2             | 33 916 N                   |
| I <sub>x</sub> | 29 402 785 mm <sup>4</sup> |
| E              | 2e5 MPa                    |

Very good compliance of numerical calculations results and analytical stresses is noticeable (Fig. 4). Differences result only from simplifications of analytical model based on skipping of local changes of stiffness caused by joining of main supporting structure of the forage trailer with other constructional elements. It is important that maximum values of stresses, which decide about the frame supporting ability, differ only by ca. 3%.

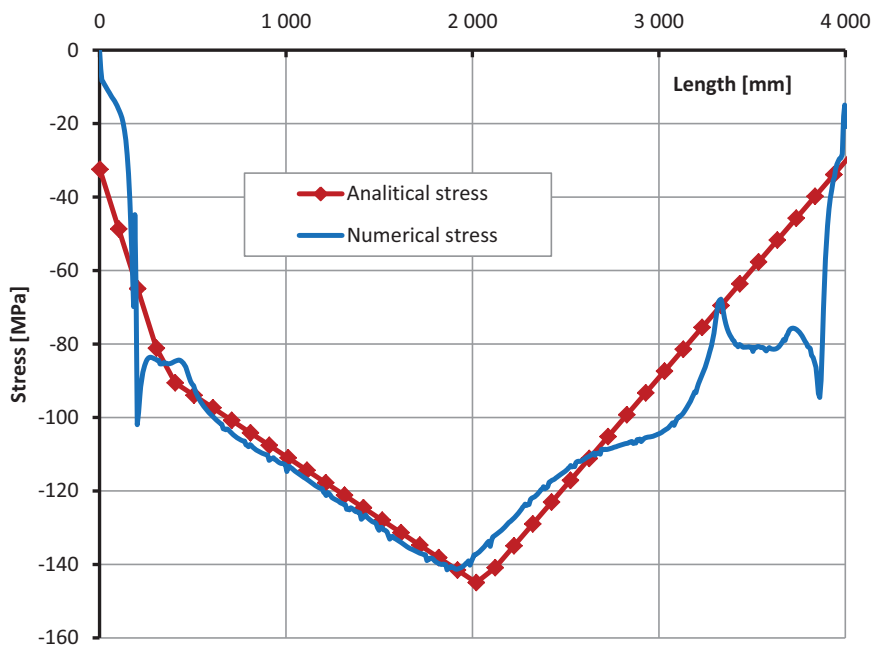


Fig. 4. Set of results of analytical calculations and numerical analyses for stresses in supporting beam of low EVO 12 frame

In case of deflections nature of changes in both cases of analyses is identical. Local stiffness do not influence the change of nature of function of forage trailer deflections. Value of deflections calculated numerically is only by 5% higher than the one obtained analytically.

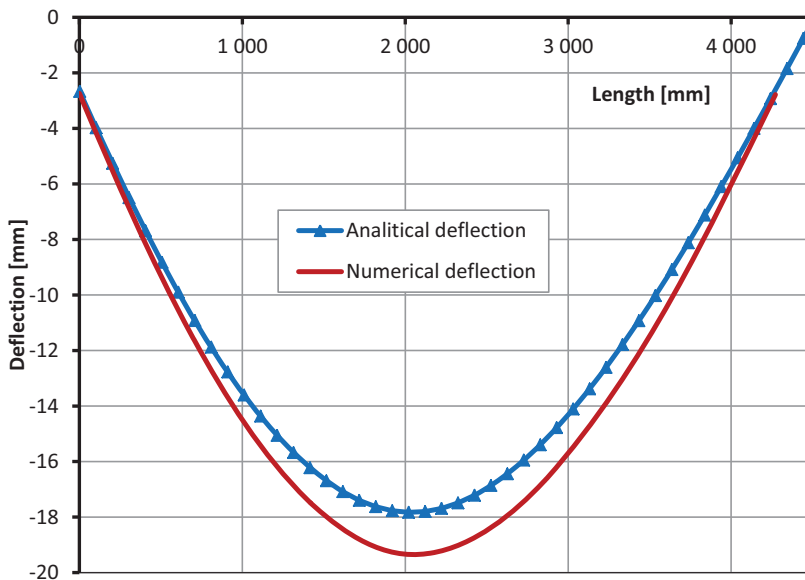


Fig. 5. Set of results of analytical calculations and numerical analyses for deflections in supporting beam of EVO 12 frame

## 5. Summary

The paper presents modelling manner and results of analytical analyses of modified forage trailer supporting structure. Calculation results were compared with results of numerical MES calculations. Very good compliance of analytically calculated stresses and deflections with the ones obtained based on MES calculations was achieved. Thus, it should be stated that even in case of complex technical objects, correctly performed modelling process of analytical model allows for obtaining correct results. Despite significant simplifications at construction of analytical mathematical model, achieved results are useful for initial verification of numerical model.

## References

- [1] Cichański A., Burak M., Skibicki D., Stopel M., *Numeryczna analiza konstrukcji nośnej wozu paszowego*, Journal of Polish CIMAC, Gdańsk, 2012.
- [2] Siołkowski B., Holka H., Malec M., *Zbiór zadań ze statyki i wytrzymałości materiałów*, Akademia Techniczno-Rolnicza w Bydgoszczy, Bydgoszcz, 1988.



## STRAIN GAUGE VERIFICATION OF NUMERICAL ANALYSIS OF FORAGE TRAILER SUPPORTING STRUCTURE

Artur Cichański, Michał Burak, Dariusz Skibicki, Zbigniew Lis

University of Technology and Life Sciences in Bydgoszcz  
ul. Kaliskiego 7, 85-789 Bydgoszcz, Poland  
tel.: +48 52 3408235, fax: +48 52 3408245  
e-mail: artur.cichanski@utp.edu.pl

### Abstract

*The paper presents experimental verification of forage trailer supporting structure. Conditions for performance of strain gauge measurements of stresses at selected frame points were presented. Results of strain gauge measurements were compared with results of calculations by method of complete elements. Dozen percentage compliance of results of numerical calculations and experimental measurements was obtained. Maximum stresses were specified with accuracy of ca.2%. During measurements asymmetrical distribution of load in the frame was stated.*

**Keywords:** agricultural machinery, forage trailers, strain gauge measurements, numerical analyses

### 1. Introduction

At the stage of constructional works numerical analyses are conducted in order to evaluate structure. Such tests are mostly performed with the finite elements method FEM. Results, obtained during analysis, refer to boundary conditions specified for FEM and in particular they assume that tested objects did not indicate any process defects and material they are made of met continuum criterion continuum and criterion of isotropy of mechanical properties [3]. Thus, distribution of stresses in real constructional elements can differ from values set numerically. In order to estimate the scale of such differences, experimental tests are performed on stress state in constructional elements. One of most widely used measurement methods in this respect is resistance strain gauge measurement. [2].

The paper undertakes verification tests of numerical analyses of the structure of modified supporting frame of forage trailer. For the frame a discrete model of geometric shape was prepared and boundary conditions were proposed. [1]. As a result of solving FEM issue, distributions of deflections and stresses were set. Based upon distributions of stresses specified in the paper [1] characteristic points of supporting frame were specified at which strain gauge measurements were performed.

### 2. Object of tests

The object of tests was supporting frame of a low forage trailer EVO Fig. 1. Geometric form of tested trailer was described in detail in the paper [1]. Main supporting beams are made of closed profiles x160. The frame is made of S235JR steel. On two rear holders and one front holder. (Fig. 1) basket filled with feed is installed. Moreover a screw for infeed mixing is installed in the

basket. Frame load results from the mass of the very basket and its filling. The frame is supported on two supports located in rear part at height of head of supporting beam. Rear supports are used for mounting of axis with wheels. Trailing hook acts as the front support.

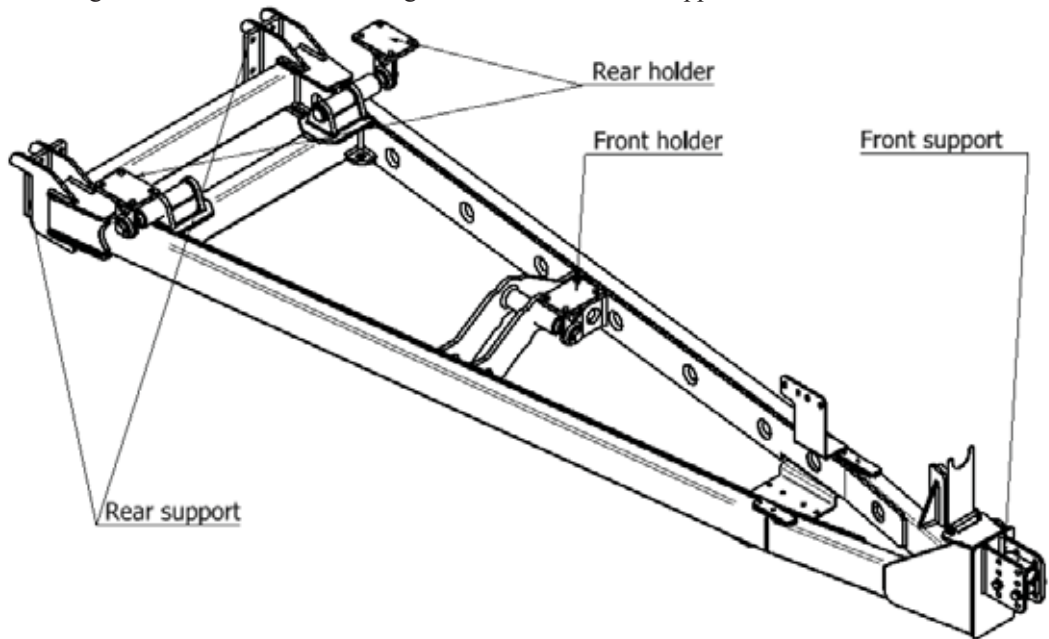


*Fig. 1. Object of tests*

### 3. Conditions for performance of tests

Based upon results of numerical analyses, characteristic points on the surface of supporting beam were indicated and strain gauge measurements were performed at these points. The scheme of numbering of strain gauges is presented at Fig. 2.

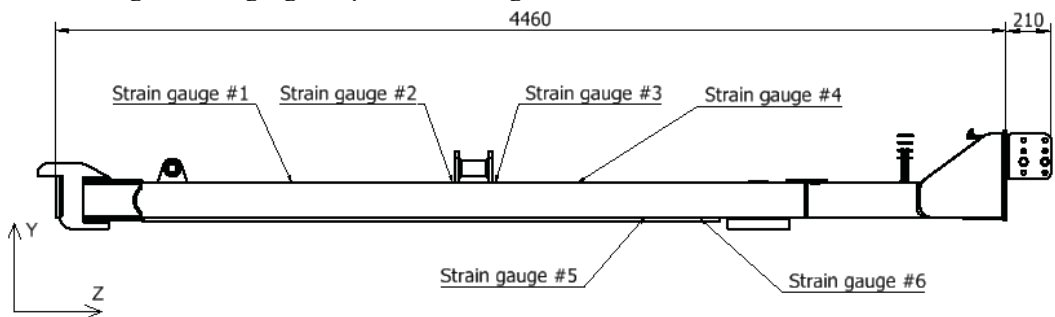


*Fig. 2. Scheme of numbering of strain gauges*

On upper shelf of right beam there are strain gauges located at locations no 1 to 4. on lower shelf of right beam there are strain gauges located at locations no 5 and 6. In addition, on left beam there are strain gauges located at locations no 3 and 4. The system located on right beam was specified as strain gauge no 3 and on left beam as no 3L. Similar convention was adopted for labelling of strain gauges no 4. Location of strain gauges no 1 to 4 in relation to component elements of frame is presented at Fig. 3.

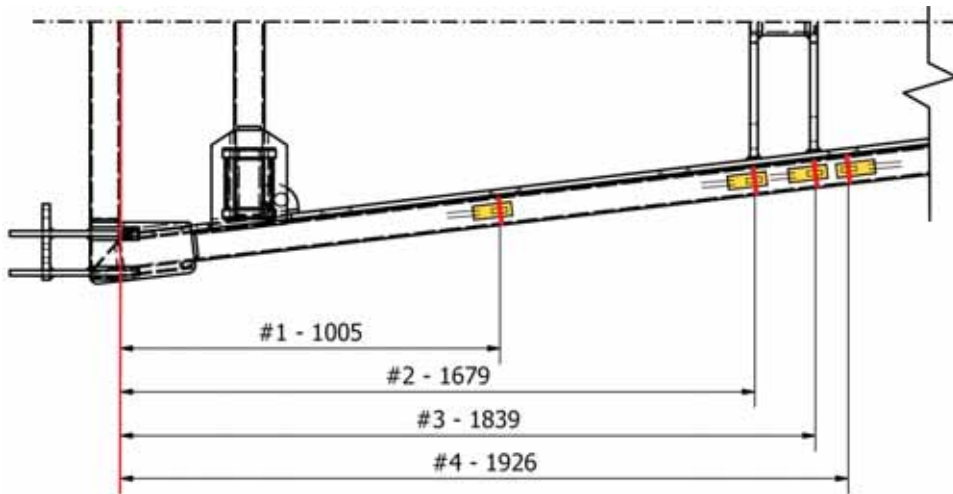


*Fig. 3. Scheme of location of strain gauges 1 to 4*

Location of strain gauges no 5 and 6 in relation to component elements of frame is presented at Fig. 4.

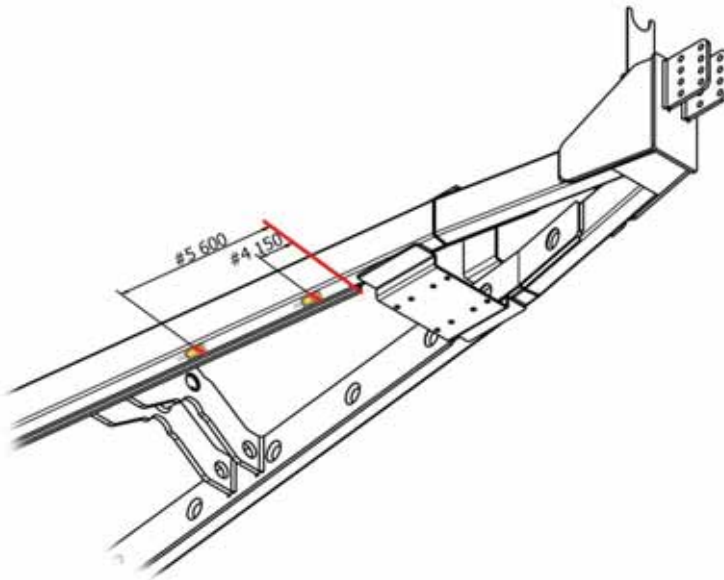


*Fig. 4. Scheme of location of strain gauges 5 and 6*

Measurements were performed on a complete forage trailer (Fig. 5). Load was applied to forage basket and measured with a scale included in the trailer equipment. Strain gauge tests were performed with 8 channel universal strain gauge bridge made by National Instruments – NI SCXI-1520 and USB module for data acquisition with 13bits resolution and sampling frequency of 200 kS/s – NI SCXI-1600. Strain gauges made by HBM – 1-LY11-6/120-3-3m were used, with measurement base of 6 mm and fast drying glue 1-Z70. Data was recorded with NI LabVIEW SignalExpress software.



Fig. 5. Conditions for performance of strain gauge measurements

#### 4. Results of strain gauge measurements

Results of strain gauge measurements and their corresponding values of stresses set numerically for load of 2 000kg are presented in table 3, for load of 3 350kg in table 4 and for load of 2 000kg in table 5. Percentage error of measurements is specified from dependencies (1).

$$\delta = \left| \frac{\sigma_{FEM} - \sigma_{gauge}}{\sigma_{FEM}} \right| * 100\% \quad (1)$$

Table. 3. Stresses set strain gauge and numerically for load of 2000kg

| Strain gauge | Set no 1  |                  |              | Set no 2  |                  |              |
|--------------|-----------|------------------|--------------|-----------|------------------|--------------|
|              | FEM [MPa] | Measuremen [MPa] | $\delta$ [%] | FEM [MPa] | Measuremen [MPa] | $\delta$ [%] |
| 1            | -26.89    | -21.0            | 21.9         | -26.89    | -22.5            | 16.3         |
| 2            | -33.37    | -26.0            | 22.1         | -33.37    | -27.0            | 19.1         |
| 3            | -34.60    | -30.0            | 13.3         | -34.60    | -30.0            | 13.3         |
| 3L           | -34.60    | -32.5            | 6.1          | -34.60    | -32.5            | 6.1          |
| 4            | -33.37    | -35.0            | 4.9          | -33.37    | -34.0            | 1.9          |
| 4L           | -33.37    | -35.0            | 4.9          | -33.37    | -36.0            | 7.9          |
| 5            | 28.24     | 27.5             | 2.6          | 28.24     | 27.5             | 2.6          |
| 6            | 23.64     | 22.5             | 4.8          | 23.64     | 22.5             | 4.8          |

Table. 4. Stresses set strain gauge and numerically for load of 3350kg

| Strain gauge | Set no 3  |                  |              | Set no 4  |                  |              |
|--------------|-----------|------------------|--------------|-----------|------------------|--------------|
|              | FEM [MPa] | Measuremen [MPa] | $\delta$ [%] | FEM [MPa] | Measuremen [MPa] | $\delta$ [%] |
| 1            | -45.04    | -36.0            | 20.1         | -45.04    | -36.0            | 20.1         |
| 2            | -55.90    | -41.5            | 25.8         | -55.90    | -42.0            | 24.9         |
| 3            | -57.96    | -46.0            | 20.6         | -57.96    | -47.0            | 18.9         |
| 3L           | -57.96    | -52.0            | 10.3         | -57.96    | -52.0            | 10.3         |
| 4            | -55.90    | -55.0            | 1.6          | -55.90    | -55.0            | 1.6          |
| 4L           | -55.90    | -57.0            | 2.0          | -55.90    | -57.0            | 2.0          |
| 5            | 47.30     | 46.0             | 2.8          | 47.30     | 46.0             | 2.8          |
| 6            | 39.59     | 35.0             | 11.6         | 39.59     | 35.0             | 11.6         |

Table. 5. Stresses set strain gauge and numerically for load of 2000kg

| Strain gauge | Set no 5  |                  |              | Set no 6  |                  |              |
|--------------|-----------|------------------|--------------|-----------|------------------|--------------|
|              | FEM [MPa] | Measuremen [MPa] | $\delta$ [%] | FEM [MPa] | Measuremen [MPa] | $\delta$ [%] |
| 1            | -26.89    | -22.5            | 16.3         | -26.89    | -22.5            | 16.3         |
| 2            | -33.37    | -26.0            | 22.1         | -33.37    | -26.0            | 22.1         |
| 3            | -34.60    | -29.0            | 16.2         | -34.60    | -29.5            | 14.7         |
| 3L           | -34.60    | -32.0            | 7.5          | -34.60    | -32.0            | 7.5          |
| 4            | -33.37    | -34.0            | 1.9          | -33.37    | -34.0            | 1.9          |
| 4L           | -33.37    | -35.0            | 4.9          | -33.37    | -36.0            | 7.9          |
| 5            | 28.24     | 28.0             | 0.9          | 28.24     | 28.0             | 0.9          |
| 6            | 23.64     | 22.5             | 4.8          | 23.64     | 22.5             | 4.8          |

For each tested levels of load two series of measurements were performed. Averaged values of percentage error at load level for individual strain gauges are presented in the form of a graph at Fig. 6.

Comparison of measurement error for strain gauges no 3 and 4 indicates asymmetrical distribution of load on the frame. Stresses set at selected points located on right frame side (Fig 4) reach higher values than analogical stresses at left frame side. This can be due to inaccuracy in structure engineering of the welded frame. Maximum stresses each time were measured in strain gauges no 4 and 4L. values read on these strain gauges at maximum load of 3350kg are characterised with low value of error, ca. 2%. Maximum error for the whole analysis does not exceed dozen of percentage. Higher error values occur at the side of overestimation and lower at

the side of underestimation of numerically set stresses. Along with the load increase, underestimation error of stresses decreases.

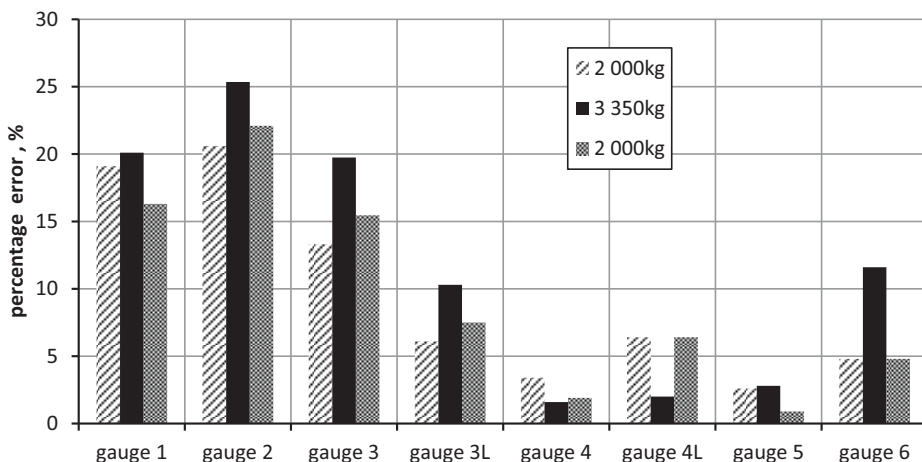


Fig. 6. A set off errors in strain gauge measurements

## 5. Summary

The paper presents conditions for performance and results of strain gauge tests of forage trailer supporting structure. Measurement results were compared with results of numerical calculations FEM. Good compliance of experimentally set stresses with the ones obtained from FEM calculations was achieved. FEM analyses error does not exceed dozen of percentage in the whole measurement range. For maximum measured stress values FEM analyses error does not exceed several of percentage. During measurements asymmetrical distribution of load in supporting structure was observed.

## References

- [1] Cichański A., Burak M., Skibicki D., Stopel M., *Numeryczna analiza konstrukcji nośnej wozu paszowego*, Journal of Polish CIMAC, Gdańsk, 2012.
- [2] Roliński Z., *Tensometria oporowa : podstawy teoretyczne i przykłady zastosowań*, Warszawa : WNT, 1981
- [3] Ugural A.C., *Mechanics of materials*, John Wiley&Sons, 2008.



## The effect of a welding method on the structure of a welded joint

Krzysztof Ciechacki\*, Tadeusz Szykowny

*University of Technology and Life Sciences  
al. Prof. S. Kaliskiego 7, 85-789 Bydgoszcz, Poland  
tel.: +48 52 3408748, fax: +48 52 3408244  
\*e-mail: krzysztof.ciechacki@utp.edu.pl*

### Abstract

*This work explains the influence of a local structural heterogeneity and resulting mechanical heterogeneity in welded joints on the location and nature of welded joint failure. Toughened structural steel S355 with a thickness of 7mm, welded using laser beam or gas metal arc welding (GMAW) was used for the purposes of this analysis. Hardness penetration pattern in welded joint cross-section was defined and mechanical properties of a welded joint in static tensile test ( $R_e$ ,  $R_m$ ,  $A_5$ ,  $Z$ ) were determined. Microstructure and microfractographic tests of fractures were performed.*

**Key words:** laser beam welding, GMAW, hardness, macrostructure, microstructure

### 1. Introduction

Welding methods use heat sources with a different level of energy flux concentration. Particularly difficult to establish are relations between local structural changes and mechanical properties of welded joints. From a practical point of view, these relations have a decisive effect on the weldability of metals, as well as affecting welding technology itself and, ultimately, working properties.

Finding solutions to complex technical problems, dependent on the identification of both physical processes related to welding and its effects within a welded joint and the entire structure is the subject of numerous experimental and theoretical studies [1,3-6,9].

The current knowledge based on the studies of heat-induced structural changes which accompany welding is insufficient to provide an in-depth analysis of the influence of microstructure differences in the vicinity of a welded joint on the mechanical properties [1,3]. According to E. Ratanowski [8,9], the differences of the microstructure within a welded joint area lead to changes of the local stresses and mechanical properties, as well as determining location and nature of welded joint failure.

The aim of this study is to analyse the structure and properties of a welded joint obtained at significantly different values of heat energy concentrations.

### 2. Material, programme and testing methodology

Toughened structural steel S355 with chemical composition as provided in table 1 was used for the

studies.

*Table 1. Chemical composition of S355 steel (percent of mass)*

| C     | Si    | S     | P     | Mn    | Ni    | Cr    | Mo    | Cu    | Ti  | Al    | Sn    | Zn    | Mg    |
|-------|-------|-------|-------|-------|-------|-------|-------|-------|-----|-------|-------|-------|-------|
| 0.212 | 0.403 | 0.008 | 0.014 | 1.416 | 0.067 | 0.030 | 0.009 | 0.021 | 0.0 | 0.053 | 0.008 | 0.020 | 0.049 |

Mechanical properties of tested steel were defined based on a static tensile test. The properties are as follows:  $R_e=734\text{MPa}$ ,  $R_m=797\text{MPa}$ ,  $A_5=11.2\%$ ,  $Z=42.4\%$ ).

Single-run butt welding of test plates with a thickness of 7mm and dimensions of 300x100mm using GMAW or laser beam welding was performed. Transverse macroscopic welded joint microsections etched with Marble reagent were made. Hardness penetration pattern was determined using Vickers HV1 method. Flat quintuple tensile test specimens were cut from the plates. Metallographic nital etched specimens were observed under an optical microscope. Microfractographic analyses of fractures following tensile tests were performed using SEM.

### 3. Test results

Macrostructure of a welded joint made using GMAW is presented in figure 1, while that of a joint made using laser beam welding in figure 3. Hardness penetration patterns in weld cross-section (figure 2 and 4) were made in each of the areas characteristic of a welded joint (MP-HAZ-SP) halfway through the thickness of the plates.

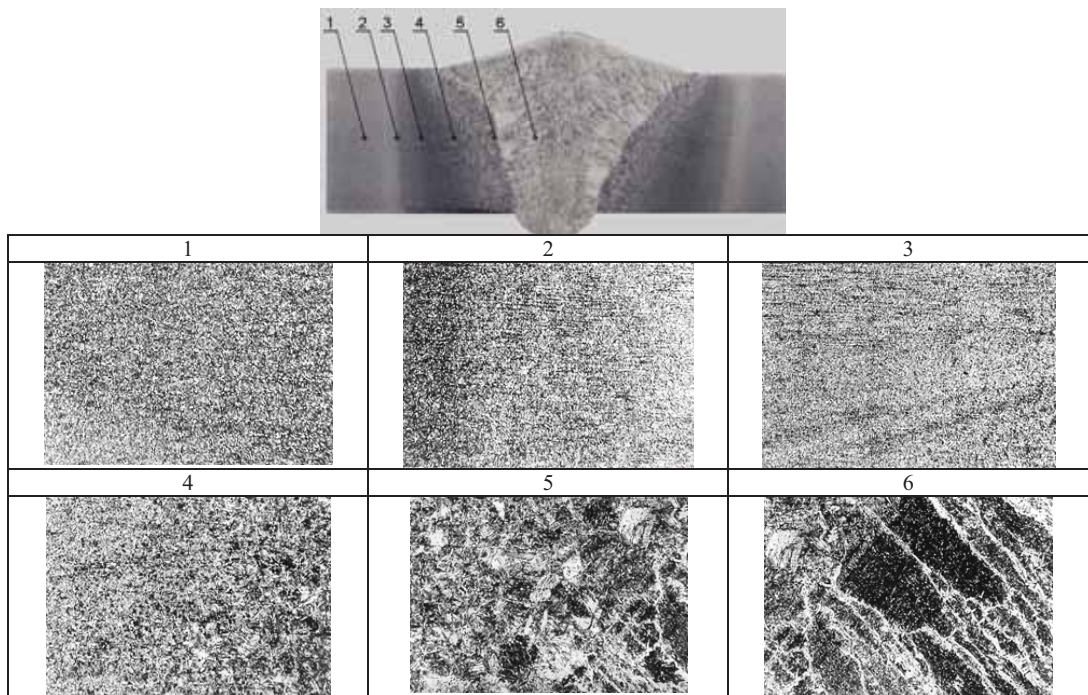


*Figure 1. Macrostructure of a joint welded using GMAW, magnified 4x times. Microstructure of numbered areas, 70x times magnified, nital etched*

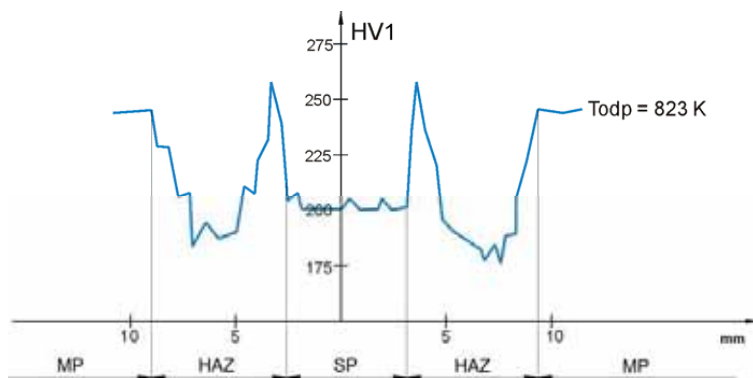


Figure 2. Hardness penetration pattern in cross-section of a joint welded using GMAW

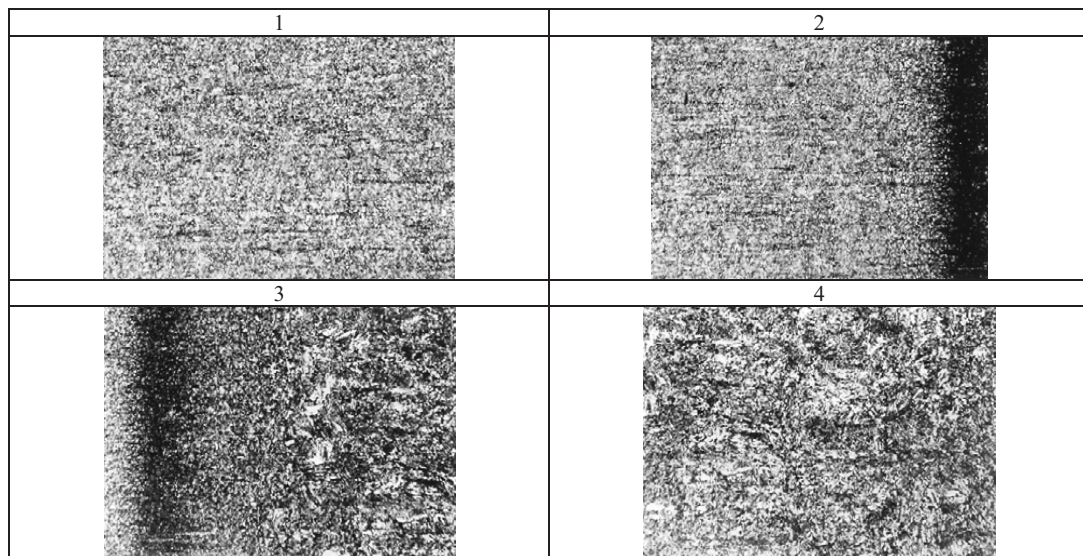
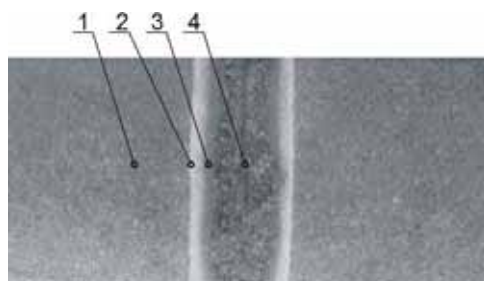


Figure 3. Macrostructure of a laser beam welded joint, magnified 6x times. Microstructure of numbered areas, 70x times magnified, nital etched

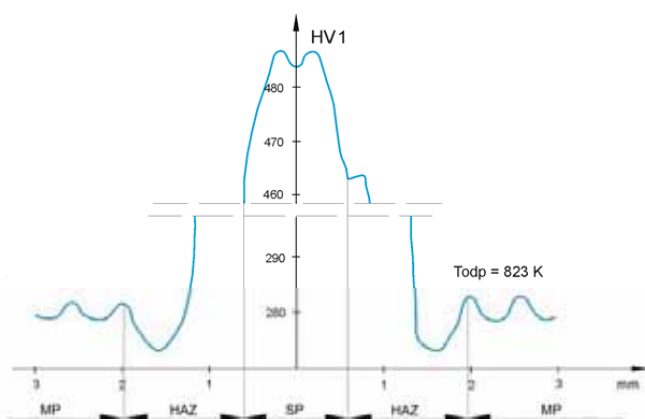


Figure 4. Hardness penetration pattern in a laser beam welded joint cross-section

Strength properties of welded joints are presented in table 2. Measurement results were given confidence interval at coefficient  $1-\alpha = 0.95$ .

Table 2. Results of welded joints static tensile test

| Welding method     | $R_{e_{sr}}$ , MPa | $R_{m_{sr}}$ , MPa | $A_{5sr}$ , %    | $Z_{sr}$ , %     |
|--------------------|--------------------|--------------------|------------------|------------------|
| GMAW               | $480.6 \pm 31.8$   | $686.0 \pm 11.8$   | $12.88 \pm 1.27$ | $38.98 \pm 6.33$ |
| Laser beam welding | $737.4 \pm 8.7$    | $793.2 \pm 4.1$    | $11.34 \pm 0.72$ | $42.77 \pm 1.97$ |

Joints made using GMAW were destroyed in the areas with reduced hardness, i.e. in the joint area or in the heat-affected zone. Laser beam welded joints become destroyed only in base metal.

As a rule, joints made using GMAW become destroyed in the areas with reduced hardness, i.e. in the joint area or in the heat-affected zone. Reduced hardness in these areas results from the microstructure that occurs there. The microstructure of an SP weld with a hardness of ca. 200HV consists of coarse-grained, column ferrite and pearlite. The narrow heat-affected zones with increased hardness adjoining the welded joint have a fine pearlite structure. During the heating, these areas had an austenitic structure. The relatively high speed of heat penetration into the inside of the material causes austenite to be converted into dense pearlite with a hardness of 255HV. The subsequent area of reduced hardness (fig. 2) results from the conversion of austenite under conditions of lower cooling and tempering speed (temperature below  $A_{r1}$ ).

In the case of laser beam welding, energy concentration within a small area of a welded joint and a very large gradient of temperature causes non-diffusive transformation to occur, which results in obtaining a maximum hardness of 490HV (fig. 4). The joint is destroyed as a consequence of tensile test only in base metal.

Morphological characteristics of the fracture surfaces in specimens depend on the location of a fracture (base metal, heat-affected zone and weld). This is closely connected with the type and quantity of structures present there.

In the case of GMAW, fractures most often run along the border of the heat-affected zone – base material or in the weld. The occurrence of a coarse-grained ferritic and pearlitic structure in these areas determines largely the nature of fractures which can be classified as transcrystalline ductile and fissile with ductile being predominant.

Laser welded specimens were destroyed in base metal. The fracture is mainly transcrystalline and ductile with small fissile fracture presence (fig. 7).

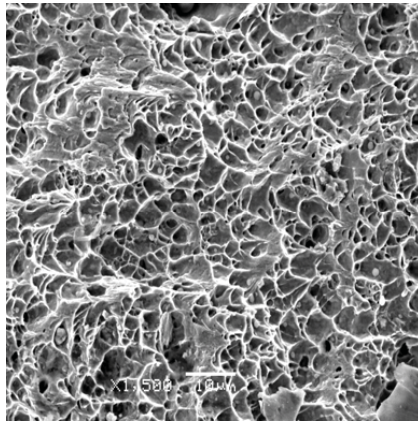


*Figure 5. Microfractography of a joint welded using GMAW, fracture in the heat-affected zone, 1500x times magnified*

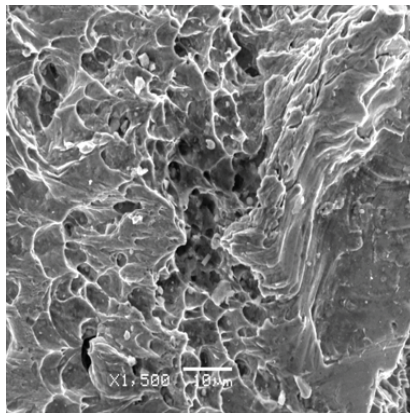


*Figure 6. Microfractography of a joint welded using GMAW, fracture in the weld, 1500x times magnified*

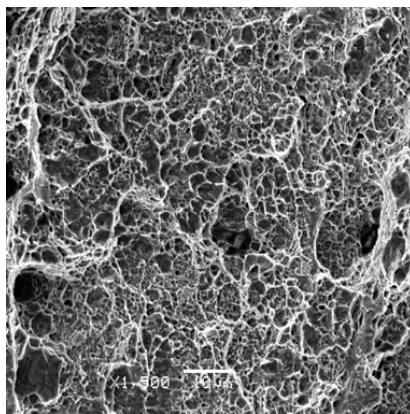


*Figure 7. Microfractography of a laser welded joint, fracture in the base metal, 1500x times magnified*

Experimental studies enabled the widths of areas with different hardness to be determined. The outcome of the experimental tests was input data for MES numeric calculations [4]. The basis for determination of the areas with a varied microstructure was the value of maximum temperature and time  $t_{8/5}$ , which was determined based on the temperature isotherms running through any given cross-section point. With time values  $t_{8/5}$  as a function of a distance from the weld axis, it was possible to set the width of respective zones using CTPc-S graphs [2,7]. The widths of the zones established based on MES and experiments, both for GMAW and laser beam welding demonstrated good compliance.

#### 4. Conclusions

A joint welded using GMAW becomes destroyed in areas with reduced hardness compared to base metal, i.e. in the weld area or in the heat-affected zone, whereas in the case of laser beam welded joints the failure is located only in base metal.

Fracture in GMA welded joints is combined, transcrystalline fissile with some ductile characteristics. Fracture in laser welded joints is transcrystalline and ductile with small fissile fracture present.

The strength of a GMA welded joint is substantially reduced compared to that made using laser beam welding. Worth noting is also much higher scatter of results around the average in the case of GMAW compared to laser beam welding.

Further tests should be focused on determining parameters of joint crack resistance.

#### References

- [1] **Bhadeshia H.K.D.H.** (1997), Models for the elementary mechanical properties of steel welds. *Mathematical Modelling of Weld Phenomena 3 Edited by Cejra H. Book 650. The Institute of Materials London.*
- [2] **Brózda J., Pilarczyk J., Zeman M.** (1983), *Welding CCT diagrams of austenite transformations-S. Ed. Katowice, Silesia.*
- [3] **Buchmayr B., Cerjak H.** (1988), Mathematical description of HAZ behaviour of low – alloyed structural steels. *Weld Quality – The Role of Computers, II W-conf. Vienna.*
- [4] **Ciechacki K.** (2005), The study of mechanical properties of the selected calls are bonded with a local variation of mechanical properties, Ph.D. Thesis, University of Technology and Agriculture in Bydgoszcz, Faculty of Mechanical Engineering.
- [5] **Goldak J. i inni** (1986), Computer Modeling of Heat Flow in Welds. *Metallurgical Transactions*, nr 9, s 587-600;
- [6] **Godlak J., Breiguine V., Dai N., Hughes E.** (1997), Thermal stress analysis in solids near the liquid region in welds. *Mathematical Modelling of Weld Phenomena 3, Institute of Materials, book 650.*
- [7] **Mikula J., Wojnar L.** (1993), The use of computational methods in the evaluation of the weldability of steel - CCT-S diagrams, *Overview of Welding*, nr 9, s. 4-7.
- [8] **Ranatowski E.** (1997), Some remarks on stress state at interface of the thin layer in metal joints under tension. *Micro Materials*, editors: B. Michel, T. Winkler, Berlin.
- [9] **Ranatowski E.** (2001), Some remarks on the relation between microstructure and mechanical properties in mismatched weld joints. *Materials Engineering*, nr 5.



## AUTOMATION OF PLASMA MACHINING IN A CONTINUOUS OPERATION LINE

Piotr Domanowski\*

\* University of Technology and Life Sciences in Bydgoszcz  
al. Prof. S. Kaliskiego 7, 85-789 Bydgoszcz, Poland  
e-mail: piotr.domanowski@utp.edu.pl

### Abstract

*The application of plasma techniques for surface modification like cleaning, activation and etching are described in this article. Technological process of glass packaging decoration takes place on a continuously operating conveyor line. A machine tool for plasma modification with a movable vacuum chamber has been designed. Construction and structure of mechanical, pumping and electric power supply systems have been described, together with machine tool operating cycle.*

**Keywords:** production automation, plasma modification, plasma cleaning, plasma activation, plasma etching, low temperature plasma

### 1. Application of plasma techniques for surface modification

Low pressure plasma allows for various possibilities of surface modification. Some of the applications are as follows: precise cleaning of dirty structural components, plasma activation, etching and coating of components [1], [2].

Plasma cleaning is a method of surface cleaning which proved to be effective, economic and safe for the natural environment. Plasma cleaning is six times more effective than traditional cleaning methods, and cleaned surface is ready for subsequent operations with no significant loss of material. Electrons are accelerated to very high velocities by oscillating electromagnetic field and excite atoms and gas molecules, which results in plasma generation. Ultraviolet radiation emitted during plasma generation very effectively breaks bonds of most organic compounds which contaminate the surface. The surface is physically cleaned using ion bombardment, and, depending on gas type, by chemical reactions. Contaminations are transformed into gaseous phase and sucked off.

Plasma cleaning has been used for:

- removal of lubricants, oils, oxides,
- pretreatment before bonding, soldering or gluing,

- pretreatment of components before lacquering [3].

Plasma activation can be used in case of surface modification of new packaging materials. Material surface is machined by plasma, using oxygen, for example. Radical points are created, ensuring good adhesiveness (which is necessary before overprinting, lacquering, gluing of components).

In the process of material structuring, creating good adhesiveness of associated materials when producing packaging materials, surface etching of such material can be useful. The surface is etched using a reactive process gas. The material is removed, converted into gaseous phase and sucked off. It may increase the area and wetting characteristic.

Plasma modification of a surface may take place on different organic materials, giving them hydrophobic, hydrophilic characteristic, resistance to external mechanical impacts. Shaping of the profile of textural surface properties of organic materials is not excluded. Moreover, plasma technology can be used to create barrier coatings, resistant to external mechanical impacts, including hydrophobic and hydrophilic coatings [1], [2], [4].

## **2. Industrial application**

The need for automated plasma treatment of bottles before their decoration resulted from insufficient quality of the process which has been realized in existing production lines in the leading company operating in Poland. Up till now, corona plasma cleaning using individually set gas burners has been used. The results of such cleaning have been unsatisfactory because of local (partial) burns of the cleaned surfaces and variations of surface adhesion.

A conveying line shown in drawing 2 is used in the automatic line for bottle decoration presented in drawing 1. Components, which are being machined, move continuously, which results from the technological process related to repeated application of paints and lacquers, and ultraviolet curing of the surface. Cleaning and activation of surface using low temperature plasma, which 'flows around' the component being cleaned in the vacuum chamber, have been proposed.

It required practical verification of proposed plasma method on specially built test stand, and designing a mechanical assembly consisting of a moving vacuum chamber, which was sequentially closing a batch of components being machined, and, after plasma treatment, was returning to initial position. Such solution has not been used on the market of vacuum devices for plasma cleaning, so it has been a subject of patent application [5].

## **3. Machine tool construction and design**

Machine tool (drawing 3) consists of a stand with guides, on which a slide 1 is placed with a vacuum chamber 2. A system of aluminium sections item<sup>®</sup> has been used to build a movable assembly. Slide 1, driven by a servo-motor 4, moves along the guides of the stand 5. Vacuum chamber has been divided into two parts, which are closed by pneumatic actuators 3. On the front of two parts of the chamber a silicone seal is placed, in which holes have been cut for spindles which fasten components to be machined (drawing 4). Because of seal durability, when the chamber is closed, spindles are centered with V-blocks elastically fastened to both sides of the chambers.

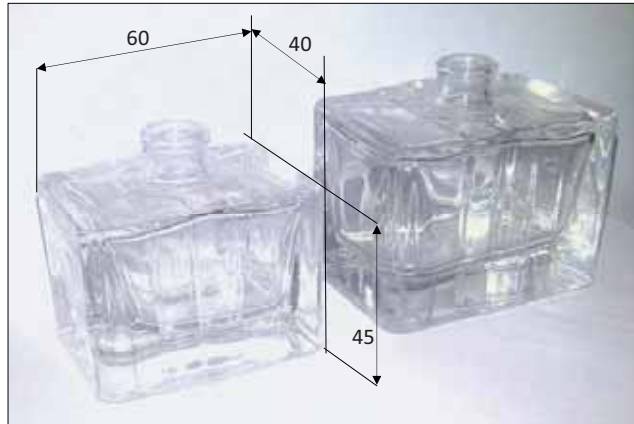


*Fig. 1. Glass packagings for machining – plasma cleaning*

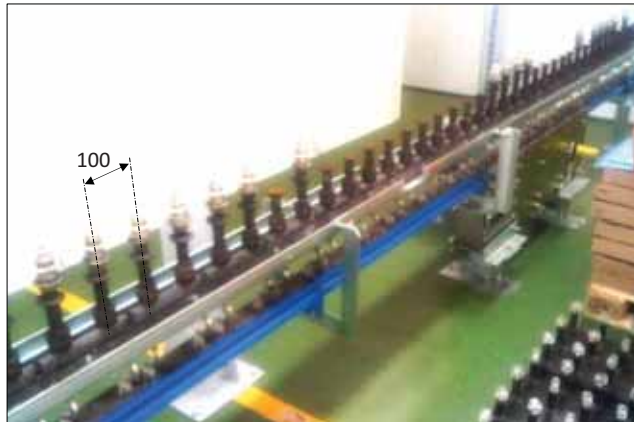


*Fig . 2. Continuously operated line*

The vacuum chamber dimensions are as follows: 1900 x 160 x 160mm. The vacuum chamber has been made as a welded structure of 1.4306 stainless steel. The slide with the vacuum chamber moves along the conveyor line, on which the cleaned elements are fastened (bottles) with a constant pitch of 100mm. The conveyor line moves with a uniform speed of 4m/min. Vacuum is created by a pump assembly, consisting of an initial rotary pump and a Root WA501 pump made by PfeiferVacuum. The pumps make it possible to achieve the vacuum of  $10^{-3}$ mbar. Fast pumping away of the chamber is necessary, so an additional ballast tank 8 is used, of 0,5m<sup>3</sup> capacity. The pump assembly is connected to the vacuum chamber with a flexible hose 12. Pressure inside the chamber is measured with a TPR Pirani gauge. Pure argon or a mixture of argon and oxygen in a ratio of 9:1 as technological gas can be supplied to the vacuum chamber. Gas flow rate is set with a mass controller Bronkhorst (18...900sccm). The control of the mechanical drive system and pump assembly is realized by a PLC with vacuum valves 9, 10, 11. Dora Power System 16 is used as a power supply for the plasma generator. It constitutes an autonomic current source, in which

the distribution of power is independent of load impedance [6], [7]. Current stabilizing takes place in the processing system without any feedback. To fulfill these conditions, a resonant circuit of power conversion with a resonant circuit quality factor stabilizing is used in DPS power supply. Energy supply is controlled discretely thanks to group modulation of generator signal which controls a bridge which keys a resonant frequency. Positive and negative poles are connected to electrodes 18 placed opposite to each other in both parts of the vacuum chamber 2 – drawing 4. Structural presentation of the machine tool with a pump system is shown in drawings 5 and 6.

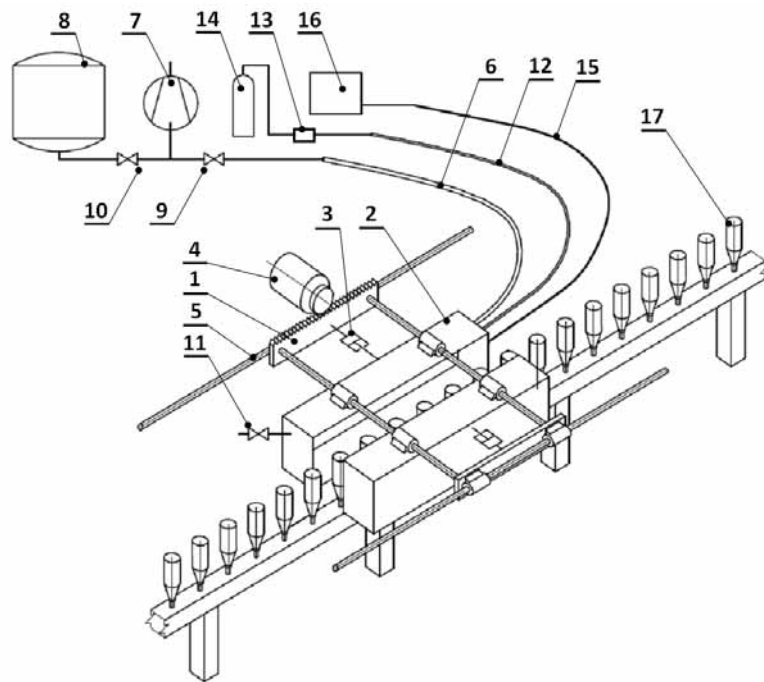


*Fig. 3. The diagram of the machine tool for plasma cleaning of the elements in continuously operated line, (description in the article)*

#### **4. Working cycle – the process of plasma cleaning and activation**

The system operates in the following way: elements which are to be machined are moved on a conveyor 17, continuous movement, at a uniform speed, and vacuum chamber 2 is opened and placed in a terminal position of the stand guides 5. Next, the vacuum chamber is moved – accelerated motion – until movement speed is equal to the line speed, and the chamber is closed. There are 19 elements fastened to the spindles in the chamber. Now, the vacuum chamber 2 with elements to be cleaned moves with a speed which is equal to the speed of the conveyor line. After closing the vacuum chamber the valve 9 is opened, so the chamber is connected with the ballast tank. Pressures are equalized to the level of approximately 450mbar within about 2,5sec.

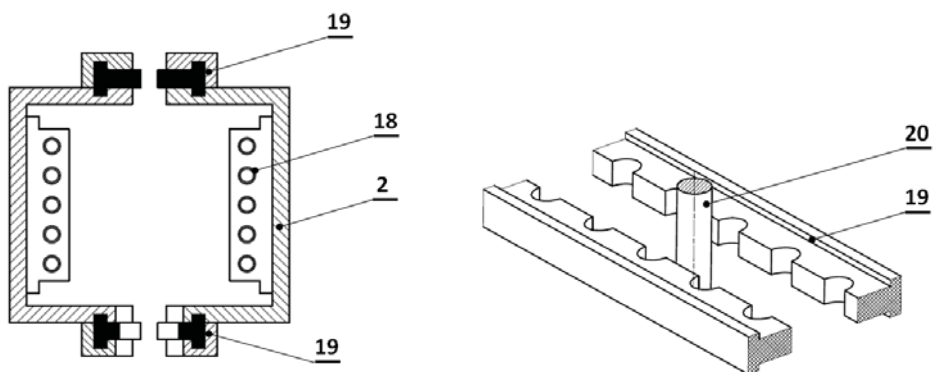


*Fig. 4. Arrangement of electrodes and sealing of the chamber and spindles*

Then the valve cuts off the ballast tank and further pumping is performed only by the pumps. After reaching the vacuum level of 100mbar, DPS power supply is switched on and plasma is initiated. Optimum time of the cleaning process is 3 seconds, and has been set on the grounds of test results. So, it is advantageous to continue vacuum pumping with simultaneous metering of the technological gas. After that time the power supply is switched off. Then vacuum pumping is switched from the vacuum chamber 2 to the ballast tank 8 by closing the valve 9 and opening the valve 10, after opening the valve 11 the air gets into the vacuum chamber. Operating time of the vacuum valves is 0,2 sec. and the time of filling with air is 2,5sec. After the air got into the chamber it is possible to open the chamber and slow down, then the chamber goes back to the initial position. Return movement time is 3 sec. Then the working cycle is repeated.

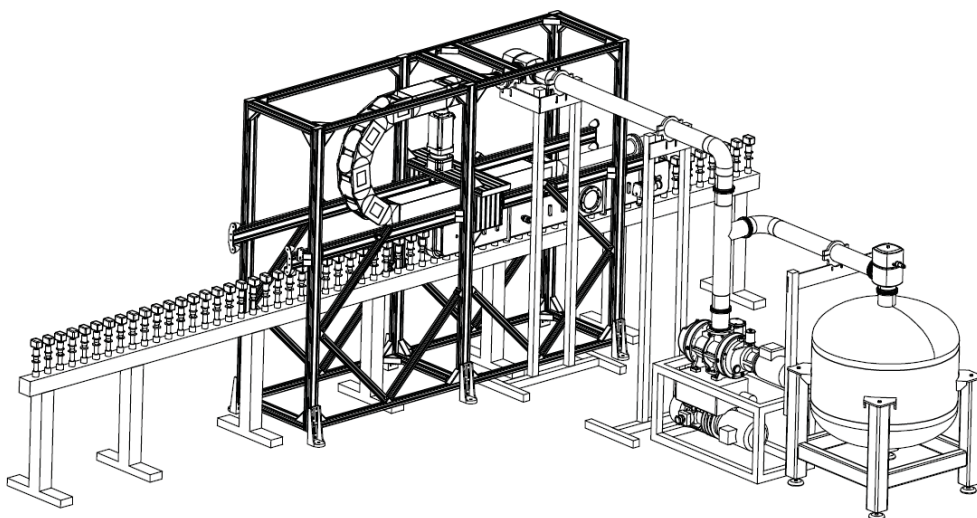


*Fig. 5. The designed machine tool for surface plasma modification in continuously operated line*

## 5. Conclusions

The machine tool has been designed and made, for modifying the surface of the elements on the continuously operating conveyor line. Machine tool has been introduced in the industrial plant in the region. Economical purposefulness of the introduction is based on the high quality of the product and the possibility of application of this technology in other production lines in the plant. It is possible to employ this solution in the production lines in the industry of glass packagings and plastic packagings, in food and pharmaceutical industries .

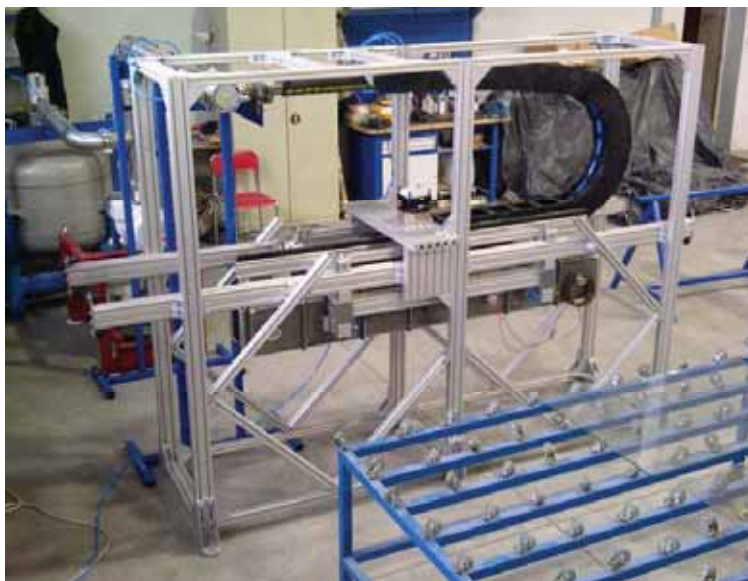


Fig. 6. Machine tool for surface plasma modification in continuously operated line

## References

- [1] Szałatkiewicz J.: *Wytwarzanie plazmy i jej zastosowania*, Pomiary Automatyka Robotyka, 3/2010.
- [2] *Plasma Technology Process Diversity + Sustainability*, German Federal Ministry of Education and Research (Bundesministerium für Bildung und Forschung – BMBF), 2001.
- [3] *Plasma technology*, Published by: Diener electronic GmbH + Co. KG, 2007. [www.diener.de](http://www.diener.de)
- [4] Kaczmarek D., Domaradzki J., Prociów E., Wojcieszak D., Mazur. M., Sieradzka K., Adamiak B., Domanowski P.: *Powłoki wielofunkcyjne dla transparentnej elektroniki*, III Sympozjum : Fotowoltaika i Transparentna Elektronika - perspektywy rozwoju, Oficyna Wydawnicza Politechniki Wrocławskiej, 2012.
- [5] Domanowski P.: *Układ i komora próżniowa do obróbki plazmowej elementów na linii o ruchu ciągłym*, Zgłoszenie patentowe nr P 399750, Urząd Patentowy RP, 2012.
- [6] Dora J.: *Zasilacz rezonansowy*. Patent PL nr 313150, Urząd Patentowy RP, 1996.
- [7] Halarewicz J., Domanowski P., Dora J., Wawrzak A., Karwowski K., Pinio P., Wiatrowski A., Posadowski W. M.: *Próżniowe otrzymywanie cienkich warstw na wielkogabarytowych, szklanych podłożach. Część 2 – linia przemysłowa*, Elektronika - Konstrukcje, 4/ 2012.



## MOTIONAL CHARACTERISTICS OF GRAINS IN THE MULTI-HOLE SPACE OF A MULTI-DISC GRINDER

Józef Flizikowski, Andrzej Tomporowski

University of Technology and Life Sciences in Bydgoszcz,  
Ul. Ks. Kordeckiego 20, 85-225 Bydgoszcz,  
tel. 048 52 340 8255,  
e'mail: fliz@utp.edu.pl

### Abstract

*It was investigated multi-disc grinders in directions knowledge of, describe and utilize, for design and structural purposes, the characteristics that indicate the relations between speeds, idle movement, loads and the indicators of motion variables in the grinding space. The mathematical description of the states of and changes in grains, their surface and volume during movement (idle and working movement) of the components and assemblies in the multi-hole grinding process was obtained as a objective of this work.*

**Keywords:** biomass grinding, square of quasi-cutting, working elements geometry

### 1. Introduction

Investigations into multi-disc grinders demonstrate that it is possible to acquire knowledge of, describe and utilize, for design and structural purposes, the characteristics that indicate the relations between speeds, idle movement, loads and the indicators of motion variables in the grinding space.

**The objective of this work** is to provide a mathematical description of the states of and changes in grains, their surface and volume during movement (idle and working movement) of the components and assemblies in the multi-hole grinding process.

### 2. Motional Characteristics

Usable characteristics and multi-disc and multi-hole grinding outcome variables: power demand ( $P_R=f(n)$ ), degree of fineness ( $\lambda=f(n)$ ) and mass target efficiency ( $Q_m=f(n)$ ,  $Q_c \leq Q_m$ ) depend on the common area of the edges of two holes ( $S_c, S_T$ ), density and volume of grain in the working space ( $\rho_m, V_g$ ), rotational, angular and linear speed of a component and time ( $n, \omega, v, \Theta, t_i$ ) -  $L(P_R, \lambda, Q_m, Q_c) = P(S_c, S_T, \rho_m^{m+1}, V_g, n, \omega, v, \Theta, t_i)$ ; they also depend on the volumetric dosing of mass feed  $q(0;1)$ .

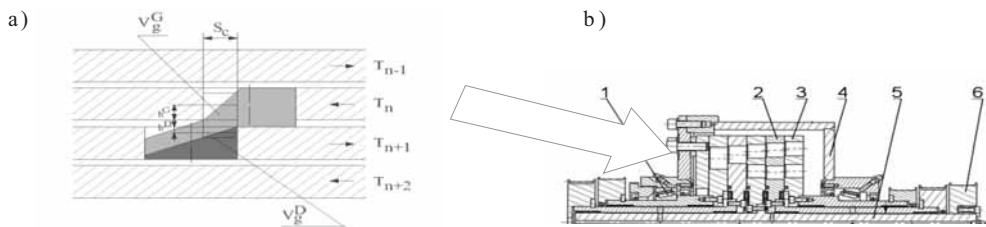


Fig.1. RWT-5KZ multi-hole five-disc grinder working unit, [8,9]: a) grain filling in two adjoining working holes of the quasi-cutting unit:  $T_{n-1}$  do  $T_{n+2}$  – subsequent grinding discs,  $h^G$  – height of material column before the cutting plane,  $h^D$  – height of material column behind the cutting plane,  $V_g^G$  – calculated volume of material before the cutting plane,  $V_g^D$  – calculated volume of material behind the cutting plane,  $S_c$  – common area of the quasi-cutting pair of holes; b) cross-section of the multi-disc unit: 1 – bearing, 2 – grinding disc (so-called „preceding” disc), 3 – grinding disc (so-called “subsequent” disc), 4 – body, 5 – shaft, 6 – pulley

The usable characteristics of grinding, dependent on the movement of grain and grinder components were named the motional characteristics of grain [1,2,7-11].

**Assumptions:** To determine motional characteristics of grain, two states were assumed which are dependent on the linear speed of the grinding holes edges (Fig. 1) [7,11]: the first one – idle state, involving only movement and mixing, exclusive of grinding (linear speed of points on edges – below  $0.7\text{m}\cdot\text{s}^{-1}$ ), second – working state, with significant grinding initiators (above  $0.7\text{m}\cdot\text{s}^{-1}$ ). The characteristics have been formulated applying the following assumptions [1,2,7,11]:

- a) the number of contacts between grains, components and particles along their pathway influences the quality and grinding effects,
- b) the positioning of holes in respective discs of the grinding unit forms a line in the internal cone that starts on the initial diameter ( $d$ ) with the pitch ( $s$ ) and the length of the helical line ( $c$ ), which increases by the thickness ( $g$ ) and the number of discs ( $n$ ) up to the length ( $C$ ) – finished with an external cone of the hole edges,
- c) movement, mixing and grinding of grains (p-m-r) depend, among other things, on friction conditions, structural features of discs and the positioning of holes in discs, with dynamic movement of the machine structural components and of grain ( $p=p_m+p_z$ ) occurring during idle movement and when working load is applied to the machine ( $p_m=p_j+p_r$ ), and of grains ( $p_z=p_o+p_p$ ) during axial and radial movement within the hole and disc space,
- d) during movement and mixing of grain (p-m), apart from following trajectory similar to the helical line (original path), grains also rotate around the centre of gravity (secondary movement); grinding dynamics does not rule out both types of movement (r),
- e) grinding on the edges of holes between adjoining discs is performed through equally split quasi-cutting,
- f) cross-section of holes in discs is dependent on the outflow and can be described using Kvapil's theory [5]:

$$S_{\min} = K \cdot n \cdot (5 \cdot d_z)^2$$

where:  $S_{\min}$  – the smallest cross-section of the hole through which grain is freely moved –  $\text{m}^2$ ,  $K$  – experimental coefficient (for corn grains  $K=1,4$ ),  $n$  – coefficient for the shape of holes in discs, for round holes  $n=0,85$ ,  $d_z$  – average size of grain –  $\text{m}$ .

In both states of component movement, in particular in the second one – depending on the shape of grain and tools (holes) and the positioning of their cutting edge in relation to the movement direction – some of the edges perform the cutting, other scratching operations and yet other the cutting of grooves in grains. Hence, what we see here is dynamic, complex and volumetric intensity of grinding per path unit. On assuming fixed reference values expressed in coefficients, grinding intensity can be expressed applying the following dependency:

$$I_{DR} = \frac{U}{L \cdot P} = c_{DR} \cdot \frac{N \cdot d \cdot x}{H \cdot y} \cdot \frac{dm^3}{m \cdot W} \quad (1)$$

where:  $U$  - volumetric loss of grain in  $\text{dm}^3$ ,  $L$  - path (p-m-r) in m,  $P = P_j + P_R$  - power supplied to the system to defeat resistance to idle and grinding motions in W,  $N$  - normal unit load in MPa,  $c_{DR}$  - factor of proportionality in  $\text{dm}^3 \cdot \text{m}^{-1} \cdot \text{W}^{-1}$ ,  $d$  - substitute height of the cutting edges measured perpendicularly to the motion direction in m,  $x = (i_{lkr}/i_{lzk})$  relation between the number of cutting edges and the total number of grains and edges on motion trajectory,  $H$  - grain hardness,  $y$  - coefficient characterising relative number of grains and holes edges in transferring discs ( $C_{kR}(\underline{S}_e, \underline{S}_T, \underline{V}_z)$ ), susceptible to load ( $y = f(C_{kR})$ ).

The positioning of grains being ground in the working space of a multi-hole grinder (Fig. 1a) is described by statistical distribution of its length. Because the material present in the holes of this same disc is characterised by the same particle size  $\rho$  and is subject to the same grinding and cutting process in each hole, its state for the purpose of this analysis is indexed with the cutting number ( $m$ ) and the disc number ( $n$ ) [7,8]:

$$\rho_n^m : [0, l_{\max}] \rightarrow [0, 1], \quad \int_0^{l_{\max}} \rho_n^m dl = 1. \quad (2)$$

The thickness of the  $n$ -th disc, for the purpose of this analysis, is marked with the symbol  $y_n$ , and the height up to which the material fills the hole in the  $n$ -th disc prior to the  $k$ -th cut by the symbol  $\tilde{y}_n^{(k)}$ .

In efficient grinding and cutting, length distribution of grains which filled the empty space in the  $(n+1)$ -th disc changes as per the following dependency (Fig. 1a):

$$\tilde{\rho}_{n+1}^m(x) = A_{n,m} \rho_n^m = \left(1 - \frac{x}{y_{n+1} - \tilde{y}_{n+1}^m}\right) \rho_n^m(x) + \frac{1}{y_{n+1} - \tilde{y}_{n+1}^m} \int_x^{l_{\max}} \rho_n^m(l) dl, \quad (3)$$

while of those left in the  $n$ -th disc as per:

$$\tilde{\rho}_n^{m+1}(x) = \tilde{B}_{n,m} \rho_n^m = \left(1 - \frac{x}{\tilde{y}_n^m}\right) \rho_n^m(x) + \frac{1}{\tilde{y}_n^m} \int_x^{l_{\max}} \rho_n(l) dl, \quad (4)$$

where:  $A$ ,  $B$  - scholastic operators for  $m$ -th cut,  $n$ -th disc.

It was assumed for simplification purposes that, subsequent to grinding, distribution of granulated product in the hole spaces of the  $(n+1)$ -th disc will be uniform (cut fraction and that present in the hole before cutting will mix) and it will therefore be the weighted average from  $\rho_{n+1}^k$  i  $\rho_n^k$ :

$$\rho_{n+1}^m(x) = \frac{\tilde{y}_{n+1}^m}{y_{n+1}} \rho_{n+1}^{m-1} + \frac{y_n - \tilde{y}_{n+1}^m}{y_{n+1}} A_{n,m} \rho_n^m(x) \quad (5)$$

During the modelling of the common part surface, integration of grinding momentary cross-section was employed [1,2,5]:

$$S_C = \int_{x_1}^{x_2} \left\{ b_2 + [R_2^2 - (x - a_2)^2]^{1/2} \right\} dx - \int_{x_1}^{x_2} \left\{ b_1 - [R_1^2 - (x - a_1)^2]^{1/2} \right\} dx \quad (6)$$

where:

$a_1, a_2, b_1, b_2$  -  $C_1$  and  $C_2$  hole centres coordinates  
 $R_1, R_2$  - holes radius vector.

Based on what has been said, distribution of grain length in ground material which filled the empty space of the  $(n+1)$ -th disc changes as follows:

$$\tilde{\rho}_{n+1}^m(x) = A_{n,m} \rho_n^m = \left(1 - \frac{x}{y_{n+1} - \tilde{y}_{n+1}^m}\right) \rho_n^m(x) + \frac{1}{y_{n+1} - \tilde{y}_{n+1}^m} \int_x^{l_{\max}} \rho_n^m(l) dl \quad (7)$$

whereas in the material left within  $n$ -th disc in the following way (analogical reasoning):

$$\tilde{\rho}_n^{m+1}(x) = \tilde{B}_{n,m} \rho_n^m = \left(1 - \frac{x}{h^D}\right) \rho_n^m(x) + \frac{1}{h^D} \int_x^{l_{max}} \rho_n(l) dl \quad (8)$$

It must be remembered that the column of the material being cut is not the entire material that has been moved to the lower hole. Its volume is  $S_c \cdot h^D$  whereas that of the entire material moved from the preceding hole to the subsequent hole is

$$V_{\frac{D}{2}}^D(\alpha_c) - V_n^m$$

It means that the second and third component in (8) must be multiplied by the relation between these volumes:

$$\tilde{\rho}_n^{m+1}(x) = \tilde{B}_{n,m} \rho_n^m = \left(1 - \frac{S_c \cdot x}{V_{\frac{D}{2}}^D(\alpha_c) - V_{n+1}^m}\right) \rho_n^m(x) + \frac{S_c}{V_{\frac{D}{2}}^D(\alpha_c) - V_{n+1}^m} \int_x^{l_{max}} \rho_n(l) dl \quad (9)$$

It was assumed for simplification purposes that, subsequent to cutting, the grain length distribution in the  $(n+1)$ -th disc will be uniform (cut fraction and that present in the hole prior to cutting will mix), and therefore it will be the weighted average from  $\rho_{n+1}^{m-1}$  and  $\tilde{\rho}_{n+1}^{m-1}$ .

$$\rho_{n+1}^m(x) = \frac{V_{n+1}^m}{V^D} \rho_{n+1}^{m-1} + \frac{V^D - V_{n+1}^m}{V^D} \tilde{B}_{n,m} \rho_n^m(x) \quad (10)$$

The filling level of the quasi-cutting unit and thus the efficiency of the cutting process depend on the value of the function  $V^D$ ,  $V^G$  and  $S_c$  which in turn depend on the direction of the effective gravitation and on the total volume of material in both holes before cutting

$$(V_{n+1}^m + V_n^m).$$

Other indicators of variables are provided based on tests.

Intensity is the measure of the reduction of initial volume of grains ( $V_g$ ) on the way from the entrance to the exit from a multi-disc unit, per unit of power consumed by the grinding drive system. The first state of multi-disc grinding, where only movement and mixing ( $v_R < 0,7 \text{ m} \cdot \text{s}^{-1}$ ) occur, does not result in explicit volume reduction (U), however, grinding elements travel a specific path (L) and the system is supplied with power ( $P_j$ ). After efficient speed is exceeded ( $v_R > 0,7 \text{ m} \cdot \text{s}^{-1}$ ), volume reductions are observed resulting from the effects of the cutting edges with grinding power ( $P_R$ ) on the path (L). Dynamic intensity of grinding is directly proportional to the unit load (N) and inversely proportional to the grain hardness (H) and the conditions of the grinding unit ( $C_{KR}(S_c, S_T, V_g), C_k$ ). The interpretation of the grinding mechanism should be that a grain with the area  $S$ , being moved between the edges of a grinding element, pressed using axial force  $N$ , is deformed elastically and plastically by the width  $b$ , becoming swollen over the volume of the front surface. After the load is removed, deformations are reduced by the value of elastic deformations to  $\sigma_1$ . Assuming that the nature of elastic deformation is analogous to that resulting from ball indentation, a different formula is obtained for grinding intensity:

$$I_{DR} = n \cdot d_z^3 \cdot \left( \frac{1}{\sigma} - \frac{1}{\sigma_1} \right) = k(S_c, S_T, V_g) \cdot \frac{N}{E}; \frac{dm^3}{m \cdot W} \quad (11)$$

where:  $n$  – number of grains carrying normal load  $N$ ,  $d_z$  – grain diameter in m,  $k$  – factor of proportionality taking account of the relations between momentary volumes, surfaces and power, in  $\text{m}^3 \cdot \text{m}^{-1} \cdot \text{W}^{-1}$ ,  $E$  – coefficient of elasticity (tensile modulus) in MPa.

Because it is difficult to precisely determine elastic and plastic deformations for grains in accordance with (11), and the grinding intensity is determinable by complex physical and mechanical processes, path and power for grinding is calculated or determined based on measurements.

Similarly, in modelling and identification of grinding with regard to grain in motion as per the dependency (1), in particular with regard to movement and mixing of grains, the effect of internal friction must be taken into account. The assumption no. b indicates that movement, mixing and

grinding involves the friction and helical trajectories, in the space described by two radial lines:  $L=C-c$  (between external and internal edges of holes in discs, e.g. along the spiral of Archimedes with the polar equation:  $r=a\varphi$ ) and thus:

$$I_{DR} = \frac{U}{L \cdot P} = \frac{U}{\lambda \cdot v_{p^*m} \cdot t_{p^*m} \cdot P}$$

or

(12a and 12b)

$$I_{DR} = c_{DR} \cdot \frac{N \cdot d \cdot x}{(C-c) \cdot P} = c_{DR} \cdot \frac{N \cdot d \cdot x}{\left( \sqrt{\pi^2 \cdot D^2 + s^2} - \sqrt{\pi^2 \cdot d^2 + s^2} \right) \cdot P} \cdot \frac{dm^3}{m \cdot W}$$

where:  $\lambda$  – coefficient determining the effect of internal friction ( $\mu_w$ ) on the grain movement speed ( $v_{p+m}$ ) in the  $t_{p+m}$  time of passage through the multi-disc unit:

$$\lambda = \frac{1}{\sqrt{2\mu_w \left( \frac{1}{\mu_w} + 2\mu_w \right) - \sqrt{1 + \mu_w^2}}},$$

$D$  – outer diameter of the helical line on which the holes are positioned in m,  $d$  – inner diameter of the helical line on which the holes are positioned in m,  $s$  – pitch equal to disc thickness – m.

It was assumed in the experimental verification that the trajectory of grain moving in the area between the radial lines of the external and internal cone (holes positioning envelope) is a continuous line – in terms of movement and mixing (first state) and continuous and disrupted (for the duration of grinding) – in the case of the second state (efficient edge speed, for e.g. corn:  $v_R > 0,7 \text{ m} \cdot \text{s}^{-1}$ ). As the speed of grains during movement and mixing is low and because grains are stopped for the duration of quasi-cutting and there is a potential increase in the flying movement of grain specks as a result of bouncing subsequent to grinding, it can be assumed for simplification purposes that the second state has the motion trajectory and time equal to  $t_{p+m+r} = t_{p+m}$ .

**Idle movement characteristics:** Characteristics that are identical for states and changes in all multi-hole spaces of multi-disc grinding units are variable power demand  $P_{R|m}$  depending on the rotational speed of units and grinder components  $n_m$  (machine idle running characteristics) – without ground material:

$$P_{R|m} = f(n_m), q(0) \quad (13),$$

which, depending on the linear speed of a grinding element  $v_R$ , takes the following form:

$$P_{R|m} = k_{1m} \cdot v_R, \text{ for: } q(0), Q_m = 0, Q_c = 0 \quad (13a)$$

Similarly, power  $P_{R|(m+z)}$  for machine idle movement with grain (feeding with grain  $q$ , movement of machine components and grain with the speed  $n_{m+z}$ , without grinding):

$$P_{R|(m+z)} = f(n_{m+z}), q(0; 1) \quad (14),$$

which leads to the dependency that takes into account the volume of grain  $V_g$  in material moved between discs:

$$P_{R|(m+z)} = k_{2(m+z)} \cdot v_R \cdot f(V_g), \text{ for: } q(0; 1), Q_m = \frac{dm}{dt}, Q_c = 0 \quad (14a)$$

Dependencies from (13) to (14a) require tests to be conducted to determine idle movement modules and calculate moved material functional volume:

$$k_{1m}, k_{2(m+z)}, f(V_g)$$

Thus, we obtain the model of power dependency for machine components movement, with or without grain feed – without grinding operation (only grain movement), on the rotational speed, at zero or constant power supply, without grain size changes, without grinding efficiency, at target efficiency equal to zero ( $Q_c=0$ ) but with movement efficiency or efficiency equal to power supply,

without grinding operation  $Q_m = \frac{dm}{dt}$ . The characteristic of idle running is a special type of load characteristics. It corresponds to the mixing power characteristics ( $P_R = P_m$ ).

**Load movement characteristics:** For different rotational speeds of discs (linear speed  $v_R$  on the radius vectors of the pass-through and grinding holes edges) and variable power supply/grain feed  $q(0;1)$ , variable degrees of fineness, mass and target efficiencies (loads with full grinding) and totally different mass  $Q_m$  and target  $Q_q$  efficiencies (of a product specified in terms of size and geometry) are obtained.

Power utilised for grinding includes components of idle and grinding loads and of dynamic increase – depending on phenomena complexity:

$$P_{Ro} = P_{Rj(m+z)} + P_{Rr} + P_{Rd}, \text{ for: } q(0;1), \\ \text{and for } \lambda = f(n, \Delta n) \neq 1, Q_m = f(n, \Delta n) = \frac{dm}{dt}, Q_q \neq 0 \quad (15),$$

Below is a proposed experimental description of power input under load relative to cross-sections of grain mass in grinding holes  $S_c$  and on the intra-disc surfaces  $S_T$ , in the form of a general dependency, dependent on the speed of the grinding edge [9]:

$$P_{Ro} = (k_{2(m+z)} \cdot f(V_g) + \tau \cdot f(S_c, \tilde{\rho}_n^{m+1}, V_g) + \varepsilon_d \cdot \tau \cdot f(S_c, S_T, \tilde{\rho}_n^{m+1})) \cdot v_R \quad (15a)$$

Dependencies (15) and (15a) require tests to be conducted to define dynamic increase module and calculate probable cross-sections participating in material grinding:

$$\varepsilon_d, S_c, S_T, \tilde{\rho}_n^{m+1}$$

### 3. Indicators analysis results

In order to determine the characteristics of idle running ( $k_{1m}, k_{2(m+z)}, f(V_g)$ ), load ( $\varepsilon_d, (S_c, S_T, \tilde{\rho}_n^{m+1})$ ), efficiency  $Q_m = \frac{f(\tilde{\rho}_n^{m+1}, S_c, S_T, V_g, n, \Delta n_{ij})}{\varepsilon_R} \rightarrow \max$  and unit power consumption

$$E_j = \frac{P_R(\tilde{\rho}_n^{m+1}, S_c, S_T, V_g, n, \Delta n_{ij})}{Q_m(\tilde{\rho}_n^{m+1}, S_c, S_T, V_g, n, \Delta n_{ij})} \rightarrow \min, \text{ power demand of a five-disc grinder was tested in the cutting}$$

operation, both with and without ground material. In this work, an analysis was conducted to determine substitute function  $F_r$  (Fig.2), which takes into account the complexity of  $F_r = f(S_c, S_T, \tilde{\rho}_n^{m+1}, V_g)$ . Sample results are presented in figure 2.

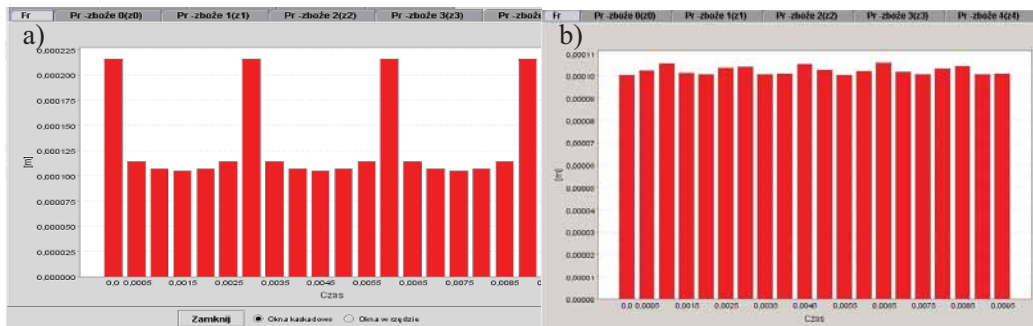


Fig. 2. Momentary function of  $F_r$  cross-section substitute function, dependent on the surface and volume of the adjacent working holes in discs  $S_c, S_T, \tilde{\rho}_n^{m+1}, V_g$  for a) increase in the number of holes between discs  $PLOT=2$ , b)  $PLOT=1$

Active power  $P$ , consumed depending on the number of holes, angular speed of discs and under conditions of the programmed feeding of triticale, maize and rice grains (working movement, under load) are shown in figure 3.

The power demand function (Fig. 3 - mathematical description of states and changes of grinding power) obtained from a statistical analysis, movement of the multi-hole grinding components and units in the triticale and rice grinding process demonstrate percentage compliance of model and process response:  $Q=14,7$ . On the other hand, in the case of maize, quality function reaches on average slightly lower percentage compliance of results:  $Q=19,2$ .

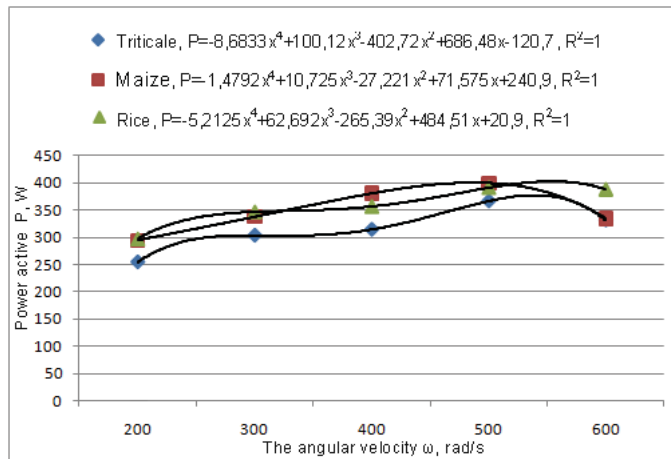


Fig 3. Active power consumed by drive units ( $P_d$ ) utilized for the grinding of triticale, maize and rice grains, depending on the angular speed [8]

The results of machine tests of the grinding process were also estimated with momentary characteristics of their surface and grinding volume (e.g. as per Fig. 2). Here too the quality function reaches relatively high values as far as the model's quality estimator is concerned, which indicates that there is significant discrepancy between the response of the model and the actual object:  $Q=39,6$  - in the case of an increase in the number of holes between discs (in rows)  $PLOT=2$ , and in the case of  $PLOT=1$ ,  $Q=16,8$ , which can be considered a value that coincides with the evaluations of the power function ( $Q=14,7$ ) of rice and triticale.

The results obtained from the machine test, the function of cross-section and momentary volumes in the form of dependencies (11) are sufficient for a general function of grinding intensity in grain motion to be formulated:

$$I_{DR} = k \left( \left( 1 - \frac{Sc \cdot x}{V_{\frac{D}{2}}^D(\alpha_c) - V_{n+1}^m} \right) \rho_n^m(x) + \frac{Sc}{V_{\frac{D}{2}}^D(\alpha_c) - V_{n+1}^m} \int_x^{t_{max}} \rho_n(l) dl \right) \cdot \frac{N}{E} \cdot \frac{dm^3}{m \cdot W} \quad (16)$$

This function can form the basis for further optimisation or modernisation of the multi-disc and multi-hole grinding structure used for the grinding of e.g. triticale and rice, with high level of its compliance with experimental results.

#### 4. Results analysis

With the stabilised motion of grinding components ( $(n,\omega,v)=\text{const}$ ), for the analysed scope of grain movement and with the use of functional models, it is possible to acquire knowledge of and design mutual relations within the multi-hole and multi-disc system of the grinder working unit: filling of the transport and grinding area, power, process target and mass efficiency as well as linear (circumferential) and rotational speeds of operating discs.

The systematised characteristics of idle running and load, based on specialist calculations and investigations into grinders, indicate that the filling of the quasi-cutting unit, and therefore efficient, power demand and energy consumption in the grain cutting process, depend on the values of operating speeds of both quasi-cutting and feeding. These, in turn, depend on motional and drive parameters of individual grinding units and the sum of momentary cross-sections, material volume in adjacent holes, making up a grinding unit. The grain motion characteristics, at various stages of disintegration and movement, depend on the common areas of the preceding and subsequent holes and their filling level with material both before and behind the cutting plane.

Applying a practical approach related to the structure and operation of food machines—assuming a design solution (as a logical conjunction of criteria and structural features of a quasi-cutting unit) within the conceptual space, providing an optimal solution from the point of view of the selected criteria including objective, minimum power, auto-adjustment and multi-level structure—it is possible to propose a new pro-developmental solution with regard to further analyses of the integrated grinding system in the field of permissible variability of structural features and processing parameters.

#### 5. Conclusions

The methodology of calculations and examination of the characteristics of grain motion, for idle and loaded grinding, may lead to improvement and development of processing machines.

The selected characteristics of grain motion point to the need for reaching a compromise between the two basic functions: movement and grinding within the intra-hole working space. Proposed and partly verified models will facilitate selection of optimal structural features and multi-disc grinding process parameters. It is a useful and desired course, resulting ultimately in obtaining a nutritious/high energy product with a defined form, structure and repeatable dimensions.

The analysis of the current studies and structural basics of triticale, maize and rice grain grinders, as well as detailed mathematical descriptions of the grinding process in relation to the structure of disintegrating units confirm the possibility of development and experimental verification of mathematical models useful for optimisation (modernisation and advancement) of multi-disc grinding structures. Models and corresponding mathematical dependencies facilitate efficient designing and planning of multi-hole grinding systems utilisation.

#### References

- [1] Flizikowski, J. B., *Intelligent grinding system*, Inżynieria i Aparatura Chemiczna nr 3/2011, Poland: SIGMA-NOT Sp. z o.o., (pp.22-23), Warszawa 2011a.
- [2] Flizikowski, J. B., *Levels of intelligent grinding system*, Inżynieria i Aparatura Chemiczna nr 3/2011, Poland: SIGMA-NOT Sp. z o.o., (pp.24-26), Warszawa 2011b.
- [3] Knosala, R. i Zespół, *Zastosowanie metod sztucznej inteligencji w inżynierii produkcji*, WNT, Warszawa 2002.

- [4] Niederliński, S., *System i sterowanie*, Poland, PWN, Warszawa 1987.
- [5] Macko, M., Boniecka, M. & Drop, A., *Life cycle assessment of grinders Rusing SoliWorks Sustainability application (in polish)*. Inżynieria i Aparatura Chemiczna nr 3/2011, Poland: SIGMA-NOT Sp. z o.o., (pp.49-50), Warszawa 2011.
- [6] Powierża, L., *Zarys inżynierii systemów bioagro-technicznych*, Wydawnictwo ITE, Radom 1997.
- [7] Tomporowski, A., *Structure development of biological material shredders, Part I and II (in polish)*, Inżynieria i Aparatura Chemiczna nr 3/2011, Poland: SIGMA-NOT Sp. z o.o., (pp.75-78), Warszawa 2011a.
- [8] Tomporowski, A., *Studium efektywności napędu i rozwiązań innowacyjnych konstrukcji wielotarczowych rozdrabniaczy ziaren biomasy*, LTN, Lublin 2011b.
- [9] Tomporowski, A., *Filling model for the working multi-disc biomass grain grinding unit*, The Archive of Mechanical Engineering; vol. LIX, number 2, pp. 155-174, Warszawa 2012a.
- [10] Tomporowski, A., *Stream of efficiency of rice grains multi-disc grinding*, Eksploatacja i Niezawodność – Maintenance and Reliability; 14(2), pp.150-153, Lublin 2012b.
- [11] Tomporowski, A., Opielak, M., *Structural features versus multi-hole grinding efficiency*, Eksploatacja i Niezawodność – Maintenance and Reliability; 14(3), pp. 223-228, Lublin 2012.

***This work was financially supported by the Polish National Centre for Research and Development in 2010-2013***





## MACHINE VIBRATIONS ON A FLEXIBLE ROOF

Henryk Holka, Tomasz Jarzyna

*University of Technology and Life Sciences*  
ul. Ks. Kordeckiego 20, 85-225 Bydgoszcz, Poland  
tel.: +48 52 373-02-80, fax: +48 52 374-93-27  
e-mail: holka@utp.edu.pl, tomasz\_jarzyna@o2.pl

### Abstract

*The paper presents the synthesis of the receptance by using the block diagrams. The presented method is also very useful when the machine or a group of machines is mounted on a flexible roof which is hard to describe analytically. Such a case occurred while analyzing vibrations of a group of pumps installed on a floor of an assembly hall. Pumps, apart from excitations generated by the operation, are subjected to kinematic excitations from a vibrating foundation. A synthesis of the pump connection with a flexible base has been presented in this paper.*

**Keywords:** pump, vibrations, structural synthesis, flexible foundation

### 1. Introduction

In paper [3] vibrations of a mixed flow pump rotor shaft seated with neighboring machines on a susceptible floor. The vibrating shaft generated the pump vibrations which through the susceptible roof were transferred onto the neighboring machines causing a kinematic excitation, Figure 1.



Fig. 1. A group of pumps installed on the first floor of an assembly hall

Thus, there was crated a dynamic system consisting of the pump and roof for which, due to an unknown flexible continuous system, the analytic description is difficult. A interesting method of analysis discrete and flexible systems is structural synthesis of their receptance, [1, 2]. The simplification of a description is based on the idea that the unknown and difficult for fully identification flexible sub-system is replaced by its receptance, obtained by experiments, only in the points of connection.

A structural scheme of connection built this way can be treated as the object of control and is completely ready for the analysis which are used in the control engineering by means of the matrix transfer function [4]. The method will be illustrated using the example.

## 2. The synthesis of the receptance

Let us consider the system presented in Fig. 2.

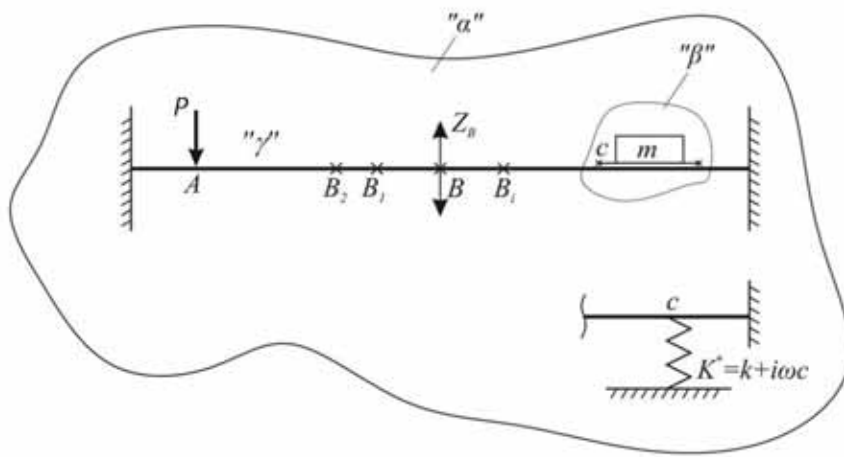


Fig. 2. The model of the system

In the point A of analyzed system the input force  $P(t)$  is acted. On point C there is the mass  $m$  or spring  $k$ . The aim of this work is minimization of vibration of the point B.

This model consists of the flexible sub-system " $\gamma$ " and discrete " $\beta$ ". Because the continuous sub-system  $\gamma$  is very difficult for analytical description, the unknown data of this receptances were determined experimentally.

The matrix receptance  $\gamma$  has the form

$$\gamma(i\omega) = \begin{bmatrix} \gamma_{AA} & \gamma_{AB} & \gamma_{AC} \\ \gamma_{BA} & \gamma_{BB} & \gamma_{BC} \\ \gamma_{CA} & \gamma_{CB} & \gamma_{CC} \end{bmatrix}, \quad (1)$$

where:  $\gamma_{ij} = \gamma_{ji}$ .

After connection the block diagram can be drawn (Fig. 3).

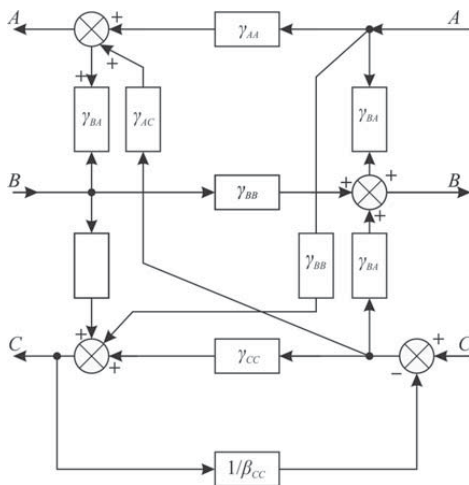


Fig. 3. Synthesis of the receptances

From above structure the receptance  $\alpha$  after connection has the form:

$$\alpha(i\omega) = \begin{bmatrix} \alpha_{AA} & \alpha_{AB} & \alpha_{AC} \\ \alpha_{BA} & \alpha_{BB} & \alpha_{BC} \\ \alpha_{CA} & \alpha_{CB} & \alpha_{CC} \end{bmatrix}. \quad (2)$$

System response is obtained from the equation

$$\begin{bmatrix} Z_A \\ Z_B \\ Z_C \end{bmatrix} = \begin{bmatrix} \alpha_{AA} & \alpha_{AB} & \alpha_{AC} \\ \alpha_{BA} & \alpha_{BB} & \alpha_{BC} \\ \alpha_{CA} & \alpha_{CB} & \alpha_{CC} \end{bmatrix} \begin{bmatrix} P(t) \\ 0 \\ 0 \end{bmatrix}, \quad (3)$$

or in shorten notation

$$\mathbf{Z} = \boldsymbol{\alpha} \mathbf{P}, \quad (4)$$

where:  $\mathbf{Z}$  is column vector including outputs  $z_A, z_B, z_C$ ,  
 $\boldsymbol{\alpha}$  is the matrix of receptances of the whole system after connection,  
 $\mathbf{P}$  is the column vector of input forces.

From equation (4) one can write:

$$z_B(i\omega) = \alpha_{BA} P(t), \quad (5)$$

where:  $\alpha_{BA}$  is the receptance between points B and A.  
The receptance  $\alpha_{BA}$  is obtained from above general presented diagram - Fig. 4.

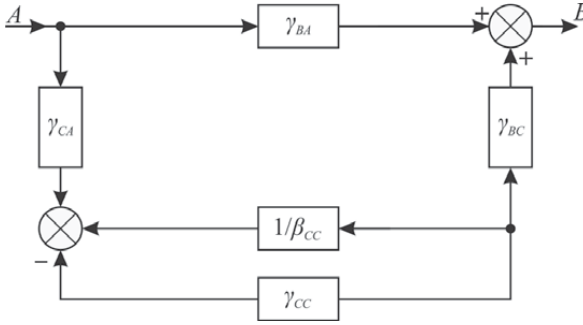


Fig. 4. The block diagram of the  $\alpha_{BA}$

Solving above diagram we have:

$$\alpha_{BA} = \frac{\gamma_{BA}(\gamma_{CC} + \beta_{CC}) - \gamma_{BC}\gamma_{CA}}{\gamma_{CC} + \beta_{CC}} = \frac{L_{BA}(i\omega)}{M(i\omega)}. \quad (6)$$

The coordinate  $z_B$  is zero when  $\alpha_{BA} = 0$ , that is mean when  $L_{BA} = 0$

$$\gamma_{BA}(\gamma_{CC} + \beta_{CC}) - \gamma_{BC}\gamma_{CA} = 0, \quad (7)$$

now

$$\beta_{CC} = \frac{\gamma_{BC}\gamma_{CA} - \gamma_{BA}\gamma_{CC}}{\gamma_{BA}}. \quad (8)$$

The receptance  $\beta_{CC}$  can get the following forms:

$$\text{mass } \beta_{CC} = -\frac{1}{m \cdot \omega^2}, \quad (9)$$

$$\text{spring } \beta_{CC} = \frac{1}{k}. \quad (10)$$

Substituting equations (9) and (10) to (8) we can calculate mass the  $m$  or stiffness  $k$ :

$$m(\omega) = \frac{\gamma_{BA}}{\gamma_{BA}\gamma_{CC} - \gamma_{BC}\gamma_{CA}}, \quad (11)$$

$$k(\omega) = \frac{\gamma_{BA}}{\gamma_{BC}\gamma_{CA} - \gamma_{BA}\gamma_{CC}}. \quad (12)$$

### 3. Calculation

The sub system  $\gamma$  was experimentally described (Tab. 1) and graphically presented in Fig. 5.

Tab. 1. The experimentally determined receptances  $\gamma$

| $\omega$ | $\gamma_{BC}$ | $\gamma_{CA}$ | $\gamma_{BA}$ | $\gamma_{CC}$ |
|----------|---------------|---------------|---------------|---------------|
| 50       | $10^{-6}$     | $50^{-6}$     | $50^{-6}$     | $70^{-6}$     |
| 60       | $14^{-6}$     | $60^{-6}$     | $60^{-6}$     | $82^{-6}$     |

|     |            |           |           |            |
|-----|------------|-----------|-----------|------------|
| 70  | $20^{-6}$  | $66^{-6}$ | $66^{-1}$ | $89^{-6}$  |
| 80  | $26^{-6}$  | $72^{-6}$ | $72^{-6}$ | $95^{-6}$  |
| 90  | $33^{-6}$  | $76^{-6}$ | $76^{-6}$ | $100^{-6}$ |
| 100 | $41^{-6}$  | $80^{-6}$ | $80^{-6}$ | $110^{-6}$ |
| 110 | $50^{-6}$  | $83^{-6}$ | $83^{-6}$ | $120^{-6}$ |
| 120 | $58^{-6}$  | $85^{-6}$ | $85^{-6}$ | $135^{-6}$ |
| 130 | $67^{-6}$  | $86^{-6}$ | $86^{-6}$ | $140^{-6}$ |
| 140 | $78^{-6}$  | $87^{-6}$ | $85^{-6}$ | $148^{-6}$ |
| 150 | $88^{-6}$  | $87^{-6}$ | $80^{-6}$ | $150^{-6}$ |
| 160 | $100^{-6}$ | $87^{-6}$ | $73^{-6}$ | $140^{-6}$ |
| 170 | $113^{-6}$ | $86^{-6}$ | $64^{-6}$ | $130^{-6}$ |
| 180 | $110^{-6}$ | $85^{-6}$ | $55^{-6}$ | $120^{-6}$ |

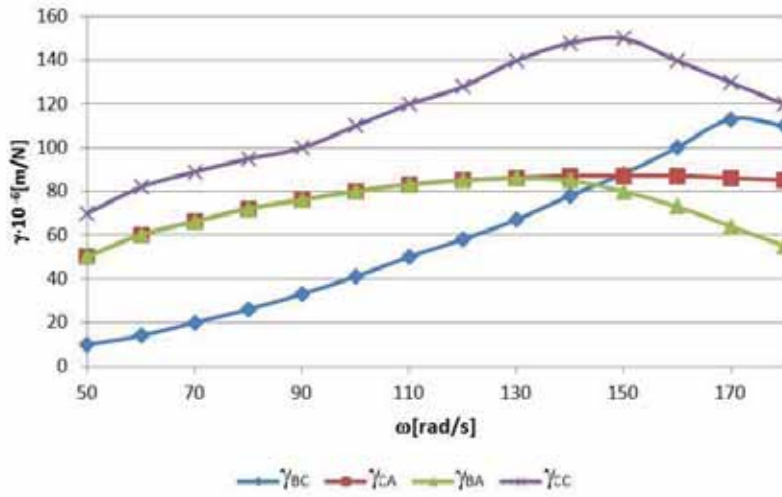


Fig. 5. The receptances of sub-system  $\gamma$

Substituting the values of the receptances  $\gamma_{BC}$ ,  $\gamma_{CA}$ ,  $\gamma_{BA}$  and  $\gamma_{CC}$  from Tab. 1 to equation 11 the mass of subsystem  $\beta$  is obtained, Fig. 6.

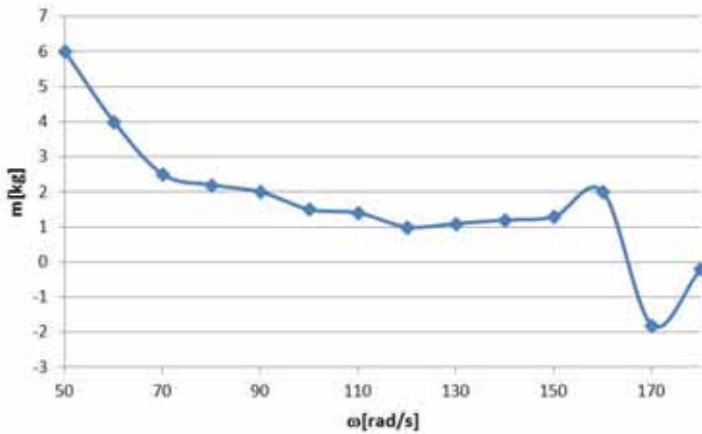


Fig. 6. The mass of the subsystem  $\beta$

Now one can check the result of calculation, for  $\omega=60$  rad/s and 100 rad/s,  $m(60)=4$  kg and  $m(100)=1,5$  kg.

If the calculation is correctly done, the receptance  $\alpha_{BA}$  (equ. 6) should be zero for above masses, Fig. 7.

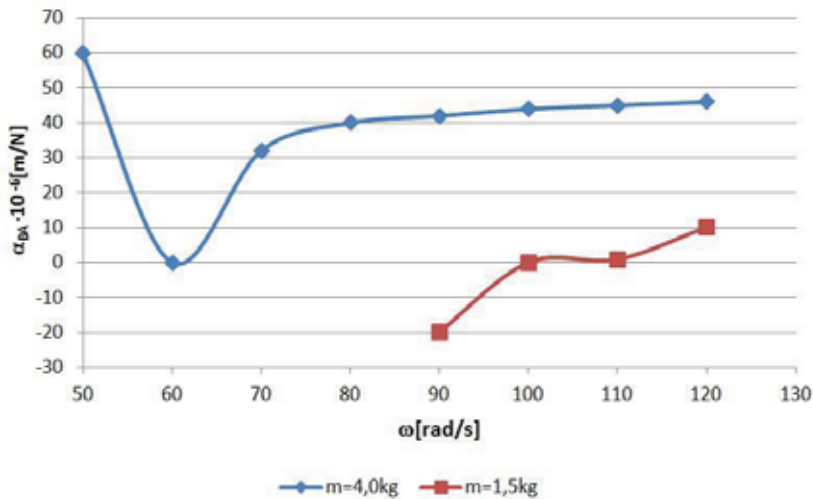


Fig. 7. The receptance  $\alpha_{BA}$  for  $m=4$  kg and  $m=1,5$  kg

From presented diagrams (Fig. 7) one can see that really for  $\omega=60$  rad/s and  $\omega=100$  rad/s the receptance  $\alpha_{BA} = 0$ , that means  $z_B = 0$ .

#### 4. Conclusion

As the result of the above work the following conclusion have been drawn:

1. As it has been demonstrated the method is very useful for systems in which the continuous system is difficult to describe analytically. In such a case the continuous system can be described by the experiment only in the points of connection with the discrete system.
2. On the basis of this example, it can be said that reduction of vibrations in selected points of the continuous system is possible and it is even possible to seat the machines in such a way that vibrations can reduce each other.
3. For large roofs the equipment for taking dynamic characteristics is expensive and, above all, needs to have relatively high power. It is usually used in construction engineering.

#### References

- [1] Holka H., *Receptance synthesis by means of block diagrams*, 7th World Congress of IFTTooMM, Sevilla 1987.
- [2] Holka H., Peszyński K., *Minimize of vibration by means of the structure synthesis of the receptances*, Engineering Mechanics 2003, Svratka, Czech Republic, 2003.
- [3] Jarzyna T., *Analiza dynamiczna pionowej dwustopniowej pompy diagonalnej*, Inżynieria i Aparatura Chemiczna, pp. 13–15, 2012, 51, nr 1.
- [4] Kaczorek A.: *Teoria sterowania i systemów*, WNT, Warszawa 2003.



## APPLICATION A LABORATORY STAND FOR MULTI-SYMPTOMS TESTS FOR HIGH CYCLIC FATIGUE OF CONSTRUCTIONAL MATERIAL

Andrzej Kaczmarek

Gdansk University of Technology  
Faculty of Ocean Engineering and Ship Technology  
G. Narutowicza 11/12, 80-233 Gdansk, Poland  
phone: +48 58 347 24 30, email: andrew925@wp.pl

### Abstract

*This paper describes a need of diagnostics present ship plants according to current technical state. In order to reach competent physical quantity describing fatigue of materials by congregated energy. This paper describes using some diagnostics methods (acoustic emission AE, vibration, thermovision, deformation) in order to definition fatigue state of construction material. The author tries to find correlation between measured quantities which describe continuous process of fatigue wear. Innovation of this research allows use a new, little-know and little-recognized acoustic emission method by energetic fatigue research. Besides the results of AE will verified by use well-knowing and described research methods that are using to appreciate fatigue materials (vibration, thermovision, deformation). Used diagnostic methods were verified with photos of cracked scrap. The conclusion describes suggestion of research results. They will be needed to classification of fatigue symptoms that are measured by the above methods and are giving competent diagnostic dependence. This paper deals the results of elementary research on laboratory stand. They will be used to diagnostic of ship plants and their driving elements (shafts, cams, valves).*

**Keywords:** ship plants, drive elements, energetic methods for fatigue materials, vibration methods, acoustic emission

### 1. Introduction

The fatigue of materials is continuous process that attends maintenance of machines. It is in all constructional element working with changeable loading so it is in many working machines. Present researches and experiences show that elements work in loading area making stresses under durable value of fatigue stresses is non-failure. The breakage is at the time result of wear or excessive loading [1, 2, 3] (fig. 1, fig. 2). It should think however how can determine technical state of device or its individual parts, if they were exposed for excessive loading or bad maintenance (f.e. disappearance of oil lubrication), appearance of notch or concentration stresses. This situation concerns especially driving elements of machines working with changeable loading. In this situation would be local weakness of material and start of crack. The breakage influences for shorter time of maintenance, less reliability and uncertainty of technical state.

Continuous monitoring of susceptible and important machine's elements is realized in lots of devices and constructions. For reliability very important is determination technical state according to continuous monitoring (maintenance according to present technical state). It concerns devices that demand high reliability like marine power plants and turbogenerators. According to this

knowledge user can provide next sensible maintenance and moment of damage. This measuring technique is helpful to prevent and decrease damage and accidents. This technique and automatic systems can create modern diagnostic systems and limit human's mistakes.

## **2. The purpose of test stand building**

The purpose of test stand building has been determination the degradation of material's property (especially constructional materials used to driving elements of marine power plants). This test stand is used to determination of fatigue strength limit for standard test pieces. In this case we can get Wöhler characteristic of material that is loaded of oscillatory bending moment. The method of making fatigue tests on this test stand is knowing very well and described at national standard PN-76/H-04326. The test stand is now provided with modern measuring apparatus that can describe fatigue state. This test stand is very useful to making basic tests by use apparatus detect fatigue of material at first time loading.

The tests making on this test stand have the purpose that we can describe a fatigue state of material by use present apparatus and methods. The described test stand is introduction to next experiments that are realized as doctorate study. A topic of the doctorate study includes diagnostic of some driving elements of marine power plants that are hazarded oscillatory loading, especially by use Acoustic Emission's parameters as diagnostics symptom.

## **3. The test stand and the using measuring apparatus**

The test stand was built probably in 50'th year XX century by workers and lectors worked on Mechanical Department of Gdansk University of Technology for making fatigue tests. The appearance and construction is similar to any test stands had been described on speciality literature [4]. The test stand was renovated and accommodated for test of fatigue process by use modern apparatus.

For recording quantities describing fatigue state of material's test piece the test stand is provided with following measuring apparatus:

- Acoustic Emission (AE-system AMSY-5 of Vallen),
- vibration (vibration meter SVAN 956 of Svantek),
- temperature (thermovision camera of FLIR),
- deflection (dial indicator [0,01mm]),
- basic quantity (loading, number of cycles, time, rotational speed).

The sensors were installed with directions for use for measure quantity that describe actual fatigue state. It is especially important a graduation of measuring apparatus because they have to inform about actual material's property. This attention concerns especially Acoustic Emission and thermovision camera

The Acoustic Emission apparatus is provided with right filters that can record (after right process) frequency spectrum of material's cracks. Classification of right signals and random noises is laborious and demands right experience. Application of Acoustic Emission in described tests was possible only with experience that were got in earlier projects. This experience allows right correct Acoustic Emission apparatus and its software [5]. By temperature measurement we should especially attention that the measurement of emitted radiation spectrum informs about right temperature of test piece (the correct emission factor). The tests had show that the warmest point is not in this same side and "drifts". The fig. 1 shows a side where the sensors were installed:

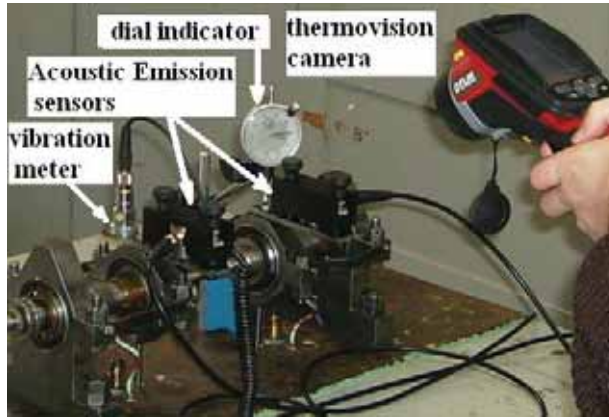


Fig. 1. Installation of sensors

The loading of test piece is caused by weights that are hung under test stand and make constant bending moment by stiff string system – fig. 2:

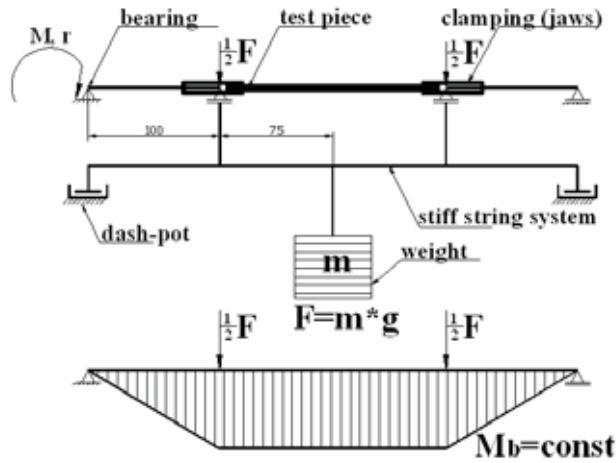


Fig. 2. The loading of test piece

The oscillatory stresses are caused by rotation of test piece that is loaded bending moment. If we know the properties of material we can count a number of cycles (fatigue life) and vice versa. The properties of material and chemical constitution were identified by tension test in certification laboratory of Gdansk University of Technology. The tension test helped to identify the right material of test pieces. The material of test pieces is unalloyed weldable fine-grained steel S355N. If we know dimensions of the stiff string system (fig. 2) we can count very easy stresses that are in test piece. The final relation is following:

$$\sigma_b = \frac{M_b}{W_x} \cong \frac{\frac{1}{2} F \cdot l}{0,1 d^3} = \frac{\frac{1}{2} \cdot 22 \text{ kg} \cdot 9,81 \frac{\text{m}}{\text{s}^2} \cdot 100 \text{ mm}}{0,1 \cdot (8 \text{ mm})^3} = 9,58 \cdot 22 = 211 \text{ MPa} \quad (1)$$

The installation of Acoustic Emission sensor and vibration sensor together on one bearing housing causes to get comparable information (fig. 1). The information will analyse in the next experiment. This method allows to locate cracks of test piece. The time of cracks and velocity of wave propagation (steel) allow to count the place of cracks (fig. 5, fig. 6). The two-dimensional analysis (two Acoustic Emission sensors) was made by use special Visual Class program.

The results of tests, experience and literature show high scatter of Wöhler characteristic for oscillatory bending test. A number of cycles for constant loading (fatigue life) differs over 100%. It is necessary to make statistical verification.

#### 4. Tests

The tests were made according to Wöhler characteristic. The fatigue strength limit was determined according to literature, experience and material's certificate. The next step consisted in start from high loading and reduce it and observe the parameters. The range of loading and measurements was determined after break a few test pieces. The test was made for fifteen test pieces and makes introduction to the next tests and statistical verification.

The measurement of vibration, deflection and temperature were taken reading after particular number of cycles (discrete measurement). The characteristic of measurement for particular test pieces was described on this way (fig. 4). The test was planned in this case, that reading of parameters were made for every test pieces after particular number of cycles. In this way we can get comparable information about analysis of fatigue process. The measurement for parameters of Acoustic Emission (AE) was read continuous off. This way caused get the quantities describe a shape of AE wave (RMS, number of level's overflows).

The analysis of results allows to state that amount of dissipative energy in cyclic loaded driving elements could be a information about fatigue state of material. The range of hysteresis lop (co-ordinate system stress - strain) describes amount of energy  $U$  that is necessary to deformation of material at every cycle. Some of energy is wasted for internal friction in microstructure of material [2,8]. In this case losses of energy make increase of temperature. The final relation between the total losses of energy in material  $W$  and strain's energy  $U$  is following 2 [8]:

$$W = U \left( \frac{\sigma_{rz-z}}{\sigma_a} \right)^\Theta \quad (2)$$

where:

$\sigma_{rz-z}$  – true stresses by break (by tensile test),

$\sigma_a$  – amplitude of stresses,

$\Theta$  – factor describes intensity of increase of energy  $W$  with energy  $U$  together with increase of cycle's number  $N_f$  described relation for plastic materials 3,

$\epsilon_{rz}$  – true strain for  $\sigma_{rz-z}$ .

$$\frac{1}{\Theta} = 0,085 + 0,37e_{rz} \quad (3)$$

Every loss of energy is described range of hysteresis lop and is propagated as elastic wave in material. A shape and parameters of this wave are measured by AE sensors. The results of test show that for low number of cycles the energy at one cycle is “sufficient high”. The signal

generated of this way is measured by AE sensors. The results of test show that for big number of cycles the energy at one cycle is “low” and the crack’s energy losses in material could not measure by AE sensors. The temperature and AE are good correlation of parameters that describe losses of energy in cyclic loaded test piece. The fig. 3 shows increase of temperature for one test piece measured by use the thermovision camera for followed cycles. The fig. 4 shows characteristic of temperature and strain cycles-dependet for four test pieces loaded the same weight. The table 1 includes basic data and results of tests.

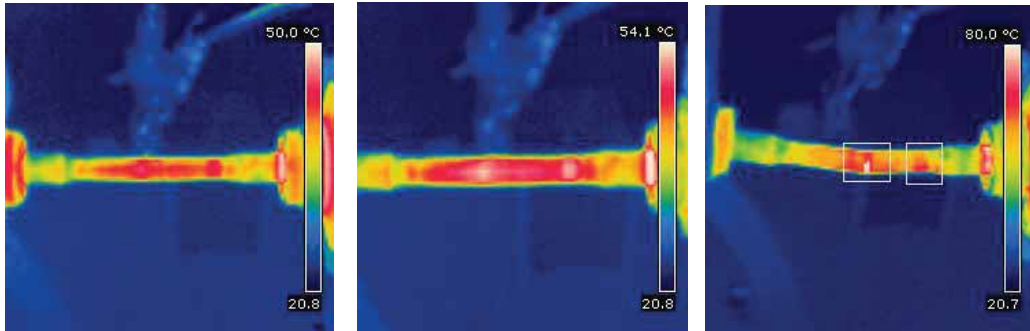


Fig. 3. Increase of temperature for followed cycles and moment of crack

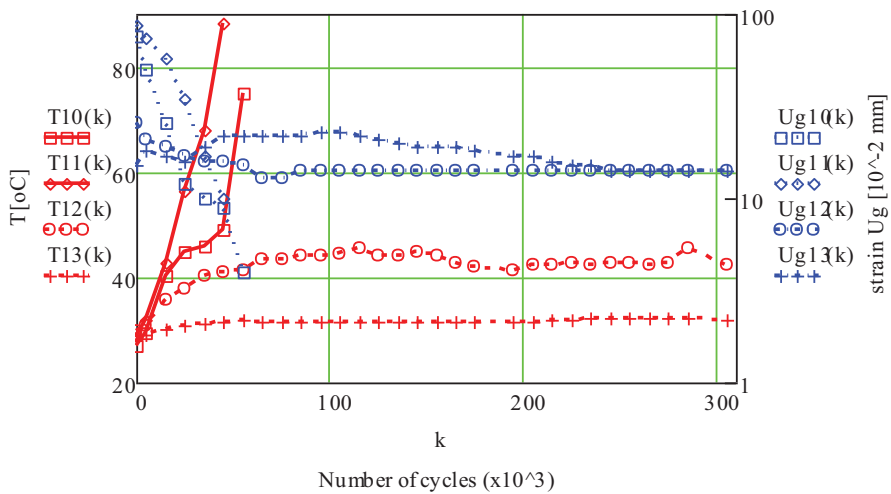


Fig. 4. The temperature  $T[^{\circ}\text{C}]$  (red line) and strain  $U_g[10^{-2}\text{mm}]$  (blue line) cycles-dependet  $k$  for four test pieces: 10, 11, 12 i 13 (loading 22kg)

Tab. 1. Basic data and results of tests for four test pieces

|  | Test piece 10    | Test piece 11    | Test piece 12     | Test piece 13                      |
|--|------------------|------------------|-------------------|------------------------------------|
| number of cycles until crack                                       | $55 \times 10^3$ | $45 \times 10^3$ | $509 \times 10^3$ | $1450 \times 10^3$<br>didn't crack |
| max. temperature after $20 \times 10^3$ cycles                     | 48,1 °C          | 53,6 °C          | 39,0 °C           | 31,3 °C                            |
| strain after $20 \times 10^3$ cycles                               | 0,59 mm          | 0,42 mm          | 0,09 mm           | 0,08 mm                            |
| absolute change of AE amplitude (after moment of strain hardening) | 4,4%             | 4,2%             | 1,5%              | 0,1%                               |
| visible crack's location (AE signal)                               | YES              | YES              | WEAKLY            | NO                                 |
| amplitude of stresses  | 211 MPa          | 211 MPa          | 211 MPa           | 211 MPa                            |

The results show that thanks to AE method is possible separation of signal that genesis is from fatigue source. High elementary energy which is emitted in one cycle is measured by AE apparatus. Fig. 6 shows signal location described by number of location events and measure by AE sensors. For 10 and 11 test pieces (short fatigue life) we can very clearly see the signals generated in the middle range of test piece between AE sensors (the crack place). For 12 test piece (fig. 5, fig. 6) we can see this same signal generated in middle range but noise from bearings is stronger. In this case we could not detect a material defect and a crack location. The signal of 14 test piece doesn't show fatigue cracks. This analysis is acknowledged by temperature, strain and basic data in table 1.

This results show that loss of energy in cyclic loaded material describe its duration (fatigue life). We can very right measure this process by use Acoustic Emission. A low diagnosticability is for test pieces have long fatigue life (big number of cycles until crack) and low storage of energy in material.

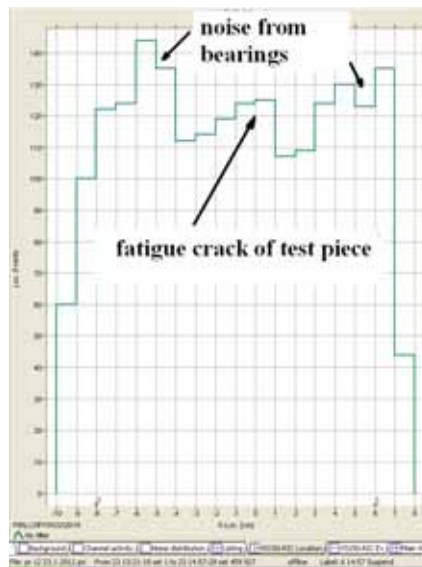


Fig. 5. The number of location events were measured in range between AE sensors

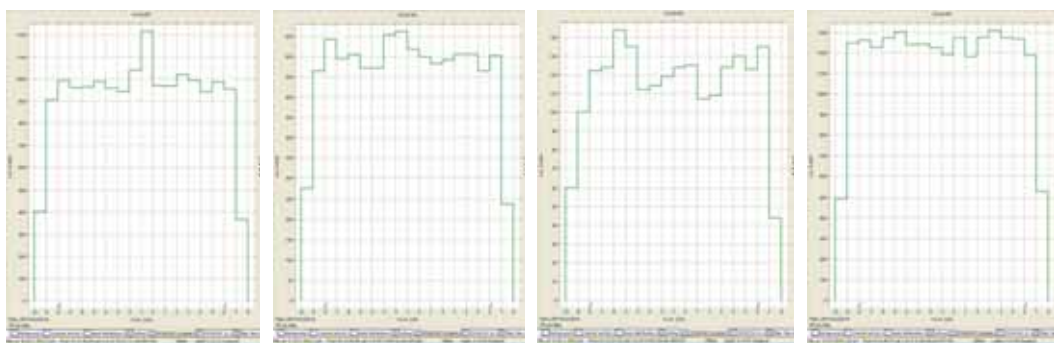


Fig. 6. The location of crack range (from left: test piece 10, 11, 12, 13)

It is a correlation between amplitude of AE signal and fatigue state of material. At the moment of strain hardening (point on characteristic where strain-line is curved) the amplitude of AE is decreasing (tab. 1, fig. 7, fig. 8). The decrease is more clear for test pieces which have a low fatigue life (10 and 11 test piece). The decrease is weakly clear for test pieces which have a high fatigue life and unclear strain hardening (12 test piece). A change of AE amplitude is not visible for uncracked test piece (13 test piece). The moment of crack is described increase of AE amplitude. The general rule for energetic evaluation of multi-symptoms tests of fatigue material is described following: strain hardening – decrease of strain – lower energy – lower AE amplitude – stabilization of temperature.

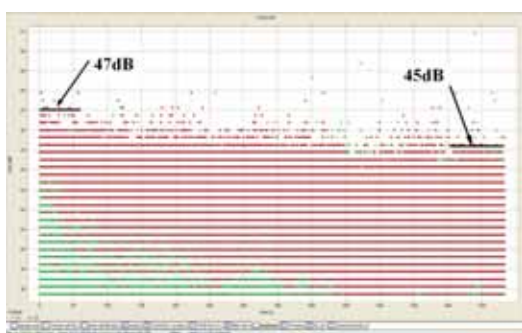


Fig. 7. The change of AE amplitude [dB] at moment of the strain hardening – 10. test piece

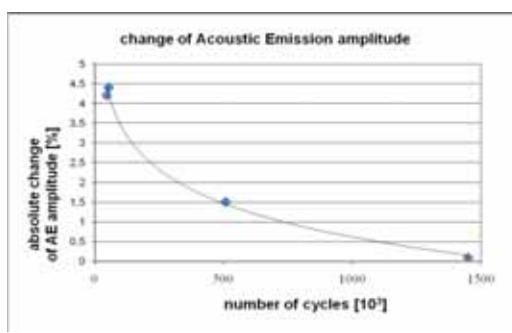


Fig. 8. The change of AE amplitude at moment of the strain hardening cycles-dependent

The process of fatigue material can be described by frequency spectrum of vibration. A measurement was taken reading after particular number of cycles because a memory of vibration meter was limited (discrete measurement). With following decrease of section of test piece a rigidity of joint is decreasing. This process shows high amplitude in particular frequency spectrum of vibration (analysis FFT fig. 9, fig. 10). Spectrum of high amplitude of frequency is in the range of first harmonic (after noise's filtering - noises from bearings). The next analysis can find range of frequency which is symptom of fatigue material. The frequency: second harmonic (100Hz) and four'th harmonic (200Hz) are symptoms of following fatigue crack of material.

A visible increase of energy signal which is measured by AE sensors is not sufficient measure by vibration sensors. Fig. 9 shows frequency spectrum of vibration before loading. With following degradation of material (fatigue material) the second harmonic (100Hz) and four'th harmonic (200Hz) are more visible – harmonic which are characteristic for fatigue crack of shafts. The measurement for four test pieces loading this same weight (tab. 1) does not show increase of

amplitude in frequency spectrum of vibration for second harmonic and four'th harmonic (analysis FFT - fig. 10) – however the increase of AE parameters is visible. This measure shows that vibration method is useful for diagnostic of technical state at the final life of devices (10 - 20% life before break-down). The vibration method is useful because by use analysis FFT we can recognize defect (characteristic frequency spectrum of vibration) but we can not describe quantitative (by amount) damage or sufficient describe diagnostic of fatigue state of material.

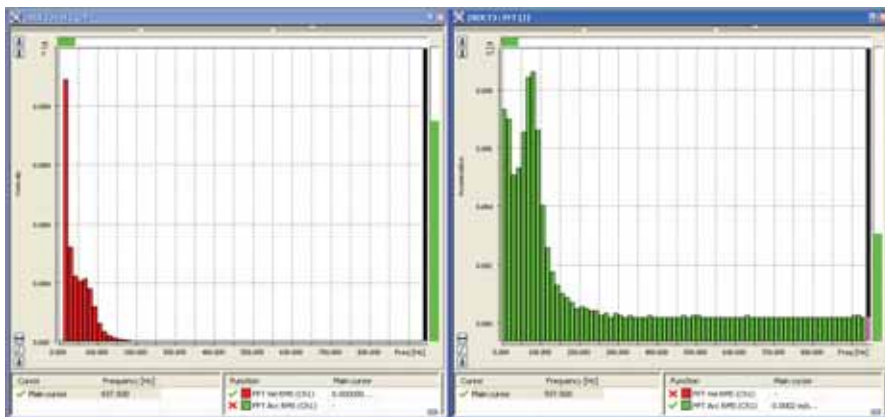


Fig. 9. Analysis FFT for test piece before loading (spectrum): velocity (left) and acceleration (right)

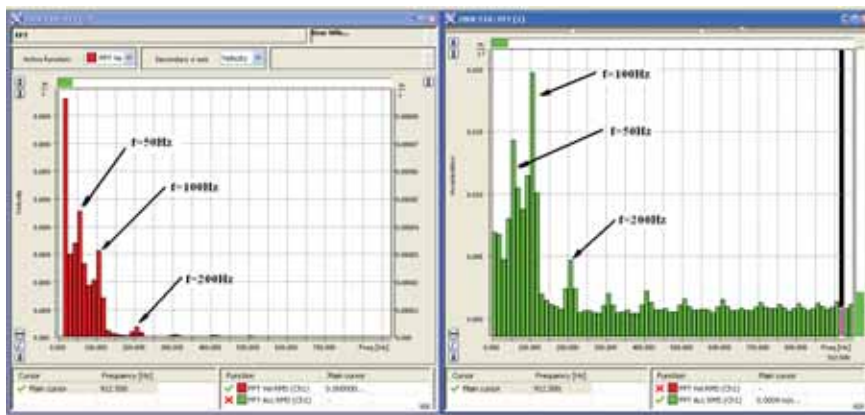
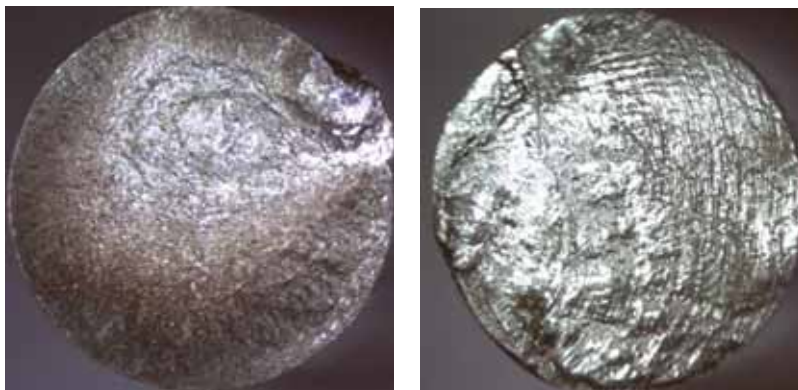


Fig. 10. Analysis FFT for test piece during test: velocity (left) and acceleration (right)

The used parameters give diagnostics information about progress of fatigue material and its quantitative describing. However for describing structure of material were made metallographic photos of fatigue scrap (fig. 11). They were useful for verification of measured parameters and for more precise describing of fatigue process and for explanation their run. This procedure can help to describe state of material in crack point together with results of measurement. This procedure can help to compare fatigue scrap with run of measured parameters.

The parameters of overnamed apparatus and fatigue scraps show loss of energy in one cycle and describe state of material. Fig. 11 shows 10 and 12 test piece. The fatigue scrap for 12 test piece is characterized small spacing between crack's lines and big ratio between fatigue range and plastic-brittle range. This fatigue scrap shows big number of cycles to break-down and small loss of energy in one cycle. This statement is described by results of AE, strain and temperature. The fatigue scrap for 10 test piece is characterized for low cyclic test. A big loss of energy in one cycle

is characterized big spacing between crack's lines. This statement is described by results of AE, strain and temperature (very clear location of crack – fig. 6).



*Fig. 11. Metallographic photos of fatigue scrap (left: 10. test piece; right: 12. test piece)*

The metallographic photos show that diagnostic of technical state for machines by use loss of energy in cyclic loading material is very useful. The used apparatus is very useful for this tests.

A right shape of AE wave and its characteristic frequency (analysis FFT), amplitude and RMS will be helped in next tests to associate in individual groups for common runs of waves. In this process will be made classifiers which could help to separation a individual frequency responsible for useful signal (fatigue material) and noises. The next analysis of results will be made by use special Visual Class program.

## **5. Conclusion**

The results of made tests give interesting conclusions. It is common correlation between measured parameters: Acoustic Emission, vibrations, temperature and deflection. This statement was very probable because process of fatigue material is continuous process and following degradation of structure of material has to give changeable symptoms. Moreover fatigue material is energetic process which is characterized cyclic strain that makes increase of temperature and strain hardening. It should mark that the highest temperature which is measured at test is not always in crack point. This observation could show that material has internal defects or heterogeneous structure. However at the moment of crack the highest temperature was always in crack point. The strain hardening is characterized decrease of strain and this makes less deflection and less moment of inertia (less moment of rotational mass) and increase of rotational speed.

A previous tests give information that we can see relation between AE and vibration parameters [6]. The frequency and amplitude which are results of fatigue material are visible by use AE apparatus more earlier. A fatigue material which is energetic process is characterized for loss of energy in material and change its properties which are recording by use AE apparatus. The Acoustic Emission gives information about damage location and amplitude's value. Thanks to this information we can estimate state of fatigue material as function of loss of energy in material. Thanks to this information we can decide about maintenance and work of drive system in the future. When we compare a vibration method and Acoustic Emission we have to make statement that the vibration method allows to estimate a fatigue material by use a characteristic frequency (frequency spectrum) and not by use change of amplitude (RMS).

A big scatter of number of cycles until crack for test pieces loaded this same weight was caused probably influence of strain hardening of primary material during rolling. All test pieces were cut and made from the one steel plate (this same material S355N). The test pieces were

turned in this cause that axis of test piece is parallel to direction of rolling. The test pieces which were cut from surface layer had a higher internal work-hardening (internal stresses and direction of grains as a result of plastic working) that could be a reason of higher fatigue strength [8] (fig. 4).

It is relation between number of cycles and measured parameters. This is a general statement and true for all test pieces. We can make statement that we can predict a future time for crack of test piece on the basis of measured parameters. This statement says measured parameters give information about quantitative (by amount) description of fatigue material and how many cycles a test piece can work.

In the next part of test will be introduced changes in material (cut notch) and continuous change of loading for test pieces work over a fatigue strength. This method will show technical state of machines or their parts work with overloading and with internal preliminary fatigue wear. This method will allow determine a relationship between diagnostic parameters and predict possibility of fatigue life.

## Bibliography

- [1] Korczewski, Z., Rudnicki, J., *Stability evaluation of the marine propulsion unit mechanical system by means of vibrations measurement and their analysis*, 5th International Conference, Maritime Transport 2012, Barcelona, 27-29 June 2012.
- [2] Szala, J., Boroński, D., *Ocena stanu zmęczenia materiału w diagnostyce maszyn i urządzeń*, Wydawnictwo Naukowe Instytutu Technologii Eksploatacji – PIB, Radom 2008.
- [3] Gajewski, M., *Zmęczeniowe niszczenie metalowych elementów konstrukcyjnych. Zmęczenie i mechanika pękania: Materiały XXII Sympozjum Zmęczenie i Mechanika Pękania*, Wydawnictwa Uczelniane Uniwersytetu Technologiczno-Przyrodniczego, Bydgoszcz 2008.
- [4] Katarzyński, S., Kocańda, S., Zakrzewski, M., *Badanie własności mechanicznych metali*. WNT, Warszawa 1969.
- [5] Girtler, J., i inni, *Emisja akustyczna w procesach uszkodzeń układów korbowo-tłokowych silników o zapłonie samoczynnym – ocena, analiza, metodyka badań*, Sprawozdanie z realizacji projektu badawczego, grant nr N504 043 31/3480, Gdańsk 2006, 49-65.
- [6] Report, *Pomiary parametrów emisji akustycznej generowanej przez zmęczeniowe uszkodzenia panwi łożysk MB50, MB02 na stanowisku badawczym SMOK Część VIII (wykonanie pomiarów na stanowisku, opracowanie wyników, wnioski z badań)* about research project Ministry of Science and Informatics (nr. 3480/TO2/2006/31): *Identyfikacja stanu technicznego układów korbowo-tłokowych silników o zapłonie samoczynnym ze szczególnym uwzględnieniem emisji akustycznej jako sygnału diagnostycznego*. Research project for Faculty of Ocean Engineering and Ship Technology Gdansk University of Technology nr 05/2009/PB, Gdańsk 2008.
- [7] Lipski, A., *Monitorowanie procesu zmęczenia z zastosowaniem kamery termowizyjnej: Materiały XXII Sympozjum Zmęczenie i Mechanika Pękania*, Wydawnictwa Uczelniane Uniwersytetu Technologiczno-Przyrodniczego, Bydgoszcz 2008.
- [8] Kocańda, S., Szala, J., *Podstawy obliczeń zmęczeniowych*, Wydawnictwo Naukowe PWN, Warszawa 1997.



## NEW, ENERGY SAVING ROTOR SOLUTION OF BEATER GRINDER FOR CORN GRAIN

Jerzy Kalwaj

University of Technology and Life Sciences  
Prof. S. Kaliskiego 7, 87-763 Bydgoszcz, Poland  
e-mail: kal97@wp.pl

### Abstract

*The permanent rise of consumption and price of feed products over the world have created necessity of looking for every possibility decrease cost of feed production, in this range, first of all, process machines.*

*15 mln ton corn grains was milled for feed every year by beater grinder. This part of machines characterize substantial energy consumption from 36 to 72 kJ/kg [1,2].*

*Analysis of literature and own investigation over grinders proved, that modernization of working unit may be reason to importance of energy saving in the process. To put into changes of beaters geometric, which consideration the structure of grain grinding. The verify of test the new rotor solution show advantage energetic compare to traditional one about 24%.*

**Keywords:** beater, grinder, corn grain, rotor, modernization, energy saving

### 1. Introduction

Grain's grinding is the main technological operation in mixed feed production. It is achieved with the help of beater grinder (Fig. 1), which are commonly used owing to their all-purpose employment as far as the feeding stuff raw material is concerned, their simple structure and service. The essential fault of these machines is high energy consumption [1, 2].

The technological process in the grinder is as follows, a weighed and placed in tank sample of the raw material is delivered to hammer mill encharging hopper at uniform rate through feeder. Next, it is transported gravitationally to the operation chamber where it is subjected to the percussive action of hammers. The kinetic energy of particles is used for their division, their collisions among them on the screen. The difference between grinders and grain must be 42 m/s – it is condition of shock defragmentation. Successive division of the particle takes place until its size is equal to the diameters of holes in the screen. Such particles leave the hammer mill, next they are transported by the air stream through special short channel to aerocyclone where they are separated from the air. In order to increase the efficiency of separation, the aerocyclone is provided with fibrous filter. The ground particles fall to product tank.

For example, grinding barley using screen 4 mm needed from 8 to 12 collision with beaters. The time of one contact being  $10 \cdot 10^{-5}$  s. Great value of unit energy consumption (about 60 kJ/kg) is causes too long time of staying grains in working chamber. This phenomenon cause of produce too much fraction of dust (particle less than 0,5 mm) what is physiologically undesirable quality of feed is lower [3].

Continuous development of beater grinders don't solve problem of high energy consumption in this machines.

Betterment of working parameters take place with modernization. Changes of beater grinder dedicated to corn grains is a complex scientific problem, who contain three factors: corn grain (feed material), process of fragmentation and build of the machine.

General may be accept, that the structure of corn grains is inhomogeneous and have two parts: fibrous cover with high strength and unregulary interior represent fragile mass. Optimal way of grinding this material would be connecting of two methods: cutting for covered and beat for interior.

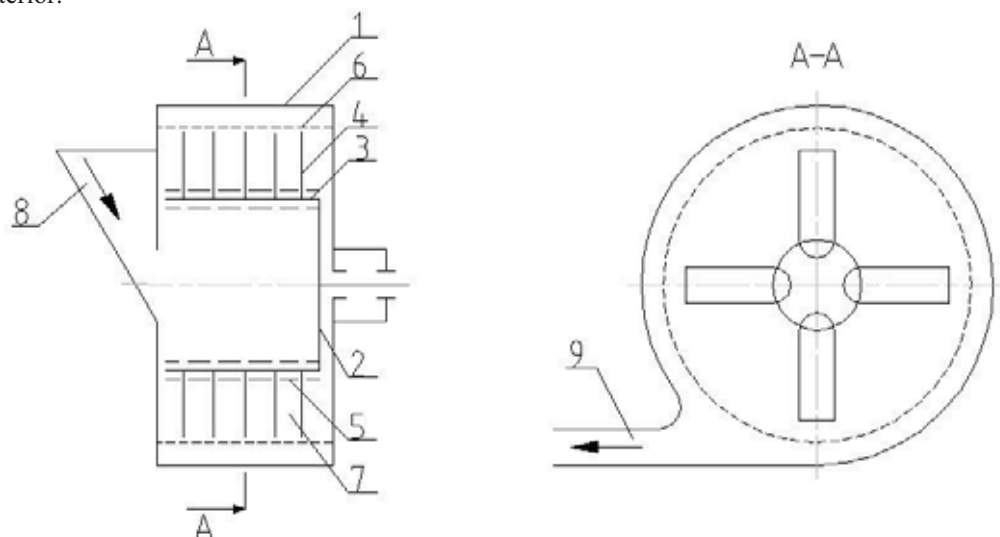


Fig. 1. Scheme of beater grinder :1 – housing, 2 – rotor, 3 – bolt, 4 – beater, 5 – sleeve, 6 – screen, 7 – working chamber, 8 – charge, 9 – outlet [1]

The second reason of high energy consumption by grinder is low efficiency of collisions in grinding chamber. It has been observed, that there grains take rotates motion. The consequence of this phenomenon is that not all collisions lead to fragmentation of particles. Compare to author of this article using in grinder rotor beater with different length: longer, which take place at outside of chambers and short one at the middle of working area. That solution generation speed gradient of particle to central part of chamber – braking circulation of collection grain. Consequential, quantity of efficiency collisions increase.

## 2. Object and methods

Description of grinder construction modernization, generates to the following research problems:

- does application of the thin and thick beaters in grinder rotor, lead to reduction of energy consumption? The supposition is that the thin beater, can intense cutting cover of grain, while this beaters make collision process in grain interior area more effective.
- does application of the long and short beaters in grinder rotor lead to less energy consumption? The supposition is that makes axis vector of particle speed, what provoke higher speed of collision.

Veryfication of this problems have needed experiment. The physical model of traditional and modernization grinder was made, next special system and measure instruments were installed. Barley was used like test material. Traditional beaters was perpendicular plate begin 4 mm-thickness and 80 mm- length.

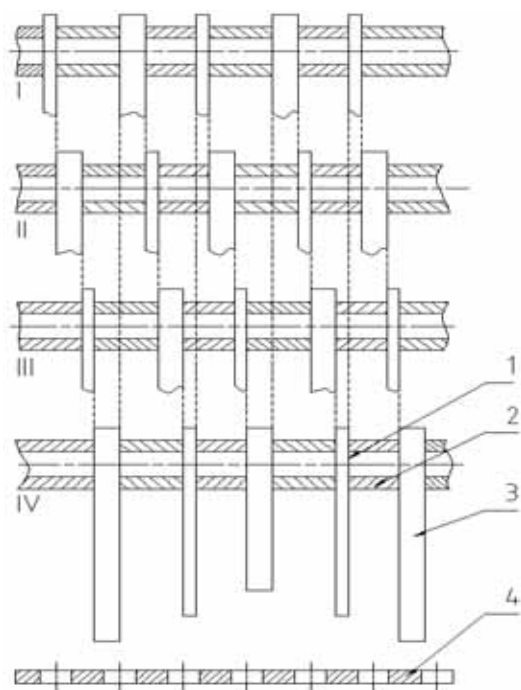


Fig. 2. Scheme of working set of grinding rotor, after modernization (unfold version):

1 – bolt, 2 – sleeve, 3 – beater, 4 – screen

Idea of the improved rotor with modified beaters is presented in Fig. 2,. Beaters is separated by special sleeve, which are fixed on the bolts I – IV. The following changes have been done according to traditional solution:

- application “cutting” beater being 2mm,, and “shock” beaters being 4mm – divide of working process on two ways – cutting cover and defragmentation inside area by shock.
- locate by turns five piece of beaters at four bolts with special sleeve, which make the next principle – one full turn of rotor determine that maximum area of chamber take place in process,
- use the beaters having variable length and location the with principles – the shorter one put in the middle of the working chamber. The end points of beaters create parabolic line at one belt.

Laboratory grinder with change of constructional elements was build and installed in system consist – fedder, grinder and collect unit. Special solution make possible fast change of elements – rotors and screens. Screen who surround chamber has 3, 4, 5, 6 mm wholes diameter (according to norms). This parameters contains variable not-dependent in experiment.

In the test put to trial following function:

$$E = \frac{P_c - P_j}{Q_m} = f(g, l, d), \quad (1)$$

where:

E – unit energy consumption kJ/kg,

$P_c$  – summary power in the process, W,

$P_j$  – power of idle running, W,

$Q_m$  – mass output, kg/n

g – thickness of beaters, mm,

l – length of beaters, mm,

d – diameter of holes screen, mm

The unit energy consumption was defined as the quantity of energy necessary to obtain a unit of the ground product mass. It was calculated from the ratio of power consumption to the hammer mill efficiency. The power was determined by an indirect method by means of the moment measured and the rotational speed of the hammer mill shaft.

### 3. Results and conclusions

Obtained results are presented in Fig. 3. Four curves show relations for various rotors. The first is base for compare investigations. Next numbers two and three show results individual solution of rotor and last – four is summary function for new construction of rotor at all.

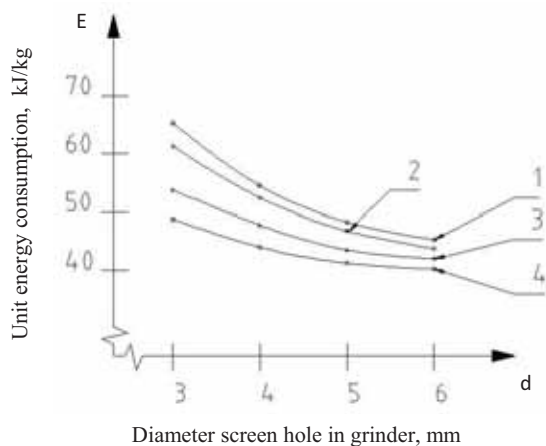


Fig. 3. Relationship between energy consumption  $E$  and diameter screen hole in grinder  $d$  for various rotor solution

Carried out experiment and analyses of curves in Fig. 3 entitle to formulate the following conclusions:

- the independent variable in examination has proved essential influence on energy consumption of grinding process,
- test results positive verify investigation problems in this experiment,
- application beaters which various length leads to reduction of energy consumption from 11 – 14%,
- application beaters with various thickness leads to reduction of energy consumption up to 18%. The reduction is largest for inside diameter of screen being 3mm,
- the largest row of grinding energetic is observed for completely redesigned rotor. The observed reduction is not as sum of applications, that is result of interaction between independent variables. Maximum reduction of energy consumption comparing with traditional solution is about 24%
- the problems need optimization test.

### References

- [1] Osiński J., *Projektowanie i konstrukcja*, WNT, Warszawa 1994.
- [2] Flizikowski J.: *Rozprawa o konstrukcji*, Bydgoszcz - Radom 2002.
- [3] Kalwaj J., *Wpływ konstrukcji bijaków na efektywność rozdrabniania udarowego*, Inżynieria i aparatura chemiczna, nr. 5/2010.



## ANALYSIS OF THE QUALITY OF ELECTRICITY ON THE BASIS OF THE RESULTS OF THE RESEARCH MODEL OF LOW VOLTAGE LINE

Piotr Kolber, Daniel Perczyński, Bogdan Landowski

Uniwersytet Technologiczno-Przyrodniczy  
ul. S.Kaliskiego 7, 85-796 Bydgoszcz, Polska  
tel.: 052 3408297, fax: 052 3408495  
e-mail: pkolber@utp.edu.pl

### Summary

*The work shows a model of a low voltage line (LV), loaded asymmetrical (asymmetry load), feeding scattered customers. The object of the research is an LV line supplying rural customers. Analysis of the tests results of the built model allows among others, evaluation of the values that characterise the quality of the electricity supplied to customers and the parameters that describe the objective of the research. In order to assess the quality of electricity (provided to customers) the algorithm calculation was compiled and on the basis of the developed model, it is possible to calculate the values of voltage sags and deviations on the individual points of the line. In addition, it enables the designation of the asymmetry of voltage (the coefficients of voltage asymmetry). The figures characterising the quality of electricity can be appointed to different parameters describing an LV, inter alia, distribution of customers along the line, what type of customers are connected to the line (productive and unproductive), the nature and extent of the load and the degree of load asymmetry.*

**Keywords:** low voltage line, loads asymmetry, voltage drops, voltage deviations, voltage asymmetry

### 1. Introduction

The reasons for the presence of currents and voltages asymmetry in three-phase grids are primarily non-symmetrical loads and non-symmetrical transmission devices. The work three-phase electrification system is called asymmetrical or non-symmetrical when the work conditions of one or all phases are different. In three-phase systems there are short-term and long-term operational, asymmetrical modes of work. Short-term asymmetry is usually caused by emergency processes. These are primarily asymmetrical short circuit and disconnections of one phase in the cycle of automatic re-connection. Long-term asymmetry in a transmission system can occur when you enable the network an asymmetrical load, with the presence of asymmetrical elements or asymmetric work of transmission system.

Asymmetry caused by an asymmetrical load is called the transverse asymmetry. Asymmetry caused by an asymmetrical transmission element (dissimilar own impedances and interactions of the lines) or asymmetric and cross currents flowing in this element is called the longitudinal asymmetry [3].

Asymmetrical states of work are present especially in rural distribution networks of low-voltage power systems. Such states of work follow from asymmetry of loads in phases, caused by

an unbalanced power distribution for each phase of single-phase receivers and random enable receivers to the network.

In the designing and construction of a rural network efforts are made to proportionally and evenly connect all single-phase receivers to the individual phases, but it does not always meet this criterion.

Even in conditions of balanced connection of receivers, an asymmetry occurs in low-voltage lines. This is because each of receivers can be enabled or disabled from the network depending on changing situation. Usually a load of each phase changes in time, regardless of other phases load.

Asymmetry of line caused by dissimilar reciprocal impedances has caused a negative impact on the quality of electricity, particularly in the case of overhead low-voltage lines, built with flat laid cables. In the lines of higher voltages (above 15 kV) the asymmetry is reduced by changes in the mutual positions of the cables.

## 2. The object of research

The object of research is a low voltage line, loaded asymmetrical, supplying rural customers. The analysis adopted a line model of 2<sup>nd</sup> type, characterised by zero values of crosswise parameters in the substitute scheme (crosswise parameters: unit conductance of  $G_0$  line, unit susceptance of  $B_0$  line, takes into account medium and high-voltage lines) [1]. This type of line is characteristic of rural areas; four-cables and overhead line, with flat laid cables, and as the most widespread, is also the most unfavourable, due to mutual impedance of line in terms of asymmetry loads, the quality of the power is thus supplied to customers. Different values of mutual impedances make that line as an asymmetrical element of electricity transmission. In addition, assumed that receptions have a resistance-induction character.

Test Object Model is presented in the Figure 1.

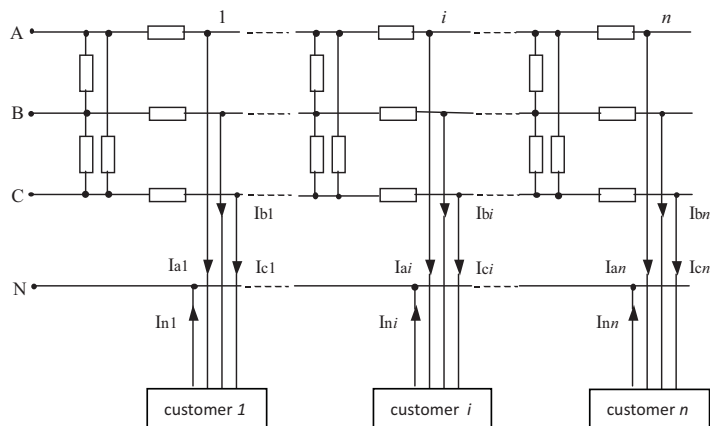


Fig.1. Model of low voltage line asymmetrical loaded

## 3. Model of low voltage line

Model of low voltage line include, inter alia:

1) Fixed parameters:

- $f$  – network frequency ( $f = 50$  Hz),
- $U_{st}$  – voltage phase at the beginning of the line (in a station);  $U_{st} = 240$  V,
- $\gamma$  – wire conductivity (for Al.  $\gamma = 34,8$  m/ $\Omega \cdot \text{mm}^2$ ),

$s, s_N$  – cross-section of the phase and neutral wires;,  
 $b_{AN}, b_{BN}, b_{CN}$  – distance between the wires A i N, B i N, C i N,  
 $b_{AB}, b_{BC}, b_{AC}$  – distance between wires A and B, B and C, A and C,

2) Data determining the topology of the line:

$l$  – length of the line [m],

$n$  – number of receipt points,

$l_i$  – distance of  $i$ -th receipt point from the beginning a line; [m].

3) Resistance values on sections between receipt points; [ $\Omega$ ]

a) for a phase wire

$$R_{(k-1)k} = \frac{l_k - l_{k-1}}{\gamma S} \quad (1)$$

b) for a neutral wire

$$R_{N(k-1)k} = \frac{l_k - l_{k-1}}{\gamma S_N} \quad (2)$$

4) Unit reactances, own and mutual of loops wire; [ $\Omega/m$ ]

a) reactances of loops wire respectively A and N, B and N, C and N

$$\begin{aligned} X_{AN} &= \left( 0,15 \log \frac{b_{AN}^2}{r_A \cdot r_N} \right) \cdot 10^{-3}, \\ X_{BN} &= \left( 0,15 \log \frac{b_{BN}^2}{r_B \cdot r_N} \right) \cdot 10^{-3}, \\ X_{CN} &= \left( 0,15 \log \frac{b_{CN}^2}{r_C \cdot r_N} \right) \cdot 10^{-3}, \end{aligned} \quad (3)$$

where:

$r_A, r_B, r_C, r_N$  – radii of cross-sections phase and zero wires

b) reactances of loop wire A and B, B and C, C and A

$$\begin{aligned} X_{ANB} &= \left( 0,15 \log \frac{b_{AN} \cdot b_{BN}}{b_{AB} \cdot r_N} \right) \cdot 10^{-3}, \\ X_{BNC} &= \left( 0,15 \log \frac{b_{BN} \cdot b_{CN}}{b_{BC} \cdot r_N} \right) \cdot 10^{-3}, \\ X_{ANC} &= \left( 0,15 \log \frac{b_{AN} \cdot b_{CN}}{b_{AC} \cdot r_N} \right) \cdot 10^{-3}. \end{aligned} \quad (4)$$

5) The power values at individual receipt points

In every group of value of three powers phase at receipt points, you can separate:  $P_{maxi}$  – power of the most loaded phase,  $P_{pi}$  – power of indirectly loaded phase,  $P_{mini}$  – power of the least loaded phase.

$$P_{\max i} = \frac{1}{1 + k_{1i} + k_{2i}} P_{si} = w_i P_{si}, \quad (5)$$

where:

- maximum load factor [2]

$$w_i = \frac{P_{\max i}}{P_{si}}, \quad (6)$$

- intermediate load factor

$$k_{1i} = \frac{P_{pi}}{P_{\max i}}, \quad (7)$$

- minimum load factor

$$k_{2i} = \frac{P_{\min i}}{P_{\max i}}, \quad (8)$$

- peak power in the  $i$ -th receipt point

$$P_{si} = \sum_{f=1}^3 U_{fi} I_{fi} \cos \varphi_{fi} = P_{\max i} + P_{pi} + P_{\min i}, \quad (9)$$

where:

$U_{fi}, I_{fi}, \cos \varphi_{fi}$  – phase values of: voltage, current and the cosine at the  $i$ -th receipt point  
(f = A,B,C).

6) The values of phase currents measured in individual connections:

$$\begin{aligned} \underline{I}_{Ai} &= \frac{P_{Ai}}{U_n \cdot \cos \varphi_{Ai}} e^{-j\varphi_{Ai}}, \\ \underline{I}_{Bi} &= \frac{P_{Bi}}{U_n \cdot \cos \varphi_{Bi}} e^{-j\varphi_{Bi}} e^{j240^\circ}, \\ \underline{I}_{Ci} &= \frac{P_{Ci}}{U_n \cdot \cos \varphi_{Ci}} e^{-j\varphi_{Ci}} e^{j120^\circ}, \end{aligned} \quad (10)$$

where:

$U_n$  – value of nominal voltage.

7) The phase current values in a line between  $(k-1)$  and  $k$ -th receipt point

$$\underline{I}_{A(k-1)k} = \sum_{i=k}^n \underline{I}_{Ai}, \quad \underline{I}_{B(k-1)k} = \sum_{i=k}^n \underline{I}_{Bi}, \quad \underline{I}_{C(k-1)k} = \sum_{i=k}^n \underline{I}_{Ci}. \quad (11)$$

8) Resistance phase losses of voltage on the section: phase wire – neutral wire between  $(k-1)$ , and  $k$ -th receipt point

$$\begin{aligned} \Delta \underline{U}_{AN(k-1)k}^R &= \Delta \underline{U}_{A(k-1)k}^R - \Delta \underline{U}_{N(k-1)k}^R, \\ \Delta \underline{U}_{BN(k-1)k}^R &= \Delta \underline{U}_{B(k-1)k}^R - \Delta \underline{U}_{N(k-1)k}^R, \\ \Delta \underline{U}_{CN(k-1)k}^R &= \Delta \underline{U}_{C(k-1)k}^R - \Delta \underline{U}_{N(k-1)k}^R, \end{aligned} \quad (12)$$

where:

- resistance phase losses of voltage between receipt points

$$\begin{aligned}\Delta \underline{U}_{A(k-1)k}^R &= \underline{I}_{A(k-1)k} \cdot R_{(k-1)k}, \\ \Delta \underline{U}_{B(k-1)k}^R &= \underline{I}_{B(k-1)k} \cdot R_{(k-1)k}, \\ \Delta \underline{U}_{C(k-1)k}^R &= \underline{I}_{C(k-1)k} \cdot R_{(k-1)k},\end{aligned}\quad (13)$$

- resistance losses of voltage in neutral wire

$$\Delta \underline{U}_{N(k-1)k}^R = -(\underline{I}_{A(k-1)k} + \underline{I}_{B(k-1)k} + \underline{I}_{C(k-1)k}) \cdot R_{N(k-1)k}. \quad (14)$$

9) Inductive phase losses of voltage on the section: phase wire – neutral wire ( $k-1$ ) and  $k$ -th receipt point

$$\begin{aligned}\Delta \underline{U}_{AN(k-1)k}^X &= \Delta \underline{U}_{A(k-1)k}^X - \Delta \underline{U}_{N(k-1)k}^X, \\ \Delta \underline{U}_{BN(k-1)k}^X &= \Delta \underline{U}_{B(k-1)k}^X - \Delta \underline{U}_{N(k-1)k}^X, \\ \Delta \underline{U}_{CN(k-1)k}^X &= \Delta \underline{U}_{C(k-1)k}^X - \Delta \underline{U}_{N(k-1)k}^X,\end{aligned}\quad (15)$$

- inductive phase losses of voltage between neighboring receipt points

$$\begin{aligned}\Delta \underline{U}_{A(k-1)k}^X &= \frac{l_{(k-1)k}}{2} (\underline{I}_{A(k-1)k} \cdot jX_{AN} + \underline{I}_{B(k-1)k} \cdot jX_{ANB} + \underline{I}_{C(k-1)k} \cdot jX_{ANC}), \\ \Delta \underline{U}_{B(k-1)k}^X &= \frac{l_{(k-1)k}}{2} (\underline{I}_{A(k-1)k} \cdot jX_{ANB} + \underline{I}_{B(k-1)k} \cdot jX_{BN} + \underline{I}_{C(k-1)k} \cdot jX_{BNC}), \\ \Delta \underline{U}_{C(k-1)k}^X &= \frac{l_{(k-1)k}}{2} (\underline{I}_{A(k-1)k} \cdot jX_{ANC} + \underline{I}_{B(k-1)k} \cdot jX_{BNC} + \underline{I}_{C(k-1)k} \cdot jX_{CN}),\end{aligned}\quad (16)$$

- inductive loss of voltage in neutral wire on the section as above

$$\Delta \underline{U}_{N(k-1)k}^X = -\frac{l_{(k-1)k}}{2} (\underline{I}_{A(k-1)k} \cdot jX_{AN} + \underline{I}_{B(k-1)k} \cdot jX_{BN} + \underline{I}_{C(k-1)k} \cdot jX_{CN}). \quad (17)$$

10) Phase losses of voltage from the beginning of the line to the  $i$ -th receipt point

$$\begin{aligned}\Delta \underline{U}_{ANi} &= \sum_{k=1}^i (\Delta \underline{U}_{AN(k-1)k}^R + \Delta \underline{U}_{AN(k-1)k}^X), \\ \Delta \underline{U}_{BNi} &= \sum_{k=1}^i (\Delta \underline{U}_{BN(k-1)k}^R + \Delta \underline{U}_{BN(k-1)k}^X), \\ \Delta \underline{U}_{Cni} &= \sum_{k=1}^i (\Delta \underline{U}_{CN(k-1)k}^R + \Delta \underline{U}_{CN(k-1)k}^X).\end{aligned}\quad (18)$$

11) Phase voltages and between wires in the  $i$ -th point of receipt point

a) phases voltages

- vectors

$$\begin{aligned}\underline{U}_{Ai} &= \underline{U}_{st} - \Delta \underline{U}_{ANi}, \\ \underline{U}_{Bi} &= \underline{U}_{st} \cdot e^{j240^\circ} - \Delta \underline{U}_{BNi}, \\ \underline{U}_{Ci} &= \underline{U}_{st} \cdot e^{j120^\circ} - \Delta \underline{U}_{Cni},\end{aligned}$$

- modules

$$\begin{aligned}U_{Ai} &= |\underline{U}_{Ai}|, \\ U_{Bi} &= |\underline{U}_{Bi}|, \\ U_{Ci} &= |\underline{U}_{Ci}|,\end{aligned}\quad (19)$$

b) voltages between wires

- vectors

$$\begin{aligned}\underline{U}_{ABi} &= \underline{U}_{Ai} - \underline{U}_{Bi}, \\ \underline{U}_{BCi} &= \underline{U}_{Bi} - \underline{U}_{Ci},\end{aligned}$$

- modules

$$\begin{aligned}U_{ABi} &= |\underline{U}_{ABi}|, \\ U_{BCi} &= |\underline{U}_{BCi}|,\end{aligned}\quad (20)$$

$$\underline{U}_{CAi} = \underline{U}_{Ci} - \underline{U}_{Ai} ,$$

$$U_{CAi} = |\underline{U}_{CAi}|.$$

12) Phase drops and voltage deviations [4]

a) voltage drops

$$\Delta U_{Ai} = U_{st} - U_{Ai} ,$$

$$\Delta U_{Bi} = U_{st} - U_{Bi} ,$$

$$\Delta U_{Ci} = U_{st} - U_{Ci} ,$$

b) voltage deviations

$$\delta U_{Ai} = \frac{U_{Ai} - U_n}{U_n} \cdot 100\% ,$$

$$\delta U_{Bi} = \frac{U_{Bi} - U_n}{U_n} \cdot 100\% , \quad (21)$$

$$\delta U_{Ci} = \frac{U_{Ci} - U_n}{U_n} \cdot 100\% .$$

13) Coefficients of voltage asymmetry [3]

a) opposite order

$$\alpha_{U_2}(i) = \frac{U_{2i}}{U_{1i}} \cdot 100\% ,$$

b) zero order

$$\alpha_{U_0}(i) = \frac{U_{0i}}{U_{1i}} \cdot 100\% , \quad (22)$$

where:

$U_{2i}$ ,  $U_{1i}$ ,  $U_{0i}$  – symmetrical components of voltage; in opposite order, matching, and zero order

$$\begin{aligned} U_{2i} &= \frac{1}{3} \sqrt{U_{Ai}^2 + U_{Bi}^2 + U_{Ci}^2 - 2U_{Ai}U_{Bi} \cos(\alpha_i - \frac{\pi}{3}) - 2U_{Bi}U_{Ci} \cos(\beta_i - \frac{\pi}{3}) - 2U_{Ci}U_{Ai} \cos(\alpha_i + \beta_i + \frac{\pi}{3})} , \\ U_{1i} &= \frac{1}{3} \sqrt{U_{Ai}^2 + U_{Bi}^2 + U_{Ci}^2 - 2U_{Ai}U_{Bi} \cos(\alpha_i + \frac{\pi}{3}) - 2U_{Bi}U_{Ci} \cos(\beta_i + \frac{\pi}{3}) - 2U_{Ci}U_{Ai} \cos(\alpha_i + \beta_i - \frac{\pi}{3})} , \\ (23) \quad U_{0i} &= \frac{1}{3} \sqrt{U_{Ai}^2 + U_{Bi}^2 + U_{Ci}^2 + 2U_{Ai}U_{Bi} \cos \alpha_i + 2U_{Bi}U_{Ci} \cos \beta_i + 2U_{Ci}U_{Ai} \cos \beta_i} , \\ \alpha_i &= \arccos \frac{U_{Ai}^2 + U_{Bi}^2 - U_{ABi}^2}{2U_{Ai}U_{Bi}} , \quad \beta_i = \arccos \frac{U_{Bi}^2 + U_{Ci}^2 - U_{BCi}^2}{2U_{Bi}U_{Ci}} . \end{aligned} \quad (24)$$

In the case of an angle symmetry:  $\alpha = 2\pi/3$ ,  $\beta = 2\pi/3$

According to PN-EN 50160 standards, values of deviations should be within the limits of:

$$-10\% < \delta U_f < +10\% \quad (25)$$

while the value of the coefficient of voltage asymmetry (for the network, restrictions concern only the values of the asymmetry coefficient of the opposite order)

$$\alpha_{U2} < \alpha_{dop} = 2\% \quad (26)$$

#### 4. Selected results of simulations

Examples of calculations carried out for overhead line LV with simple track, specified cross-section wires ( $s = s_n = 50 \text{ mm}^2$ ) and a fixed topology, so the length  $l = 1080 \text{ m}$ , the number of receipt points of  $n = 10$ . Assume customers evenly along the line. At the beginning, values of the peak power  $P_{si}$  were generated for the individual connections and its average value was  $P_{sg} = 5,753 \text{ kW}$  (on the basis of research results in rural customers). Distribution of the power on

time stages was implemented by determining the values of coefficients described in formulas (6), (7), (8).

For several values of the maximum load factor obtained on the basis of research results concerning loads in rural customers:

$$w_i = \bar{w} - \sigma_w = 0,406 \quad w_i = \bar{w} = 0,541 \quad w_i = \bar{w} + \sigma_w = 0,675 \quad w_i = \bar{w} + 2\sigma_w = 0,709$$

values of coefficient  $k_{1i}$  were generated. On the basis of mutual relations between the asymmetry loads factors resulting from the formula (5), fixed the value of the coefficient  $k_{2i}$  in individual receipt points of the line. On this basis, obtained values of coefficients, values of peak power and phase powers were calculated in individual connections. Values of phase coefficients were generated on the basis of measurements carried out in a transformer station MV/LV (average value of the  $\cos\varphi = 0,923$ ). This enabled the calculation of phase currents in receipt points according to the formula (10). These currents corresponding to the phase powers at random, were attributed to the phases of the line. This allowed us to define the value of currents in the line, drops and levels of phase voltages and therefore values of voltage deviations and coefficients of voltage asymmetry, which are among the parameters which characterise the quality of electricity in low-voltage power line. Table 1. shows the values of coefficient voltage asymmetry and voltage deviations for the most loaded phase and at the end of the line for a specific level of loads asymmetry in customers, which largely are characterised by the coefficient of maximum load  $w_i$  (it determines a level of phase load as dominant in relation to the remaining phase loads).

*Tab. 1. Results of qualitative parameters of electricity at the end of the line for a specific level of asymmetry loads in customers for the peak of load.*

| $w_i$                         | $\alpha_{U2}$ | $\alpha_{Uo}$ | $\delta U_{f \max}$ |
|-------------------------------|---------------|---------------|---------------------|
| $\bar{w} - \sigma_w = 0,406$  | 1,12          | 5,41          | -11,9               |
| $\bar{w} = 0,541$             | 2,00          | 9,85          | -20,1               |
| $\bar{w} + \sigma_w = 0,675$  | 2,08          | 10,67         | -21                 |
| $\bar{w} + 2\sigma_w = 0,709$ | 2,77          | 14,39         | -23,1               |

where:

$\bar{w}$ ,  $\sigma_w$  - mean value and standard deviation of the maximum load factor ( $w_i$ ) on the basis of research concerning phase loads in rural customers for the peak of load,

$\alpha_{U2}$ ,  $\alpha_{Uo}$  - values of coefficients of voltage asymmetry for opposite order and zero-order,

$\delta U_{f \max}$  - value of voltage deviations in the most loaded stage.

## 5. Conclusions

Analysis of the results of simulation studies allows us to determine the sensitivity of the system of low voltage line, on a degree of asymmetry loads of customers in terms of the quality of

supplied electricity. For a relatively moderate asymmetry of loads occurring in customers ( $w = 0,406$ ; for the symmetry of the phase loads  $w = 0.33$ ), value of the coefficient of voltage asymmetry, ranged limits ( $\alpha_2 = 1,12\%$   $\alpha_{dop} = 2\%$ ), which took place, overrun limit of voltage deviations in the phase of the most loaded ( $\delta U_{fmax} = -11.9\% < -10\%$ ). It must be noticed that asymmetry loads overlapped the asymmetry of line as a transmission element. In the case of very explicit asymmetry customer loads ( $w = 0.709$ ) the value of coefficient exceeded the limit value of the asymmetry voltage ( $\alpha_{U2} = 2.77\% > \alpha_{dop} = 2\%$ ) and moreover, the limit value of voltage deviations in two phases were exceeded as well, while in one of them - very strongly ( $\delta U_{fmax} = -23,1\% < -10\%$ ).

Due to the complexity of the phenomenon of load asymmetry, it is necessary to develop simulation models that using the data of a network, customers and the results of measurements which representative customers, allows us to assess risk of exceeded limit values of selected parameters of electricity in the LV line. Then, it enables us to take into consideration the asymmetry loads to design a new network (e.g. choice cross-section of wires), quality control of electricity in existing and potential of its modernisation.

## References

- [1] Bolkowski, St., *Elektrotechnika teoretyczna*, Tom 2, WNT, Warszawa 1986.
- [2] Kolber, P., Perczyński, D., Bojar, P., *Voltage unbalance model in a rural low voltage power line*, 11<sup>th</sup> International Conference on Developments in Machinery Design and Control Vol.9, Cervený Kláštor 2007.
- [3] Kowalski, Zb., *Asymetria w układach elektroenergetycznych*, PWN, Warszawa 1987.
- [4] Kowalski, Zb., *Wyznaczanie odchyleń i spadków napięcia w sieciach niskiego napięcia zasilających niesymetryczne i nieliniowe odbiorniki energii elektrycznej*, Jakość i użytkowanie energii elektrycznej Tom 2, 1996.
- [5] Polska Norma PN-EN 50160, *Parametry napięcia zasilającego w publicznych sieciach rozdzielczych*, 1998.



## OPTIMAL CONTROL ALGORITHMS FOR TRANSMISSIONS IN CITY BUSES

Grzegorz Koralewski

*University of Economics and Innovation in Lublin  
ul. Melgiewska 7-9, 20-209 Lublin, Poland  
tel.: + 48 81 7493243, fax: + 48 81 7491777  
e-mail: grzegorz.koralewski@wsei.lublin.pl*

### **Abstract**

*The article presents a mathematical model of motion of a car equipped with the automatic hydromechanical transmission. All possible conditions of transmission operation during car acceleration have been analysed. The model has been applied in a computer program for city bus acceleration simulation. Also the methodology of defining optimal gear shift algorithms for the automatic hydro mechanical transmission has been presented. There have been used two optimization criteria: acceleration time minimization and fuel consumption minimization in the acceleration phase. The methodology has been illustrated by an example of optimal control algorithms synthesis of the automatic hydromechanical transmission in a city bus.*

**Keywords:** city bus, automatic hydromechanical transmission, control algorithms, optimization criteria, acceleration time, fuel consumption

### **1. Introduction**

Nowadays production of buses and other automotive vehicles is very often based on compiling a complete product of sub-assemblies and parts supplied by other automotive companies specialized in a given field. Even small production plants undertake the task of building buses and use sub-assemblies and parts from recognized automotive business companies.

Such a strategy of designing and producing buses tailored to meet an individual client's requests and using sub-assemblies and parts from famous automotive companies is applied by Polish bus and coach manufacturer Solaris Bus & Coach S.A. [6]. Their offer of a wide range of bus models for various purposes and with different equipment is a technological and commercial success. Buses from Solaris & Coach S.A. can be seen on the roads in Poland, Western and Central-Western Europe and the Middle East. They are mainly city buses.

### **2. City bus gearboxes**

Public transport buses are continually improved to make them more comfortable for passengers, safer for the traffic, less burdensome for their drivers and more environmentally friendly. Because of all these aspects it is vital to replace bus manual mechanical drive system with an automatic system as well as continue work on improving the bus body design and modernizing its engine.

Automatic gearboxes are standard equipment of currently produced city buses [7]. They are automatic hydromechanical transmissions which bring many advantages to them.

The only important disadvantage of automatic hydromechanical transmissions applied in bus drive systems has so far been their less efficient exploitation compared to those with mechanical gearboxes and resulting a few per cent higher fuel consumption.

At present this essential drawback is successfully eliminated by means of:

- improving the transmission design with the aim of increasing its mean exploitation efficiency by optimization of the hydrokinetic transmission, the possibility of blocking it at top gears and the possibility of two-stream torque transmission at medium gears,
- optimizing transmission control programmes which realize assigned criteria of bus (car) motion quality with self-adaptation to variable exploitation factors.

These are also current tendencies in the development of automatic hydromechanical transmissions in world-wide known automotive companies with three companies dominating in the field of bus transmissions: Allison (USA), Zahnradfabrik Friedrichshafen AG (ZF) and Voith (Germany) [4, 5, 7].

### **3. Motion modelling for a bus with an automatic hydromechanical transmission**

Bus drive system made up of ready-made sub-assemblies i.e. the engine, the gearbox, the drive shaft, the driving axle, axle shafts, road wheels, retarders etc. requires that they not only match mechanically and are properly situated in the body or chassis of a bus but also that their technical parameters and functional characteristics are chosen correctly and programs controlling cooperation of sub-assemblies prepared. This is especially true about algorithms of shifting gears control in a hydromechanical transmission in relation to the engine control and other bus parameters such as: mass, gearbox and main gear ratio, road wheels parameters, air resistance, road resistance and inertia resistance etc. There is a large dispersion of gear shift moments in transmission systems of automotive vehicles with manual mechanical gearboxes especially under city traffic conditions [2].

Incorrect algorithms for hydromechanical transmission gear shift control may lead to such undesired phenomena as:

- bus combustion engine operating at ranges undesired with respect to fuel consumption, dynamic properties or fumes toxicity,
- considerable variations in bus acceleration at adjacent gears which negatively influence passengers' comfort and cause dynamic overload in the torque converting system which reduces drive system life.

In order to improve hydromechanical transmission design and optimize its control programs through computer simulations of bus motion it is necessary to employ mathematical models describing processes of the bus motion.

### **4. Research object characteristics**

The studied object is a city bus Solaris Urbino 12 weighing 13200 kg (at the time of research) with a 9.2 dm<sup>3</sup> compression-ignition supercharged engine DAF PR183 [6] of the power of 183 kW at 2200 rpm and the torque 1050 Nm at 1100 – 1700 rpm, equipped with an automatic hydromechanical transmission ZF 5HP500 [7] with the maximum transformation coefficient of 2.5 and a possibility of blocking the hydrokinetic transmission if its operation is not indispensable under given traffic conditions. This contributes to increasing average exploitation efficiency of the hydromechanical transmission. The kinematic diagram of the hydromechanical transmission is presented in fig. 1 and the sequence of elements shifting respective gears in tab. 1.

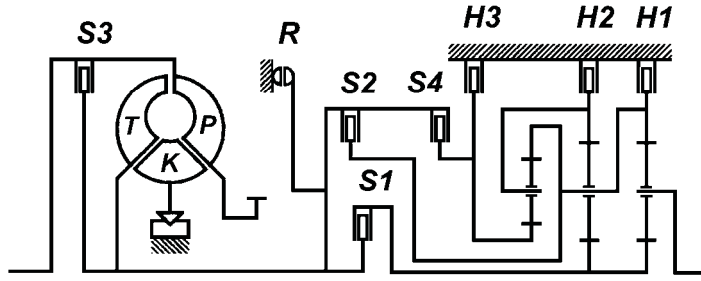


Fig. 1. The kinematic diagram of the automatic hydromechanical transmission ZF 5HP500 [7]

Tab. 1. The operation sequence of elements shifting gears in the hydromechanical transmission ZF 5HP500 [7]

| Gear | Switched element |    |    |    |    |    |    | Speed ratio |
|------|------------------|----|----|----|----|----|----|-------------|
|      | S1               | S2 | S3 | S4 | H1 | H2 | H3 |             |
| N    |                  |    |    |    |    |    |    | –           |
| 1    | •                |    |    |    | •  |    |    | 3,43        |
| 2    | •                |    |    |    |    | •  |    | 2,01        |
| 3    | •                |    | •  |    |    |    | •  | 1,42        |
| 4    | •                | •  | •  |    |    |    |    | 1,0         |
| 5    |                  | •  | •  |    |    |    | •  | 0,83        |
| R    |                  |    |    | •  | •  |    |    | 4,84        |

## 5. Acceleration model of a bus with the automatic hydromechanical transmission

In the process of car acceleration the power stream transmission in the hydromechanical transmission can be realized in the following way: as a one stream flow through the hydrokinetic transmission in the first, second (and reverse) gears and mechanically with a blocked hydrokinetic transmission in the third, fourth and fifth gears. In each of the above mentioned situations mechanical transmission gear shifts can be accomplished. The mathematical specification of the dynamics of the equivalent model of a car drive with a hydromechanical transmission will also change accordingly.

Following d'Alembert's principle and skipping transitional transformations we get the following mathematical dependences which represent the bus acceleration model for respective operation conditions of the hydromechanical transmission [1]:

- Monotonic acceleration with full-stream power transmission through the hydrokinetic transmission in between gear shifts:

$$\left\{ \begin{array}{l} M_S - M_P = I_S \frac{d\omega_S}{dt} \\ \left( F_n - \Psi mg - c_x \frac{\gamma A}{2} v^2 \right) \frac{i_0 i_i}{r_d} = \left[ m + \frac{\sum I_k}{r_d^2} + I_{un} \left( \frac{\eta_m i_0 i_i}{r_d} \right)^2 \right] \frac{d\omega_T}{dt} \\ i_d M_P \frac{\eta_m i_0 i_i}{r_d} - \Psi mg - c_x \frac{\gamma A}{2} v^2 = \left[ m + \left( i_d I_S \frac{d\omega_S}{dn_T} + I_{un} \right) \left( \frac{\eta_m i_0 i_i}{r_d} \right)^2 + \frac{\sum I_k}{r_d^2} \right] \frac{dv}{dt} \end{array} \right. , \quad (1)$$

where:

$M_S$  – engine torque,

$M_P$  – output torque on hydraulic converter pump impeller,

$I_S$  – moment of inertia of engine crankshaft together with the flywheel, pump impeller and the liquid connected to it,

$I_{un}$  – moment of inertia of the masses of power transmission system elements between converter output shaft and driven road wheels,

$I_k$  – moment of inertia of a single wheel together with rotating brake elements,

$F_n$  – driving force,

$\Psi$  – road resistance coefficient  $\Psi = f \cos \alpha + \sin \alpha$ ,

$m$  – bus total weight,

$g$  – gravitational acceleration,

$c_x$  – air resistance coefficient,

$\gamma$  – air density,

$A$  – car side face,

$v$  – car velocity,

$r_d$  – wheel dynamic radius,

$i_0$  – final drive ratio,

$i_i$  – ratio of shifted reduction gear,

$\eta_m$  – mechanical efficiency of car power transmission system,

$\omega_S$  – engine angular velocity,

$\omega_T$  – angular velocity of hydraulic converter turbine wheel,

$i_d$  – dynamic ratio of hydraulic torque converter (transformation coefficient).

- Monotonic acceleration in case of the blocked hydromechanical transmission is similar to the one for the car with a mechanical gearbox in respect of mathematical specification:

$$M_S \frac{\eta_m i_0 i_i}{r_d} - \Psi mg - c_x \frac{\gamma A}{2} v^2 = \left[ m + (I_S + I_{un}) \left( \frac{\eta_m i_0 i_i}{r_d} \right)^2 + \sum I_k \right] \frac{dv}{dt}. \quad (2)$$

- Gear shifts during the full-stream torque transmission in the hydrokinetic transmission:

$$\left\{ \begin{array}{l} M_S - M_P = I_S \frac{d\omega_S}{dt} \\ i_d M_P - \frac{M_{ti}}{i_i^c} - \frac{M_{ti-1}}{i_{i-1}^c} = I_T \frac{d\omega_T}{dt} \\ \left( M_{ti} i_i^b + M_{ti-1} i_{i-1}^b \right) \frac{\eta_m i_0}{r_d} - \Psi mg - c_x \frac{\gamma A}{2} v^2 = \left[ m + I_{un} \left( \frac{\eta_m i_0 i_i}{r_d} \right)^2 + \sum I_k \right] \frac{dv}{dt} \end{array} \right., \quad (3)$$

where:

$M_{ti}, M_{ti-1}$  – friction torque on the clutches shifting  $i$ -th and  $i-1$ -st gear,

$i_i^c, i_{i-1}^c$  – ratios of transmission reduction gear in the sector between turbine wheel and active (attacking) clutch plates shifting  $i$ -th and  $i-1$ -st gear,  
 $i_i^b, i_{i-1}^b$  – ratios of transmission reduction gear in the sector between passive (being attacked) clutch plates shifting  $i$ -th and  $i-1$ -st gear and converter output shaft,  
 $I_T$  – moment of inertia of hydraulic torque converter turbine wheel and the liquid connected to it.

– The hydrokinetic transmission blockade at  $i$ -th gear:

$$\left\{ \begin{array}{l} M_S - M_P - M_{bl} = I_S \frac{d\omega_S}{dt} \\ (i_d M_P + M_{bl}) \frac{\eta_m i_0 i_i}{r_d} - \Psi mg - c_x \frac{\gamma A}{2} v^2 = \left[ m + \left( i_d I_S \frac{d\omega_S}{d\omega_T} \right) \left( \frac{\eta_m i_0 i_i}{r_d} \right)^2 + \frac{\sum I_k}{r_d^2} \right] \frac{dv}{dt} \end{array} \right. \quad (4)$$

where:

$M_{bl}$  – friction torque on the clutch blocking hydraulic torque converter.

– Gear shifting when the hydrokinetic transmission is blocked:

$$\left\{ \begin{array}{l} M_S - \frac{M_{ti}}{i_i^c} - \frac{M_{ti-1}}{i_{i-1}^c} = (I_S + I_{un}) \frac{d\omega_S}{dt} \\ \left( M_{ti} i_i^b + M_{ti-1} i_{i-1}^b \right) \frac{\eta_m i_0}{r_d} - \Psi mg - c_x \frac{\gamma A}{2} v^2 = \left[ m + I_{un} \left( \frac{\eta_m i_0 i_i}{r_d} \right)^2 + \frac{\sum I_k}{r_d^2} \right] \frac{dv}{dt} \end{array} \right. \quad (5)$$

Dependences (1)-(5) were applied while the program for computer simulation of acceleration of a bus with an automatic hydromechanical transmission was worked out, then it was realized and initially verified experimentally in operation [3].

## 6. Algorithms of shifting gears in the automatic hydromechanical transmission

As a rule popular methods of defining gear shift algorithms for an automatic gearbox refer to car motion maximally similar to steady motion. Difficulties with direct application of car theory criteria like fuel consumption economy and acceleration dynamics but also applied imperfect mathematical methods have determined a variety of additional factors which show graphically or graphically and analytically optimal gear shifts moments. An assessment of these factors and the physical reason behind them can be found in this study [1].

First of all, recommended gear shifts which ensure the highest dynamics of acceleration should be performed when the engine reaches its rotational speed equal to its maximum power or they can be described as crossing points of engine power curves in the function of motion velocity at two adjacent gears. Moreover, drive power on driven wheels curves, dynamic and car acceleration characteristics and engine maximum rotational speed moments can also be applied as economical optimality factors of this gear shift strategy.

Gear shift moments which guarantee the least fuel consumption are defined as crossing points of hourly fuel consumption curves in the function of vehicle motion velocity at stable fuel intake or unitary fuel consumption curves at adjacent gears. Other factors in optimally economical car acceleration are unitary amount of fuel consumption with regard to hydrokinetic transmission efficiency or drive power on car wheels with equal fuel consumption per hour at adjacent gears of

hydromechanical transmission or else hydrokinetic transmission efficiency in the function of motion velocity.

Such variety of applied factors and therefore many different methods of setting gear shift optimal moments obviously leads to vital differences between gear shift moments algorithms defined for the same hydromechanical transmission. This is a result of different approximation of the above mentioned factors in relation to initial optimization criteria and this contributes to significant divergences between hydromechanical transmission algorithms based on the same optimization criteria. Hence the need arises to assess them from the point of view of ensuring required results extremum and to see to what extent the applied factors meet the original optimization criteria.

## 7. Optimization criteria and acceleration quality functionals

Determining optimal gear shift moments in a hydro-mechanical transmission at constant position of the throttle pedal means finding such car motion velocity values  $V_p$ , at which gear shifts should be done – shifts from lower to higher gears. This should ensure obtaining functional extremum of the quality of car acceleration. Because of the well-known diversity between acceleration dynamics and fuel economy it seems justified to employ a few criteria simultaneously. This allows them to complement each other and makes control of the obtained results possible. Analysis of similar studies indicates that the following initial criteria of car acceleration optimization should be adopted:

- acceleration time  $T$  necessary to reach the assigned terminal acceleration velocity  $V_k$ ,
- distance covered  $S$  at accelerating up to assigned terminal velocity  $V_k$ ,
- fuel consumption  $Q$  necessary to reach the assigned terminal acceleration velocity  $V_k$ ,
- variational criterion  $\varepsilon$  of fuel consumption at accelerating with acceleration dynamics taken into account [1].

Appropriate bus acceleration quality functionals for argument  $v$  can be presented as [1]:

- for acceleration dynamics:

$$J_T = \sum_{i=1}^n \int_{V_0}^{V_k} \frac{1}{a_i(v)} dv = \sum_{i=1}^n \left( \int_{V_0}^{V_p} \frac{1}{a_i(v)} dv + \int_{V_p}^{V_k} \frac{1}{a_{i+1}(v)} dv \right) \rightarrow \min, \quad (6)$$

$$J_S = \sum_{i=1}^n S_i = \sum_{i=1}^n \left[ \int_{V_0}^{V_p} \frac{v}{a_i(v)} dv + \int_{V_p}^{V_k} \frac{v}{a_{i+1}(v)} dv - V_k \left( \int_{V_0}^{V_p} \frac{1}{a_i(v)} dv + \int_{V_p}^{V_k} \frac{1}{a_{i+1}(v)} dv \right) \right] \rightarrow \min, \quad (7)$$

- for fuel consumption:

$$J_Q = \sum_{i=1}^n \int_{V_0}^{V_k} \frac{(g_e N_e)_i}{a_i(v)} dv = \sum_{i=1}^n \left[ \int_{V_0}^{V_p} \frac{(g_e N_e)_i}{a_i(v)} dv + \int_{V_p}^{V_k} \frac{(g_e N_e)_{i+1}}{a_{i+1}(v)} dv \right] \rightarrow \min, \quad (8)$$

$$J_{\varepsilon} = \sum_{i=1}^n Q_i - \sum_{i=1}^n \frac{(g_e N_e)_k}{V_k} S_i = \sum_{i=1}^n \left\{ \int_{V_0}^{V_p} \frac{(g_e N_e)_i}{a_i(v)} dv + \int_{V_p}^{V_k} \frac{(g_e N_e)_{i+1}}{a_{i+1}(v)} dv - \right. \\ \left. - \frac{(g_e N_e)_k}{V_k} \left[ \int_{V_0}^{V_p} \frac{v}{a_i(v)} dv + \int_{V_p}^{V_k} \frac{v}{a_{i+1}(v)} dv \right] \right\} \rightarrow \min \quad , \quad (9)$$

where:

$a$  – bus acceleration,

$v$  – motion velocity actual value,

$V_0, V_k$  – initial and terminal acceleration velocity,

$i, n$  – index and number of gears in hydromechanical transmission, respectively,

$S_i, t_i$  – distance covered and acceleration time at  $i$ -th shift gear, respectively,

$g_e$  – specific fuel consumption of engine,

$N_e$  – engine power output.

In order to analytically investigate extremum of expressions (6)-(9) the integrand was expressed in bus motion velocity function  $v$  by design parameters and functional dependences characteristic of the studied object.

A mathematical model of car acceleration described by dependences (1)-(5) and an assumption that bus motion is a particle motion has been used to define optimal gear shift moments of the hydromechanical transmission at constant throttle pedal position. This can be expressed as follows:

$$a = \frac{F_n - F_{op}}{m_{red}}, \quad (10)$$

where:

$F_{op}$  – motion resistance force,

$m_{red}$  – bus reduced mass including inertia in the acceleration process.

Reduced mass of a car with hydrokinetic transmission in the drive system is defined as:

$$m_{red} = m\delta = m \left\{ 1 + \frac{1}{mr_d^2} \left[ \left( I_p i_d \frac{d\omega_p}{d\omega_T} + I_T \right) (i_g i_i)^2 \eta_m + \sum I_k \right] \right\}, \quad (11)$$

where:

$\delta$  – reduced mass coefficient,

$I_p$  – inertia moment of a hydrokinetic transmission pump impeller and engine rotating elements,

$d\omega_p, d\omega_T$  – angular acceleration of pump and hydrokinetic transmission turbine impellers, respectively.

With the use of prepared mathematical model of bus acceleration (of a bus with hydromechanical transmission) and determined motion quality functionals the conditions of their extremum existence were defined by computer simulations. Optimal gear shifts of the hydromechanical transmission should take place at the moment when the accelerating vehicle reaches such velocity  $V_p$  at which the following conditions are fulfilled:

- for acceleration time criterion  $T$  to assigned velocity  $V_k$ :

$$\frac{d}{dv} \left[ \int_{V_0}^{V_p} \frac{1}{a_i(v)} dv - \int_{V_p}^{V_k} \frac{1}{a_{i+1}(v)} dv \right] = \frac{1}{a_i(V_p)} - \frac{1}{a_{i+1}(V_p)} = 0, \quad (12)$$

- for acceleration distance covered criterion  $S$  to assigned velocity  $V_k$ :

$$\begin{aligned} \frac{d}{dv} \left\{ \int_{V_0}^{V_p} \frac{v}{a_i(v)} dv - \int_{V_p}^{V_k} \frac{v}{a_{i+1}(v)} dv - V_k \left[ \int_{V_0}^{V_p} \frac{1}{a_i(v)} dv - \int_{V_p}^{V_k} \frac{1}{a_{i+1}(v)} dv \right] \right\} = \\ = \frac{V_p}{a_i(V_p)} - \frac{V_p}{a_{i+1}(V_p)} - V_k \left[ \frac{1}{a_i(V_p)} - \frac{1}{a_{i+1}(V_p)} \right] = 0 \end{aligned} \quad , \quad (13)$$

- for fuel consumption  $Q$ :

$$\frac{d}{dv} \left[ \int_{V_0}^{V_p} \frac{(g_e N_e)_i}{a_i(v)} dv - \int_{V_p}^{V_k} \frac{(g_e N_e)_{i+1}}{a_{i+1}(v)} dv \right] = \frac{(g_e N_e)_i}{a_i(V_p)} - \frac{(g_e N_e)_{i+1}}{a_{i+1}(V_p)} = 0, \quad (14)$$

- for variational fuel consumption  $\epsilon$ :

$$\begin{aligned} \frac{d}{dv} \left\{ \int_{V_0}^{V_p} \frac{(g_e N_e)_i}{a_i(v)} dv - \int_{V_p}^{V_k} \frac{(g_e N_e)_{i+1}}{a_{i+1}(v)} dv - \frac{(g_e N_e)_k}{V_k} \left[ \int_{V_0}^{V_p} \frac{v}{a_i(v)} dv - \int_{V_p}^{V_k} \frac{v}{a_{i+1}(v)} dv \right] \right\} = \\ = \frac{(g_e N_e)_i}{a_i(V_p)} - \frac{(g_e N_e)_{i+1}}{a_{i+1}(V_p)} - \left[ \frac{V_p}{V_k} \frac{(g_e N_e)_i}{a_i(V_p)} - \frac{V_p}{V_k} \frac{(g_e N_e)_{i+1}}{a_{i+1}(V_p)} \right] = 0. \end{aligned} \quad (15)$$

Conditions (12) and (13) concerning acceleration dynamics can be expressed as:

$$[a_i(V_p) - a_{i+1}(V_p)](V_p - V_k) = 0. \quad (16)$$

Similarly gear shift optimality conditions with regard to fuel consumption can be formulated as:

$$\left[ \frac{(g_e N_e)_i}{a_i(V_p)} - \frac{(g_e N_e)_{i+1}}{a_{i+1}(V_p)} \right] \left( 1 - \frac{V_p}{V_k} \right) = 0. \quad (17)$$

Optimal gear shift moments in the hydromechanical transmission for a bus acceleration process can be received by finding the extremum of the above presented functionals. According to dynamics criteria they will be defined as crossing points of the vehicle acceleration curves in the function of motion velocity at adjacent gears. If there are no such crossing points, gear shift moments will be defined as limit points of the interval of possible velocity variability  $V_p$  at the preceding gear.

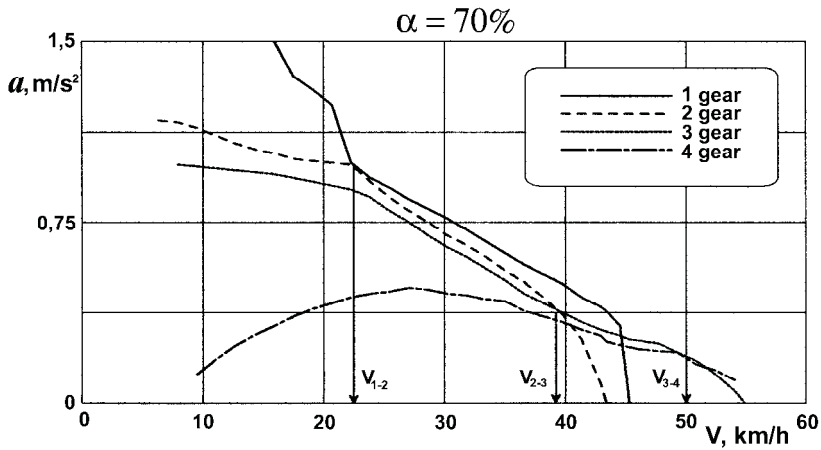


Fig. 2. Graphic interpretation of seeking optimal for acceleration dynamics gear shift moments of the city bus hydromechanical transmission

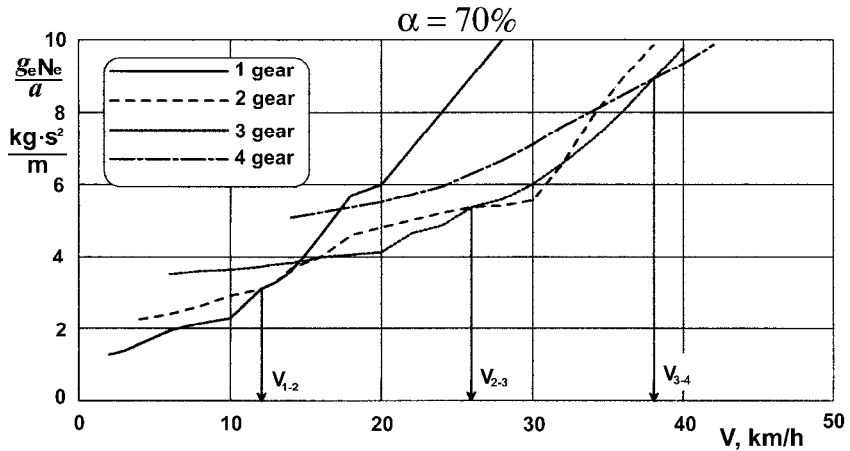


Fig. 3. Graphic interpretation of seeking optimal with regard to fuel consumption gear shift moments in the automatic hydromechanical transmission of a city bus

This procedure strategy is illustrated in fig. 2 where acceleration curves at respective gears of the Solaris bus equipped with an automatic hydromechanical transmission ZF 5HP500 have been shown. The crossing points of these accelerations mark mechanical reducer gear shift moments which ensure maximum bus acceleration dynamics.

According to optimal economy criterion moments of gear shifts are defined by the crossing points of factors curves expressed as:  $\frac{g_e N_e}{a}$  in the function of the vehicle motion velocity at adjacent gears in the hydromechanical transmission or as border range of possible velocity variability interval  $V_p$ . Fig. 3 shows graphically how optimal gear shift moments are determined so that they minimize fuel consumption of the Solaris bus equipped with automatic transmission ZF 5HP500 and yet required acceleration dynamics is preserved.

Optimal algorithms for gear shift control in the hydromechanical transmission ZF 5HP500 of the Solaris city bus based on such strategies have been graphically illustrated in fig. 4 as gear shift lines for the bus acceleration phase. Both algorithms realizing maximum bus acceleration

dynamics and those ensuring minimisation of fuel consumption in the process of acceleration have been distinguished.

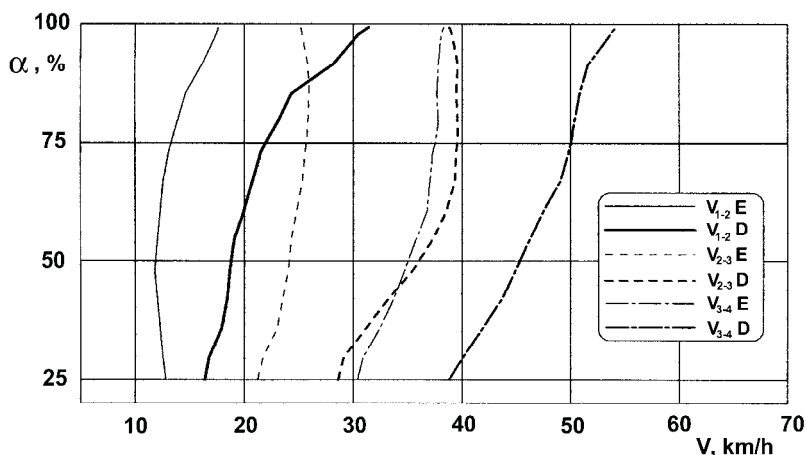


Fig. 4. Algorithms of automatic hydromechanical transmission ZF 5HP500 control in the Solaris city bus

## 8. Conclusions

According to various criteria of analyzing acceleration dynamics or fuel consumption conditions of optimal gear shift moments are the only ones and they are not contradictory in terms of quality. Employing various criteria leads only to diversifying quantity assessment of motion dynamics or fuel consumption in the same bus acceleration process under study.

Undertaken analytical and experimental [1, 3] studies applied to automatic hydromechanical transmissions have confirmed optimality of gear shift moments defined by this method. A set of such moments in the whole area of engine power control defines gear shift algorithms in the hydromechanical transmission and they in turn define the control programs. The hydromechanical transmission control programs have a considerable impact on fuel-traction properties of the bus cyclical motion and thus on technical and economical effectiveness of its exploitation.

## References

- [1] Koralewski, G., *Metodologiczieskije aspekty optimizacji zakonov upravlienija i parametrov gidromiechanicznych pieriedacz avtomobiliej*, NVF Ukrainski tehnologii, Lwów 2000.
- [2] Koralewski, G., Wrona, R., *Evaluation of optimality of car mechanical gearbox steering under urban traffic conditions*, XIII International Scientific Meeting Motor Vehicles & Engines MVM'2004, pp. 27–32, Kragujevac 2004, Yugoslavia.
- [3] Koralewski, G., Wrona, R., *Modelling of acceleration of the city bus with hydromechanical automatic transmission*, Naukovo-vyrobnychnyj žurnal "Problemy Techniki" № 2/2004, pp. 109–114 Odessa 2004.
- [4] Micknass, W., Popiol, R., Springer, A., *Sprzęgła, skrzynki biegów i pólósie napędowe*, Wydawnictwa Komunikacji i Łączności, Warszawa 2005.
- [5] Siedlecki, A., *Skrzynie biegów ZF Ecomat*, Transport – Technika Motoryzacyjna nr 5/2000, pp. 69–70.
- [6] [www.solarisbus.pl](http://www.solarisbus.pl) – strona internetowa firmy Solaris Bus & Coach S.A.
- [7] Zajac, M., *Układy przeniesienia napędu samochodów ciężarowych i autobusów*, Wydawnictwa Komunikacji i Łączności, Warszawa 2003.



## INVESTIGATION OF THERMAL PROPERTIES OF SELECTED POLYMER BLENDS

**Bogusław Królikowski**

*Institute for Engineering of Polymer Materials and Dyes  
ul. M. Curie-Skłodowskiej 55, 87-100 Toruń, Poland  
e-mail: b.krolikowski@impib.pl*

**Joachim Zimniak**

*University of Technology and Life Sciences,  
Faculty of Mechanical Engineering  
ul. Kaliskiego 7, 85-789 Bydgoszcz, Poland  
e-mail: zimniak@utp.edu.pl*

### **Abstract**

*The influence of co-rotating twin-screw extrusion of polymer blends on their thermal properties has been presented in this paper. The polymer blends that have been taken into consideration consisted of PE and PP processed by BTSK 20 without any compatibilizer. The contents of minor phase, i.e. PP in polymer matrix, i.e. PE in wt. % ranged from: 95/5, 90/10, 85/15 to 15/85, 10/90, 5/95 [1 – 4, 9 – 11]. The main idea of this work was verification of what changes the co-rotating twin-screw extrusion may cause in thermal properties of above mentioned polymer blends as well as polymers used separately. The DSC and TGA methods have been chosen for this purpose. The results may be applied for recycling purposes of mixed plastics, however, in this work the primary polymers have been used to avoid any undesired influence of recycling operations for blends' properties.*

**Keywords:** PE, PP, co-rotating twin-screw extrusion of polymers, polymer composites, thermal properties

### **1. Introduction**

The enhanced interest in application of different compositions of polymers can be observed lately. The analysis of literature reveals that such compositions are thermodynamically immiscible (incompatible) [2 – 4]. It turns out however that the most advantageous content of (MP) positively influencing the properties of (PM) is no more than 15 wt.% to avoid undesirable coalescing phenomena of the (MP) particles at higher concentrations. The advantageous particle size is 1  $\mu\text{m}$ .

It is sometimes estimated that presently 30 % of all produced plastic products are made of polymer mixtures and compositions. The enhancement of this production is of ever growing tendency.

### **2. Objective of the work**

The objective of the present work was to investigate the influence of selected screw configuration of the co-rotating twin-screw extruder type BTSK-20 of very good dispersive – distributive performance on some thermal properties [2 – 4, 10, 11]. The scheme of the segments arrangement has been presented in fig. 1. In spite of practical application for plastics recycling, the

investigation has been conducted using primary granulates of polymers including processing conditions for simulation of the real recycling procedure.

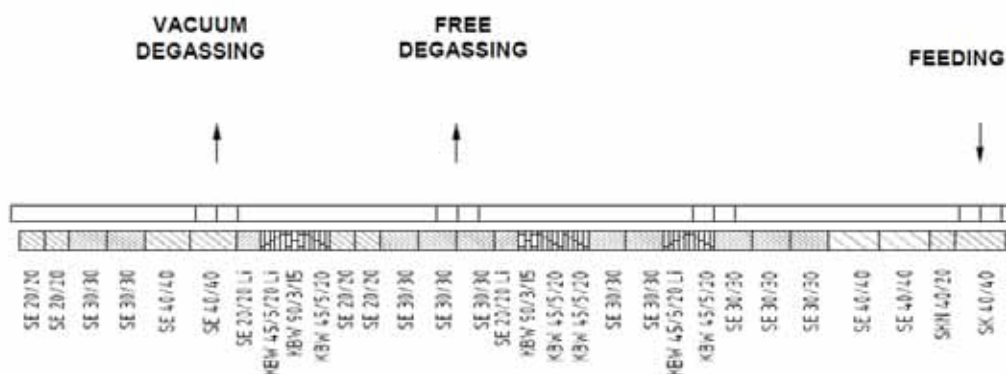


Fig. 1. The scheme of the plasticizing system of the co-rotating twin-screw extruder type BTSK  $\Phi 20 \times 40 D$ : SK – single winding transport segment, SE – double winding transport segment, SKN – transition segment (single-winding), Numbers: 1.Winding pitch, mm, 2.Length of the segment, mm, KBW – kneading segments, Numbers: 1.Angle between eccentric axes, 2.Number of eccentrics, 3.Length of the segment, mm, Letters: direction of the segment inclination: Li – left-handed segment, no letter – right-handed

### 3. Experimental

#### Materials

The polymers that have been chosen for tests were PE and PP of domestic production (Basell Orlen S.A.), of type FGAN 18-D003 and Moplen HP 456J, respectively.

#### Processing conditions

The component polymers were mixed together and processed twice simulating the real recycling procedure of the single component in conditions as follows:

primary granulate  $\rightarrow$  1<sup>st</sup> processing to get the product I  $\rightarrow$  size reduction, cleaning, a.s.o.  $\rightarrow$  2<sup>nd</sup> processing to get the product II

When recycling the single component is subjected to two thermal attacks. The simulation of the above mentioned polymer blends also concerns the two reprocessing steps. The processing temperature all over the heating zones did not exceed 190°C, (both for extrusion and injection molding operation), the usual processing temperature of PP and PE. The products of this recycling procedure were polymer compositions in pelletized form. For better understanding of the idea the primary polymers were also subjected to this above mentioned reprocessing [5 – 8].

The configuration used in this work, consisting of transporting, kneading and returning (braking) segments of strong mixing and dispersive function was thought for good homogenizing effect of polymer blends. The problem relies on using four special left – handed screw segments acting as returning (braking) segments, (marked as Li), situated just before the degassing points that enhance the effectiveness of the mixing function.

### Test methods

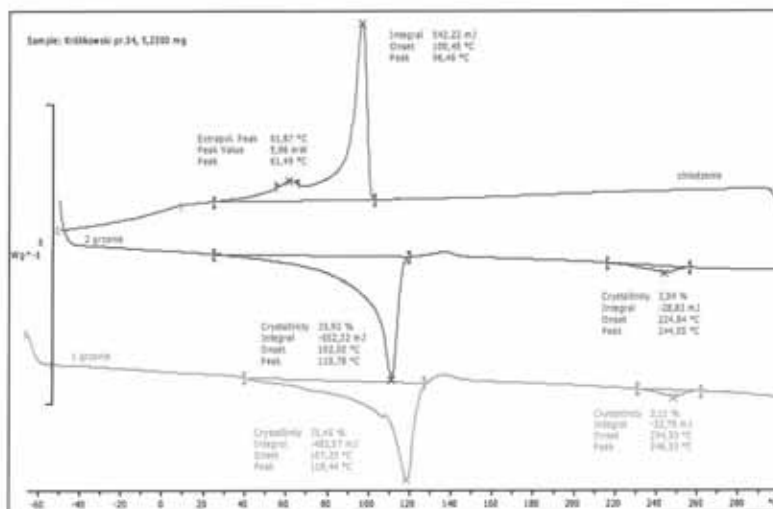
The selected parameters that have been taken into consideration during the investigation were as follows:

- DSC values using Mettler – Toledo calorimeter type DSC 822<sup>o</sup>/700 after PN-EN ISO 11357-1:2002 standard,
- TGA values using thermogravimetric device Mettler – Toledo type TGA/SDTA 851<sup>o</sup>/1100 after PN-EN ISO 11358:2004 standard.

## 4. Results and discussion

The results of investigation have been gathered and presented on figures 2 – 5. They concern results of thermal properties for polymer blends, primary polymers and primary polymers reprocessed with this configuration. The results after selected parameter values give information how far double reprocessing using a selected screw configuration can influence the above mentioned properties of investigated separate polymers as well as in blends compared to primary polymers.

$S_K$  investigation of the mixture PE/PP after DSC shows two separated phases of different crystalline degree (scheme 1). Both polymers PE and PP, being of crystalline structure show strong mutual influence of (PM) on (MP) (fig. 2) depending on what polymer prevails as a polymer matrix. It confirms the immiscibility of PE and PP.



Scheme 1. The example of the run of DSC analysis of a polymer blend showing characteristic parameter values including  $S_K$

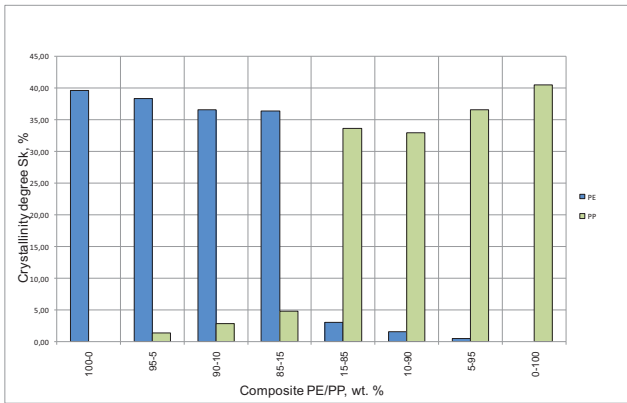
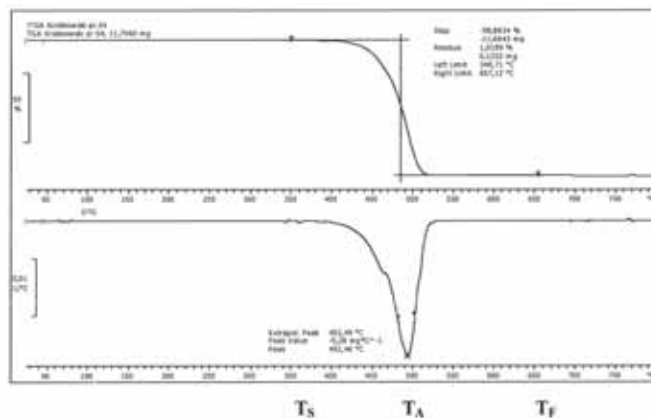


Fig.2. The influence of MP on crystalline degree  $S_K$  of PM after DSC

The thermal results, i.e. melting temperature as well as crystalline degree for single polymers (not presented in the work) show slight changes when reprocessing and may be neglected in further discussion.

The problem of TGA analysis (scheme 2) is shown on figs. 3 and 4 presenting starting  $T_S$  and average  $T_A$  temperatures of blends' decomposition when heating samples up to 600°C.



Scheme 2. The example of the run of the TGA analysis of a polymer blend showing characteristic temperature points

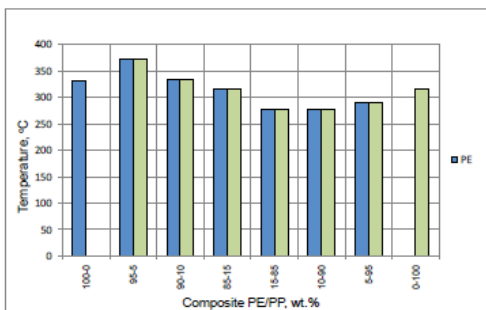


Fig.3. The influence of MP on starting temperature  $T_S$  of decomposition of PM after TGA

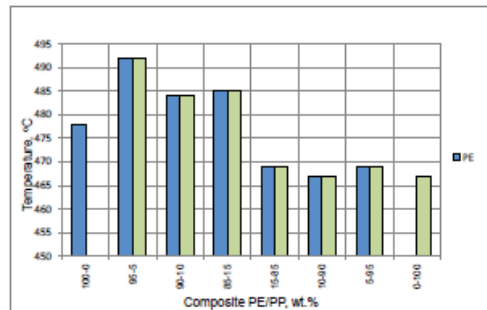


Fig.4. The influence of MP on average temperature  $T_A$  of decomposition of PM after TGA

The diagrams do not show any phase separation. The analysis only confirms the homogenization of the components, not miscibility. The enhancement of  $T_S$  and  $T_A$  in almost all cases of PE/PP compositions may indicate the arising of new fractions shifting both temperatures in higher values. The mixtures PP/PE indicate shifting  $T_S$  and  $T_A$  towards lower temperatures what may indicate quicker decomposition of PP/PE compositions because of PP matrix. The changes in  $T_S$  values are much stronger than in case of  $T_A$  for compositions PE/PP (scale comparison).

On the other hand, the fig. 5 shows the differences in decomposition temperatures  $T_S$ ,  $T_A$  and  $T_F$  for pure separate primary polymers compared to reprocessed ones. Starting temperature may differ by 80°C and final ones even by 150°C.

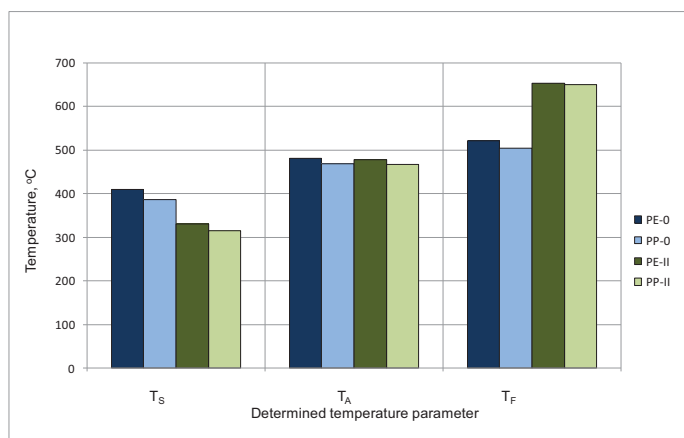


Fig. 5. Comparison of TGA results for primary and reprocessed separate polymers used in the work

The fall of  $T_S$  means that a new polymer fraction of lower decomposition temperature may arise. On the other hand, the increase of  $T_F$  temperature indicates a presence of the new fraction of higher decomposition temperature. The average temperature  $T_A$  however varies very little. So, it may be considered as a resultant temperature for above mentioned polymers and all thermal phenomena arising in polymers when reprocessing. Such great differences are not observed for blends. The changes in above mentioned temperature values vary stronger for PP resin than for PE, indicating higher susceptibility of PP to thermal decomposition and to possible mechanochemical reactions than PE. The same case may concern PE/PP and PP/PE compositions after figs. 3 and 4.

## 5. Conclusions

The conclusions that may be drawn from the above mentioned results are following:

- the thermal behaviour of the tested samples shows immiscibility of both components, however their homogeneity is quite well and they may be processed together,
- in spite of possible formation of different fractions in reprocessed polymers the average as a “resultant” temperature of the blend decomposition ( $T_A$ ) remains almost unaffected,
- the results may be very interesting for the recyclers dealing in processing of recovered plastics, because the presented idea may help to influence the final costs connected with plastics recycling.

Some abbreviations used in the text:

|                                      |   |
|--------------------------------------|---|
| (MP) – minor phase                   | S <sub>K</sub> – crystalline degree       |
| (PM) – polymer matrix                | T <sub>S</sub> – starting TGA temperature |
| PE – low density polyethylene (LDPE) | T <sub>A</sub> – average TGA temperature  |
| PP – polypropylene                   | T <sub>F</sub> – final TGA temperature    |

## References

- [1] Banasiak, A., Sterzyński T., *Morfologia kompozycji polimerowej PP/talk*, Polimery, 2005, **49**, 6, s. 442.
- [2] Bastian, M., *Melting of Polymer Blends In Co-rotating Twin Screw Extruders*, Intern. Polym. Processing, A review, 2001, **16**, s. 124-130.
- [3] Delamare, L., Vergnes, B., *Computation of the Morphological Changes of the Polymer Blend Along the Twin Screw Extruder.*, Polym. Eng. Sci., 1996, **36**, s. 1685-1693.
- [4] Huneault, M.A., Champagne, M.F., Luciani, A., *Polymer Blend Mixing and Dispersion in the Kneading Section of a Twin Screw Extruder*, ibidem, 1996, **36**, s. 1694-1706.
- [5] Jakubowska, P., Sterzyński T., Królikowski B., *Struktura i właściwości mieszaniny polipropylenu z pulweryzowanym PET*, Inż. i Ap. Chem., 2005, **44**, nr 3s, s. 33.
- [6] Jakubowska, P., Sterzyński, T., Królikowski, B., *The Properties of Polyolefins Modified with PET Powder*, J. of Appl. Polymer Sci., 2008, **109**, 3, s. 1993-1999.
- [7] Jurkowski, B., Jurkowska B., *Sporządzanie kompozycji polimerowych*, WNT Warszawa, 1995.
- [8] Królikowski, B., *Wpływ rozdrabniania PET i PE na właściwości mechaniczne oraz termiczne kompozycji polimerowych*, Polimery, 2007, **52**, 10, s. 752 – 759.
- [9] Manas-Zloczower, J., Tadmor, Z., *Mixing and Compounding of Polymers*, Carl Hanser Verlag, Munich, Vienna, New York, 1994, s. 692 – 696.
- [10] Potente, H., Bastian, M., Bergemann, K., Senge, M., Scheel, G., Winkelmann, Th., *Melting of Polymer Blends in Co-rotating Twin Screw Extruder*, ibidem, **16**, 2001, s. 143-150.
- [11] Utracki, L.A., Shi, Z.H., *Development of Polymer Blend Morphology Duri Compounding in a Twin Screw Extruder*, Polym. Eng. Sci., 1992, **32**, s. 1824-1833.

## Acknowledgments:

This research work was supported by Polish Ministry of Education and Science (**Project No. 6170/B/T02/2011/40**).



## INFLUENCE OF COOLING AND LUBRICATION ON SELECTED FEATURES OF GEOMETRICAL STRUCTURE OF SURFACES TURNED AT HIGH CUTTING SPEEDS

Tadeusz Leppert

University of Technology and Life Sciences  
ul. Kordeckiego 20, 85-225 Bydgoszcz, Poland  
e-mail: [tleppert@utp.edu.pl](mailto:tleppert@utp.edu.pl)

### Abstract

*The article presents research results on the influence of cooling and lubrication of the cutting zone as well as an impact of cutting parameters on the surface roughness and material bearing ratio of the roughness profile of a turned 18G2A steel surface. The goal of the research was to determine effects of elimination or reduction of a cooling and lubricating fluid in the process of high speed turning. It has been concluded that in high speed machining conditions, the influence of the used modes of cooling and lubrication in the cutting zone is limited. Eliminating or reducing the quantity of the cooling and lubricating medium in the process of turning does not cause worsening of the geometrical characteristics of a machined surface which, together with environmental reasons, makes dry/MQL machining highly justifiable.*

**Keywords:** cutting, cooling, lubrication; dry cutting; surface roughness

### 1. Introduction

Cooling and lubrication of the cutting zone have a considerable influence on the longevity of tools' cutting edges, dimensional accuracy, characteristics of the surface layer of machined pieces as well as shaping conditions and chip removal from the cutting zone. Because of high costs of cooling and lubricating fluids, their impact on the environment and on machine operators' health, the machining industry more and more often prefers machining without such fluids. This is called dry machining or machining with a minimal quantity of lubrication (MQL machining) [1,3-5,8]. This is further encouraged by the development of tool materials and coatings, and new designs of tools and machining devices. Unfortunately, strict requirements related to dimensional and shape accuracy as well as to surface roughness accompanied by a strong feeling that cooling and lubrication fluids are absolutely necessary effectively block a more widespread use of such machining methods. Their popularity requires an in-depth knowledge of the machining process and optimal cutting parameters for particular materials [7,11].

The need to reduce costs and increase overall manufacturing efficiency caused that high speed machining (HSM) is becoming more and more popular in the industry, especially because machining time constitutes a significant part of the total manufacturing time. There are several definitions of high speed machining. An important factor that allows to regard a particular value of

the cutting speed as high speed machining is a type and characteristics of the machined material [6]. This type of machining has many advantages: high efficiency of removing machining allowance, higher quality of the machined surface, shorter manufacturing time, decreased cutting force, more effective thermal energy transfer through chip removal, decreased deformation of the machined piece and others [10,11,12].

The fact that comparative studies into the influence of cooling and lubrication modes on the geometrical characteristics of surfaces machined at high cutting speeds are far and between justifies the presented research. Its primary aims were to determine the influence of eliminating the cutting fluid (dry machining) or reducing its quantity (MQL) on selected characteristics of the geometrical structure after turning 18G2A steel and to compare these values with those after machining with emulsion.

## 2. Experimental procedure

The research was performed on a CNC turning machine made by A. Monforts Werkzeugmaschinen GmbH & Co, type RNC 400 with the primary drive of 18,5 kW. The machined piece (turned longitudinally) was a pipe made of 18G2A construction steel of higher quality, 75 mm in diameter with a wall thickness of 10 mm and a length of 150 mm. The pipe had 10 mm measurement zones. The choice of steel was dictated by its narrow limits of carbon and manganese content as well as low quantities of impurities, mainly silicon and phosphorus. The chemical composition is shown in table 1.

*Tab.1. Chemical composition of 18G2A steel (PN-H 74245:1996)*

| C   | Mn  | Si      | P           | S           | Cr          | Ni          | Mo | W | V | Al.     | Cu      |
|-----|-----|---------|-------------|-------------|-------------|-------------|----|---|---|---------|---------|
| 0,2 | 1,5 | 0,2-0,5 | max<br>0,04 | max<br>0,04 | max<br>0,03 | max<br>0,03 | -  | - | - | max 0,2 | max 0,3 |

The following modes of cooling and lubrication were used:

- S – no cutting fluid, dry,
- MQL – minimal lubrication with oil fog quantity of  $0,014 \text{ mm}^3/\text{s}$ ,
- E – 14% cutting fluid, based on Super Oil EP emulgating oil by Oilcom, designed for steel and cast iron machining with a  $0,07 \text{ dm}^3/\text{s}$  flow,

The oil fog was made from Acu-Lube LB8000 vegetable oil with a Minibooster MBII device by Acu-Lube (fig.1).

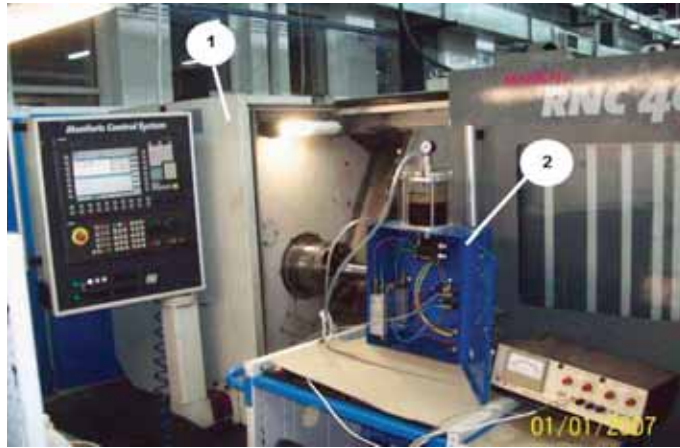


Fig. 1. Workplace, 1- machine, 2- Minibooster II oil fog generator

The cutting tool used in the research was MSS 2525–12-EB produced by Mikrona, with oil fog access channels and interchangeable SNMG 120408TF cutting edges by ISKAR. The edge geometry:  $\gamma_0=5^\circ$ ,  $\alpha_0=10^\circ$ ,  $\chi_r=45^\circ$ ,  $\lambda_s=0^\circ$ ,  $r_\epsilon=0,8$  mm, covered with TiAlN and TiN coating by means of the PVD method.

The turning tests were performed with a complete static program [9] with changeable cutting speed and feed with three value levels and a permanent cutting depth  $a_p$  1 mm. The values assigned to the cutting parameters are presented in table 2.

Tab. 2. Working conditions

| sample No      | 1    | 2    | 3    | 4    | 5    | 6    | 7    | 8    | 9    |
|----------------|------|------|------|------|------|------|------|------|------|
| $v_c$<br>m/min | 418  |      |      | 511  |      |      | 581  |      |      |
| $f$<br>mm/rev  | 0,08 | 0,15 | 0,30 | 0,08 | 0,15 | 0,30 | 0,08 | 0,15 | 0,30 |

The analysis of the influence of cooling and lubrication modes in the cutting zone on the geometrical structure of the machined surface was performed based on measurements of the  $Ra$  parameter and material bearing ratio curves of the surface roughness. The measurements were made on a Hommelwerke T2000 profilographometer, with a M1 DIN-4777 filter and a TK300 sensor with the following parameters: measuring range: 20  $\mu\text{m}$ , measured length: 4,8 mm, elementary measuring length: 0,8 mm, measuring speed: 0,50 mm/s. The measurements were repeated 5 times and mean values were calculated.

### 3. Results and discussion

The results shown in fig. 2 reveal a significant influence of the cooling and lubrication modes of the cutting zone on the measured characteristics of the geometrical structure of the machined

surface, which depended on the employed cutting parameters. In turning at a low feed rate ( $f=0,08$  mm/rev), the influence of cooling and lubrication on the surface roughness was limited. Eliminating the emulsion led to slight decrease of the  $Ra$  parameter value, compared with turning with emulsion whereas the application of MQL resulted in the lowest value of the surface roughness ( $Ra=0,37$   $\mu\text{m}$ ). Along with an increase of the feed rate, the diversification of the  $Ra$  value increased, depending on the cooling and lubrication mode with the relation of the interaction between the conditions of cooling and lubrications maintained. The greatest differences in the values of the  $Ra$  parameters, depending on the cooling and lubrication in the cutting zone, appeared in turning at a feed rate of  $f=0,30$  mm/rev. The limited diversity of the surface roughness values, depending on the cooling and lubrication mode, may have resulted from hindered access of the emulsion/oil fog to the cutting zone at high cutting speeds [4,6]. The lowest values of the  $Ra$  parameter after MQL turning may have come from decreased friction between the moving edge and machined piece surfaces and better conditions of chip creation and removal. The increased roughness after turning with emulsion, compared with dry turning may have resulted from the cooling action of the emulsion which decreased plastic properties of the material with the decrease of the temperature.

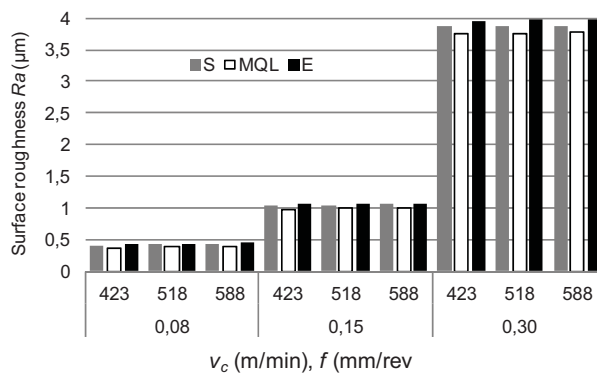


Fig. 2. Influence of cooling and lubrication mode surface layer roughness

Out of all the cutting parameters, the greatest influence on the increase of the  $Ra$  parameter was exerted by the feed rate (fig. 3). The relations between the cooling and lubrication mode and the surface roughness as the feed rate increased showed that the increase in the  $Ra$  parameter value was conditioned by kinematic-stereometric impression of the cutting edge on the machined surface. The influence of the cutting speed on the surface roughness when the speed changed from 423 to 581 m/min was insignificant, which points to relatively comparable cutting conditions in the used range of cutting speeds.

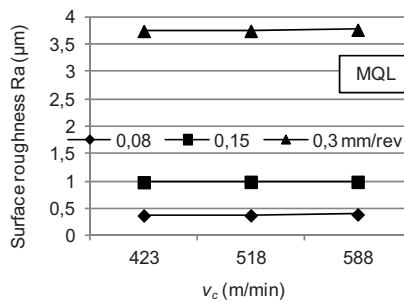
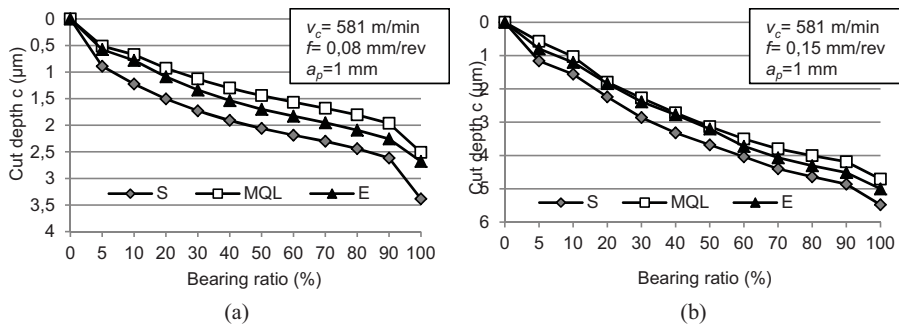


Fig. 3. Influence of cutting speed and feed rate on surface layer roughness in MQL turning

The material bearing ratio is also of great importance due to functional characteristics of the machined surface [2]. The performed research did not reveal any significant influence of the cooling and lubrication mode on the bearing ratio curves and bearing ratio itself in the used range of cutting parameters (fig. 4). Only after turning at a speed of 581 m/min and a feed rate of 0,08 mm/rev (fig. 4a) was it clearly observed that the Abbott-Fireston curve became more diversified. The greatest bearing ratio was observed in surfaces machined in the MQL mode. The height of the roughness profile above the roughness core was smaller than that after turning dry and with emulsion. This points to a greater resistance of the surface layer to wear. A similar shape of the Abbott-Fireston curve was observed after turning with emulsion. The surfaces machined dry had a lower material bearing ratio than the ones mentioned above. The heights above and below the roughness core were greatest and pointed to a lower resistance to wear as well as a greater ability to hold fluid in micro pits below the roughness core. With an increase of the feed rate, the bearing ratio of the machined surfaces decreased and the differences in the shape of the Abbott-Fireston curve became less obvious.



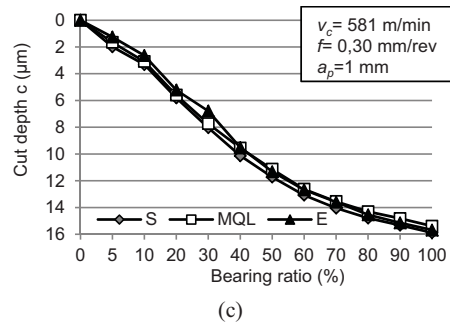


Fig. 4. Influence of cooling and lubrication mode on bearing ratio curve, (a)  $f=0,08$  mm/rev; (b)  $f=0,15$  mm/rev; (c)  $f=0,30$  mm/rev)

The research showed that in the used cooling and lubrication conditions of the cutting zone, the influence of the cutting speed and feed rate on the Abbott-Firestone curve and bearing ratio was similar. The cutting speed did not significantly influence the bearing ratio. An increase in the feedrate caused the Abbott-Firestone curves to diversify in terms of their shape and bearing ratio, which became worse. The dependence of the bearing ratio of the machined surface on the cutting speed and feedrate in MQL turning is presented in fig. 5.

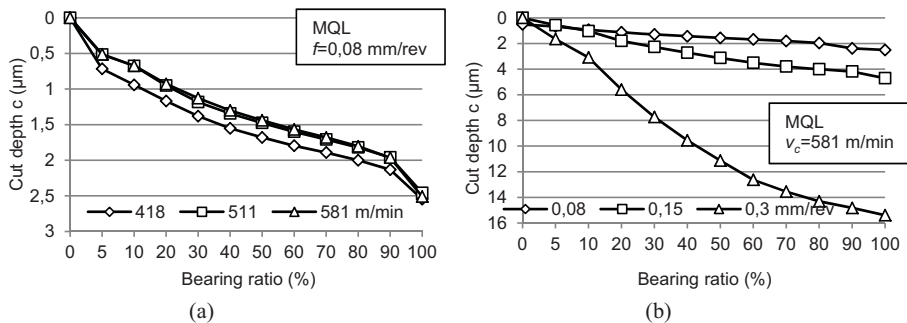


Fig. 5. Influence of cutting speed (a) and feed rate (b) on bearing ratio curve of roughness profile after MQL turning

#### 4. Conclusions

The performed research has revealed that the influence of the cooling and lubrication mode on the geometrical structure of surfaces machined at a wide range of cutting speeds is limited and depends on the used cutting speed and feedrate values. This may result from hindered access of the cooling and lubricating medium to the cutting zone.

In the used range of cutting parameters, the lowest roughness value was observed on surfaces machined in the MQL mode, after dry turning and finally after machining with emulsion. As the feed rate increased, the action of the cooling and lubricating medium increased as well. So did the differences in the roughness values, depending on the cooling and lubricating mode.

The greatest influence on the surface roughness was exerted by the feed rate whereas the influence of the cutting speed on the same parameter was insignificant.

The research did not prove a significant influence of the cooling and lubrication mode on the Abbott-Firestone curve shape nor on the bearing ratio in the used range of the cutting parameters. A greater value of the bearing ratio, compared to other cooling and lubrication modes, was recorded for MQL turning and turning at a speed of 581 m/min and a feed rate of 0,08 mm/rev. The cutting speed did not influence the bearing ratio, which became significantly lower as the feed rate increased.

## References

- [1] Brinksmeier, E., Walter, A., Janssen, R., Diersen, P., *Aspects of cooling lubrication reduction in machining advanced materials*, Proceedings of the Institution of Mechanical Engineers-Part B-Engineering Manufacture, 12/1, vol. 213, pp. 769-779, 1999.
- [2] Cirstoiu, A.C., *Surface roughness evaluation in turning based on Abbott–Firestone curve*, Int. Conference ECAHITECH'10, Bucharest, pp.223-231, 2010.
- [3] Dhar, N.R., Kamruzzaman, M., Ahmed, M., *Effect of minimum quantity lubrication (MQL) on tool wear and surface roughness in turning AISI-4340 steel*, Journal of Materials Processing Technology, 172, pp. 299–304, 2006.
- [4] Dhar, N.R., Ahmed, M.T., Islam, S., *An experimental investigation on effect of minimum quantity lubrication in machining AISI 1040 steel*, Int. J. Mach. Tool Manuf. 47, pp. 748–753, 2007..
- [5] Klocke, F., Eisenblaetter, G., *Dry Cutting*, Annals of the CIRP 46/2, pp. 519 – 526, 1997.
- [6] Lin, W.S., *The study of high speed fine turning of austenitic stainless steel*, J. Achievements Mater. Manuf. Eng. 27/2, pp. 191-194, 2008.
- [7] Machado, A.R., Wallbank, J., *The effect of extremely low lubricant volumes in machining*, Wear 210, pp. 76-82, 1997.
- [8] M'Saoubi, R. M., Outeiro J.C., Chandrasekaran H., Dillon O.W., Jawahir I.S., *A review of surface integrity in machining and its impact on functional performance and life of machined products*, International Journal of Sustainable Manufacturing, Inderscience Publishers, 1 (1/2) pp. 203-236, 2008.
- [9] Polański, Z., *Metody optymalizacji w technologii maszyn*, PWN, Warszawa 1977.
- [10] Sales, F.W., Diniz, A.E., Machado, A.R., *Application of cutting fluids in machining processes*, Journal of the Brazilian Society of Mechanical Sciences 23(2), pp. 227-240, 2001.
- [11] Sreejith, P.S., Ngoi, B.K.A., *Dry machining: Machining of the future*, Journal of Materials Processing Technology, Elsevier, 101, pp. 287-291, 2000.
- [12] Wienert, K., Inasaki, I., Sutherland, J.W., Wakabayashi, T., *Dry machining and minimum quantity lubrication*, Annals of the CIRP 53/2, 511-537, 2004.





## SURFACE LAYER PROPERTIES IN DRY TURNING OF C45 STEEL

Tadeusz Leppert

University of Technology and Life Sciences  
ul. Kordeckiego 20, 85-225 Bydgoszcz, Poland  
e-mail: [tleppert@utp.edu.pl](mailto:tleppert@utp.edu.pl)

### Abstract

*In machining operations cooling and lubrication liquids perform significant technological functions such as reducing temperature of the cutting area and determine machined surface layer characteristics. However their negative ecological effects force the industrial and scientific community to find an alternative means of cooling and lubrication of the cutting zone. The article shows the results of performed experiments of the influence of cooling and lubrication methods on the machined surface layer roughness and bearing ratio after turning C45 steel. The experimental results indicate that in correct chosen cutting parameters, the elimination of cutting liquids does not have to decrease the machined surface quality and makes it possible to reduce ecological burdens imposed by wet machining processes.*

**Keywords:** cutting, cooling, lubrication; dry cutting; surface roughness

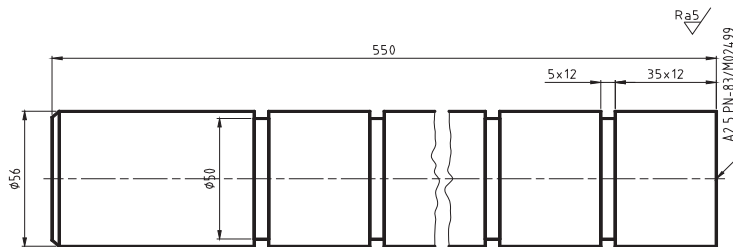
### 1. Introduction

In machining operations cooling and lubrication liquids perform many important functions, mainly reducing temperature of the cutting tool point and work piece as well as removing chips from the machining area. More over liquids influence the tool life, dimension accuracy and machined surface quality. However the ecological awareness of machining processes motivated many scientific investigations, performed in order to determine the results of cutting liquids elimination and replace them with other cutting fluids [1,3,4,6]. The development in cutting tool materials and coatings made it possible to increase of the tool point toughness and resistance to high temperatures required in machining without cooling. Contemporary cutting tool materials enable dry cutting of different work piece materials both in the soft and hardened state [2,6]. Particularly important is the correct selection of tool's substrate and coating which in dry machining should give comparable tool life with that of wet cutting. The optimised cutting point geometry ought to reduce contact surface among tool, chip and work piece in order to minimize cutting friction, which is one of the main factors affecting the tool live and work piece temperature.

Elimination of cutting liquids from machining processes makes it possible to reduce costs associated with coolants purchase, exploitation and maintenance as well as with machining processes. Dry cutting is more environmental friendly and decreases health hazards induced by contact with cutting liquids. Practical applications however make sense when all tools engaged in the machining process can work dry, otherwise an intermittent flow of coolant can lead to numerous cracks and chippings on the cutting edge, which is made of material sensitive to high temperature shocks.

An important issue in dry machining is rapid chips removal from the cutting zone and machine tool. Slow chips disposal may cause a temperature increase of work piece material and machine tool elements, which in turn bring about deterioration of dimensional accuracy and surface layer properties.

## 2. Experimental procedure



The experiments were performed according to the static determined complete program [5]. The selected cutting parameters comprised three levels of cutting speed and feed rate and constant depth of cut  $a_p=1$  mm (tab. 1).

Sintered carbide inserts SPUN 120308 (production of Pramet –Czech Republic) covered by PVD method with (TiAlSi)N coating were employed, fixed in a tool holder CSSPR 20 x 20mm. The following cutting point geometry was applied:  $\gamma_0=5^\circ$ ,  $\alpha_0=10^\circ$ ,  $\chi_r=45^\circ$ ,  $\lambda_s=0^\circ$ ,  $r_\varepsilon=0,8\text{mm}$ . Quoted inserts were recommended for machining of anticorrosive or heat resistance steels as well as soft steels machined with medium cutting speeds. The influence of the cutting tool wear on investigated factors was minimized by changing the cutting edge for each specimen.

Mineral oil ARTEkat Super VG-32 consists of highly refined mineral oil with lubricity increasing additives in concentration of 9-11 %, designed for turning, milling, drilling and other operations of machining steel, and cast iron.

Measurements of surface finish parameters:  $Ra$  and the profile bearing ratio were performed on a profilographometer Hommel-Tester T2000 with Tk300 sensor and the following parameters: evaluation length 4,8 mm, sampling length 0,8 mm. Tests were repeated 5 times and then the mean values determined.

### 3. Results and discussion

Experimental results indicated a substantial relationship between cutting conditions and geometrical properties of the surface layer. The influence of feed rate exceeded that of cutting speed, and at constant feed rates an increase of cutting speed caused a decrease of surface roughness parameter  $Ra$  or its value remained on the same level (fig. 2, 3).

At the feed rate of 0,08 mm/rev and in the used range of cutting speed, the biggest differences of  $Ra$  parameter appeared at  $v_c=120$  m/min. The differences of  $Ra$  during turning with application of emulsions as well as with dry cutting were insignificant. A better surface finish was achieved when compressed air was engaged. The use of oil caused an increase of surface roughness. At the feed rate of 0,27 mm/rev and cutting speed of 76 m/min compressed air reduced values of surface roughness. At a speed range of 120 to 237 m/min and feed rate 0,27mm/rev the best surface finish was obtained using the ARTEkat Super VG-32 oil. The other methods of applying cutting fluids led to much the same results. A further increase of feed rate to 0,47mm/rev did not bring about significant differences in surface finish when cutting dry or with emulsion. The application of compressed air in these conditions produced an increase of surface roughness. On the contrary the application of non emulsifying oil brought the best results.

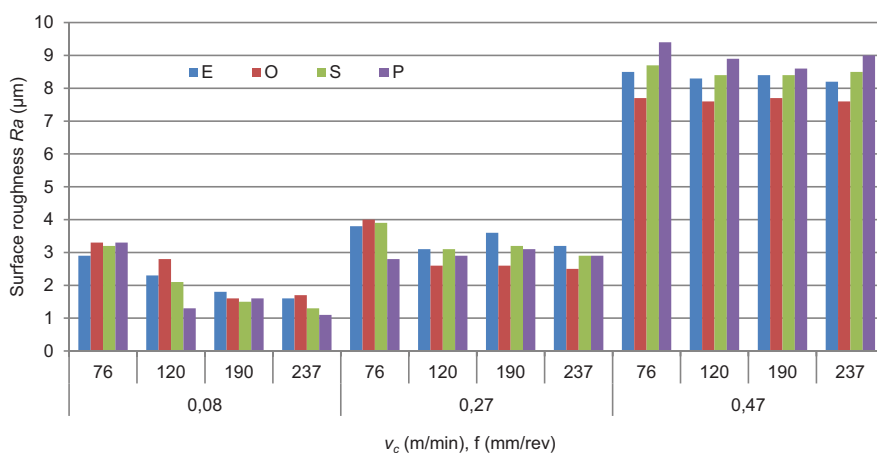


Fig. 2. Influence of cooling and lubrication conditions on surface roughness

The experiments showed that with the increase of speed, differences in surface roughness between dry cutting and with application of cutting liquids undergo diminishing tendency, especially when using small feed rates. An increasing pressure on the chip-tool point interface, at the higher speeds and feed rates, made the penetration of cutting liquids between rubbing surfaces of chip and tool point difficult or at least restricted at the same time reducing their lubricating effect and a positive influence on the surface finish. A higher cutting zone temperature in dry

cutting facilitated the chip formation and separation and reduced material cutting resistance. The influence of the disturbing cutting process factors on the theoretical surface finish, ensuing from the geometric and kinematical reproduction of the tool point on the machined surface was also restricted [3,6].

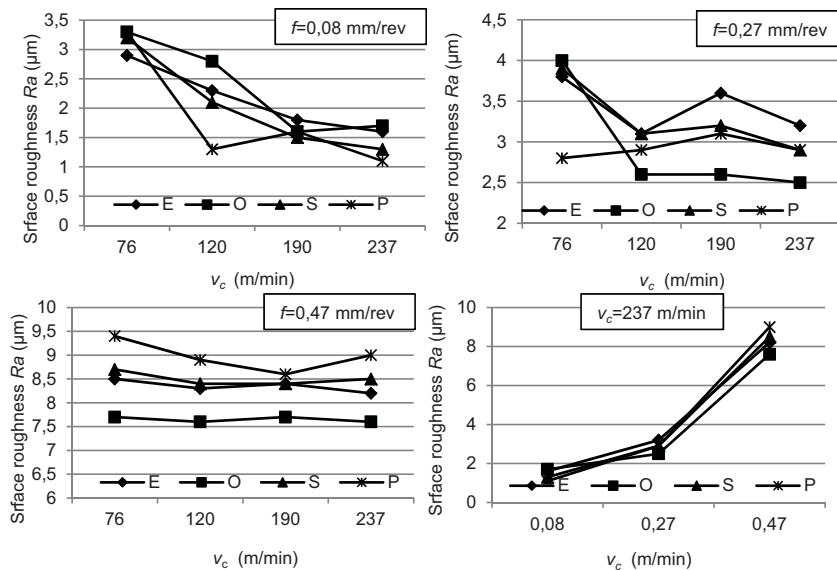


Fig. 3. Influence of cooling and lubrication on: surface roughness  $R_a$

The increase of cutting speed at low feed rate made the influence of applied liquids on the quality of machined surfaces less significant, what could indicate on lack of reasons for their usage in finish turning of C45 steel. The reduction of surface roughness in the case of turning with the ARTEkat Super VG oil in increased feed rates could be due to the oil lubricating qualities and the used additives in its composition.

The positive impact of compressed air in the range of small speeds and feeds indicated on the existence of advantageous distribution of temperature in the cutting zone, which made the generated chips shorter and easier to transfer from the cutting area. The compressed air due to reduced cooling capacity did not induce such a temperature lowering effect in the tool-work piece interface as emulsion or oil, which could facilitate the separation of chip from the machined material and increase of surface finish. Therefore at lower cutting speeds and feed rates it seems advisable to apply compressed air as a factor improving dry cutting process and chip disposal. The increase of speed and feed rate limited positive effect of compressed air on surface roughness.

The investigations did not reveal any significant impact of applied cutting fluids on the surface roughness profile shape (fig. 4) and the bearing ratio (fig. 5, 6). The digressive-progressive shape of the surface bearing ratio curves indicated small values of core roughness depth and reduced peak height. The reduced valley depth values exceeded the peak height, which pointed out to a good load bearing capacity, wear ability and oil retaining capability of the machined surfaces.

An increase of the cutting speed did not only reduce the surface roughness but also contributed to the improvement of the surface bearing ratio (fig. 5). With an increase of feed rate a negative change in the profile bearing ratio occurred which caused a reduction of surface bearing ratio (fig. 6). The lower feed rate contributed to an increase in the bearing ratio especially after turning with compressed air. The shape of the profile bearing ratio curves after turning with emulsion and oil were similar depending on the applied feed rate.

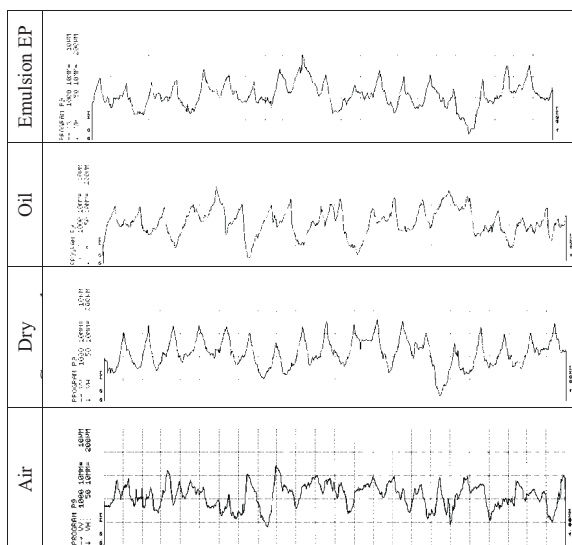


Fig. 4. Profilogram of surface roughness:  $V_c=76$  m/min,  $f=0,27$  mm/rev

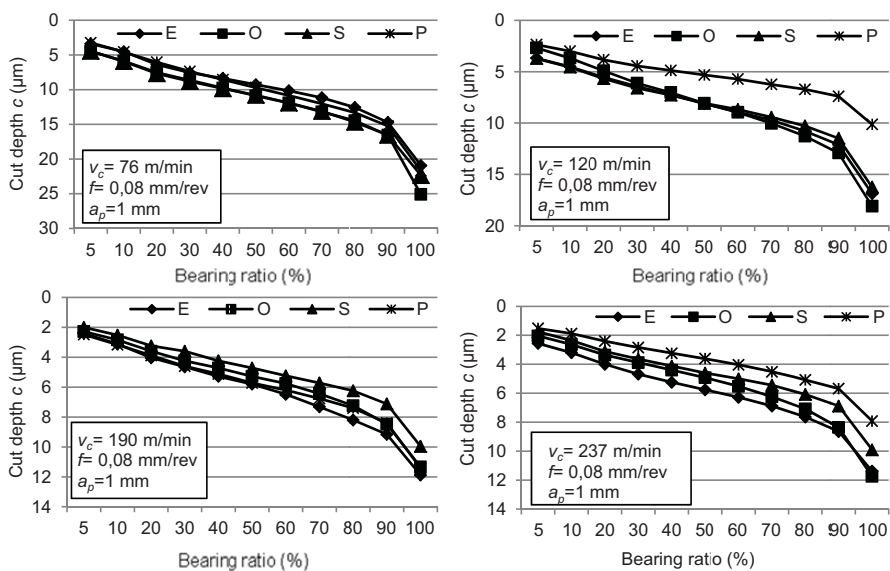


Fig. 5. Influence of cooling, lubrication and cutting speed on surface bearing ratio

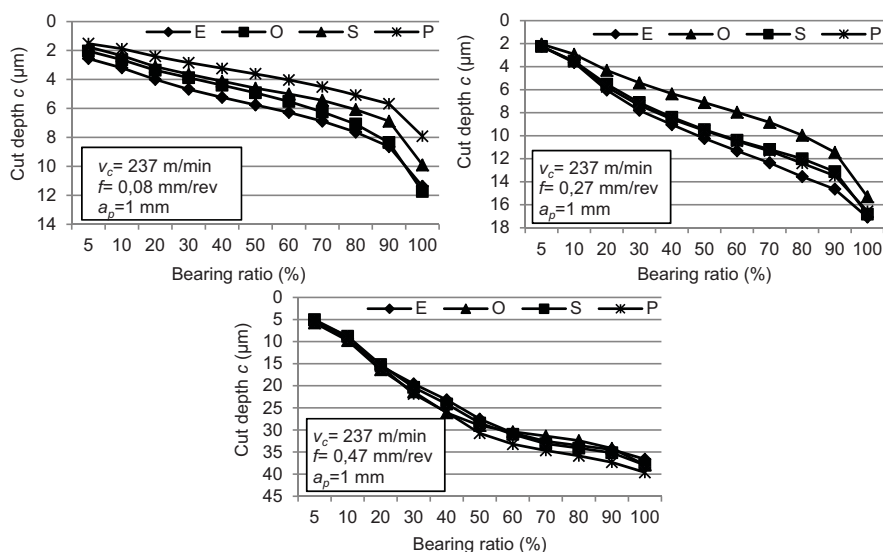


Fig. 6. Influence of cooling, lubrication and feed rate on surface bearing ratio

#### 4. Conclusions

The experiments confirmed a significant influence of cutting parameters on geometric characteristics of a machined surface. The largest influence is exerted by feed rate, and with constant feed rate, the increase of cutting speed caused a reduction of surface roughness and bearing ratio or they remain on near the same level.

Differences between particular surface roughness values depending on cutting fluids were not significant, especially in the range of small cutting feed rates. It is possible to obtain in dry turning of C45 steel comparable surface geometrical characteristics to that of wet machining.

The application of compressed air in the range of low cutting speeds and feed rates influenced favourably geometrical surface parameters in dry turning and can support cutting process and chip disposal.

The applied methods of cooling and lubrication did not show a significant influence on the shape and bearing ratio of surface roughness profile. With the increase of feed rate the bearing ratio underwent negative changes.

#### References

- [1] Avila R.F., Abrao A.M., *The effect of cutting fluids on the machining of hardened AISI 4340 steel*, Journal of Materials Processing Technology, 119 (2001), 21-26
- [2] Byrne G., Dornfeld D., Denkena B., *Advancing cutting technology*, Annals of the CIRP 52/2/2003 483-507.
- [3] Diniz A. E., Micaroni R., *Cutting conditions for finish turning process aiming: the use of dry cutting*, International Journal of Machine Tools & Manufacture 42 (2002) 899-904.
- [4] Machado A.R., Wallbank J., *The effect of extremely low lubricant volumes in machining*, Wear 210 (1997) 76-82.
- [5] Polański Z., *Metody optymalizacji w technologii maszyn*, PWN Warszawa 1977
- [6] Vieira J.M., Machado A.R., Ezugwu E.O., *Performance of cutting fluids during face milling of steels*, Journal of Materials Processing Technology 116 (2001) 244-251.



## INFLUENCE OF STRESS AND STRAIN CONTROL ON CYCLIC PROPERTIES OF AW-2017A ALUMINIUM ALLOY

Bogdan Ligaj

*University of Technology and Life Sciences in Bydgoszcz, Faculty of Mechanical Engineering,  
Department of Machine Design, ul. Prof. S. Kaliskiego 7, 85-789 Bydgoszcz, Poland  
phone number: +48 52 340 82 53, fax: +48 52 340 82 71  
e-mail: bogdan.ligaj@utp.edu.pl*

### Abstract

*The work presents test results of aluminium alloy AW-2017A in variable constant amplitude loading conditions with the cycle asymmetry coefficient  $R = -1$ . Tests were performed independently for stress and strain control. Obtained test results enabled to determine Manson-Coffin (M-C) and Wöhler (W) fatigue life curves as well as Ramberg-Osgood (R-O) cyclic strain curve. The aim of the paper is to present differences between M-C and W fatigue characteristics determined in stress and strain conditions. Differences between mentioned characteristics were evaluated on the base of a relative difference. In case of Wöhler (W) curves the value of differences depends on the stress amplitude level  $S_a$  and it is between -1.0 to 1.9.*

**Keywords:** low-cycle fatigue, diagrams of fatigue life, AW-2017A aluminium alloy.

### Nomenclature

- $2N_f$  – the number of reversals to failure,  
 $N_{(s)}$  – fatigue life read from Wöhler curve determined with stress controlled conditions for defined value of stress  $S_a$ ,  
 $N_{(\varepsilon)}$  – fatigue life read from Wöhler curve determined with strain controlled conditions for defined value of stress  $S_a$ ,  
 $S$  – specimen stress – general notation [MPa],  
 $S_a$  – sinusoidal cycle stress amplitude [MPa],  
 $S_{a(\varepsilon)}$  – stress amplitude read from Ramberg-Osgood cyclic strain curve determined with strain controlled conditions for defined  $\varepsilon_{ac}$  value [MPa],  
 $S_{a(\sigma)}$  – stress amplitude read from Ramberg-Osgood cyclic strain curve determined with stress controlled conditions for defined  $\varepsilon_{ac}$  value [MPa],  
 $\varepsilon$  – strain – general notation,  
 $\varepsilon_{ac}$  – total strain amplitude,  
 $\varepsilon_{ac(\varepsilon)}$  – total strain amplitude read from Manson-Coffin curve with strain controlled conditions for the defined number of reversals of loading  $2N_f$ ,  
 $\varepsilon_{ac(\sigma)}$  – total strain amplitude read from Manson-Coffin curve with stress controlled conditions for the defined number of reversals of loading  $2N_f$ ,  
 $\delta_{(S_a)}$  – relative difference of stress amplitude value for Ramberg-Osgood curves determined with stress and strain controlled conditions,

- $\delta_{(e)}$  – relative difference of total strain amplitude value for Manson-Coffin curves determined with stress and strain controlled conditions,
- $\delta_{(N)}$  – relative difference of fatigue life for Wöhler curves determined with stress and strain controlled conditions.

## 1. Introduction

Fatigue life calculations of structural elements in variable loading conditions are performed with an application of fatigue life curves: Wöhler (W) or Manson-Coffin (M-C). In the range of high cycle fatigue (HCF) life the Wöhler curve is applied while in the range of low cycle fatigue life the Manson-Coffin one. The mentioned W and M-C curves are determined in variable test conditions. The first of them is determined in stress controlled conditions ( $S_a = \text{const.}$ ) whereas the second one in strain controlled conditions ( $\epsilon_{ac} = \text{const.}$ ) [2].

In the work [4] there were presented results of C45 steel (softening-hardening steel,  $R_m/R_e = 1.6$ ) performed on plain steel specimens in strain and stress controlled conditions. The comparative analysis between Wöhler and Manson-Coffin fatigue life curves was performed. Differences of fatigue lives between W curves for stress and strain control are: for  $S_a = 550 \text{ MPa}$  –  $\delta_{550} = 21.6 \%$ , for  $S_a = 250 \text{ MPa}$  –  $\delta_{250} = -36.1 \%$ . In case of M-C curves fatigue life differences are: for  $\epsilon_{ac} = 0.03$  –  $\delta_{0.03} = 51.4 \%$ , for  $\epsilon_{ac} = 0.0015$  –  $\delta_{0.0015} = -190.1 \%$ . Concluding the author points relatively small differences between fatigue life curves W and M-C determined in  $S_a = \text{const.}$  and  $\epsilon_{ac} = \text{const.}$  conditions what enables their interchangeable application.

The goal of the work [3] was to compare Ramberg-Osgood (R-O), Wöhler and Manson-Coffin curves determined in stress and strain controlled conditions. There was tested austenitic steel X5CrNi18-10 (steel that undergo cyclic hardening,  $R_m/R_{0.2} = 2.0$ ) and tests were performed on plain specimens. Relative differences among R-O, M-C and W characteristics were presented as diagrams and the range of their changes is: for R-O –  $\delta_{(S_a)} = -0.15 \div 0.16$ , for M-C –  $\delta_{(e)} = -0.20 \div -0.02$ , for W –  $\delta_{(N)} = -0.90 \div 0.55$ . In the summary authors indicate that the value of differences is connected with the type of material and the value of stress amplitudes  $S_a$  or the total strain amplitude  $\epsilon_{ac}$ .

On the base of works [3] and [4] one can state that differences among R-O, M-C and W curves are connected with cyclic properties of a material. Therefore the aim of this work is the evaluation of values of relative differences among R-O, M-C and W characteristics determined in stress controlled ( $S_a = \text{const.}$ ) and strain controlled ( $\epsilon_{ac} = \text{const.}$ ) conditions for AW-2017A aluminium alloy.

The scope of the work covers the presentation of test results in static and variable loading conditions and the comparative analysis of Ramberg-Osgood, Manson-Coffin and Wöhler curves.

## 2. Experimental tests

### 2.1. Material for test

For tests there was assumed magnesium and copper aluminium alloy AW-2017A (alloy indication AlCu4MgSi (A)) in accordance with PN-EN 573-3:2010 and PN-EN 573-3/AK:1998 standards. Increased constituents of copper and magnesium in the alloy results in increase of strength properties and decrease of plastic properties [1]. Chemical composition of the alloy and percentage of individual constituents was presented in tab. 1.

Material for specimens was bought in a form of a round bar with 25 mm diameter. Material condition was defined as T4 what indicates that aluminium alloy undertook solution heat treatment and aging to obtain stable state.

Table 1. Chemical composition of AW-2017A T4 aluminium alloy

|                                      | Percentage of constituents, % |     |         |         |         |      |     |     |      |             |
|--------------------------------------|-------------------------------|-----|---------|---------|---------|------|-----|-----|------|-------------|
|                                      | Cu                            | Fe  | Si      | Mn      | Mg      | Zn   | Cr  | Ni  | Ti   | Inne        |
|                                      |                               | max |         |         |         | max  | max | max | max  |             |
| In accordance with PN-EN 573-3: 2010 | 3.5÷4.5                       | 0.7 | 0.2÷0.8 | 0.4÷1.0 | 0.4÷1.0 | 0.25 | 0.1 | 0.1 | 0.15 | Zr+Ti ≤ 0.2 |

## 2.2. Test results in static loading conditions

Tests in static loading conditions were performed in accordance with PN-EN ISO 6892-1:2010 standard. Obtained test results are included in table 2 where mean values as well as standard deviations of determined parameters are given. The exemplary course of  $S = f(\epsilon)$  dependance was presented in fig. 1a. Additionally there was presented a fragment of dependance  $S = f(\epsilon)$  for the limited strain range ( $\epsilon = 2\%$ ) in order to present the shape of characteristic in the range of elastic limit (fig.1b). The value of relation  $R_m/R_e = 1.48$ .

Table 2. Static properties of AW-2017A alloy in tensile loading conditions

|                           | Static properties of AW-2017A alloy |           |       |       |       |      |
|---------------------------|-------------------------------------|-----------|-------|-------|-------|------|
|                           | $R_e$                               | $R_{0.2}$ | $R_m$ | E     | $A_5$ | Z    |
|                           | MPa                                 | MPa       | MPa   | MPa   | %     | %    |
| Mean values               | 316.7                               | 320.1     | 469.5 | 73077 | 16.1  | 23.0 |
| Standard deviation values | 1.3                                 | 0.6       | 4.5   | 1304  | 0.8   | 0.8  |

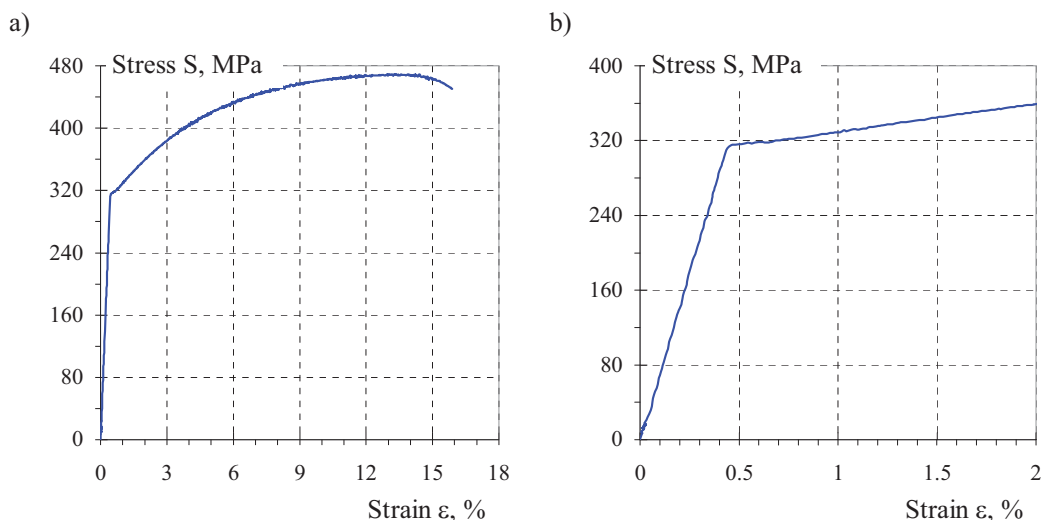


Fig. 1. The exemplary dependance  $S = f(\epsilon)$  for aluminium alloy AW-2017A (a) and its fragment limited to  $\epsilon = 2\%$  (b)

## 2.3. Cyclic properties of aluminium alloy in stress and strain controlled conditions

Tests of steel cyclic properties under stress and strain control was performed in sinusoidal loading conditions characterized by the cycle asymmetry coefficient  $R = -1$ . Realization of a loading cycle was performed in accordance with the scheme presented in fig. 2. In tests tere were applied specimens with 10 mm diameter and meseasurement base length 18 mm that fulfill requirements of PN-84/H-04334 standard.

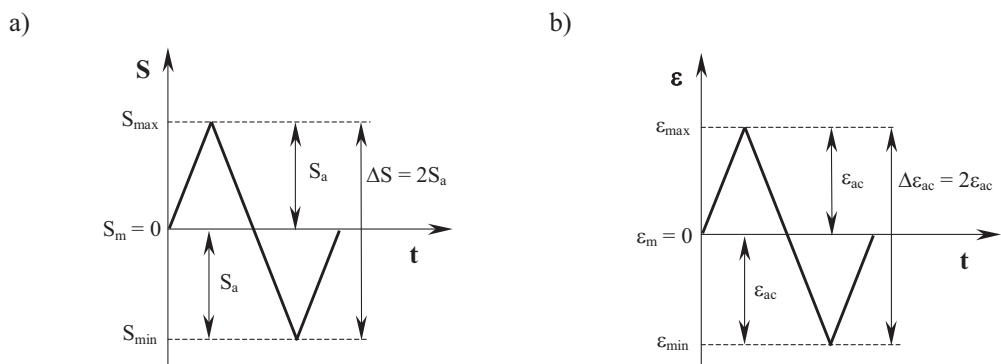


Fig. 2. Loading cycle scheme applied in fatigue tests with control: a – stress, b – strain

Obtained fatigue test results enabled to determine Ramberg-Osgood ( $S_a$ - $\epsilon_{ac}$ ) cyclic deformation curve described with the formula:

$$\epsilon_{ac} = \frac{S_a}{E} + \left( \frac{S_a}{K'} \right)^{\frac{1}{n'}} \quad (1)$$

Manson-Coffin fatigue life curve ( $\epsilon_{ac}$ - $2N_f$ )

$$\frac{\Delta \epsilon_{ac}}{2} = \epsilon_f' (2N_f)^c + \frac{\sigma_f'}{E} (2N_f)^b \quad (2)$$

and Wöhler fatigue life curve ( $S_a$ - $N$ )

$$\log S_a = -\frac{1}{m_{(-1)}} \log N + b_{(-1)} \quad (3)$$

Values of parameters appearing in equations (1), (2) and (3) were presented in the table 3.

Table 3. Parameters of equations describing Ramberg-Osgood, Manson-Coffin and Wöhler curves for AW-2017A aluminium alloy

|                               |     |               |     | Test conditions                             |   |
|-------------------------------|-----|---------------|-----|---|---|
|                               |     |               |     | Stress-controlled ( $S_a = \text{const.}$ ) | Strain-controlled ( $\epsilon_{ac} = \text{const.}$ ) |
| Equation parameters of curves | M-C | E             | MPa | 73077                                       | 73077   |
|                               |     | c             |     | -1.1871                                     | -1.3979   |
|                               |     | b             |     | -0.1091                                     | -0.0737   |
|                               |     | $\epsilon_f'$ |     | 2.406                                       | 12.505  |
|                               |     | $\sigma_f'$   | MPa | 836   | 632   |
|                               | R-O | $n'$          |     | 0.0741                                      | 0.0514  |
|                               |     | $K'$          | MPa | 640   | 556   |
|                               | W   | $m_{(-1)}$    |     | 8.64  | 13.79   |
|                               |     | $b_{(-1)}$    |     | 2.9230                                      | 2.7817  |

### 3. Analysis of test results

Evaluation of obtained test results strain and stress controlled conditions was based on the comparative analysis of Ramberg-Osgood, Manson-Coffin and Wöhler curves that led to determine differences of relative values.

Analysis of Ramberg-Osgood cyclic deformation was conducted on the base of relative difference of amplitudes of nominal stress  $\delta_{(S_a)}$  determined from the equation:

$$\delta_{(S_a)} = \frac{S_{a(\sigma)} - S_{a(\varepsilon)}}{S_{a(\varepsilon)}} \quad (4)$$

Results of amplitudes  $S_{a(\sigma)}$  and  $S_{a(\varepsilon)}$  were read from the Ramberg-Osgood curve for  $\varepsilon_{ac}$  specific values. Strain-controlled test results were a reference point in the conducted analysis.

Comparison of Mason-Coffin fatigue life curves was conducted on the base of the analysis of difference value of relative total strain amplitude  $\delta_{(\varepsilon_{ac})}$  determined from the equation:

$$\delta_{(\varepsilon)} = \frac{\varepsilon_{ac(\sigma)} - \varepsilon_{ac(\varepsilon)}}{\varepsilon_{ac(\varepsilon)}} \quad (5)$$

Values of total strain amplitudes  $\varepsilon_{ac(\sigma)}$  and  $\varepsilon_{ac(\varepsilon)}$  were read from the Mason-Coffin curve for specific values of the number of reversals of loading  $2N_f$ . Strain-controlled test results were a reference point in the conducted analysis.

Differences among test results, shown in a form of Wöhler curves for stress and strain-controlled conditions, were analyzed on the base of a value of relative difference of fatigue lives  $N$  calculated from the equation:

$$\delta_{(N)} = \frac{N_{(\sigma)} - N_{(\varepsilon)}}{N_{(\varepsilon)}} \quad (6)$$

Values of fatigue life  $N_{(s)}$  and  $N_{(\varepsilon)}$  were read from Wöhler curves for specific value of stress amplitude  $S_a$ . Strain-controlled test results were a reference point in the conducted analysis.

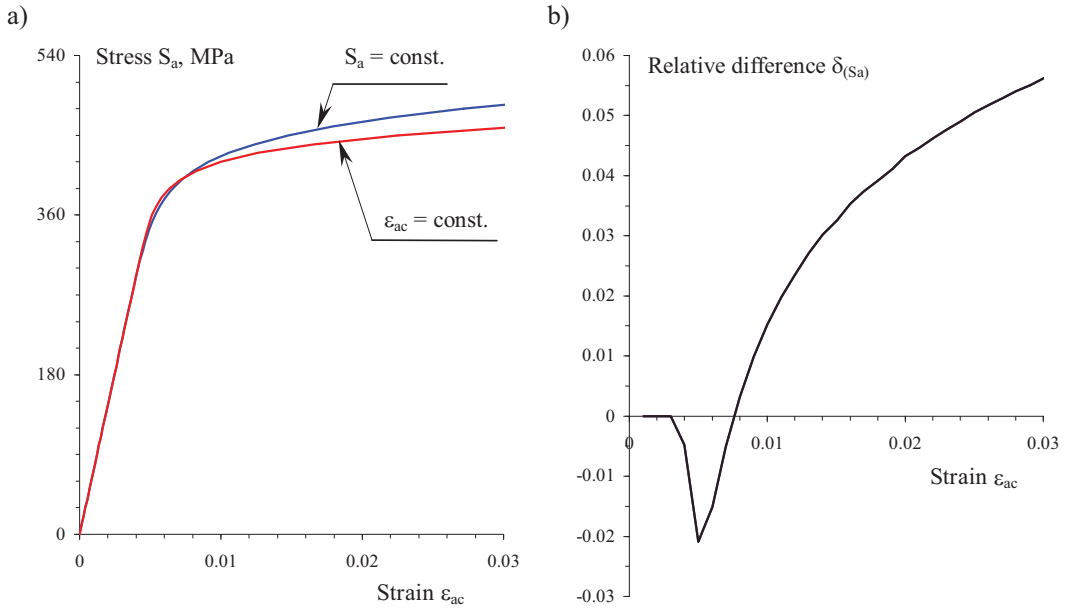


Fig. 3. Comparison of Ramber-Osgood cyclic hardening curves in stress and strain controlled conditions (a) leading to determination of relative difference of nominal stress amplitude  $S_a$  (b)

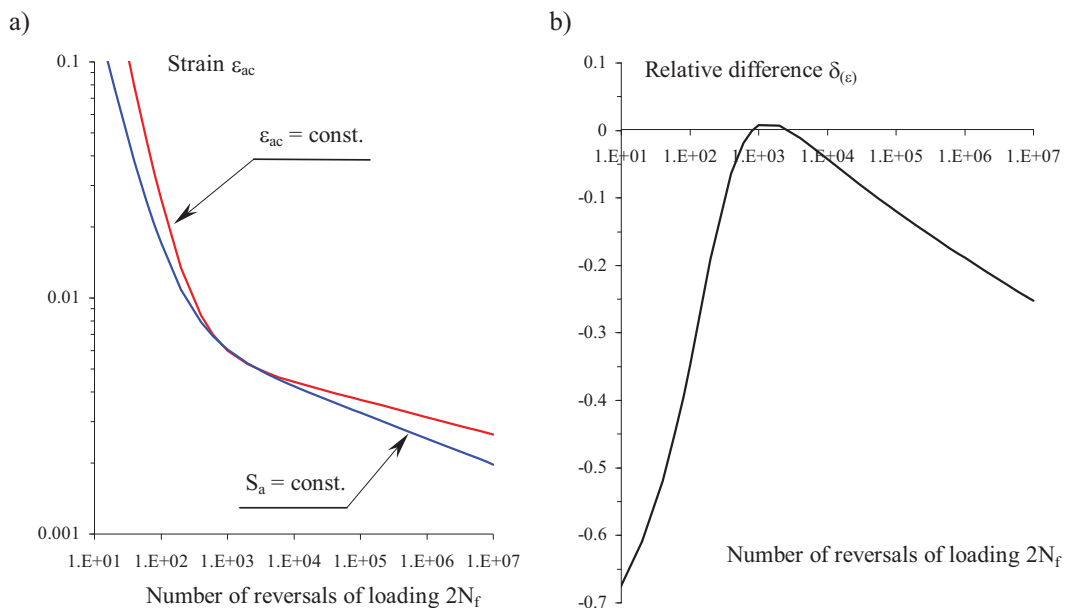


Fig. 4. Comparison of Mason-Coffin fatigue life curves in stress and strain controlled conditions (a) leading to determination of relative difference of total strain amplitude  $\epsilon_{ac}$  (b)

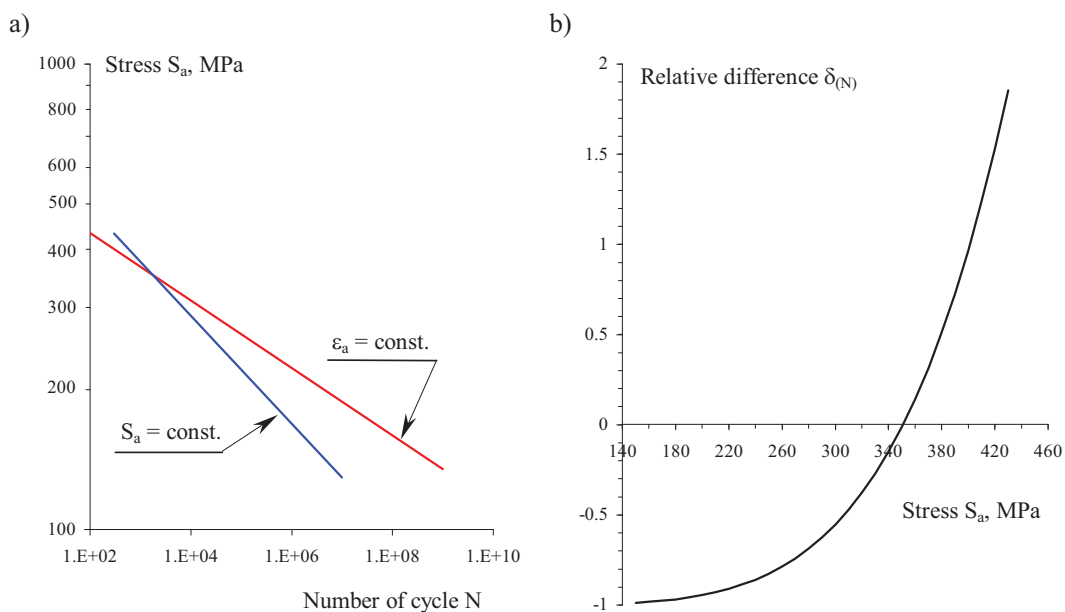


Fig. 5. Comparison of Wöhler fatigue life curves in stress and strain controlled conditions (a) leading to determination of relative difference of number of cycles  $N$  (b)

In fig. 3a there were presented test results in the form of R-O curves determined in stress controlled ( $S_a = \text{const.}$ ) and strain controlled ( $\epsilon_{ac} = \text{const.}$ ) conditions. Mutual position of curves indicates their high conformity. It is confirmed by the diagram of relative value difference of stress

amplitude  $\delta_{(S_a)}$  that was presented in fig. 3b. In the range of  $\varepsilon_{ac} < 0.003$  curves of R-O indicates high conformity ( $\delta_{(S_a)} = 0$ ). In the range from  $\varepsilon_{ac} = 0.003$  to  $\varepsilon_{ac} = 0.0077$  the curve for  $\varepsilon_{ac} = \text{const.}$  is characterized by higher values of  $S_a$ . Maximum value of relative difference is  $\delta_{(S_a)} = -0.021$ . In the range of  $\varepsilon_{ac} \geq 0.0077$  the curve R-O determined for  $S_a = \text{const.}$  is characterized by higher values of  $S_a$ . Maximum value of relative difference is  $\delta_{(S_a)} = 0.056$ .

Mutual position of Mason-Coffin fatigue life curves for stress and strain control is presented in fig. 4a whereas values of relative difference determined from the formula (5) in fig. 4b. For the range of number of reversals  $2N_f < 800$  and  $2N_f > 2100$  higher values of total strain amplitude  $\varepsilon_{ac}$  are connected with the fatigue life curve obtained in strain controlled conditions. The highest values of relative difference were obtained for  $2N_f = 10^1$  ( $\delta_{(\varepsilon)} = -0.67$ ) and for  $2N_f = 10^7$  ( $\delta_{(\varepsilon)} = -0.25$ ). For the range of reversals  $800 < 2N_f < 2100$  there were obtained higher values  $\varepsilon_{ac}$  for  $S_a = \text{const.}$  Value of relative difference is  $\delta_{(\varepsilon)} \approx 0.008$ .

In fig. 5a there is presented mutual position of Wöhler curves that were determined in dynamic and kinematic controlled conditions. Determined values of relative difference  $\delta_{(N)}$  (fig. 5b) for the analyzed range of stress amplitude changes  $S_a$ , limit from  $\delta_{(N)} \approx -1.0$  (dla  $S_a = 150$  MPa) to  $\delta_{(N)} \approx 1.9$  (dla  $S_a = 430$  MPa). Fatigue life curves cross in a point that refers to a value of  $S_a = 350$  MPa. For the value  $S_a < 350$  MPa the curve determined in conditions of  $\varepsilon_{ac} = \text{const.}$  is characterized by higher values of fatigue life  $N$  whereas for  $S_a > 350$  MPa higher values of  $N$  were obtained for the curve determined for  $S_a = \text{const.}$

#### 4. Summary

Performed analysis of test results of AW-2017A aluminium alloy enables to formulate following remarks:

- a. Comparative analysis of R-O, M-C and W curves determined in stress ( $S_a = \text{const.}$ ) and strain ( $\varepsilon_{ac} = \text{const.}$ ) controlled conditions indicated ranges of changes of relative values that are for:
  - cyclic strain curves wykresów R-O:  $\delta_{(S_a)} = -0.021 \div 0.056$ ,
  - fatigue life curves M-C:  $\delta_{(\varepsilon)} = -0.67 \div 0.008$ ,
  - fatigue life curves W:  $\delta_{(N)} = -1.0 \div 1.9$ .
- b. Curves of relative differences ( $\delta_{(S_a)}$ ,  $\delta_{(\varepsilon)}$ ,  $\delta_{(N)}$ ) for AW-2017A aluminium alloy are characterized by similar change of values as for X5CrNi18-10 austenitic steel [3]. Concurrence of results can be caused by similar cyclic properties of mentioned alloys because the materials can be classified as the ones that undergo cyclic hardening.

#### References

- [1] Dobrzański L.A., *Metal engineering materials*, WNT, Warszawa, 2004.
- [2] Kocańda S., Szala J., *Fundamentals of fatigue calculations, (in Polish)*, PWN, Warszawa 1997.
- [3] Ligaj B., Szala G., *The comparison of cyclic properties of X5CrNi18-10 steel in the range of low-cycle fatigue in conditions of stress and strain control*, Fatigue Failure and Fracture Mechanics, Trans Tech Publications, Switzerland, 2012.
- [4] Szala G., *Comparative analysis of cyclic properties of metals obtained conditions of stress and strain range diversification control on the example of C45 steel*, Journal of Polish CIMAC, vol.6, no.3, 2011, pp. 305-312.

**Note: This work has been elaborated in the frame of the project No. 2221/B/T02/2010/39 financed by Polish Ministry of Sciences and Higher Education.**





## EVALUATION OF THE SELECTED FACTORS EFFECT ON THE FATIGUE LIFE OF SPECIMENS WITH SIZED AND RIVETED HOLE PART I. DESIGN OF EXPERIMENT AND TESTS RESULTS

Adam Lipski

*University of Technology and Life Sciences in Bydgoszcz*  
*Faculty of Mechanical Engineering*  
*Al. Prof. S. Kaliskiego 7, 85-789 Bydgoszcz, Poland*  
*tel.: +48 52 3408220, fax: +48 52 3408271*  
*e-mail: adam.lipski@utp.edu.pl*

### **Abstract**

*Evaluation of the fatigue load, the rivet squeezing force, the velocity of rivet close up and the hole diameter before sizing (after drilling) effect on the fatigue life of specimens with sized and riveted hole was presented in this paper. The work contains two parts. Design of experiment and the results of the fatigue tests performed by the described experiment plan was presented in the first part. The statistical analyses and examples of using the mathematical model of the experimental unit were presented in the second part.*

**Keywords:** riveted joints, fatigue life, rivet hole sizing, design of experiment

### **1. Introduction**

The fatigue strength of riveted joints is influenced by a number of design, process and material-related factors. Design factors include e.g. the type of the connection, size of the riveted joint, thickness of the connected metal plates, the rivet diameter and type or applied pitch of the joint [1]. Fatigue strength is also significantly influenced by rivet holes preparation process. This results from the fact that rivet holes are areas where local stress concentration occur. It is the place where fatigue cracks are initiated which may subsequently develop and lead to disasters.

Rivet holes may be subjected to special processing in order to increase their resistance to fatigue cracking. The most important processes of that kind include reaming and sizing. Reaming reduces the scatter of hole diameters and increases hole surface smoothness. While sizing introduces compressive stress to internal layers of the material. This stress hinders initiation of fatigue cracks on the hole surface. Holes may be sized using special burnishing heads (for holes of 3 mm diameter and bigger) or small holes can be sized using mandrels of appropriate diameter. Achieved surface cold work degree depends on the difference between the diameter of the sized hole and the diameter of the sizing mandrel. Those problems were analysed in paper [5].

The fatigue strength of sized rivet holes is influenced by a number of factors. The experimental analysis of those factors from fatigue point of view is very long-lasting and expensive. Efficiency and informative are very significant in this type of experiments. Experimental design methods are particularly useful in this case.

The example of evaluation of the selected factors effect on the fatigue crack initiation in the area of sized rivet hole by using experimental design was presented in this paper. The analysis was performed by using results obtained from the experiment plan developed on the basis of [2-4,6]. Specimens for tests were made of 1.27 mm thick non-clad plates of aluminium grade 2024-T3 [5] with sized hole riveted by using snap head rivet for aircraft with 3 mm diameter and 5 mm length compatible with Polish Standard BN-70/1121-03 (3517A-3-6). Rivets were made of aluminium grade PA24.

## 2. Experimental design

### 2.1. Classification of quantity describing the experimental unit

#### 2.1.1. Independent (input) variables

A set of the independent variables was assumed on the base of preliminary tests described in [5]:

- $x_1$  - a nominal fatigue load in a hole section described by maximal tension stress in a cycle (the cycle asymmetry factor  $R=0$ )  $S_{max}$ , MPa,
- $x_2$  - a rivet squeezing force  $P$ , kN,
- $x_3$  - a velocity of rivet close up  $v$ , mm/s,
- $x_4$  - a hole diameter before sizing (after drilling)  $d_w$ , mm.

#### 2.1.2. Control variables

A set of control variables was assumed:

- $c_1$  - a rivet diameter  $d_n = 3.0$  mm,
- $c_2$  - a sheet thickness  $g = 1.27$  mm,
- $c_3$  - type of the rivet – snap head rivet for aircraft [7],
- $c_4$  - a rivet length  $l_n = 5$  mm,
- $c_5$  - a load frequency  $f = 10$  Hz,
- $c_6$  - drilling and sizing process conditions,
- $c_7$  - sheet and rivet material.

#### 2.1.3. Disturbing variables

As the basic disturbing variables were assumed:

- $z_1$  - hole drilling and sizing inaccuracy,
- $z_2$  - rivet dimensions inaccuracy.

#### 2.1.4. Dependent (output) variable

Fatigue life (number of the constant amplitude cycles to the failure) was assumed as the dependent variable:

- $y$  - the common logarithm of the fatigue life  $N_c$ , cycle:

$$y = \log N_c . \quad (1)$$

The dependent variable in logarithmic form was assumed by analogy to Wöhler's equation in semi-logarithmic scale. The dependent variable without logarithmic form was also previously analysed but statistical analyses demonstrated no adequacy of this mathematical model.

## 2.2. Ranges of independent variables

The minimum and maximum value were assumed for particular independent variables:

- for the maximum tension stress in a cycle ( $R=0$ )  $S_{max}$ :

$$x_{1 \min} = 150 \text{ MPa}, \quad (2)$$

$$x_{1 \max} = 250 \text{ MPa}, \quad (3)$$

- for the rivet squeezing force  $P$ :

$$x_{2 \min} = 8.5 \text{ kN}, \quad (4)$$

$$x_{2 \max} = 12.9 \text{ kN}, \quad (5)$$

- for the velocity of rivet close up  $v$ :

$$x_{3 \min} = 0.02 \text{ mm/s}, \quad (6)$$

$$x_{3 \max} = 0.14 \text{ mm/s}, \quad (7)$$

- for the hole diameter before sizing  $d_w$ :

$$x_{4 \min} = 2.9 \text{ mm}, \quad (8)$$

$$x_{4 \max} = 3.1 \text{ mm}. \quad (9)$$

## 2.3. Mathematical model of the experimental unit

It was assumed in this work that the relationship between fatigue life and riveting process factors and fatigue load can be described by the equation in the form of the second-degree polynomial with dual interactions:

- in the sum form:

$$\hat{y} = b_0 + \sum_{i=1}^n b_i \cdot x_i + \sum_{i=1}^n b_{ii} \cdot x_i^2 + \sum_{i=1, j=1, i < j}^n b_{ij} \cdot x_i \cdot x_j, \quad (10)$$

- in the expanded form:

$$\begin{aligned} \hat{y} = & b_0 + b_1 \cdot x_1 + b_2 \cdot x_2 + b_3 \cdot x_3 + b_4 \cdot x_4 + \\ & + b_{11} \cdot x_1^2 + b_{22} \cdot x_2^2 + b_{33} \cdot x_3^2 + b_{44} \cdot x_4^2 + \\ & + b_{12} \cdot x_1 \cdot x_2 + b_{13} \cdot x_1 \cdot x_3 + b_{14} \cdot x_1 \cdot x_4 + \\ & + b_{23} \cdot x_2 \cdot x_3 + b_{24} \cdot x_2 \cdot x_4 + \\ & + b_{34} \cdot x_3 \cdot x_4. \end{aligned} \quad (11)$$

The assumed mathematical model of the experimental unit has 15 unknown coefficients of equation (11).

## 2.4. Independent variables coding

It was assumed five values for each independent variable.

The independent variables were coded by using the following equations:

a) centre points of the independence variables:

$$x_{i0} = \frac{x_{i\max} + x_{i\min}}{2}, \quad \text{for } i = 1, 2, \dots, n, \quad (12)$$

hence:

$$x_{10} = \frac{x_{1\max} + x_{1\min}}{2} = \frac{250 + 150}{2} = 200 \text{ MPa}, \quad (13)$$

$$x_{20} = \frac{x_{2\max} + x_{2\min}}{2} = \frac{12.9 + 8.5}{2} = 10.7 \text{ kN}, \quad (14)$$

$$x_{30} = \frac{x_{3\max} + x_{3\min}}{2} = \frac{0.14 + 0.02}{2} = 0.08 \text{ mm/s}, \quad (15)$$

$$x_{40} = \frac{x_{4\max} + x_{4\min}}{2} = \frac{3.1 + 2.9}{2} = 3.0 \text{ mm}, \quad (16)$$

b) an axial point:

$$\alpha = \sqrt[4]{2^n} = \sqrt[4]{2^4} = 2, \quad (17)$$

c) variability units of independence variables:

$$\Delta x_i = \frac{x_{i\max} - x_{i0}}{\alpha}, \quad \text{for } i = 1, 2, \dots, n, \quad (18)$$

hence:

$$\Delta x_1 = \frac{x_{1\max} - x_{10}}{2} = \frac{250 - 200}{2} = 25 \text{ MPa}, \quad (19)$$

$$\Delta x_2 = \frac{x_{2\max} - x_{20}}{\alpha} = \frac{12.9 - 10.7}{2} = 1.1 \text{ kN}, \quad (20)$$

$$\Delta x_3 = \frac{x_{3\max} - x_{30}}{\alpha} = \frac{0.14 - 0.08}{2} = 0.03 \text{ mm/s}, \quad (21)$$

$$\Delta x_4 = \frac{x_{4\max} - x_{40}}{\alpha} = \frac{3.1 - 3.0}{2} = 0.05 \text{ mm}, \quad (22)$$

d) coding and decoding relations:

– a coding relation:

$$\tilde{x}_i = \frac{x_i - x_{i0}}{\Delta x_i}, \quad \text{for } i = 1, 2, \dots, n, \quad (23)$$

– a decoding relation:

$$x_i = x_{i0} + \tilde{x}_i \cdot \Delta x_i, \quad \text{for } i = 1, 2, \dots, n, \quad (24)$$

e) real values corresponding to coded values of independent variables:

– for  $\tilde{x}_i = -\alpha$ :

$$x_{1(-\alpha)} = x_{10} + \tilde{x}_1 \cdot \Delta x_1 = 200 - 2 \cdot 25 = 150 \text{ MPa} , \quad (25)$$

$$x_{2(-\alpha)} = x_{20} + \tilde{x}_2 \cdot \Delta x_2 = 10.7 - 2 \cdot 1.1 = 8.5 \text{ kN} , \quad (26)$$

$$x_{3(-\alpha)} = x_{30} + \tilde{x}_3 \cdot \Delta x_3 = 0.08 - 2 \cdot 0.03 = 0.02 \text{ mm/s} , \quad (27)$$

$$x_{4(-\alpha)} = x_{40} + \tilde{x}_4 \cdot \Delta x_4 = 3.0 - 2 \cdot 0.05 = 2.9 \text{ mm} , \quad (28)$$

– for  $\tilde{x}_i = -1$ :

$$x_{1(-1)} = x_{10} + \tilde{x}_1 \cdot \Delta x_1 = 200 - 1 \cdot 25 = 175 \text{ MPa} , \quad (29)$$

$$x_{2(-1)} = x_{20} + \tilde{x}_2 \cdot \Delta x_2 = 10.7 - 1 \cdot 1.1 = 9.6 \text{ kN} , \quad (30)$$

$$x_{3(-1)} = x_{30} + \tilde{x}_3 \cdot \Delta x_3 = 0.08 - 1 \cdot 0.03 = 0.05 \text{ mm/s} , \quad (31)$$

$$x_{4(-1)} = x_{40} + \tilde{x}_4 \cdot \Delta x_4 = 3.0 - 1 \cdot 0.05 = 2.95 \text{ mm} , \quad (32)$$

– for  $\tilde{x}_i = 0$ :

$$x_{1(0)} = x_{10} + \tilde{x}_1 \cdot \Delta x_1 = 200 \text{ MPa} , \quad (33)$$

$$x_{2(0)} = x_{20} + \tilde{x}_2 \cdot \Delta x_2 = 10.7 \text{ kN} , \quad (34)$$

$$x_{3(0)} = x_{30} + \tilde{x}_3 \cdot \Delta x_3 = 0.08 \text{ mm/s} , \quad (35)$$

$$x_{4(0)} = x_{40} + \tilde{x}_4 \cdot \Delta x_4 = 3.0 \text{ mm} , \quad (36)$$

– for  $\tilde{x}_i = +1$ :

$$x_{1(+1)} = x_{10} + \tilde{x}_1 \cdot \Delta x_1 = 200 + 1 \cdot 25 = 225 \text{ MPa} , \quad (37)$$

$$x_{2(+1)} = x_{20} + \tilde{x}_2 \cdot \Delta x_2 = 10.7 + 1 \cdot 1.1 = 11.8 \text{ kN} , \quad (38)$$

$$x_{3(+1)} = x_{30} + \tilde{x}_3 \cdot \Delta x_3 = 0.08 + 1 \cdot 0.03 = 0.11 \text{ mm/s} , \quad (39)$$

$$x_{4(+1)} = x_{40} + \tilde{x}_4 \cdot \Delta x_4 = 3.0 + 1 \cdot 0.05 = 3.05 \text{ mm} , \quad (40)$$

– for  $\tilde{x}_i = +\alpha$ :

$$x_{1(+\alpha)} = x_{10} + \tilde{x}_1 \cdot \Delta x_1 = 200 + 2 \cdot 25 = 250 \text{ MPa} , \quad (41)$$

$$x_{2(+\alpha)} = x_{20} + \tilde{x}_2 \cdot \Delta x_2 = 10.7 + 2 \cdot 1.1 = 12.9 \text{ kN} , \quad (42)$$

$$x_{3(+\alpha)} = x_{30} + \tilde{x}_3 \cdot \Delta x_3 = 0.08 + 2 \cdot 0.03 = 0.14 \text{ mm/s} , \quad (43)$$

$$x_{4(+\alpha)} = x_{40} + \tilde{x}_4 \cdot \Delta x_4 = 3.0 + 2 \cdot 0.05 = 3.1 \text{ mm} , \quad (44)$$

f) summary of real and coded values of independence variables (tab. 1)

*Tab. 1. Summary of values of independence variables for the assumed plan of experiment*

| Parameter level   | Real values |       |       |       | Coded values  |               |               |               |
|-------------------|-------------|-------|-------|-------|---------------|---------------|---------------|---------------|
|                   | $x_1$       | $x_2$ | $x_3$ | $x_4$ | $\tilde{x}_1$ | $\tilde{x}_2$ | $\tilde{x}_3$ | $\tilde{x}_4$ |
|                   | MPa         | kN    | mm/s  | mm    | -             | -             | -             | -             |
| axial lower point | 150         | 8.5   | 0.02  | 2.90  | $-\alpha$     | $-\alpha$     | $-\alpha$     | $-\alpha$     |
| lower point       | 175         | 9.6   | 0.05  | 2.95  | -1            | -1            | -1            | -1            |
| central point     | 200         | 10.7  | 0.08  | 3.00  | 0             | 0             | 0             | 0             |
| upper point       | 225         | 11.8  | 0.11  | 3.05  | +1            | +1            | +1            | +1            |
| axial upper point | 250         | 12.9  | 0.14  | 3.10  | $+\alpha$     | $+\alpha$     | $+\alpha$     | $+\alpha$     |

g) the mathematical model of the experimental unit in the expanded coded form:

$$\begin{aligned}
\hat{y} = & k_0 + k_1 \cdot \tilde{x}_1 + k_2 \cdot \tilde{x}_2 + k_3 \cdot \tilde{x}_3 + k_4 \cdot \tilde{x}_4 + \\
& + k_{11} \cdot \tilde{x}_1^2 + k_{22} \cdot \tilde{x}_2^2 + k_{33} \cdot \tilde{x}_3^2 + k_{44} \cdot \tilde{x}_4^2 + \\
& + k_{12} \cdot \tilde{x}_1 \cdot \tilde{x}_2 + k_{13} \cdot \tilde{x}_1 \cdot \tilde{x}_3 + k_{14} \cdot \tilde{x}_1 \cdot \tilde{x}_4 + \\
& + k_{23} \cdot \tilde{x}_2 \cdot \tilde{x}_3 + k_{24} \cdot \tilde{x}_2 \cdot \tilde{x}_4 + \\
& + k_{34} \cdot \tilde{x}_3 \cdot \tilde{x}_4,
\end{aligned} \tag{45}$$

where:

$$\begin{aligned}
k_0 = & b_0 + \sum_{i=1}^4 b_i \cdot x_{i0} + \sum_{i=1}^4 b_{ii} \cdot x_{i0}^2 + \sum_{i=1, i < j}^4 b_{ij} \cdot x_{i0} \cdot x_{j0} = \\
= & b_0 + b_1 \cdot x_{10} + b_2 \cdot x_{20} + b_3 \cdot x_{30} + b_4 \cdot x_{40} + \\
& + b_{11} \cdot x_{10}^2 + b_{22} \cdot x_{20}^2 + b_{33} \cdot x_{30}^2 + b_{44} \cdot x_{40}^2 + \\
& + b_{12} \cdot x_{10} \cdot x_{20} + b_{13} \cdot x_{10} \cdot x_{30} + b_{14} \cdot x_{10} \cdot x_{40} + \\
& + b_{23} \cdot x_{20} \cdot x_{30} + b_{24} \cdot x_{20} \cdot x_{40} + \\
& + b_{34} \cdot x_{30} \cdot x_{40},
\end{aligned} \tag{46}$$

$$\begin{aligned}
k_1 = & b_1 \cdot \Delta x_1 + b_{12} \cdot x_{20} \cdot \Delta x_1 + b_{13} \cdot x_{30} \cdot \Delta x_1 + b_{14} \cdot x_{40} \cdot \Delta x_1 + \\
& + 2 \cdot b_{11} \cdot x_{10} \cdot \Delta x_1,
\end{aligned} \tag{47}$$

$$\begin{aligned}
k_2 = & b_2 \cdot \Delta x_2 + b_{12} \cdot x_{10} \cdot \Delta x_2 + b_{23} \cdot x_{30} \cdot \Delta x_2 + b_{24} \cdot x_{40} \cdot \Delta x_2 + \\
& + 2 \cdot b_{22} \cdot x_{20} \cdot \Delta x_2,
\end{aligned} \tag{48}$$

$$\begin{aligned}
k_3 = & b_3 \cdot \Delta x_3 + b_{13} \cdot x_{10} \cdot \Delta x_3 + b_{23} \cdot x_{20} \cdot \Delta x_3 + b_{34} \cdot x_{40} \cdot \Delta x_3 + \\
& + 2 \cdot b_{33} \cdot x_{30} \cdot \Delta x_3,
\end{aligned} \tag{49}$$

$$\begin{aligned}
k_4 = & b_4 \cdot \Delta x_4 + b_{14} \cdot x_{10} \cdot \Delta x_4 + b_{24} \cdot x_{20} \cdot \Delta x_4 + b_{34} \cdot x_{30} \cdot \Delta x_4 + \\
& + 2 \cdot b_{44} \cdot x_{40} \cdot \Delta x_4,
\end{aligned} \tag{50}$$

$$k_{12} = b_{12} \cdot \Delta x_1 \cdot \Delta x_2, \tag{51}$$

$$k_{13} = b_{13} \cdot \Delta x_1 \cdot \Delta x_3, \tag{52}$$

$$k_{14} = b_{14} \cdot \Delta x_1 \cdot \Delta x_4, \tag{53}$$

$$k_{23} = b_{23} \cdot \Delta x_2 \cdot \Delta x_3, \tag{54}$$

$$k_{24} = b_{24} \cdot \Delta x_2 \cdot \Delta x_4, \tag{55}$$

$$k_{34} = b_{34} \cdot \Delta x_3 \cdot \Delta x_4, \quad (56)$$

$$k_{11} = b_{11} \cdot \Delta x_1^2, \quad (57)$$

$$k_{22} = b_{22} \cdot \Delta x_2^2, \quad (58)$$

$$k_{33} = b_{33} \cdot \Delta x_3^2, \quad (59)$$

$$k_{44} = b_{44} \cdot \Delta x_4^2. \quad (60)$$

## 2.5. Plan of the experiment

The fatigue tests were made in agreement with the static determined five level  $(-\alpha, -1, 0, +1, +\alpha)$  plan of the experiment PS/DS-P: $\lambda$  (in Polish classification) [2-4,6]. The static determined full factorial plan PS/DK-2<sup>n</sup> was the base for this plan.

Required number of independent variables sets:

$$N = n_k + n_\alpha + n_0 = 2^n + 2 \cdot n + n_0 = 2^4 + 2 \cdot 4 + 7 = 31, \quad (61)$$

where:

$n_k = 2^n$  – a number of sets for full factorial plan PS/DK-2<sup>n</sup>,

$n_\alpha = 2 \cdot n$  – a number of sets for axial points,

$n_0 = 7$  – a number of sets for central points (for  $n = 4$ ).

Summary of sets for the experiment was presented in tab. 2.

The plan of experiment has  $N = 31$  sets. The minimum number of repetition of each set was assumed as  $r = 3$ . Hence, the total number of fatigue tests for assumed plan of experiment is

$$N_r = N \cdot r = 93. \quad (62)$$

The presented plan of experiment make possible analysis of non-linear response surface of the experimental unit (characteristic for fatigue) and thanks to this it has high informativeness close to the static determined full factorial plan PS/DK.

Moreover the advantage of this plan is the high efficiency factor described by relation

$$e_N = \frac{N}{N_k} = \frac{31}{625} = 0.0496, \quad (63)$$

where

$$N_k = 5^4 = 625 \quad (64)$$

is the number of sets for the static determined full factorial plan PS/DK-5<sup>4</sup> with 4 independent variables and 5 values for each independent variable. It means that comparable information about the experimental unit can be obtain from less than a 5% of the static determined full factorial plan sets.

The realizability criterion for the proposed plan was meet because of an axial point has a value equal 2 (see (17)). By reason of this it is possible to select appropriate pitch diameter of drills for drilling holes for sizing.

## 3. Results of the experiment

The results of the fatigue tests performed by the described plan of the experiment were presented in tab. 3. The results were presented as the mean fatigue life calculated from 3 repetition of each set of independent variables.

#### 4. Summary

The plan of experiment as an example of using the design of experiment were presented in this paper. The obtained results are the basis for the next stage of evaluation of the selected factors effect on the fatigue life of specimens with sized and riveted hole: statistical analyses for determining the adequacy of the proposed mathematical model of the experimental unit. Those analyses were presented in the second part of this paper.

Tab. 2. Summary of sets for experiment (the template of the experiment)

| Number of sets | No. of set $u$ | Independent variables |               |               |               |       |       |       |       |
|----------------|----------------|-----------------------|---------------|---------------|---------------|-------|-------|-------|-------|
|                |                | coded                 |               |               |               | real  |       |       |       |
|                |                | $\tilde{x}_1$         | $\tilde{x}_2$ | $\tilde{x}_3$ | $\tilde{x}_4$ | $x_1$ | $x_2$ | $x_3$ | $x_4$ |
|                |                | -                     | -             | -             | -             | MPa   | kN    | mm/s  | mm    |
| $n_k = 16$     | 1              | -1                    | -1            | -1            | -1            | 175   | 9.6   | 0.05  | 2.95  |
|                | 2              | +1                    | -1            | -1            | -1            | 225   | 9.6   | 0.05  | 2.95  |
|                | 3              | -1                    | +1            | -1            | -1            | 175   | 11.8  | 0.05  | 2.95  |
|                | 4              | +1                    | +1            | -1            | -1            | 225   | 11.8  | 0.05  | 2.95  |
|                | 5              | -1                    | -1            | +1            | -1            | 175   | 9.6   | 0.11  | 2.95  |
|                | 6              | +1                    | -1            | +1            | -1            | 225   | 9.6   | 0.11  | 2.95  |
|                | 7              | -1                    | +1            | +1            | -1            | 175   | 11.8  | 0.11  | 2.95  |
|                | 8              | +1                    | +1            | +1            | -1            | 225   | 11.8  | 0.11  | 2.95  |
|                | 9              | -1                    | -1            | -1            | +1            | 175   | 9.6   | 0.05  | 3.05  |
|                | 10             | +1                    | -1            | -1            | +1            | 225   | 9.6   | 0.05  | 3.05  |
|                | 11             | -1                    | +1            | -1            | +1            | 175   | 11.8  | 0.05  | 3.05  |
|                | 12             | +1                    | +1            | -1            | +1            | 225   | 11.8  | 0.05  | 3.05  |
|                | 13             | -1                    | -1            | +1            | +1            | 175   | 9.6   | 0.11  | 3.05  |
|                | 14             | +1                    | -1            | +1            | +1            | 225   | 9.6   | 0.11  | 3.05  |
|                | 15             | -1                    | +1            | +1            | +1            | 175   | 11.8  | 0.11  | 3.05  |
|                | 16             | +1                    | +1            | +1            | +1            | 225   | 11.8  | 0.11  | 3.05  |
| $n_\alpha = 8$ | 17             | $+\alpha$             | 0             | 0             | 0             | 250   | 10.7  | 0.08  | 3.0   |
|                | 18             | $-\alpha$             | 0             | 0             | 0             | 150   | 10.7  | 0.08  | 3.0   |
|                | 19             | 0                     | $+\alpha$     | 0             | 0             | 200   | 12.9  | 0.08  | 3.0   |
|                | 20             | 0                     | $-\alpha$     | 0             | 0             | 200   | 8.5   | 0.08  | 3.0   |
|                | 21             | 0                     | 0             | $+\alpha$     | 0             | 200   | 10.7  | 0.14  | 3.0   |
|                | 22             | 0                     | 0             | $-\alpha$     | 0             | 200   | 10.7  | 0.02  | 3.0   |
|                | 23             | 0                     | 0             | 0             | $+\alpha$     | 200   | 10.7  | 0.08  | 3.1   |
|                | 24             | 0                     | 0             | 0             | $-\alpha$     | 200   | 10.7  | 0.08  | 2.9   |
| $n_0 = 7$      | 25             | 0                     | 0             | 0             | 0             | 200   | 10.7  | 0.08  | 3.0   |
|                | 26             | 0                     | 0             | 0             | 0             | 200   | 10.7  | 0.08  | 3.0   |
|                | 27             | 0                     | 0             | 0             | 0             | 200   | 10.7  | 0.08  | 3.0   |
|                | 28             | 0                     | 0             | 0             | 0             | 200   | 10.7  | 0.08  | 3.0   |
|                | 29             | 0                     | 0             | 0             | 0             | 200   | 10.7  | 0.08  | 3.0   |
|                | 30             | 0                     | 0             | 0             | 0             | 200   | 10.7  | 0.08  | 3.0   |
|                | 31             | 0                     | 0             | 0             | 0             | 200   | 10.7  | 0.08  | 3.0   |

Tab. 3. Summary of the results of the experiment

| No. of set<br><i>u</i> | Independent variables |               |               |               |       |       |       |       | Mean fatigue<br>life | Dependent<br>variable    |
|------------------------|-----------------------|---------------|---------------|---------------|-------|-------|-------|-------|----------------------|--------------------------|
|                        | coded                 |               |               |               | real  |       |       |       |                      |                          |
|                        | $\tilde{x}_1$         | $\tilde{x}_2$ | $\tilde{x}_3$ | $\tilde{x}_4$ | $x_1$ | $x_2$ | $x_3$ | $x_4$ | $\bar{N}$            | $\bar{y} = \log \bar{N}$ |
|                        | -                     | -             | -             | -             | MPa   | kN    | mm/s  | mm    | cycle                | -                        |
| 1                      | -1                    | -1            | -1            | -1            | 175   | 9.6   | 0.05  | 2.95  | 609 489              | 5.785                    |
| 2                      | 1                     | -1            | -1            | -1            | 225   | 9.6   | 0.05  | 2.95  | 119 939              | 5.078                    |
| 3                      | -1                    | 1             | -1            | -1            | 175   | 11.8  | 0.05  | 2.95  | 625 525              | 5.796                    |
| 4                      | 1                     | 1             | -1            | -1            | 225   | 11.8  | 0.05  | 2.95  | 121 441              | 5.083                    |
| 5                      | -1                    | -1            | 1             | -1            | 175   | 9.6   | 0.11  | 2.95  | 614 175              | 5.788                    |
| 6                      | 1                     | -1            | 1             | -1            | 225   | 9.6   | 0.11  | 2.95  | 115 099              | 5.061                    |
| 7                      | -1                    | 1             | 1             | -1            | 175   | 11.8  | 0.11  | 2.95  | 620 271              | 5.793                    |
| 8                      | 1                     | 1             | 1             | -1            | 225   | 11.8  | 0.11  | 2.95  | 124 273              | 5.094                    |
| 9                      | -1                    | -1            | -1            | 1             | 175   | 9.6   | 0.05  | 3.05  | 169 358              | 5.228                    |
| 10                     | 1                     | -1            | -1            | 1             | 225   | 9.6   | 0.05  | 3.05  | 48 896               | 4.684                    |
| 11                     | -1                    | 1             | -1            | 1             | 175   | 11.8  | 0.05  | 3.05  | 192 778              | 5.285                    |
| 12                     | 1                     | 1             | -1            | 1             | 225   | 11.8  | 0.05  | 3.05  | 54 597               | 4.734                    |
| 13                     | -1                    | -1            | 1             | 1             | 175   | 9.6   | 0.11  | 3.05  | 163 210              | 5.212                    |
| 14                     | 1                     | -1            | 1             | 1             | 225   | 9.6   | 0.11  | 3.05  | 45 667               | 4.657                    |
| 15                     | -1                    | 1             | 1             | 1             | 175   | 11.8  | 0.11  | 3.05  | 185 947              | 5.269                    |
| 16                     | 1                     | 1             | 1             | 1             | 225   | 11.8  | 0.11  | 3.05  | 51 635               | 4.711                    |
| 17                     | $+\alpha$             | 0             | 0             | 0             | 250   | 10.7  | 0.08  | 3.0   | 48 512               | 4.680                    |
| 18                     | $-\alpha$             | 0             | 0             | 0             | 150   | 10.7  | 0.08  | 3.0   | 1 163 303            | 6.065                    |
| 19                     | 0                     | $+\alpha$     | 0             | 0             | 200   | 12.9  | 0.08  | 3.0   | 192 974              | 5.284                    |
| 20                     | 0                     | $-\alpha$     | 0             | 0             | 200   | 8.5   | 0.08  | 3.0   | 171 473              | 5.234                    |
| 21                     | 0                     | 0             | $+\alpha$     | 0             | 200   | 10.7  | 0.14  | 3.0   | 195 577              | 5.291                    |
| 22                     | 0                     | 0             | $-\alpha$     | 0             | 200   | 10.7  | 0.02  | 3.0   | 199 007              | 5.298                    |
| 23                     | 0                     | 0             | 0             | $+\alpha$     | 200   | 10.7  | 0.08  | 3.1   | 43 414               | 4.636                    |
| 24                     | 0                     | 0             | 0             | $-\alpha$     | 200   | 10.7  | 0.08  | 2.9   | 365 636              | 5.562                    |
| 25                     | 0                     | 0             | 0             | 0             | 200   | 10.7  | 0.08  | 3.0   | 208 829              | 5.319                    |
| 26                     | 0                     | 0             | 0             | 0             | 200   | 10.7  | 0.08  | 3.0   | 191 698              | 5.282                    |
| 27                     | 0                     | 0             | 0             | 0             | 200   | 10.7  | 0.08  | 3.0   | 202 717              | 5.306                    |
| 28                     | 0                     | 0             | 0             | 0             | 200   | 10.7  | 0.08  | 3.0   | 187 171              | 5.271                    |
| 29                     | 0                     | 0             | 0             | 0             | 200   | 10.7  | 0.08  | 3.0   | 190 578              | 5.279                    |
| 30                     | 0                     | 0             | 0             | 0             | 200   | 10.7  | 0.08  | 3.0   | 205 034              | 5.312                    |
| 31                     | 0                     | 0             | 0             | 0             | 200   | 10.7  | 0.08  | 3.0   | 188 257              | 5.274                    |

## References

- [1] Jachimowicz J., Szymczyk E., Sławiński G., *Analiza wpływu technologii nitowania na stan przemieszczeń, odkształceń i naprężeń wokół nitu*, Mechanik Nr 4/2008, ss. 332-337.
- [2] Klonecki W., *Statystyka dla inżynierów*, PWN, Warszawa 1999.
- [3] Korzyński M., *Metodyka eksperymentu*, WNT, Warszawa 2006.
- [4] Kukielka L., *Podstawy badań inżynierskich*, PWN, Warszawa 2002.
- [5] Lipski A., Mroziński S., Lis Z., *Evaluation of the rivet hole sizing degree effect on the fatigue life*, Journal of Polish CIMAC, Vol. 6, No. 3, 2011, pp. 119-125.
- [6] Polański Z., *Planowanie doświadczeń w technice*, PWN, Warszawa 1984.
- [7] Norma branżowa BN-70/1121-03 *Nity lotnicze ze łbem kulistym*.

Scientific work financed from the funds of Polish Ministry of Science and Higher Education in the years 2006-2010 as a research project No. 61/EUR/2006/02.





## EVALUATION OF THE SELECTED FACTORS EFFECT ON THE FATIGUE LIFE OF SPECIMENS WITH SIZED AND RIVETED HOLE PART II. STATISTICAL ANALYSES OF EXPERIMENTAL RESULTS

Adam Lipski

University of Technology and Life Sciences in Bydgoszcz  
Faculty of Mechanical Engineering  
Al. Prof. S. Kaliskiego 7, 85-789 Bydgoszcz, Poland  
tel.: +48 52 3408220, fax: +48 52 3408271  
e-mail: adam.lipski@utp.edu.pl

### Abstract

*Evaluation of the fatigue load, the rivet squeezing force, the velocity of rivet close up and the hole diameter before sizing (after drilling) effect on the fatigue life of specimens with sized and riveted hole was presented in this paper. The work contains two parts. Design of experiment and the results of the fatigue tests performed by the described experiment plan was presented in the first part. The statistical analyses and examples of using the mathematical model of the experimental unit were presented in the second part.*

**Keywords:** riveted joints, fatigue life, rivet hole sizing, design of experiment

### 1. Introduction

The second part of the work about evaluation of the selected factors effect on the fatigue life of specimens with sized and riveted hole was presented in this paper. The part contains the statistical analyses of experimental results and examples of using the mathematical model of the experimental unit.

### 2. Statistical analyses

#### 2.1. Elimination of results with gross error

The Grubbs' test was used to elimination of results with gross error. The mean value of the dependent variable for each set of the independent variables  $u$  was determined by using following equation

$$\bar{y}_u = \frac{\sum_{i=1}^r y_{u/i}}{r} \quad (1)$$

and standard deviation

$$s_u = \sqrt{\frac{\sum_{i=1}^r (y_{u/i} - \bar{y}_u)^2}{r-1}} \quad (2)$$

where:

$r = 3$  – a number of repetition the same for each set,

$y_{u/i}$  – a result number  $i$  from  $r$  repetitions for set number  $u$ .

The test statistic was determined separately for the maximum and the minimum value of the dependent variable for each set of the independent variables. It was determined for the largest and for the least value of the dependent variable by using an equation

$$B_{\max} = \frac{\max(y_{u/i}) - \bar{y}_u}{s_u}, \quad B_{\min} = \frac{\bar{y}_u - \min(y_{u/i})}{s_u}. \quad (3)$$

The critical value of the test statistic  $B_{\alpha,r} = 1.412$  was determined for the number of repetition  $r = 3$  and the significance level  $\alpha = 0.05$  [3]. Results of calculation were presented in tab. 1.

Because for each set of independent variables

$$B_{\max} < B_{\alpha,r} \quad (4)$$

and

$$B_{\min} < B_{\alpha,r}. \quad (5)$$

there is no reason to rejection the maximal and minimal values for each set as gross error results.

Tab. 1. Summary of calculation for results with gross error elimination

| No. of set $u$ | Coded independent variables |               |               |               | Dependent variable       |       | Grubbs' statistics |            |
|----------------|-----------------------------|---------------|---------------|---------------|--------------------------|-------|--------------------|------------|
|                | $\tilde{x}_1$               | $\tilde{x}_2$ | $\tilde{x}_3$ | $\tilde{x}_4$ | $\bar{y} = \log \bar{N}$ | $s_u$ | $B_{\max}$         | $B_{\min}$ |
| 1              | -1                          | -1            | -1            | -1            | 5.785                    | 0.007 | 0.852              | 1.101      |
| 2              | 1                           | -1            | -1            | -1            | 5.078                    | 0.038 | 0.895              | 1.079      |
| 3              | -1                          | 1             | -1            | -1            | 5.796                    | 0.013 | 1.104              | 0.846      |
| 4              | 1                           | 1             | -1            | -1            | 5.083                    | 0.044 | 0.914              | 1.068      |
| 5              | -1                          | -1            | 1             | -1            | 5.788                    | 0.009 | 0.880              | 1.088      |
| 6              | 1                           | -1            | 1             | -1            | 5.061                    | 0.027 | 1.115              | 0.818      |
| 7              | -1                          | 1             | 1             | -1            | 5.793                    | 0.009 | 1.055              | 0.935      |
| 8              | 1                           | 1             | 1             | -1            | 5.094                    | 0.033 | 0.819              | 1.115      |
| 9              | -1                          | -1            | -1            | 1             | 5.228                    | 0.030 | 1.087              | 0.881      |
| 10             | 1                           | -1            | -1            | 1             | 4.684                    | 0.084 | 1.011              | 0.989      |
| 11             | -1                          | 1             | -1            | 1             | 5.285                    | 0.018 | 1.133              | 0.758      |
| 12             | 1                           | 1             | -1            | 1             | 4.734                    | 0.060 | 0.793              | 1.123      |
| 13             | -1                          | -1            | 1             | 1             | 5.212                    | 0.022 | 0.853              | 1.101      |
| 14             | 1                           | -1            | 1             | 1             | 4.657                    | 0.055 | 0.801              | 1.121      |
| 15             | -1                          | 1             | 1             | 1             | 5.269                    | 0.029 | 0.858              | 1.098      |
| 16             | 1                           | 1             | 1             | 1             | 4.711                    | 0.052 | 1.121              | 0.801      |
| 17             | $+\alpha$                   | 0             | 0             | 0             | 4.680                    | 0.087 | 1.022              | 0.977      |
| 18             | $-\alpha$                   | 0             | 0             | 0             | 6.065                    | 0.036 | 0.823              | 1.113      |
| 19             | 0                           | $+\alpha$     | 0             | 0             | 5.284                    | 0.042 | 1.079              | 0.895      |
| 20             | 0                           | $-\alpha$     | 0             | 0             | 5.234                    | 0.026 | 1.022              | 0.976      |
| 21             | 0                           | 0             | $+\alpha$     | 0             | 5.291                    | 0.027 | 0.886              | 1.084      |
| 22             | 0                           | 0             | $-\alpha$     | 0             | 5.298                    | 0.026 | 1.073              | 0.907      |
| 23             | 0                           | 0             | 0             | $+\alpha$     | 4.636                    | 0.048 | 0.959              | 1.036      |
| 24             | 0                           | 0             | 0             | $-\alpha$     | 5.562                    | 0.033 | 1.119              | 0.806      |
| 25             | 0                           | 0             | 0             | 0             | 5.319                    | 0.031 | 0.976              | 1.023      |
| 26             | 0                           | 0             | 0             | 0             | 5.282                    | 0.023 | 0.897              | 1.078      |
| 27             | 0                           | 0             | 0             | 0             | 5.306                    | 0.029 | 1.026              | 0.972      |
| 28             | 0                           | 0             | 0             | 0             | 5.271                    | 0.038 | 0.862              | 1.096      |
| 29             | 0                           | 0             | 0             | 0             | 5.279                    | 0.038 | 0.980              | 1.019      |
| 30             | 0                           | 0             | 0             | 0             | 5.312                    | 0.018 | 1.127              | 0.782      |
| 31             | 0                           | 0             | 0             | 0             | 5.274                    | 0.025 | 1.084              | 0.887      |

## 2.2. Inter-row variance and standard deviation

Inter-row variance was calculated from equation [3]

$$s_u^2 = \frac{\sum_{i=1}^r (y_{u/i} - \bar{y}_u)^2}{r-1}, \quad (6)$$

and standard deviation from

$$s_u = \sqrt{s_u^2}. \quad (7)$$

Homogeneity of variance in a sample was checked with Cochran's C-test (the same number of repetition for each set of independent variables  $r = 3$ ).

The test statistic was determined by equation

$$G = \frac{\max(s_u^2)}{\sum_{j=1}^u s_u^2} = 0.1610, \quad (8)$$

where  $\max(s_u^2) = 0.007530$  and  $\sum_{j=1}^u s_u^2 = 0.046778$  were determined by using results of equations (6) and (7).

The Cochran's test critical value  $g_{\alpha,k;\nu} = 0.1940$  was determined for the significance level  $\alpha = 0.05$  and degrees of freedom  $k = N = 31$  and  $\nu = r - 1 = 2$  [3].

Because

$$G < g_{\alpha,k;\nu}, \quad (9)$$

there is no reason to rejection the hypothesis about homogeneity of variance.

## 2.3. Determination of coefficients in regression function in coded form

Coefficients in regression function in coded form were determined by following equations:

$$k_0 = D \cdot (0\bar{y}) + E \cdot \sum_{s=1}^4 (s\bar{s}\bar{y}), \quad (10)$$

$$k_s = \frac{(s\bar{y})}{e} = (s\bar{y}) \cdot e^{-1}, \quad (11)$$

$$k_{(s-1)s} = \frac{((s-1)s\bar{y})}{n_k} = ((s-1)s\bar{y}) \cdot n_k^{-1}, \quad (12)$$

$$k_{ss} = (F - G) \cdot (s\bar{s}\bar{y}) + G \cdot \sum_{s=1}^3 (s\bar{s}\bar{y}) + E \cdot (0\bar{y}), \quad (13)$$

where auxiliary factors values  $D = 0.1428$ ,  $E = -0.0357$ ,  $F = 0.035$ ,  $G = 0.0037$  oraz  $e^{-1} = 0.0416$  were selected from [4] and with agree with the plan of the experiment  $n_k^{-1} = 0.0625$ .

Auxiliary factors values were calculated from equations:

$$(0\bar{y}) = \sum_{u=1}^N y_u = 162.35, \quad (14)$$

$$(1\bar{y}) = \sum_{u=1}^N x_{1u} \cdot y_u = -7.824, \quad (15)$$

$$(2\bar{y}) = \sum_{u=1}^N \bar{x}_{2u} \cdot \bar{y}_u = 0.372, \quad (16)$$

$$(3\bar{y}) = \sum_{u=1}^N \bar{x}_{3u} \cdot \bar{y}_u = -0.104, \quad (17)$$

$$(4\bar{y}) = \sum_{u=1}^N \bar{x}_{4u} \cdot \bar{y}_u = -5.549, \quad (18)$$

$$(12\bar{y}) = \sum_{u=1}^N \bar{x}_{1u} \cdot \bar{x}_{2u} \cdot \bar{y}_u = 0.014, \quad (19)$$

$$(13\bar{y}) = \sum_{u=1}^N \bar{x}_{1u} \cdot \bar{x}_{3u} \cdot \bar{y}_u = -0.025, \quad (20)$$

$$(14\bar{y}) = \sum_{u=1}^N \bar{x}_{1u} \cdot \bar{x}_{4u} \cdot \bar{y}_u = 0.639, \quad (21)$$

$$(23\bar{y}) = \sum_{u=1}^N \bar{x}_{2u} \cdot \bar{x}_{3u} \cdot \bar{y}_u = 0.024, \quad (22)$$

$$(24\bar{y}) = \sum_{u=1}^N \bar{x}_{2u} \cdot \bar{x}_{4u} \cdot \bar{y}_u = 0.164, \quad (23)$$

$$(34\bar{y}) = \sum_{u=1}^N \bar{x}_{3u} \cdot \bar{x}_{4u} \cdot \bar{y}_u = -0.075, \quad (24)$$

$$(11\bar{y}) = \sum_{u=1}^N \bar{x}_{1u}^2 \cdot \bar{y}_u = 126.236, \quad (25)$$

$$(22\bar{y}) = \sum_{u=1}^N \bar{x}_{2u}^2 \cdot \bar{y}_u = 125.328, \quad (26)$$

$$(33\bar{y}) = \sum_{u=1}^N \bar{x}_{3u}^2 \cdot \bar{y}_u = 125.614, \quad (27)$$

$$(44\bar{y}) = \sum_{u=1}^N \bar{x}_{4u}^2 \cdot \bar{y}_u = 124.049, \quad (28)$$

Coefficients in regression function in coded form were determined by equations (10)÷(13):

$$k_0 = D \cdot (0\bar{y}) + E \cdot \sum_{s=1}^3 (s\bar{y}) = D \cdot (0\bar{y}) + E \cdot (11\bar{y} + 22\bar{y} + 33\bar{y} + 44\bar{y}) = 5.290, \quad (29)$$

$$k_1 = (1\bar{y}) \cdot e^{-1} = -0.3255, \quad (30)$$

$$k_2 = (2\bar{y}) \cdot e^{-1} = 0.01546, \quad (31)$$

$$k_3 = (3\bar{y}) \cdot e^{-1} = -0.004326, \quad (32)$$

$$k_4 = (4\bar{y}) \cdot e^{-1} = -0.2308, \quad (33)$$

$$k_{12} = (12\bar{y}) \cdot n_k^{-1} = 0.0008602, \quad (34)$$

$$k_{13} = (13\bar{y}) \cdot n_k^{-1} = -0.001541, \quad (35)$$

$$k_{14} = (14\bar{y}) \cdot n_k^{-1} = 0.03996, \quad (36)$$

$$k_{23} = (23\bar{y}) \cdot n_k^{-1} = 0.001480, \quad (37)$$

$$k_{24} = (24\bar{y}) \cdot n_k^{-1} = 0.01023, \quad (38)$$

$$k_{34} = (34\bar{y}) \cdot n_k^{-1} = -0.004681, \quad (39)$$

$$k_{11} = (F - G) \cdot (11\bar{y}) + G \cdot (11\bar{y} + 22\bar{y} + 33\bar{y} + 44\bar{y}) + E \cdot (0\bar{y}) = 0.009829, \quad (40)$$

$$k_{22} = (F - G) \cdot (22\bar{y}) + G \cdot (11\bar{y} + 22\bar{y} + 33\bar{y} + 44\bar{y}) + E \cdot (0\bar{y}) = -0.01858, \quad (41)$$

$$k_{33} = (F - G) \cdot (33\bar{y}) + G \cdot (11\bar{y} + 22\bar{y} + 33\bar{y} + 44\bar{y}) + E \cdot (0\bar{y}) = -0.009661, \quad (42)$$

$$k_{44} = (F - G) \cdot (44\bar{y}) + G \cdot (11\bar{y} + 22\bar{y} + 33\bar{y} + 44\bar{y}) + E \cdot (0\bar{y}) = -0.05862. \quad (43)$$

## 2.4. Statistical analysis of regression function

The Student's t-test was used for significance rating of coefficients in regression function. The inter-row variance in the centre of the experiment plan was determined by equations

$$s_e^2 = \frac{S_E}{f_E} = 0.000388985, \quad (44)$$

and

$$S_E = \sum_{u=n_k+n_\alpha+1}^N (\bar{y}_{0u} - \bar{\bar{y}}_0)^2, \quad (45)$$

$$\bar{\bar{y}}_0 = \frac{\sum_{u=n_k+n_\alpha+1}^N \bar{y}_{0u}}{n_0}, \quad (46)$$

$$f_E = n_0 - 1 = 6, \quad (47)$$

where:

- $\bar{y}_{0u}$  – the mean values of the dependent variable in the centre of experiment plan,
- $\bar{\bar{y}}_0$  – the mean value of the dependent variable values in the centre of experiment plan,
- $n_k$  – a number of sets for full factorial plan PS/DK-2<sup>n</sup>,
- $n_\alpha$  – a number of sets for axial points,
- $n_0$  – a number of sets for central points,
- $N$  – a total number of sets in the plan of experiment,
- $f_E$  – degrees of freedom.

Auxiliary factors values for calculations were presented in tab. 2.

The variance of coefficients in regression function were calculated by following equations

$$s^2(k_0) = D \cdot s_e^2 \quad (48)$$

$$s^2(k_s) = \frac{s_e^2}{e} = s_e^2 \cdot e^{-1} \quad (49)$$

$$s^2(k_{(s-1)s}) = \frac{s_e^2}{n_k} = s_e^2 \cdot n_k^{-1} \quad (50)$$

$$s^2(k_{ss}) = F \cdot s_e^2 \quad (51)$$

Tab. 2. Auxiliary factors values for variance in the centre of experiment plan determination

| No. of set<br>$u$ | Coded independent variables |               |               |               | Dependent variable        | Auxiliary factors                    |
|-------------------|-----------------------------|---------------|---------------|---------------|---------------------------|--------------------------------------|
|                   | $\tilde{x}_1$               | $\tilde{x}_2$ | $\tilde{x}_3$ | $\tilde{x}_4$ | $\bar{y}_{0u}$            | $(\bar{y}_{0u} - \bar{\bar{y}}_0)^2$ |
| 25                | 0                           | 0             | 0             | 0             | 5.319                     | 0.000 736                            |
| 26                | 0                           | 0             | 0             | 0             | 5.282                     | 0.000 094                            |
| 27                | 0                           | 0             | 0             | 0             | 5.306                     | 0.000 205                            |
| 28                | 0                           | 0             | 0             | 0             | 5.271                     | 0.000 432                            |
| 29                | 0                           | 0             | 0             | 0             | 5.279                     | 0.000 168                            |
| 30                | 0                           | 0             | 0             | 0             | 5.312                     | 0.000 387                            |
| 31                | 0                           | 0             | 0             | 0             | 5.274                     | 0.000 312                            |
|                   |                             |               |               |               | $\bar{\bar{y}}_0 = 5.292$ | $S_E = 0.002\ 334$                   |

The standard deviation of coefficients in regression function were calculated by equations

$$s(k_0) = \sqrt{s^2(k_0)} \quad (52)$$

$$s(k_s) = \sqrt{s^2(k_s)} \quad (53)$$

$$s(k_{(s-1)s}) = \sqrt{s^2(k_{(s-1)s})} \quad (54)$$

$$s(k_{ss}) = \sqrt{s^2(k_{ss})} \quad (55)$$

The test statistic was determined by equation

$$t_0 = t(k_0) = \frac{|k_0|}{s(k_0)} \quad (56)$$

$$t_s = t(k_s) = \frac{|k_s|}{s(k_s)} \quad (57)$$

$$t_{(s-1)s} = t(k_{(s-1)s}) = \frac{|k_{(s-1)s}|}{s(k_{(s-1)s})} \quad (58)$$

$$t_{ss} = t(k_{ss}) = \frac{|k_{ss}|}{s(k_{ss})} \quad (59)$$

The significance rating of coefficients in regression function were presented in tab. 3.

The critical value of Student's t-test  $t_{\alpha; f_E} = 2.45$  was determined for the significance level  $\alpha = 0.05$  and degrees of freedom  $f_E$ .

If following equation is satisfied

$$t_i \geq t_{\alpha; f_E} \quad (60)$$

then there is no reason to reject null hypothesis about insignificance of a coefficient in regression function i.e. the coefficient is significant for dependent variable.

If following equation is satisfied

$$t_i < t_{\alpha; f_E} \quad (61)$$

then there is the reason to accept null hypothesis about insignificance of a coefficient in regression function in statistical sense with the significance level i.e. the coefficient is insignificant for dependent variable and it can be omit in regression function.

Tab. 3. The significance rating of coefficients in regression function

| Coefficient | Variance of coefficient | Standard deviation | Test statistic | Student's t-test                  | Test results  |
|-------------|-------------------------|--------------------|----------------|-----------------------------------|---------------|
| $k_i$       | $s^2(k_i)$              | $s(k_i)$           | $t_i = t(k_i)$ |                                   |               |
| $k_0$       | 0.000 055 547           | 0.007 453          | 709.76         | $t_i \geq t_{\alpha; f_E} = 2.45$ | significant   |
| $k_1$       | 0.000 016 182           | 0.004 023          | 80.91          | $t_i \geq t_{\alpha; f_E} = 2.45$ | significant   |
| $k_2$       | 0.000 016 182           | 0.004 023          | 3.84           | $t_i \geq t_{\alpha; f_E} = 2.45$ | significant   |
| $k_3$       | 0.000 016 182           | 0.004 023          | 1.08           | $t_i < t_{\alpha; f_E} = 2.45$    | insignificant |
| $k_4$       | 0.000 016 182           | 0.004 023          | 57.38          | $t_i \geq t_{\alpha; f_E} = 2.45$ | significant   |
| $k_{12}$    | 0.000 024 312           | 0.004 931          | 0.17           | $t_i < t_{\alpha; f_E} = 2.45$    | insignificant |
| $k_{13}$    | 0.000 024 312           | 0.004 931          | 0.31           | $t_i < t_{\alpha; f_E} = 2.45$    | insignificant |
| $k_{14}$    | 0.000 024 312           | 0.004 931          | 8.10           | $t_i \geq t_{\alpha; f_E} = 2.45$ | significant   |
| $k_{23}$    | 0.000 024 312           | 0.004 931          | 0.30           | $t_i < t_{\alpha; f_E} = 2.45$    | insignificant |
| $k_{24}$    | 0.000 024 312           | 0.004 931          | 2.07           | $t_i \geq t_{\alpha; f_E} = 2.45$ | insignificant |
| $k_{34}$    | 0.000 024 312           | 0.004 931          | 0.95           | $t_i < t_{\alpha; f_E} = 2.45$    | insignificant |
| $k_{11}$    | 0.000 013 614           | 0.003 690          | 2.66           | $t_i \geq t_{\alpha; f_E} = 2.45$ | significant   |
| $k_{22}$    | 0.000 013 614           | 0.003 690          | 5.04           | $t_i \geq t_{\alpha; f_E} = 2.45$ | significant   |
| $k_{33}$    | 0.000 013 614           | 0.003 690          | 2.62           | $t_i \geq t_{\alpha; f_E} = 2.45$ | significant   |
| $k_{44}$    | 0.000 013 614           | 0.003 690          | 15.89          | $t_i \geq t_{\alpha; f_E} = 2.45$ | significant   |

## 2.5. Significance rating of multivariate correlation coefficient

The multivariate correlation coefficient can be the fitting measure of regression function to experiment results

$$R = \sqrt{1 - \frac{\sum_{u=1}^N (\hat{y}_u - \bar{y}_u)^2}{\sum_{u=1}^N (\bar{y}_u - \bar{y})^2}} = \sqrt{1 - \frac{0.024133}{3.996}} = 0.997, \quad (62)$$

where the mean value of dependent variable for set  $u$  with  $r$  number of repetition

$$\bar{y}_u = \frac{\sum_{i=1}^r y_{u/i}}{r}, \quad (63)$$

and the mean value of dependent variable for experimental unit for  $N$  sets

$$\bar{\bar{y}} = \frac{\sum_{u=1}^N \bar{y}_u}{N} . \quad (64)$$

The output variable values of mathematical model of experimental unit for set  $u$  of input variables were calculated by regression function (without insignificant coefficients rejection)

$$\begin{aligned} \hat{y} = & k_0 + k_1 \cdot \hat{x}_1 + k_2 \cdot \hat{x}_2 + k_3 \cdot \hat{x}_3 + k_4 \cdot \hat{x}_4 + \\ & + k_{11} \cdot \hat{x}_1^2 + k_{22} \cdot \hat{x}_2^2 + k_{33} \cdot \hat{x}_3^2 + k_{44} \cdot \hat{x}_4^2 + \\ & + k_{12} \cdot \hat{x}_1 \cdot \hat{x}_2 + k_{13} \cdot \hat{x}_1 \cdot \hat{x}_3 + k_{14} \cdot \hat{x}_1 \cdot \hat{x}_4 + \\ & + k_{23} \cdot \hat{x}_2 \cdot \hat{x}_3 + k_{24} \cdot \hat{x}_2 \cdot \hat{x}_4 + k_{34} \cdot \hat{x}_3 \cdot \hat{x}_4 . \end{aligned} \quad (65)$$

The Snedecor's F-test was used for the multivariate correlation coefficient significance determination.

The test statistics was determined by equation

$$F = \frac{N-L}{L-1} \cdot \frac{R^2}{1-R^2} = 188.11 , \quad (66)$$

where:

$N = 31$  – the total number of sets in experimental plane,

$L = 15$  – a number of coefficients in regression function.

The critical Snedecor's F-test value  $F_{\alpha; r_1; r_2} = 2.37$  was determined for the significance level  $\alpha = 0,05$  and degrees of freedom  $r_1 = L - 1 = 14$  and  $r_2 = N - L = 16$ .

Because

$$F > F_{\alpha; r_1; r_2} \quad (67)$$

there is no reason to rejection the hypothesis about the multivariate correlation coefficient significance and simultaneously about correctness of coefficients in regression function.

## 2.6. Adequacy of the mathematical model of experimental unit

The adequacy of the mathematical model of experimental unit rating was determined by using Snedecor's F-test [4].

The test statistics was determined by equation

$$F = \frac{s^2(y)_a}{s^2(y)} = 3.74 . \quad (68)$$

The adequacy variance characterised approximation accuracy

$$s^2(y)_a = \frac{SQ_a}{f_2} = 0.001453 , \quad (69)$$

where  $f_2 = N - L - 1 = 15$  and the tests accuracy variance was determined on the base of results for central point's sets  $n_0 = 7$  from plane of experiment (tab. 2):

$$s^2(y) = \frac{\sum_{u=n_k+n_a+1}^N (\bar{y}_{0u} - \bar{\bar{y}}_0)^2}{n_0 - 1} = \frac{S_E}{n_0 - 1} = 0.000389 . \quad (70)$$

The numerator value in (54) was determined by equation

$$SQ_a = n_0 \cdot (\bar{\bar{y}}_{0u} - \hat{y}_{0u})^2 + \sum_{u=1}^{N-n_0} (\bar{y}_u - \hat{y}_u)^2 = 0.021799, \quad (71)$$

where  $\bar{\bar{y}}_{0u} = 5.292$  (from tab. 4) and  $\hat{y}_u = 5.290$  (from tab. 6).

The critical Snedecor's F-test value  $F_{\alpha; f_1; f_2} = 3.94$  was determined for the significance level  $\alpha = 0,05$  and degrees of freedom  $f_1 = n_0 - 1 = 6$  and  $f_2 = N - L - 1 = 15$ .

Because

$$F < F_{\alpha; r_1; r_2} \quad (72)$$

there is no reason to rejection the hypothesis about adequacy of the mathematical model of experimental unit to the experimental results from statistical point of view.

## 2.7. Decoding of coefficients in regression function

Decoding of coefficients in regression function was made by using following relations:

$$\begin{aligned} b_0 = & k_0 - k_1 \cdot \frac{x_{10}}{\Delta x_1} - k_2 \cdot \frac{x_{20}}{\Delta x_2} - k_3 \cdot \frac{x_{30}}{\Delta x_3} - k_4 \cdot \frac{x_{40}}{\Delta x_4} + k_{12} \cdot \frac{x_{10} \cdot x_{20}}{\Delta x_1 \cdot \Delta x_2} + \\ & + k_{13} \cdot \frac{x_{10} \cdot x_{30}}{\Delta x_1 \cdot \Delta x_3} + k_{14} \cdot \frac{x_{10} \cdot x_{40}}{\Delta x_1 \cdot \Delta x_4} + k_{23} \cdot \frac{x_{20} \cdot x_{30}}{\Delta x_2 \cdot \Delta x_3} + k_{24} \cdot \frac{x_{20} \cdot x_{40}}{\Delta x_2 \cdot \Delta x_4} + \\ & + k_{11} \cdot \left( \frac{x_{10}}{\Delta x_1} \right)^2 + k_{22} \cdot \left( \frac{x_{20}}{\Delta x_2} \right)^2 + k_{33} \cdot \left( \frac{x_{30}}{\Delta x_3} \right)^2 + k_{44} \cdot \left( \frac{x_{40}}{\Delta x_4} \right)^2 = -166.15, \end{aligned} \quad (73)$$

$$\begin{aligned} b_1 = & \frac{k_1}{\Delta x_1} - k_{12} \cdot \frac{x_{20}}{\Delta x_1 \cdot \Delta x_2} - k_{13} \cdot \frac{x_{30}}{\Delta x_1 \cdot \Delta x_3} - k_{14} \cdot \frac{x_{40}}{\Delta x_1 \cdot \Delta x_4} + \\ & - 2 \cdot k_{11} \cdot \frac{x_{10}}{\Delta x_1^2} = -0.11539, \end{aligned} \quad (74)$$

$$\begin{aligned} b_2 = & \frac{k_2}{\Delta x_2} - k_{12} \cdot \frac{x_{10}}{\Delta x_1 \cdot \Delta x_2} - k_{23} \cdot \frac{x_{30}}{\Delta x_2 \cdot \Delta x_3} - k_{24} \cdot \frac{x_{40}}{\Delta x_2 \cdot \Delta x_4} \\ & - 2 \cdot k_{22} \cdot \frac{x_{20}}{\Delta x_2^2} = -0.22485, \end{aligned} \quad (75)$$

$$\begin{aligned} b_3 = & \frac{k_3}{\Delta x_3} - k_{13} \cdot \frac{x_{10}}{\Delta x_1 \cdot \Delta x_3} - k_{23} \cdot \frac{x_{20}}{\Delta x_2 \cdot \Delta x_3} - k_{34} \cdot \frac{x_{40}}{\Delta x_3 \cdot \Delta x_4} \\ & - 2 \cdot k_{33} \cdot \frac{x_{30}}{\Delta x_3^2} = 10.867, \end{aligned} \quad (76)$$

$$\begin{aligned} b_4 = & \frac{k_4}{\Delta x_4} - k_{14} \cdot \frac{x_{10}}{\Delta x_1 \cdot \Delta x_4} - k_{24} \cdot \frac{x_{20}}{\Delta x_2 \cdot \Delta x_4} - k_{34} \cdot \frac{x_{30}}{\Delta x_3 \cdot \Delta x_4} \\ & - 2 \cdot k_{44} \cdot \frac{x_{40}}{\Delta x_4^2} = 127.94, \end{aligned} \quad (77)$$

$$b_{12} = \frac{k_{12}}{\Delta x_1 \cdot \Delta x_2} = 0.000031279, \quad (78)$$

$$b_{13} = \frac{k_{13}}{\Delta x_1 \cdot \Delta x_3} = -0.0020547, \quad (79)$$

$$b_{14} = \frac{k_{14}}{\Delta x_1 \cdot \Delta x_4} = 0.031969 \quad (80)$$

$$b_{23} = \frac{k_{23}}{\Delta x_2 \cdot \Delta x_3} = 0.044834, \quad (81)$$

$$b_{24} = \frac{k_{24}}{\Delta x_2 \cdot \Delta x_4} = 0.18592, \quad (82)$$

$$b_{34} = \frac{k_{34}}{\Delta x_3 \cdot \Delta x_4} = -3.1208, \quad (83)$$

$$b_{11} = \frac{k_{11}}{\Delta x_1^2} = 0.000015726, \quad (84)$$

$$b_{22} = \frac{k_{22}}{\Delta x_2^2} = -0.015359, \quad (85)$$

$$b_{33} = \frac{k_{33}}{\Delta x_3^2} = -10.735, \quad (86)$$

$$b_{44} = \frac{k_{44}}{\Delta x_4^2} = -23.448. \quad (87)$$

The mathematical model of the experimental unit has finally following form:

$$\begin{aligned} \hat{y} = & \underline{-166.15} - \underline{0.11539} \cdot x_1 - \underline{0.22485} \cdot x_2 + 10.867 \cdot x_3 + \underline{127.94} \cdot x_4 + \\ & + \underline{0.000015726} \cdot x_1^2 - \underline{0.015359} \cdot x_2^2 - \underline{10.735} \cdot x_3^2 - \underline{23.448} \cdot x_4^2 + \\ & + 0.000031279 \cdot x_1 \cdot x_2 - 0.0020547 \cdot x_1 \cdot x_3 + \underline{0.031969} \cdot x_1 \cdot x_4 + \\ & + 0.044834 \cdot x_2 \cdot x_3 + 0.18592 \cdot x_2 \cdot x_4 + 3.1208 \cdot x_3 \cdot x_4. \end{aligned} \quad (88)$$

The above-mentioned relations can be write with independent variables denatation:

$$\begin{aligned} \log N_c = & \underline{-166.15} - \underline{0.11539} \cdot S_{\max} - \underline{0.22485} \cdot P + 10.867 \cdot v + \\ & + \underline{127.94} \cdot d_w + \underline{0.000015726} \cdot S_{\max}^2 - \underline{0.015359} \cdot P^2 + \\ & - \underline{10.735} \cdot v^2 - \underline{23.448} \cdot d_w^2 + 0.000031279 \cdot S_{\max} \cdot P + \\ & - 0.0020547 \cdot S_{\max} \cdot v + \underline{0.031969} \cdot S_{\max} \cdot d_w + \\ & + 0.044834 \cdot P \cdot v + 0.18592 \cdot P \cdot d_w + 3.1208 \cdot v \cdot d_w. \end{aligned} \quad (89)$$

Underlined terms of equation (74) or (75) are significant in a statistical sense.

The equation (75) allows to estimate the fatigue life depending on the significant process parameters (the rivet squeezing force  $P$ , the hole diameter before sizing  $d_w$  and velocity of rivet close up  $v$ ) and the nominal fatigue load in a hole section described by maximal tension stress in a cycle (the cycle asymmetry factor  $R=0$ )  $S_{max}$ .

### 3. Examples of using the mathematical model of experimental unit

Sample fatigue life plots obtained from the mathematical model of experimental unit (equation (75)) were presented in Fig. 1÷3. As it can be seen the fatigue load  $S_{max}$  has the largest influence on fatigue life of tested specimens. The hole diameter before sizing  $d_w$  is the second important factor (Fig. 1).

The rivet squeezing force  $P$  (in range of 8,5÷12,9 kN) has the least influence on fatigue life (Fig. 2) especially for large values of sizing degree (smaller hole diameter before sizing  $d_w$ ). It can be connected with high work hardening around hole after sizing.

Velocity of rivet close up  $v$  has the significant influence on fatigue life too (Fig. 3). It may be concluded that the velocity of rivet close up, the higher the fatigue life.

### 4. Summary

The example of evaluation of the selected factors effect on the fatigue crack initiation in the area of sized rivet hole by using experimental design was presented in this paper. The analyses were performed by using results obtained with the static determined five level plan of the experiment called PS/DS-P:λ in Polish classification. The advantage of this plan is high efficiency factor that means that comparable information about experimental unit can be obtain from less than a 5% of the static determined full factorial plan sets. It has special importance in case of very long-lasting and expensive fatigue tests.

The statistical analyses were presented that there are no results with gross error. The most significant coefficients in the regression function is the fatigue load  $S_{max}$ . The least significant coefficient is the rivet squeezing force  $P$ . The multivariate correlation coefficient value  $R = 0.997$  is significant for the regression function and finally the mathematical model of experimental unit is adequate to the experimental results from statistical point of view.

### References

- [1] Klonecki W., *Statistics for engineers*, PWN, Warszawa 1999 (in Polish).
- [2] Korzyński M., *Design of experiment*, WNT, Warszawa 2006 (in Polish).
- [3] Kukielka L., *Fundamentals of engineering research*, PWN, Warszawa 2002 (in Polish).
- [4] Polański Z., *Design of experiment in technics*, PWN, Warszawa 1984 (in Polish).
- [5] Branch standard BN-70/1121-03 *Snap head rivet for aircraft* (in Polish).

Scientific work financed from the funds of Polish Ministry of Science and Higher Education in the years 2006-2010 as a research project No. 61/EUR/2006/02.

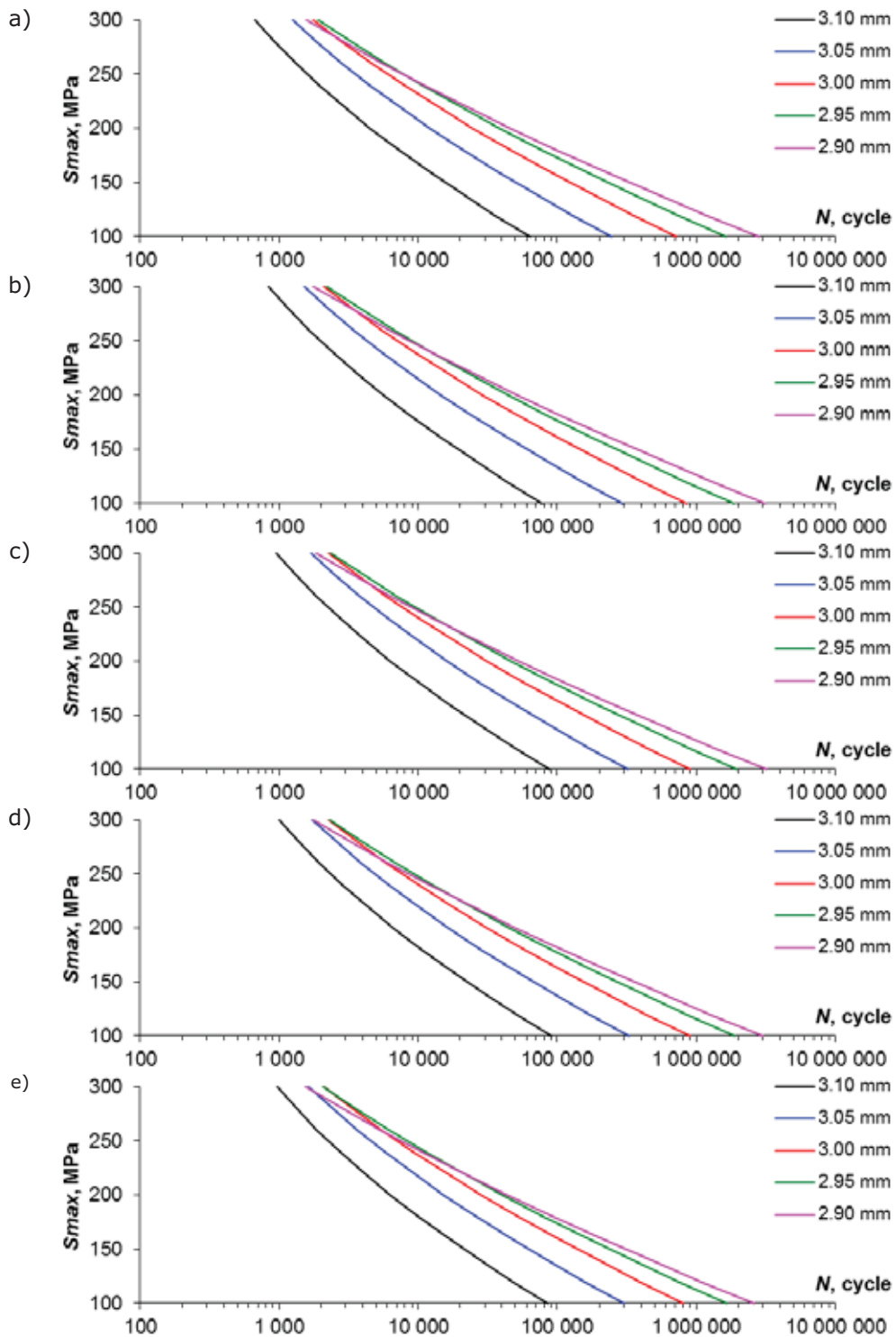


Fig. 1. Sample fatigue life plots with extrapolation outside of  $S_{max}$  range in plan of experiment obtained from the mathematical model of experimental unit depending on the hole diameter before sizing  $d_h$ , and the rivet squeezing force  $P$ : a) 8.5 kN, b) 9.6 kN, c) 10.7 kN, d) 11.8 kN, e) 12.9 kN (velocity of rivet close up  $v = 0.08$  mm/s = const)

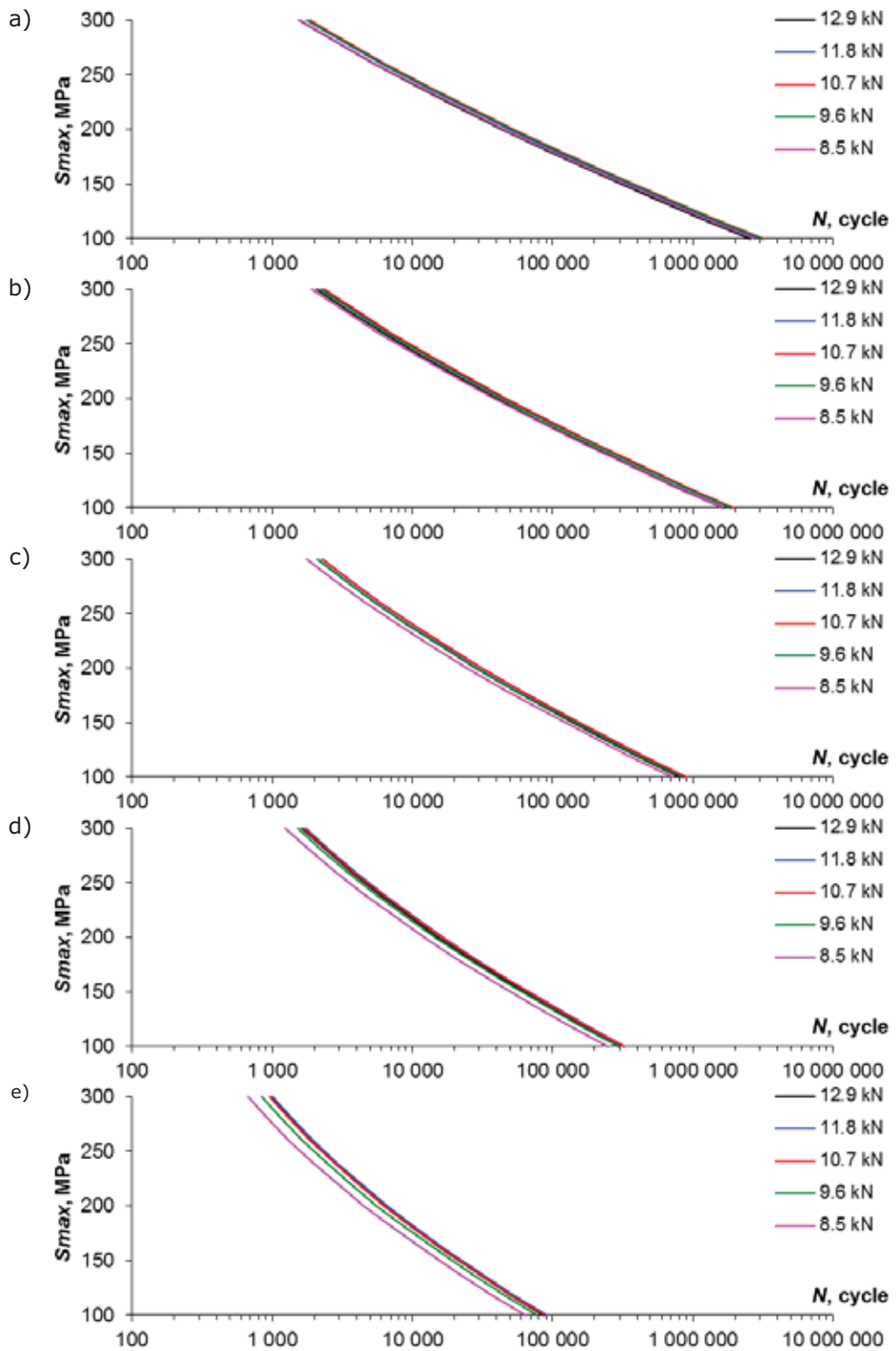


Fig. 2. Sample fatigue life plots with extrapolation outside of  $S_{max}$  range in plan of experiment obtained from the mathematical model of experimental unit depending on the rivet squeezing force  $P$  and the hole diameter before sizing  $d_w$ : a) 2.90 mm, b) 2.95 mm, c) 3.00 mm, d) 3.05 mm, e) 3.10 mm (velocity of rivet close up  $v = 0.08$  mm/s = const)

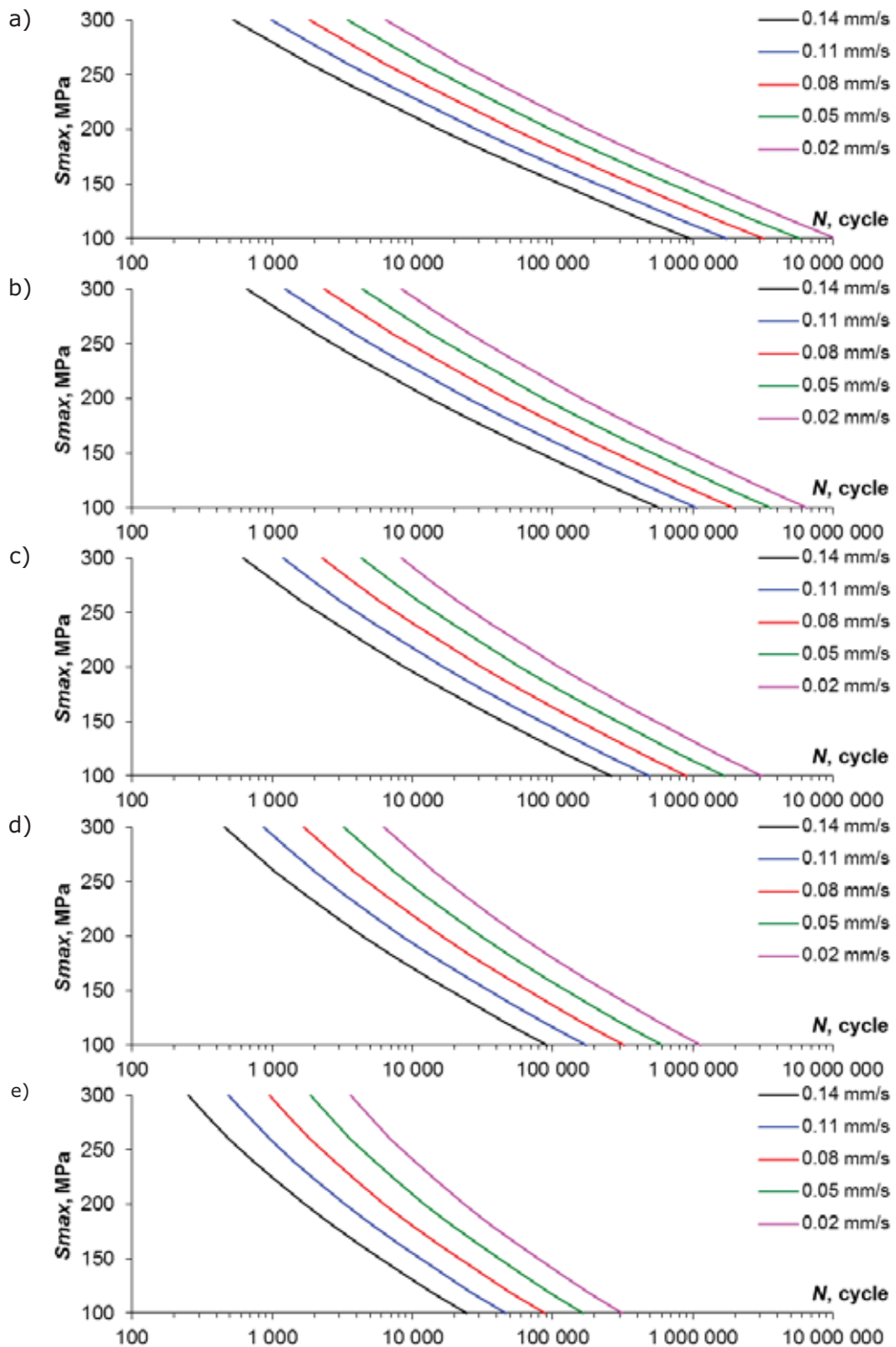


Fig. 3. Sample fatigue life plots with extrapolation outside of  $S_{max}$  range in plan of experiment obtained from the mathematical model of experimental unit depending on velocity of rivet close up  $v$  and the hole diameter before sizing  $d_w$ : a) 2.90 mm, b) 2.95 mm, c) 3.00 mm, d) 3.05 mm, e) 3.10 mm (the rivet squeezing force  $P = 10.7$  kN = const)



## DETERMINATION OF INPUT DATA FOR THE PROCESS OF VALIDATION OF OWN CALCULATION SOFTWARE FOR BASIC MATERIAL DATA IN STATIC STRENGTH TESTS

Zbigniew LIS<sup>1</sup>, Marek SZCZUTKOWSKI<sup>2</sup>

<sup>1,2</sup> University of Technology and Life Sciences in Bydgoszcz  
ul. Prof. Kaliskiego 7 85-789 Bydgoszcz, Poland  
phone: +48 52 340 82 55, fax: +48 52 340 82 55  
e-mail: m.szczutkowski@utp.edu.pl

### *Abstract*

*The paper deals with the idea of validation of own application software related to data analysis in conditions of an accredited laboratory. Defined conditions require suitable approach to the chosen problem. While the accreditation process is directly connected with ISO/IEC 17025:2005 which refers to ISO 9001:2000 standards the quality management approach has been proposed in order to perform suitable requirements. Tensile testing method sets an example for the discussed topic as well as the application software supporting the method. Among various input data authors do mention i.e. environmental and organizational conditions, personnel qualifications or measurement equipment.*

**Keywords:** laboratory, accreditation, data analysis software, software validation, tensile testing

### 1. Introduction

A testing laboratory fulfills requirements of customers from the point of view of reliability of test results. Actually this is not always an issue from legal point of view but in general each customer of the laboratory needs as reliable results as possible. To support both practical and legal requirements of clients ISO/IEC 17025:2005 standard [2] has been elaborated. The standard [2] specifies the general requirements for the competence to carry out tests. It covers testing performed using standard methods, non-standard methods, and laboratory-developed methods. The standard is applicable to all laboratories regardless of the number of personnel or the extent of the scope of testing activities. As it is stated in the document it is for use by laboratories in developing their management system for quality, administrative and technical operations. Laboratory customers, regulatory authorities and accreditation bodies may also use it in confirming or recognizing the competence of laboratories. The term 'management system' used in the standard means the quality, administrative and technical systems that govern the operations of a laboratory. Moreover if testing laboratories comply with the requirements of the standard, they will operate a quality management system for their testing and calibration activities that also meets the principles of ISO 9001 [2].

Authors' professional and scientific experience is connected with testings performed in conditions of an accredited laboratory. Especially having in mind requirements of customers mentioned in the first indention the usage of ISO/IEC 17025 is an essential advantage in testing

services.

As technology develops more and more IT tools are used in testing processes. They support various tests on different stages i.e. data analysis. In such a case one can discuss commercial software that requires payment before it can be used or own software developed by the laboratory itself. In the second case the developed applications needs to be validated. Validation can be discussed from the point of view of information technology as well as ISO 17025:2005 requirements.

The aim of the paper is to discuss the process of determination of input data for validation of own software application in an accredited testing laboratory on the example of the calculation software for basic material data in strength static tests.

## 2. Software validation as a requirement of software engineering as well as quality management

In software engineering validation for software, in its simplest terms, is the demonstration that the software implements each of the software requirements correctly and completely. In other words, the right software product was built. In the United States since the mid-1980s, for example, the Food and Drug Association (FDA) has enforced validation of software and computer systems in pharmaceutical manufacturing for consumers' safety. In response to this important industry need, the industry has created special task forces with the primary mission of developing guidelines for computer and software validation - known as the Computer System Validation Committee of the Pharmaceutical Research and Manufacturing Association (PhRMA) [9].

Discussing benefits of the validation process the document [6] states that software validation is a critical tool used to assure the quality of device software and software automated operations. Software validation can increase the usability and reliability of the device, resulting in decreased failure rates, fewer recalls and corrective actions, less risk to patients and users, and reduced liability to device manufacturers. Software validation can also reduce long term costs by making it easier and less costly to reliably modify software and revalidate software changes. Software maintenance can represent a very large percentage of the total cost of software over its entire life cycle. An established comprehensive software validation process helps to reduce the long-term cost of software by reducing the cost of validation for each subsequent release of the software.

Sometimes it is hard to find the difference in terms validation and verification. The terms are frequently used in the software testing world but the meaning of those terms are mostly vague and debatable. One encounter all kinds of usage and interpretations of those terms, and it is our humble attempt here to distinguish between them as clearly as possible [10]. Table 1 presents basic differences.

*Table 1. Differences between validation and verification [10]*

| Criteria   | Verification  | Validation   |
|------------|---|--|
| Definition | The process of evaluating work-products (not the actual final product) of a development phase to determine whether they meet the specified requirements for that phase. | The process of evaluating software during or at the end of the development process to determine whether it satisfies specified business requirements.        |
| Objective  | To ensure that the product is being built according to the requirements and design specifications. In other words, to ensure that work products meet their specified    | To ensure that the product actually meets the user's needs, and that the specifications were correct in the first place. In other words, to demonstrate that |

|                  |  |  |
|------------------|--|--|
|                  | requirements.  | the product fulfills its intended use when placed in its intended environment. |
| Question         | Are we building the product right?                       | Are we building the right product?   |
| Evaluation items | Plans, Requirement Specs, Design Specs, Code, Test Cases | The actual product/software.   |
| Activities       | Reviews, Walkthroughs, Inspections                       | Testing  |

It is entirely possible that a product passes when verified but fails when validated. This can happen when, say, a product is built as per the specifications but the specifications themselves fail to address the user's needs [10] .

The basic principles behind software validation are as follows[9]:

- a) specify the intended use of the software and user requirements;
- b) verify that the software meets the requirements through proper design, implementation, and testing;
- c) and maintain proper use of the software through an ongoing performance program.

It has to be noticed that the document [6] bases on quality system issues and refers to various quality management standards i.e. AS 3563.1-1991 "Software Quality Management System, Part 1: Requirements" published by Standards Australia [1] or to ISO 9000-3:1997 "Quality management and quality assurance standards - Part 3: Guidelines for the application of ISO 9001:1994 to the development, supply, installation and maintenance of computer software" [4] published by International Organization for Standardization.

Discussing the point of view of quality management systems the base standard ISO 9000:2005 [3] defines validation as a confirmation with the use of objective evidence that the requirements for an intended use or application have been fulfilled. In the standard [2] the definition states that validation is the confirmation by examination and the provision of objective evidence that the particular requirements for a specific intended use are fulfilled.

Considering the IT difference in terms between verification and validation it has to be stated that such a diversification can be also seen in quality standards. Standard [3] defines verification as a confirmation, through the provision of objective evidence, that specified requirements have been fulfilled.

From the point of view of the standard [2] according to authors [7] the parallels with validation are obvious as verification is also confirmation, also based on objective evidence and also tested against specified requirements but apparently without a specific use in mind that is part of the definition of validation. In practice the difference lies in the fact that validation is cited in connection with test methods, while verification is used in connection with the confirmation of data.

Although various definitions may be confusing it is obvious that own application software has to fulfill requirements of laboratory personnel to provide reliable data analysis results. Therefore objective evidence has to be provided so that the software validation process has to be designed in details.

On the base of such an assumption, with knowledge on IT and quality management systems from the range of validation, the plan for the validation process can be set.

As the first stage in the process there should be defined input data.

### 3. Input data in reference to designed software

Considering the assumption made before it seems the the obvious step to take would be to

define the validation process in accordance with ISO 9000:2005 model of the process approach (fig. 1).

One of key roles in the model is played by input data. Discussing static tensile tests and computer application software that supports the analysis of data it is essential to answer the question what would be the content of the input data. Basing on the scientific and professional experience authors of this work decided to define the content as following elements:

- a) testing method,
- b) environmental and organizational test conditions,
- c) measurement equipment,
- d) test piece material,
- e) personnel qualifications,
- f) software for machine.

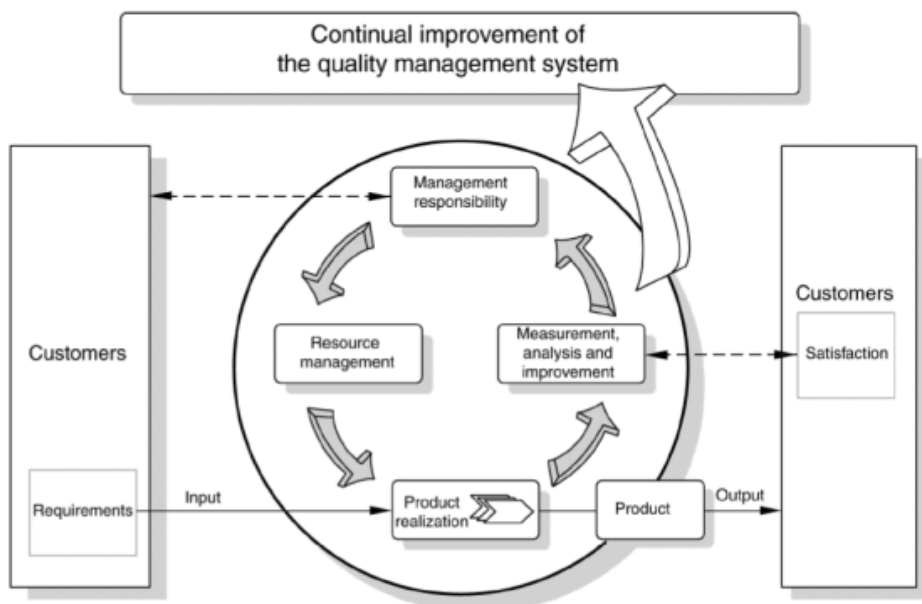


*Fig. 1. Model of the process approach in accordance with [3]*

At first the test method is an issue. The question is whether it is based on an international standard. Obviously it is easier to perform test on the base of standard or other specifications from the organizational point of view. There is no need to perform extra documentation as well as the method does need to be validated. In such a situation the first impression is that taking into consideration standard tests is more efficient form the financial point of view. However, considering both technical and organizational issues, the problem seems to be more complicated. For example standard test are limited to special environmental conditions or defined test pieces. It requires purchasing of i.e. new equipment. On the other hand sometimes customer needs non-standard materials or elements to be tested.

From the point of view of validation of own software the second option is much more sophisticated. While standard testing methods give limits and requirements strictly defined the non-standard methods that use own application software require cooperation with an author of the

method and laboratory personnel that uses it. The more unique testing method the less chance to find the reliable comparison tool. The easiest way to deliver objective evidence is to compare test results obtained with different (2 or more) data analysis software. For instance the commercial one and the new elaborated tool of the laboratory. Objective evidence is easy to get while previously the laboratory used commercial software that underwent verification as an element of the testing method during the accreditation process.

In static tensile tests authors assume that designing software for data analysis makes sense while a machine provides data in digital form. What is more any machine (type, producer etc.) able to cooperate with own software should provide the same data.

While for tensile tests there are needed various physical quantities such as temperature or length it is essential to define precisely requirements for measurement instruments. Cooperation of measurement instruments and own application software surely affect measurement uncertainty.

Test pieces usually depend on customer's needs. It is more comfortable for the laboratory while specimens are based on the standard as it is presented in fig. 2 (main types of test pieces according to [5]. B – A refer to annexes published with the standard). However it needs to be discussed if our software limits to such situations or also reflects non-standard requirements of the customer.





| Type of product  |   | Corresponding Annex |
|--|---|---------------------|
| <b>Sheets — Plates — Flats</b><br><br><b>Thickness</b><br>$a$ | <b>Wire — Bars — Sections</b><br>  <br><b>Diameter or side</b> |                     |
| $0,1 \leq a < 3$   | —   | B                   |
| —  | $< 4$   | C                   |
| $a \geq 3$   | $\geq 4$  | D                   |
| <b>Tubes</b>   |   | E                   |

Fig. 2. Main types of test piece according to product type [5]

There is also the problem of personnel qualifications. It can be discussed from different points of view as well: technical in the range of testing method (how experienced and efficient he/ she is in his/ her everyday work related directly to specific tests), technical in the range of usage of IT tools (gaining quickly new knowledge and skills from the area) or organizational (new methods of work vs. old habits and complaints on changes).

Finally the own application software has to cooperate, as it was noticed before, with the testing machine. The machine has to provide data in digital form but it is impossible to require more from machine producers. That is why the software has to be as efficient as possible in data processing on the way machine – user – software.

#### 4. Summary

Reliable test results depend on many organizational and technical issues. It is very hard to design and build such a unique organization as a testing laboratory. Quality management standards, especially the ones dedicated strictly to special types of organizations, can be useful in organizational and technical development. ISO/IEC 17025:2005 standard directly refers to testing

laboratories. Therefore it can be applied in material testing units as well.

Different tests methods should undergo the process of validation. While the method is based on the standard the laboratory does not need to perform the process. If the method is elaborated as a unique one for the laboratory validation is necessary. In both cases laboratories nowadays use more and more IT tools to develop testing processes. If the software supporting the process is new it has to be validated as well.

Authors proposed the quality management approach which corresponds also to software engineering basics. In such a case it is essential to define input data. In the paper input data were defined in the form of different elements such as: testing method, environmental and organizational test conditions, measurement equipment, test piece material, personnel qualifications, software for machine. The content of input data bases on scientific and organizational experience in the range of material strength tests.

The screenshot shows the 'Tensile Report' application window. It features a table for inputting test data with columns for displacement [mm], force [kN], elongation [%], and stress [MPa]. Below this is a section for material properties with fields for Ae, Su, L0, and an 'Input' field. Another table is provided for results with columns for E, Ap, Z, and Rm. At the bottom, there are five buttons: 'Load data', 'Show plot', 'Calculate', 'Generate HTML report', and 'About'.

|   | [mm] | [kN] | [%]   | [MPa] |
|---|------|------|-------|-------|
| 1 | 0.02 | 0.15 | -0.01 |       |
| 2 | 0.04 | 0.51 | 0.02  |       |
| 3 | 0.05 | 0.81 | 0.01  |       |

|       | Ae   | Su | L0 |
|-------|------|----|----|
| Input | 50.3 |    |    |

|         | E [10 <sup>4</sup> MPa] | Ap [%] | Z [%] | Rm [MPa] |
|---------|-------------------------|--------|-------|----------|
| Results |                         |        |       |          |

Buttons: Load data, Show plot, Calculate, Generate HTML report, About

Fig. 3. "Tensile report". Main window [8]

On the base of the defined content authors are planning to perform validation of own software application "Tensile report". The software was developed as a result of cooperation between an academic teacher (one of the authors of this paper) and a student and finally became a base for a graduation project [8]. Results of the validation process in accordance with the proposed approach will be presented in further publications.

## References

- [1] AS 3563.1-1991 - Software Quality Management System, Part 1: Requirements.

- [2] ISO/IEC 17025:2005 - General requirements for the competence of testing and calibration laboratories.
- [3] ISO 9000:2005 - Quality management systems - Fundamentals and vocabulary.
- [4] ISO 9000-3:1997 - Quality management and quality assurance standards - Part 3: Guidelines for the application of ISO 9001:1994 to the development, supply, installation and maintenance of computer software.
- [5] ISO 6892-1:2009 - Metallic materials - Tensile testing - Part 1: Method of test at room temperature.
- [6] U.S. Department Of Health and Human Services, Food and Drug Administration, Center for Devices and Radiological Health, Center for Biologics Evaluation and Research.: *General Principles of Software Validation; Final Guidance for Industry and FDA Staff*, 2002.
- [7] Czichos, H., Saito, T., Smith, L.: *Springer Handbook of Materials Measurement Methods*, Springer, 2006
- [8] Reinke, D.: *Computer-aided standard test method for tensile strength – application software implementation*, Graduation project, Univeristy of Technology and Life Sciences in Bydgoszcz, 2011.
- [9] <http://computer.yourdictionary.com/validation>, 06.2012
- [10] <http://softwaretestingfundamentals.com/verification-vs-validation>, 06.2012





## CARBON PARTITIONING AND MECHANISM OF BAINITE REACTION IN EXPERIMENTAL Fe-Cr-Mo-C STEEL

**Zdzisław Ławrynowicz**

*University of Technology and Life Sciences, Mechanical Engineering Faculty  
Department of Materials Science and Engineering  
av. Kaliskiego 7, 85-789 Bydgoszcz, Poland  
E-mail: lawry@utp.edu.pl*

### **Abstract**

*Carbon partitioning and mechanism of bainite transformation have been studied in Fe-Cr-Mo-C steel using high speed dilatometry backed by thermodynamic analysis. Obtained results confirm the incomplete reaction phenomenon with the cessation of the bainite transformation well before paraequilibrium is achieved. These experimental data indicate that bainitic ferrite forms by a displacive transformation mechanism, but soon afterwards, excess of carbon is partitioned into the residual austenite. The results are discussed in terms of the mechanism of bainite transformation.*

**Keywords:** carbon partitioning, mechanism of bainite transformation

### **1. Introduction**

Carbon concentration in the residual austenite at the termination of the bainitic reaction and the mechanism of bainite transformation in steels remain still controversial and involves two general concepts, that bainitic reaction occurs via a diffusional mechanism [1], and that bainitic reaction occurs in a displacive mechanism as far as the substitutional elements are concerned [4]. Aaronson and co-workers introduced hypothesis that occurrence of bainitic "bay" on *TTT* diagrams many commercial steels and incomplete reaction phenomenon (transformation stasis) are attributed to a special effect of alloying elements on the growth kinetics, which was termed as a solute drag-like effect (SDLE) [3,6,9,17]. However, atom probe experiments reveal the absence of any substitutional alloying element partitioning at the bainitic ferrite/austenite interface during bainitic transformation. It is usually assumed that the point where dimensions cease to change represents full transformation. But in case of bainitic transformation, reaction ceases before the parent phase has completely transformed what is known as an incomplete reaction phenomenon. It means that at any temperature below  $B_S$  and in the absence of any interfering secondary reactions only a limited quantity of bainitic ferrite forms before the reaction terminates. The role of carbon in the growth of bainite, is difficult to resolve directly, because even if the ferrite is supersaturated during growth, the relatively high transformation

temperatures provide an opportunity for the excess of carbon to diffuse rapidly into residual austenite before any experimental measurements can be made [2]. There are indirect methods of determining the carbon concentration of bainitic ferrite during growth, e.g. dilatometry method. This paper attempts to investigate the mechanism of the bainite transformation in 15HM2 steel and to clarify the bainitic ferrite formation mechanism from the thermodynamic point of view.

## 2. Experimental procedures

A high-speed Adamel Lhomargy LK-02 dilatometer was used to establish change of length ( $\Delta L/L$ ) during isothermal bainitic transformation. In order to ensure rapid cooling ( $\sim 300\text{Ks}^{-1}$ ) from austenitizing temperature ( $1000^\circ\text{C}$ , 10 minutes), the specimens were 13mm in length and 1.1mm in diameter. Lattice parameter measurements were carried out using a X-ray diffractometer with Fe-filtered  $\text{CoK}_\alpha$  radiation. The precision ferrite lattice parameter determination included a knowledge of the angular positions of the (110), (200), (211) and (220) peaks. The data were analysed using a Taylor-Sinclair function to extrapolate the values of the ferrite parameter to angular position of  $\Theta=90^\circ$ . The linear expansion coefficient of ferrite ( $e_\alpha$ ) was determined by annealing a specimen at  $650^\circ\text{C}$  for 30 minutes to decompose any retained austenite and then recording the change of length during slow cooling. The linear expansion coefficient of austenite ( $e_\gamma$ ) was measured after cooling from temperature of  $1100^\circ\text{C}$  while the specimen was in the single  $\gamma$  phase field. Determination of the linear expansion coefficients was carried out in a UBD Leitz-Wetzlar dilatometer. Thin foils were stored in ethanol and subsequently examined in a Tesla BS-540 electron microscope at an operating voltage of 120 kV.

## 3. Conversion of dilatometry data

For the transformation of austenite into a mixture of bainitic ferrite and carbon enriched residual austenite and assuming isotropic strain the relationship between dimensional changes  $\Delta L$  and volume changes  $\Delta V$  is given by the equation [4]:

$$\frac{\Delta V}{V} \approx 3 \frac{\Delta L}{L} \quad (1)$$

Where  $L$  is the specimen length at the transformation temperature. The lattice parameters of bainitic ferrite and untransformed austenite at the reaction temperature,  $a_\alpha$  and  $a_\gamma$ , can be calculated from the values of lattice parameters at ambient temperature ( $25^\circ\text{C}$ ,  $298\text{K}$ ) using the linear thermal expansion coefficients  $e_\alpha$  and  $e_\gamma$ :

$$a_\alpha = a_{0\alpha} [1 + e_\alpha (T - 298)] \quad (2)$$

$$a_\gamma = a_{0\gamma} [1 + e_\gamma (T - 298)] \quad (3)$$

where  $T$  is the absolute temperature. The room temperature lattice parameter of austenite ( $a_{0\gamma}$  in nm) at the mean steel composition (i.e. when  $V_\alpha = 0$ ) can be calculated using equation determined by Dyson and Holmes [8]:

$$a_{o\gamma} = 0.3578 + \sum_{i=1}^n C_i x_i \quad (5)$$

where  $C_i$  are coefficients and  $x_i$  is the weight fraction of alloying element in phase  $\gamma$ , where  $i = 1, 2, \dots, n$  represents alloying elements ( $i = 1$  for carbon,  $i > 1$  for substitutional solutes). The ferrite lattice parameter  $a_{o\alpha}$  was determined by X-ray analysis and for ascertain it was calculated using following equation [4]:

$$a_{o\alpha} = 0.28664 + (3a_{Fe}^2)^{-1} \cdot [(a_{Fe} - 0.0279x_c^\alpha)^2 (a_{Fe} + 0.2496x_c^\alpha) - a_{Fe}^3] - 0.003x_{Si}^\alpha + 0.006x_{Mn}^\alpha + 0.007x_{Ni}^\alpha + 0.031x_{Mo}^\alpha + 0.005x_{Cr}^\alpha + 0.0096x_V^\alpha \quad (6)$$

The lattice parameter of pure ferrite was taken as  $a_{Fe} = 0.28664 \text{ nm}$  [16]. The terms  $x_i^\alpha$  represent the mole fraction of the species  $i$  in phase  $\alpha$ . The carbon concentration of the residual austenite  $x_1^\gamma$  increases during bainitic transformation as a consequence of the increasing volume fraction of bainitic ferrite. Given that the excess carbon in the bainite ferrite partitions into the residual austenite and assuming that the final microstructure consists of only bainitic ferrite and residual austenite it is possible to estimate the carbon concentration according to the following relationship derived from mass balance considerations [4]:

$$x_1^\gamma = \frac{2a_\alpha^3 \bar{x} (1 - x_1^\alpha)(1 - V_\alpha) + a_{e\gamma}^3 (\bar{x} - x_1^\alpha) V_\alpha}{2a_\alpha^3 (1 - x_1^\alpha)(1 - V_\alpha) + a_{e\gamma}^3 (\bar{x} - x_1^\alpha) V_\alpha} \quad (7)$$

The carbon content of the ferrite  $x_1^\alpha$ , is a very small and is approximated by the  $A_1 \alpha/(\alpha+\gamma)$  phase boundary of the Fe-C phase diagram (since of its smallness ignoring the effect of substitutional elements). The value of carbon in bainitic ferrite was taken to be  $x_1^\alpha = 0.00139$  (0.03 wt.%) [16]. The calculated carbon concentrations of residual austenite at the point where the formation of bainite terminates will be next compared against the extrapolated  $T_0$ ,  $T_0'$  and  $A_3'$  phase boundaries.

#### 4. Material, results and discussion

The composition of the steel investigated is given in Tab. 1.

Tab. 1. Chemical compositions of the steel used in this study.  
All concentrations are given in wt.% and at.% ( $\times 10^{-2}$ )

| Steel |       | C     | Si    | Cr    | Mn    | Mo    | Al    |
|-------|-------|-------|-------|-------|-------|-------|-------|
| 15HM2 | wt. % | 0.14  | 0.23  | 0.88  | 0.73  | 2.4   | 0.03  |
|       | at. % | 0.651 | 0.457 | 0.945 | 0.729 | 1.397 | 0.062 |

The dilatometry results showed that the relative length change during the formation of bainite at selected temperatures increases as the isothermal transformation temperature decreases below the  $B_S$  (Fig. 1), then the amount of bainite formed is dependent on the transformation temperature. The lattice parameters of ferrite and austenite and values of linear expansion coefficients are given in Tab. 2. The

details for calculation of volume fraction of transformation are given in Tab. 3.

Calculated and measured the carbon concentration of the residual austenite ( $x_\gamma$ ) and carbon concentration at the interphase boundaries in Fe-Cr-Mo-C steel are given in Tab. 4.

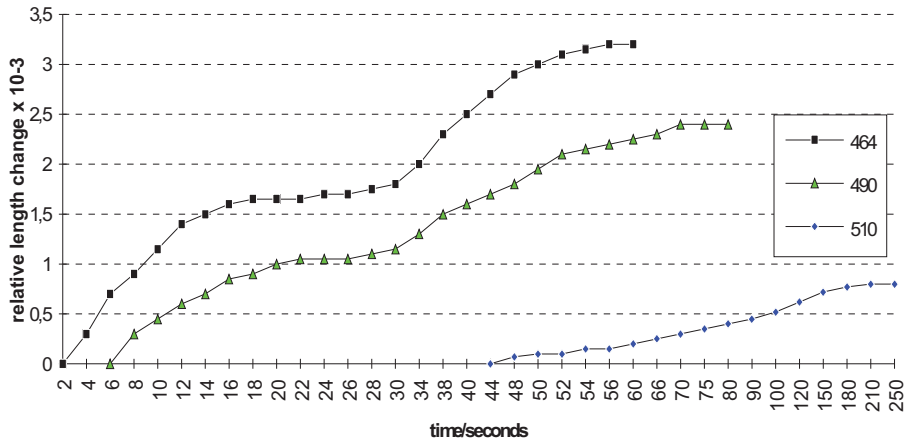


Fig. 1. The relative length change ( $\Delta L/L$ ) observed by dilatometry during isothermal transformation at selected temperatures below  $B_s$  temperature in Fe-Cr-Mo-C steel

Tab. 2. Lattice parameters and linear expansion coefficients of ferrite and austenite

| Steel      | Lattice parameter of ferrite $a_{\alpha}$<br>nm | Lattice parameter of austenite $a_{\gamma}$<br>nm | Ferrite $e_{\alpha}$<br>$^{\circ}\text{C}^{-1}$ ,<br>$\times 10^{-5}$ | Austenite $e_{\gamma}$<br>$^{\circ}\text{C}^{-1}$ ,<br>$\times 10^{-5}$ |
|------------|---|---|---|---|
| Fe-Cr-Mo-C | 0.2872<br>0.2871 *                              | 0.35910   | 1.627   | 2.317   |

\* The ferrite lattice parameter determined using a X-ray diffractometer

Tab. 3. Parameters for determination of volume fractions of bainite ( $V_B$ ) in Fe-Cr-Mo-C steel

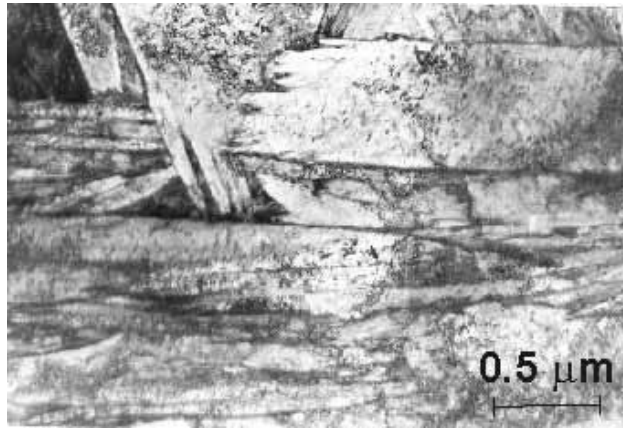
| Transformation temperature, $^{\circ}\text{C}$ | $a_{\gamma}$<br>nm | $a_{\alpha}$<br>nm | $\Delta L/L^*$<br>$\times 10^{-3}$ | $V_B$ |
|--|--------------------|--------------------|------------------------------------|-------|
| 464  | 0.3627             | 0.2893             | 4.88                               | 0.66  |
| 475  | 0.3628             | 0.2893             | 4.52                               | 0.62  |
| 490  | 0.3629             | 0.2894             | 4.56                               | 0.53  |
| 500  | 0.3630             | 0.2894             | 4.35                               | 0.22  |
| 510  | 0.3631             | 0.2895             | 4.46                               | 0.18  |

\* Values of the dimensional changes accompanying the transformation of austenite to bainitic ferrite measured at transformation temperature,

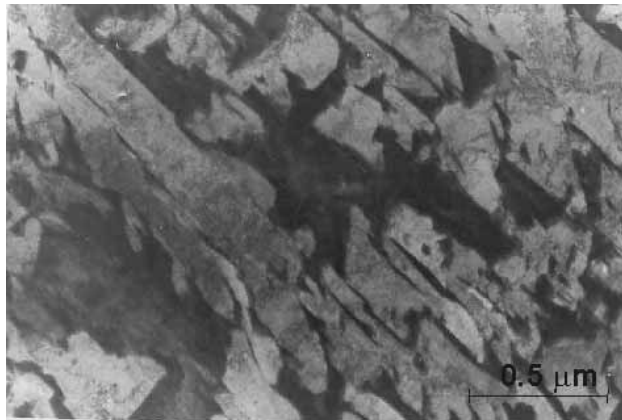
$V_B$  Measured volume fraction of transformation.

Fig. 2 shows the general morphology of the microstructure in 15HM2 steel after austenitization at 1200°C and isothermal transformation at 450°C for 600s. The morphology of the bainite is similar to low carbon lath martensite, where dislocated laths are separated by films of retained austenite. No blocky austenite was observed in this structure. Careful examination of this microstructure shows small precipitated carbides laying inside bainitic ferrite laths. No significant changes in morphology with increasing reaction time were observed after isothermal transformation at 450°C. This structure, therefore, belongs to lower bainite assuming that lower bainite in this steel is a structure composed of carbides within bainitic laths with interlath retained austenite films [11-15].

After austenitization at 1200°C and at higher transformation temperature (550°C), bainite changes into a morphology without carbides within the laths but with blocky retained austenite (Fig. 3).



*Fig. 2. Morphology of the microstructure in 15HM2 steel after austenitization at 1200°C and isothermal transformation at 450°C for 600s. Thin foil*



*Fig. 3. Microstructure of 15HM2 steel after austenitization at 1200°C and isothermal transformation at 550°C for 1800s. Thin foil*

Tab. 4. Calculated and measured the carbon concentration of the residual austenite ( $x_\gamma$ ) and carbon concentration at the interphase boundaries in Fe-Cr-Mo-C steel

| Phase      | Transformation temperature, °C / Carbon concentration at the interphase, mol |        |        |        |        |        |        |        |
|------------|--|--------|--------|--------|--------|--------|--------|--------|
|            | 700  | 600    | 510    | 500    | 490    | 475    | 464    | 400    |
| $A_3'$     | 0.0233   | 0.0520 | 0.0840 | 0.0878 | 0.0918 | 0.0978 | 0.1023 | 0.1257 |
| $x_{T_0}$  | 0.008  | 0.0157 | 0.0243 | 0.0253 | 0.0261 | 0.0277 | 0.0293 | 0.0384 |
| $x_{T_0'}$ |  | 0.0033 | 0.0135 | 0.0147 | 0.0160 | 0.0179 | 0.0194 | 0.0267 |
| $x_\gamma$ |  |        | 0.0076 | 0.0079 | 0.0121 | 0.0146 | 0.0162 |        |

The determined carbon concentrations of the residual austenite at the point where the formation of bainite ceases are compared with the  $T_0$ ,  $T_0'$  and  $A_3'$  phase boundaries for examined 15HM2 steel in Fig. 4. The diagram was calculated using a model developed by Bhadeshia [4,5] based on the McLellan and Dunn quasi-chemical thermodynamic model [16]. The  $T_0$  curve represents the locus of all points where austenite and ferrite of the same composition have equal free energy [1,4]. The  $T_0'$  curve allows for 400J/mol of stored energy in the bainitic ferrite to take account of the strain energy due to the invariant-plane strain shape change that accompanies the growth of bainitic ferrite [5,7]. The  $A_3'$  curve is the calculated paraequilibrium ( $\alpha+\gamma$ )/ $\gamma$  phase boundary indicating equilibrium between ferrite and austenite when the ratio of substitutional alloying elements to iron is constant everywhere. The bainite and martensite reactions start temperatures  $B_S$  and  $M_S$  are also marked on that diagram.

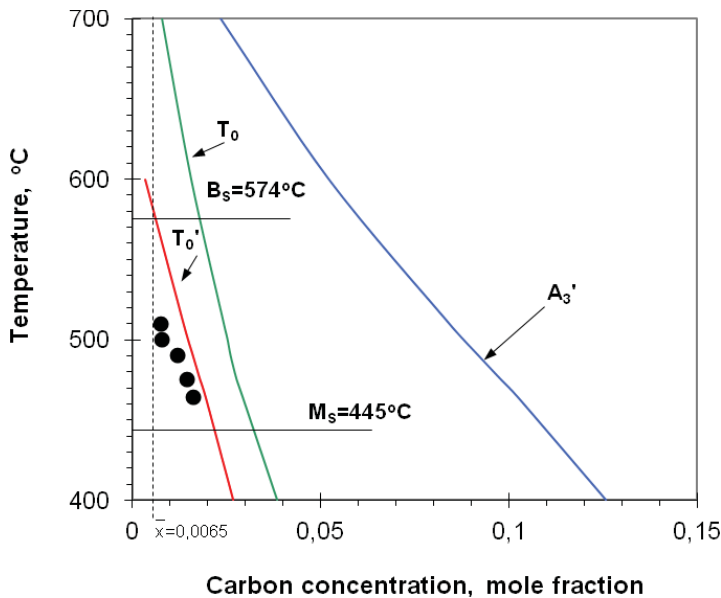


Fig. 4. Calculated phase diagram with experimental data of carbon concentration of residual austenite at the termination of isothermal bainite formation for Fe-Cr-Mo-C steel (black circles represent experimental data)

Paraequilibrium is a constrained equilibrium in which only carbon atoms are free to partition between ferrite and austenite. The ratio of the substitutional solute concentration to the iron concentration is the same in ferrite and in austenite, the chemical potential of carbon is equal in the two phases [6]. The paraequilibrium phase boundary is chosen because no substitutional alloying element partitioning occurs during bainite formation.

If the hypothesis that paraequilibrium exists during all stages of transformation is correct, then the reaction should stop when the carbon concentration of the austenite is given by the  $A_3'$  curve. In presented experiment the reaction is found to stop when the average carbon concentration of the residual austenite is close to the  $T_0$  curve than the  $A_3'$  boundary (black circles in Fig. 4). Note that the difference in carbon concentrations between the  $T_0'$  and  $A_3'$  curves at the chosen temperatures of bainitic reaction is very large, so the presented experiment is a sensitive indication of the failure of the transformation to reach paraequilibrium. The  $T_0'$  curve has a negative slope, so the austenite can tolerate more carbon before diffusionless transformation becomes impossible, as the transformation temperature is reduced.

The presented above results can be explained when it is assumed that bainitic ferrite grows without diffusion, but any excess of carbon is soon afterwards rejected into the residual austenite by diffusion [9-13]. This makes more difficult for subsequent bainitic ferrite to grow, when the austenite becomes stabilised by increased carbon concentration. The maximum extent to which the bainite reaction can proceed is therefore determined by the composition of the residual austenite. A stage where diffusionless growth becomes thermodynamically impossible and the formation of bainitic ferrite terminates is where the carbon concentration of the austenite reaches the  $T_0'$  curve. The incomplete reaction phenomenon supports the hypothesis that the growth of bainitic ferrite occurs without any diffusion with carbon being partitioned subsequently into the residual austenite. There is as yet no reasonable alternative explanation of this phenomenon.

## 5. Conclusions

The austenite to bainite transformation was studied in Fe-Cr-Mo-C steel using dilatometry backed by thermodynamic analysis. The results obtained are summarized as follows:

1. The reaction terminates prematurely as the carbon content of the residual austenite reaches the  $T_0'$  curve well before the paraequilibrium carbon concentration is achieved (given by the extrapolated  $A_3'$  phase boundary) which indicates that the growth of bainitic ferrite is diffusionless.
2. The maximum extent of bainite formation in 15HM2 steel is dependent on the transformation temperature and the degree of transformation strongly decreases with approaching the bainite start temperature.

## References

- [1] Aaronson, H.I., Reynolds, W.T., Shiflet, G.J., Spanos, G., *Bainite Viewed Three Different Ways*, Metall. Trans. A, 21A, 1343-1380, 1990.
- [2] Aaronson, H.I., *The proeutectoid ferrite and the proeutectoid cementite reactions*, In: Aaronson HI, Zackay VF, editors. *Decomposition of Austenite by Diffusional Processes*. New York: Interscience Publishers, 387-546, 1962.
- [3] Aaronson, H.I., *The Mechanism of Phase Transformations in Crystalline Solids*, The Institute of Metals, London, 1969, p.270.
- [4] Bhadeshia, HKDH, Christian, JW., *Bainite in steels*, Metall Trans. A, 21A, 767-797, 1990.

- [5] Caballero, F.G., Miller, M.K., Babu, S.S., Garcia-Mateo, C., *Atomic scale observations of bainite transformation in a high carbon high silicon steel*, Acta Materialia, 55, 381-390, 2007.
- [6] Chen, J.K., Vandermeer, R.A., Reynolds, W.T., JR., *Effect of Alloying Elements upon Austenite Decomposition in Low-C Steels*, Metall. Mater. Trans.A, 25A, 1367-1379, 1994.
- [7] Christian J.W., Edmonds D.V., *Int. Conf. on Phase Transformations in Ferrous Alloys*, A.R. Marder, J.I. Goldstein, ASM, Metals Park, OH, 1984, p.293.
- [8] Dyson D.J., Holmes, B., *Effect of alloying additions on the lattice parameter of austenite*, J. Iron Steel Inst., 208, 469-474, 1970.
- [9] Hehemann, R.F., Kinsman, K.R., Aaronson, H.I., *A debate on the bainite reaction*, Metall. Trans., 3, 1077-94, 1972.
- [10] Hillert, M., Höglund, L., Ägren, J., *Escape of carbon from ferrite plates in austenite*, Acta Metall Mater., 41, 1951-7, 1993.
- [11] Ławrynowicz, Z., Barbacki, A., *Carbides precipitation in bainite in an experimental Mo-Cr-V-Ti steel*, Conference Proceedings of the 6-th International Conference "Carbides, Nitrides, Borides," Poznań-Kołoźbrzeg, pp. 42-47, 1993.
- [12] Ławrynowicz, Z., *Ausferritic or Bainitic Transformation in ADI*, Proceedings of the 12th International Symposium on Advanced Materials, Paper No: 98, ISAM2011-98, Rawalpindi, Pakistan.
- [13] Ławrynowicz, Z., *Decarburisation of bainitic ferrite laths and its influence on the microstructure in Fe-Cr-Si-C steel*, Advances in Materials Science, 2011, Vol. 11, No. 2 (28), June pp. 56-64, 2011.
- [14] Ławrynowicz, Z., *Affect of decarburisation times of bainitic ferrite laths on the microstructure in Fe-Cr-C steel*, Journal of Polish CIMAC, Vol. 6, No. 3, pp. 127-136, 2011.
- [15] Ławrynowicz, Z., *Affect of cementite precipitation on the extend of bainite transformation in Fe-Cr-C steel*, Advances in Materials Science, Vol. 11, No. 3 (29), pp.13-19, September 2011.
- [16] McLellan, R.B., Dunn, W.W., J.Phys.Chem. Solids, 30, 2631-2637, 1969.
- [17] Reynolds, W.T. et al., *An investigation of the Generality of Incomplete Transformation to Bainite in Fe-C-X Alloys*, Metall. Trans.A, 21A, 1479-1491, 1990.



## BAINITE MORPHOLOGY IN EXPERIMENTAL Fe-Mo-Cr-V-Ti-C STEEL

**Zdzisław Ławrynowicz**

*University of Technology and Life Sciences, Mechanical Engineering Faculty  
Department of Materials Science and Engineering  
av. Kaliskiego 7, 85-789 Bydgoszcz, Poland  
E-mail: lawry@utp.edu.pl*

### **Abstract**

*The development of bainitic transformation was studied using TEM, dilatometry and thermodynamic calculations, both from a fully austenitic microstructure ( $T_A=1200^\circ\text{C}$ ) and from a microstructure containing a mixture of austenite and undissolved carbides ( $T_A=1000^\circ\text{C}$ ). The amount, distribution and morphology of retained austenite, bainitic ferrite and precipitation of carbides strongly depends on both; prior austenitization and isothermal transformation temperatures within the bainitic range.*

**Keywords:** bainite morphology, bainitic transformation, low alloy steel

### **1. Introduction**

The present paper attempts to investigate the morphology of bainite formation in laboratory prepared low alloy Cr-Mo-V-Ti (signed as 15HM2VT steel). Vanadium and titanium are present to refine the austenite grain size, resulting in a fine grained ferritic structure. Low carbon content promotes good toughness and weldability by elimination the volume fraction of carbide containing microconstituents (e.g. pearlite). In Fe-C-X steels, when X is a strong carbide forming alloying element, interphase boundary carbides and fibrous carbides were present after isothermal reaction at temperatures above the bay temperature [1,2,7,8]. This type of high strength low alloy (HSLA) steels are supposed to have the requisite good combination of strength, toughness and weldability for many industrial applications.

The main aim of the present investigation was to investigate the influence of austenitizing temperature (changing the volume of dissolved carbides and from this the chemical composition of austenite) and temperature of isothermal transformation on bainite transformation.

### **2. Material and experimental procedure**

The composition of the alloy investigated is given in Tab. 1. The specimens were austenitized for 20 minutes at 1000 and 1200°C. A coating layers were used to protect the specimens against decarburization. After isothermal transformation, the specimens were water quenched.

Tab. 1. Chemical compositions of the investigated steel (Wt Pct)

| Steel   | C    | Si   | Cr   | Mn   | Mo  | V    | Ti   | P     | S     | Al   |
|---------|------|------|------|------|-----|------|------|-------|-------|------|
| 15HM2VT | 0.15 | 0.24 | 0.84 | 0.92 | 2.6 | 0.24 | 0.12 | 0.022 | 0.019 | 0.06 |

Dilatometric analysis was carried out on a Leitz-Wetzlar vacuum dilatometer using a 20 mm by 3.5 mm dia. specimens to establish the  $A_1$  and  $A_3$  temperatures (Tab. 2). A high-speed LK-02 Adamel Lhomargy dilatometer was used to establish the  $M_S$  temperature (Tab. 2). In order to ensure rapid quenching ( $300 \text{ K s}^{-1}$ ) the specimens were 12mm in length and 1.0mm in diameter. The specimens were austenitized for 10 min. at  $1000^\circ\text{C}$  in dilatometry furnace and subsequently gas quenched to the isothermal transformation temperature by an automatically controlled high-pressure helium jet.

Tab. 2.  $A_1$ ,  $A_3$ ,  $B_S$  and  $M_S$  temperatures

| Steel   | Temperature, $^\circ\text{C}$ |          |          |          | Experimentally determined |       | Thermodynamically calculated |         |
|---------|-------------------------------|----------|----------|----------|---------------------------|-------|------------------------------|---------|
|         | $A_{c1}$                      | $A_{c3}$ | $A_{r1}$ | $A_{r2}$ | $M_S$                     | $B_S$ | $M_S^*$                      | $B_S^*$ |
| 15HM2VT | 807                           | 969      | 730      | 896      | 453                       | -     | 423                          | 555     |

\*Assuming full austenitization ( $1200^\circ\text{C}$ ) ensuring complete dissolving of carbides in austenite

The specimens for transmission electron microscopy (TEM) were machined to 3mm dia. rod, carefully avoiding any heating. The rods were sliced into 0.35mm thick discs while being kerosene cooled. The discs were subsequently ground down to a thickness of 40-50  $\mu\text{m}$  on 500 grid paper. These foils were finally electropolished in a twin-jet at room temperature and at 55-60V using a 25-pct glycerol, 5 pct perchloric acid and 70 pct ethanol mixture. Thin foils were stored in ethanol and subsequently examined in a Tesla BS-540 electron microscope at an operating voltage of 120 kV. Optical microscopy was used to examine etched structures. Specimens were etched in 2% nital solution.

### 3. Results and discussion

To plan the heat treatments a time-temperature-transformation (TTT) diagrams (Fig. 1) were calculated for the composition given in Tab. 1. The calculation was done using a method developed by Bhadeshia [3,4].

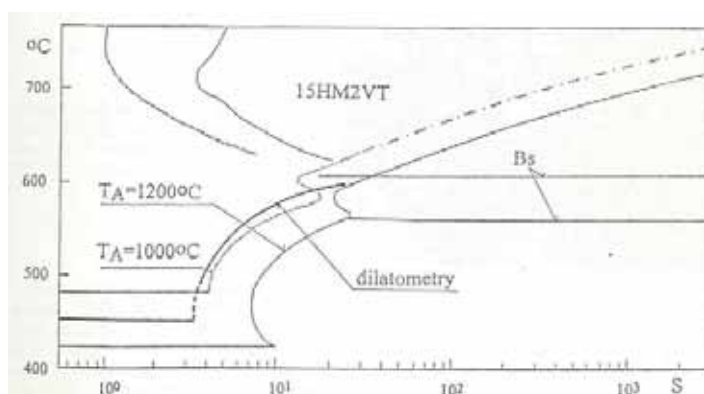


Fig. 1. Time-temperature-transformation (TTT) diagram of investigated 15HM2VT steel [10]

In that method the TTT diagram has been treated as being composed of two separate C curves, one of which represents diffusional transformations and the other, displacive reactions (Widmanstätten ferrite and bainite). The technique is capable of correctly generating the bay region of time-temperature-transformation diagrams, while at the same time allowing relative shifts in the shear and diffusional C curves, as a function of alloying element content. The bainitic ferrite  $B_S$  and martensitic  $M_S$  start temperatures were also calculated using the same method. The bainite start temperature  $B_S$  is the temperature corresponding to the upper part of the shear transformation C curve and it strictly refers to the point at which the nucleation of ferrite that grows displacively first becomes possible [3,5]. The transformation temperature data are given in Tab. 2.

Based on the dilatometry data and the data from the calculated TTT diagram heat treatment of 15HM2VT steel was planned as follows: two austenitizing temperatures 1000 and 1200°C/20minutes, and two utmost temperatures of bainite range, e.g. 575 – 500°C and 550 – 450°C respectively. Austenitizing temperature 1200°C was required for complete dissolution of VC carbides [2]. Isothermal reaction temperatures were chosen to lie above the  $M_S$  temperature to avoid formation of martensite during the isothermal heat treatment, and below the bay temperature of investigated steel.

Optical microscopy was carried out in order to observe any variations in the gross features of microstructure, e.g. prior austenite grain size, bainitic packet size and distribution of blocky austenite with heat treatment. The microstructural dimensions are given in Tab. 3.

Tab. 3. Microstructural parameters of 15HM2VT steel

| Microstructural parameters                  | Austenitization temperature:       |                   |                                  |                                  |
|---|------------------------------------|-------------------|----------------------------------|----------------------------------|
|   | 1200°C                             |                   | 1000°C                           |                                  |
|   | Transformation temperature, °C     |                   | Transformation temperature, °C   |                                  |
|   | 550                                | 450               | 575                              | 500                              |
| Average austenite grain size, $\mu\text{m}$ | 50                                 | 50                | 17                               | 17                               |
| Volume of bainite in the form of packets, % | 45                                 | 50                | 40                               | 45                               |
| Packet length, $\mu\text{m}$                | 40                                 | 40                | -                                | -                                |
| Packet width, $\mu\text{m}$                 | 30                                 | 36                | -                                | -                                |
| Width of bainite lath, $\mu\text{m}$        | 0.5                                | 0.4               | 0.6                              | 0.5                              |
| Morphology of retained austenite            | thin films, also irregular islands | mainly thin films | irregular islands and thin films | irregular islands and thin films |
| Volume fraction of retained austenite, % *  | 5.0                                | 8.6               | -                                | -                                |

\* Volume fraction of retained austenite were determined by rtg diffractometer on samples quenched to ambient temperature after isothermal transformation for 6h at temperature 550°C and for 3h at temperature 450°C

Optical micrographs of the partially reacted specimens of the 15HM2VT steel are shown in figures 2 and 3. Only large individual carbides TiC, regardless of austenitization temperature, can be detected in micrograph of the 15HM2VT steel (TiC carbides are arrowed). In observed microstructures the bainite reaction has not proceeded to completion, and large pools of residual austenite have subsequently transformed to martensite on water quenching.

There is a general tendency for structural refinement with decreasing austenitizing temperature.

The packet size after austenitization at 1200°C is coarser than that of 1100°C, which can be related to the larger austenite grain size (Tab. 3).

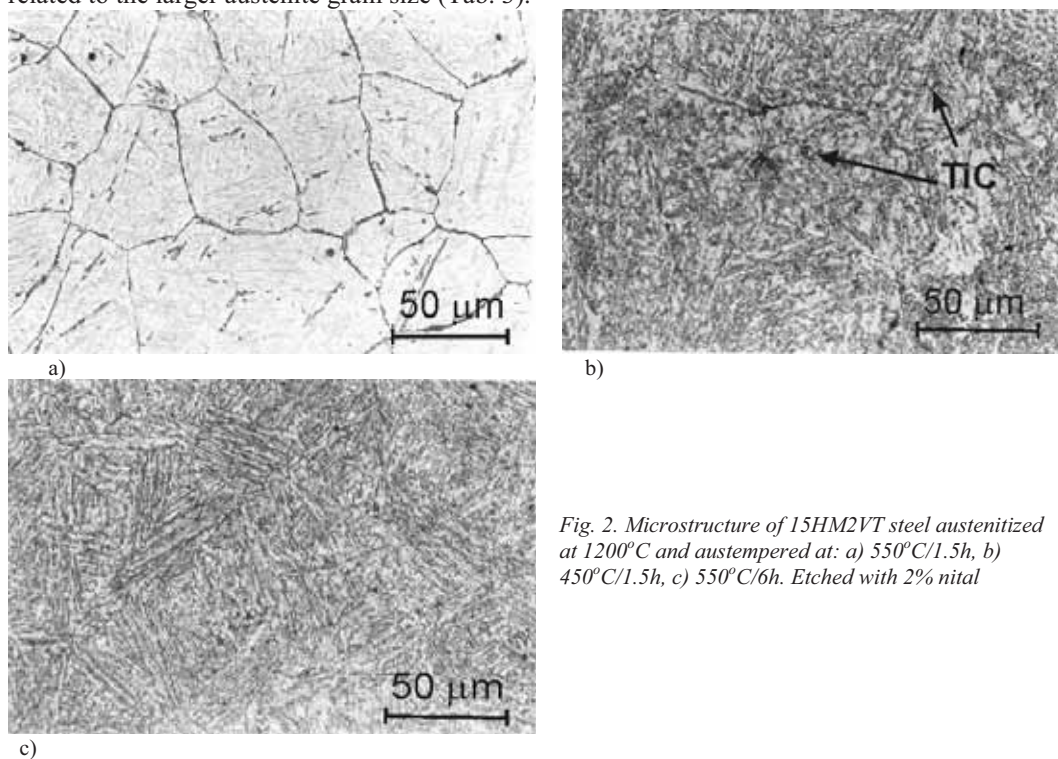


*Fig. 2. Microstructure of 15HM2VT steel austenitized at 1200°C and austempered at: a) 550°C/1.5h, b) 450°C/1.5h, c) 550°C/6h. Etched with 2% nital*

After transformation to bainite at higher temperature retained austenite exhibited a blocky, triangular shape. It was found that for 15HM2VT steel the volume fraction of retained austenite increased with decreasing of the isothermal transformation temperature (Tab. 3). The volume fraction of retained austenite after austenitization at 1000°C was beneath the level of resolution of applied X-ray diffractometer. When temperature of isothermal transformation was decreased the blocky morphology of retained austenite was replaced by films of retained austenite separated by platelets of bainitic ferrite. This film austenite, since it is trapped in the immediate vicinity of bainite laths is known to contain a higher carbon content than blocky austenite has and it is difficult to transform to martensite [6,8]. Therefore an increase in the volume fraction of retained austenite with an decrease in isothermal transformation temperature results as a higher amount of residual austenite with a higher carbon content.

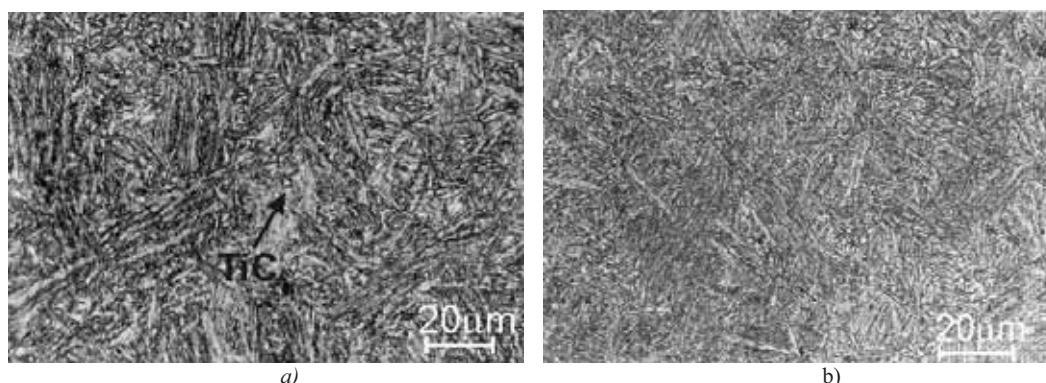


Fig. 3. Microstructure of 15HM2VT steel austenitized at 1000°C and austempered at: a) 575°C/1.5h, b) 500°C/1.5h. Etched with 2% nital

The fine details of the microstructure were examined by TEM. Fig. 4 shows a morphology of blocky austenite in 15HM2VT steel after heat treatment at 1000°C following isothermal transformation at 500°C for 120s. Beside blocky austenite, interlath films of retained austenite in the bainitic regions were also observed after this treatment. In 15HM2VT steel after austenitization at higher temperature (1200°C), retained austenite occurs mainly as interlath films (Fig. 5). As the austenitization temperature increases from 1000 to 1200°C the structure changes from upper (granular) bainite to upper lath bainite. It is assumed that upper bainite in these steel is a structure composed of carbide free bainitic ferrite laths with interlath retained austenite films replacing the interlath cementite of the classical upper bainitic microstructure. The interlath retained austenite films are stable and there is no apparent decomposition to martensite.

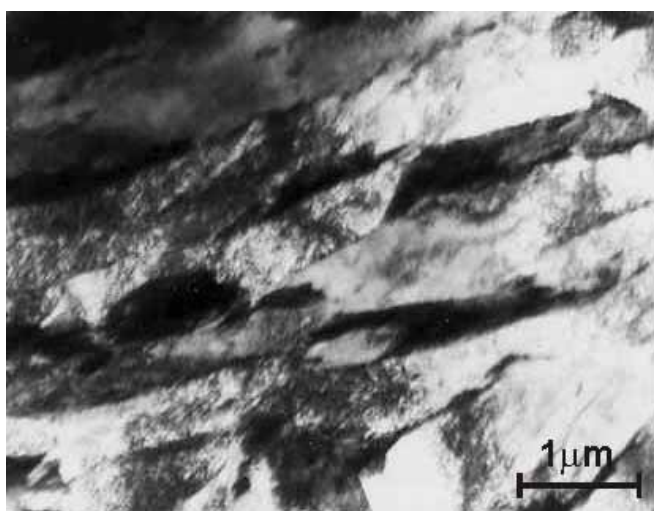
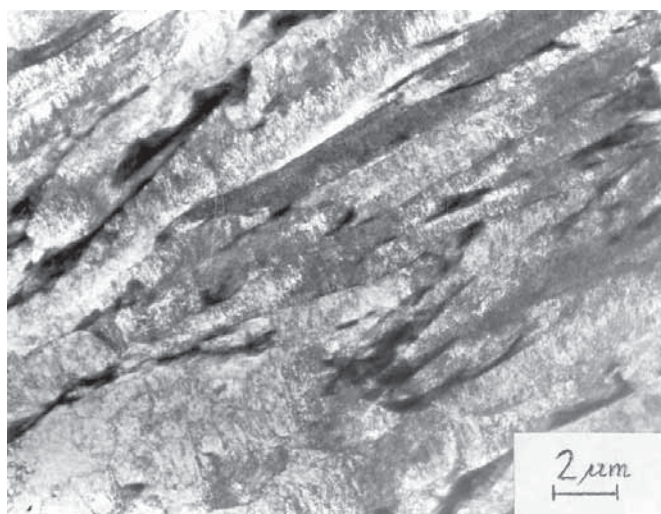


Fig. 4. Microstructure of 15HM2VT steel after austenitization at 1000°C following isothermal transformation at 500°C for 120s. Thin foil



*Fig. 5. Microstructure of 15HM2VT steel after austenitization at 1200°C following isothermal transformation at 550°C for 3600s. Thin foil*

Fig. 6 shows the general morphology of the microstructure in 15HM2VT steel after austenitization at 1200°C and isothermal transformation at 550°C for 7200s. The morphology of the bainite is similar to low carbon lath martensite, where dislocated laths are separated by films of retained austenite. No blocky austenite was observed in this structure. Careful examination of this microstructure shows no evidence of carbides precipitation. No significant changes in morphology with increasing reaction time were observed after isothermal transformation at 550°C. This structure, therefore, belongs to upper bainite assuming that upper bainite in this steel is a structure composed of carbide free bainitic laths with interlath retained austenite films [5,12].

After austenitization at 1200°C and at lower transformation temperature (450°C), bainite changes into a morphology with carbides within the laths (Fig. 7). It is also seen that carbide particles within ferrite laths and the long axis of the laths are at angles of 55 to 60 deg, as observed in lower bainite [13]. On the presently widely accepted view [5,11,13], in lower bainite carbides precipitate from highly supersaturated ferrite laths. During a progress of bainitic reaction the excess of carbon in bainitic ferrite may partition eventually into the residual austenite or precipitate from the ferrite in the form of carbides. If the latter process is dominant, then lower bainite is obtained [13].

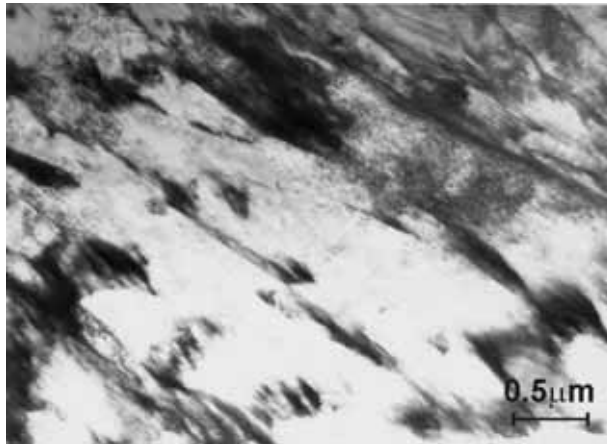


Fig. 6. Microstructure of 15HM2VT steel after austenitization at 1200°C and isothermal transformation at 550°C for 7200s. Thin foil

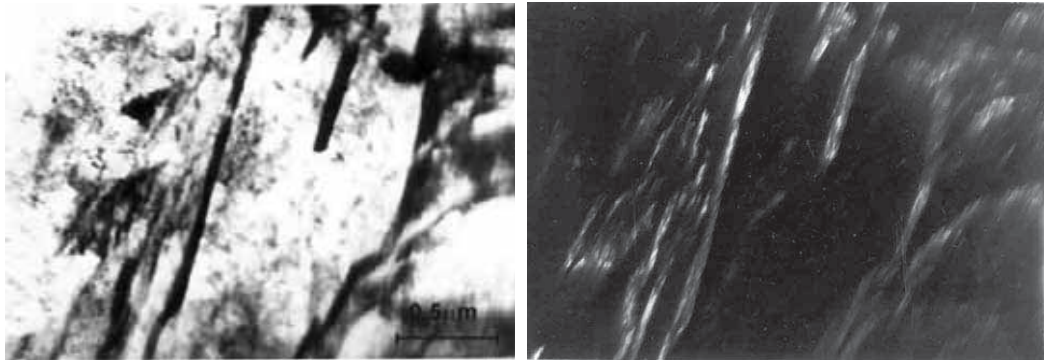


Fig. 7. Microstructure of 15HM2VT steel after austenitization at 1200°C and isothermal transformation at 450°C for 7200s. Bright and dark field from residual austenite. Thin foil

Thus the amount, distribution and morphology of retained austenite and occurrence of carbides vary with the austenitizing and transformation temperatures. The dispersed and ductile austenite films between the ferrite platelets (Fig. 7) can be expected to have a crack blunting effect. But the blocks of austenite tend to transform to high carbon untempered martensite under the influence of small stresses and consequently have an embrittling effect. Also other intrinsic components of the microstructure, such as particles of cementite laying especially in the interlath regions can be responsible for damage initiation.

#### 4. Conclusions

The development of bainitic transformation was studied using TEM, dilatometry and thermodynamic calculations, both from a fully austenitic microstructure ( $T_A=1200^\circ\text{C}$ ) and from a microstructure containing a mixture of austenite and undissolved carbides ( $T_A=1000^\circ\text{C}$ ).

Transmission electron microscopy revealed that after isothermal transformation the microstructure within the prior austenite grains consists of a mixture of ferritic bainite, residual austenite and/or carbides. After austenitization at 1200°C followed by bainitic reaction, the bainite was in the form of classical sheaves. The amount, distribution and morphology of retained

austenite, bainitic ferrite and precipitation of carbides strongly depends on both; prior austenitization and isothermal transformation temperatures within the bainitic range.

## References

- [1]Aaronson, H.I., Reynolds, W.T., Shiflet, G.J.,Spanos, G. *Bainite Viewed Three Different Ways*, Metall. Trans. A, 21A, pp. 1343-1380, 1990.
- [2]Barbacki A. *Próba uogólnienia mechanizmu wydzielania węglików stopowych podczas przemiany austenitu w ferryt na przykładzie węglików wanadu i molibdenu*. Rozprawy nr 73, Politechnika Poznańska, Poznań, 1976.
- [3]Bhadeshia, H.K.D.H., *Diffusional and Displacive Transformations*, Scripta Metall. 21, pp. 1017-1022, 1987.
- [4]Bhadeshia, H.K.D.H., *Thermodynamic analysis of isothermal transformation diagrams*, Metal Science, 16, pp. 159-165, 1982.
- [5]Bhadeshia, H.K.D.H., Christian, J.W., *Bainite in steels*, Metall Trans. A, 21A, pp. 767-797, 1990.
- [6]Hillert, M., *Paradigm shift for bainite*, Scripta Materialia, 47, pp. 175-180, 2002.
- [7]Honeycombe, R.W.K., *Ferrite*, Met. Sci., 6, pp. 201-214, 1980.
- [8]Honeycombe, R.W.K., Bhadeshia, H.K.D.H., *Steels, microstructure and properties*, London: Edward Arnold; 1995.
- [9]Honeycombe, R.W.K., Bhadeshia, H.K.D.H., *Steels, microstructure and properties*, London: Edward Arnold; 1995.
- [10]Ławrynowicz, Z., Barbacki, A., *Carbides precipitation in bainite in an experimental Mo-Cr-V-Ti steel*, Conference Proceedings of the 6-th International Conference "Carbides, Nitrides, Borides, " Poznań-Kołobrzeg, pp. 42-47, 1993.
- [11]Ławrynowicz, Z., *Mechanism of bainite transformation in Fe-Cr-Mo-V-Ti-C steel*, International Journal of Engineering, 12, pp. 81-86, 1999.
- [12]Ławrynowicz, Z., Barbacki, A., *Features of Bainite Transformation in Steels*, Advances in Materials Science, vol. 2, no 1,pp. 5-32, 2002.
- [13]Ławrynowicz, Z., *Transition from Upper to Lower Bainite in Fe-C-Cr Steel*, Materials Science and Technology, 20, pp. 1447-1454, 2004.



## PCB EXPOSURE AND DATA MATRIX BASED JOB VERIFICATION

**Adam Marchewka<sup>1)</sup>, Ryszard Wocianiec<sup>2)</sup>, Jarosław Zdrojewski<sup>3)</sup>**

<sup>2)</sup> *University of Technology and Life Sciences*

Faculty of Mechanical Engineering

ul. Prof. Sylwestra Kaliskiego 7, 85-791 Bydgoszcz,

*e-mail: ryw@utp.edu.pl*

<sup>1,3)</sup> *University of Technology and Life Sciences*

Faculty of Telecommunications and Electrical Engineering

ul. Prof. Sylwestra Kaliskiego 7, 85-791 Bydgoszcz,

e-mail<sup>3)</sup>: [jaz@utp.edu.pl](mailto:jaz@utp.edu.pl)

e-mail <sup>1)</sup>: [adimar@utp.edu.pl](mailto:adimar@utp.edu.pl)

## Abstract

*This article presents a Data Matrix based system for selecting and controlling jobs for the exposure machine. Job selection and proper choice selection and use of phototools are automatically supervised with a help of information transported inside data part of the code. Description, films verification, field id to retrieve information from the database as well is included. Presented method can help to the operator to choose automatically proper settings and transmission of needed parameters for the performed task.*

**Keywords:** PCB production, automatic parameters selection, image recognition, Data Matrix

## 1. Introduction

Using the "Code Image" is receiving more and more attention in the systems saving and transferring information. Code Image in this case Data Matrix (DM) technique is defining a way for saving array of data (Fig. 1) using a digital image, and next faultlessly and automatically inputting them into a desired process. The authors took up the subject of application of such transfer of parameters in the process of printed circuit manufacturing, or more specifically, during the exposure process, which will transfer the responsibility and fault risk from the machine's operator to the team supervisor, preparing the production and limiting process parameters to the required values.

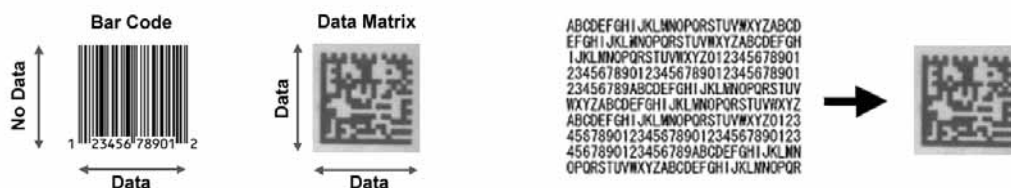


*Fig. 1. Comparison between Bar Code and Data Matrix with its ability to keep information in two dimensional structure*

Latest exposure machines are more and more sophisticated. Bare material, photopolymer, film and a light source is still a base but new technology exposure machine can measure, align material, and generate feedback data documenting a production cycle. Moreover, the analyzed system will ensure correctness of machine settings and it will help to verify a film choice, along with a possibility to set its critical parameters related to registration and exposure process (Fig. 2).

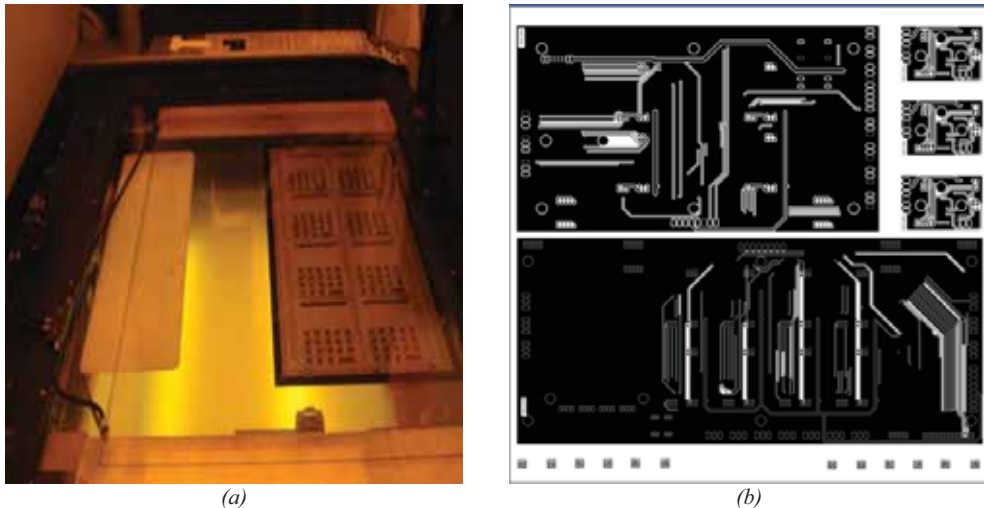


Fig. 2. Exposure Frame with a films and panel loaded (a). Data Matrix placed on the film in predefined location film choice (b), along with a possibility to set its critical parameters related to positioning and exposure

Over the years several image processing algorithms decode and encode data in DM were recreated. These methods provide way to process correctly an input image with a quality do not allowing the encoded information to be read automatically.

Data Matrix is two-dimensional bar code which may have a form of square or rectangular symbol build up of individual cells usually dots or squares. In such form it is a prearranged grid of dark and light cells bordered by a structure of finder pattern (Fig. 3a). The structure of finder pattern is used to detect the orientation and structure of the 2D code symbol. Data encoding process use a series of dark or light cell over a pre-determined size. Size of the cell is called the X-dimension and usually is limited by the parameters of the camera optical channel.

Data Matrix can carry variable amount of data (Fig. 3b). Usually if more data encoded then the size of the resulting DM symbol gets bigger. To keep 1kB of data – it also depends if they numerical or alphanumerical - size of a given Data Matrix approximately will be 96x96.

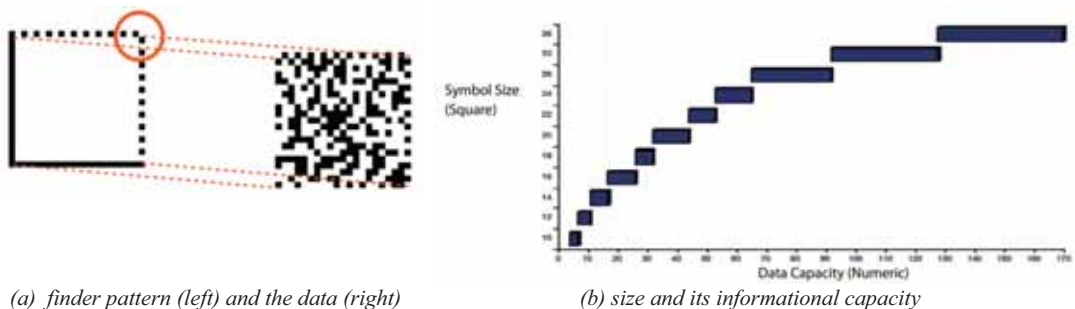


Fig. 3. Structure and capacity of Data matrix

The issues related to proper decoding of encoded information arise when defining:

- the size of the image containing information;
- Data Matrix capacity and image resolution (size of a single point);
- uneven light conditions during image acquisition;
- possible mark contamination observed by the camera, as well as on the camera's lens.

The proposed by us method uses the Radon transformation. In the past, there were attempts to use this transformation to analyze and recognize Data Matrix [2, 8]. In this paper authors are describing modified algorithm introducing new improved classifier for a method presented in [8].

## 2. Data Matrix image analyze characteristics

The registration system, usually has inbuilt set of cameras, used as a part of alignment subsystem of the exposure machine. Every camera has calibrated position and is placed perpendicularly to the observed mark and is an integral part of the whole device (Fig. 4).

Such camera has several tasks and one of them is reading Data Matrix to encode the data contained in the given symbol. Despite it unclear working conditions, which are unfavorable for a correct reading of the data printed on the film may occur frequently.

Therefore a proposed vision system has to be transparent to dynamic lighting changes of the registered scene, regular occurrence of various film defects, and quality of code printed onto the film. Because in most cases – very close to 99% - two films plotted on the internal side are used. Because of their relation to the panel being exposed one of them will provide mirrored images of the DM. Moreover, the size of information portion of the code varies. In most cases DM will be used only for identification, but it can contain information specific for a job including registration and exposure parameters (Fig. 5). Due to this requirement, even knowing the camera's relation to the observed scene it is difficult to define the size of cell carrying information in DM. As a result, system has to automatically calculate the size of the cell using DM finder pattern.

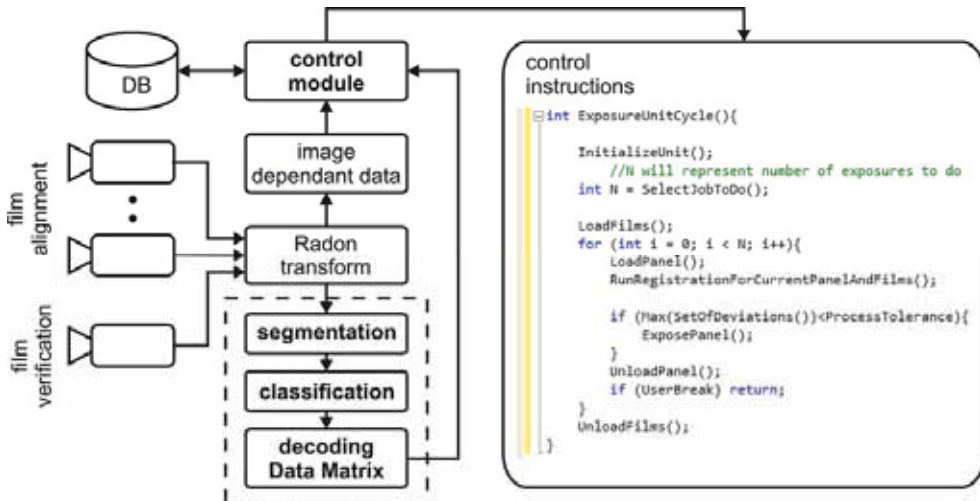


Fig. 4. Simplified exposure unit registration system diagram: set of movable industrial cameras, PC based control controller, database to exchange and carry system data

In the considered arrangement (Fig. 5) image  $I[x, y]$  will have blocks  $B[x_0, y_0]$  of a constant, undefined but detectable size. Moreover, every such block adheres to the next one. While adjacent blocks possess a noticeable different and at the same time they represent significant insensitivity

function value, the boundaries between them can be determined easily. However, for DM it is not a rule. Very often adjacent blocks have same insensitivity function value. While analyzing an input image, that is filtering a given image with an edge filter, regularity can be observed, where every set of blocks (of the same or similar insensitivity function value) is demarcated from other sets with straight, mutually perpendicular sections. Thanks to such assumption existing algorithm of searching of straight lines in the picture can be used.

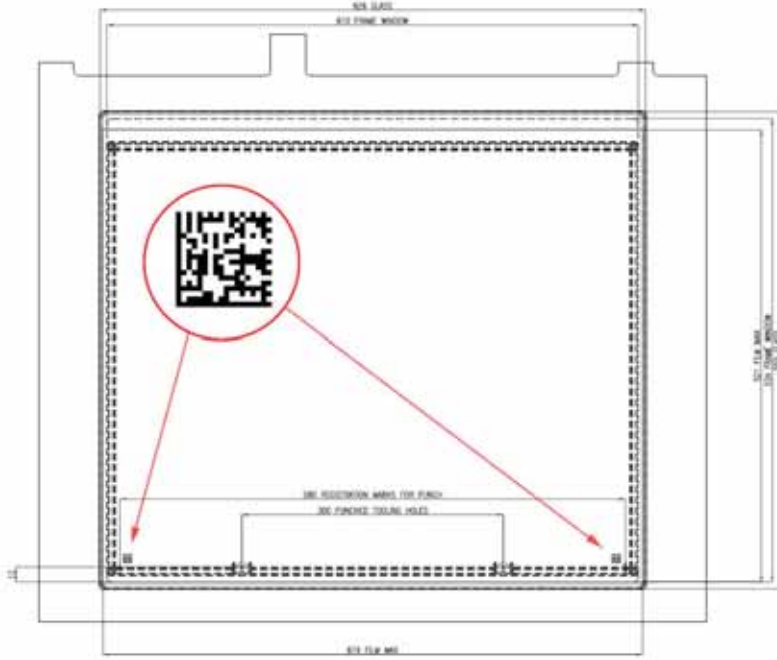


Fig. 5. Film definition presenting predefined DM location in relation to the frame limits [8]

The Radon Transform (1) is defined as [1, 6]:

$$R_{\theta}(\rho) = \int_{-\infty}^{+\infty} f(x' \cos \theta - y' \sin \theta, x' \sin \theta + y' \cos \theta) dy', \quad (1)$$

where

$$\delta > 0 \text{ and } \begin{bmatrix} x' \\ y' \end{bmatrix} = \begin{bmatrix} \cos \theta & \sin \theta \\ -\sin \theta & \cos \theta \end{bmatrix} \begin{bmatrix} x \\ y \end{bmatrix}.$$

The Radon operator maps the spatial domain  $f(x, y)$  to the projection domain  $(\rho, \theta)$ , in which  $\theta$  is the angle and  $\rho$  the smallest distance to the origin of the coordinate system.

Detection of straight lines in the picture is performed through finding in the domain maxima transforms, which clearly indicate the angle of the straight line and its distance from the center of the image [3, 4, 5].

It means that performing a Radon transform for an edge image and finding a maximum value for this function we can define the angle of our image. However, any occurrence of contamination on the lens or film (scratches etc.), can induce serious errors.

In the process of angle analysis of the image we look for a pair of values  $R_{\theta_1}(\rho)$  and  $R_{\theta_2}(\rho)$  where the image angle is expressed as  $\theta_l = \max(R_{\theta_1}(\rho), R_{\theta_2}(\rho))$  under assumption  $\theta_1 = \theta_2 + 90^\circ$ .

Such approach allows finding the demarcation lines of the individual cells, even with a high noise. However, for specific cases, it is likely to not find a line of demarcation. This can occur when two columns, or two rows, next to each other are similar to each other. It means that the  $\sum |R_{\theta_1}(\rho_n) - R_{\theta_1}(\rho_{n+1})| = k$  where  $k \ll N$  ( $N$  - number of cells) Fig. 6 or when the edge of cells is not blurred (edge operators can't detect).

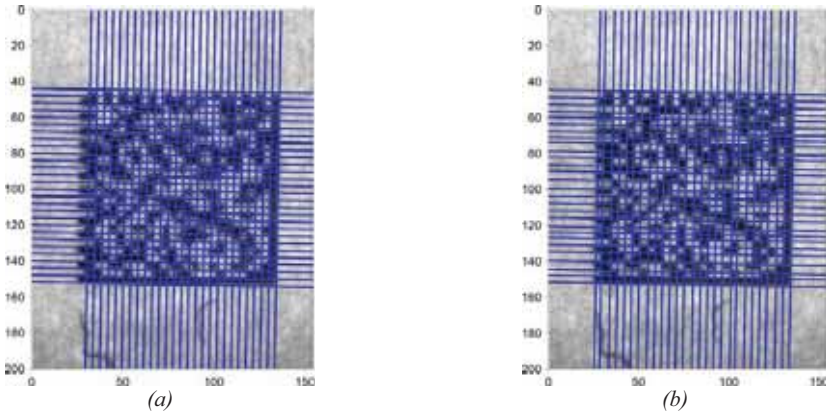


Fig. 6. Some segmentation process results (a) without tolerance (b) using analyze of local Radon transform maximum

In order to eliminate uncertainty of the presented method we suggest certain modifications in our implementation. They are possible only under such conditions:

- the camera is perpendicular to the observed surface (only insignificant deviations are allowed);
- the dimensions of a single cell in Data Matrix are known.

The first assumption permits upholding the condition that Radon transform maximum values which indicate cell demarcation lines are distributed for angles that fulfill a condition:  $\theta_1 = \theta_2 + 90^\circ$ .

In practice there exists high probability that demarcation lines designated using edge detecting filters (Sobel, Roberts, Canny) will be not parallel to each other, which means the conditions cannot be fulfilled. That is why during the implementation of algorithm insignificant deviations of designated edges being unparallel on the  $\pm 1^\circ$  level were taken into consideration (Fig. 7).

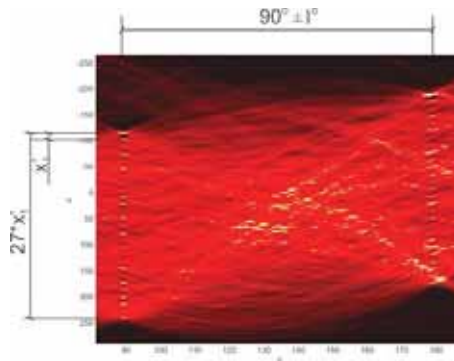


Fig. 7. Radon Transform of Data Matrix Using 110 Projections

Second assumption allows us to limit the amount of calculated lines separating cells. Let  $N$  be a number of cells in a row or a column in Data Matrix, then  $\rho_a = \{x', x' + nx'_1\}$  and  $\rho_b = \{x', x' + nx'_1\}$  where  $n = \{1, 2, \dots, N+1\}$ . However even here difficulties concerning quality of image acquired from the camera can be encountered. Due to used camera resolution and electronic noise introduced during video signal transmission, the dimensions of individual cells, both horizontal and vertical, can vary. It is a crucial aspect during classification process for very small cells, 5x5 pixels and smaller. That is why introductory assessment of  $\theta_l$ , on the basis of aforementioned conditions, and then a search in the nearest vicinity i.e.  $\theta_l \pm 1^\circ$  and  $x'_1 \pm 1px$  for  $\rho_a$  and  $\theta_2 = \theta_2 \pm 90 \pm 1^\circ$  and  $x'_1 \pm 1px$  for  $\rho_b$  is advised, a result of which is a division of the image (Fig. 8b).

On the base of such a demarcation line set, a set of image points belonging to a given cell (classification process) can be specified.

Despite the specific assumptions in the segmentation process (Fig. 8), we are not able to fully eliminate image pixels whose brightness value of the function clearly represents the value of a cell. Therefore, the DM shall be determined by the classifier (2):

$$M_{DM} = \begin{cases} 0 & \text{for } median(B[x, y]) > \tau \\ 1 & \text{for } \text{other} \end{cases}, \quad (2)$$

where  $B[x, y]$  is a block of image appointed by the demarcation lines,  $\tau$  is a threshold defined as  $\tau = \min(R_{\theta_1}(\rho_a), R_{\theta_2}(\rho_b))$ .

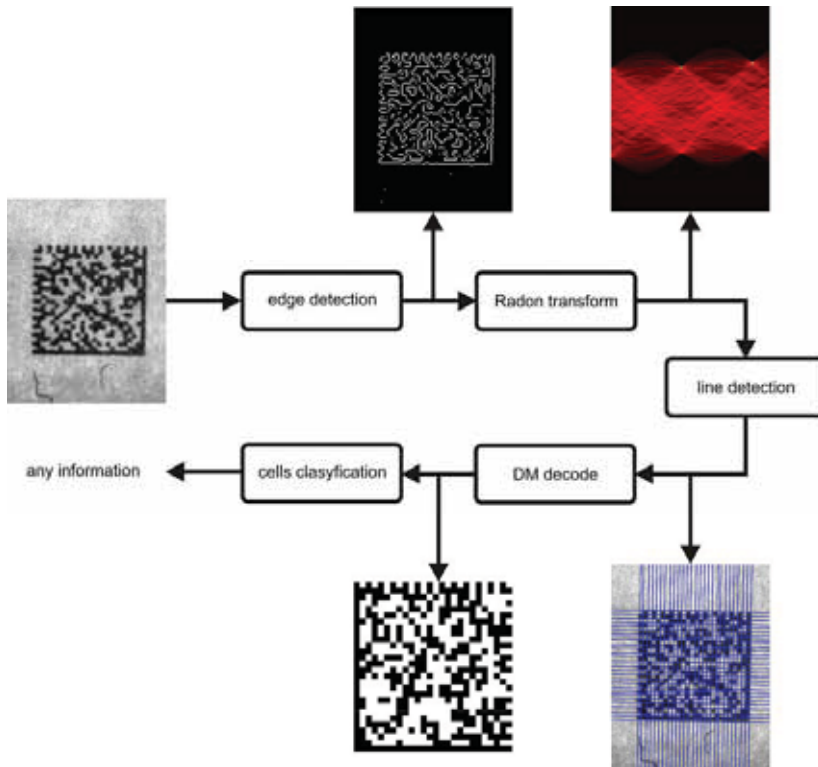


Fig. 8. DM information image recognition algorithm diagram. On the left main system elements, on the right effects visualization of subsequent process steps

### 3. Experimental results

Series of trials for real images registered by the exposure machine were conducted; however, the preliminary research was conducted for synthetic images. The group contained images whose single Data Matrix cell dimensions were 5x5 pixels. For this group trials were conducted (Fig. 10). In order to define the method's sensitivity for every synthetic image a Gaussian white noise with different mean and variance values is added. In this way both the image's PSNR level and the size of a single mark for which the algorithm recognizes the code was estimated.

In Tab.1 PSNR values were included along with recognition of image code sequence percentile. Additionally, series of trials for real images registered by the exposure machine were conducted. This way an impressive outcome of 98% of correctly recognized marks on the images was obtained.

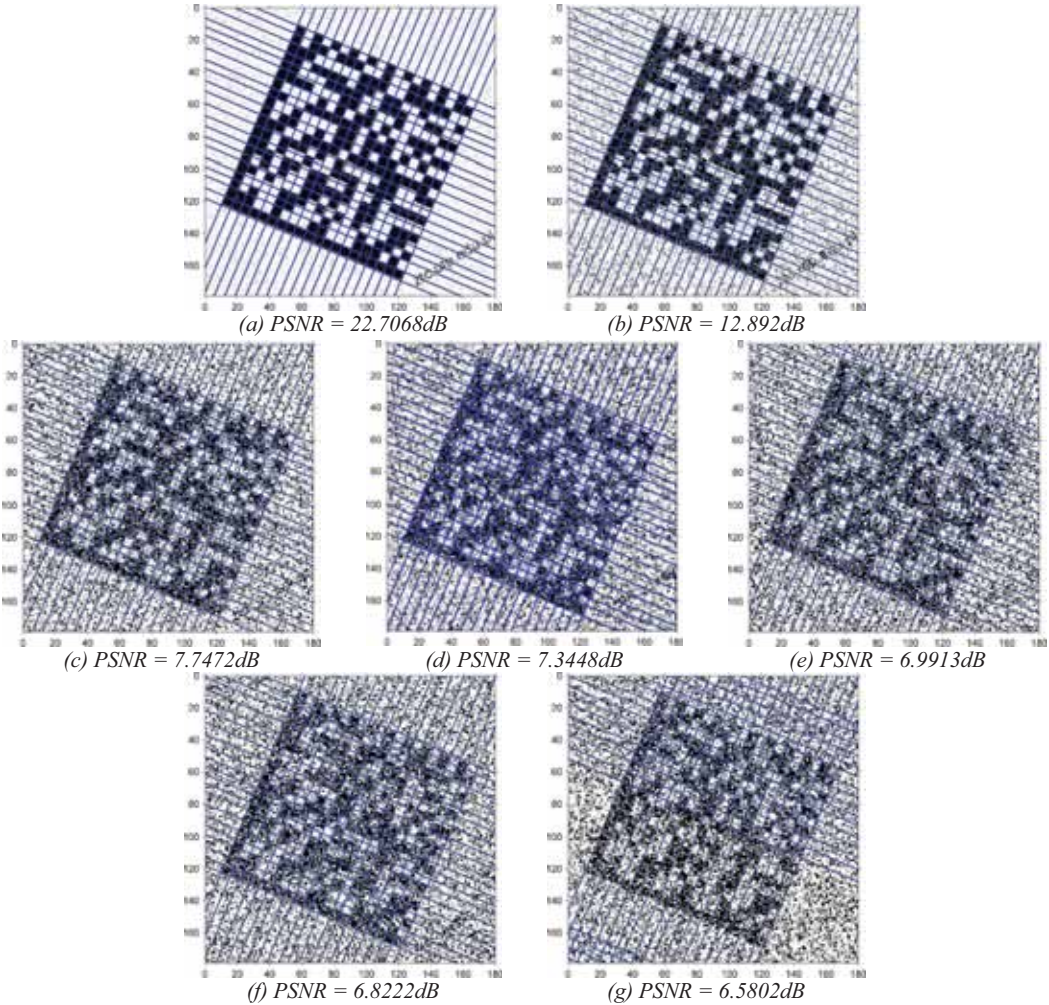


Fig. 10: Sample results of PSNR impact on image recognition capacity

Tab. 1. Results for code cell based on 5x5 pixels

|             |         |        |        |        |        |        |        |
|-------------|---------|--------|--------|--------|--------|--------|--------|
| PSNR        | 22.7068 | 12.892 | 7.7472 | 7.3448 | 6.9913 | 6.8222 | 6.5802 |
| Recognition | 100%    | 100%   | 100%   | 94%    | 83%    | 67%    | 26%    |

#### 4. Conclusions

This article presents a approach to Data Matrix code analysis using new optimized new improved classifier. In the case of exposure unit proper DM detection is considered as start point of the unit setup procedure. Decoded data is verified over the information saved in the database and is leading to the quick and reliable process of setting up the exposure machine parameters. The proposed method of getting inputs from DM is based on Radon Transform. Beside image analyze, research process was extended by fallowing decoding step and extracting stored encoded information. Acquired results are promising. Proposed algorithm can detect and decode barcode fast and correctly. It allows eliminating mistakes resulting from image processing methods' imperfections. Of course, the presented method was tested with DM symbols with a low modulation grade and blurred symbol images. DM with damaged borders, uneven illumination, omni-directional symbol recognition can be processed as well. In any case it is necessary to remember stability of the process can be illumination dependent especially in the production conditions of a yellow room. Because of the specific setup of the camera and artwork including DM, issues like perspective and significant geometric distortions was assumed to not be a case for this system. The results showing algorithm limitations will be presented in next articles.

#### References

- [1] Yu Hai-peng, Liu, Yi-xing, Liu, Zhen-bo., *Auto detection of wood texture orientation by radon transform*, Journal of Forestry Research, 16:1–4, 2005.
- [2] Tarłowski, R., Choraś, M., *Digital Analysis of 2D Code Images Based on Radon Transform*, Computer Recognition Systems 3, Advances in Intelligent and Soft Computing, Kurzynski, Marek and Wozniak, Michal, Springer Berlin / Heidelberg, pp.143-150, vol.57, 2009.
- [3] Toft, P., *Detection of lines with wiggles using the radon transform*, Submitted to NORSIG'96, Preprint from Department of Mathematical Modelling, Technical University of Denmark, (1996)
- [4] Leavers, V.F., Boyce, J.F., *The radon transform and its application to shape parameterization in machine vision*. Image Vision Comput, 5:161–166, May 1987.
- [5] Gur, E., Weizman, Y., Zalevsky, Z., *Radon transform based image enhancement for microelectronic chips inspection*. IEEE Transactions on Device and Materials Reliability, 2010.
- [6] Radon, J., *On the determination of functions from their integrals along certain manifolds*, in: The radon transform and some of its applications, annexe a. Wiley, New York, 1983, (translation of Radon's 1917 paper by R. Lohner), 1917.
- [7] Information technology - *Automatic identification and data capture techniques - Data Matrix bar code symbology specification*, ISO/IEC 16022:2006(E), 2006.
- [8] Marchewka A., Zdrojewski J., *Data Matrix in the PCB production*. Image Processing & Communications 16(3-4):31-36, 2011, DOI: 10.2478/v10248-012-0009-z, Versita, Warsaw 2012.
- [9] GS1 Data Matrix An introduction and technical overview of the most advanced GS1 Application Identifiers compliant symbology; <http://www.gs1.org>.



## APPLICATION OF SPECTRAL ANALYSES FOR SURFACE LAYER CHANGES ESTIMATION OF CO-OPERATING UNITS WITH CONFORMAL CONTACT

Maciej Matuszewski, Marcin Łukasiewicz, Janusz Musiał

*University of Technology and Life Science  
ul. S. Kaliskiego 7, 85-796 Bydgoszcz, Poland  
tel.: +48 52 3408656, fax: +48 52 3408245  
e-mail: matus@utp.edu.p*

### **Abstract**

*The qualitative opinion of the surface layer condition was introduced in this paper. The usefulness of spectral analyses was analysed to the opinion of changes proceed in the surface layer of co-operating units. The functions of the power spectral density and autocorrelation which were used to analyses were self- characterized.*

*The structures of the surface after tribology investigations were accepted to the opinion of proceeding changes. Spectral graphs were analysed for structures without the co-operation (directly after the finishing processing) and after the various roads of the friction. The following intervals of the road of the friction were used to the qualitative opinion: 100, 200, 300, 500 metres – there are most intensive changes and 2000 metres – the stabilization of changes follows. The conditions during tribology investigations were accepted as stable. The received graphs of the power spectral density and autocorrelation function approve oneself useful in the opinion of the changes proceed of surface layer during her transformation.*

**Keywords:** *qualitative analysis, surface layer, spectral analysis, tribology investigations, conformal contact*

### **1. Introduction**

The properties of surface layer (SL) created as a result of the established technological process realization in the largest mark influence on the tribology profiles of the machine engines co-operating units [3, 7, 10, 12]. About the properties of surface layer generally decides the surface stereometry that is the external top section of surface layer. The stereometry form of the surface defines itself as the surface geometrical structure (SGS). The stereometry structure of the surface is the ridges set of the surface, being the realized processing traces or the results of the wear process. Describing SGS admits as basic quantities: the surface roughness, the wavy finish, the stage of surface isotropy – the directive tendency of the processing feed ridge, the deviation of shape and the surface defects [1].

The surface could have the anisotropic character in dependence from the location of SGS characteristic elements – with steered location of eminences and depressions (the surface directive tendency) or isotropic – not showing the steering location. The geometrical structure of the units of kinematic pair's surface has the essential influence on the friction processes proceeds in these pairs, and on the kinematic pair's waste intensity.

The estimation of co-operating units surface layer proceeds changes describes quantitative and qualitative values changes. The description of quantitative changes expresses quantities: the various parameters of roughness, the mass decrease, the change of linear dimensions [3, 9, 10, 11]. However the opinion of qualitative changes takes place among others on the basis of the studied surfaces photos or also basis on the spectral analyses of the surfaces [2, 6, 8]. We receive the information on the basis of the qualitative analysis about general sights of SGS and about the wear effects and also about the kind of possible damages.

In this paper to the qualitative analysis of the condition of the surface geometrical structure were accepted the spectral analyses which describe the frequencies structure of studied surfaces.

## **2. SGS function used for spectral analysis**

The functions of power spectral density (PSD) and autocorrelation (AC) were used to the spectral analysis of surface layer changes estimation. The functions of power spectral density and autocorrelation describe the frequencies structure of the surface. These functions are very usefulness in analysing the surface topography during production and constitution of the geometrical surface, and surface waste process estimation.

During investigations, one from above mentioned functions is generally used in dependence from the aim of the tests. This results from the mutual statements between these functions, because the power spectral density function is Fourier transformation of the autocorrelation function. The power spectral density function illustrates how the surface irregularity deviation spreads together with the frequency.

In the practise of investigations the PSD function is used more often, because among others basis on this function we could estimate the influence the component strength of cutting forces or the condition of cutting edge on the surface geometrical structure. In this case the autocorrelation function is used as the opinion supplementary parameter because it reacts very sensible on any structure surface disturbances [4, 5].

In generally basis on the surface spectral analysis we could draw out following conclusions [4, 5]:

- the largest signification in the spectral analysis have component with low frequency, the high frequency component signification is insignificant,
- on the periodical surfaces in one or two perpendicular directions the power of energy focuses in the areas of proper frequency along these same senses,
- on the anisotropic surfaces the energy of the power focuses along the perpendicular sense to the directive direction (symmetrical) of the surface,
- in case of anisotropic surfaces mixed with participation of the random component with short-wave character, the decisive part keep long-wave periodical components that defining the anisotropy of the structure,
- in case of anisotropic random surfaces appear the characteristic sights of the random hum on the background of clear predominant components with low frequency beside this the surface structure keeps anisotropy and directive tendency,
- in case of random isotropic structures clearly predominates the random hum and sights of anisotropy are insignificant.

## **3. The analysis of the example surface structures**

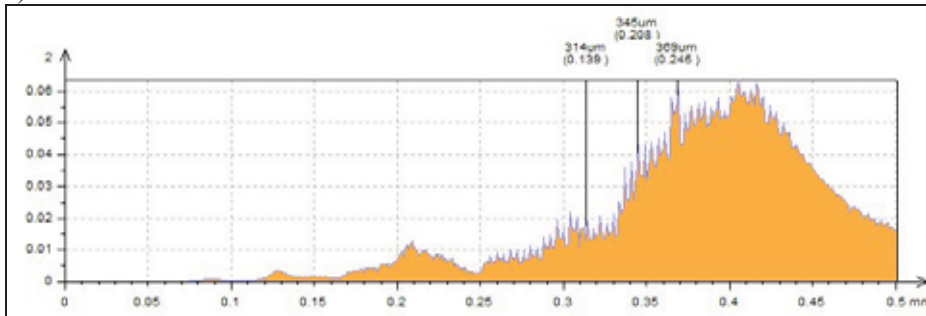
To analyse of the spectral analyses usefulness for the qualitative opinion of co-operating surfaces layer changes the experimental investigations were conducted. Studied samples were subjected tribology investigations, and the point of the contact of co-operating surfaces during investigations was conformal, i.e. he was spread on the whole co-operating surface of samples.

One of analysed structures came directly from the finishing processing, this surface was without the co-operation, but remaining structures were after tribology investigations with the various roads of the friction. The following intervals of the road of the friction were chosen to the qualitative opinion: 100, 200, 300, 500 - there are most intensive changes and 2000 metres – the stabilization of changes follows. Conditions during tribology investigations were accepted as stable.

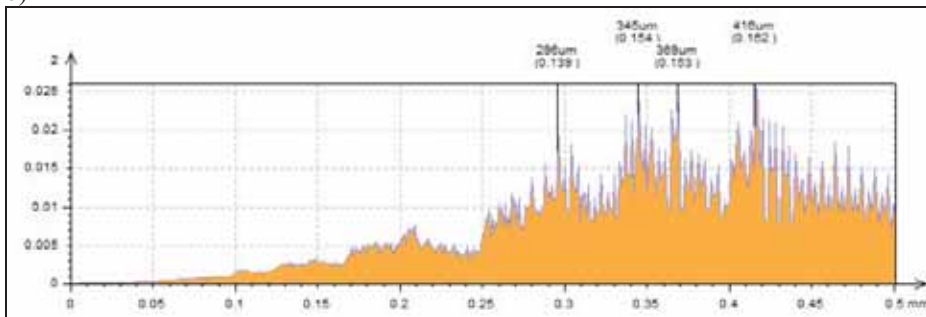
The samples with counter-sample co-operated in the centre oiling which was machine oil (L-AN 68), and values of parameters exploational were following: the speed of the relative movement: 2,9 m/min (0,05 m/s), burden 600 N (theoretical pressures in the zone of the contact point 2 MPa). The angle of co-operation between the characteristic directive tendency of samples and counter-sample was 0°. Samples were made from steel 102Cr6, counter-samples were made from steel X210Cr12. Hardness of counter-sample visibly exceed (about 50 %) the hardness of samples – the changes should proceeds firstly on the samples surface. The values of hardness were suitably 60 HRC and 40 HRC.

The graphs of the power spectral density function for put measuring points were introduced on pictures below.

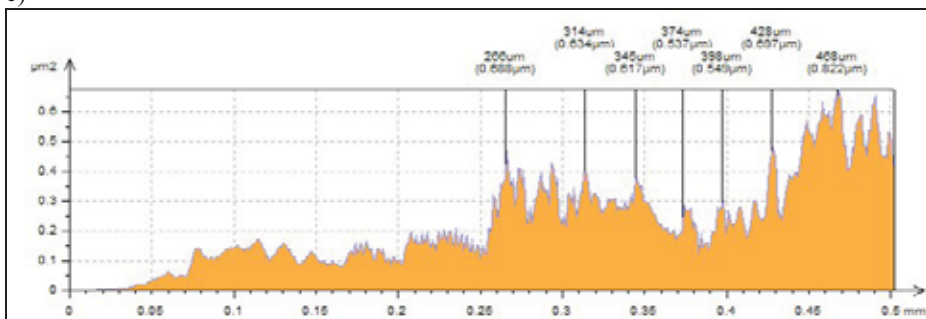
a)



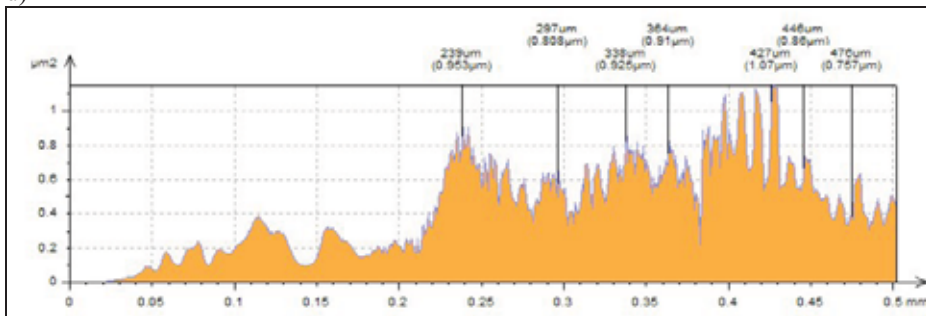
b)



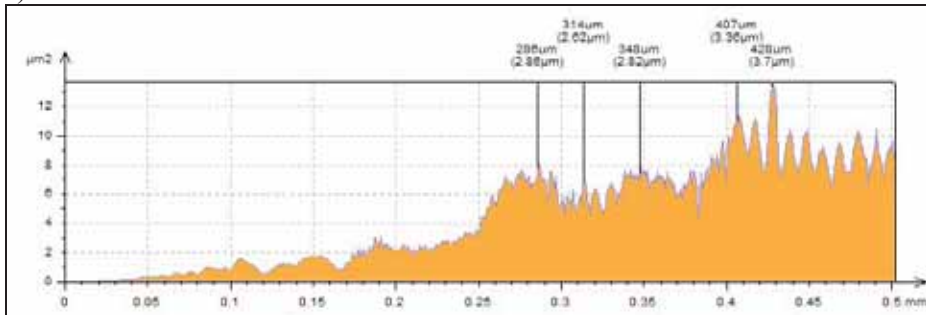
c)



d)



e)



f)

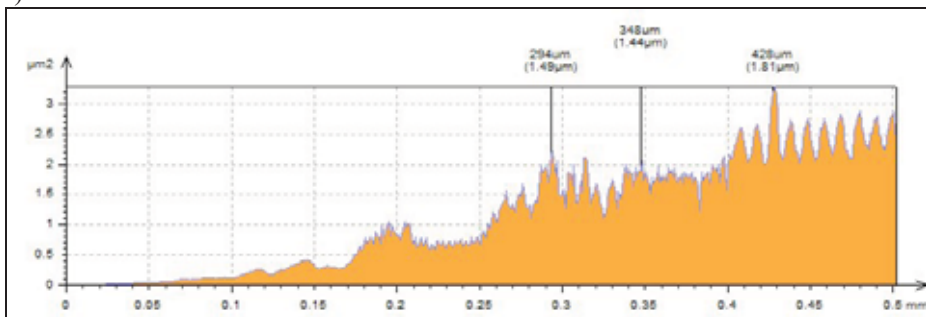


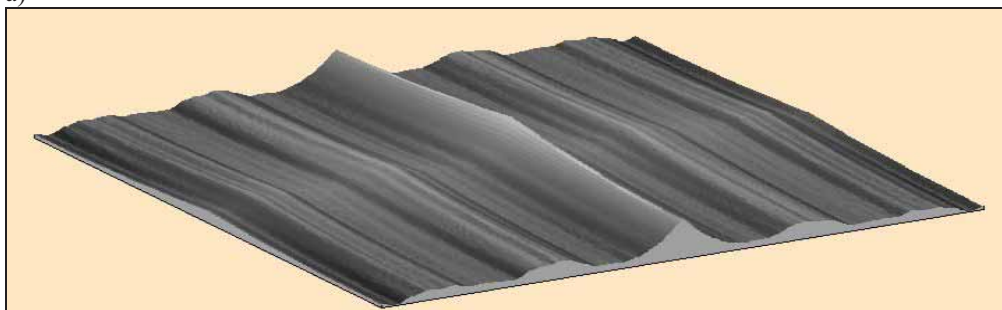
Fig.1. The graphs of the power spectral density function for the following intervals of the friction:  
a) 0 (without co-operation), b) 100, c) 200, d) 300, e) 500, f) 2000 meters

As it was introduced on the graphs the function of power spectral density changes on the individual stages of the co-operation. On the picture 1a, when the sample did not co-operate yet, we could observe one modal value on the graph. This value becomes from the surface character (definite directive tendency SGS) and from determined way of processing and established parameters.

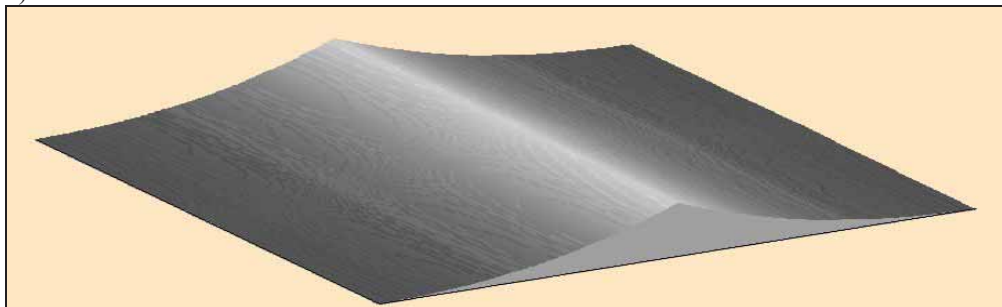
On remaining graphs we don't have one modal value any more this causes from changes formed in the result of the surfaces co-operation. The traces of the processing disappear and the direction of these traces isn't so clearly privileged any more.

The graphic figure of the autocorrelation function of studied structures was introduced on picture 2.

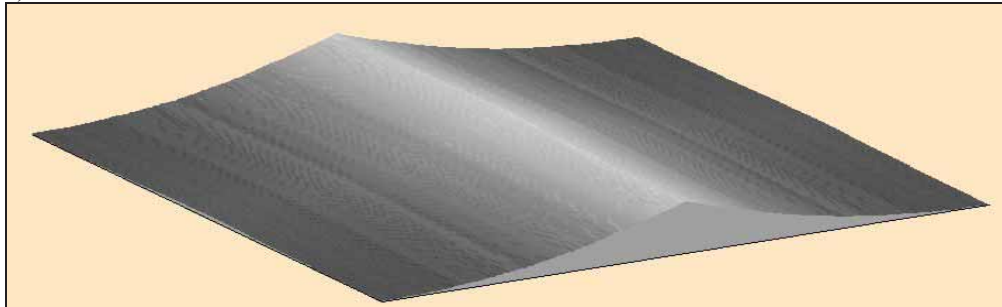
a)



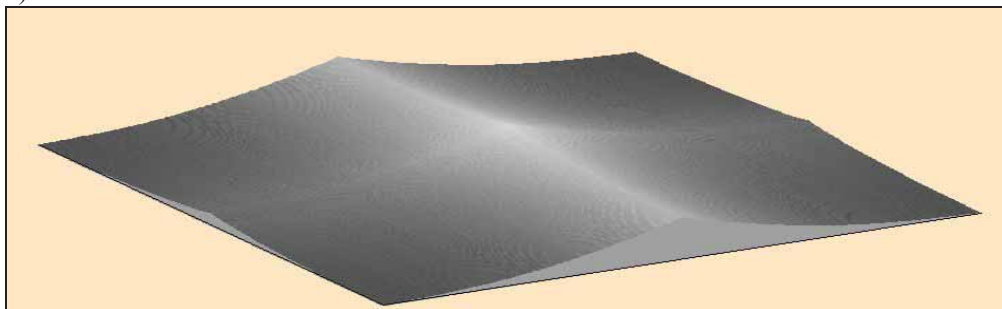
b)



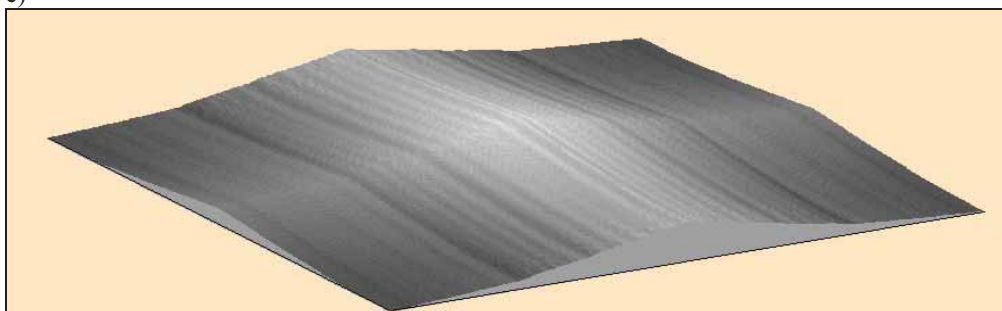
c)



d)



e)



f)



*Fig. 2. The graphs of the autocorrelation function for the following intervals of the friction:  
a) 0 (without co-operation), b) 100, c) 200, d) 300, e) 500, f) 2000 meters*

As it was introduced on the graphs we could observe the surface geometrical structure with anisotropic character (introduced on figure 2a) changes into mixed character structure without the clearly privileged directions, but with occurrence directive tendency of SGS shown in figure 2f. We could not observe the full passage into structure with isotropic character with total fading of directive tendency SGS.

#### 4. Conclusion

Basis on conducted analyses in this paper the usefulness of spectral analyses was affirmed in tribology investigations. The received results and graphs of the power spectrum density and

autocorrelation functions were very useful in the qualitative opinion of the surface structure. Basis on these functions we could analyse the changes of surface layer during their transformation.

For fuller qualitative opinion of the surface layer condition for studied surfaces of co-operating units it would also execute other analysis basis on the 2D or 3D pictures. It could help with diagnosing about the surface stereometry.

## References

- [1] Burakowski T., Wierzchoń T., *Inżynieria powierzchni metali*, WNT, Warszawa 1995.
- [2] Górecka R., Polański Z., *Metrologia warstwy wierzchniej*, WNT, Warszawa 1983.
- [3] Matuszewski M., *Badanie wpływu wybranych parametrów struktury geometrycznej powierzchni elementów par kinematycznych na proces ich zużywania*, Praca doktorska, Uniwersytet Technologiczno-Przyrodniczy, Bydgoszcz 2008.
- [4] Oczóś K. E., Liubimow W., *Determinowość i losowość struktur geometrycznych powierzchni (SGP)*, Pomiary Automatyka Kontrolna nr 10/2002, s. 4÷6.
- [5] Oczóś K. E., Liubimow W., *Struktura geometryczna powierzchni*, Oficyna Wydawnicza Politechniki Rzeszowskiej, Rzeszów 2003.
- [6] Pawlus P., *Topografia powierzchni: pomiar, analiza, oddziaływanie*, Oficyna Wydawnicza Politechniki Rzeszowskiej, Rzeszów 2006.
- [7] Pietruszewicz W., *Parametry powierzchni i ich przydatność do określenia cech użytkowych przedmiotu*, Materiały Konferencji N-T „Wpływ technologii na stan warstwy wierzchniej”, s. 631÷646, Poznań – Gorzów Wlkp. 1985.
- [8] PN – 87/M – 04250, *Warstwa wierzchnia. Terminologia*.
- [9] Styp-Rekowski M., *Geometrical constructional features of special rolling bearings against their exploitational properties*, Proceedings of IV<sup>th</sup> Symposium INTERTRIBO '90, Vol. C, pp. 93÷96.
- [10] Styp-Rekowski M., *Znaczenie cech konstrukcyjnych dla trwałości skośnych łożysk kulkowych*, Wydawnictwo Uczelniane ATR, seria Rozprawy nr 103, Bydgoszcz 2001.
- [11] Zwierzycki W., Grądkowski M. (redakcja), *Fizyczne podstawy doboru materiałów na elementy maszyn współpracujących tarcioowo*. Wydawnictwo Instytutu Technologii Eksploatacji, Radom 2000.
- [12] Żurowski W., Sadowski J., *Badania maksymalnej odporności układów ciał metalicznych na zużywanie*. Inżynieria Powierzchni nr 1/2001.





## PC CONTROLLED TURNING TOOL

**Tadeusz Mikołajczyk, Łukasz Kamieniecki**

*University of Technology and Life Sciences  
Prof. S. Kaliskiego Str. 7, 85-796 Bydgoszcz, Poland  
Tel. 48 52 3408743, fax: 48 52 3408743  
e-mail [tami@utp.edu.pl](mailto:tami@utp.edu.pl), [luke\\_4don@wp.pl](mailto:luke_4don@wp.pl)*

### *Abstract*

*Design of PC controlled turning tool is presented in paper. Tool placed in the guides was driving using the stepper motor and a screw cooperating with the nut joined with the tool. To control of the tool was used PC with the step motor interface connected to the LPT port. Mounted to the holder tool allows machining shape surface using the universal lathe.*

**Keywords:** *mechatronics tool, turning process, lathe, step motor*

### **1. Introduction**

There are many small companies providing services in machining. To be competitive, they must offer short lead times, high quality and repeatability of the details. In the case of machinery equipment in a conventional machine, it involves the employment of large numbers of skilled workers, or the purchase of modern machining centers, which usually goes beyond the financial capacity of the company. To maintain the competitiveness of these companies, they have to use cheap and flexible as possible universal tool [3-6].

In cutting tools area the new direction are mechatronics tools (fig. 1) [1,2,6-8].

This special tools equipped with own engine and special control system made possible change its geometry. KOMET KomTronic [8] system add the special U-axis included in tool (fig. 1). This change are possible by using mechatronics system in process cutting. Mechatronics tools and its control system cooperate with the control system of numerical machine tools. In the industrial mechatronics tool are used to machine tools possibilities increase and automates the process machining.

The paper presents elaborated in University of Technology and Life Sciences (Bydgoszcz, Poland) the design of controlled PC turning tool, which makes the new possibility of machining using conventional lathes.



Fig. 1. KOMET KomTronic U-Axis system [8]

## 2. Mechatronics turning tool idea

In the Department of Production Engineering and Mechanical Students Scientific Division our University conceived the idea of creating an intelligent tool, which can be fitted with any conventional lathe (fig. 2). The role of the operator have expired only in the material change in machine holder and start of machining process.

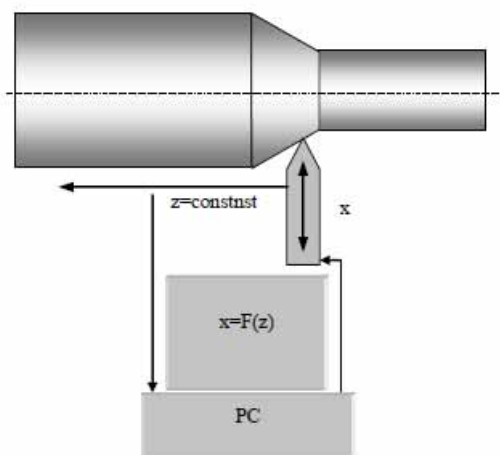


Fig. 2. Idea of mechatronics PC controlled turning tool

This mechatronics tool will be controlled using PC and connected to special interface which can control of  $x$  position of tool edge synchronically to change the  $z$  coordination changed with constant feed. PC controlled turning tool will be mounted in lathe holder and allows machining shaped surface as numerical control process.

## 3. Tool control system

To solve the problem of mechatronics tool construction was elaborated control system of this tool.

The concept of building system based on special tool that can be placed in the holder conventional lathe (fig. 3). The task was to prepare the tool object. Rotational speed of the object should be controlled using the inverter in such a way as to be able to change right / left turns, which make working retail in a few passages. The tool should consist of a with turning tool in a rigid body. Extension of the tool will take place through a transmission with a computer-controlled motor with a precise number of revolutions.

To control position of tool in  $z$  axis may be use many solutions:

- counter of gear ratio revolutions,
- precision interface for measure tool holder motion ex. digital calliper with computers interface.
- optical measure system with using computers mouse.

In first proposition computer software by counting the number of lathe spindle revolutions and using feed monitor the tool will monitor its position.

Second proposition is using digital calliper. It is the best solution with high accuracy.

In first experiments, very simple measuring system with optical mouse was used (fig. 3). Because this signal will be measured using pixels of screen its resolution will be 0.264 mm (Thinkpad tablet X41).

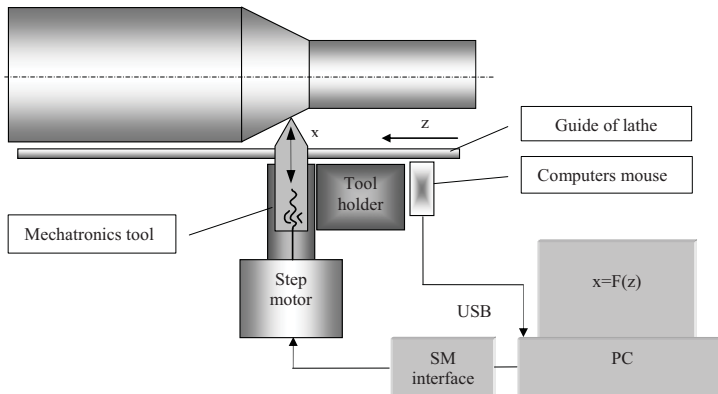


*Fig. 3. Control system of mechatronics turning tool with using of computer mouse to measure  $z$  position*

The control system task is: generation of surface machining program and control the machining process.

To control of the tool  $x$  position was used PC with the motor control interface. In first probe to stepper motor control was used USB interface, but this driver were able to obtain low level of motor control steps frequency. In control stepper motor better use LPT interface. In VB6 environment we can control this port using In and Out procedures. With using special software for NC machining it is possible to achieve very high-frequency pulses to ensure a very high rotational speed of stepper motors [9,10]. For this purpose with Windows platform, programs such as Mach3 [9], STEP2CNC [10], use special handling procedures to LPT port.

Pulse frequency of step-motor control is essential particularly important in the case of surface processing wide angle of inclination. Due to the constant feed in the direction of the used system allows to obtain maximum surface angle depends of radial feed (Fig. 4). More and more radial feed value make possibility to get more surface inclination angle. In presented location of  $x$  tool axis not possible is getting the surface perpendicular to axis of lathe. This requires positioning edge of mechatronics tool at an angle to the axis of lathe or stop of axial feed.

For the purposes of the model has been created using Microsoft Visual Basic 6.0 *TurnTool* software to control the machining process. The main aim before emerging software was simple and intuitive interface (fig. 5), which allows CNC programming tools for person with a basic knowledge of technical drawing and machining. Elaborated software make possible to do:

- design and visualize items model using simple CAD system,
- set the basic parameters of machining,
- generating machining program,

- simulation of machining on the basis of input data,
- control tool retrieval of data from sensors,
- control of turning process.

The program uses advanced procedures for creating an optimal program for machining of the workpiece in many passages, and its simulation on a computer screen. In the future it is planned to develop the system by using G-code editor, which allows to load an external program of treatment or manual modification, which is useful for advanced users.

#### 4. Tool model

Tool design was developed using the Solid Works program (fig. 6).

Cutting tool with a threaded hole in the axle shaft was placed in a steel fence, which at the same time corps of tool. Tool placed in the guides was driving using the stepper motor. The stepper motor is coupled with axis of the threaded nut cooperating with the tool. The three-dimensional model of the tool used to generate drawings of individual parts, check and investigate the kinematics and calculate the tool stiffness. It was carried out in ANSYS environment (fig. 7).

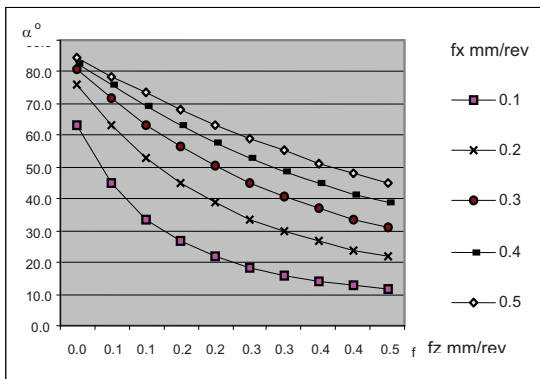


Fig. 4. Axial feed -  $f_z$  influence on surface angle for another radial feed -  $f_x$

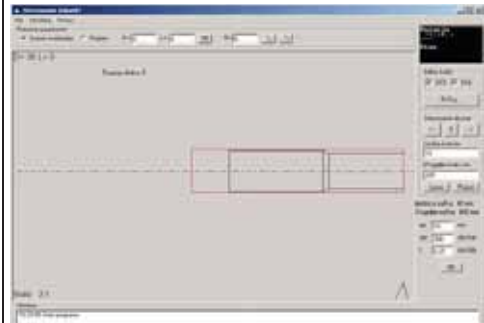


Fig. 5. Main form of TurnTool software

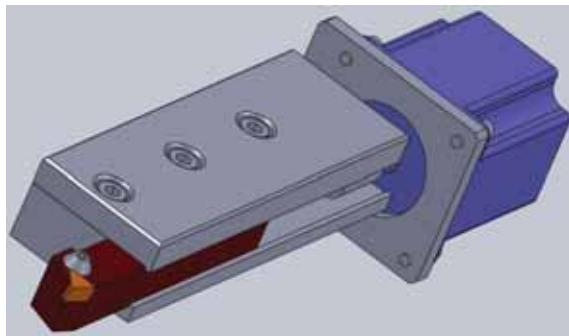


Fig. 6. Virtual model of mechatronics tool

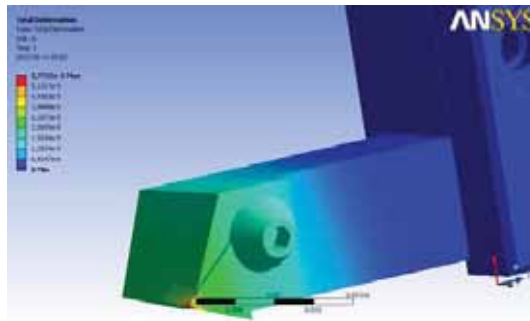


Fig. 7. Results of FEM calculation

## 5. Tools testing s

Tool designed and executed, was used to practical attempt to turning aluminium detail (fig. 8). Elaborated tool fitted to the lathe holder. The tool edge was situated on the axis of the lathe. To power the stepper motor controller uses a stabilized laboratory power supply (fig. 8).

Preset shape drawn in the *TurnTool* software, then generated  $x=f(z)$  control file. Shaping workpiece surface turning was carried out automatically switched axial feed. Conducted tests confirmed the correctness of the tool motion speed without load. Then attempts were cutting the sample. Obtained as expected shaping surface treatment.

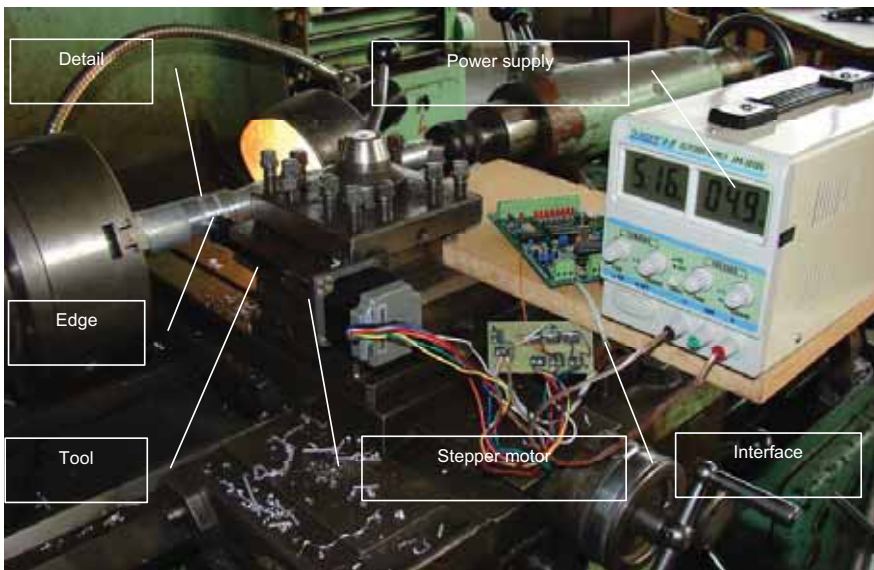


Fig. 8. Turning using controlled PC mechatronics tool

Because of the presence of radial cutting forces were clearing the slack due to gear favorable exacitude of processing.

Resulting of machining experiments showed no surface defects, and the dimensions correspondent to the values given. It confirms sufficient stiffness of the developed tool.

## 6. Conclusions

Showed in paper the controlled PC turning tool is a new idea in mechatronics tool. Presented design of tool and its control system and software show the new possibilities of automation machining using conventional lathe. Developed construction is very cheap – implemented easy to control stepper motor providing of process machining control. In the developed tools design equipping it will be useful with in trapezoidal screws, or even spherical. This increase the accuracy and correctness of the sustainability drive.

The mechatronics turning tool approach to building intelligent tool. The use of specialized tools mechatronic allows partial automation of machine tools conventional development by promoting efficiency and productivity.

The construction of such tools is now easier due to the widespread presence in the market of components for construction of such tools and especially the stepper motor including built-in gear, stepper motor controllers. There are also available other driving and the position measuring systems.

It is expedient to carry out further work and tools development including with the use of the second controlled axis. The next step in development of mechatronic tool will be the modernisation of tools software in direction of G-code file using to control machining process.

## References

- [1] CICHOSZ P.: Narzędzia skrawające, WNT Warszawa, 2006
- [2] CICHOSZ P., KUZINOWSKI M.: Narzędzia mechatroniczne w skrawaniu. W Obróbka skrawaniem tom 3, Zaawansowana technika. pod redakcją H. Latosia. Wyd. uczelniane UTP Bydgoszcz, 2009, 259-274
- [3] LATOS H.: Elastyczność geometryczno-kinematyczna narzędzi skrawających. Wydawnictwo Uczelniane Akademii Techniczno-Rolniczej, Bydgoszcz, 1997
- [4] LATOŚ H., MIKOŁAJCZYK T.: Surface shaping with industrial robot. 1st International Conference "Optimization of the Robots and Manipulators" OPTIROB-2006, Predeal, Romania, University "POLITEHNICA" of Bucharest, Faculty IMST, Department MSP, 2006, 265-269
- [5] LATOŚ H., MIKOŁAJCZYK T., Virtual aid design of geometric and kinematics flexible tools. XII Workshop on Supervising and Diagnostics of Machining Systems. Virtual Manufacturing, Karpacz, Poland, 2001, 145-152
- [6] MIKOŁAJCZYK T.: Mechatroniczny nóż tokarski o elastyczności kinematyczno-geometrycznej. W. Obróbka skrawaniem - tom 2 Innowacje pod redakcją M. Stósa, IZTW Kraków, 2008, 113-119
- [7] [www.dandrea.com](http://www.dandrea.com)
- [8] [www.komet.com/tools-navigation/tools/mechatronic.html](http://www.komet.com/tools-navigation/tools/mechatronic.html)
- [9] [www.machsupport.com/](http://www.machsupport.com/)
- [10] [www.cnc.info.pl](http://www.cnc.info.pl)



## INFLUENCE OF TEMPERATURE ON MATERIAL DATA DETERMINED ON THE BASE OF LOW CYCLE FATIGUE TESTS

Stanisław Mroziński, Radosław Skocki, Zbigniew Lis

University of Technology and Life Sciences in Bydgoszcz  
ul. Prof. Kaliskiego 7 85-789 Bydgoszcz, Poland  
phone: +48 52 340 82 12, fax: +48 52 340 82 71  
e-mail: stmpkm@utp.edu.pl

### Abstract

*The work deals with the method of fatigue life calculations with application of material characteristics determined during low cycle fatigue tests [7]. Analysis of obtained results enables to state that values of parameters  $n'$  and  $K'$  change and depend on fatigue life period  $n/N$  as well as temperature. Values of parameters  $n'$  and  $K'$  determined in half of fatigue life ( $n/N=0,5$ ) are not mean values for the whole range of fatigue life. The comparative analysis of obtained results indicates the scale of simplification by assumption, as results of elaboration, of values of parameters  $n'$  and  $K'$  from the one period of fatigue life  $n/N=0,5$ .*

**Keywords:** fatigue life, cyclic properties

### 1. Introduction

In the fatigue life calculation method that bases on the local strain and stress analysis [7] there are used material data determined during fatigue life tests in the range of low cycle fatigue life. The method of tests as well as elaboration of test results are covered by the standard [1]. In accordance with guidelines included in the mentioned document low cycle properties of metals are defined on the base of constant amplitude tests on several (minimum 5) levels of controlled stress or strain [1]. At each level of strain or stress there are processed at least three fatigue life tests. During tests there are recorded, for chosen cycles of loading, temporary values of loading force and strain of a specimen. Recorded values of force and strain enable, after the end of tests, to perform the analysis of basic parameters of a hysteresis loop and define their correlations.

One of two characteristics defined on the base of performed tests is the cyclic stain curve describing a dependence between the plastic strain amplitude  $\varepsilon_{ap}$  and the stress amplitude  $\sigma_a$ . During the elaboration of test results it is assumed that between these parameters, from the stabilization period, appear the power relationship. In double logarithmic coordinates it is described by the Morrow equation [3] that is:

$$\lg \sigma_a = \lg K' + n' \lg \varepsilon_{ap} \quad (1)$$

where:  $K'$  - the curve exponent,  
 $n'$  - the gradient of the curve (the strain hardening coefficient)

Parameters  $n'$  and  $K'$  of the equation (1) are basic material data used during fatigue life calculations. The presented method of elaboration of test results does not arouse doubts in case of cyclically stable materials. Doubts do appear in case of materials characterized by changes of cyclic properties that do not show stabilization period.

On the base of the analysis of works on low cycle test on metals [2] it can be stated that the period of stabilization may appear in short term or does not appear at all [4]. For such materials necessary parameters of the hysteresis loop ( $\sigma_a$  and  $\varepsilon_{ap}$ ) are assumed from the period responding to half of fatigue life  $n/N=0,5$ , where:  $N$ - fatigue life on the defined loading level to the failure appearance while,  $n=0,5N$ . The processing during determination of hysteresis loop parameters in the case of the lack of stabilization period is shown in Fig. 1. In the figure there are schematically shown exemplary curves of changes of one of parameters ( $\sigma_a$ ) appearing in the equation (1) on five levels of total strain  $\varepsilon_{ac}$  during tests of alloy steel [4].

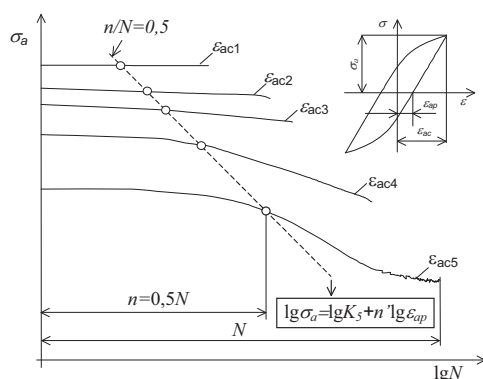


Fig. 1. Processing during elaboration of test results with the classic method (material with the lack of stabilization period) [4]

From the course of curves ( $\sigma_a$ ) it results that tested steel undergoes essential softening. Points marked on individual stress curves mean half of fatigue life ( $0,5n/N$ ) on each level of total strain  $\varepsilon_{ac}$ . Values of parameters  $n'$  and  $K'$  obtained as a result of approximation of hysteresis loops parameters ( $\sigma_a$ ,  $\varepsilon_{ap}$ ) with the equation (1) describe only temporary cyclic properties of material for the fatigue life period  $n/N=0,5$ . During fatigue life calculations they undergo an informal transposition (approximation) on the whole range of fatigue life. Such an attitude during determination of material data can be one of reasons of diversification of tests and calculation results observed for many metals and their alloys [4]. The problem especially refers to determination of material data of metals in increased temperatures.

The main aim of the work is the analysis of influence of temperature as well as the level of failure of cast steel on material data determined during low cycle fatigue tests.

## 2. Description of experimental tests

Experimental tests were performed with the usage of specimens made of martensitic cast steel GX12CrMoVNb9-1 (GP91). The shape of specimen and its dimensions are shown in Fig. 2.

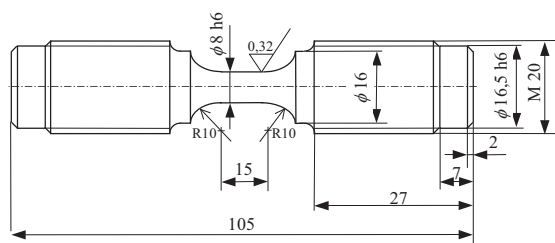


Fig. 2. Specimen for test

Tests were performed on five levels of strain  $\varepsilon_{ac}$  ( 0,25; 0,3; 0,35; 0,5; 0,6 %). The total strain amplitude was the controlled parameter during tests ( $\varepsilon_{ac}=\text{const}$ ). During fatigue life tests for chosen cycles there were recorded temporary values of loading force as well as strain of specimen. As a criterion of test of the fatigue life test end on all levels of strain  $\varepsilon_{ac}$  there was assumed a deformation of the hysteresis loop in the half-cycle of tension.

### 3. Test results and their analysis

Values of loading force and strain recorded for chosen cycles were elaborated in order to determine the course of changes of basic parameters of the hysteresis loop that are  $\varepsilon_{ap}$  and  $\sigma_a$ . Temporary stress in specimen  $\sigma$  was determined by division the value of temporary loading force by the specimen cross-sectional area. Using maximum  $\sigma_{\max}$  and minimum  $\sigma_{\min}$  values of stress there was determined the amplitude value  $\sigma_a$ . Similar approach was applied while determining the value of the total strain amplitude  $\varepsilon_{ap}$ .

As it was expected increased temperature caused decrease of fatigue life. Influence of temperature on fatigue life depends on the strain level. It is small in the area of the largest levels of strain and increases as strain decreases. In Fig. 3 there are shown exemplary curves of two parameters of the hysteresis loop ( $\varepsilon_{ap}$  and  $\sigma_a$ ) in the function of number of loading cycles.

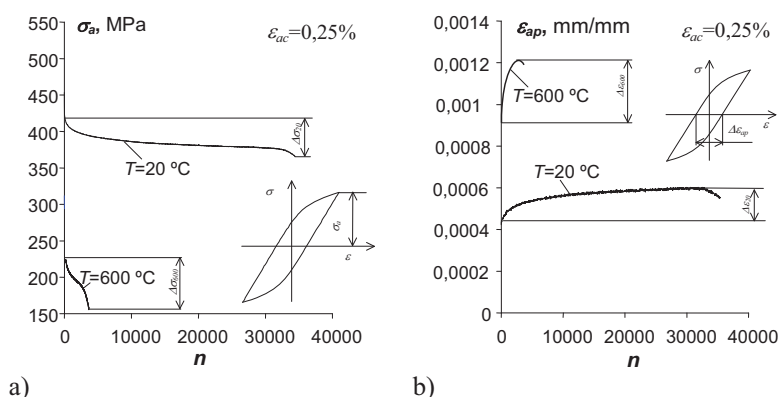


Fig. 3. Changes of parameters of the hysteresis loop on the level  $\varepsilon_{ac}=0,25\%$ : a)  $\sigma_a$ , b)  $\varepsilon_{ap}$

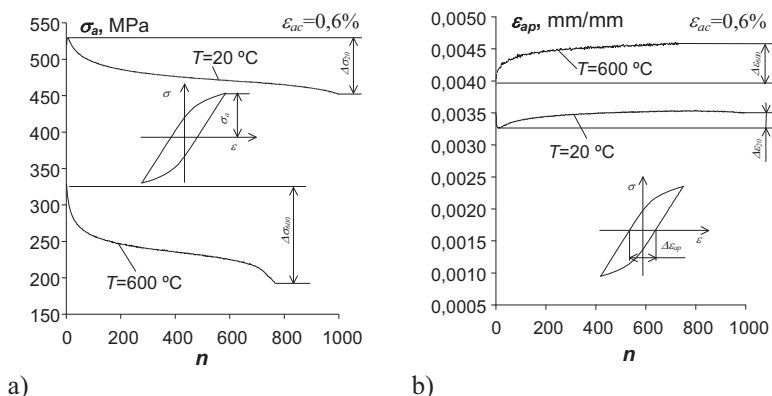


Fig. 4. Changes of parameters of the hysteresis loop on the level  $\varepsilon_{ac} = 0,6\%$ : a)  $\sigma_a$ , b)  $\varepsilon_{ap}$

On the base of obtained curves it can be stated that there is no clear stabilization period of cyclic properties on any of loading levels. As the  $n$  number of loading cycles increases parameters of the hysteresis loop change. The stress amplitude  $\sigma_a$  (fig. 3a and 4a) decreases and at the same time the plastic strain amplitude increases  $\varepsilon_{ap}$  (fig. 3b, 4b). The pattern of changes of mentioned parameters attests to cyclic softening of the cast steel. In figures 3 and 4 ranges of courses of parameters recorded in the fatigue test were marked. On the base of the analysis of determined curves it can be stated that the range of changes of  $\Delta\sigma$  and  $\Delta\varepsilon$  parameters increases with the number of loading cycles and the strain level. Moreover the course of changes of parameters increases as temperature increases. The problem of softening of the cast steel in increased temperature was discussed in details in works [5, 6].

The method proposed in the work [4] was used to evaluate influence of temperature and fatigue failure level. Its pith is in usage of parameters of the hysteresis loop from different periods of relative fatigue life  $n/N$  during approximation of hysteresis loop parameters ( $\varepsilon_{ap}$ , and  $\sigma_a$ ) with straight lines described by the equation (1).

The above was schematically shown in Fig. 5. During elaboration of test results on each of loading levels there were separated 10 periods of relative fatigue life  $n/N$ . Periods were defined with the usage of parallel lines  $L_1$ - $L_{10}$ . Lines stand for fatigue life periods where values of strain  $\varepsilon_{ap}$  were assumed. Analogically  $\sigma_a$  stresses were determined in the same periods of fatigue life.

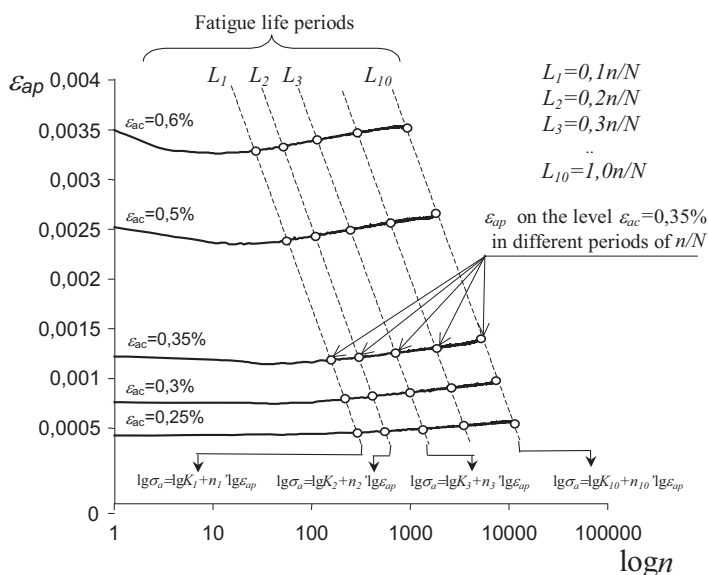


Fig. 5. Changes of plastic strain of the cast steel in temperature 600°C, the method of elaboration of test results

Values of coefficient  $n'$  and exponent  $K'$  of the equation (1) obtained in different fatigue life periods were analyzed in the function of relative fatigue life  $n/N$ . Curves of changes of  $n'$  and  $K'$  are shown in Fig. 6. In order to illustrate the simplification performed during elaboration of test results in the figure there were also marked values of mentioned parameters for the one period of fatigue life ( $n/N=0,5$ ).

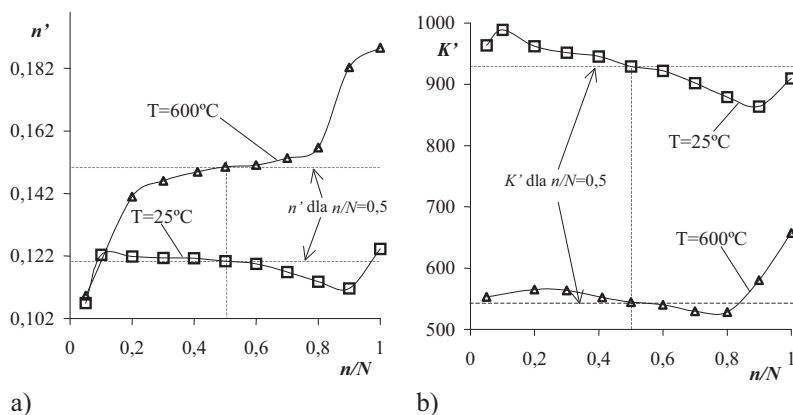


Fig. 6. Elaboration results of low cycle tests of the cast steel obtained in two temperatures: a) value of the exponent  $K'$ , b) value of the coefficient  $n'$

As it was expected values of parameters  $n'$  and  $K'$  change and depend on the fatigue life period  $n/N$ . Bigger changes of material data are a consequence of the bigger range of changes of parameters of the hysteresis loop in the function of the number of loading cycles in increased temperature. The comparative analysis of material data  $n'$  and  $K'$  in both temperatures indicates the scale of the performed simplification by assuming, as elaboration results, values of parameters  $n'$  and  $K'$  from the one period of fatigue life  $n/N=0,5$ .

#### 4. Summary

Martensitic cast steel during low cycle loading in ambient temperature and in temperature 600 °C undergoes cyclic softening without clear stabilization period. Temperature and total strain level influence on the value of appearing softening.

Material data ( $n'$  and  $K'$ ) used in fatigue life calculations essentially depend on fatigue life in which they were determined. Bigger range of changes of loop parameters in temperature 600 °C causes that the range of material data changes in increased temperature is also bigger than in ambient temperature.

Material data of martensitic cast steel ( $n'$  and  $K'$ ), obtained as a result of elaboration of fatigue life tests with the method given in the standard [1], describe only temporary cyclic properties. Values of data determined in half of fatigue life ( $n/N=0,5$ ) are not mean values for the whole range of fatigue life.

Material data ( $n'$  and  $K'$ ) obtained in different fatigue life periods enable a design engineer to estimate the range of possible changes of cyclic properties. In case of essential machine elements it is possible to perform calculations that verify extreme values of those parameters.

#### References

- [1] ASTM E606-92: *Standard Practice for Strain -Controlled Fatigue Testing*
- [2] Kocańda, S., Kocańda, A., *Niskocyklowa wytrzymałość zmęczeniowa metali*, PWN, Warszawa 1989
- [3] Morrow, J.D.W., *Internal Friction, Damping and Cyclic Plasticity: Cyclic Plastic Strain Energy and Fatigue of Metals ASMT STP-378* Philadelphia 1965 s. 45-84
- [4] Mroziński, S., (2008), *Stabilizacja własności cyklicznych metali i jej wpływ na trwałość zmęczeniową*, Wydawnictwa Uczelniane Uniwersytetu Technologiczno-Przyrodniczego w Bydgoszczy, Rozprawy Nr 128, Bydgoszcz 2008
- [5] Mroziński, S., Skocki, R., *Softening of Martensitic Cast Steel*, Journal of Polish CIMAC tom 6 zeszyt 1-3, poz. 21, 2011
- [6] Mroziński, S., Skocki, R., *Wpływ temperatury na zmiany właściwości cyklicznych staliwa martenzytycznego*, XXIV Sympozjum Zmęczenie i Mechanika Pękania Bydgoszcz - Pieczyńska, maj 2012
- [7] Tucker, L.E., *Procedure for Designing Against Fatigue Failure of Notched Parts*, Society of Automotive Engineers, Inc., SAE Paper No 720265, New York 1972

*Scientific work financed by the Ministry of science in the years 2011 - 2013 as a research project No. 1215/B/T02/2011/40*



## EXAMINATION OF CAST STEEL IN TERMS OF THERMO-MECHANICAL FATIGUE

Stanisław MROZIŃSKI<sup>1</sup>, Sławomir WŁODARCZYK<sup>2</sup>

<sup>1,2</sup> *University of Technology and Life Sciences in Bydgoszcz, Faculty of Mechanical Engineering, Al. Prof. S. Kaliskiego 7, 85-789 Bydgoszcz,  
tel.: 48 52 340-82-64, fax: 48 52 340-82-71, e-mail: mrozinski.stanislaw@utp.edu.pl*

### Abstract

*The paper presents experimental verification of experimental tests methodology on the testing machine in the range of thermal and thermo-mechanical fatigue. Test samples were made of martensitic cast steel. Control parameter of the tests was temperature of the sample whereas there were recorded parameters as follows: loading force and temperature of the specimen. In this study it was stated that the temperature decreases the strength parameters of the cast steel and an increase its elongation. As the results of the changes of the temperature occurred loading may exceed yield strength.*

**Keywords:** *thermo-mechanical fatigue, fatigue life, cyclic properties, martensitic cast steel*

### 1. Introduction

The endless tendency to increase the performance of devices in the energy industry, aviation makes it necessary to determine the material characteristics in terms of thermo-mechanical fatigue. Complexity of tests in terms of thermo-mechanical fatigue and difficult interpretation of results caused that the basic guidelines for such testing were collected in the form of standards [1,2]. The thermal stress occurs when in operating conditions the deformation of component is inhibited due to an increase of temperature. Cyclic changes of the temperature may cause variable stress which may lead to the, so-called, thermal fatigue.

Thermal fatigue can be classified as thermal fatigue with external constraints (constraint reactions, the forces applied to the surface) or internal constraints (temperature gradient, anisotropy of the structure and the different thermal expansion values of coefficients adjacent grains, phases or composite components) [3,4,5,6].

Thermal load cycle can be divided into characteristic stages: heating up to the maximum temperature  $T_{max}$  in a time of  $t_1$ , withstand the maximum temperature during  $t_{Tmax}$ , cooling to minimum temperature  $T_{min}$  in a time of  $t_2$ , withstand a minimum temperature during the  $t_{Tmin}$  (Fig. 1). Stresses in machine parts undergoing mechanical loads during machine operation in conditions of temperature changes are interaction between stresses resulting from mechanical and thermal loads.

The aim of this study was an experimental verification of the methodology of experimental research in the field of thermal and thermo-mechanical fatigue on the testing machine. The scope of the work was to investigate the effect of temperature on the strength parameters which are

determined in static tensile tests and stresses which generate in the metal under conditions of external constraints.

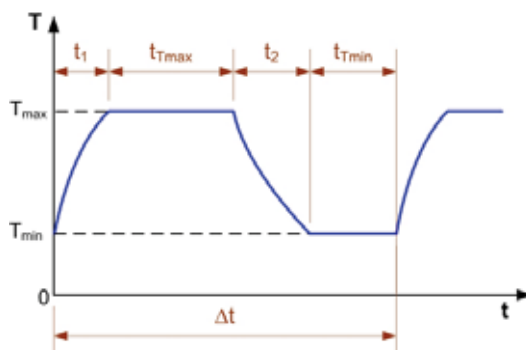


Fig. 1. Cycle stages of heat load

## 2. Description of tests

Martensitic cast steel GX12CrMoVNB9-1 was used during verification tests. The chemical composition of the cast steel is given in table. 1.

Table 1. The chemical composition of cast steel GX12CrMoVNB9-1 in%.

| C    | Mn   | Si   | P     | S     | Cr   | Mo   | V    | Nb   | N    |
|------|------|------|-------|-------|------|------|------|------|------|
| 0.12 | 0.47 | 0.31 | 0.014 | 0.004 | 8.22 | 0.90 | 0.12 | 0.07 | 0.04 |

Specimens were prepared according to the standard [7]. Static and cyclic tests were carried out under conditions of mechanical stress and under thermal load. Static tests were performed according to the standard [8] for the four levels of temperature. During the tests actual values of the loading force and deformation of the specimen were recorded. Fig. 2 presents the specimen fixed in the grips of the testing machine prepared for the static tensile tests.



a)



b)

Fig. 2. Tests at elevated temperatures: a) Fixing of the extensometer, b) The specimen in the heating chamber

Test was carried out under the heat load on the testing machine equipped with a heating chamber. Chamber heating elements are the resistive coils. Power of the installed heating elements allow to warm up the specimen with the speed of about  $10^{\circ}\text{C} / \text{min}$ . The temperature of the specimen was monitored using a thermocouple mounted to the measuring part of the specimen.

Specimen temperature was changed according to the program shown in Fig. 3. Recorded values during heating and cooling of the chamber was the force which loaded the specimen and specimen's temperature. The parameter which was maintained during the tests was the level of specimen deformation ( $\varepsilon=\text{const}$ ). Deformation of the specimen was monitored using an extensometer with a measuring base of 12.5 mm.

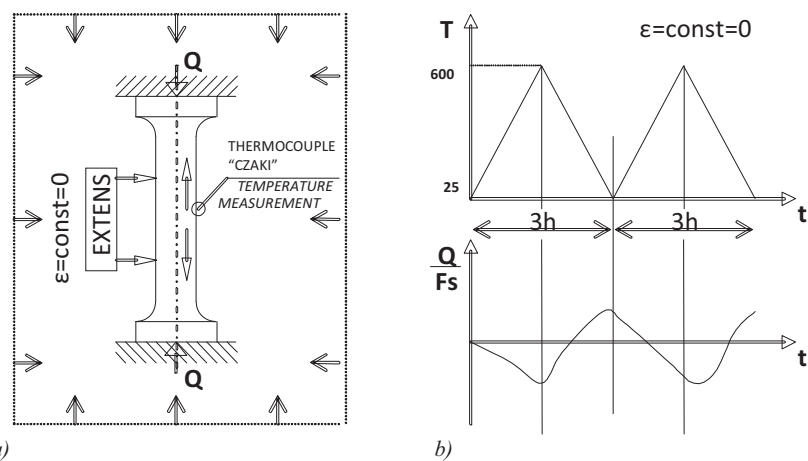


Fig. 3. Thermal fatigue tests: a) measuring system b) program of changes of temperature and stresses

### 3. Test results

#### 3.1. Mechanical stress

The results obtained under conditions of mechanical loading at different temperatures are presented in graphs, static stretching of the coordinate system of the stress-elongation (Fig. 4). Stresses in the specimen were calculated as the ratio of momentary value of loading force per cross-sectional area before the specimen loading.

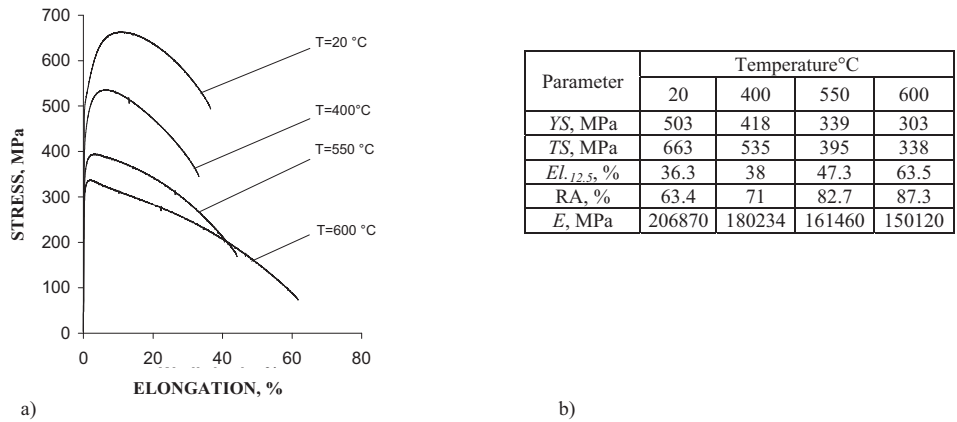


Fig. 4. The results of static tests: a) tensile graphs, b) influence of temperature on strength parameters

The results of static tensile tests were analyzed in the context of the effect of temperature on basic strength parameters. Fig. 5 summarizes the basic values of strength parameters in the

function of temperature.

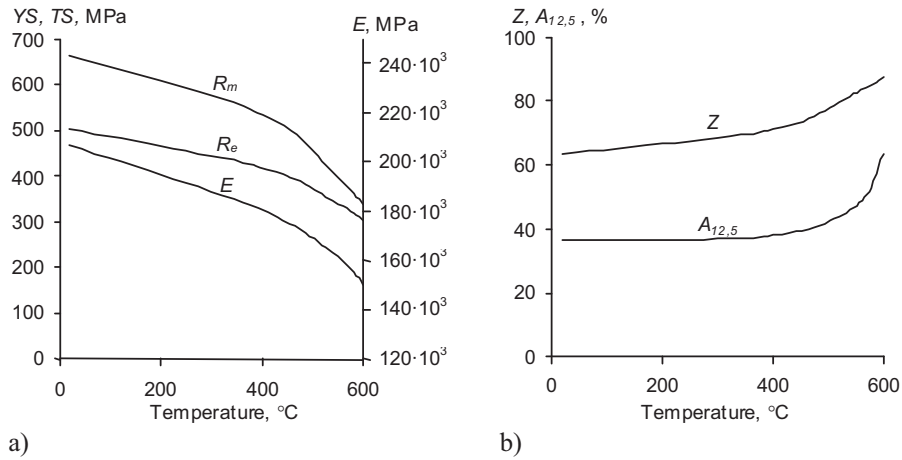


Fig. 5. Influence of temperature on strength parameters: a) YS, TS, E, b)  $A_{12,5}$ , Z

As expected, the increase in temperature decreases the strength parameters  $R_m$  and  $R_e$ , and slightly increases in elongation. Analysis of the graphs shows that the temperature exceeding about 450°C enhances the effect of temperature on the parameters.

### 3.2. Thermal loads

Recorded strength values and temperature during the tests allowed to the analysis of the courses of the stresses in the specimen. Selected results of thermal load conditions are shown in Fig. 6 in the form of graphs of changes in function of temperature stress ( $\sigma=f(T)$  - Figure 6a) and the stress time ( $\sigma=f(T)$ -Fig. 6b).

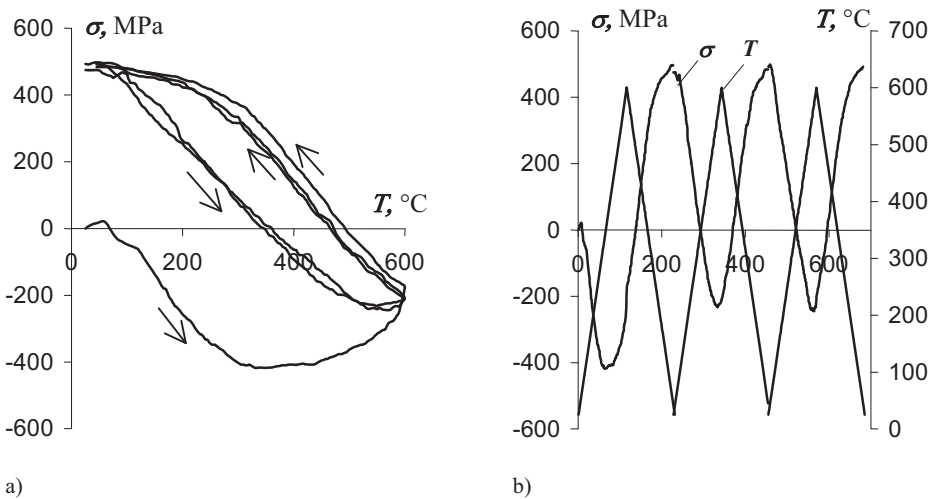


Fig. 6. Changes in stress in the function of temperature and time

On the basis of the changes of waveform of stress in the function of time it can be stated that until the temperature of about 450°C changes of stress are linear. Above this temperature plasticity of the specimen occurs and the relationship between stresses and the temperature is no longer linear. Obtained results of verification tests show possibility to realize the tests in terms of thermo mechanical fatigue on standard testing machine.



*Fig. 7. Picture of specimens after tests of thermal fatigue*

In order to implement long-term fatigue tests it is necessary to elaborate and implement the system which would control the temperature of the specimen. Guidelines for the construction of such a system can be found in the work [2.9].

#### **4. Summary**

Elevated temperature causes decrease of the strength parameters of cast steel. In the temperature of 600°C ultimate tensile strength equals about 50%; yield strength equals 60% of ultimate tensile strength cast steel determined at room temperature.

From zero pulsating temperature changes may lead to the occurrence varying stresses in the material shuttles (tension-compression). The value of maximum stress variables depends on the level temperature. Tension in the material as a result changes in temperature may exceed the yield strength.

#### **References**

- [1] Chakraborti, P.C.; Mitra, M.K., 2005. Room temperature low cycle fatigue behaviour of two high strength lamellar duplex ferrite–martensite (DFM) steels. *International Journal of Fatigue* Volume: 27, Issue: 5, p. 511-518
- [2] Collins J.A., 1993. *Failure of Materials in Mechanical Design, Analysis, Prediction, Prevention*. John Wiley & Sons, New York.
- [3] Kocańda S., Kocańda A., 1989. *Niskocyklowa wytrzymałość zmęczeniowa metali*. PWN Warszawa.
- [4] Manson S.S., Halford G.R., 1986. Re-Examination of Cumulative Fatigue Damage Analysis – an Engineering Perspective. *Engineering Fracture Mechanics* 25(5/6), p. 539-571.
- [5] Mroziński S., 2008. Stabilizacja własności cyklicznych metali i jej wpływ na trwałość zmęczeniową. *Wydawnictwo Uczelniane Uniwersytetu Technologiczno-Przyrodniczego w Bydgoszczy*, Rozprawy Nr 128.
- [6] Mughrabi, Hael; Höppel, Heinz Werner, 2010. Cyclic deformation and fatigue properties of very fine-grained metals and alloys. *International Journal of Fatigue*. Volume: 32, Issue: 9, p. 1413-1427
- [7] Plumtree, A.; Abdel-Raouf H.A., 2001. Cyclic stress–strain response and substructure. *International Journal of Fatigue* Volume: 23, Issue: 9, p. 799-805.
- [8] PN-84/H-04334 *Badania niskocyklowego zmęczenia metali*.

- [9] Xianjie Yang, 2005. Low cycle fatigue and cyclic stress ratcheting failure behavior of carbon steel 45 under uniaxial cyclic loading. International Journal of Fatigue Volume: 27, Issue: 9, p. 1124-1132.

*Scientific work financed by the Ministry of science in the years 2011 - 2013 as a research project No. 1215/B/T02/2011/40*



## A PROPOSAL OF MODIFICATION OF THE ZENNER'S FATIGUE CRITERION FOR THE CASE OF NON-PROPORTIONAL LOADING

Lukasz Pejkowski, Dariusz Skibicki

University of Technology and Life Sciences  
al. Prof. S. Kaliskiego 7, 85-789 Bydgoszcz  
tel.: +48 52 3408202, +48 52 3408247

e-mail: lukasz.pejkowski@utp.edu.pl, dariusz.skibicki@utp.edu.pl

### Abstract

In this paper, a modification of the Zenner's fatigue criterion has been proposed. The modification changes the value of "effective shear stress" amplitude for the case of non-proportional load. In this work there's also verification of proposed modification has been made for 4 kinds of materials. In the conclusions, distinctive features of results obtained by using these methods have been pointed out.

**Keywords:** fatigue of materials, fatigue curves, accelerated methods

### 1. The Idea of Integral Criteria

The Integral approach assumes that an appropriate description of fatigue behavior of a structural element involves summing the damage parameters on all the physical planes, running through the considered point  $P$  of the material [3]. Location of these planes is described by means of a sphere representing the material elementary volume (fig.1b). The planes are tangent to the sphere surface in point  $P$ . Coordinates of point  $P$  are determined by radius vector  $\vec{n}$ . In turn, the location of vector  $\vec{n}$  is determined by angles  $\gamma$  and  $\varphi$  (fig.1).

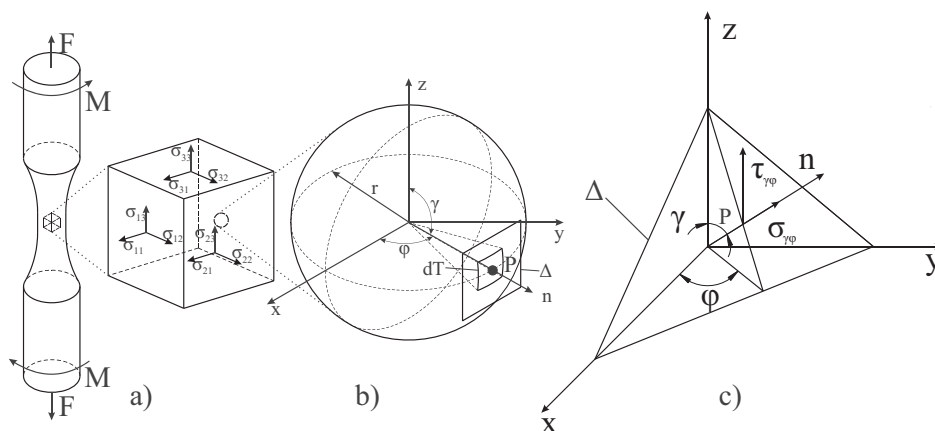


Fig. 1 - A way of description of a physical plane location

The integral approach was used for the first time by Novoshilov [8]. He identified the second invariant of the stress tensor deviator with the square mean from shear stresses acting on all planes running through a given point. The mean can be expressed in the following way:

$$\tau_{RMS} = \sqrt{\frac{1}{T} \int_T \tau_{\gamma\varphi}^2 dT}. \quad (1)$$

If the location of a sectional plane is described in the way given in figure 1, then  $dT$  is an elementary surface of sphere with radius  $r = l$  and is equal to:

$$dT = r^2 \sin \gamma d\varphi d\gamma = \sin \gamma d\varphi d\gamma, \quad (2)$$

a  $T$  is the sphere equal surface, that is, the shear stress acting on plane as  $\Delta$  has been denoted as  $\tau_{\gamma\varphi}$ . After taking into consideration all the notations, the root mean square from all the stresses has the form:

$$\tau_{RMS} = \frac{1}{4\pi} \int_{\gamma=1}^{\pi} \int_{\varphi=0}^{2\pi} \tau_{\gamma\varphi}^2 \sin \gamma d\varphi d\gamma. \quad (3)$$

For a plane stress state the formula for  $\tau_{\gamma\varphi}^2$  can be given as:

$$\begin{aligned} \tau_{\gamma\varphi}^2 = & \sin^2 \gamma [(\sigma_x^2 + \tau_{xy}^2) \cos^2 \varphi + \tau_{xy}^2 \sin^2 \varphi + 2\sigma_x \tau_{xy} \sin \varphi \cos \varphi] - \\ & - \sin^4 \gamma [\sigma_x^2 \cos^4 \varphi + 4\sigma_x \tau_{xy} \sin \varphi \cos^3 \varphi + 4\tau_{xy}^2 \sin^2 \varphi \cos^2 \varphi]. \end{aligned} \quad (4)$$

After substituting formula (4) to (3) and integration we receive:

$$\tau_{RMS} = \left[ \frac{2}{15} (\sigma_x^2 + 3\tau_{xy}^2) \right]^{\frac{1}{2}}. \quad (5)$$

It can be noticed that the expression in round brackets is equal to square of equivalent stress according to the hypothesis of Huber-Mises-Hencky (HMH):

$$\sigma_{HMH} = \sqrt{\sigma_x^2 + 3\tau_{xy}^2}. \quad (6)$$

Formulas (3) and (5) can be compared in the following way:

$$\left[ \frac{2}{15} \sigma_{HMH}^2 \right]^{\frac{1}{2}} = \left[ \frac{1}{4\pi} \int_{\gamma=0}^{\pi} \int_{\varphi=0}^{2\pi} \tau_{\gamma\varphi}^2 \sin \gamma d\varphi d\gamma \right]^{\frac{1}{2}}. \quad (7)$$

The formula of equivalent stress according to HMH hypothesis can be derived from the above equation, for constant-amplitude fatigue loads:

$$\sigma_{HMH} = \sqrt{\frac{15}{8\pi} \int_{\gamma=0}^{\pi} \int_{\varphi=0}^{2\pi} \tau_{\gamma\varphi}^2 \sin \gamma d\varphi d\gamma} \leq Z_{rc}, \quad (8)$$

where  $Z_{rc}$  is fatigue limit for fully reversed tension-compression.

## 2. Zenner's criterion in terms of integral criteria

The idea of integral approach to HMM hypothesis was developed by Zenner [9]. He notes that, firstly, HMM hypothesis assumes the same ratio  $Z_{so}/Z_{rc} = 1/\sqrt{3}$  for all the materials. Actually, this ratio occupies interval  $0,5 < Z_{so}/Z_{rc} < 0,8$  for ductile materials, which should be taken into account in the calculations. Secondly, Zenner says that notation (8) accounts only for shear stress. Experimental tests show that also mean stresses and normal stress amplitudes have an influence on the material fatigue life.

With regard to these observations Zenner formulated a criterion in which  $\tau_{\gamma\varphi}^2$  replaces the so called 'effective amplitude'. The criterion can be written in the form [9]:

$$\sigma_Z = \sqrt{\frac{15}{8\pi} \int_{\gamma=0}^{\pi} \int_{\varphi=0}^{2\pi} (a\tau_{\gamma\varphi,a}^2(1 + m\tau_{\gamma\varphi,m}^2) + b\sigma_{\gamma\varphi,a}(1 - n\sigma_{\gamma\varphi,a})^2) \sin \gamma d\gamma d\varphi} \leq Z_{rc}. \quad (9)$$

In the above notation  $a$ ,  $b$ ,  $m$  and  $n$  are coefficients dependent on the material constants. In order to calculate them it is necessary to have: tensile – compressive fatigue strength  $Z_{rc}$ , torsional fatigue strength  $Z_{so}$ , pulsating tensile strength  $Z_{rj}$ , pulsating torsional  $Z_{sj}$ . The constants are calculated on the basis of the formulas:

$$a = \frac{1}{5} \left( 3 \left( \frac{Z_{rc}}{Z_{so}} \right)^2 - 4 \right), \quad b = \frac{2}{5} \left( 3 - \left( \frac{Z_{rc}}{Z_{so}} \right)^2 \right), \quad (10)$$

$$a \cdot m = \frac{Z_{rc}^2 - \left( \frac{Z_{rc}}{Z_{so}} \right)^2 \left( \frac{Z_{sj}}{2} \right)^2}{\frac{12}{7} \left( \frac{Z_{sj}}{2} \right)^4}, \quad b \cdot n = \frac{Z_{rc}^2 - \left( \frac{Z_{rj}}{2} \right)^2 - \frac{4}{21} a m \left( \frac{Z_{rj}}{2} \right)^4}{\frac{15}{4} \left( \frac{Z_{rj}}{2} \right)^3} \quad (11)$$

For load without mean stresses, expression (9) is reduced to the form:

$$\sigma_Z = \sqrt{\frac{15}{8\pi} \int_{\gamma=0}^{\pi} \int_{\varphi=0}^{2\pi} (a\tau_{\gamma\varphi,a}^2 + b\sigma_{\gamma\varphi,a}^2) \sin \gamma d\gamma d\varphi} \leq Z_{rc}. \quad (12)$$

Thanks to this, it is enough to know values of  $Z_{rc}$  and  $Z_{so}$ .

## 3. Zenner's criterion for nonproportional loads

In case of non-proportional loads, that is, when sinusoidal variables of stress are out-of-phase phase, the vector of shear stress on a sectional plane changes not only its module but also its direction, drawing a hodrograph (fig.2).

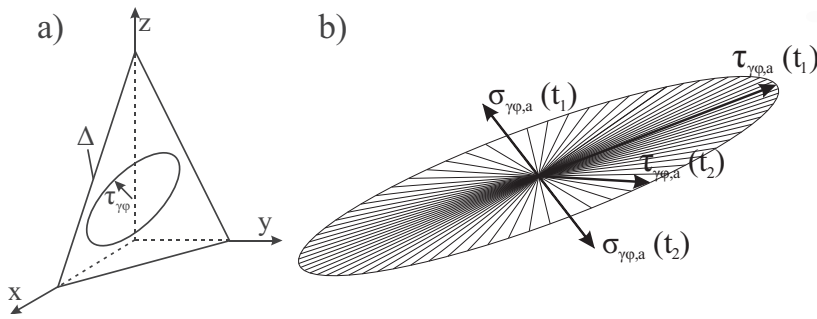


Fig. 2 - Changes of the and normal stress vector during a non-proportional load cycle: a) hodograph of a shear stress vector, b) subsequent positions of a shear stress vector

Zenner's criterion, given in form (12), accounts only for maximal values of modules for normal and shear stress vectors, whereas, tests of micro-structure and fractures of materials exposed to non-proportional load [3] indicate that not only the change of shear stress vector module but also the change of its direction has a large influence on fatigue behavior.

#### 4. Modification of Zenner's criterion due to load non-proportionality

In the proposed modification of Zenner's criterion, the maximal module of shear stress  $\tau_{\gamma\phi,a}$  has been replaced in formula (12) with a quantity accounting for changes of the action course of the shear stress vector.

For tension-compression and torsion, when the components of load are sinusoidal and out-of-phase, the path drawn by the vector of shear stress is an ellipse, as in figure 2. In such a situation it is convenient to describe the changes of shear stress vector location in a system of coordinates, determined by the course of a vector with maximal module  $\bar{k}$  and direction perpendicular to it  $\bar{n}$  (fig. 3).

Coordinates of unit vectors determining these directions can be obtained from the formulas:

$$\bar{k} = \frac{\bar{\tau}_{\gamma\phi,max}}{\|\bar{\tau}_{\gamma\phi,max}\|}, \quad \bar{n} = \bar{k} \begin{bmatrix} \cos \frac{\pi}{2} & -\sin \frac{\pi}{2} \\ \sin \frac{\pi}{2} & \cos \frac{\pi}{2} \end{bmatrix}. \quad (13)$$

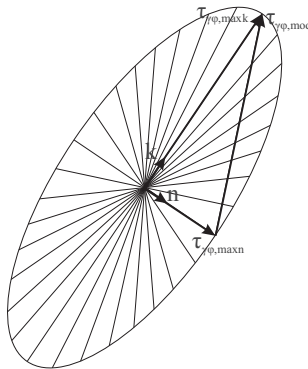


Fig. 3 - Unit vectors  $\bar{k}$  and  $\bar{n}$  determining directions used for a description of the tangent stress vector location changes and the proposed quantity  $\tau_{\gamma\phi,mod}$

The proposed quantity, substituting  $\tau_{\gamma\varphi,a}$  in Zenner's criterion, is a module of vector which is the result of the sum of vectors whose projections on directions  $\bar{k}$  and  $\bar{n}$  reach the highest values during the cycle of loading (fig.3). This quantity can be expressed by the formula:

$$\tau_{\gamma\varphi,mod} = \|\bar{\tau}_{\gamma\varphi,max\bar{k}} + \bar{\tau}_{\gamma\varphi,max\bar{n}}\|. \quad (14)$$

When there is no phase shift between the components of loading, the value of  $\tau_{\gamma\varphi,mod} = \tau_{\gamma\varphi,a}$  is identical as in an unchanged Zenner's criterion.

A similar solution to the description of non-proportionality was used by Freitas and others [5], as a measurement of the loading path non-proportionality on an octahedral plane.

Eventually, a modified Zenner's criterion is expressed by the dependence:

$$\sigma_Z = \sqrt{\frac{15}{8\pi} \int_{\gamma=0}^{\pi} \int_{\varphi=0}^{2\pi} (a \|\bar{\tau}_{\gamma\varphi,max\bar{k}} + \bar{\tau}_{\gamma\varphi,max\bar{n}}\|^2 + b \sigma_{\gamma\varphi,a}^2) \sin \gamma \, d\gamma d\varphi} \leq Z_{rc}. \quad (15)$$

## 5. Verification of Modified Zenner's criterion

Modified Zenner's criterion was verified for the aluminum alloy 7075-T651 [1], steel 1045 for the data from works [2] and [6] as well as tests of steel X2CrNiMo17-12-2 [7].

The verification involves comparing experimental fatigue life with the computing one. Statistical parameters used for the comparison are: the mean scatter of fatigue life  $T_N$  and the mean-square error of fatigue life estimation  $T_{RMS}$ , which has been calculated according to formulas [7]:

$$T_N = 10^{\bar{E}}, \quad (16)$$

$$\bar{E} = \frac{1}{n} \sum_{i=1}^n \log \left( \frac{N_{exp,i}}{N_{cal,i}} \right), \quad (17)$$

$$T_{RMS} = 10^{E_{RMS}}, \quad (18)$$

$$E_{RMS} = \sqrt{\frac{\sum_{i=1}^n \log^2 \left( \frac{N_{exp,i}}{N_{cal,i}} \right)}{n}}. \quad (19)$$

It has been assumed that acceptable results should be included in interval  $0,5 \div 2$  for and  $1 \div 2$  for  $T_{RMS}$ . Verification results have been presented below in the form of charts of comparison between calculated life  $N_{cal}$  and experimental  $N_{exp}$  and tables with values  $T_N$  and  $T_{RMS}$ .

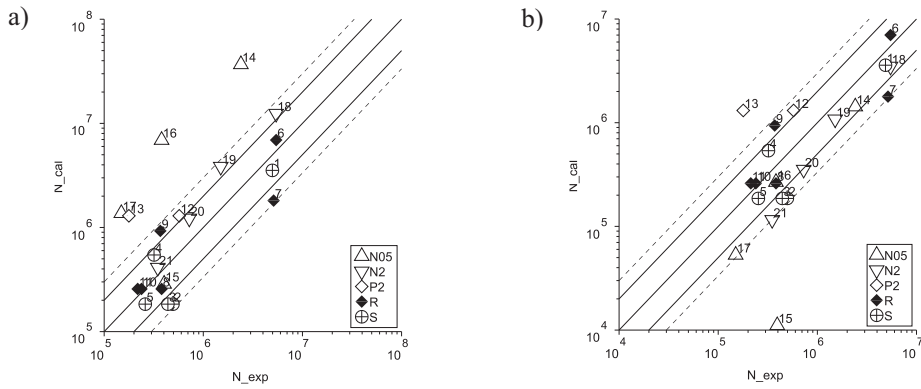


Fig. 4a - Chart of comparison between experimental fatigue life and calculated obtained for: a) Zenner's criterion for 1045 steel [6], b) modified Zenner's criterion for 1045 steel [6]

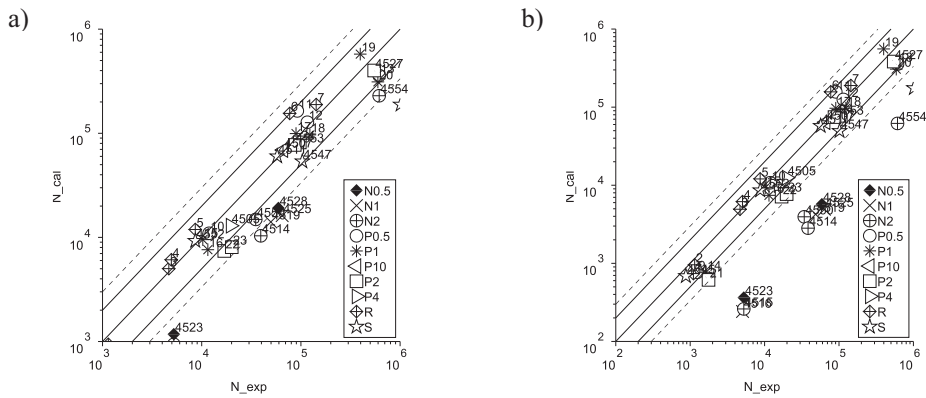


Fig. 5a - Chart of comparison between experimental fatigue life and calculated obtained for: a) Zenner's criterion for 1045 steel [2], b) modified Zenner's criterion for 1045 steel [2]

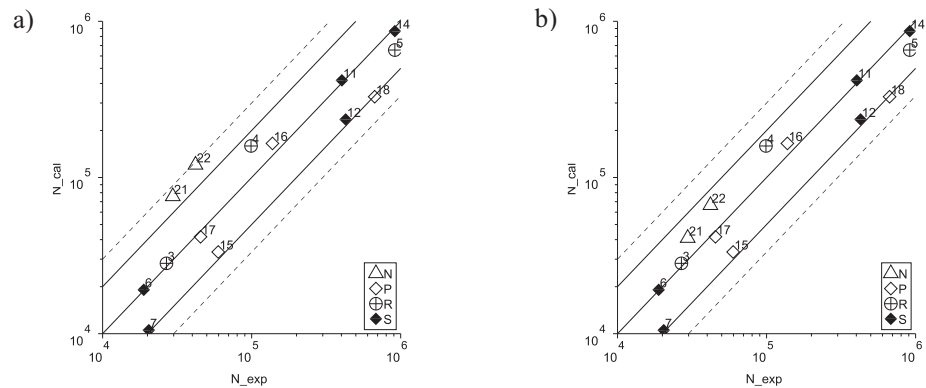


Fig. 6a - Chart of comparison between experimental fatigue life and calculated obtained for: a) Zenner's criterion for 7075-T651 aluminum alloy [1], b) modified Zenner's criterion for 7075-T651 aluminum alloy [1]

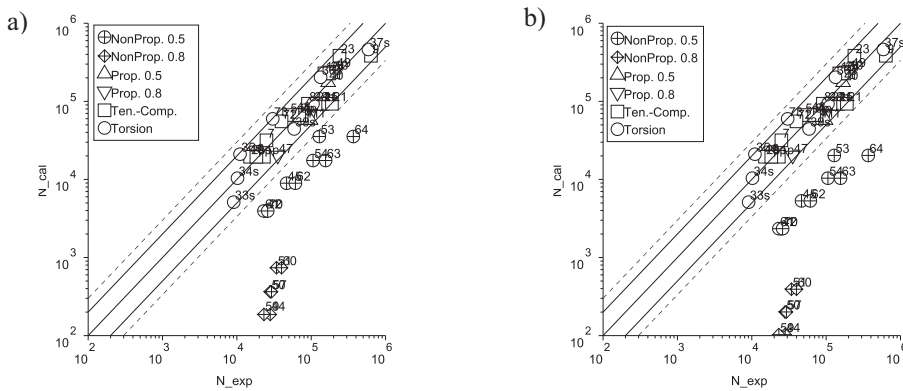


Fig. 7a - Chart of comparison between experimental fatigue life and calculated obtained for: a) Zenner's criterion for X2CrNiMo17-12-2 steel [7] b) modified Zenner's criterion for X2CrNiMo17-12-2 steel [7]

Tab 1. Comparison of  $T_N$  and  $T_{RMS}$  parameters for Zenner's criterion before and after modification for 1045 steel [6]

|                                       | Zenner's criterion |           | Modified Zenner's criterion |           |
|---------------------------------------|--------------------|-----------|-----------------------------|-----------|
|                                       | $T_N$              | $T_{RMS}$ | $T_N$                       | $T_{RMS}$ |
| Tension                               | 1,00               | 1,84      | 1,00                        | 1,84      |
| Torsion                               | 1,49               | 1,95      | 1,49                        | 1,95      |
| Proportional load $\lambda = 2$       | 0,24               | 4,61      | 0,24                        | 4,61      |
| Non-proportional load $\lambda = 0,5$ | 0,15               | 9,73      | 3,97                        | 6,63      |
| Non-proportional load $\lambda = 2$   | 0,54               | 1,97      | 1,90                        | 2,03      |

Tab 2. Comparison of  $T_N$  and  $T_{RMS}$  parameters for Zenner's criterion before and after modification for 1045 steel [2]

|                                       | Zenner's criterion |           | Modified Zenner's criterion |           |
|---------------------------------------|--------------------|-----------|-----------------------------|-----------|
|                                       | $T_N$              | $T_{RMS}$ | $T_N$                       | $T_{RMS}$ |
| Tension                               | 1,00               | 1,60      | 1,00                        | 1,60      |
| Torsion                               | 1,62               | 2,25      | 1,73                        | 2,34      |
| Proportional load $\lambda = 0,5$     | 1,09               | 1,51      | 1,10                        | 1,51      |
| Proportional load $\lambda = 1$       | 1,27               | 1,56      | 1,3                         | 1,57      |
| Proportional load $\lambda = 2$       | 1,75               | 1,95      | 1,83                        | 2,02      |
| Proportional load $\lambda = 4$       | 1,54               | 1,54      | 1,60                        | 1,60      |
| Proportional load $\lambda = 10$      | 0,97               | 1,03      | 1,03                        | 1,03      |
| Non-proportional load $\lambda = 0,5$ | 3,72               | 3,77      | 12,16                       | 12,24     |
| Non-proportional load $\lambda = 1$   | 5,36               | 5,60      | 17,51                       | 17,98     |
| Non-proportional load $\lambda = 2$   | 3,39               | 3,54      | 12,44                       | 12,70     |

Tab 3. Comparison of  $T_N$  and  $T_{RMS}$  parameters for Zenner's criterion before and after modification for 7075-T651 aluminum alloy [1]

|                       | Zenner's criterion |           | Modified Zenner's criterion |           |
|-----------------------|--------------------|-----------|-----------------------------|-----------|
|                       | $T_N$              | $T_{RMS}$ | $T_N$                       | $T_{RMS}$ |
| Tension               | 1,00               | 1,36      | 1,00                        | 1,36      |
| Torsion               | 1,05               | 1,71      | 1,05                        | 1,71      |
| Proportional load     | 1,22               | 1,53      | 1,22                        | 1,53      |
| Non-proportional load | 0,62               | 2,4       | 1,13                        | 2,11      |

Tab 4. Comparison of  $T_N$  and  $T_{RMS}$  parameters for Zenner's criterion before and after modification for X2CrNiMo17-12-2 steel [7]

|                                       | Zenner's criterion |           | Modified Zenner's criterion |           |
|---------------------------------------|--------------------|-----------|-----------------------------|-----------|
|                                       | $T_N$              | $T_{RMS}$ | $T_N$                       | $T_{RMS}$ |
| Tension                               | 1,00               | 1,41      | 1                           | 1,41      |
| Torsion                               | 0,94               | 1,54      | 0,94                        | 1,54      |
| Proportional load $\lambda = 0,5$     | 1,14               | 1,45      | 1,14                        | 1,45      |
| Proportional load $\lambda = 0,8$     | 1,09               | 1,40      | 1,09                        | 1,40      |
| Non-proportional load $\lambda = 0,5$ | 6,34               | 6,49      | 10,83                       | 11,02     |
| Non-proportional load $\lambda = 0,8$ | 99,76              | 101,92    | 185,43                      | 188,97    |

## 6. Conclusions

On the basis of the carried out analysis it can be said that in case of steel 1045 [6] the proposed modification of Zenner's criterion improved the obtained values of equivalent stresses for non-proportional loads. In case of steel 1045 [2] there occurred a re-estimation of equivalent stresses which caused smaller values of computing fatigue lives as compared to the experimental ones. For aluminum alloy 7075-T651 [1] the results obtained with the use of the modification indicate improvement in the obtained equivalent values. However, for austenite steel X2CrNiMo17-12-2 [7] the obtained results turned out to be not acceptable.

## References

- [1] Mamiya E.N., Castro F.C., Algarte R.D., Araújo J.A., *Multiaxial fatigue life estimation based on a piecewise ruled S - N surface*, International Journal of Fatigue 33, pp. 529-540, 2011.
- [2] McDiarmid D. L., *Multiaxial fatigue life prediction using a shear stress based critical plane failure criterion*, Fatigue design Vol. 1 Technical Research Center of Finland, pp. 21-33, 1992.
- [3] Skibicki D., *Kryteria zmęczenia dla obciążeń nieproporcjonalnych*, Wydawnictwa Uczelniane Uniwersytetu Technologiczno-Przyrodniczego, pp. 47 - 49, Bydgoszcz 2009.
- [4] Skibicki D., Sepmrich J., Pejkowski Ł., *Steel X2CrNiMo17-12-2 Testing for Uniaxial, Proportional and Non-Proportional Loads as delivered and in the Annealed Condition*, Materials Science Forum, 2012.
- [5] Skibicki D. i inni, *Metody doświadczalne w zmęczeniu materiałów i konstrukcji*, Wydawnictwo Naukowe Instytutu Technologii Eksploatacji, pp. 249-303, Radom 2009.
- [6] Verreman Y., Guo H., *High-cycle fatigue mechanisms in 1045 steel under non-proportional axial-torsional loading*, Fatigue & Fracture of Engineering Materials & Structures 30, pp. 932-946, 2007.
- [7] Walat K., Łagoda T., 2011, *Trwałość zmęczeniowa elementów maszyn w płaszczyźnie krytycznej wyznaczonej przez ekstremum kowariancji naprężeń*, Oficyna wydawnicza Politechniki Opolskiej, pp. 99-104.
- [8] Zenner H., Richter I., *Eine Festigkeitshypothese für die Dauerfestigkeit bei beliebigen Beanspruchungskombinationen*, Konstruktion 29, pp. 11 – 18, 1977.
- [9] Zenner H., Simbürger A., Liu J., *On the fatigue limit of ductile metals under complex multiaxial loading*, International Journal of Fatigue 22, pp. 137 – 145, 2000.



## SIMULATION OF BLOWING PREFORM AND OPTIMIZATION THEIR THICKNESS DISTRIBUTION FOR FINAL TARGET SHAPE OF IN CONTAINER

Karol Pepliński, Artur Kubielski

Bydgoszcz University of Technology and Agriculture  
ul. Aleja Prof. S. Kaliskiego 7, 85-789 Bydgoszcz, Poland  
tel.: +48 52 3408224, fax: +48 52 3408222  
e-mail: karolpep@utp.edu.pl

### Abstract

*Injection blow molding is a manufacturing process widely used to produce thin thermoplastic parts and it is best suited to smaller containers ranging in capacity from 1 ml to about 1.5 liters, typically for medical, pharmaceutical, and personal care application [3]. In this paper was presented numerical simulation of the inflation phase of an injection blow molding process under which a polymer preform is deformed into a mould under the action of applied pressure. Two cases of blowing preform were considered: for blowing pressure 4MPa and 2MPa. Simulation starts with constant thickness preform geometry. There has been excessive difference of thickness distribution (about  $0,6 \pm 1,6\text{mm}$ ) in the bottle after forming. On this basis, was made optimization of the preform profile geometry to remove thickness differences. It was assumption one optimization step to obtain final thickness distribution about 0.3mm and next to optimization steps to obtain hypothetical thickness about 0.1 mm. Noted was a significant effect of the initial preform thickness distribution on the final desirable wall thickness distribution (0.3 mm or 0.1mm) in the considered container. The Ansys Polyflow procedure of optimizing the preform thickness distribution allowed eliminating excessive differences in injection blow molding container.*

**Keywords:** injection blow molding, Ansys Polyflow simulation, optimization preform geometry

### 1. Introduction

In the last 35 years plastics manufacturing technology grow rapidly. The result of this development is a significant increase manufacturing of different product, example injection blowing bottle. According to statistic data, in 2010, Europe processed 46,6 million tons of plastics. The demand of packaging producers accounted for 39% of European market for plastics processing [8]. These data show that the manufacturing of packaging technology, in particular injection blow molding process, is a vital direction of progress of polymer processing. Blowing techniques have some of the greatest opportunities for the manufacturing hollow product example for cosmetics, childes and pharmaceuticals [2]. Blowing containers can be produce by popular following resins [3]: HDPE, LDPE, PS, ABS, PP, PVC, PET and polycarbonate.

One of the most important key components during the production of these methods is appropriate selection of technological parameters of processing, as well as initial geometrical features of preform (thickness distribution), to provide positive functional characteristics of final products. Classically in industrial situation required distribution of preform thickness is obtained by the trial and error method. However, this process is monotonous, time dependent and cost of

obtaining satisfactory results is usually very high. A good course of action for the proper selection of perform geometric features is the use of computer-aided processing of polymeric materials such as Ansys-Polyflow.

This article is a continuation of the blowing simulation task presented in [5, 6], but here for the first time will be presented blowing preform with is situated in injection blow molding technology.

## **2. Description injection blowing molding process and simulation task**

The injection molding process produces a molded part called a preform. This method is preferred over extrusion blow molding for making small parts that require high production volumes and closer quality dimensions. Injection blow molding consists of injecting a thermoplastic material into a cavity and around a core rod producing a hollow test tube (preform). The preform can be injection molded in a profiled shape that corresponds to the requirements of the blow mold form. The molded preform still on the core rod is transferred to the blow mould. The mould is clamped around the preform and air is blown to shape of the cavity. The preform is injected onto a support pin or core, which forms a neck with threads to their required dimensions. The preform is then blown against the cavity wall to its final shape [2, 3, 4].

The information contained in the literature position [1, 2] shows that there are not possible to obtain injection blowing products with a uniform wall thickness distribution on the basis of preform with constant thickness. Additionally preform diameter and geometry influence on final product feature.

Computer-aided design can give many useful facts. One of this is reduce plastics consumption for final bottle. Excessive thick of the bottle wall is not desirable. One of the assumptions of bottle design stage is uniform thickness of final bottle which was brief foredesign. Ansys-Polyflow can eliminate trial and error stage and help minimize the time and energy using for starting and realizing production stage. One of the most important element of the injection blow molding process is initial state of perform (geometry and temperature distribution). Each final shape of container should have preform with individual range of geometry and plastics processing parameters. Improper selection of perform geometric features may result in lack of a precise blow mold mapping, poor distribution of wall thickness, or too little of the final strength of the product. Ansys Polyflow software allows determining the appropriate distribution of wall thickness in preform by realizing the blowing simulation.

The aim of this study was to simulate blowing preforms for the real model deodorants roll-on (Fig. 1) using different blowing pressures and optimization perform test for final wall thickness distribution of bottle. Much more information about Polyflow applications was described in previous author publications [5, 6].

The aim of this paper is to stage two series of CAE simulations of blowing preform for different blowing pressures and some optimization stages for preform geometry: first task include changing geometry for final uniform container distribution about 0.3 mm and second for the 0.1 mm. The final effect will be to find preform geometry, providing the product about these values.



Fig. 1. Considered real roll-on bottle geometry

### 3. Process description

The study object to realizing simulation stages was draft on the CAD system (surface model), but the geometry was be simplification to shape seeing on Fig. 2. Preform height is 90 mm and their diameter is  $d_1=20$  mm. Height of container is 93 mm. The hoop ratio (HR) [3] in our analyzed object has average value  $HR=1,2\div1,5$ . For the standard injection blow molding process preform height should be similar to the height of container but always little shorter [2]. For the study model assumed only a "quarter-object", because it was symmetrical about two planes perpendicular to each other. The initial thickness of the preform was  $g = 2$  mm. The material for perform is PEHD, which have a temperature of  $T = 120$  °C, viscosity  $\mu = 7350$  Pa•s and density  $\rho = 0.96$  g/cm<sup>3</sup> at the moment of blowing stage. On the first stages of simulation value of blowing pressure was 4 MPa (Fig. 3-4) and for the second stage: 2 MPa (Fig. 5b,d).

The simulation blowing time for standard power computer depended on grid layouts, which on this item were about 65 thousand MES elements. For the corresponding grid (about 215 thousand elements) a container calculations are taking too long to be able to be carried out to the end (within 18 hours converted just 15 simulation steps by the program with about 250 expected).

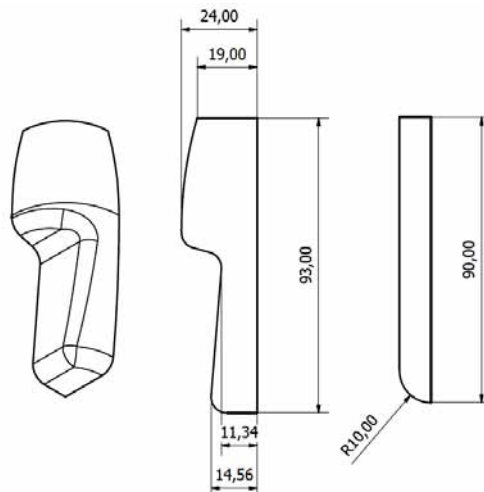


Fig. 2. Simplification bottle CAD geometry conmtainer model (left) and initial preform shape (right) with dimensions

#### 4. Simulation results and their analyses

Realized simulations generated series of results, which the selected part is presented below. Figure 2 shows a comparison the distribution of thickness container obtained from the preform with constant thickness. It was observed non-uniform thickness distribution (Fig. 3b). Excessive thickness can cause some minimal deformation of container in this place. Also it can generate so long cycle time in cooling process and unnecessary consumption of energy using. Preform with different initial geometry (Fig. 3c) help obtain final container with much more uniform thickness distribution (Fig. 3d).

First of all, showing the perform wall thickness distribution and final bottle for subsequent optimization steps for the first (Fig. 3b) and second (Fig. 4a). Each perform optimization step (first and next second) changes the form of perform geometry. The program adjusts the preform so that the largest possible part of the final container surface has reached the desired thickness. Already the first optimization allows reducing the consumption of polymer material. The greatest preform thickness are on the place when the blowing time is longer and depend on blowing ratio and bottle geometry.

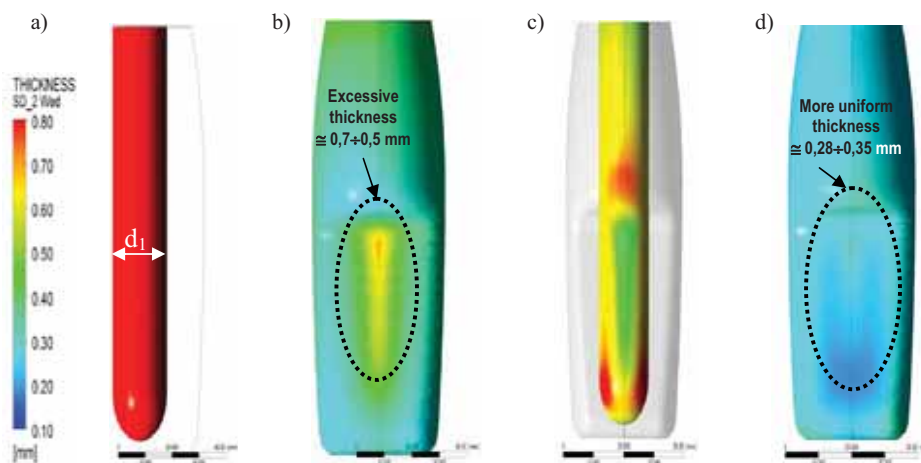


Fig. 3. Comparison part thickness distribution as a result of different preform geometry for optimization assumption 0,3 mm: a) preform with constant thickness geometry  $g=2$ , b) container with non-uniform thickness, c) preform with optimized thickness geometry  $g=0,8\div0,45\text{mm}$ , d) container with much more uniform thickness distribution  $g=0,28\div0,35\text{mm}$

For final desirable final hypothetical wall thickness distribution about 0,1 mm it was realized two stage of preform optimization (Fig. 4). It can be seen that each steps give different preform geometry and final wall thickness distribution in container. For the first optimization average wall thickness is  $(0,20\div0,29\text{mm})$ . After second optimization the container has a thickness value  $(0,1\div0,25)$  near to desirable, but still it is not uniform. In this situation it can be positive reaction to tray change diameter geometry of preform  $d_2=1,5d_1$  or realized third stage of optimization. But this can be done in the future research.

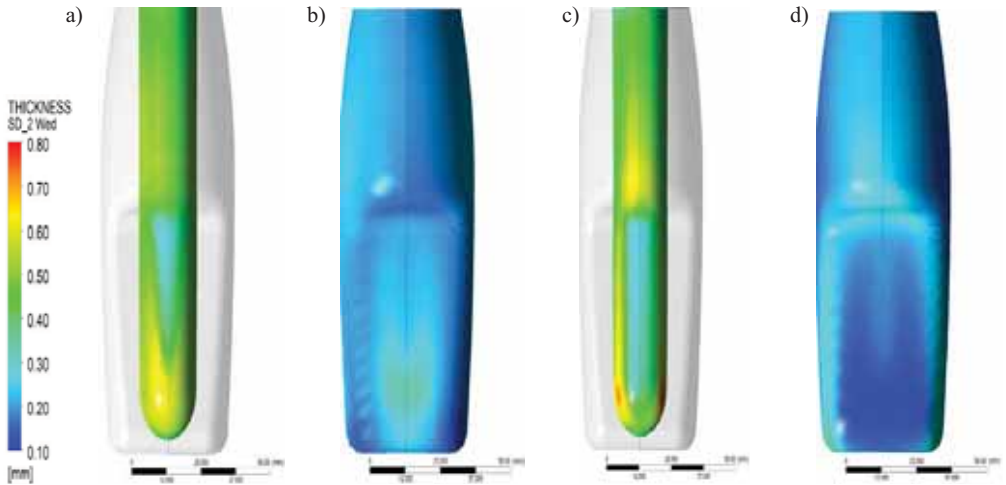


Fig.4. Contrast part thickness distribution as a result of different evaluation perform geometry for optimization assumption 0,1 mm: a) perform in the first optimization stage, b) container as an effect of first preform optimization, c) perform in the second optimization stage, d) container as an effect of first preform optimization

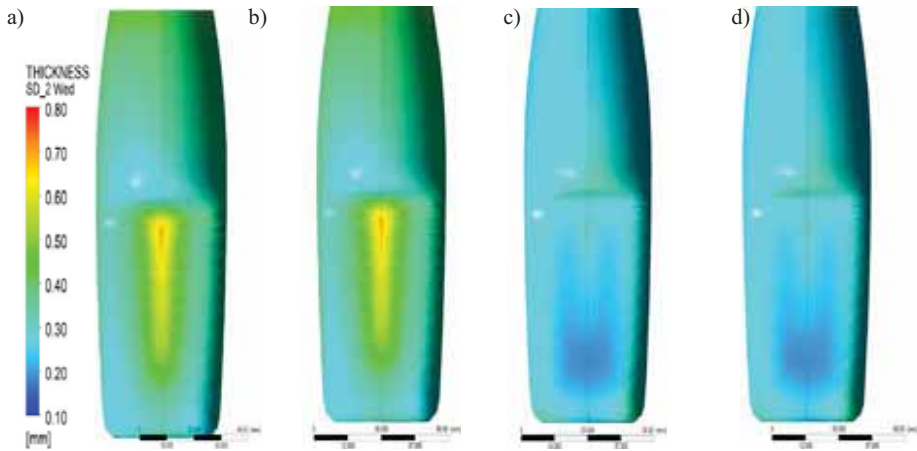


Fig.5. Compare of part thickness distribution as a function of different blowing pressure: a-b) container as a result of constant initial preform geometry and blowing pressure 4MPa and 2MPa, c-d) container as a result of optimization initial preform geometry and blowing pressure 4MPa and 2MPa

Finally, it should be added that the software also allows the presentation of a given stage of blowing in a certain time moment, as illustrated on the Fig. 6.

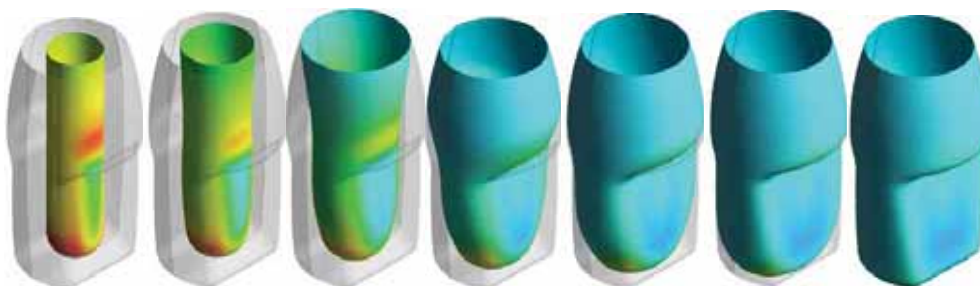


Fig. 6. Simulation stages during preform blowing in different time stages

## 5. Final consideration and summary

An optimization technique for injection blow molded products was made in Ansys Polyflow software. It was shown that the technique could be useful to design the preform wall thickness distribution such that the final product was at a target thickness. Research has allowed optimizing the geometry shape of the preform to the desired shape of the container. It was obtained the distribution of wall thickness, which helped achieve the goals of research (wall thickness product - WTP  $g_1 = 0.3$  mm and  $g_2 = 0.1$  mm). These thickness assumptions in the optimization simulation stages can have different values, ex.  $g_1 = 0.5$  mm. It is only dependent on author assumption.

Software Ansys Polyflow, enables to carry numerical experiment in the range of phenomena modeling during the injection blowing process. By steering wall thickness distribution on initial preform it is possible to get the more profitable wall thickness distribution of formed containers. Especially in the case of complex geometry in blowing product we have new opportunity of applying the technology of blowing forming. Numerical analyses can reduce energy consumption during injection and cooling stage as an effect of more uniform thickness distribution of final container.

## References

- [1] Dees J.: Preform Optimization Using Non-linear Finite Element Simulations, ANTEC 2003 Plastics: Annual Technical Conference, Volume 1: Processing, pp. 842-849
- [2] Belcher S.L.: *Practical guide to injection blow molding*, Taylor & Francis Group, 2007.
- [3] Kutz M.: *Applied plastics engineering handbook*, 1<sup>st</sup> ed., pp. 280 – 284, Elsevier 2011
- [4] Norman, C. L., *Practical guide to blow moulding*, Smithers Rapra Technology, 2006.
- [5] Pepliński, K., Bieliński, M. *Polyflow software use to optimize the parison thickness in blowing extrusion*, Journal of Polish CIMAC, 4, Gdańsk 2009.
- [6] Pepliński K., Mozer A.: Ansys-Polyflow software use to select the parison diameter and its thickness distribution in blowing extrusion, Journal of Polish CIMAC, 5, Gdańsk 2010.
- [7] Pepliński, K., Bieliński, M., *Processing and functional properties of the containers prepared by blowing extrusion in variable processing conditions, and evaluation of yield and quality of the process*, Polimery, 54, nr 6, pp. 448-456, 2009.
- [8] www.plasticseurope.org, The Compelling Facts About Plastics 2010, Plastics Europe, Brussels – Belgium 2011.



## COMPARISON OF BOTTLE WALL THICKNESS DISTRIBUTION OBTAIN IN REAL MANUFACTURING CONDITIONS AND IN ANSYS POLYFLOW SIMULATION ENVIRONMENT

Karol Pepliński, Arkadiusz Mozer

*Bydgoszcz University of Technology and Agriculture  
ul. Aleja Prof. S. Kaliskiego 7, 85-789 Bydgoszcz, Poland  
tel.: +48 52 3408224, fax: +48 52 3408222  
e-mail: karolpep@utp.edu.pl*

### **Abstract**

*Extrusion blow molding (EBM) is a widely used and known manufacturing process to produce thin or thick thermoplastic hollow object like cosmetics container or big drums. This process can be realized on extrusion blow molding machine and tooling. Each extrusion blow molding machine has a programming die head. The initial parison thickness distribution should be depended on final bottle geometry. However, to determine the proper distribution of parison thickness to get the most uniform thickness of the container wall, it is not an easy task. In order to precisely define this distribution is simple using Ansys Polyflow. The article includes a comparison of bottle wall thickness distribution obtain in real manufacturing conditions and in realizing Polyflow simulation. Also it will be propose an initial parison thickness distribution (programming) for the bottle design, which is manufacturing in the industry to pack nail polish remover. This will allow the packaging manufacturer to produce a bottle of a higher quality in terms of distribution of wall thickness.*

**Keywords:** *extrusion blow molding, parison programming, wall thickness distribution, Ansys-Polyflow*

### **1. Introduction**

Design of extrusion blow molding process for a specific product is aided by various computer techniques. One of the most advanced processes, allowing assessment of blowing and shaping the final selected features of the products, is using CAE software Ansys Polyflow [7]. It allows you to establish multiple relationships running during the consideration process. One of them is able to determine the initial distribution of wall thickness of extruded parison so as to obtain the most uniform distribution of wall thickness in container. It is extremely important for the plastics unit consumption on the blowing product, as well as achieving a more even distribution of cooling rates, which may prevent distortion and deformation products [6]. If the product has a uniform distribution of wall thickness of the container, you can shorten the cooling time in a bottle, so you can improve the energy efficiency [5] of the process realized, that a year can bring significant economical savings.

Wider information about extrusion blow molding process and assumptions to Polyflow simulate are available in the position [2, 4].

## 2. Determination of parison thickness distribution for blowing product

The articles produced by non unbounded extrusion blow molding process are large differences in wall thickness distribution of the product, but it is depended on production process. In order to ensure uniform wall thickness of the blowing product, extruded parison should have a thicker wall, where the later is more blow ratio, including the stretch in the longitudinal direction. This is achieved by changing the width of the gap between the moveable mandrel and die [1].

Consequently, one of the most important aspects in the extrusion blow molding process is the identification and selection of the initial parison geometry, in order to obtain the desired products of locally constant or variable wall thickness distribution with a minimum weight of the blowing product [2].

Utmost helpful step in the determination of correct geometric parison profile is realized blowing simulations for the initial constant thickness of parison [4], in order to achieve a specific distribution of the final container wall thickness, which is then used by the mathematical Polyflow solver to optimization an initial profile of the parison, for example, on its length (Vertical Wall Distribution System).

It is usually so that the largest thinning is formed at the corners in blowing product [3]. Using a larger parison thickness makes thinned areas are thicker, but too much plastic (which is not needed) is located in other place of the product. Ultimately, the parison of variable thickness allows obtaining the greatest wall thickness distribution ratio of the bottle. It also allows, for example, reduce the amount of plastic waste from about 20 to 40% (depending on the geometrical characteristics of the blowing product: oval, rectangular, 'sharp' corners, handle, etc.), thus making the product lighter and more economical in production. It should be further noted that carrying out a series of successive Polyflow optimization (number 3÷4) gives the best results [4].

It should be mentioned that the available methods to control the parison thickness distribution systems (also possible to use in the Polyflow simulation), include: Vertical Wall Distribution System (VWDS), Static Flexible Deformable Ring (SFDR), Partial Wall Distribution System, (PWDS) [6], Three Dimensional Wall Distribution System (3DWDS).

## 3. Realized task

The realized tasks aims to make the bottle wall thickness measurements obtained under real production conditions, and computer simulation. Also, the goal is assumed to propose an optimized thickness distribution of extrudate parison to obtain a product with more uniform wall thickness over the entire surface of the bottle. Considered bottles capacity is 150 ml.

In the engagement on the blowing simulation software Ansys-Polyflow, first prepared a virtual model of the cavity and parison (Fig. 1). Due to lack of die land geometry and parameters of the extrusion head, computer simulations have been limited to the closing stage of the parison in the mold and its blow. On the basis of traces of the upper and lower 'tail' waste bottles obtained under real conditions and the initial simulation, establish the initial diameter of the parison,  $d = 24\text{mm}$ . On the other hand, knowing that the die land of the head gap is 2 mm, it was assumed that the initial thickness of the parison is  $g = 2,3\text{ mm}$ .

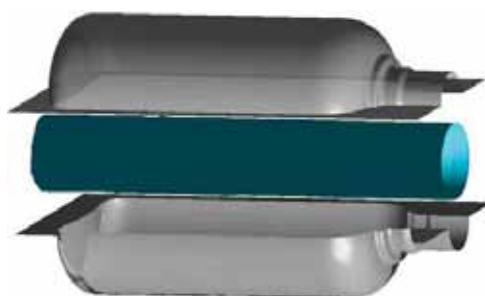


*Fig. 1. Virtual model of the cavity and parison*

In the next stage of the geometric model has been imported into the program Ansys Polyflow, which successively applied FEM mesh for the cavity and parison, specified boundary conditions, blowing conditions, contact conditions for the parison and mold, mold closing conditions, plastics HDPE properties, running computational module, to obtain the thickness distribution of the bottle, read the results from the simulation.

Also for fifteen selected bottles received in terms of real production grid points was applied in two sections for each of the bottles. One of the sections was placed at a distance of 3 mm from the parting line, while the second was applied in the plane turned 90 degrees from the parting plane. Moreover this some points were measure in Polyflow environment (Fig. 2).

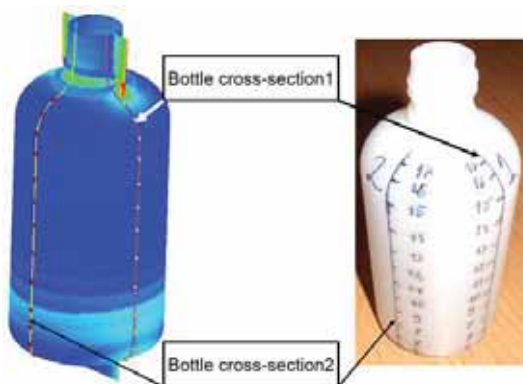


*Fig. 2. Bottle cross section: (on the left) virtual model, (on the right) real model of 150 ml HDPE container*

With the help of a measuring device the Magna-Mike 8500 (Hall Effect thickness gage), were measured wall thicknesses of bottles, at the designated points of measurement. The results were averaged for each section and included in the research protocol, and the results are shown in Fig. 3–4 (line – wall thickness results of real bottle). This results comparison with Polyflow outcome (see line – wall thickness results for Polyflow simulation).

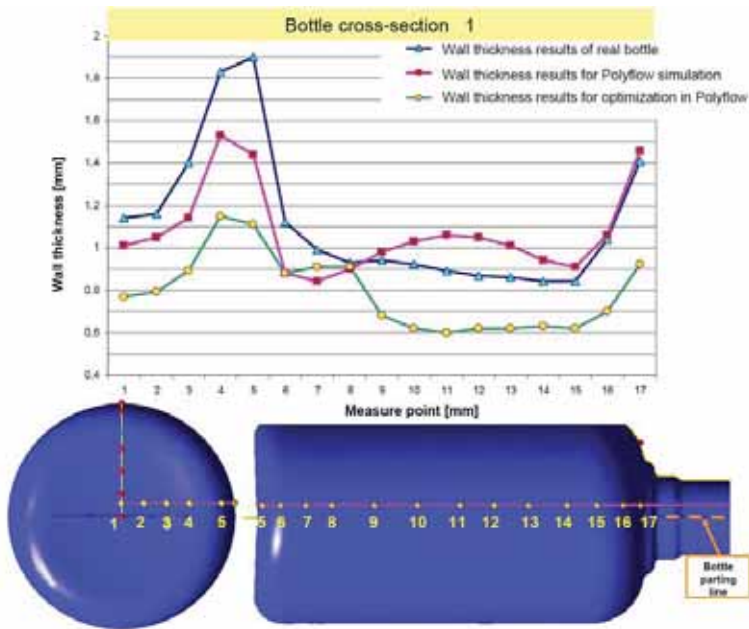


Fig. 3. Comparison part thickness distribution along the measurement line in cross section 1

Additionally, in order to obtain a more uniform wall thickness distribution in the bottles were realized Polyflow simulations to optimize the initial parison thickness distribution (Fig. 5) in the axial direction (method VWDS), to obtain the bottle of the assumed thickness of 0.6 mm (in the entire volume of the bottle).

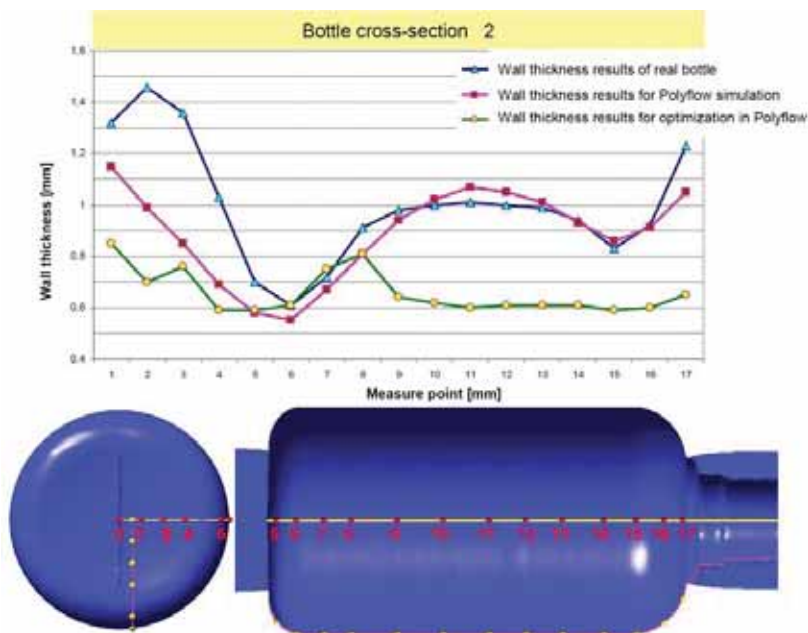


Fig. 4. Comparison part thickness distribution along the measurement line in cross section 2

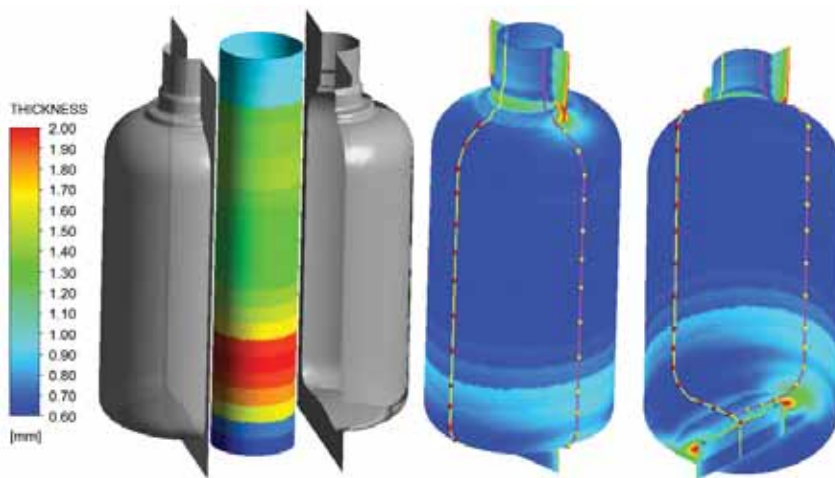


Fig. 5. Final part thickness distribution for optimized parison diameter 24 mm: (on the left) optimized parison thickness distribution, (on the right) visible final bottle wall thickness distribution after realized task

#### 4. Final consideration and summary

Comparing the thickness distributions of products obtained in the first section and second, we can conclude that the results of measurements and simulations of actual bottles are mostly close to each other, but especially in bottom zone of the bottle (points 1-6) are greater discrepancies. The resulting differences may result from the inability to simulate the plastic flow in pinch off section when mold close, which in real life takes place, to ensure adequate strength weld line bottom of the bottle. It should also be noted that the simulation assumes a certain initial diameter and thickness of the parison, which may differ from reality.

Implemented to optimize the simulation can be a kind of guideline for changing the geometric of extrudate parison to achieve greater uniformity of real bottle wall thickness distribution. This determination can be more helpful for more complex geometry of blowing product.

For increased confidence (accuracy) of the simulation results, further work on such simulation of polymer flow through the die head and land length, take a picture of real parison and measure its diameter, and comparison with simulations.

#### References

- [1] Kazmer D. O.: *Plastics Manufacturing Systems Engineering – A Systems Approach*, pp. 25–46 Carl Hanser Verlag, Munich 2009
- [2] Kutz M.: *Applied plastics engineering handbook*, 1<sup>st</sup> ed., pp. 267–280, Elsevier 2011
- [3] Norman, C. L., *Practical guide to blow moulding*, Smithers Rapra Technology, 2006.
- [4] Pepliński K., Mozer A.: *Ansys-Polyflow software use to select the parison diameter and its thickness distribution in blowing extrusion*, Journal of Polish CIMAC, 5, Gdańsk 2010.
- [5] Pepliński K.: *Microcellular monolayer extrusion blow molding for hollow object*, Journal of Polish CIMAC, 7, Gdańsk 2012 (in print).
- [6] Rosato, D.V.: *Blow Molding Handbook*, Hanser Publisher 2nd edit., Munich 2004.
- [7] Ansys Polyflow User's Guide, Ansys Inc., 2011.





## MICROCELLULAR MONOLAYER EXTRUSION BLOW MOLDING FOR HOLLOW OBJECT

Karol Pepliński

Bydgoszcz University of Technology and Agriculture  
ul. Aleja Prof. S. Kaliskiego 7, 85-789 Bydgoszcz, Poland  
tel.: +48 52 3408224, fax: +48 52 3408222  
e-mail: karolpep@utp.edu.pl

### Abstract

*Microcellular monolayer extrusion blow molding (MM-EBM) is a relatively new manufacturing process which can be used to produce thin thermoplastic hollow object with lower weight and new inside wall structure of container. This process can be realized on standard extrusion blow molding machine and tooling: extruder and blow mold. On the world are know other similar process like MuCell Foam for Blow-Molding [1], but this process required some modification of extrusion blow molding system: SCF injection system. Our considered process base on standard extrusion blow molding process and can give similar results with using expandable microspheres. In this article the main Author assumption is describe and show some results of realizing this MM-EBM process with using standard polymer (HDPE) and Expancel microspheres for blow molding. Also during manufacturing on mass scale can be seen that MM-EBM process is energy effective because can be realize at lower plastics processing temperature and blowing pressure.*

**Keywords:** microcellular extrusion blow molding, expandable microspheres, container weight, energy effectiveness

### 1. Introduction

Blow molding covers three main thermoplastic processes: extrusion blow molding, stretch blow molding, and injection blow molding. Extrusion blow molding is the largest and most popular for other blowing process like injection blow molding and stretch blow molding. The whole blow molding industry is growing approximately in stabile rate 3÷5 % yearly. According to statistic data, in 2010, Europe processed 46,6 million tons of plastics. The demand of packaging producers accounted for 39 % of European market for plastics processing [8]. These data show that the manufacturing of packaging technology, in particular extrusion blow molding process, is a vital direction of progress of polymer processing. Blowing containers can be produce by popular following resins for container below and over five liters [3]: HDPE and PP. Nowadays it is very popular trend in plastics and design industry to minimize weight of the product and energy consumption during their manufacturing. Rise of energy, material and transport cost demand new approach to manufacturing process like it is extrusion blow molding. In order to comply with these requirements can apply specialized foam additives like available special blowing agents – Expancel [2], which mainly contribute to the reduction hollow container weight and help achieve other benefits such as reduced energy demand per blowing unit during realizations of the process and minimizing the consumption of plastics for an individual blowing product.

In the world literature on the realized subject in this article is contained only very sparse information of a vague and advertising on the MM-EBM process, especially HDPE modified special agent in the form of microspheres. Brand is the lack of research results to modify the impact of this material on the course and efficiency of MM-EBM, which raises the need for the implementation of the theme of this issue. In this article the Author presents selected the first stage of their research, which concerns selection of the ranges processing of MM-EBM conditions in terms of accepted criteria: minimize the weight of the product, reduce temperature profile on the plasticizing and extrusion head system and also to cut the demand for compressed air consumption during inflation and blowing parison. Like it is obviously known producing compressed air form most standard EBM systems which need value range about 4÷6 bars it is cost. It is well known that the loss in pressure of 1 bar results in a loss of energy equivalent to 7÷8 % of power consumed by air compressor manufacturers. Therefore, the lower blowing pressure value from 5 to 3 bar reduces the generation of compressed air at about 21÷26 %. Hence it is advisable to make attempts to blow molded parison at lower pressures. These requirements are very good for idea of material and energy-consuming systems [4]. The manufacturer's data Expancel that such blowing pressure reduction is possible, however, information on the MM-EBM is elementary (in a few sentences). Other general information is that Expancel in most plastics technology can be processed on the temperature range 140÷220 °C [2]. It should also be noted that for the standard process of extrusion blow molding HDPE extruded parison temperature is about 190 °C (similar to the plasticizing unit – 180÷190 °C) and the blowing pressure is 5 bar. These assumptions are by no means true for containers with an average thickness of the extruded parison wall thickness 2÷3 mm. For these assumptions can be realized first try of microcellular monolayer extrusion blow molding process which task range will be describe in process description.

## 2. Extrusion blow molding process

Extrusion blow molding is a manufacturing technique used to quickly form hollow object like blown bottles and containers of different geometry and volume. It has alternative glass and metal containers. The fast developments in BM polymers, additives and EBM equipment technology give whole spectrum to blowing product like: multilayered fuel tanks, spoilers, and drums. It does mean that consumer product industries (beverage, cosmetics) are the prime users of blow molding. Diagram of an extrusion blow molding process is visible on Fig. 1. Blow molding involves a tube of hot thermoplastic being extruded continuously downward from the die. When the extruded parison is of the accurate length, the mold is closed, squeeze and pinching off the top and bottom ends (sometimes in a different place or in each place) and a cutoff knife cuts the parison at the near die face [3]. Next the blow mold is going to the blow pin station. Compressed air is injected into the molten parison and then expands to contact with mold cavity and starts cooling cycle to moment when hollow object solidifies. The cooling action is realized by water mold cooling and dry purge of compressed air. Subsequently article is then ejected. The excessive amount of plastics material (“tail”) created in the pinch off section is automatically trimmed. For bigger parts this operations are made manual by an operator.

Machines with programming head can extrude a controlled variable-wall-thickness parison using the moveable core which is inside die head. In place where container will be have higher blow ratio parison should be thicker then other place. For complex geometry it is not to easy predict the parison profile thickness distribution. The programmable parison extrusion program for thickness utilizes just the correct amount of material for the container. Wall thickness can be controlled in almost all sections of the container [3]. In this place can be very helpful CAE programs like Ansys-Polyflow [6], which assist to obtain proper parison shape to final blowing hollow object.

Blow molded parts are made with undercuts and are easily removed from the mold, eliminating the need for expensive in-mold cams and slides. Blow molds are also less expensive and need not have in-mold cams and slides (they are cost) [5] because containers are easily removed from the mold. In extrusion blowing molds forces and pressures are much more smaller then the high injection and packing pressures of injection moldings. Therefore, cast aluminum, steel alloys plus beryllium copper molds are used [7].

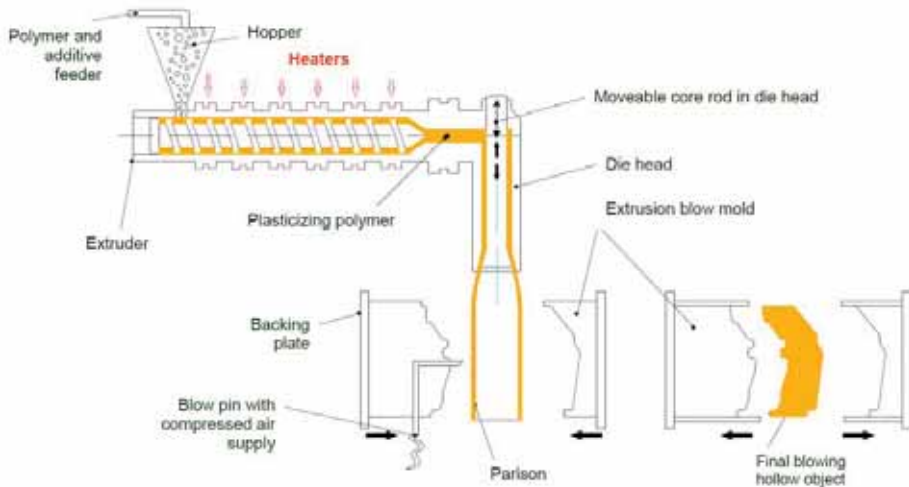


*Fig. 1. Idea of extrusion blow molding proces*

### 3. MM-EBM process description

MM-EBM process consists in adding microspheres granules to the plastics material, also known as the blowing agent which include a gas, which under appropriate conditions of extrusion blow molding process is expanded, and the microspheres increasing its size several times. As a result of MM-EBM a received hollow container suitable two-phase structure, changing it structure from solid to the microporous.

The microcellular monolayer extrusion blow molding process was carried out using an industrial blow molding machine Battenfel Fischer (Fig. 2). To the realizing of MM-EBM was used the following initial conditions:

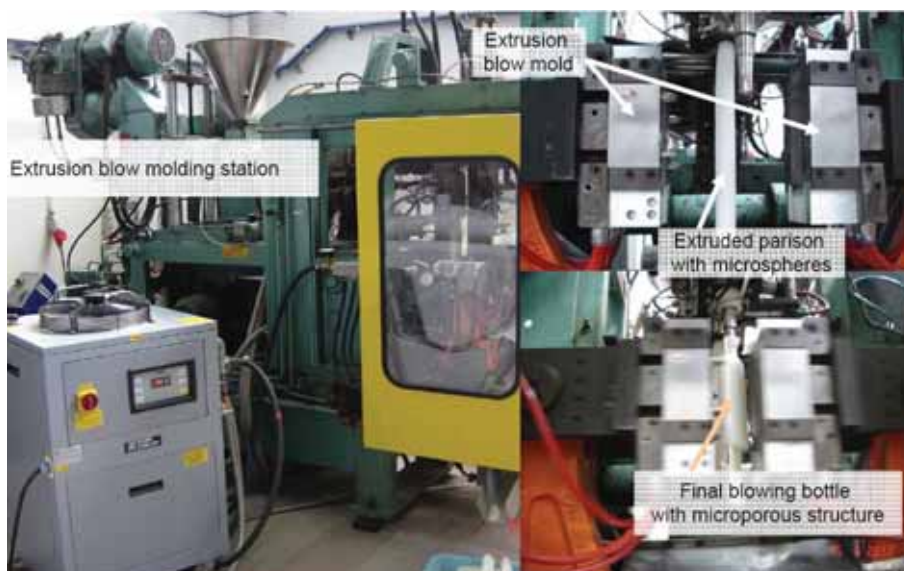


Fig. 2. Extrusion blow molding machine to realizing MM-EBM process

- the temperature in each heating zones: (plasticizing unit)  $T_1 = 170\text{ }^{\circ}\text{C}$ ,  $T_2 = 175\text{ }^{\circ}\text{C}$ ,  $T_3 = 175\text{ }^{\circ}\text{C}$ ,  $T_4 = 175\text{ }^{\circ}\text{C}$ , (die head)  $T_5 = 180\text{ }^{\circ}\text{C}$ ,  $T_6 = 175\text{ }^{\circ}\text{C}$ ,
- screw speed during extrusion blow molding  $n_s = 1.8\text{ min}^{-1}$
- two different percentage value of blowing agent in the material ( $e_1 = 0,5\text{ }%$  and  $e_2 = 1,2\text{ }%$ ) at constant blowing pressure  $p_{b1} = 4\text{ bar}$ .
- overall blow molding cycle time  $t_c = 15,46\text{ s}$ ,
- mold temperature during cooling  $T_c = 15\text{ }^{\circ}\text{C}$

Also began to produce bottles in the MM-EBM at a reduced blowing pressure  $p_{b2} = 2\text{ bar}$ . It should be mentioned that the process of extrusion blow molding has also been made for standard processing conditions without blowing agent (standard profile temperature in plasticizing and die head unit for PE-HD processing is  $20\text{ }^{\circ}\text{C}$  higher, and blowing pressure is  $5\text{ bar}$ ). After the MM-EBM processes began to assess the weight and inside structure of blowing container, using a laboratory microscope MN800 EPI/DIA. Results is presented in the next chapter.

#### 4. Research results and their analyses

After completing the extrusion blow molding process, for standard EBM terms and terms for MM-EBM, began to assess the weight of blowing products. This assessment was realized according to accepted criteria (% amount of the special blowing agent – microspheres and blowing pressure). Normally, in the standard extrusion blow molding condition, the average weight of the bottle was  $16,2 \pm 0,25\text{ g}$ . The addition of special blowing agent in the amount of  $e_1 = 0,5\text{ }%$  and  $e_2 = 1,2\text{ }%$  leads to a successive reduction of the bottle weight: respectively value of  $14,4 \pm 0,16\text{ g}$  and  $11,8 \pm 0,14\text{ g}$ . Also should be noted that the use of higher content of blowing agent, for example, in an amount of  $1.5\text{ }%$  did not bring positive results in the considered MM-EBM process conditions. These dependencies can be clearly seen in Fig. 3. In conclusion, the uses of special blowing agent in an amount of  $1,2\text{ }%$ , to significant reduce ( $27\text{ }%$ ) the weight of the bottle.

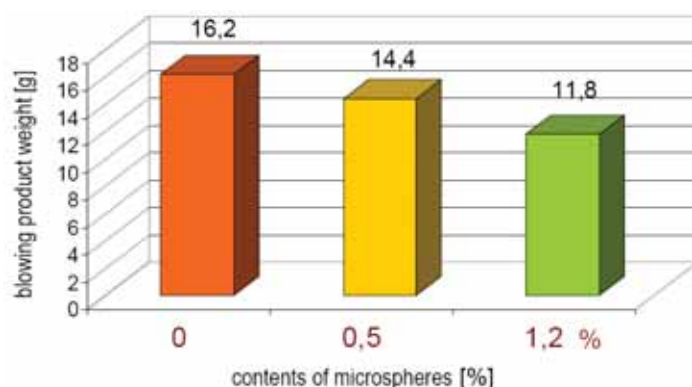


Fig. 3. Blowing product weight reduction as a effect of using microspheres

The next step concerned the evaluation of the bottle wall microstructure in the accepted convention area, as indicated in Fig. 4. As a result of forty times magnification were assessed an average microsphere size. The average pore size determined based connected twenty measurements on samples taken from bottles, where in each sample was measured most visible microspheres. With the Expancel blowing agent in the number of  $e_1 = 0,5 \%$ , average microsphere size of about  $L_{\mu p} = 80 \mu m$ , and in turn for  $e_2 = 1,2 \%$  of the value of  $L_{\mu p} = 120 \mu m$  (see Fig. 4). The study was conducted for blowing pressure of 4 bar. Also clearly shows that the higher the content of the Expancel the denser pore distribution in the structure of the bottle wall, which also determines a significant reduction in the bottle weight. In each case under consideration, it is noted that the lower blowing pressure  $p_2 = 2$  bar generates about 10% lower value of microspheres size  $L_{\mu p}$ . For lower blow pressures notes are visually much denser distribution (in each  $1 \text{ cm}^2$ ) of microspheres in the inside of bottle wall.

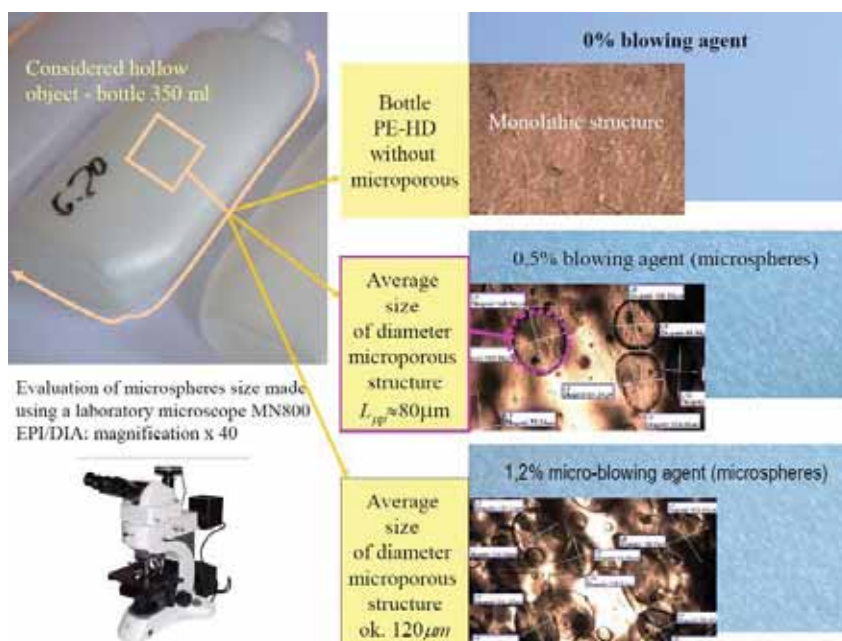


Fig. 4. The evaluation of the bottle wall microstructure in the accepted convention area: (on the left) considered and analysed area, (on the right) microstructure of bottle wall with visible microspheres

#### 4. Final consideration and summary

The use of special blowing agent – microspheres, called Expancel, allows to the production of hollow object with reduced weight. This can be extremely promising in the case of the measure used to produce object of a much larger size, even drums (200 liters) or canisters (20÷40 liters). However, in this case would include a separate practical study in industrial conditions. Assuming that the average drums weight is 5 kg, object is theoretically able to reduce its weight by up to about 1300 grams, which can be extremely important for the unit consumption of plastics materials for a given product, and also as well as reducing transport costs.

With regard to the management of energy resources should be noted that use of a special blowing agent – microspheres allows you to significantly reduce energy demand for the plasticizing material – on average by reduced processing temperature about 20 °C. Also reduced the demand for compressed blowing air by lowering the pressure with value 4 bar to 2 bar. As a result of the calculations, the author has noted, that despite the relatively high price of Expancel is possible to reduce material consumption at the global scale and doesn't increase the global cost of processing materials. All the more should be considered highly advantageous, that the microcellular monolayer extrusion blow molding process can be implemented on standard extrusion blow molding machines.

#### References

- [1] Anderson J.: *MuCell Foam for Blow-Molding*, Trexel Inc.
- [2] *Expancel microspheres in thermoplastics*, Technical bulletin no 24, 2005.
- [3] Kutz M.: *Applied plastics engineering handbook*, 1<sup>st</sup> ed., pp. 280 – 284, Elsevier 2011
- [4] Michael F. Ashby: *Materials Selection in Mechanical Design*, 4th ed., Elsevier 2011
- [5] Norman, C. L., *Practical guide to blow moulding*, Smithers Rapra Technology, 2006.
- [6] Pepliński K., Mozer A.: *Ansys-Polyflow software use to select the parison diameter and its thickness distribution in blowing extrusion*, Journal of Polish CIMAC, 5, Gdańsk 2010.
- [7] Pepliński K., Ohla A., Bieliński M.: *Design and manufacturing mold for extrusion blow molding* (part 1), Przetwórstwo Tworzyw, 2006, 1–2, p. 12–19
- [8] [www.plasticseurope.org](http://www.plasticseurope.org), *The Compelling Facts About Plastics 2010*, Plastics Europe, Brussels – Belgium 2011.



## SPATIAL APPROXIMATION OF IMPACT TEST RESULTS OF UNIT LOAD

Tomasz Piątkowski, Janusz Sempruch, Tomasz Tomaszewski

*University of Technology and Life Sciences*  
ul. Prof. S. Kaliskiego 7, 85-789 Bydgoszcz, Poland  
tel.: +48 52 3408145  
e-mail: [topiat@utp.edu.pl](mailto:topiat@utp.edu.pl)

### Abstract

*The paper presents an application proposal of B-spline surface of third order in the approximation of test results of unit load impact. The accelerations appearing during tests of free fall of the object from the height on undeformable ground were recorded by means of tri-axial acceleration sensor placed inside the tested load. An approximation was realized with the help of numeric optimization using the SQP method. The control points, forming initially the sphere surface, are the decision variables of the optimization task. The spatial visualization of data (using B-spline surface) is developed to streamline an interpretation and analysis of results recorded during tests. It allows precise load places determination, which require introduction of constructional modifications to improve the protective packaging properties.*

**Keywords:** unit load, free fall test, B-spline surface, numerical optimization, impact

### 1. Introduction

All consumer goods, before they are delivered to the end user, have to travel the distance between the supplier and the final recipient. In order to improve their transportability, the goods are enclosed in protecting packaging – the packaging having the form of cuboidal parcels – that are treated as transport units. During travel, the unit loads are subjected to manipulation operations (e.g. loading, unloading, picking, positioning, sorting, etc.), which create a danger of mechanical damage of the package and its content. Among the most dangerous causes of the load safety infringement are the mechanical hazards of the impact character caused by fall of the load on the ground or on other loads, as well as the impacts that take place when the load interacts with manipulators – for example, realizing sorting process of load streams transported on conveyors [13], [15], [16].

Protection of the load content against mechanical damage can be achieved by properly packaging application that alleviates the dynamic effect of impact [10].

Scientific works dealing with the problem of investigation and analysis of the constructional packaging properties focus mainly on the use of computational numeric methods – the finite element method especially [12]. Packaging and their content are treated, as non-homogenous bodies. However, this attitude is not commonly applied in engineering practice. On the needs of classic packaging design, during their structural features modelling, it is sweeping simplification accepted and used guidelines and recommendations determined on the basis of manufacturers' practical experiences [7].

In view of the lack of the possibility of the precise and exact prediction of the actual mitigating impact properties of the packaging, while their design, the experimental investigations of the unit loads prototypes is necessary carrying out.

The free fall tests of loads from height are one of the main methods of the investigations of the packaging's protective ability. The programme of tests is defined on the basis of guidelines presented in standards, e.g. [8], [9], [5], [4]. This program consists in fall of the load (with suitable oriented walls, edges, and corners) from assumed height on smooth and undeformable ground. The visual inspection of the packaging and its content, performed after series of tests, make up the basis of effectiveness assessment of packaging's protective property. An appearance of any damages of the load content, causing lack of the addressee acceptance (or final consumer), is connected with an introduction necessity of the constructional changes to the packaging (or to the packaging content also).

The experimental investigations of the free fall do not require applying any specialist laboratory devices which are necessary, e.g. in case of the product damage boundary determination [3] or during the cushion curve development for packaging material [2]. In the simplest version of the free fall tests, the load can be positioned manually. In order to improve the repeatability of the test results, the positioning of unit loads before the fall, can be aided by simple devices – drop testers [17].

The constructional-design-test process is realized iteratively, on the basis of the trial-and-error method, till the packaging's protective properties are accepted. This process is considerably more predictable and precise, if the course of the experimental investigations of the impact is recorded by the tri-axial acceleration recorder installed in the load inside [14]. The recorder's data permit the packaging places identification, which require additional introduction of springy-damping or stiffening elements. It is also possible to indicate places, where the cushion material is applied in excess, causing the groundless growth of cost and mass of the packaging. The packaging property investigations with the use of the acceleration recorder make it possible to replace the load content with the substitute material of equivalent mass, geometry and consistency. This approach has economic meaning, especially in case of packaging design for costly or dangerous articles. The analysis of non-processed data written by tri-axial acceleration recorder during series of tests is difficult and non-effective. The spatial data approximation (proposed in presented work) can help to solve this problem. The recorder's data are subjected to approximation by means of B-spline surface of third order ( $m=n=3$ ) using numeric optimization. This surface takes into consideration the recorder orientation with relation to the load edges, enabling the intuitive identification of packaging's characteristic places.

## 2. Basic description of B-spline surface

The B-spline surface is one of more often applied surface representation in the engineering graphics. There is capable of presenting complex, 3D solids using a little number of variables. The B-spline surface of order ( $n, m$ ) is assigned through the grid of control points  $P_{i,j}$  (Fig. 1) according to the expression [6], [11], [19]:

$$p(s, t) = \sum_{i=0}^{z_n} \sum_{j=0}^{z_m} P_{i,j} N_i^n(s) N_j^m(t) \quad (1)$$

where:

$s \in [0,1], t \in [0,1]$  – parameters,

$z_n+1, z_m+1$  – number of control points  $P$  placed along rows and columns of the grid (Fig. 1),

$m, n$  – order of B-spline surface,

$P_{i,j}$  – control points,

$i=0,1,2,\dots,z_n, j=0,1,2,\dots,z_m$  – indexes of row and column grid of control points (Fig. 1),  
 $N_i^n(s)$ ,  $N_j^m(t)$  – basis B-spline functions.

The function  $N_i^n(s)$  (and  $N_j^m(t)$ ) can be effectively assigned on the basis of recurrent Mansfield-de Boor-Cox formula [18]:

$$\begin{cases} N_i^n(s) = \frac{s-u_i}{u_{i+n}-u_i} N_i^{n-1}(s) + \frac{u_{i+n+1}-s}{u_{i+n+1}-u_{i+1}} N_{i+1}^{n-1}(s) & \text{if } n > 1 \\ N_i^1(s) = \begin{cases} 1 & \text{dla } s \in [u_i, u_{i+1}) \\ 0 & \text{otherwise} \end{cases} & \text{otherwise} \end{cases} \quad (2)$$

where:

$u_k$  – knot of B-spline curve ( $k=0,1,2,\dots,z_n+n$ ):

$$u_k = \begin{cases} 0 & k < n \\ \frac{k-n+1}{z_n-n+2} & n \leq k \leq z_n \\ 1 & \text{otherwise} \end{cases} \quad (3)$$

Knots determined according to formula (3) are uniformly spaced out in the range of  $u_k \in [0; 1]$  in non-descending order. First and last knot are duplicated as many times as B-spline curve order is. This condition allows to obtain the tangency of beginning and end of B-spline curve to the grid of control points.

The steps in determining the function  $N_j^m(t)$  are analogous.

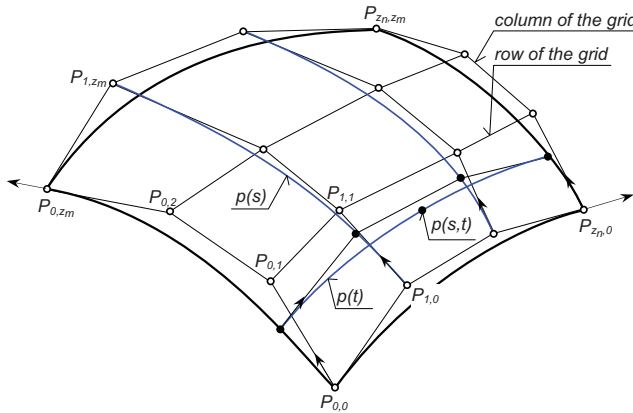


Fig. 1. The surface point  $p(s,t)$  as a point on the curve [11]

The point  $p(s,t)$  assignment, which lies on B-spline surface, can be reduced to the calculation of point on the B-spline curves. The points of surface can be determined using any algorithm designed for calculation of point on the curve, e.g. de Boor algorithm [11].

### 3. Method of experimental impact tests

For recording the course of the impact process during free fall of the object onto rigid ground, a tri-axial acceleration recorder type SAVER 3L30 made by Lansmont, was placed inside the load. The recorder, equipped with a built-in operational memory, was powered from a lithium battery. The device makes it possible to record up to 100 courses of acceleration whose values do not

exceed 100 g (g – acceleration of gravity). Acceleration signal is sampled with the rate of 1 kHz, and the error of measurement does not exceed 0.1 g. The recorder communicates with a PC computer through a serial port RS-232, which allows for data acquisition and control. The instrument is enclosed in an aluminium casing having the form of rectangular prism of dimensions 0.076x0.076x0.04 m and mass of 0.4 kg. When registering the course of events during the impact process, the recorder placed within the load is set to operate in event recording mode, and works as an autonomous system, without the need of external control and supply.

To perform the free fall drop tests we prepared unit load of dimensions 0.136x0.136x0.1 m and total mass 0.5 kg (Fig. 2). The load consisted of a box made of corrugated board, inside of which was filled with expanded polystyrene (EPS). The cushion material, whose function was shock protection, had a thickness of 0.03 m.

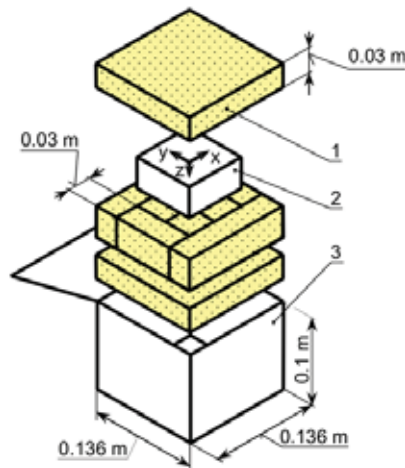


Fig. 2. Unit load prepared to the tests of free fall on rigid ground; 1 – cushion elements, 2 – acceleration recorder, 3 – cardboard box

The load with the acceleration recorder embedded inside it, was subjected to a series of tests of free fall on a smooth, rigid ground. Taking into account the condition of not exceeding the  $\pm 100$  g acceleration value admissible for the recorder, we selected drop heights for load:  $h = [0.30; 0.45; 0.60]$  m. The hazard of falling from the assumed heights was consistent with real hazards in the actual process of transportation from the supplier to the final recipient [7]. The load during tests was manipulated manually and it was dropped four times from the selected height  $h$ , on each of corner, edge and wall. Moreover, in case of the load fall on the edge or corner, it was tried to place the gravity centre of the load on the normal of impact, and in case of the fall on the wall – the surface of the chosen wall of the load was parallel positioned to the rigid ground. The height of the free fall was related to the distance between the lowest point of the packaging and the surface of the rigid ground.

#### 4. Proposition of spatial approximation of experimental test results

The data written in the acceleration recorder memory are represented in the rectangular coordinate system (Fig. 3b). Due to planned approximation of the results of experimental investigations, the spherical coordinate system is the more effective representation of these data (Fig. 3a, Fig. 4).

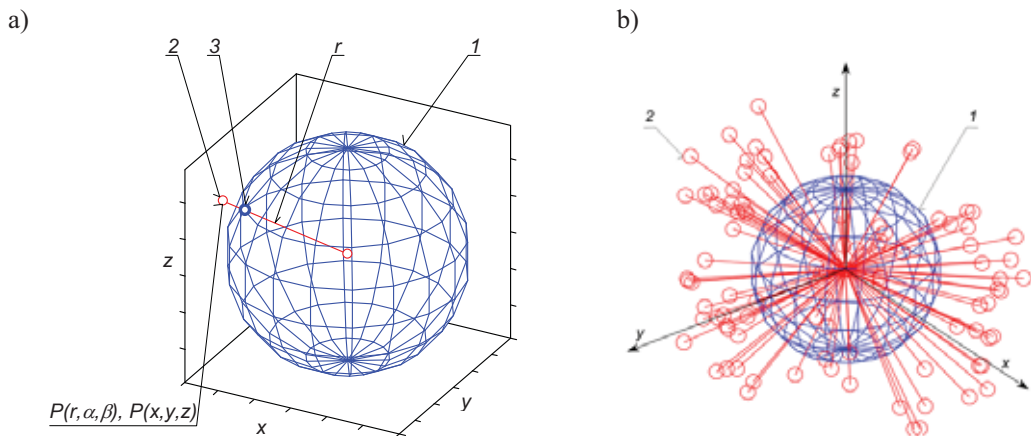


Fig. 3. Data registered during experimental investigations: a) singly impact test, b) series of 100 impact tests; 1 – initial grid of control points of B-spline surface, 2 – acceleration registered during experimental investigations, 3 – projection of point (2) on B-spline surface in radius-vector  $r$  direction

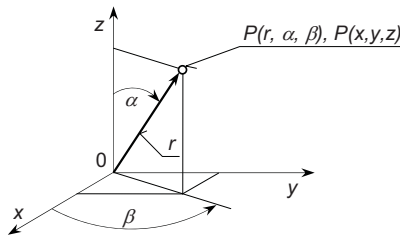


Fig. 4. Spherical and rectangular systems of coordinates

The conversion from the rectangular coordinate system to spherical is defined by dependences:

$$r = \sqrt{x^2 + y^2 + z^2}, \quad \beta = \arctg\left(\frac{y}{x}\right), \quad \alpha = \arccos\left(\frac{z}{r}\right) \quad (4)$$

$$r \geq 0, \quad 0 \leq \alpha \leq \pi, \quad 0 \leq \beta \leq 2\pi \quad (5)$$

and renewed transition from the spherical system to rectangular is described by formulas:

$$x = r \sin \alpha \cos \beta, \quad y = r \sin \alpha \sin \beta, \quad z = r \cos \alpha \quad (6)$$

The results  $(x_i, y_i, z_i)$  of experimental investigations of the unit load impact (data in Fig. 3 marked out by the reference 2) are subjected to approximation by means of B-spline surface of third order (1÷3). This approximation was performed using the numeric optimization, whose objective function is the minimization of the sum of squares of relative differences between real accelerations (registered during investigations) and their approximations [1]:

$$\min Q(X) = \sum_{i=1}^w \left( \frac{\hat{r}_i - r_i}{\hat{r}_i} \right)^2 \quad (7)$$

where:

$X = [r_1, r_2, \dots, r_v]$  – decision variables (radius-vectors of independent control points of B-spline surface in spherical co-ordinate system),

$v = (z_n - 1)(z_m - 1) + 2$  – number of independent control points ( $v=146$ , if  $\Delta\alpha=\pi/9$  and  $\Delta\beta=\pi/9$ )

$z_m + 1 = \pi/\Delta\alpha + 1$  – number of control points of meridian,

$z_n + 1 = 2\pi/\Delta\beta + 2$  – number of control points of equator,

$w=100$  – number of registered impact tests,

$r_i, \hat{r}_i$  –  $i$ -th resultant of object acceleration assigned during experimental research and projection of this resultant on B-spline surface.

During optimization, the SQP method (Sequential Quadratic Programming) was used – offered in the Matlab environment.

The initial values of the vector components of decision variables define the grid of control points assigning the sphere surface (Fig. 3a – marked by reference 1). The poles of this grid are common points for all meridians. From this reason, among control points, we can distinguish so-called dependent and independent points.

It is assumed, during the optimization, that the position of the control points of B-spline surface can be modified only through length change of the radius-vectors. The  $\alpha$  and  $\beta$  angles of these radius-vectors' position are constant – they are accepted during decision variables vector  $X$  defining.

## 5. Research results

In Fig. 5÷Fig. 10 the investigation results of the free fall of the unit load from the height  $h=0.3$  m,  $h=0.45$  and  $h=0.6$  m are shown. The data registered during experimental investigations are presented by means of markers in the shape of circles. An approximation of these data is represented with the help of B-spline surface. The grid of control points is also shown in these figures. The surface colours are connected with the value of an acceleration resultant. The bigger an acceleration of the load content, the more intensive red colour of the surface. To do correlation of B-spline surface position with respect to the load walls, the drawings contain the load edges and an indication of one of its corners (point in the black colour). The Fig. 5, Fig. 7 and Fig. 9 represent the oblique projection of the surface, and Fig. 6, Fig. 8, Fig. 10 – their orthogonal projections (main, top and left-side views). Numerical values showed in the graphs concern object accelerations in  $m/s^2$ .

From the analysis of presented data results, that the effectiveness of mitigation of overloads exerted on the load content is bigger, when the packaging impacts in the corners, than in the walls. The packaging shows larger stiffness of walls (the wall bottom especially – Fig. 8, Fig. 10) than corners. Increased flexibility of the load corners can be caused by the fact that cushion elements and the recorder don't constitute an uniform whole.

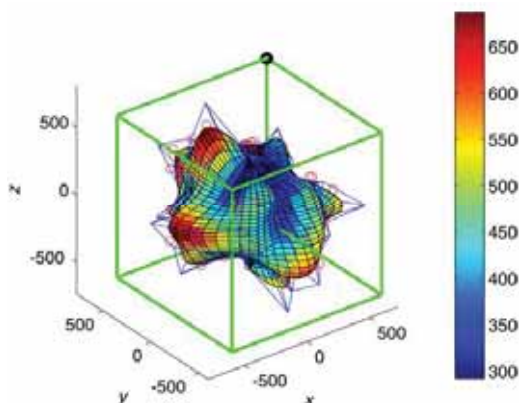


Fig. 5. Result of approximation (in isometric projection) of the of load accelerations registered during free fall from height  $h=0.3$  m

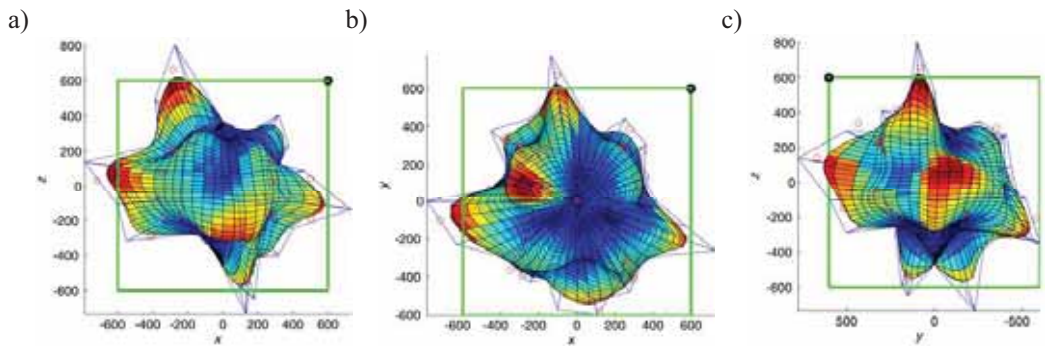


Fig. 6. Orthogonal projection of chart from Fig. 5: a) in the  $xz$  plane (main view), b) in the  $xy$  plane (top view), c) in the  $yz$  plane (left-side view)

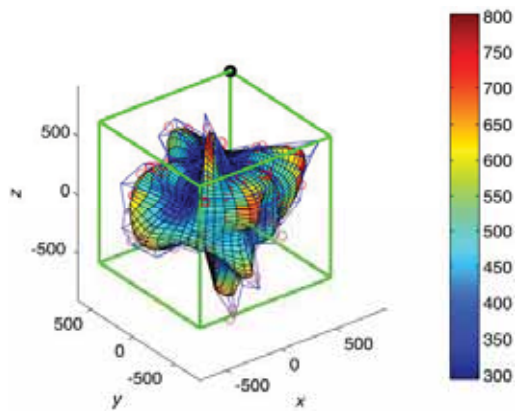


Fig. 7. Result of approximation (in isometric projection) of load accelerations registered during free fall from height  $h=0.45$  m

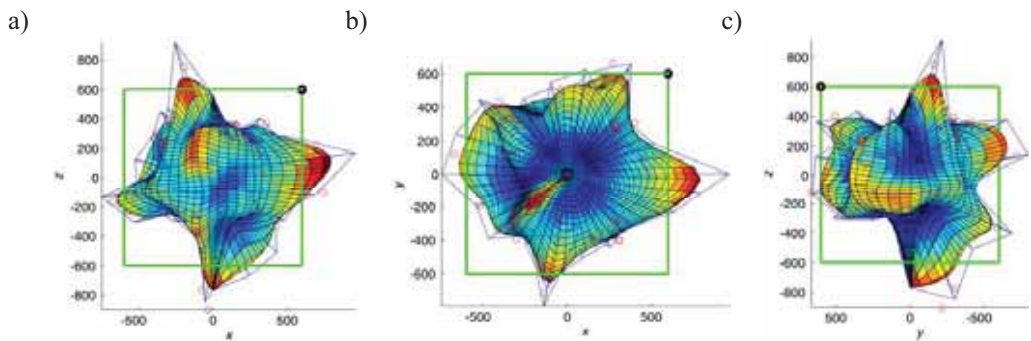


Fig. 8. Orthogonal projection of chart from Fig. 7: a) in the  $xz$  plane (main view), b) in the  $xy$  plane (top view), c) in the  $yz$  plane (left side view)

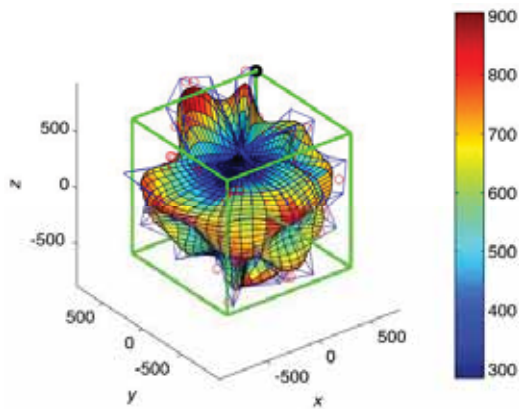


Fig. 9. Result of approximation (in isometric projection) of load accelerations registered during free fall from height  $h=0.6$  m

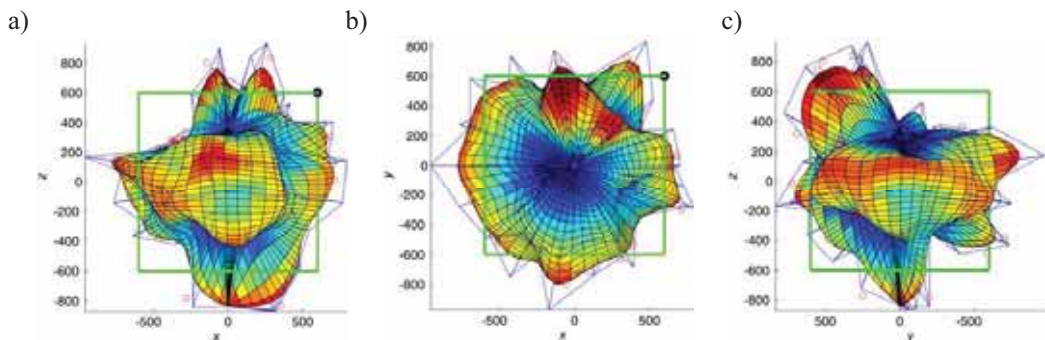


Fig. 10. Orthogonal projection of chart from Fig. 9: a) in the xz plane (main view), b) in the xy plane (top view), c) in the yz plane (left side view)

## 6. Summary

The following final attentions were formulated:

- Use of B-spline surface makes possible to reproduce complex solid geometry with an application of little number of decision variables.
- B-spline surface approximation enables an intuitive analysis of data obtained during experimental free fall tests of unit loads.
- 3D visualization of acceleration allows precise packaging places identification (in the three-dimensional space) which are critical for the safety of the load content and require constructional improvements.
- Proposed approximation of discrete data recorded by tri-axial sensor enables assigning the closed continuous surface that permits to determine acceleration of load during impact against an obstacle in any direction in 3D space.

## References

- [1] Arnold B.F., Stahlecker P., *Relative squared error prediction in the generalized linear regression model*, Statistical Papers 44, 2003, 107-115.
- [2] ASTM D1596 – 97(2003), *Standard test method for dynamic shock cushioning characteristics of packaging material*.
- [3] ASTM D3332 – 99(2010), *Standard test methods for mechanical-shock fragility of products, using shock machines*.
- [4] ASTM D4169 – 09, *Standard practice for performance testing of shipping containers and systems*.
- [5] ASTM D5276 – 98(2009), *Standard test method for drop test of loaded containers by free fall*.
- [6] Foley JD., Dam A., Hughes J., Phillips R., *Introduction to computer graphics*, WNT, Warsaw, 2001.
- [7] Herbert H., Schueneman H., *Packaging engineering, design and testing. A step-by-step approach for protection of fragile products*, Package Test Laboratory Westpak, Inc., San Jose, CA95119, USA, 2000, [www.westpak.com/techpapers/08\\_package\\_engineering\\_design\\_testing.pdf](http://www.westpak.com/techpapers/08_package_engineering_design_testing.pdf) (accessed: 2010-09-04).
- [8] ISO 2248:1985, *Packaging – Complete, filled transport packages – Vertical impact test by dropping*.
- [9] ISO 4180:2009, *Packaging – Complete, filled transport packages – General rules for the compilation of performance test schedules*.
- [10] Khangaldy P., Schueneman H., *Design parameters for deformable cushion systems. Package, Test Laboratory Westpak, Inc., San Jose, CA95119, USA, 2000, [www.westpak.com/techpapers/02\\_design\\_parameters\\_de\\_formable\\_cushion\\_systems.pdf](http://www.westpak.com/techpapers/02_design_parameters_de_formable_cushion_systems.pdf)* (accessed: 2010-09-04).
- [11] Kiciak P., *Basis of curves and surfaces modeling, An application in computer graphics*. WNT, Warsaw, 2005.
- [12] Low K.H., *Drop-impact cushioning effect of electronics products formed by plates*. Advances in Engineering Software 34, 2003, 31-50.
- [13] Piatkowski T., *Active fence with flexible link*, Journal of Theoretical and Applied Mechanics 48(6), 2010, 87-109.
- [14] Piatkowski T., Sempruch J., *Model of inelastic impact of unit loads*, Packaging Technology and Science, 22(1), 2009, 39-51, DOI: 10.1002/pts.825.
- [15] Piatkowski T., Sempruch J., *Model of the process of load unit stream sorting by means of flexible active fence*, Mechanism and Machine Theory, 43(5), 2008, 549-564, DOI:10.1016/j.mechmachtheory.2007.05.004.
- [16] Piatkowski T., Sempruch J., *Ranges of application of sorting manipulators*, Journal of POLISH CIMAC, 3 (6), 2011, 235-244.
- [17] *Precision Drop Tester PDT56ED*, <http://www.lansmont.com/DropTest/PDT56ED/Default.htm> (accessed: 2011-06-15).
- [18] Shene CK, *De Boor's algorithm*, <http://www.cs.mtu.edu/~shene/COURSES/cs3621/NOTES/spline/de-Boor.html> (accessed: 2011-04-14).
- [19] Xu X., Huang W., Russell R. D., Williams J. F., *Convergence of de Boor's algorithm for the generation of equidistributing meshes*, IMA Journal of Numerical Analysis 31, 2011, 580-596.





## MINIMIZATION OF NOISE IN FOUNDRIES ON THE EXAMPLE OF THE IRON FOUNDRY IN BYDGOSZCZ

**Jan Sadowski**

*University of Technology and Life Sciences in Bydgoszcz  
Faculty of Mechanical Engineering  
ul. Kaliskiego 7, 85-789 Bydgoszcz  
tel.: +48 52 3408418  
e-mail: [sadjan@utp.edu.pl](mailto:sadjan@utp.edu.pl)*

### *Abstract*

*In this article, a negative impact of noise in foundries on both physical and mental abilities of the workers have been discussed on the basis of the authors own implementation solution. The result is work efficiency decrease and quality determination. On the example of Iron Foundry at PESA works in Bydgoszcz (former ZNTK). The effects of minimalization of the loudest noise sources in different departments of the factory have been presented along with the assessment of noise reduction effectiveness rate. The presented solutions can have applications in other casting foundries in the whole country.*

**Keywords:** *noise in foundries and its minimalization*

### **1. Introduction**

Protecting environment against all kinds of harmful factors, including noise, is a necessity of our times. Noise is one of the factors of the environment which in a significant way shapes living and working conditions of human beings. An obligation to evaluate the occupational risk related to the noise exposure and to reduce this risk to the lowest possible level taking into consideration technical progress and the possibility to reduce noise at its source is one of the main obligations of an employer. The above obligation results from the European legislation (Directive 86/188/EEC, Directive proposal 94/C230/03 and the project of a new Directive adopted in June 2002 by the EU Social Policy Council) and Polish legislation: Labour Code, Regulation of the Minister of Economy and Labour as of 5<sup>th</sup> August 2005 on occupational health and safety of work involving exposure to noise or mechanical vibrations.

One of the important problems is the noise in the work environment, especially at the foundries where the level of noise at the posts often exceeds permissible limits and the machines operating in this sector of the industry are one of the loudest. On one hand, they create difficulties for the employees operating them (fatigue, risk of hearing loss, reduction of speech intelligibility and perception of signals), on the other hand, the noise created by these machines and emitted through the openings of the buildings and warehouses is usually sensed in the neighbourhood as very disruptive [2,4].

Progress in recognizing the dependencies between the influence of noise and health condition of an employee and their psychomotor features should contribute to undertaking more and more effective projects in the field of protection against noise. The main direction of activities related to

noise should be fighting against noise on the legal, technical and organizational level. This is not the task to be achieved in near future since it involves spending large amounts of money e.g. for construction of noise protections already at the stage of designing and operating noisy equipment (machine). On the other hand, failure to undertake protective actions causes huge losses difficult to be measured directly or even immeasurable [1,2,5].

The article presents the analysis of the problem related to the industrial noise at foundries and the possibilities of its minimization illustrated with an example of Bydgoszcz Iron Foundry at PESA Plant (formerly ZNTK) in Bydgoszcz.

## **2. Negative influence of the industrial noise on the employees of a foundry and its effects**

According to the estimates presented by the National Labour Inspectorate [3,5], noise in the foundry industry is one of the biggest industrial dangers and it constitutes 45% of all dangers. In the second place is dust 25% and subsequently toxic compounds 6%, vibrations 7% while the remaining 25% are factors of the work environment (mechanical dangers, lighting, microclimate, biological pollution, electromagnetic fields etc.).

Machinery and equipment used in the foundry industry are the loudest of all industry sectors and these are: jolt moulding machines, shake-out grids, tumbling barrels, conveyor systems, ventilation systems, forming machines, compressed air dischargers, grinding machines etc. The average sound level for this group of machines is 90 to 125 dB(A) [1,6,7,9, 10].

Therefore the noise at foundries is a danger of the work environment which exceeds the permissible limits the most often. Its presence, which has been proved [2,5,7], contributes to the high number of accidents and injuries, sickness absences (also not related to accidents) and, what is the most important economically, to low productivity and poor quality of work.

The losses incurred by the management of foundries, insurance companies and health care centres as a result of occupational diseases, accidents and injuries are relatively significant, but the losses related to the fact that people working in a noisy environment will do less, worse and will damage more castings are at least ten times bigger [5,8,11].

Harmfulness and onerousness of the noise at foundries depend on its physical features and on parameters such as: sound level, frequency, spectral characteristics, nature and time ranges of acoustic vibrations as well as on the relation between the machine operator and the source of the noise.

Table 1 shows that the harmful influence of acoustic vibrations related to the noise at foundries can affect health and when it comes to the productivity and work quality at foundries it can also have functional effects [2,5 10].

Health effects are: a psychomotor performance of an employee, their mental (emotional) state, their mood and health, quality of hearing and their diseases. Functional effects which influence productivity and work quality are: lack of independence, insecurity, loss of orientation in the environment, lack of comfort and understanding.

Figure 1 presents health and functional aspects during work of employees of foundry industry [3,9].

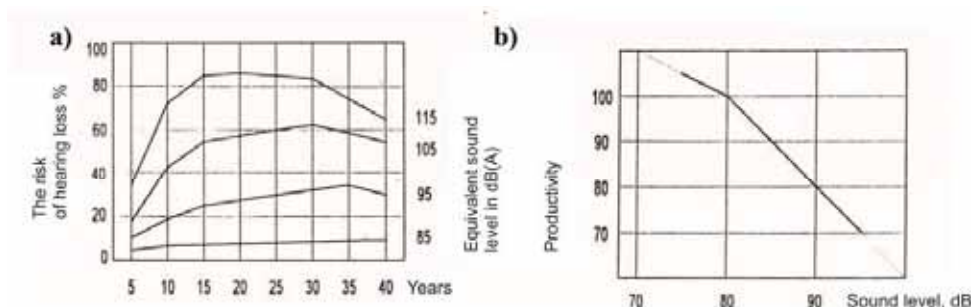


Fig. 1. Effects: a) on health; b) on the people's work effectiveness in the casting industry depending on the noise level

Tab. 1. Impact of noise on the employees health and work efficiency

| Ref. no. | Equivalent sound A level (dB) | Impact on a human being  |
|----------|-------------------------------|--|
| 1        | up to 35 dB                   | Harmless but irritating  |
| 2        | from 35 to 75 dB              | Exhausts nervous system, lowers productivity, influences speech intelligibility, reduces the effectiveness of perception, difficulties with concentration  |
| 3        | from 75 to 85 dB              | Makes it difficult to sleep and rest, longer exposure causes headaches and has negative influence on nervous system, it causes hearing impairment, makes remembering difficult, reduces the efficiency of the process of thinking and reasoning        |
| 4        | from 85 to 130 dB             | It causes permanent hearing damage, disorders of cardiovascular, nervous and balance system, makes speech intelligibility from a distance of 0,5m impossible, reduces the efficiency of solving problems, increases sensitivity to confounding factors |
| 5        | over 130 dB to 150 dB         | It stimulates vibration of some internal organs of a human body and causes their chronic diseases and sometimes complete destruction of internal organs of a human being.  |

To estimate financial effects achieved thanks to reducing the noise we can use the notion of the so called effectiveness of noise reduction which is described by the formula [5]:

$$E = \frac{M \cdot \Delta L}{\Delta C} \quad (1)$$

where:

E – the effectiveness of noise reduction in the object, in dB (A) x person/1000 PLN or average gross salary,

M – the number of people for whom the noise has been reduced,  
 $\Delta L$  – estimated or actual value of noise reduction, in dB(A) reaching the above-mentioned group of people,  
 $\Delta C$  – the costs of the noise reduction, PLN.

The higher the value of effectiveness E is, the better the results of the implemented solutions reducing the noise attributable to one person exposed to the above-average sound level are.

It is estimated that [2,5,9] the reduction of noise at foundries by only 1dB(A) gives an average increase in productivity by 1,5%, reduces the number of deficiencies, accidents and injuries by 10%, reduces sickness absences not related to accidents by 4% and generally reduces the risk of occupational hearing loss.

### 3. Examples of the noise minimization at Bydgoszcz iron foundry

Below you can see examples of the noise minimization at Bydgoszcz Iron Foundry at PESA Rail Plant (formerly ZNTK) in Bydgoszcz, introduced in 1999 [12]. Bydgoszcz Iron Foundry casts brake pads from grey iron with the addition of phosphorus.

The sound levels of the main noise sources located in different Divisions of the Foundry are presented in Table 2.

The analysis of the noise sources shows that the sound level at different divisions and posts is significant and sometimes very high, exceeding the permissible limits and reaching up to 115 dB(a). Spectra of the main noise sources in octave bands of 63÷8000 Hz center frequency were also identified by making at each point of the post from 4 to 15 detailed measurements.

The results of the research were used to develop soundproofing constructions and to select appropriate absorbing and insulating materials for sound-absorbing structures for particular noise sources (Table 2).

The reduction of the noise of OPB tumbling barrel (point I, Table 2) used for cleaning brake pads of total length 9m and diameter of 2,5m was difficult to achieve. This noise decided about its output value on the conveyor belt 67 placed outside the room in which the barrel was placed. An important issue was to reduce the energy caused by hitting of the finished castings against metal resonant cavity of the barrel. It was soundproofed by putting another sound-absorbing and insulating layers on the body of the barrel using channel sections to connect them [50 according to Fig. 2.

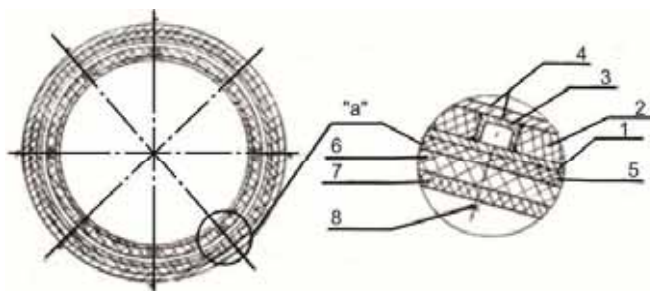


Fig. 2. Silencing the tumbling barrel noise: 1 - the barrel outer coat; 2 - mineral wool layer; 3 - fastening channel; 4 - inner coat; 5 - inner gum coat; 6 - mineral wool layer; 7 - outer gum coat; 8 - a screw with spring washers connecting gum coats with the main body

What is more, insulation of the walls of the room where a tumbling barrel was placed was reinforced by putting soundproofing curtains made of rubber coats and thick canvas on the walls.

For the reduction of noise of metal conveyor systems and of dropping of castings, scrap-metal and coke to cupola (point II, III, V, XIII, XV, Tab. 2) hard rubber  $\neq 10\text{mm}$  was used which not only reduced material vibrations of the dropped mass caused by the impact, movement and friction of the transported castings (charge material), but also served as a great protection for a metal load-bearing construction of the transporting and dropping equipment before expenditure which is presented in Fig. 3.

The reduction of noise in the pipeline systems transporting heated air from the heaters to cupolas (point XIV, Tab. 2) and at the production halls of the foundry adjacent to the station was achieved thanks to the increase of attenuation of pipeline channels (the use of absorption silencers), stiffening pipelines and acoustic adaptation of the hall where heaters are placed (hanging appropriately selected spatial cone-shaped absorbers and wall insulation), but also thanks to placing the heaters on the soundproof rubber plates.

*Tab. 2. Effectiveness results of noise minimalization solutions applied in the Foundry in Bydgoszcz*

| Ref. No. | Source of the noise                 | Average sound level before soundproofing $L_1$ , dB(A) | Average sound level after soundproofing $L_2$ , dB(A) | Effects of soundproofing $\Delta\text{dB} = L_1 - L_2$ | Runtime of a device per shift in hours | Estimated equivalent sound level $L_{\text{eq}2}$ dB(A) (after soundproofing) | Equivalent sound level according to the norm $L_{\text{eq}}$ , dB(A) | The variation from the norm, dB(A) | Effectiveness of soundproofing, E#<br>$\left[ \frac{\text{person} \cdot \text{dB(A)}}{\text{PLN}} \right]$ |
|----------|-------------------------------------|--|---|--|--|---|--|------------------------------------|--|
| 1        | I – tumbling barrel                 | 114,9  | 103,8   | 11,1   | 5                                      | 100,2   | 87   | -13,2                              | 2,21   |
| 2        | II – receipt of insertions, belt 67 | 103,8  | 92,0  | 11,8   | 5                                      | 88,3  | 87   | -1,3                               | 2,84   |
| 3        | III – chute 67/68                   | 98,7   | 92,3  | 6,4  | 4                                      | 87,8  | 88   | -0,2                               | 1,76   |
| 4        | V – chute 64/65                     | 107,5  | 95,1  | 12,4   | 4                                      | 93,8  | 88   | -5,8                               | 3,32   |
| 5        | VI – DISAMATIC A                    | 88,2   | 82,8  | 5,4  | 4                                      | 80,5  | 88   | 7,5                                | 1,63   |
| 6        | VII – DISAMATIC B                   | 87,5   | 82,1  | 5,4  | 4                                      | 80,5  | 88   | 7,5                                | 1,63   |
| 7        | XIII - gantry                       | 105,7  | 88,2  | 21,6   | 2                                      | 84,5  | 94   | 9,5                                | 3,81   |
| 8        | XIV – turbo blowers                 | 99,2   | 84,1  | 15,1   | 8                                      | 83,5  | 85   | 1,5                                | 3,46   |
| 9        | XV – coke loading                   | 87,4   | 80,5  | 6,9  | 1                                      | 81,5  | 94   | 12,5                               | 1,95   |
|          |                                     |  |   |  |  |   |  | $E_{\text{sr}}$                    | 2,51   |

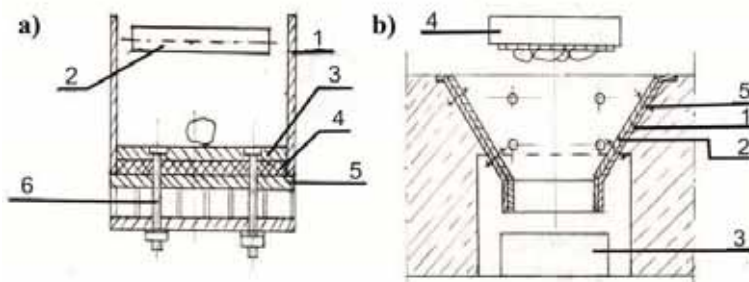


Fig. 3. Silencing scheme of shutes

a) transport shute: 1 - shute silenced; 2 - transport series; 3 - upper steel board; 4 - lower gum board; 5 - lower steel board; 6 - fastening screws with spring washers

b) charging hopper: 1 - metal housing; 2 - gum boards; 3 - receiver device; 4 - electromagnets; 5 - fastening screws with spring washers

Pneumatic (aerodynamic) noise caused by a sudden exhaust of the compressed air into the atmosphere from the control system of the machine used to form brake pads of two lines DISAMATICA A and B (points VI, VII, Tab. 2) was reduced by directing the exhaust air using appropriately selected (of a specific length and section) wires into the inner space of the body of the forming machine bearing and by using several individual expansion silencers with small measurements which is presented in Fig. 4.

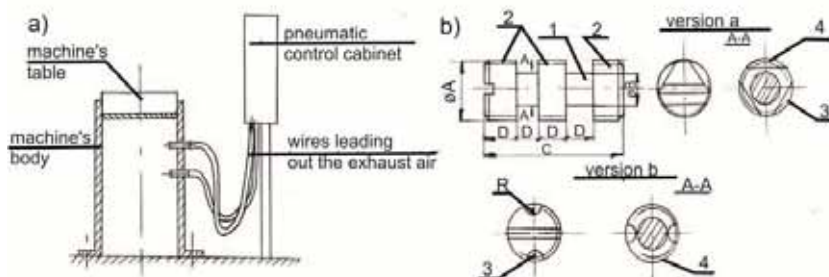


Fig. 4. Pneumatic noise silencing of the DISAMATIC line:

a) directing the air flow into the space of the body

b) small expand silencers: 1 - cylindrical bolt; 2 - gummed collar; 3 - prismatic or grooved cuts

After substantial soundproofing the devices minimizing the noise were subject to practical verification in the production environment in terms of mechanical durability, resistance to attrition (transporting and dropping equipment) and cracking caused by impact loading for the period of 2 years. It was found that too high temperature of brake pads coming out of the barrel and production line destroyed after around 1 year the hard rubber. Therefore, even harder, easily replaceable vibroacoustic plates were used.

#### 4. Evaluation of the achieved effects

After introduction of the devices minimizing the noise the measurements were made at the same points as initial measurements. At each point several series of measurements were conducted. The purpose of such detailed measurements was to determine total acoustic effect of soundproofing works as well as to objectively determine the equivalent sound level at the posts and in the places where the employees exposed to noise spend time.

To estimate the equivalent sound level at the post  $L_{eq2}$  (after soundproofing) the norms PN-EN ISO 3744, PN-EN ISO 3746, PN-EN ISO 11201 were used including runtime (technological

time) of the devices at the foundry during one shift and compared it with the standardized equivalent sound level  $L_{eq}$  (PN-ISO-01307) which is presented in Table 2. Table 2 presents also the values of effectiveness of noise reduction  $E$  calculated using the formula (1) at particular Foundry Divisions.

The results presented in Table 2 show that high acoustic effectiveness of the devices minimizing the noise installed at the Iron Foundry was achieved. There was a great decrease of the noise at particular points: at point II (belt 67), where employees are most exposed to the noise, it decreased by around 12 dB(A), at other points by average  $5 \div 8$  dB(A) and at some points even by  $15 \div 20$  dB(A). The achieved average rate of effectiveness  $E=2,51$  is also high. It means that by spending on soundproofing 1000 PLN per employee of the foundry working in a noisy environment (exposed to noise) we receive the noise reduction of around 2,5 dB(A) which means that the energy of the noise reaching an employee is two times lower [5,11].

## 5. Summary

Although high acoustic effectiveness was achieved some of the achieved results did not meet the requirements of the PN-ISO-01307 norm, this applies especially to point I (tumbling barrel), IV (chute 64/65) and to some extent to point II (belt 67). The noise exceeds the limit at these points by around  $13 \div 1,3$  dB(A) (Table 2).

Further soundproofing of these points is possible by, for example, increasing insulation and acoustic absorption of the post at the belt and its surroundings, by hanging appropriately selected absorbing and insulating structures and additionally by covering the inner part of a steel coat of a tumbling barrel with very hard rubber (resistant to high temperatures).

However, besides the effects strictly acoustic achieved at the foundry we should not overestimate related to this decrease functional effects.

The increase of the quantitative effect of work (productivity and work quality) at particular posts at the foundry while decreasing sound level by 5 dB(A) in appropriate time ranges will amount to [5]:

- from 100 dB(A) to 95 dB(A)                       $\sim 10\%$
- from 95 dB(A) to 90 dB(A)                       $\sim 7\%$
- from 90 dB(A) to 85 dB(A)                       $\sim 6\%$
- from 85 dB(A) to 70 dB(A)                       $\sim 10,5\%$

Together it can give an estimated increase in productivity up to around 23%.

The influence of noise reduction on the number of accidents, injuries and sickness absences not related to accidents as well as on the number of cases of occupational deafness can be estimated as even greater i.e. by reducing the noise by 5 dB(A) [5] the number of accidents and injuries should decrease approximately to:  $(1 \div 10\%) \cdot (1 \div 10\%) \cdot (1 \div 10\%) \cdot (1 \div 10\%) \cdot (1 \div 10\%) = 0,9^5 = 0,59 \approx 60\%$  of the previous number of accidents and injuries while reducing the noise by 10 dB(A) can decrease their number to  $0,9^{10} = 0,35 \approx 35\%$  which means around 1/3 of their number before soundproofing.

A significant decrease of sickness absences not related to accidents at the foundry while reducing the noise by 5 dB(A) can be estimated as the value equal:  $(1 \div 4\%) \cdot (1 \div 4\%) \cdot (1 \div 4\%) \cdot (1 \div 4\%) \cdot (1 \div 4\%) = 0,96^5 = 0,82 \approx 82\%$  of the sickness absences before soundproofing while reducing the noise by 10 dB(A) as the value equal  $0,96^{10} = 0,66 \approx 66\%$  of the initial sickness absences at the foundry which means by 1/3. Observations of the management of the foundry made over a long period of time (around 3 years after implementation) confirmed the above estimations and proved practical increase in productivity and work quality and decrease of the accident rate within 10% at the discussed Foundry.

From the presented above results and facts it can be concluded that the noise at the posts in the foundry industry affects health and availability of employees causing lower and poorer effects of work regardless of their will.

As we can see there are important economical, medical and ecological reasons why the noise in the foundry industry should be reduced.

## References

- [1] Engel Z., *Ochrona środowiska przed drganiami i hałasem*. PWN, Warsaw 2001.
- [2] Sadowski J., *Wybrane przykłady minimalizacji hałasu środowiskowego*. Materials from the 5<sup>th</sup> Noise-Health-Prevention Conference, Kołobrzeg 2001, p.159-177.
- [3] Collective work, *Uszkodzenia słuchu wywołane ekspozycją na hałas przemysłowy*. Bezpieczeństwo Pracy 12/1997, p.14-19.
- [4] Lipiński J., *Zjawiska wibroakustyczne a środowisko naturalne*. Materials from the 3<sup>rd</sup> New Directions of the Development of Mechanics Conference. AGH Scientific Journals, No. 14 2000, p.177-180.
- [5] Rybarczyk W., *Hałas w przemyśle i jego ograniczenie*. Centrum Zastosowań Ergonomii. Zielona Góra, 1999, ISBN 83-906348-2-1.
- [6] Giergiel J., *Hałas i wibracje w przemyśle odlewniczym*. Part I, AGH Scientific Journals No. 1301, 1998, p.187-195.
- [7] Stolarski B., Szczybura H., Tabor A., *Hałas w przemyśle odlewniczym*. Materials-Castings-Quality 1<sup>st</sup> National Scientific Conference, Cracow 1998, p.325-331.
- [8] Cempel Cz., *Wibroakustyka stosowana*. PWN, Warsaw 2001.
- [9] Wątyły J., *Próba ekonomicznej oceny zabezpieczeń przed hałasem*. Applications of Ergonomics No. 2/3, 1995, p. 36-41.
- [10] Sadowski J., Szykowny T., *Zagrożenia hałasem w przemyśle odlewniczym i metalurgicznym*, Archives of Foundry, Volume 5, No. 17, 2005, p. 253 – 262.
- [11] Sadowski J., Wernerowski K., *Przyczyny i możliwości zmniejszenia hałasu technologicznego na prasach mechanicznych*. Applications of Ergonomics No. 3, 1997, p.19-29.
- [12] Wernerowski K., Sadowski J., Report on scientific and implementation work entitled "Wyciszenie hałasu w Odlewni Żeliwa ZNTK w Bydgoszczy"-(1999) -not published work.



## COMPUTER AIDED ELECTROCHEMICAL SHAPING OF CURVILINEAR SURFACES

Jerzy Sawicki <sup>1)</sup>, Tomasz Paczkowski <sup>2)</sup>

<sup>1)</sup>University of Technology and Life Sciences  
Faculty of Mechanical Engineerin  
ul. Prof. Sylwestra Kaliskiego 7, 85-791 Bydgoszcz,  
e-mail: [sawik@utp.edu.pl](mailto:sawik@utp.edu.pl)

<sup>2)</sup>University of Technology and Life Sciences  
Faculty of Mechanical Engineerin  
ul. Prof. Sylwestra Kaliskiego 7, 85-791 Bydgoszcz,  
e-mail: [tompacz.@utp.edu.pl](mailto:tompacz.@utp.edu.pl)

### Abstract

*Machining involves removing a surface layer from an object with the use of mechanical energy. It often happens that this process is very difficult or even impossible due to technical and economic problems ( big strength and tear resistance of the machined material). Therefore, new technological processes of removing the material from the machined object, have been developed. They involve, e.g. dissolution, melting or the material vaporization. These processes need energy of electric discharge, chemical reaction energy, and energy carried by a stream of particles. the material destruction which occurs, then, are called the material dissolution (erosion). There are different classifications of dissolution machining The most popular one is electro discharge machining (EDM), electrochemical machining (ECM), stream-dissolution machining (i.e. electron-machining (EBM) and ion- machining (IBM).*

*The purpose of this work is to present the problems connected with the computer aided electrochemical (ECM) as one of a few kinds of dissolution machining.*

**Keywords:** ECM, computer simulation

### 1. Electrochemical shaping

Electrochemical machining with the use of a tool electrode is today one of the basic electrochemical technological operations for machining tools and machines. Electrochemical machining (ECM) has been developed as a machining method for alloys of high strength and heat resistant, whose shaping with the use of traditional methods was very complicated and extremely hard [7, 13].

During this constant process the tool electrode performs most frequently a progressive motion in the direction toward the machined surface. The inter-electrode gap is supplied with electrolyte with high speed, causing carrying away of the dissolution products from the machined surface. These are mainly hydrogen particles and ions of the dissolved metal. In such conditions we can talk about a multi-phase flow and generally, three-dimensional [1, 12].

The flow hydrodynamic parameters and the medium properties determine the processes of mass, energy, momentum and energy exchange in the inter-electrode gap. Properly chosen they prevent from formation of cavitation zones, critical flow, circulation, excessive increase of the electrolyte temperature and void fraction of the gas [3, 11, 14].

The above mentioned processes have a significant influence on the electrochemical dissolution velocity and usability of the dissolved surface.

The following tasks should be dealt with during the design of the technological machining process [2, 4, 5, 6]:

- choice of ECM process conditions (electrolyte composition, machining parameters, technological requirements),
- design of the tool-electrode,
- analysis of the machining process accuracy.

It should be noted that the listed tasks are closely related to each other, and their solution is connected with prediction in time of the machined surface shape evolution, i.e. anode.

The choice of ECM process conditions is concerned with:

- material and the kind of semi-product, (dimensions defining allowance, shape),
- requirements concerning accuracy,
- requirements concerning the top surface,
- technical-economic requirements (work consumptions, cost and energy consumption)
- requirements concerning the type of the cutting machine e.( type of driving machine, supplied current, the electrolyte flow pressure, range of electrical intensity control and voltage, efficiency control, range of the feed rate, the working size of the chamber, kind of control, temperature regulation, the tool machine stiffness, etc.),
- choice of electrolyte,
- choice of machining parameters,

Design of the tool electrode involves:

- determination of the working part profile,
- arrangement of the electrolyte inlets and outlets from the inter electrode area),
- construction of the electrode (e.g. folding, all in one piece),
- technical conditions (material, accuracy, smoothness).

It is also significant to predict whether the final shape of the machined object can be obtained in the final or temporary state.

Looking for the proper shape of the electrode involves a necessity of determination of physical-chemical conditions occurring in the inter-electrode gap. These conditions depend on ECM machining parameters.

Therefore, designing tools (tool electrode) is connected with active control of the criteria restricting ECM conditions. If the accepted conditions do not yield the expected final effect, a correction of accepted quantities of ECM parameters is carried out (working voltage, the pressure of progressive motion etc.)

The process of tool designing is connected with an analysis of electrochemical shaping which covers:

- determination of the influence of the main factors on the shaping and dimensional inaccuracy,
- determination of permitted changes of parameters (ECM parameters allowance).

## **2. Modeling of the shaping electrochemical machining process**

The process of ECM electrochemical machining treated as a series of simplifications is shown in Fig. 1. The real object is replaced with a physical model, in the first stage. This model is a certain

simplification of the real object but with maintenance of its significant features. The model can have a different degree of simplification. Complications of the model can lead to complication of the equations which describe it. Choice of the right physical model providing sufficient computing accuracy requires long experience.

Mathematical model as a system, most often of integral differential equations, describes the real model resulting from the physical one, always, in some approximation.

On the basis of the mathematical model and data resulting from the physical model there emerges a given computational algorithm, whose result is computer program in a given programming language.

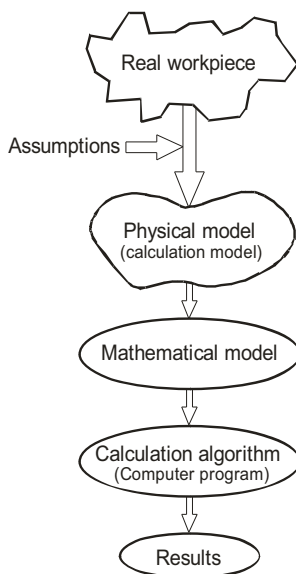


Fig. 1. Mathematical modeling algorithm

In order to carry out the algorithm (Fig. 1) it is necessary to define conditions of the electrochemical machining.

The electrochemical machining conditions are described by means of the following data [7, 13]:

- kind of electrolyte (chemical composition) and its properties:

- $\kappa_0$  - electrolyte conductivity,
- $\alpha$  - temperature coefficient of the electrolyte electrical conductivity,
- $\rho_e, \rho_H$  - electrolyte density, hydrogen,
- $c_p$  - electrolyte specific heat,
- $\mu_e, \mu_H$  - dynamic viscosity coefficient of the electrolyte and hydrogen,
- $\eta_H$  - electrochemical equivalent of hydrogen,
- $k_H$  - current dissolution efficiency,
- $\beta$  - void fraction,
- $p_H$  - pressure of hydrogen,
- $v_x, v_y$  - velocity,
- $T_i$  - temperature of the electrolyte on the inlet,

- the machined material ( chemical composition),

- the machining parameters:

- $v_f$  - feed rate of the tool electrode,
- $U$  - working voltage between the electrodes,
- $p_w$  - the electrolyte pressure on the inlet to the inter-electrode gap,
- $p_z$  - the electrolyte pressure on the outlet to the inter-electrode gap,
- $Q_v$  - volume stream,

- characteristics of the electrochemical system: cathode-electrolyte-anode:

- $k_v$  - coefficient of electrochemical machinability,
- $E_a-E_k$  - fall of the potential in near electrode layers,
- $x_i$  - coordinate of the inter-electrode gap beginning,
- $x_o$  - coordinate of the inter-electrode gap,
- $T_0$  - the temperature of electrodes,

Modeling of ECM machining involves predicting the machined surface shape evolution in time, changes of the inter-electrode gap thickness and distributions of physical-chemical conditions in the machining area, such as: distribution of static pressure, the electrolyte flow velocity, temperature, and void structure.

General differential equation describing evolution of the machined surface shape, in result of anode dissolution, according to the ECM dissolution theory, has the form [5, 11].

$$\frac{\partial F}{\partial t} + k_v \vec{j}_A \nabla F = 0 \quad (1)$$

with the initial condition  $F(x, y, 0) = F_0$

where:

- $j_A = j(X_A, Y_A, t)$  - current density distribution on the machined surface
- $k_v$  - is equal to volume of the material removed by anode dissolution during flow of a unit electrical load
- $F_0(x, y) = 0$  - equation describing the machined output surface
- $F(x, y, t) = 0$  - equation describing the anode surface in time t

Current density on the anode is expressed in the following way [4, 5]:

$$j_A = \kappa_0 \Phi_{TG}^{-1} \frac{U - E}{h} \quad (2)$$

Function  $\Phi_{TG}$  describes the influence of conductivity change inside the inter-electrode gap and is determined from the balance of voltage fall along the way.

$$\Phi_{TG} = \frac{1}{h} \left[ \int_0^h \frac{dy}{(1 + \alpha(T - T_0))(1 - \beta)^{3/2}} \right] \quad (3)$$

In order to finish the equations system describing electrochemical shaping it is necessary to determine temperature distributions and void fraction. It is connected with solution of an integral differential equations system describing the electrolyte flow through the inter-electrode gap. Equations governing the flow movement through the inter-electrode gap result from basic principles of conservation, i.e. principles of mass, current, momentum and energy conservation. In literature we can find approaches to the subject in one dimensional terms, [2, 4, 5], two-dimensional terms [6], [8]. Differences between solutions result from simplification assumptions and mathematical methods used for solution of the above problem.

For the purpose of predicting the tool electrode shape, an analysis is performed which is called a reverse issue.

The reverse issue, in electrochemical machining, whose aim is to obtain the proper shape of the tool electrode ER consists in comparing the results of simulation of the machined object shape evolution with the  $i$ -th iteration of the final shape [4, 5].

After performing simulation computing the distribution of  $\Delta F$  shape deflections from the expected shape is defined [2, 4, 5]:

$$\Delta \tilde{F} = \tilde{F}_i - F \quad (5)$$

then, the shape of tool-electrode is corrected by moving its profile points in the proper direction(Fig.2):

$$\Delta h = \alpha \Delta \tilde{F} \quad (5)$$

here:  $\alpha$  – is a coefficient conditioning velocity of the iteration process convergence.

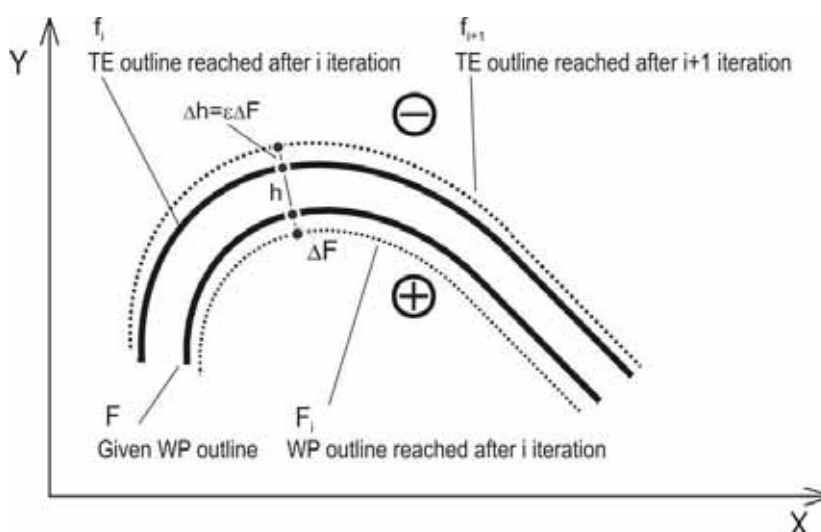


Fig.2. Scheme of the tool electrode correction

### 3. Algorithm of the shaping machining process computer simulation

Computer simulation is carried out with the use of successive approximation method [6, 14] regardless of the methods used for the solution of equation system which describe the flow hydrodynamics and they result from the principles of mass, momentum energy conservation.

Simulation of the machined object shape evolution is based on a method of, the so called, time steps. This means that equation (1) is approximated by differential quotient. The end of the simulation process takes place with practical stabilization of the ECM process. In the stable state there follows stabilization of the inter-electrode gap thickness distribution and the physical flow field, as well as the medium properties in the gap.

The course of computer simulation of the shaping machining have been presented in the form of an algorithm [8, 9, 10] (Fig3).



- element methods*, J. Electrochem. Soc. 125. 1978, s. 1981-1988.
- [2] Dąbrowski L., *Podstawy komputerowej symulacji kształtowania elektrochemicznego*, Pr. Naukowe PW, Mechanika nr 154, Wydawnictwo Politechniki Warszawskiej, Warszawa, 1992.
  - [3] Jain, V. K., Pandey. P. C., *Tooling design for ECM-A finite element approach*. Trans. ASME. J. Engng Industry 103, 1981, s. 183-191.
  - [4] Kozak J., *Kształtowanie powierzchni obróbką elektrochemiczną bezstykową (ECM)*, Pr. Naukowe PW, Mechanika nr 41, Wydawnictwo Politechniki Warszawskiej, Warszawa, 1976
  - [5] Kozak J., *Mathematical Models for Computer Simulation of Electrochemical Machining Process*, Journal of Materials Processing Technology, Vol. 76, 1998, N. 1-3.
  - [6] Łubkowski K., *Stany krytyczne w obróbce elektrochemicznej*, Prace naukowe, Mechanika, z.163, Oficyna Wydawnicza PW, Warszawa, 1996.
  - [7] McGeough, J.A., *Principles of Electrochemical Machining*, London: Chapman & Hall, 1974.
  - [8] Paczkowski T., Sawicki J., *Electrochemical machining of curvilinear surfaces*, Journal of Machining Science and Technology, vol. 12 (1), Philadelphia 2008, s. 33-52.
  - [9] Paczkowski T., Sawicki J., *Wpływ koncentracji wodoru w elektrolicie na ewolucję kształtu przedmiotu obrabianego*, wybrane zagadnienia obróbek skoncentrowaną wiązką energii, Praca zbiorowa pod red. Michała Styp-Rekowskiego, BTN, Bydgoszcz. 2003, s. 62-69.
  - [10] Paczkowski T., Sawicki J., *Zagadnienie odwrotne w modelowaniu obróbki Elektrochemicznej kształtowej*, Zagadnienia Mechaniki Stosowanej, T. 1, UTP, 2007, s. 83-95.
  - [11] Prentice, G. A., Tobias, C. W., *Simulation of changing electrode profiles*, J. Electrochem. Soc. 129(1), 1982, s. 78-85.
  - [12] Sautebin, R., Froidevaux. H., Landolt. D., *Theoretical and experimental modeling of surface leveling in ECM under primary current distribution conditions*, J. Electrochem. Soc. 127(5), 1980, s.1096-1100.
  - [13] Wilson J.F., *Practice and Theory of Electrochemical Machining*, New York, Wiley, 1971.
  - [14] Zhou. Y., *Finite element analysis of elcctrochemical machining problems validity of elcctroneutrality assumption. and flow in solution erystal growth system*, Ph.D. thesis. Department of Chemical Engineering and Materials Science, University of Minnesota. Minneapolis. MN. 1995.





## FEM CALCULATION OF RESIDUAL STRESS AFTER PULSED CURRENT ARC WELDING OF ALUMINUM ALLOY

Andrzej Skibicki

University of Technology and Life Sciences in Bydgoszcz, Faculty of Mechanical Engineering  
Prof. S. Kaliskiego 7, 85-796 Bydgoszcz  
e-mail: askibic@utp.edu.pl

### Abstract

Construction made of aluminium alloy is lighter than of steel. The use of pulsed arc for welding is helpful, but has influence on structure and residual stresses after welding. FEM model of the welded plate made of aluminium alloy was used here. The 2D model, lying on the surface of welded sheets, was used. Because of the models symmetry only  $\frac{1}{2}$  of the surface was calculated. The calculations were done with ANSYS in two phases, as uncoupled thermal and mechanical calculations. The iterative calculations of deformations and stresses are non-linear with temperature dependent material properties. The mesh of 1337 finite thermal elements SHELL57 was used. Simulation has 10,3 s of welding time followed by cooling until 800 s. Different type of pulse was used. One single period of current pulse was all the time 0,5 s. This time was divided into 5 equal sub-periods. The heat source (current of welding) was switched on for some sub-periods. The power of heat source was multiplied by factor 1,2 or 3. Distributed volume heat source was moving along of weld line. Results from temperature analysis were used in stress calculation. Elements type and material properties were changed to structural PLANE42. The results show that some residual stresses after pulsed arc welding were higher as after constant. The maximums of tensile stresses were concentrated at small, perpetual areas. They are too small for experimental measuring, but together significantly sufficient for crack propagation or local stress corrosion.

**Keywords:** welding, stress, FEM, aluminum, pulsed arc

### 1. Introduction

The welding is one of the basic techniques of connecting metals. For melting metal, which make the weld, the great amount of heat is needed. The weld is heated as well as all construction. In the results of it the structural changes appear, which makes the mechanical properties of metal lower. The results in the deformation and residual stresses category are also important. They can be dangerous for the construction. If the thickness of the material is small while the plasticity high – there are also big additional loads needed to destroy the construction. The risk is higher for the fragile materials. The thick metal sheets are during and after welding in 3 dimensional (3D) stress state. For both of those cases chance of the appearance of crack is possible. The residual deformation changes the form of construction. It can unable their operating. The shrinkage and deformation make it difficult to keep the tolerances. The practical ways for reduction of deformation and stress are the results of long-term experience. The technical development and economy introduces new technologies and materials. In this case new experience can be not long-term enough.

Construction made of aluminium alloy is lighter than made of steel. The welding of aluminium is difficult however. The use of pulsed arc is helpful, but has influence on structure and residual stresses after welding [4,7]. Its important to check this influence at some cases of welding. FEM

model of the welded plate made of aluminium alloy was used here. The 2D model, lying on the surface of welded sheets, was used. Because of the models symmetry only  $\frac{1}{2}$  of the surface was calculated.

## 2. The numerical research

The bases of the FEM calculations are shown in [1,6]. The calculations were done in two phases, as uncoupled thermal and mechanical calculations. The scheme is shown in Fig.1.

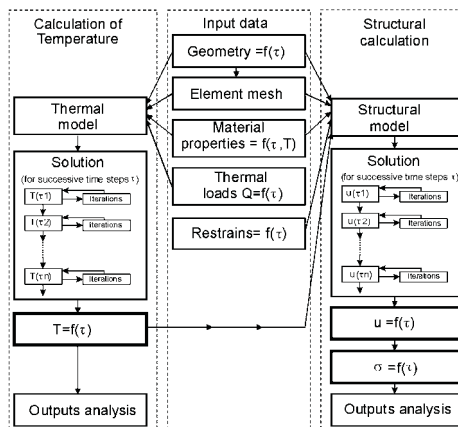


Fig. 1. Schematic diagram of uncoupled thermal-structural calculations [6]

The correct calculations are possible (especially for deformations and stresses) only with the use of non-linear, dependent on the temperature physical material properties (Fig.2)[1,2,6,8]. The material properties are dependent also on deformation. Here used properties are elastic-plastic, with isotropic hardening. The process of looking for the FEM solution is iterative (Fig. 1). The modelling welding process lasted for 10.3 s, with cooling time (until 800 s). At this time heating (loading) and cooling of models occurred. The position of the heat source was changing in following time steps. This way the “step by step” technique was used [1,6]. The results of the step (1) were necessary for the calculation of the step “2”, results of the step “2” will be necessary for the calculation of the step “3”, etc. until last step. Both of above processes strongly (factor  $10^5$ ) lengthen the process of solving the problem.

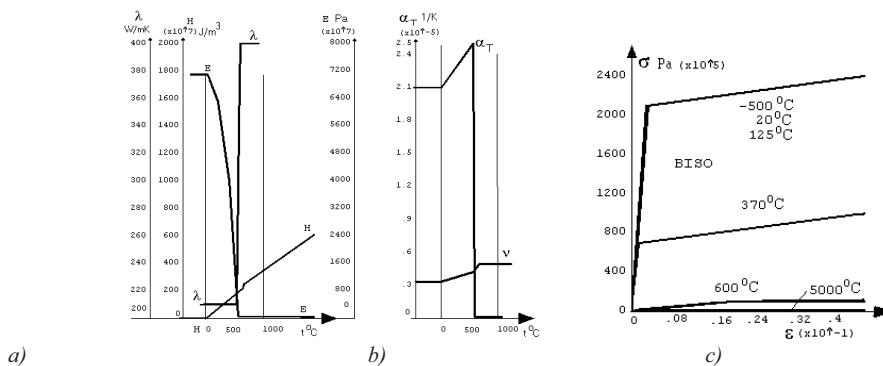


Fig. 2. Properties of the aluminium alloy, as function of the temperature. a) Specific enthalpy and thermal conductivity  $\lambda$ , b) Elastic modul  $E$ , Poisson ratio  $\nu$ , thermal dilatation  $\alpha_T$ , c) yield stress  $R_e$ , hardening modul  $E_T$ , BISO-Bilinear ISotropic hardening[1,2,3,6]

The full 3D calculations require very efficient computers. The 2D model was then used, lying on the surface of welded sheets. The aim of it was the best possible formulation of welding physics. For example on the 2D geometry, the higher perpendicular thickness of grain and root of weld was declared. Because of the models symmetry only  $\frac{1}{2}$  of the surface was calculated. The appropriate boundary conditions were used. This way the time of the calculations was shortened. Finite elements were used from the library of the program ANSYS13: SHELL57 in thermal calculations and PLANE42 in the structural calculations. 1337 elements with 1430 nodes were used. The mesh of the elements was shown in Fig.3. The size of elements is smaller near the welding lines, because of existing here high gradients (of degrees of freedom, eq. temperature or deformation).

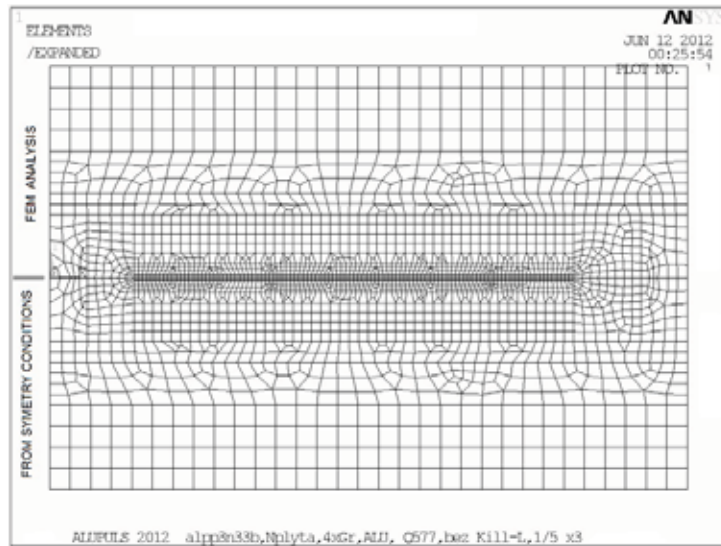


Fig. 3. Finite element mesh

Distributed, volume heat source (suggested by Goldak, [3], for MIG/MAG) was moving along the line of the weld. There were welds in the place of grooves. It happened because of completing the model by the previously removed finite elements from model ("killed"). On both surfaces (upper and bottom) the loss of heat through convection was taken into account. The convection near the weld was intensified to taken into account the heat radiation.

In the analysis different type of pulse was used. One single period of current pulse was all the time 0,5 s. This time was divided into 5 equal sub-periods. Except one, non-pulsed analysis, the heat source (corresponding to current of welding arc) was switched on for some sub-periods. The initial power of heat source ( $Q_0=3.4$  kW) was multiplied by factor  $D=1$  or 2 or 3 (Table 1 and Fig.4).

Tab. 1. Calculated residual stress (maximum)

| No | Power source<br>( $Q=D Q_0$ ) | Pulsation of arc power<br>during 0,5s period, s | Residual stress ( 800 s), MPa |              |             |
|----|-------------------------------|---|-------------------------------|--------------|-------------|
|    |                               |   | Huber-Misses                  | longitudinal | transverse  |
| 1  | $2 Q_0$                       | 0,3   | 0 +250                        | -151 / +283  | -198 / +158 |
| 2  | $Q_0$                         | 0,5   | 0 +245                        | -117 / +272  | -197 / +160 |
| 3  | $Q_0$                         | 0,4   | 0 +246                        | -91 / +265   | -187 / +164 |
| 4  | $2 Q_0$                       | 0,2   | 0 +245                        | -98 / +263   | -193 / +175 |
| 5  | $Q_0$                         | 0,3   | 0 +246                        | -66 / +264   | -183 / +183 |
| 6  | $3 Q_0$                       | 0,1   | 0 +252                        | -80 / +261   | -183 / +193 |
| 7  | $Q_0$                         | 0,2   | 0 +230                        | -42 / +258   | -146 / +195 |
| 8  | $2 Q_0$                       | 0,1   | 0 +260                        | -73 / +275   | -186 / +203 |
| 9  | $Q$                           | 0,1   | 0 +247                        | -58 / +274   | -173 / +214 |

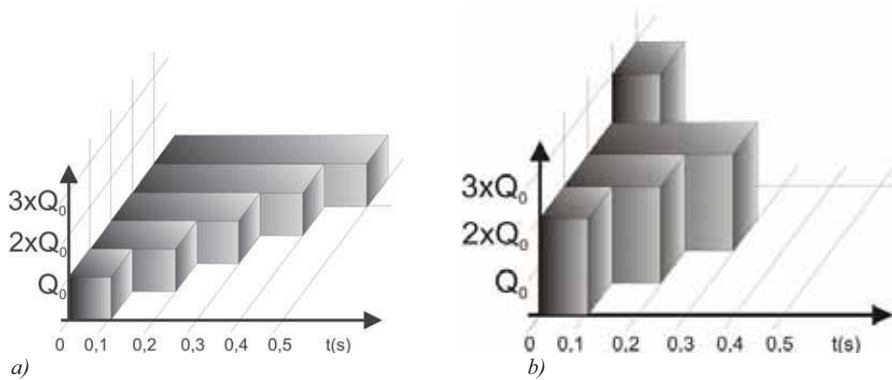


Fig. 4 Scheme of arc pulsation from tab.1 : a) for 9,7,5,3,2 , b) for 8,4,1,6.

Distributed volume heat source was moving along the line of the weld. On both surfaces the convection heat loss was set. The calculation was done in hundreds of time steps. In Fig. 5 example results, one of calculated temperature field, are shown.

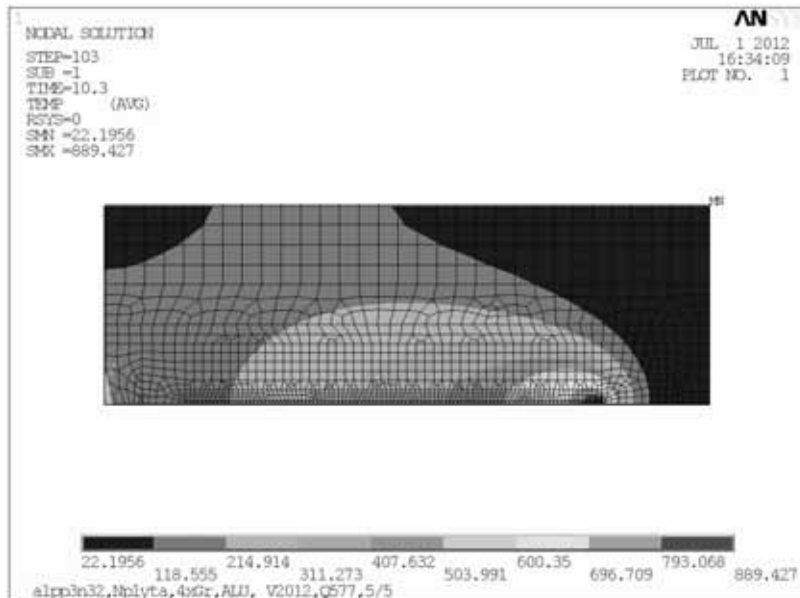


Fig. 5. Calculated temperature field, [ $^{\circ}\text{C}$ ], at time  $t=10.3$  s.

Results from temperature analysis were used in stress calculation. Elements type and material properties were changed to structural. Transient and residual stresses are calculated. In Fig. 6 are shown residual stresses for constant current arc analysis and in Fig.7 for pulsed current arc analysis.

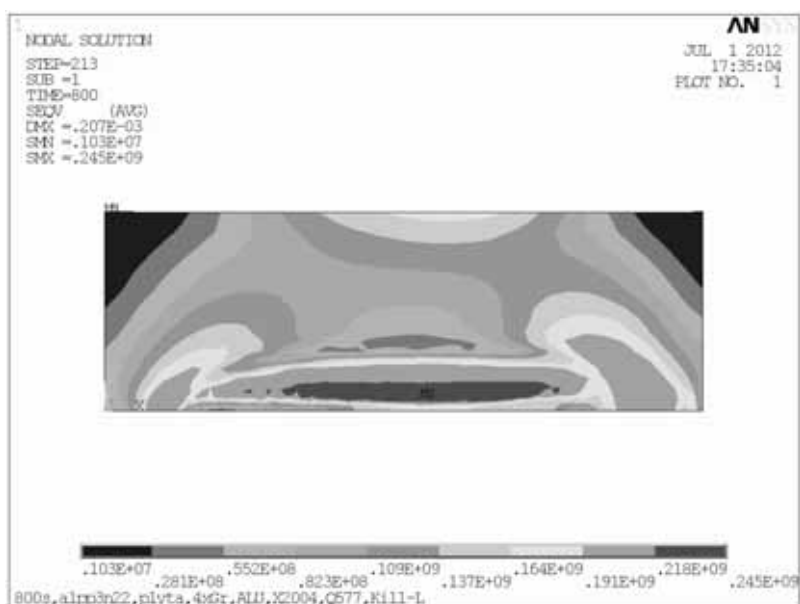


Fig. 6. Calculated residual stress (reduced von Misses) Pa, constant current arc welding (Tab.1 p.2)

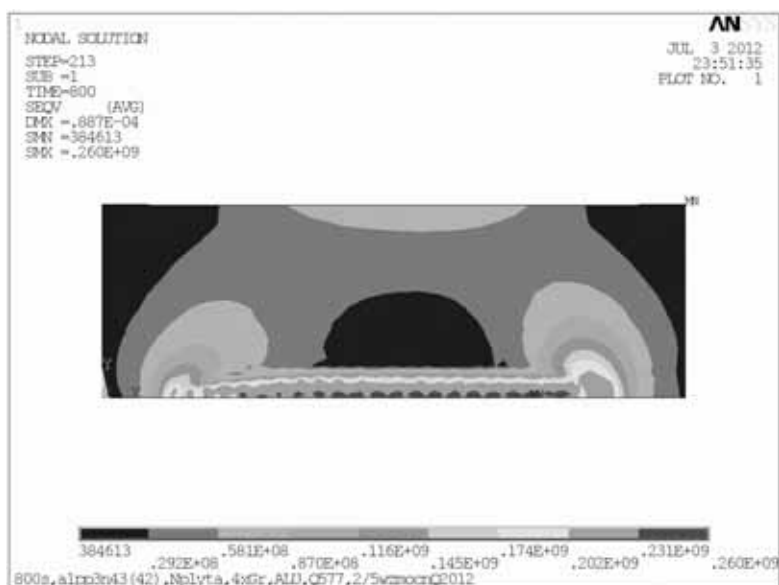


Fig. 7. Calculated residual stress (reduced Huber-Mises) Pa, pulsed current arc welding (see Tab.1 p.6)

The results are presented in Table 1. Here are show the maximum of longitudinal, transverse and reduced (Huber-Mises) residual stresses after many pulsed and constant arc welding.

The stability of solution was weak because of often, rapidly activation and deactivation of heat source [5]. The FEM program ANSYS was used.

### 3. Observations and conclusions

- 3.1 The results presented in Table 1 and in Fig.6 show that some residual stresses after pulsed arc welding were greater as after constant arc welding.
- 3.2 The maximum of tensile stresses were concentrated at small, perpetual areas.
- 3.3 These areas are too small for experimental measuring, but together significantly sufficient for crack propagation or local stress corrosion.
- 3.4 FEM is suitable for the calculation of the residual and transient welding stress.
- 3.5 The application of frequently met program ANSYS makes possible to practically use the suggested method of calculations.
- 3.6 Values of transient residual stresses are very difficult to obtain in experiment, and can be very useful. The use of FEM is very reasonable and effective.
- 3.7 Residual stresses were the greatest after spot-weld pulsed arc welding (Table 1 pos.9).

### References

- [1] Argyris, J.H., Szimmat J., Willam K.J., *Finite Element Analysis of Arc-welding Process*. Numerical Methods in Heat Transfer, 1985.vol. III.
- [2] Goldak J. et al., *Computer Modeling of Heat Flow in Welds*. Metallurgical Transactions B. 1986, nr 9, s 587-600.
- [3] Radaj D., *Heat effects of welding*, Springer Verlag,Berlin,1992.
- [4] Ranatowski E., *Elementy fizyki spajania metali*, Wyd. ATR Bydgoszcz, 1999.
- [5] Frewin M.R., Scott D.A., *Finite element model of pulsed laser welding*, Welding Research Supplement, I 1999,p. 15s-21s.
- [6] Skibicki A., *Identyfikacja stanu termicznych i mechanicznych skutków procesu spawania wybranych elementów z uwzględnieniem metod numerycznych*, Doctor's thesis. ATR Bydgoszcz. Wydział Mechaniczny 1998.
- [7] Skibicki A., *Numeryczna ocena wpływu pulsacji łuku na naprężenia pospawalnicze w stopach aluminium*. Materiały i Technologie. Roczniki Naukowe PTM. Nr 3 (3), str. 213 ÷ 216. 2005
- [8] Vishnu, R.P.,Easterling, K.E., *Phenomenological modeling of heat flow and microstructural hanges in pulsed GTA welds in a quenched and tempered steel*. Mathematical Modeling of weld Phenomena.MP,p.241-270,London,1993.



## THE INFLUENCE OF BURNISHING ON SURFACE TEXTURE OF REGENERATIVE Ni-Al-15%Al<sub>2</sub>O<sub>3</sub> PLASMA SPRAYED COATINGS

Robert Starosta

Gdynia Maritime University, Department of Marine Maintenance  
Morska Street 81-87, 81-225 Gdynia, Poland  
tel. +48 58 6901249, fax +48 58 6901399  
e-mail: starosta@am.gdynia.pl

### Abstract

The purpose of this study was the selection of roller- burnishing parameters of surface Ni-Al-15%Al<sub>2</sub>O<sub>3</sub> composite coatings obtained by "PN 120" plasma torch. Coatings with low surface roughness could be applied as layers increase the service life of torque pumps shaft used on vessels in the sea water systems.

After turning, the average surface roughness of plasma sprayed Ni-5%Al-15%Al<sub>2</sub>O<sub>3</sub> coatings was  $R_a = 1.06 \mu\text{m}$ . Their average hardness was equal to the 272 HV 2. After pre-treatment, plasma sprayed Ni-Al- 15%Al<sub>2</sub>O<sub>3</sub> coatings were burnishing. Burnishing parameters were as follows:  $V_n=28,26 \text{ m/min}$ ,  $F_n=700\text{N}$ ,  $f_n=0,044 \text{ m/rev}$ . Burnishing reduces the surface roughness of coatings as compared to machining. After the plastic working, the  $R_a$  parameter was reduced to a value of  $0.77 \mu\text{m}$ . Total height of waviness profile of machined coatings was  $6.23 \mu\text{m}$ . After burnishing, the value of  $W_t$  decreased by  $0.22 \mu\text{m}$ , to the value of  $6.01 \mu\text{m}$ . Studies burnished surface topography of coatings of Ni-5% Al15%Al<sub>2</sub>O<sub>3</sub> overlaid by "PN 120" torch revealed the presence of defects stereometric structure. There are the spalling. After plastic working of plasma coatings, decrease of parameters of the material ratio curve values were observed. For example, the reduced peak height of cut coatings were  $1.11 \mu\text{m}$ , after burnishing  $R_{pk}$  value fell to  $0.64 \mu\text{m}$ .

**Keywords:** plasma spraying, burnishing, Ni-Al-15%Al<sub>2</sub>O<sub>3</sub> coatings, regenerative coatings, torque pump

### 1. Introduction

Use of machines and equipments is associated with wear of machine parts by a process of corrosion, tribological and fatigue. This forces a periodical survey and verification of dimensional, sometimes replacement or regeneration of worn parts. The processes of wear can be reduced by shaping an appropriate surface layer of machine parts or applying coatings. In the construction of machines are commonly used electrolytic chromium coatings, cladded layer of stellite or nimonic alloys and chemical Ni-P coatings. Flame sprayed coatings can meet the performance requirements and extend the life of machine parts [1-3].

Plasma and flame sprayed coatings are characterized by porosity, oxide inclusions presence and large real area of surface. In order to obtain adequate surface roughness coatings must be applied finishing. For this purpose, the turning and grinding are used. In the paper a burnishing to finishing thermal sprayed coatings was proposed. In the literature found few data on the burnishing processes of thermal sprayed coatings. Burnishing is not used during the processing of thermally sprayed coatings, as is commonly believed that this technology causes damage to

coatings. Low susceptibility of coatings to the surface plastic treatment arises from several reasons. These include:

- a) low adhesion of coatings to the substrate,
- b) high tensile internal stress,
- c) embrittlement of coatings resulting from the presence of "in situ" oxides and the pore in the structure.

However, due to more modern torches technology for thermal spraying, the adhesion improvement and oxidation reduction of the coating material are observed. This is due to obtain the higher speeds the movement of particles in the stream of sprayed.

Franzen [4, 5] proposes the use of burnishing to forming of geometric structure of coatings WC-Fe (50% tungsten carbide) obtained by arc spraying and WC-Co coatings imposed by supersonic spraying (HVOF). There are used as a coating to increase durability of press-forming dies. Efforts are also trying to obtain the relevant surface properties of thermal sprayed coatings by rolling and pressing. Plastic working of coatings based on nickel (Ni-Al, NiAl and Ni<sub>3</sub>Al) allowed to reduce the roughness without loss of its adhesion [6]. The Szczepanik [7, 8] proposes to use burnishing process as a finishing treatment and forming of Al-SiC composites sinters. After the surface plastic treatment  $R_a = 0.12 \div 0.75 \mu\text{m}$  surface roughness were obtained.

Burnishing may also be used for surface treatment of materials prior to application of galvanic coatings, thermal sprayed and clad. Nadasi [9] proposed the use of rolling of coatings to reduce their porosity.

In the articles [10], the use of burnishing to the surface finishing flame sprayed coatings are proposed. The Ni-5%Al coatings were studied. Coatings were deposited by oxy-acetylene „Roto-Teck 80” torch. Finishing allowed obtaining a surface with small roughness for both types of coatings. Arithmetic mean roughness value of the surface alloy coatings was  $R_a = 0.27 \mu\text{m}$ . Influence of burnishing process parameters on the value of roughness reduction index ( $K_{Ra}$ ) present the regression equation (1):

$$K_{Ra} = -0,03V_n - 3,6f_n + 0,013F_n - 3,2 \pm 1,6, \quad (1)$$

where:

$V_n$  - burnishing speed, m/min,

$f_n$  - feed, mm/rev,

$F_n$  - burnishing force, N,

The lowest value of surface roughness of Ni-5%Al coating were obtained, when the following parameters burnishing was used: burnishing force  $F_n = 1100 \text{ N}$ , feed  $f_n = 0.08 \text{ mm/rev}$ , burnishing speed  $V_n = 28.26 \text{ m/min}$ . It was found that the greatest influence on reducing the roughness of the surface coating has force burnishing. The greater the forces used during the burnishing operation, the arithmetic mean roughness value  $R_a$  is lower. Feed rate of roller is inversely proportional effect on the coatings surface roughness. Studies demonstrated a statistically insignificant effect of burnishing speed on surface roughness [10].

The roller-burnishing influences not only on the reduction of surface roughness, but also on strain hardening of the processed surface. The largest influence on the hardness of the coatings has burnishing speed. The relationship between these variables is inversely proportional. The least influences on the strengthening have the feed. When the feed is a smaller the coating surface hardness is higher. On the strain hardening is also influenced by the force of burnishing. The increase in the value of the burnishing force causes an increase in hardness of the coatings. The operation of burnishing caused an increase in the hardness about 20% for Ni-Al coatings [10].

In this article the results of measurements of surface coatings roughness after the plastic working are presented. Coatings were obtained by plasma spraying method, using the "PN-120". Coatings obtained using plasmatron should be characterized by lower porosity and the less numbers of interphases oxide inclusions from the layers obtained by "RotoTeck 80".

The purpose of this study was the selection of roller- burnishing parameters of surface Ni-5%Al - 15%Al<sub>2</sub>O<sub>3</sub> coatings obtained by "PN-120" plasmatron. Coatings with low surface roughness could be applied as layers increase the service life of torque pumps shaft used on vessels in the sea water systems.

## 2. Preparation of pivots for burnishing

The coatings were sprayed on steel shafts pivots (X5CrNi 18-10) with diameter  $\phi = 40$  mm. To increase the adhesion of the coatings, the pivots were threaded. For spraying a "PN 120 " torch was used. Two kind of material powders were used, a) ProXon 21021 (Ni- 93.45%, Al-5%, B-0.8%, Fe-0.34%, Cr-0.18%, Si-0.15%, C-0.08%) and b) MetaCeram 28020 (Al<sub>2</sub>O<sub>3</sub>-97,7%, TiO<sub>2</sub> - 2,2%, SiO<sub>2</sub>- 0,1%). The powders made by Castolin. The 15% volume fraction of powder MetaCeram 28020 in coating material was used

The following parameters of plasma spraying have been applied:

- argon pressure: 0,35 MPa,
- the distance of the nozzle from the surface : 70 -100 mm,
- current: 450 ÷ 600 A,
- voltage arc internal: 47 ÷ 60V.

After spraying, the coating was subjected to initial treatment (turning) in order to reduce shape (roundness and cylindricity) deviations of the pivots shafts.

Ni-5%Al-15%Al<sub>2</sub>O<sub>3</sub> alloy coatings were machining by means of trigon inserts. Its catalogue number is GC 3210 (Sandvig Coromant) [11]. GC 3210 is a material based on tungsten carbide with a supplement of titanium nitride, covered with a TiN coating obtained by CVD method. In the DWLNRL-2525M08 holder a WMNG 080408-KM insert was mounted. Insert and the holder was manufactured by Sandvik Coromant. The geometry of the cutting tool, takes into account the insert and tool holder are follows:

- cutting inserts angle –  $\beta = 80^\circ$ ,
- approach angle –  $\kappa_r = 95^\circ$ ,
- rake angle –  $\gamma = - 6^\circ$ ,
- clearance angle –  $\alpha = 6^\circ$ ,
- nose radius –  $r_e = 0.8$  mm,

Turning parameters were used:

- cutting speed –  $V_c = 100$  m/min,
- feed rate  $f = 0.06$  mm/rev ,
- cutting depth  $a_p = 0,1$  mm.

## 3. Methodology of research

The burnishing process was conducted with a one-roller Yamato SRMD burnisher. The application parameters of the technological process of surface plastic treatment are presented in tab. 1. We decided upon an assessment of the impact of the burnishing on the surface roughness of the coatings by analyzing three factors associated with the operation – i.e.: pressure force  $F_n$ , speed of burnishing  $V_n$ , and feed  $f_n$ . We've omitted the variables concerning the type of material (plasticity border, extension) and the tools (radius of rounding up of the burnishing element, surface roughness of the burnishing element).



Fig.1.The one-roller Yamato SRMD burnisher

Tab. 1. Parameters of burnishing process

| Parameter                |          | Value |
|--------------------------|----------|-------|
| Burnishing force - $F_n$ | [N]      | 700   |
| Burnishing speed - $V_n$ | [m/min]  | 28.26 |
| Feed - $f_n$             | [mm/rev] | 0.044 |

Surface roughness and topography were measured with a profilometer HOMMEL TESTER T1000. The traverse length of the roughness measurement was 4.8 mm, and the sampling length was 0.8 mm. On the basis of the results achieved, the surface  $K_{Ra}$  roughness reduction index was defined:

$$K_{Ra} = \frac{Ra'}{Ra} \quad (1)$$

where:

$K_{Ra}$ - roughness reduction index,

$Ra'$  - coating surface roughness after cutting,

$Ra$  - surface roughness material after surface plastic processing.

The hardness measurement was performed by means of Vickers method with the use of FM-800 device, at thrust force amounting to 20 N. On the basis of the results achieved, the relative degree of hardness  $S_u$  was determined:

$$S_u = \frac{HV_2 - HV_1}{HV_1} 100\% \quad (2)$$

where:

$S_u$  - relative degree of strain hardening,

$HV_1$  - coating hardness before burnishing,

$HV_2$  - coating hardness after surface plastic treatment.

#### 4. Results

After turning, the average surface roughness of coatings of Ni-Al-15%Al<sub>2</sub>O<sub>3</sub> plasma sprayed was  $R_a = 1.06 \mu m$ . Average hardness equaled 272 HV<sub>2</sub>. Before machining, plasma sprayed alloy coatings were characterized by hardness equal 223 HV<sub>2</sub>. There is strain hardening after machining of coatings was observed. Fig. 2 and tab. 2 present the results of measurements of the parameters characterizing the geometric structure of the alloy coatings sprayed using the plasmatron, both after turning and burnishing. Burnishing allows get a surface which is

characterized by a lower surface roughness compared to the turning process. After the plastic surface treatment the  $R_a$  parameter was reduced to a value of  $0.77 \mu\text{m}$ . Roughness reduction index ( $K_{Ra}$ ) equaled to 1.38. Processing tool SRMD contributes to nearly 30 percent reduce the surface roughness of plasma sprayed Ni-Al-15%Al<sub>2</sub>O<sub>3</sub> coatings.

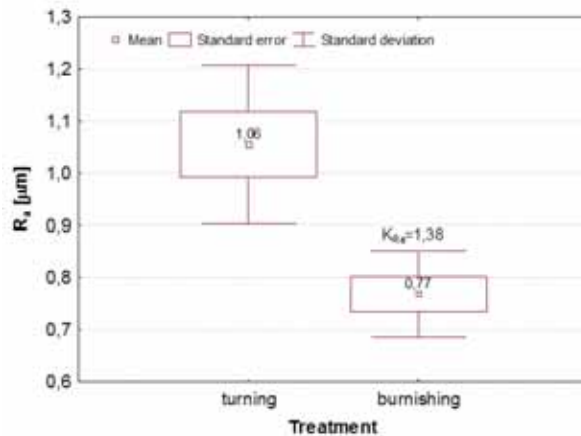


Fig. 2. Effect of treatment on  $R_a$  roughness parameter of surface Ni-Al-15%Al<sub>2</sub>O<sub>3</sub> coatings

Tab. 1. Results of basic statistical analysis of roughness ( $R_t$ ,  $R_z$ ,  $R_{Sm}$ ,  $R_{sk}$ ,  $R_{mr(50\%)}$ ), waviness ( $W_t$ ) and material ratio ( $R_{pk}$ ,  $R_k$ ,  $R_{vk}$ ) parameters of Ni-5%Al-15%Al<sub>2</sub>O<sub>3</sub> coatings obtained by plasma spraying

| parameters  | number<br>of measurements | mean  | min.  | max   | s.d   | standard<br>error |
|---|---------------------------|-------|-------|-------|-------|-------------------|
| after turning   |                           |       |       |       |       |                   |
| R <sub>t</sub> [μm]   | 6                         | 16,41 | 13,89 | 19,86 | 2,23  | 0,91              |
| R <sub>z</sub> [μm]   |                           | 8,98  | 7,55  | 10,45 | 1,24  | 0,51              |
| R <sub>Sm</sub> [mm]  |                           | 0,08  | 0,06  | 0,095 | 0,015 | 0,006             |
| R <sub>sk</sub>   |                           | -1,03 | -1,58 | -0,47 | 0,37  | 0,15              |
| W <sub>t</sub> [μm]   |                           | 6,23  | 4,31  | 7,84  | 1,35  | 0,55              |
| R <sub>pk</sub> [μm]  |                           | 1,11  | 0,87  | 1,26  | 0,15  | 0,06              |
| R <sub>k</sub> [μm]   |                           | 2,4   | 2     | 3,19  | 0,41  | 0,17              |
| R <sub>vk</sub> [μm]  |                           | 2,27  | 1,54  | 3,47  | 0,67  | 0,27              |
| R <sub>mr (50%)</sub> [μm]  |                           | 3,51  | 2,81  | 3,9   | 0,4   | 0,16              |
| After burnishing: V <sub>n</sub> =28,26 m/min, F <sub>n</sub> =700N, f <sub>n</sub> =0,044 mm/obr |                           |       |       |       |       |                   |
| R <sub>t</sub> [μm]   | 6                         | 12,28 | 10,06 | 18,01 | 2,9   | 1,18              |
| R <sub>z</sub> [μm]   |                           | 6,31  | 5,42  | 7,63  | 0,888 | 0,361             |
| R <sub>Sm</sub> [mm]  |                           | 0,043 | 0,038 | 0,051 | 0,005 | 0,002             |
| R <sub>sk</sub>   |                           | -4,15 | -6,06 | -2,33 | 1,85  | 0,69              |
| W <sub>t</sub> [μm]   |                           | 6,01  | 3,36  | 8,55  | 2,15  | 0,88              |
| R <sub>pk</sub> [μm]  |                           | 0,64  | 0,26  | 1,39  | 0,4   | 0,16              |
| R <sub>k</sub> [μm]   |                           | 1,45  | 0,93  | 2,32  | 0,58  | 0,24              |
| R <sub>vk</sub> [μm]  |                           | 2,04  | 0,98  | 4,18  | 1,04  | 0,42              |
| R <sub>mr (50%)</sub> [μm]  |                           | 2,78  | 2,15  | 3,57  | 0,54  | 0,22              |

Average value of total height of roughness profile ( $R_t$ ) of burnished coatings was equal to  $12.29\text{ }\mu\text{m}$  and  $16.41\text{ }\mu\text{m}$  after turning. Maximum height of roughness profile ( $R_z$ ) value the after plastic surface treatment decreased from  $8.98\text{ }\mu\text{m}$  to  $6.31\text{ }\mu\text{m}$ . The difference is only  $2,67\text{ }\mu\text{m}$ . Value mean of total height of waviness profile ( $W_t$ ) of turned coatings was  $6.23\text{ }\mu\text{m}$ . After burnishing the value of  $W_t$  decreased by  $0.22\text{ }\mu\text{m}$  to the value of  $6.01\text{ }\mu\text{m}$ . Statistical analysis (nonparametric tests for two dependent variables): Wilcoxon's test and sign test showed that the differences between the averages of the total height of waviness profile for both coatings of finishing processes, for a given level of significance  $\alpha = 0.05$ , is not statistically significant. The important observation is that the  $R_z$  takes the average parameter values greater than  $W_t$ . Thus, in this case the leakproofness condition is fulfilled.

There reduction of material ratio curve parameters was observed. For example, the reduced peak height of machined coatings was  $1.11\text{ }\mu\text{m}$ , and the after plastic surface treatment of  $R_{pk}$  value decreased to  $0.64\text{ }\mu\text{m}$ . Core roughness depth of machined coatings was  $2.27\text{ }\mu\text{m}$ . The average value of the  $R_k$  parameter of coatings after plastic surface treatment was  $2.04\text{ }\mu\text{m}$ .

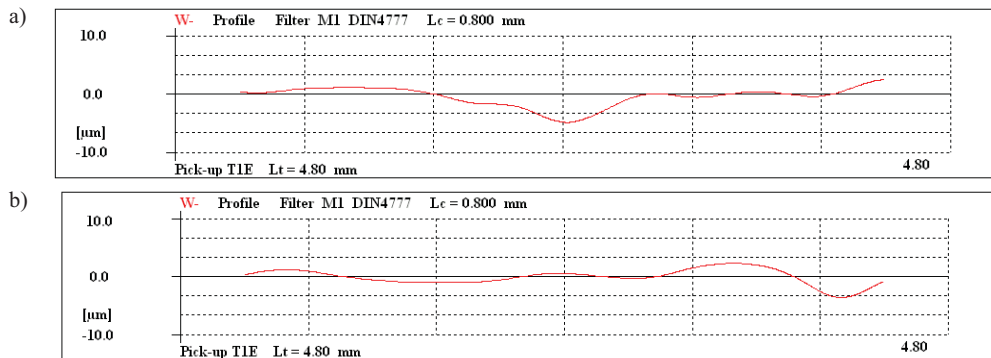


Fig. 3. Examples of waviness profiles of Ni-Al-15%Al<sub>2</sub>O<sub>3</sub> coatings obtained by plasma spraying: a) the turned ( $W_t = 7.41\text{ }\mu\text{m}$ ), b) the burnished ( $W_t = 7.13\text{ }\mu\text{m}$ ),

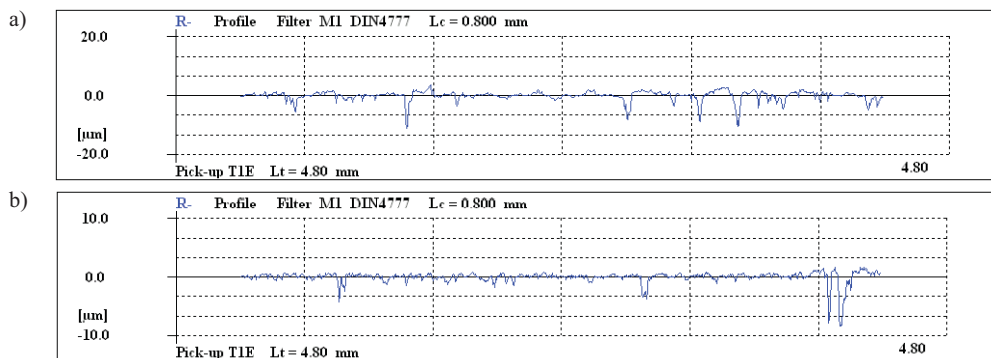


Fig. 4. Examples of roughness profiles of Ni-Al-15%Al<sub>2</sub>O<sub>3</sub> coatings obtained by plasma spraying: a) the turned ( $R_a = 1.02\text{ }\mu\text{m}$ ), b) the burnished ( $R_a = 0,71\text{ }\mu\text{m}$ ),

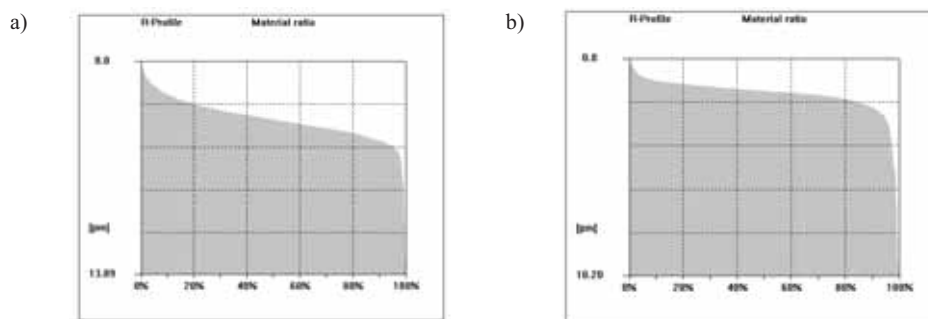


Fig. 5. Examples of material ratio curves of the surface Ni-Al-15%Al<sub>2</sub>O<sub>3</sub> coatings obtained by plasma spraying: a) the turned, b) the burnished

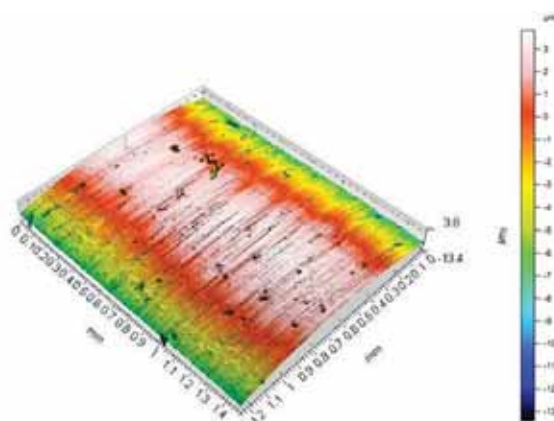


Fig. 6. Unfiltered topography of the burnished surface of plasma sprayed Ni-Al-15%Al<sub>2</sub>O<sub>3</sub> coatings

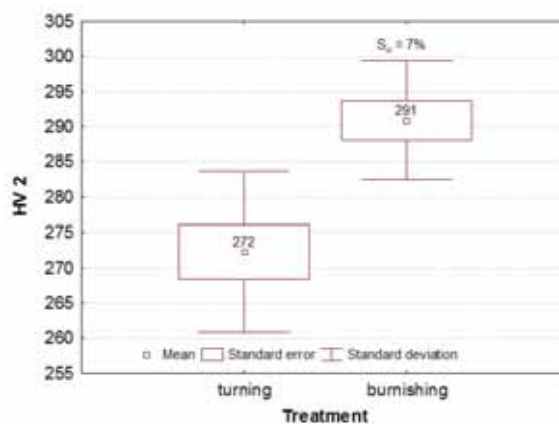


Fig. 7. Effect of treatment on hardness and relative degree of strain hardening (S<sub>0</sub>) of surface Ni-Al-15%Al<sub>2</sub>O<sub>3</sub> coatings

In figures 3, 4 and 5 examples of profiles of surface roughness, waviness and material ratio curves of Ni-Al-15%Al<sub>2</sub>O<sub>3</sub> coatings plasma sprayed by PN120 torch are presented. Studies burnished surface topography of coatings of Ni-Al-15%Al<sub>2</sub>O<sub>3</sub> overlaid by "PN 120" torch revealed the presence of defects stereometric structure. There are the spalling (fig. 6). The observed spalling on the surface of alloy coatings sprayed by plasmatron were more limited from the same geometric structure defects on the surface of coatings obtained by flame spraying methods [10].

On figure 6 presented the results of hardness measurement and estimation of the relative degree of strain hardening of plasma Ni-Al-15%Al<sub>2</sub>O<sub>3</sub> coatings. The hardness of these coatings after machining was 272 HV2. After burnishing their hardness increased to 291 HV2. Relative degree of strain hardening ( $S_u$ ) obtained a value of 7%.

## 5. Summary

- Burnishing can be used as finishing of plasma sprayed Ni-Al-15%Al<sub>2</sub>O<sub>3</sub> coatings .
- Applying to burnishing SRMD tool can be obtained to the coating surface roughness  $R_a = 0.77 \mu\text{m}$ . In comparison to the turned coatings is almost 30 percent less the  $R_a$  value ( $K_{Ra} = 1.38$ ).
- Burnished surface satisfies the tightness condition ( $W_t < R_z$ ).
- The surface structure, characterized by the material ratio curve, burnished coatings testified about: a) a small wear of shaft neck in time grinding in mated machine parts, b) large area of contact between the surface of journal with gland's packing.
- After burnishing, plasma-sprayed Ni-Al coatings can be used to regenerate journals mated water sealed gland in torque pumps (due to the surface texture).
- After burnishing, almost 7% strain hardening ( $S_u$ ) of Ni-Al -15%Al<sub>2</sub>O<sub>3</sub> coatings was observed

## References

- [1] Kung-Hsu, H., Ming-Chang, J., Ming-Der, G., *A study on the wear resistance characteristics of pulse electroforming Ni-P alloy coatings as plated*, Wear, Vol. 265, pp. 833-844, 2007.
- [2] Bolelli, G., Cannillo V., Lusvarghi L., Ricco S. *Mechanical and tribological properties of electrolytic hard chrome and HVOF-sprayed coatings*, Surface and Coatings Technology, Vol. 200, pp. 2995 – 3009, 2006.
- [3] DuraSpindle, Increasing performance, Information materials MAN B&W, 2005.
- [4] Franzen, V., Trompeter, M. Brosius, A., Tekkaya A. E., *Finishing of thermally sprayed tool coatings for sheet metal forming operations by roller burnishing*, Int J Mater Form, Vol. 3, pp. 147-150, 2010.
- [5] Franzen, V., Witulski, J., Brosius, A., Trompeter, M., Tekkaya, A.E., *Thermally sprayed coatings as effective tool surfaces in sheet metal forming applications*, Journal of Thermal Spray Technology, Vol. 20, pp. 939 -947, 2011.
- [6] Dyl, T., Starosta, R., Skoblik, R., *The effect of the unit pressure on the NiAl and Ni<sub>3</sub>Al intermetallic coatings selection parameters after plastic working*, Solid State Phenomena, Vol. 165, pp.19-24, 2010.

- [7] Szczepanik, S., *Przeróbka plastyczna materiałów spiekanych z proszków i kompozytów*, Uczelniane Wydawnictwa Naukowo-Dydaktyczne Akademii Górniczo-Hutniczej, Kraków 2003.
- [8] Szczepanik, S., Polowski, W., Czechowski, K., Wojtaszek, M., Krawiarz, J., *Badania możliwości zastosowania nagniatania tocznego do obróbki wykańczającej kompozytów Al-SiC*. Kompozyty, Vol. 7: 2, pp. 87-92, 2007.
- [9] Nadasi, E., *Nowoczesne metody metalizacji natryskowej*, Wydawnictwa Naukowo-Techniczne, Warszawa 1975.
- [10] Starosta, R., Wądołowski, D., *Wpływ nagniatania na wybrane własności powłok natryskiwanych metodą „ROTO-TECK”*. Zeszyty Naukowe. Akademia Marynarki Wojennej. Vol. 178A, pp. 275-280, 2009.
- [11] Sandvik Coromant. Katalog główny. Toczenie –frezowanie –wiercenie –wytaczanie -systemy narzędziowe, Sandviken, pp. A39-A40, 2007.

This study was a part of project no. N N504 303537, financed by Ministry of Science and Higher Education.





## ANALYTICAL-EXPERIMENTAL METHOD OF DETERMINING FATIGUE CHARACTERISTICS FOR DESIGN ELEMENTS

Przemysław Strzelecki\*, Janusz Sempruch\*\*

University of Technology and Life Sciences  
Faculty of Mechanical Engineering  
ul. Prof. S. Kaliskiego 7, 85-789 Bydgoszcz  
tel.: 693 897 581\*  
email: p.strzelecki@utp.edu.pl\*  
email: janusz.sempruch@utp.edu.pl\*\*

### Summary

*Frequently during the initial designing stage, one must use fatigue characteristics of the design element. Producing such a plot by making an experiment is not possible at most times. This paper suggests determining such characteristics based on the fatigue plot for the material. The assumptions of that method have been developed drawing on own experiment and experimental data presented in literature. The name 'analytical and experimental' assigned to the method proposed comes from the fact that it is based on the description of the fatigue properties of the material received experimentally and phenomenological properties received experimentally presented in literature. In order to verify the method proposed, a comparative plot was made for the experimental and analytical fatigue life. Based on the curve plotted, one can demonstrate that the fatigue life predicted according to own proposal range in the assumed scatter band. For the purpose of a comparison, developing the fatigue characteristics according to the FITNET method. As for this algorithm, it was found that the fatigue limit determined according to this method is much greater than the one received experimentally, which means that the method does not work for materials heavily sensitive to the effect of the notch, including e.g. material C45+C.*

**Key words:** high-cycle fatigue strength, fatigue curves, analytical methods of estimating Wöhler's curve.

### 1. Introduction

The designer, for an adequate dimensioning of a design element, must be provided with an adequate fatigue characteristics of this detail. Acquiring such experimental characteristics experimentally is time-consuming and costly. Often at the initial stage of the design, performing experiments used to acquire such characteristics is impossible.

With the above in mind, literature reports on many analytical methods to determine the approximate fatigue curve, e.g. [4] and [6]. Unfortunately there is no data on the possible error the designer can make using one of them. The attempt at verifying the above methods are given in e.g. [7,10,11,12].

This paper presents the proposal of determining the fatigue characteristics for design element based on the material characteristics. Additionally the FITNET method and the characteristics defined according to this algorithm for material C45+C.

The name 'analytical-experimental' used for the proposed method comes from the fact that it is based on the description of the material fatigue properties received experimentally and

phenomenological properties received experimentally, reported in literature.

## 2. Relationship between the fatigue characteristics of the material and a design element

Being exposed to the load variable in time, strength is of high importance, e.g. notch coefficient  $K_t$  defined as the ratio of the value of the maximum stress at the bottom of the notch to nominal stress. The value of that coefficient depends on the shape of the design element. As for the element with no change in the cross-section (e.g. smooth normative specimens) the value of the notch coefficient is  $\sim 1$ . As for the monotonic load, the effect of the changes in cross-section of the element on strength does not occur. It is common knowledge that the effect increases with the executed number of cycles until base number of cycles  $N_0$  is reached. In the publication [9] the author presents that it is possible to make an approximation stating that the effect of the notch coefficient and other factors disappears for  $10^3$  number of cycles, which is seen from the literature review involving the determination of the number of cycles at which the fatigue strength of the notched specimen and the smooth one is the same. The results are broken down in Table 1, showing that the range of variation of the number of cycles of the crossing of the curves for the notched specimens and smooth specimens ranges from  $1.15 \cdot 10^2$  to  $7.24 \cdot 10^3$ . Based on that range, it seems justifiable to assume the value of  $10^3$  cycles as the strength at which the notch effect disappears. Based on this assumption own method has been proposed to allow for determining fatigue characteristics of the design element based on the material characteristics. This proposal has been presented in the next item.

Table 1. Fatigue strength and fatigue life in the point of curves crossing for the material and the design element

| Material           | Source    | Slope coefficient for material $m$ | Notch coefficient $K_t$ | Slope coefficient for notched specimens $m_k$ | Number of cycles from the curves crossing | Strength value in the point of crossing $\sigma_p$ [MPa] | Ultimate strength $R_m$ [MPa] | Ratio $\sigma_p/R_m$ |
|--------------------|-----------|------------------------------------|-------------------------|---|---|--|-------------------------------|----------------------|
| 25CrMo4            | [9]       | 13.1                               | 2.16                    | 5.9   | 325                                       | 663  | 806                           | 0.823                |
| 25CrMo4            | [9]       | 13.1                               | 4.0                     | 4.5   | 181                                       | 693  | 806                           | 0.860                |
| 42CrMoS4           | [8]       | 14.0                               | 1.75                    | 5.55  | 3329                                      | 841  | 1100                          | 0.765                |
| 14CrMoV69          | [1]       | 16.1                               | 2.0                     | 4.5   | 1374                                      | 887  | 980                           | 0.905                |
| C45+C              | Own tests | 8.1                                | 2.2                     | 3.9   | 1068                                      | 775  | 826                           | 0.940                |
| C45+N              | [3]       | 11.0                               | 1.65                    | 4.56  | 7240                                      | 443  | 730                           | 0.607                |
| 39NiCrMo3          | [1]       | 8.2                                | 7.2                     | 4.8   | 484                                       | 884  | 995                           | 0.888                |
| En3B (C22E)        | [13]      | 19.7                               | 3.8                     | 3.75  | 4981                                      | 453  | 678                           | 0.668                |
| SUJ2 (100Cr6)      | [14]      | 21.5                               | 2.39                    | 9.0   | 465                                       | 1430   | 2241                          | 0.638                |
| 4140 (42CrMo4)     | [5]       | 13.7                               | 2.11                    | 6.3   | 115                                       | 970  | 1100                          | 0.882                |
| 4140 (42CrMo4)     | [5]       | 13.7                               | 5.03                    | 3.1   | 1565                                      | 802  | 1100                          | 0.729                |
| Low-carbon steel   | [2]       | 11.5                               | 2.5                     | 6.5   | 258                                       | 547  | 500                           | 1.094                |
| Low-carbon steel   | [2]       | 11.5                               | 2.9                     | 5.8   | 309                                       | 538  | 500                           | 1.077                |
| Range of variation |           |                                    |                         |   | 115-7240                                  |  |                               | 0.607-1.094          |

Additionally the table above presents the strength values in the point of crossing of experimental curves for smooth and notched specimens. Based on those values the ratios of strength in the point of crossing and tensile strength were calculated.

### 3. Method proposed

The method involves the determination of the points characteristic for the curve. Those are the point of crossing in the region of fatigue limit and the point limiting the range of limited fatigue life (the region of about  $10^3$  cycles).

The method proposed is based on plotting the fatigue curve for the material by making an experiment. Based on that characteristics, strength  $\sigma_3$  is determined for fatigue life of  $10^3$  number of cycles. Yet another step is determining fatigue limit for the notched element -  $Z_{Gk}$ . Next we plot the curve with two points showing coordinates  $(10^3, \sigma_3)$  and  $(10^6, Z_{Gk})$ . The schematic procedure is given in Fig. 1.

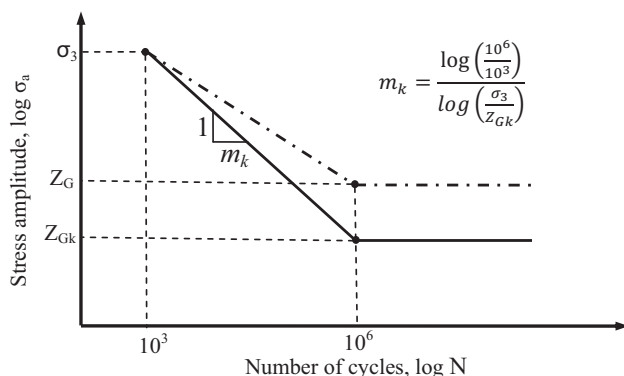


Fig. 1. Proposed method of determining the fatigue characteristics for design element (solid line) based on the fatigue characteristics of the material (dash and point line).

### 4. Method of determining the fatigue limit

The method of determining the fatigue limit for the material according to the FITNET method [6] involves multiplying tensile strength ( $R_m$ ) by coefficient  $f_{W,\sigma}$  dependent on the type of the material. The values of that coefficient are given in Table 2.

Table 2. Values of coefficient  $f_{W,\sigma}$  derived from [6]

| Material type                   | $f_{W,\sigma}$ |
|---------------------------------|----------------|
| Carburized steel                | 0.40           |
| Stainless steel                 | 0.40           |
| Forged steel                    | 0.40           |
| Cast steel                      | 0.34           |
| Steels other than above         | 0.45           |
| Sferoid cast-iron               | 0.34           |
| Malleable cast-iron             | 0.30           |
| Grey cast iron                  | 0.30           |
| Plastic-worked aluminium alloys | 0.30           |
| Cast aluminium alloys           | 0.30           |

For the notched elements, the fatigue limit for the material must be multiplied by coefficients: size  $K_d$ , surface roughness  $K_s$  and the operation of notch  $\eta$ . To determine the coefficient determined at the end, there must be calculated stress gradient at the bottom of the notch, according to the formula:

$$\chi = - \left. \frac{d\sigma_a}{dx} \right|_{x=0} \frac{1}{\sigma_{a,(x=0)}} \quad (1)$$

Then we calculate coefficient  $\eta$  according to the formula:

$$\eta = \begin{cases} 1 + \chi \cdot \text{mm} \cdot 10^{-\left[a_G - 0.5 + \frac{R_m}{b_G \text{MPa}}\right]} & \text{dla } \chi < 0.1 \text{mm}^{-1} \\ 1 + \chi \cdot \text{mm} \cdot 10^{-\left[a_G + \frac{R_m}{b_G \text{MPa}}\right]} & \text{dla } 0.1 < \chi < 1 \text{mm}^{-1} \\ 1 + \sqrt[4]{\chi} \cdot \text{mm} \cdot 10^{-\left[a_G + \frac{R_m}{b_G \text{MPa}}\right]} & \text{dla } \chi > 1 \text{mm}^{-1} \end{cases} \quad (2)$$

Coefficients  $a_G$  and  $b_G$  are read from the table below.

Table 3. Values of coefficients  $a_G$  and  $b_G$

| Material                        | $a_G$ | $b_G$ |
|---------------------------------|-------|-------|
| Stainless steel                 | 0.4   | 2400  |
| Other steels                    | 0.5   | 2700  |
| Cast steel                      | 0.25  | 2000  |
| Spheroidal cast iron            | 0.05  | 3200  |
| Malleable cast-iron             | -0,05 | 3200  |
| Grey cast iron                  | -0,05 | 3200  |
| Plastic-worked aluminium alloys | 0.05  | 850   |
| Cast aluminium alloys           | -0.05 | 3200  |

For material C45+N (the data derived from publication [3]) tested using the specimens showing coefficient  $K_t$  equal 1.65 the fatigue limit was defined according to the FITNET method. The material fatigue limit value determined was 292 MPa, calculated by multiplying tensile strength (730 MPa) by coefficient  $f_{W,\sigma}$  equal 0.45. Then there was calculated the value of gradient of stress which was  $2.4 \text{ mm}^{-1}$ . By substituting the value calculated to formula 2 we receive value of coefficient  $\eta$  equal 0.781. The fatigue limit of the notched specimen was received by multiplying the material fatigue limit by coefficient  $\eta$  and the value of 230 MPa was received. The value received differs considerably from the value received experimentally being 165 MPa considerably. With the experimental values reported, it was found that a given material shows a high value of the coefficient of material sensitivity to the effect of notch  $\eta_k$  which assumes values from 0 to 1. This coefficient is used to calculate the coefficient of the operation of notch  $K_f$  (defined as the ratio of material fatigue limit  $Z_G$  and the fatigue limit of the notched specimen  $Z_{Gk}$ ) expressed with the formula [3]:

$$K_f = 1 + \eta_k(K_t - 1), \quad (3)$$

For the material analysed, coefficient  $K_f$  when substituting  $\eta_k$  with value 1 we receive the value equal  $K_b$ , namely 1.65. Calculating the fatigue limit of the notched specimen, dividing the material fatigue limit  $Z_G$  by coefficient  $K_f$  we receive the value of 169.7 MPa (280 MPa/1.65). To provide the characteristics for the notched specimens from material C45+N according to own proposal, there was assumed the value of the fatigue limit equal 169.7 MPa.

Similar material properties was noted in material C45+C which has the same chemical composition as material C45+N, however, it is in another state of the treatment. The value of the fatigue limit for material C45+C according to the FITNET method was 330.4 MPa. As for the notched specimens with  $K_t$  equal 2.2 there was calculated the fatigue limit equal 224.7 MPa ( $R_m = 826$  MPa,  $\chi = 4.61 \text{ mm}^{-1}$ ,  $\eta = 0.77$ ). To define the fatigue limit for notched specimens applying coefficient  $K_f$  equal  $K_t$  we receive the value of 142.9 MPa (314.4 MPa / 2.2), which is closer to the experimental value of 139 MPa. To provide the characteristics according to the proposed algorithm, the fatigue limit for the notched specimens with material C45+C, the value of 142.9 MPa was assumed.

## 5. Method of verification

To verify the proposed method, there was made an experiment to determine fatigue properties of smooth and notched specimens of coefficient  $K_t$  equal 2.2 made from material C45+C. The curve is presented in Fig. 3 in which the red line stands for the results for notched specimen, while black line – for the results for smooth specimens.

With the points received from the experiment, it was possible to plot a curve to compare the experimental fatigue life with the estimated fatigue life (Fig. 4). The figure provides the black line for the situation when the experimental life equals the evaluated fatigue life (the desired situation) stand for the scatter band which was determined according to the following equations:

$$N_{pg} = s \cdot N_f \quad (4)$$

$$N_{pd} = s \cdot N_f \quad (5)$$

where:

$N_f$  – value of the fatigue life received experimentally,

$s$  – coefficient of the scatter band (there was assumed the value of 3),

$N_{pg}$  – fatigue life value for the upper interval of the scatter band,

$N_{pd}$  – value of fatigue life for the lower interval of the scatter band.

## 6. Results of the verification

Figs 2 and 3 presents fatigue curves received from the experiment for smooth and notched specimens and estimated curves according to the FITNET method and own proposal. Additionally Fig. 4 presents the curve to compare the fatigue life evaluated to the experimental fatigue life.

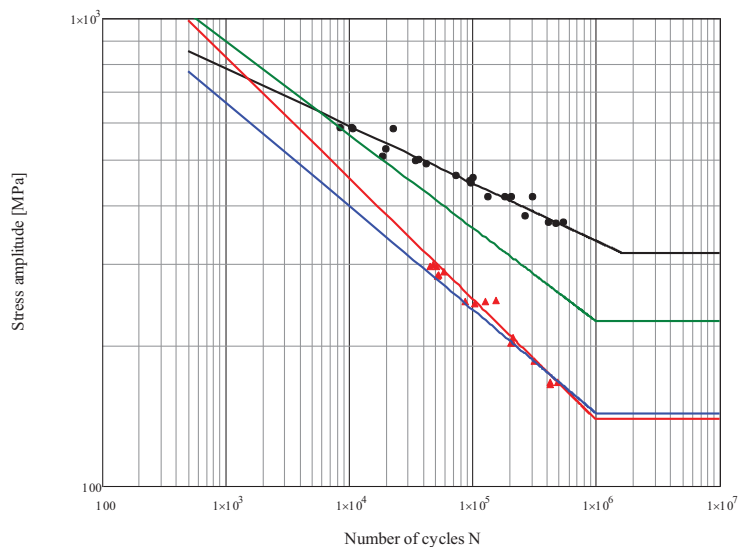


Fig. 2 Fatigue curve for steel C45+C – the black line is smooth, the red line – the circumferential notch  $K_t=2.2$ , green line stands for the green curve estimated according the FITNET method and blue line estimated according to own proposal

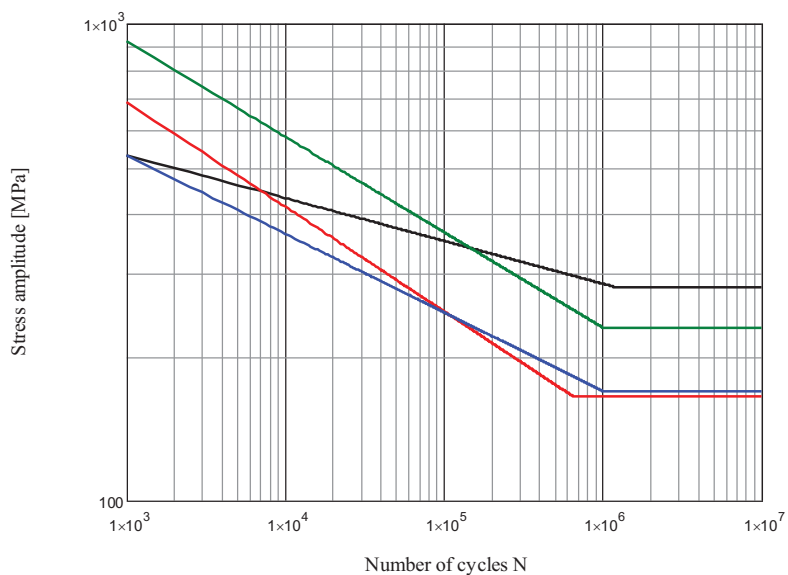


Fig. 3 Fatigue curve for steel C45+N– black line – smooth specimen [3], red line – the specimen with circumferential notch  $K_t=1.65$  [3], green line – the curve estimated according to the FITNET method and blue line estimated according to the own proposal

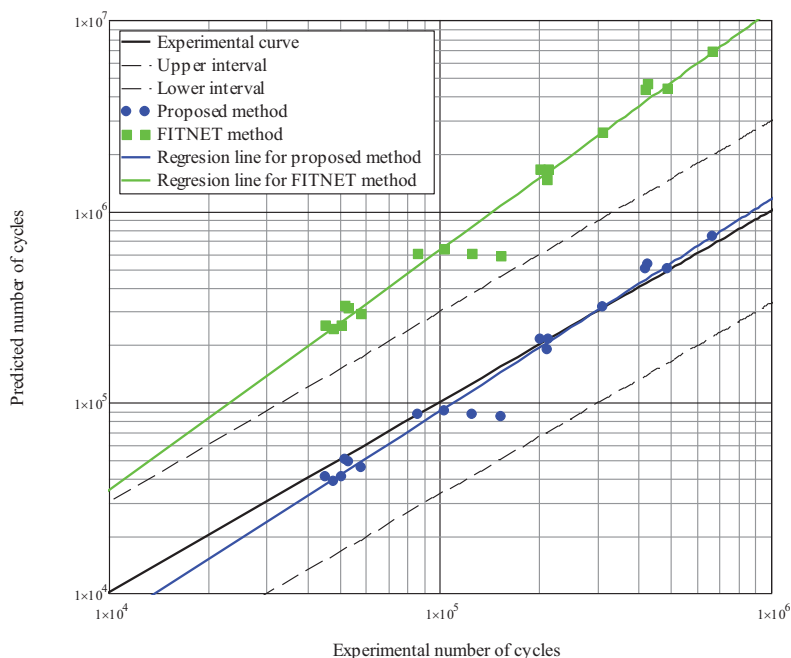


Fig. 4 Comparative curve for fatigue life received experimentally and with the estimated fatigue life according to the method proposed (blue colour) and the FITNET method (green colour)

## 7. Conclusions

Based on the curves plotted, one can state that the method of determining the fatigue limit according to the FITNET method results in a big error in the case of materials showing high sensitivity to the notch effect. Defining the characteristics for that group of materials can cause a high error in the fatigue life evaluation. Fig. 4 shows that the values estimated with that method are beyond the assumed scatter band, which means that the evaluating the fatigue life is over 3-fold of the experimental value.

As for determining the plot according to the method proposed where determining the fatigue limit the coefficient of the operation of the notch was used; it was assumed at the level equal to the notch coefficient. The characteristics provided are similar to the figure received experimentally. It is clearly visible in Fig. 4 where the points corresponding to the experimental fatigue life and the evaluated one fall within the assumed scatter band.

## Acknowledgement

The work has been co-financed by the European Union Social Fund, the state budget of Poland and the budget of the Kujawsko-Pomorskie Province as part of the project 'Krok w przyszłość – stypendia dla doktorantów', the 4<sup>th</sup> edition.

## Literature

- [1] Berto F., Lazzarin P. Yates J. R., *Multiaxial fatigue of V-notched steel specimens: a non-conventional application of the local energy method*, Fatigue & Fracture of Engineering Materials & Structures Vol. 34, Issue 11, 2011.
- [2] Qylafku G., Azari Z., Gjonaj M., Pluvinage G., On the fatigue failure and life prediction for notched specimens, Materials Science, Vol. 34, No. 5, 1998
- [3] Kocańda S., Szala J., *Podstawy obliczeń zmęczeniowych*, PWN, Warszawa, 1997.
- [4] Lee Yung-Li, Pan Jwo, Hathaway R. B., Barkey M. E., *Fatigue testing and analysis*, University of Alabama, Elsevier 2005.
- [5] Nathalie Limodin, Yves Verreman, Fatigue strength improvement of a 4140 steel by gas nitriding: Influence of notch severity, Materials Science and Engineering A 435–436 (2006) 460–467.
- [6] Neimitz A., Dzioba I., Graba M., Okrajni J., *Ocena wytrzymałości, trwałości i bezpieczeństwa pracy elementów konstrukcyjnych zawierających defekty*, Politechnika Świętokrzyska, Kielce 2008.
- [7] Pejkowski Ł., Skibicki D., *Analysis of accelerated methods for determination of fatigue curves*. Journal of Polish Cimac Selected problems of designing and operating technical systems Vol. 6 No 3; (2011). pp. 199-214.
- [8] Pyttel B., Schwerdt D., Berger Ch., *Fatigue strength and failure mechanisms in the VHCF-region for quenched and tempered steel 42CrMoS4 and consequences to fatigue design*, Procedia Engineering 2, 2010.
- [9] Schijve J., *Fatigue of structures and materials*, wyd. 2, Springer, 2009.
- [10] Sempruch J., Strzelecki P., *Error of fatigue life determination according to the FITNET method*. 17th International Conference Engineering Mechanics, 2011, pp. 531-534.
- [11] Strzelecki P., Sempruch J., *Modification of selected methods of rapid determination of fatigue characteristics in the range of limited fatigue life*, Journal of Polish Cimac Selected problems of designing and operating technical systems Vol. 6 No 3; 2011, pp. 289-296.
- [12] Strzelecki P., Sempruch J., *Verification of selected methods for rapid determination of Wöhler curve considering high-cycle fatigue*, Journal of Polish Cimac Selected problems of designing and operating technical systems, Vol. 5 No 3, 2010; ss. 177.
- [13] Susmel L., Taylor D., *The Modified Wöhler Curve Method applied along with the Theory of Critical Distances to estimate finite life of notched components subjected to complex multiaxial loading paths*, Fatigue & Fracture of Engineering Materials & Structures Vol. 31, Issue 12, 2008.
- [14] Yoshiaki Akiniwa, Nobuyuki Miyamoto, Hirotaka Tsuru, Keisuke Tanaka, *Notch effect on fatigue strength reduction of bearing steel in the very high cycle regime*, International Journal of Fatigue Vol. 28 2006 1555–1565.



## POSSIBILITIES OF SOME CONSTRUCTIONAL MATERIALS CUTTING BY MEANS OF WATER-ABRASIVE JET

Michał Styp-Rekowski<sup>1)</sup>, Maciej Matuszewski<sup>1)</sup>, Ivan L. Oborski<sup>2)</sup>

<sup>1)</sup>University of Technology and Life Sciences in Bydgoszcz, Poland  
al. Prof. S.Kaliskiego 7, 85-789 Bydgoszcz  
tel.: +48 52 3408623, e-mail: [msr@utp.edu.pl](mailto:msr@utp.edu.pl)

<sup>2)</sup>National University of Technology and Design in Kiev, Ukraine

### Abstract

*In the paper results of comparative studies concerning the possibilities of cutting of some materials by means of the AWJM method were presented. Roughness parameters (very significant technological and operational factor) of surfaces after cutting were compared. Cutting was performed on the two materials' samples: quenched and tempered alloy steel (1.2080), and natural mineral material – syenite. Variable parameters in the cutting process were accepted: pressure of water-abrasive jet and feed rate. As a result of measurements involving selected roughness parameters (Ra, Rz and Rq). It was discovered that the tested quantities have a significant effect on the state of machined surfaces.*

**Keywords:** constructional material, abrasive-water jet machining (AWJM), machine building, civil engineering, roughness parameter

### 1. Introduction

Cutting is operation very often existing in a lot of different manufacturing processes. These processes can be performed on a wide range of materials: from technical (metals, plastics) through mineral materials and derivative materials (rocks, ceramics) to biological materials (wood, straw, organic tissue) and a lot of industries, e.g.: machine building, civil engineering, extractive industry, shipbuilding industry.

Operations of cutting are applied at various stages of the production process and so the requirements concerning characteristics of cut surfaces are varied. different requirements will apply to cutting not followed by further operations or treatment and different – to cutting followed by further treatment.

Research presented in this paper involve a cutting method which uses a concentrated jet of water and abrasive material (AWJM) – the method that is developing rapidly due to its advantages [2, 4], but still defined as non-conventional treatment [7, 8].

The main aim of described experiments was to verify to what extent parameters of cutting using the AWJM method affect machined surface, especially its geometrical structure of elements made of material having very different features: steel, and natural mineral material. Surface roughness is one of the most important features of surface layer, therefore selected roughness parameters are taken as the measure for cutting results assessment.

## 2. Investigated object and range of experiments

Investigations concern samples with following geometrical features ( $l \times b \times h$ ): 30x10x5 mm, made of different materials – metallic and mineral:

- very popular constructional steel, numbered 1.2080, symbol acc. to European Standard: X210Cr12, quenched and tempered to 43 HRC,
- syenite.

Used in investigations materials have strength feature and crystalline structure quite differ. Both of chosen materials are applied in machine-tools building, nevertheless, both for different units and elements. Tested steel is used for a lot of elements produce, e.g.: elements of machines, truss construction, and mineral material – for the machine body or table and as façade elements. The main reason of such choice was need to determine the some roughness parameters obtained by abrasive-water jet cutting with defined parameters.

Cutting operations were realized using abrasive-water contour machine, made of PR China marked DWJFB 1313. As independent variables in presented investigations following quantities were accepted:

- pressure of working fluid:  $p = 200, 250$  MPa,
- feed rate:  $f = 64, 80$  and  $96$  mm/min.

According to numerous references, e.g. [1, 3, 6], these factors essentially influences cutting surfaces features.

Fluid jet consists mixture of water and Garnet abrasive, mesh 80; nozzle diameter was 1.016 mm. During machining the cutting head was 2 mm from upper machined surface.

Results of cutting process were evaluated on the base of measurements of below mentioned three chosen roughness parameters:

- $Ra$  – arithmetic mean of profile deviation from the mean,
- $Rz$  – total height of profile,
- $Rq$  – quadratic mean of profile deviation from the mean,
- $Rz/Ra$  – calculated coefficient.

Measurements using profilograph Hommelwerke T 2000.were made in three places: 0,25, 0,50 i 0,75 of  $l$  dimension (length) on measuring length (4 mm) situated on the middle of samples thickness  $b$ . Displacement of measuring lengths were presented in Fig. 1. As a final finding average value of 3 measurements ( $m_1, m_2, m_3$ ) was accepted.

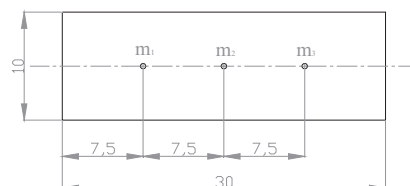


Fig. 1. Sample dimensions and measuring places on the machined samples

Presented investigations have initial character, verifying methodic possibilities, so mentioned above three elements set of roughness parameters, measured by means of mentioned metrological device one accepted as adequate.

## 3. Results of experimental investigations

Cutting surface roughness measurement findings are taken down in below tables. The values of roughness parameters provided in Table 1 refer to the cutting of steel samples quenched and

tempered up to 43 HRC. Based on the analysis of these results it was appeared that the tested cutting parameters had an effect on the obtained roughness. It was found that roughness is also higher for greater values of parameters, e.g.  $Ra$  parameter increased by 0.61 micrometer, i.e. by almost 30 % (from 2.16 to 2.77  $\mu\text{m}$ ), where there was a change in the feed rate  $f$  from 64 to 96 mm/min, i.e. for an increase by 50%.

The values roughness parameter are also caused by changes of the jet pressure. At the feed rate  $f = 64$  mm/min, an increase in the pressure  $p$  from 200 to 250 (25%) resulted in an increase in  $Ra$  parameter but only by ca. 12%. At different feed rates, an increase in roughness, expressed in a change of  $Ra$  parameter, is even lower (ca. 6%).

Table 1. Values of roughness parameters of surface cut by means of AWJM for steel sample

| Feed rate,<br>$f$ , mm/min<br>Pressure<br>$p$ , MPa | 64    | 80    | 96    |
|---|-------|-------|-------|
| $Ra$ , $\mu\text{m}$                                |       |       |       |
| 200   | 2,16  | 2,68  | 2,77  |
| 250   | 2,42  | 2,85  | 2,95  |
| $Rz$ , $\mu\text{m}$                                |       |       |       |
| 200   | 11,20 | 11,80 | 13,17 |
| 250   | 13,29 | 14,42 | 15,99 |
| $Rq$ , $\mu\text{m}$                                |       |       |       |
| 200   | 2,74  | 3,26  | 3,37  |
| 250   | 3,13  | 3,59  | 3,75  |

Changes found in the geometrical structure of the surface being cut are described by regression equations which have the following form in the analysed case:

- for  $p = 200$  MPa:
  - $Ra = -0,215 \cdot f^2 + 1,165 \cdot f + 1,21$
  - $Rz = 0,385 \cdot f^2 - 0,555 \cdot f + 11,37$
  - $Rq = -0,205 \cdot f^2 + 1,135 \cdot f + 1,81$
- for  $p = 250$  MPa:
  - $Ra = -0,165 \cdot f^2 + 0,925 \cdot f + 1,66$
  - $Rz = 0,220 \cdot f^2 + 0,470 \cdot f + 12,60$
  - $Rq = -0,150 \cdot f^2 + 0,910 \cdot f + 2,37$

Statistical calculations demonstrate that the above equations record very well observed changes, what is confirmed by the values of correlation coefficients approximating to 1,0.

The second structural material used in the study was syenite – mineral material (rock), using e.g. in very precise machine-tools and measurement machines (tables, bodies) but on the other hand – in civil engineering too. The results of measurements presented in Table 2 indicate that the surface roughness obtained as a result of abrasive-water jet cutting is similar for all analysed values of parameters. Maximum differences are in the range 5÷8%

Table 2. Values of roughness parameters of syenite samples surface cut by means of AWJM

| Feed rate,<br>$f$ , mm/min<br>Pressure,<br>$p$ , MPa | 64    | 80    | 96    |
|--|-------|-------|-------|
| $Ra$ , $\mu\text{m}$                                 |       |       |       |
| 200  | 3,93  | 3,85  | 3,78  |
| 250  | 3,87  | 3,74  | 3,70  |
| $Rz$ , $\mu\text{m}$                                 |       |       |       |
| 200  | 18,58 | 18,18 | 17,98 |
| 250  | 17,44 | 17,16 | 17,01 |
| $Rq$ , $\mu\text{m}$                                 |       |       |       |
| 200  | 4,92  | 4,82  | 4,74  |
| 250  | 4,85  | 4,69  | 4,64  |

Change in feed from 64 to 96 mm/min, i.e. by 50 % results in a change of the average value of  $Ra$  parameter from 3.93 to 3.78  $\mu\text{m}$ , i.e. its decrease but only ca. 4%. Similar situation occurs where jet pressure is changed: an increase in the value of this process parameter from 200 to 250 MPa (25%) results in  $Ra$  parameter value being decreased from 3.93 to 3.87  $\mu\text{m}$ , i.e. only 1.5%. Similar relations occur for other analysed roughness parameters. Relations for this material were described by mathematical models. Their forms are presented below:

- for  $p = 200$  MPa:
  - $Ra = 0,045 \cdot f^2 - 0,265 \cdot f + 4,09$
  - $Rz = 0,100 \cdot f^2 - 0,700 \cdot f + 19,18$
  - $Rq = 0,055 \cdot f^2 - 0,325 \cdot f + 5,12$
- for  $p = 250$  MPa:
  - $Ra = 0,005 \cdot f^2 - 0,095 \cdot f + 4,02$
  - $Rz = 0,065 \cdot f^2 - 0,475 \cdot f + 17,85$
  - $Rq = 0,010 \cdot f^2 - 0,130 \cdot f + 5,04$

The analyse indicates that in analysed range of independent variables (feed rate and jet pressure) for both materials (steel and syenite) pressure has a minor influence on the obtained roughness parameter  $Ra$  but recorded gradient is greater for the cutting of steel. Other parameters are very similar in quality. Comparison of the results obtained for two structural materials very different from each other shows that there are essential differences, see Fig.2.

An increase of steel machining parameters (feed rate and jet pressure) resulted in increase of roughness parameters in cut surfaces, whereas in the case of mineral material a reverse tendency was observed: greater values of process parameters resulted in smaller surface roughness. Such situation may result from the water and abrasive jet containing mineral grains and so, in the case of syenite, mineral machines mineral making the hardness of the tool and the hardness of the machined object similar.

As far as the cutting of steel is concerned, the difference in hardness is greater and therefore the relations between analysed factors are similar to those in traditional machining. It is assumed that the hardness of the tool should be larger than that of the machined element by at least 30 HRC.

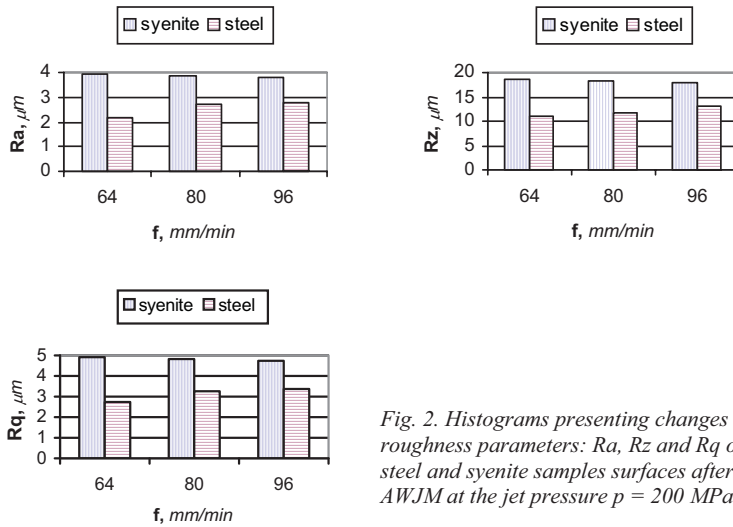


Fig. 2. Histograms presenting changes of roughness parameters:  $R_a$ ,  $R_z$  and  $R_q$  of the steel and syenite samples surfaces after AWJM at the jet pressure  $p = 200$  MPa

Comparison of histograms shown in Fig. 2 and 3 indicate that the roughness of the cut surfaces, machined with the same parameters, is much greater (even 50%) for syenite than for steel. Furthermore, it can be seen that the values of all measured parameters of cut surfaces, machined in the same parameters, are greater for mineral material than for steel.

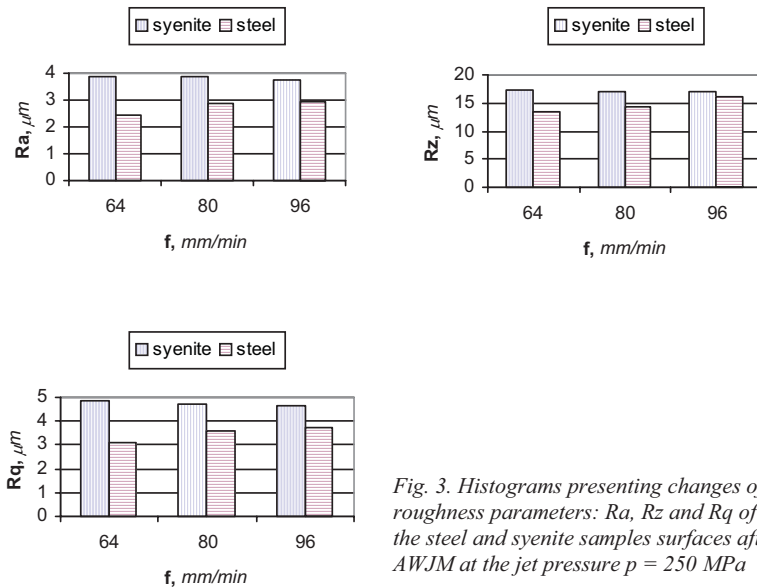


Fig. 3. Histograms presenting changes of roughness parameters:  $R_a$ ,  $R_z$  and  $R_q$  of the steel and syenite samples surfaces after AWJM at the jet pressure  $p = 250$  MPa

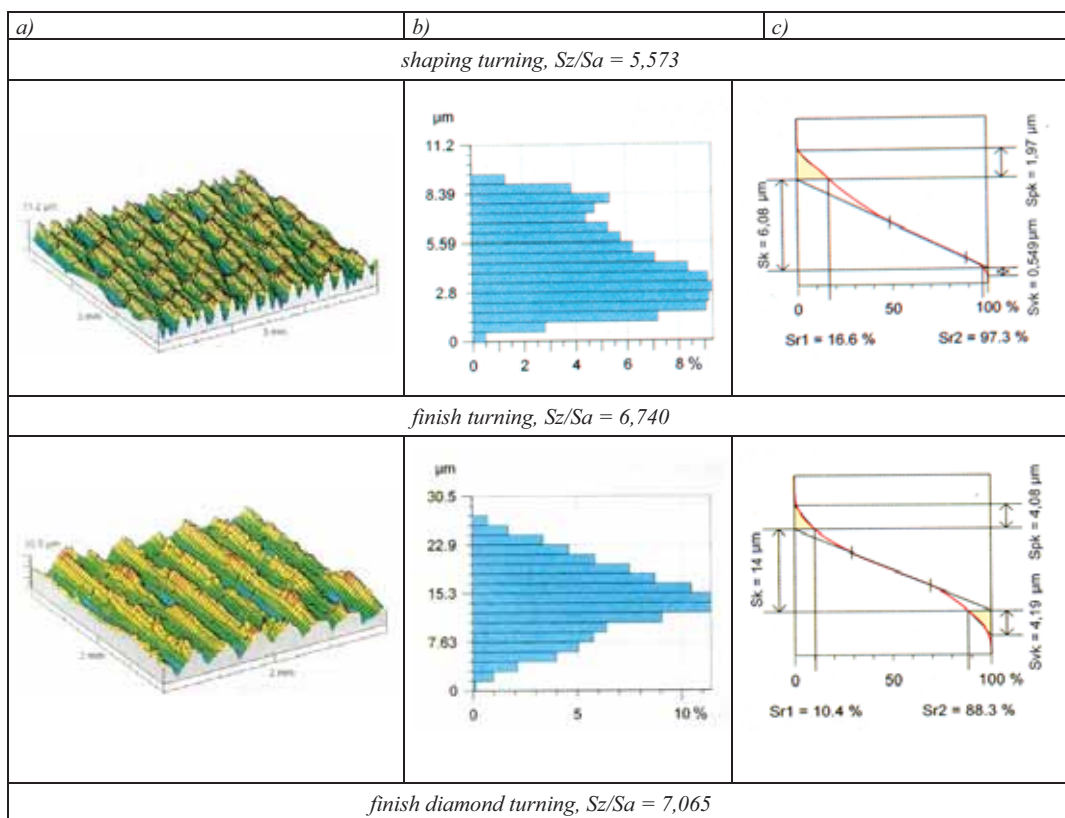
The parameters of cut surfaces roughness make this treatment to be defined as a roughing one, so it can be assumed that this method of cutting can be useful with regard to elements of which machined surfaces will be subject to further treatment. However, the AWJM method is not recommended for surfaces which are not machined after cutting.

Table 3 consists calculated quotient values of two measured roughness parameters  $Rz$  and  $Ra$ . Value of this quotient is important for various reasons, among other for tribologic features of machined surfaces what is confirmed in [5].

Table 3. Values of quotient  $Rz/Ra$  for surfaces cut with different parameters

| Jet pressure<br>MPa | Values of quotient $Rz/Ra$ |      |         |      |
|---------------------|----------------------------|------|---------|------|
|                     | steel                      |      | syenite |      |
|                     | feed rate $f$ , mm/min     |      |         |      |
|                     | 64                         | 96   | 64      | 96   |
| 200                 | 5,22                       | 4,75 | 4,68    | 4,82 |
| 250                 | 5,53                       | 5,42 | 4,49    | 4,61 |

On the ground of presented findings one can state that quotient of analysed parameters was increased together with machining accuracy increase. In Fig. 4 there were presented results of mentioned investigations. Shaping and finishing turning was compared. As the object of comparison 3D view of machined surfaces, ordinates distribution and load capacity curves were accepted.



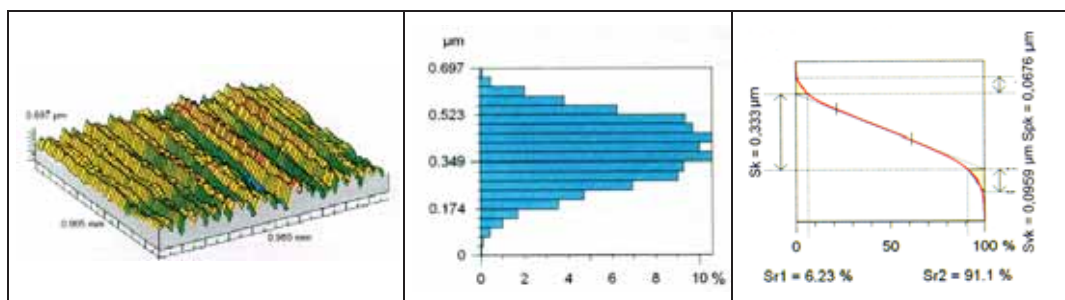


Fig 4. Comparison of turning surfaces tribology features: a) 3D surface view, b) ordinates distribution, c) load capacity curve, acc. to [5]

The views of machined surfaces are not much differentiated, besides kind of machining was differ. Visible difference were observed in ordinates distribution and load capacity curves. Allowing results of mentioned investigations, on the ground of findings contained in Table 5 one can state that for steel samples enlargement of jet pressure generates slight only (ca. 6%) increase of quotient, so load capacity of such surface will be greater too. Other relationships are for feed rate. Greater feed resulted smaller quotient value, so tribologic features will also worse.

Analysing quotient of  $Rz$  and  $Ra$  values for syenite samples inversely (than for steel) relationships were observed, namely:

- greater jet pressure – smaller quotient value – worse tribology features and
- greater feed rate – greater quotient value – better tribologic features.

#### 4. Conclusions

On the ground of presented experiments and the analysis of the selected roughness parameters measurements results obtained from such experiments, conclusions of practical nature can be formulated. The most significant of which are as follows:

- abrasive water jet method can be used for the cutting of structural materials with various chemical compositions and structure – with satisfactory efficiency,
- roughness level of the cut surface using the AWJM method defines this method as roughing,
- influence of machining parameters of AWJM is differentiate for different machined material.

As one said above, the experiments presented in this article have initial character, so on the base of obtained results one can conclude that the established aim of research was accomplished.

#### References

- [1] Holka H., Jarzyna T., Matuszewski M., Musiał J., *Wpływ stanu kwalifikacyjnego stali na efekty cięcia strugą wodno-scierną*, Inżynieria maszyn, vol. 16, z. 4/2011, p. 85-91.
- [2] Kosmol J., Wala T., Hassan A.I., *Preliminary attempt to FEM modelling of AWJM of polymeric composites*, Materiały II Międzynarodowej Konferencji „Obróbka wysokociśnieniowym strumieniem wody – WJM 2001”, p. 39-48, Kraków 2001.
- [3] Mazurkiewicz A., *Czynniki wpływające na jakość powierzchni stali po cięciu strumieniem wodno-ściernym*, Inżynieria materiałowa, nr 5/2008, p. 1-4.
- [4] Oczóś K. E., *Efektywność innowacyjnych technologii na przykładzie wybranych sposobów obróbki strumieniowo-erozyjnej*, Mechanik, vol. 76, No. 8-9/2003, p. 463-468.

- [5] Oczóś K., Lubimov W.: *Struktura geometryczna powierzchni*, Oficyna Wydawnicza Politechniki Rzeszowskiej, Rzeszów 2003.
- [6] Perec A., *Przecinanie materiałów konstrukcyjnych strugą hydro-ścierną o obniżonym ciśnieniu*. Materiały Konferencji „Mechanika’99. Nauka i praktyka”, Wydawnictwo Politechniki Gdańskiej, p. 135-136, Gdańsk 1999.
- [7] Ruszaj A., *Niekonwencjonalne metody wytwarzania elementów maszyn i narzędzi*, Instytut Obróbki Skrawaniem, Kraków 1999.
- [8] Styp-Rekowski M., *Obróbki hybrydowe i nietradycyjne jako uzupełnienie zbioru technik wytwarzania skoncentrowanymi nośnikami energii*, w: STYP-REKOWSKI M. (red.). *Wybrane zagadnienia obróbek skoncentrowaną wiązką energii*. Wydawnictwo Bydgoskiego Towarzystwa Naukowego, p. 213-216, Bydgoszcz 2003.



## RECYCLING ABILITIES OF THERMOPLASTIC IONOMERS, AS EXAMPLIFIED BY SURLYN®

**Dariusz Sykutera, Piotr Czyżewski**

*University of Technology and Life Sciences in Bydgoszcz*

*Faculty of Mechanical Engineering*

*Department of Plastics and Recycling Processing*

*ul. Kaliskiego 7, 85-796 Bydgoszcz, Poland*

*tel.: +48 52 340 82 24, fax: +48 52 340 82 22*

*e-mail: [sykutera@utp.edu.pl](mailto:sykutera@utp.edu.pl)*

### *Abstract*

*The results presented in this paper apply to the research of grinding and cutting process of ionomer copolymer (E/MAA) under the trade name Surlyn® from DuPont company. Processing of this material is difficult and its susceptibility to mechanical recycling is limited. The results presented here are an important part of research concerning management of ionomer waste formed in the injection moulding process (defective moulded pieces with and the thick-walled injection moulding waste). The plastic material under examination is applied in the line of perfume, the products are expected to have transparency of the glass and don't have disqualifying surface defects. This requires the use of non-standard conditions in the injection moulding process and the construction of complicated structures of injection moulding tools (ie, three plate mould), along with valve gate hot runner systems. In the structure of three plate mould we use cold runner system in hot runner injection moulds, the former of which forms the so-called injection waste, i.e. runner, which further increases the cost of the tool. In the case of plastics considered, injection waste constitutes up to 30 percent of the weight of the moulded piece, which, with high prices of this plastic (Surlyn® price is more than three times higher than the commonly used polyolefin materials) and reduced re-use possibilities, constitutes unaccepted, additional cost of production. This paper is an attempt to develop favorable conditions for the process of grinding of Surlyn® in terms of its re-use in secondary processing. The study shows that the temperature of feed has a significant impact on the level of thermal load of the material subjected to grinding and cutting, as well as on the effectiveness of disintegration.*

**Keywords:** *ethylene/methacrylic acid copolymers, recycling of ionomers, recycling of Surlyn (E/MAA), grinding of ionomers, cutting of ionomers,*

### **1. Introduction**

Surlyn® is the trade name of ionomer (E/MAA - *ethylene/methacrylic acid copolymers*, which has in its structure the cations of metals such as Zn and Na), produced by DuPont. Ionomers are characterized by strong electrostatic interactions between the chains of polymers and the amorphous structure. These materials have good resistance to abrasion and puncture, and good stiffness combined with the flexibility and resilience. These materials combine high tensile strength (greater than crystalline polyolefins and copolymers containing carboxylic acid groups) with good flexibility. Surlyn®, in comparison to the crystal structure of polyolefins and copolymers containing carboxylic acid groups, has much better mechanical properties, resistance to wear and damage, and good rigidity with sufficient flexibility and elasticity [1, 2].

The main areas of the application of Surlyn<sup>®</sup> are: production of cosmetic packaging (Figure 1), pharmaceutical packaging and food packaging (containers, bottles, boxes, foils, sheets, plates) and production of sports goods [1, 3, 5]. In literature, we can also find reports of attempts to use this plastic to modify the structure and properties of other thermoplastics [1, 3, 4, 8, 9]. The line of perfume expects exceptional transparency comparable to glass and moulded pieces free from visible surface defects from polymeric products. Surlyn<sup>®</sup>, with its unique properties can replace glass, giving more freedom for designing of package geometry e.g. the product with variety of wall thicknesses, sharp corners, the possibility to apply galvanic coating, the diversity in the surface finish, a wide variety of colouring, the use of overmoulding technology, safety of use) and by reducing the cost of packaging by approximately 30-40 per cent [6, 7].

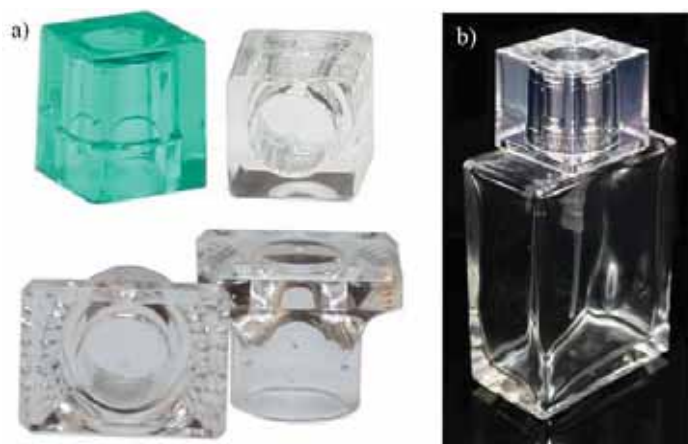


Fig. 1. Examples for using Surlyn<sup>®</sup>: a) a perfumery cap, b) complete perfumery package (bottle with cap)

Surlyn<sup>®</sup> makes lots of problems during injection moulding process, such as problems with the cooling of tool, surface defects are defects formed inside the structure of thick-walled moulded pieces. Susceptibility to mechanical recycling of ionomers is limited, due to the loss of transparency in the secondary processing (mouldings become *milky*). For these reasons, the production process often requires to apply cold runner system in hot-runner injection moulds (a three-disc mould structure arises) forming injection moulding waste, so-called "cold runner". In the case of plastics considered, injection waste constitutes up to 30 percent of the weight of the moulded piece, which, with high prices of this plastic (Surlyn<sup>®</sup> price is more than three times higher than the price of commonly used polyolefin materials) and reduced re-use possibilities, constitutes unaccepted, additional cost of production.

## 2. Methodology of research

In the research of cutting and grinding we used Surlyn<sup>®</sup> PC 2000 thermoplastic ionomer produced by DuPont (USA) in the form of injection moulding waste. It was cold runner, which, in case of Surlyn<sup>®</sup>, constituted as many as 32 per cent of the plastic entered to processing tool in one cycle. Before cutting and grinding, a part of the material under research was being frozen to temperature of -40°C within 24 hours in the freezer by Zwick (Germany). Cutting and grinding were carried out on the test stand whose description and research potential was presented in the paper [10]. Knives with a specific structure were equipped with extensometers by VISAY (Germany), stuck on in the Full Bridge Strain Gauge configuration [10]. The courses of strength and torque variations were registered with ESAM Traveller 1 converter (Germany). The angle of the edge of the cutting knives was  $\beta=60^\circ$ , while their cutting edges were inclined by  $2\lambda = 6^\circ$  to the

rotor axis (the mill by hiperboloidal rotational cutting). Tests on cutting and grinding were conducted with tangential velocity of movable knives of 3 and 6 m·s<sup>-1</sup> and by using sieves with diameters of Ø9mm of holes. Gain in weight was registered by WLC 6 scales by Radwag. Calculation of energy consumption per unit was made on the basis of a chart presenting torque variations in the realization of grinding process, according to the methodology proposed in the paper [11]. In grinding tests we also measured the temperature within the separating sieve. In order to make the data presented here more understandable, the individual cases of cutting and grinding were described in variants. Disintegration of Surlyn<sup>®</sup> with the tangential velocity of movable knives of 3 m·s<sup>-1</sup> and at ambient temperature of 20°C was described in A variant. Cutting and grinding of Surlyn<sup>®</sup> with the tangential velocity of 6 m·s<sup>-1</sup> and at ambient temperature of 20°C were described in B variant. Samples frozen to -40°C and disintegrated with the tangential velocity of 6 m·s<sup>-1</sup> of movable knives were indicated as D variant, and the ones cut with the velocity of 3 m·s<sup>-1</sup> as C variant. Proportions of graining of the recyclates obtained were estimated through sieve analyses carried out by using sieves with the diameter of holes of Ø8; 7; 6; 5; 3,5 and 2 mm. The process was realized in gyratory screen, and the analysis took 3 minutes. Moreover, recyclate grains obtained were assessed on the stand to computer analysis of view, with the help of stereo microscope with octuple magnification of the lens. Observations were made with the help of Multiscan 18 applications on Computer Scanning System from Warsaw [12].

### 3. Results of cutting

The analysis of cutting performance indicates that the freezing of the feed material to -40°C resulted in a significant increase in the values of the shear force. It seems to be the effect of an increase in hardness and stiffness of the material; this results in an increase of resistance to the effects of the cutting blades. At the same time, it was found out that the distribution of the frozen material is initiated by cutting owing to the cooperation of fixed and movable knives, and in the final phase of the process a brittle fracture of Surlyn<sup>®</sup> occurs, similar in its course to the disintegration of polystyrene at ambient temperature (see Figure 2).

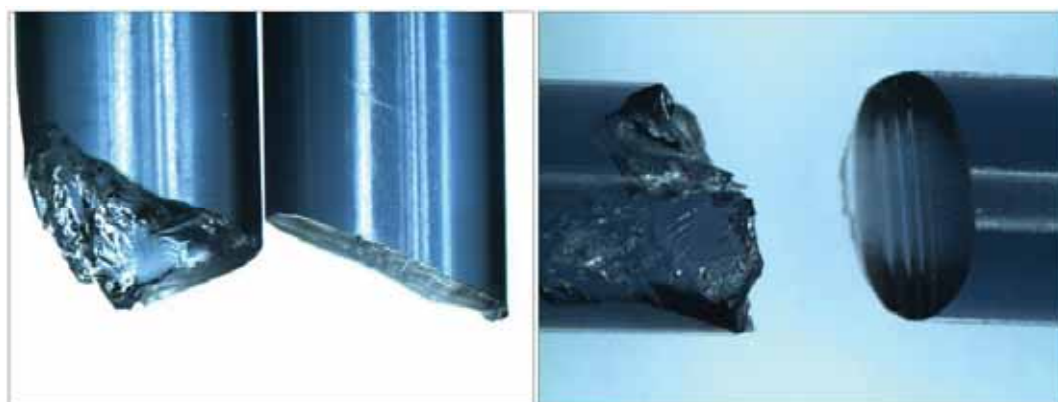


*Fig. 2. Influence of temperature on disintegration type of injection moulding waste: parts of samples after cutting in -40°C -samples on the left with frayed cutting surface- brittle cracking, parts of samples after cutting in +20°C -samples on the right with smooth cutting surface*

Reduction of the tangential velocity of the cutting blades by half to 3 m·s<sup>-1</sup> did not cause any significant changes in the course of variations of shear force or torque (see Figures 3-5). Similarly to the higher speed, the force needed to cut the sample is significantly higher for the frozen Surlyn<sup>®</sup>.

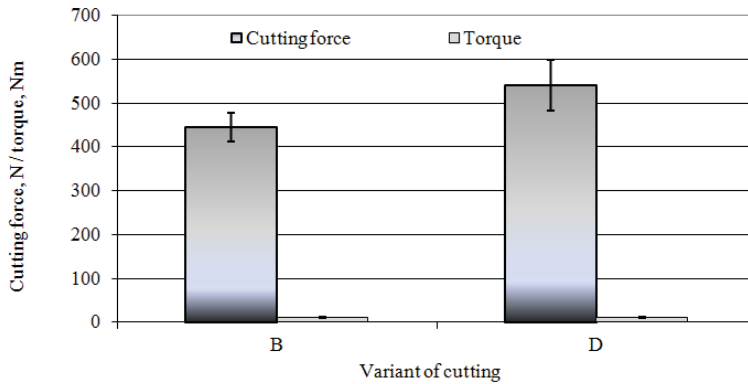


Fig. 3. Influence of the temperature of the feed on cutting force by hiperboloidal rotational cutting with tangential velocity  $6 \text{ m} \cdot \text{s}^{-1}$  (the figure shows average values and standard deviations)

The only change observed is the prolongation of cutting time from 1ms to 3ms for the tests made for the material unfrozen (see A variant). A high percentage of cracking while cutting of Surllyn® at  $-40^{\circ}\text{C}$  is evidenced by the stability of cutting time in B and D variants, despite the fact that the tangential velocity of knives was reduced twice.

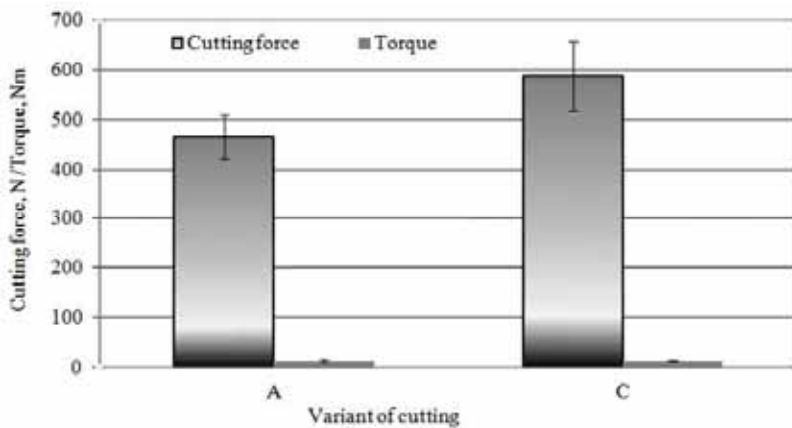


Fig. 4. Influence of temperature of the feed on cutting force by hiperboloidal rotational cutting with tangential velocity  $3 \text{ m} \cdot \text{s}^{-1}$  (the figure shows average values and standard deviations)

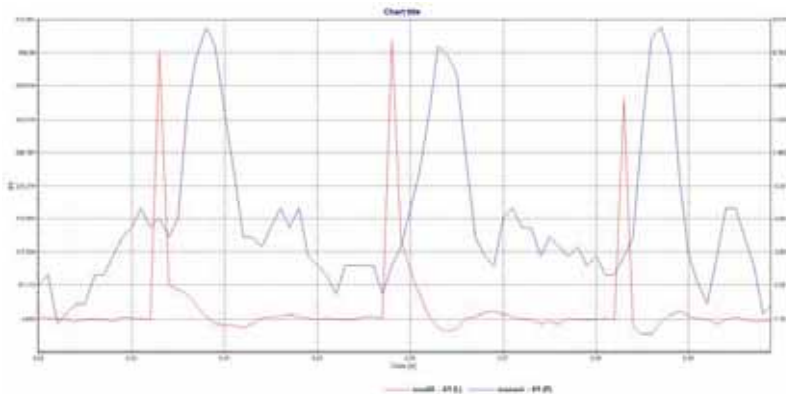


Fig. 5. Example of cutting of Surllyn® at ambient temperature with tangential velocity of  $3 \text{ m} \cdot \text{s}^{-1}$

#### 4. Results of grinding

The temperature of an input affects grinding to a significant extent (see Figures 6 and 7). Reduction of the temperature of the technological waste to  $-40^{\circ}\text{C}$  doubles the increase in performance in relation to A variant and causes an increase by 25 per cent as compared to the realization of the disintegration of Surlyn<sup>®</sup> at  $20^{\circ}\text{C}$  and at the same peripheral speed of  $6\text{ m}\cdot\text{s}^{-1}$  of movable knives. Similar changes can be observed in energy expenditures to be incurred in the process of disintegration of ionomer by knife. Reducing the temperature of the feed to  $-40^{\circ}\text{C}$  causes the decrease in energy consumption per unit used in grinding of Surlyn<sup>®</sup> from  $150\text{ kJ}\cdot\text{kg}^{-1}$  to about  $60\text{ kJ}\cdot\text{kg}^{-1}$ ; which constitutes reduction in energy input by 60 per cent. For economic purposes the cost of lowering the temperature of the feed has to be taken into account.

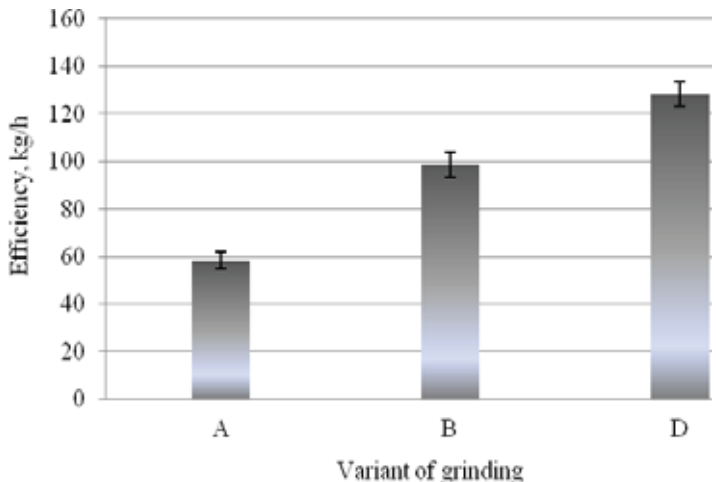


Fig. 6. Influence of conditions of grinding on efficiency during Surlyn<sup>®</sup> grinding in the cutting mill (the figure shows average values and standard deviations)

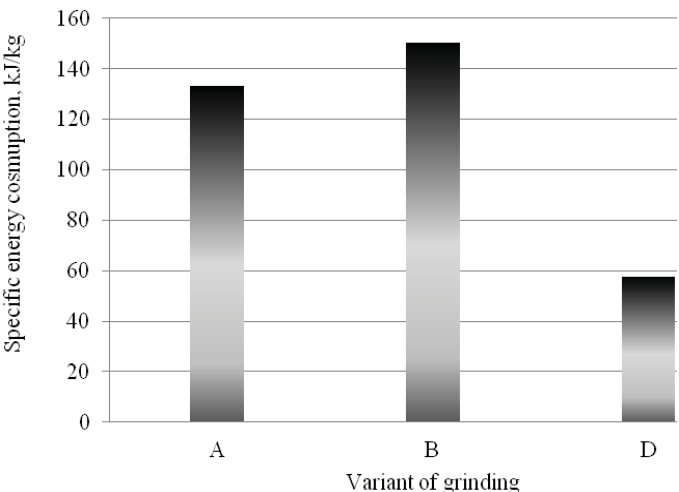


Fig. 7. Influence of conditions of grinding on energy consumption per unit during Surlyn<sup>®</sup> grinding in the cutting mill

Realization of disintegration of the material at ambient temperature is energy-consuming. Energy inputs necessary for its grinding are lower by about half when compared to a vulcanized rubber (but for graining of 1mm) and about 5 times higher then in the case of grinding of PELD to the same extent as in grinding of ionomers [11]. Using higher tangential speed of the rotor is more effective, despite the higher energy consumption per unit (see A and B variants).

Conditions for grinding processes affect temperature variations in working chamber of the tool significantly. The biggest increase of the temperature is characterized by disintegration of Surlyn<sup>®</sup> with higher tangential speed of the rotor (B variant). However, in that case, increase in temperature to about 30°C, does not constitute any thermal devastation. Freezing of the feed at -40°C caused the decrease in temperature by 10°C during grinding process, which is favourable when we take into account the sensitivity to high temperature of the disintegrated material (Figure 8). The results seem to affect the changes in structure of products obtained from recyclates. Analysis of data acquired from manufacturers of Surlyn<sup>®</sup> indicates that one of the most serious problems of recycling of Surlyn<sup>®</sup> is the loss of transparency. Thus, carefulness for maintaining relatively low temperature in a working chamber of disintegrator when carrying out the process may have a positive influence on recycling as well as on optical properties of this material.

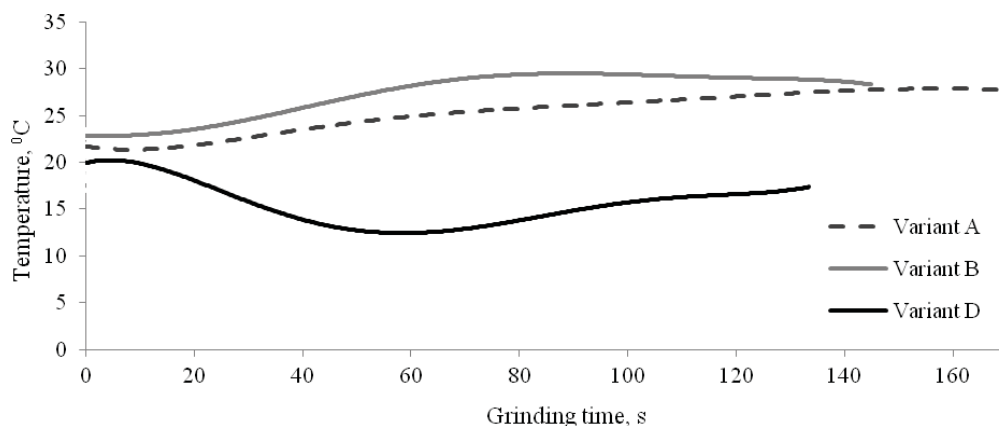


Fig. 8. Variations of temperature during the grinding process of injection moulding waste

The distribution of grains indicates that applying the Ø 9mm sieves guarantees to obtain the recyclate of the proper grinding degree. It is evidenced by the fact that for all grinding variants the dominant grain group of recyclates are grains from 3,5 to 5mm, and, as for B and D variants more than 50 per cent of the total mass is comprised of the recyclate with the grain size of less than 5mm (Figure 9). Lowering the temperature of the feed did not affect the proportions of graining to any significant extent (D variant). It is worth mentioning about the importance of tangential velocity of cutting knives, but the recyclate obtained through the velocity twice as lower is characterized with the presence of larger grains. In addition, no dust was observed, while it is common for grinding of other thermoplastic materials like polyethylene or polypropylene.

Grinding of Surlyn<sup>®</sup> at 20°C leads to creating groups of grains with flat surfaces of cutting and straight edges (Figure 10). It proves the high importance of cutting in the waste material disintegration. Lowering the temperature of the feed to -40°C caused numerous fractures and roughness on surface of the grains (Figure 10). It seems to be the effect of the growing importance of cracking in disintegration of Surlyn<sup>®</sup>, which is more stiff and brittle at this temperature.

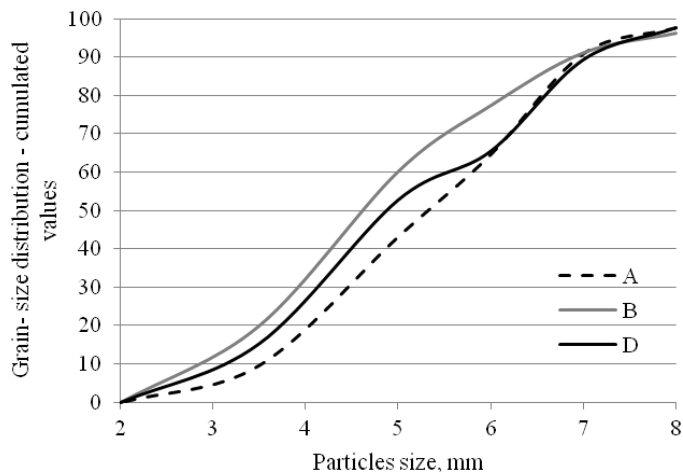


Fig. 9. Cumulated curve of ground Surlyn® PC 2000 according to grinding conditions during mill by hiperboloidal rotational cutting

| Diameter of eye in screen [mm] | Temperature of grinding of injection moulding waste [°C] |  |       |  |
|--------------------------------|--|--|-------|--|
|                                | 20°C   |  | -40°C |  |
| 8,0                            | 5,6g   |  | 3,4g  |  |
|                                | 3,7%   |  | 2,3%  |  |
| 7,0                            | 7,4g   |  | 12,3g |  |
|                                | 4,9%   |  | 8,2%  |  |
| 6,0                            | 20,0g  |  | 35,4g |  |
|                                | 13,3%  |  | 23,7% |  |
| 5,0                            | 25,0g  |  | 18,9g |  |
|                                | 16,7%  |  | 12,6% |  |
| 3,5                            | 58,4g  |  | 55,6g |  |
|                                | 38,9%  |  | 37,1% |  |
| 2,0                            | 29,1g  |  | 22,8g |  |
|                                | 19,4%  |  | 15,2% |  |

Fig. 10. Influence of temperature of the feed on geometry and surface of grains of the recyclate. All pictures are made with the use of stereoscopic microscope (8x magnification)

## 5. Conclusion

Results of cutting and grinding of Surlyn<sup>®</sup> thermoplastic ionomer show the substantial importance of temperature of the feed for the effectiveness of mechanical recycling of this material. We can assume that cutting by knife at minimum gap between the blades allows to obtain ionomer recyclate with the proper grain distributions and by the relatively acceptable effectiveness and energy consumption. There is no direct dependence between the values of the cutting force and the energy consumption per unit used for grinding. Freezing of the feed to the temperature below -40°C made grinding of the material easier, since Surlyn<sup>®</sup> was flexible at ambient temperature, owing to the growing importance of cracking in disintegration.

## References

- [1] Company information materials of DuPont, [on-line], (28, 06, 2012), access <[www2.dupont.com/Surlyn/en\\_US/](http://www2.dupont.com/Surlyn/en_US/)>
- [2] Czaja, K., *Poliolefiny*, Wydawnictwo Naukowo-Techniczne, Warszawa 2005.
- [3] Dziadur, W., Litak A., *Wpływ jonometrycznego kopolimeru etyleny na strukturę krystaliczną i własności mechaniczne poliacetalu*, Inżynieria Materiałowa 1998, R. XIX, nr 4, pp. 946 - 949.
- [4] Dziadur, W., Litak A., *Efekty modyfikacji poliacetalu kopolimerem etyleny*, Zeszyty Naukowe. Mechanika 43 (216), ATR Bydgoszcz, pp. 15-21, Bydgoszcz 1998.
- [5] Kuzia, A., *Opakowania żywności*. Praca pod red. Bohdana Czerniawskiego i Jana Michniewicza, Wydawnictwo Agro Food Technology 1998.
- [6] Information materials, *Żywica Surlyn DuPont wykorzystywana w opakowaniach*, [on-line], (27, 06, 2012), access < [http://www.plastech.pl/wiadomosci/artikul\\_1964\\_1/Zywica-Surlyn-DuPont-wykorzystywana-w-opakowaniach](http://www.plastech.pl/wiadomosci/artikul_1964_1/Zywica-Surlyn-DuPont-wykorzystywana-w-opakowaniach) >
- [7] Information materials, *DuPont: Nowa technologia obtrysku daje ogromne możliwości w dziedzinie projektowania opakowań*, [on-line], (27,06,2012), access <<http://opakowania.com.pl/Wiadomości/DuPont-Nowa-technologia-obtrysku-daje-ogromne-możliwości-w-dziedzinie-projektowania-opakowań-26378.html> >
- [8] Garcíaa, S.L., Sánchez-Valdésb, S., Ramos-Devallec, L.F., *Effect of type and concentration of ionomer compatibilizer on the HDPE/Ionomer/Clay nanocomposites morphology*, Materials Science Forum, (2010), 644, pp. 17-20.
- [9] Lim, H.T., Liu, H., Ahn, K.H., Lee, S.J., Hong, J.S., *Effect of added ionomer on morphology and properties of PP/organoclay nanocomposites*, Korean Journal of Chemical Engineering, (2010), 27 (2), pp. 705-715.
- [10] Sykutera, D., *Stanowisko badawcze i wstępne wyniki badań cięcia termoplastycznych tworzyw porowatych*, Przetwórstwo Tworzyw, 4 (136), pp. 214-217, Gliwice 2010.
- [11] Sykutera, D., *Badanie procesu rozdrabniania odpadów gumy cięciem hiperboloidalnym w aspekcie wykorzystania otrzymanego proszku gumowego do napełniania poliamidu 6*, Rozprawa doktorska, Politechnika Poznańska, Poznań 1998.
- [12] Sykutera D., *Properties of solid polyurethane recyclat obtained in the compact multistage system of cutting mills*, Journal of POLISH CIMAC, Vol.5, No. 3, pp. 201-206, Gdańsk 2010.



## POROUS POLYSTYRENE GRINDING REASERCH

**Dariusz Sykutera**

*University of Technology and Life Sciences in Bydgoszcz*  
*Faculty of Mechanical Engineering*  
*Department of Plastics and Recycling Processing*  
*ul. Kaliskiego 7, 85-796 Bydgoszcz, Poland*  
*tel.: +48 52 340 82 24, fax: +48 52 340 82 22*  
*e-mail: [sykutera@utp.edu.pl](mailto:sykutera@utp.edu.pl)*

### *Abstract*

*The aim of the research was to examine the behaviour of porous polystyrene during grinding realised in a knife grinder. The assessment of the porous structure influence on the effectiveness of polystyrene disintegration was conducted in relation to previously obtained results of knife cutting realised at the same research site. These unquestionable advantages have caused that even over  $1 \cdot 10^6$  kg of thermoplastic material includes in its structure the gas phase. The observed trend results from the tendency aiming to obtain plastic parts of light structures that may be used as construction materials. Due to the complex polymer-gaseous structure of porous materials, their mechanical recycling requires adapting special, different from typical for solid materials, cutting and grinding conditions. The behaviour of polymer materials under applied load is tightly connected with their structure. Earlier process analysis indicates that together with the cutting velocity increase, the impact cracking ratio in the material division increases. As a result of the conducted research, polystyrene recycle was obtained, which might be reused in re-processing for new product production. Polystyrene porous structure is conducive to effective grinding, which is characterised by low energy consumption for grinding and high effectiveness in relation to the grinding degree.*

**Keywords:** *recycling of polystyrene, porous polystyrene, cutting of polystyrene, grinding of porous polystyrene*

### **1. Introduction**

The use of physical or chemical pore-filling to increase the heat insulation or suppression properties of plastic materials like PELD, PP, PVC, to increase the rigidity, to replace the long-known foamed polystyrene in packaging industry by physically pore-filled polyolefin materials has also been noticed [1]. Moreover, the addition of chemical blowing agents to solid thermoplastic materials decreases the product shrinkage, improves the rheological properties as well as allows to create product geometries that so far have been considered as elements of the non-technological design (e.g. the use of different wall thicknesses) [1, 2]. It has also been found that thanks to chemical blowing agents there exists the possibility to shorten the injection cycle [1, 4]. For products of a complex shape and differentiated wall thickness the addition of even a small amount of a blowing agent decreases the shrinkage anisotropy, which eventually results in the decrease of the own tension level and deformations [1, 4]. These unquestionable advantages have caused that even over  $1 \cdot 10^6$  kg of thermoplastic material includes in its structure the gas phase. The observed trend results from the tendency aiming to obtain plastic parts of light structures that may be used as construction materials.

Due to the complex polymer-gaseous structure of porous materials, their mechanical recycling requires adapting special, different from typical for solid materials, cutting and grinding conditions

[3-7]. The behaviour of polymer materials under applied load is tightly connected with their structure. Polymer viscoelasticity causes that, apart from the grinder constructional features, also process temperature and the velocity of external forces interaction with the input material, causing its disintegration, influence the final grinding process effectiveness. Earlier process analysis indicates that together with the cutting velocity increase, the impact cracking ratio in the material division increases. This especially refers to solid thermoplastic materials [4, 7]. Basing on this, one may regard that an advantageous solution is the use of high peripheral speed of the knives. However, one should remember that high process dynamics causes the increase of powdery fraction participation and recycled material electrification. The phenomena is disadvantageous from the point of view of recycling the material. Due to low values of melting temperatures of PS, PE, and especially – of PVC, the material cutting velocity must be a compromise between the disintegration effectiveness and the recycle quality.

The aim of the research was to examine the behaviour of porous polystyrene during grinding realised in a knife grinder. The assessment of the porous structure influence on the effectiveness of polystyrene disintegration was conducted in relation to previously obtained results of knife cutting realised at the same research site [4-7].

## 2. Research methodology

Extruded parts obtained in the laboratory single-screw extruder with mounted research head of 13,5x8 mm mouthpiece cross-section were used for the research. The head was equipped in a three-zone heating system, thanks to which it was possible to achieve proper foaming of the chemical blowing agent in the solid polystyrene. The material was produced of KRASTEN 552 9002 polystyrene by the company Synthos S.A. (Czech Republic) with simultaneous Expancel 980 MBX 120 blowing agent by the company Akzo Nobel (Sweden) dosing. The blowing agent concentrate was added to PS in the amount of 4% of mass. The extrusion process was realised at the following parameters: a) extruder plasticising unit temperature: zone I - 145 °C, zone II - 215 °C, zone III - 215 °C, b) extruding head temperature: zone I - 140 °C, zone II - 140 °C, c) screw rotary velocity  $n_s = 85 \text{ rot./min}^{-1}$ . Profiles of the average cross-section of 14.5x8 mm were obtained, with final cross-section dimensions, especially for porous extruded material, controlled by the peripheral velocity of the suction cylinders. The porous material density with the content of the blowing agent of 4% in mass was estimated at the level of  $446,3 \pm 12,6 \text{ kg}\cdot\text{m}^{-3}$ , while for solid PS the obtained density equalled  $986,5 \pm 21,4 \text{ kg}\cdot\text{m}^{-3}$ . Initially cut material was disintegrated at the research site for examining the cutting and grinding processes, whose description and research capacities are included in research thesis [4, 7]. Knives of special design ensuring adequate susceptibility to deformation at the influence of the cutting force were equipped in strain gauges by company VISAY (Germany), which were stuck in the full bridge configuration. The courses of the alterations of force and torsion moment were registered by means of a converted ESAM Traveller 1 (Germany) with software, at the assumed examining time of  $10^{-2} \text{ s}$ . Cutting knives of geometrical features presented in research [4], were applied, whose cutting edges were reclined in relation to the rotor axis by the angle  $2\lambda = 6^\circ$ . The angle of the cutting knives equalled  $60^\circ$ . The tests were conducted at the peripheral velocity of the moving knives of  $3 \text{ m}\cdot\text{s}^{-1}$  and with the use of sieve of the hole diameter of  $\varnothing 9 \text{ mm}$ . The calculation of the unitary energy consumption (in relation to the ground mass) was carried out basing on the torque alteration diagram during the realisation of grinding process, according to the methodology suggested in research work [8]. The grain distribution of the obtained recycle was estimated through sieve analysis in dry conditions with the use of sieves of the hole diameter of  $\varnothing 8; 7; 6; 5; 3,5; \text{ and } 2$ . The process was realised in an eccentric sieve machine and the analysis time equalled 8 minutes. While grinding, the temperatures of the fixed knife and in the area of the separating sieve were also measured.

### 3. Results of grinding

The analysis of grinding research indicates significant influence of material structure on its mechanical recycling susceptibility. Specific energy consumption for solid polystyrene grinding is essentially lower to the energy quantity needed for grinding extruded polystyrene with 4% porophore content (Fig. 1). At the same time, no effect of porophore content on the energy level needed for material cutting was found out. In all the cases of porous polystyrene a similar level of energy consumption was obtained, slightly higher than  $40 \text{ kJ}\cdot\text{kg}^{-1}$ . Such a low level of energy consumption, when compared to other polymer materials, on porous polystyrene disintegration shows high susceptibility of this material to grinding.

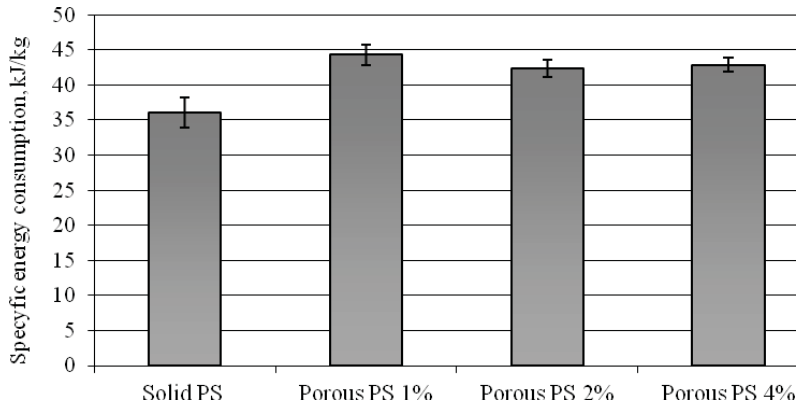


Fig. 1. Changes of the specific energy consumption during grinding polystyrene of variable pore quantity in a knife mill. The tests were conducted at the tangential velocity of the moving knives of  $3 \text{ m}\cdot\text{s}^{-1}$  and with the use of sieves of the hole diameter of  $\varnothing 9 \text{ mm}$  (the figure shows average values and standard deviations).

The changes in material grinding effectiveness can especially be noticed while analysing the mass changes during grinding (Fig. 2) as well as taking into account the changes of energy consumption, which were defined basing on the torque changes (Fig. 3).

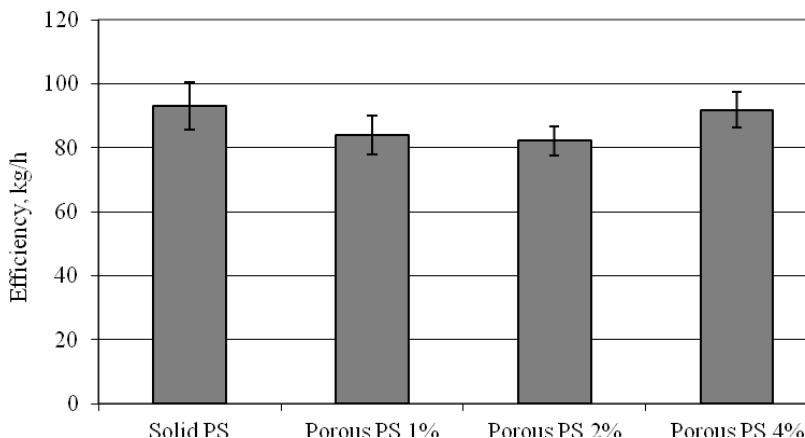


Fig. 2. Changes of the efficiency during grinding polystyrene of variable pore quantity in a knife mill. The tests were conducted at the tangential velocity of the moving knives of  $3 \text{ m}\cdot\text{s}^{-1}$  and with the use of sieves of the hole diameter of  $\varnothing 9 \text{ mm}$  (the figure shows average values and standard deviations).

The analysis of the two diagrams indicates the fact that in case of solid polystyrene grinding, due to its low toughness, the input segmentation takes place through cutting and impact cracking. The process proceeds very intensively due to the fact that in the gap between the moving and fixed knives material segmentation is initiated through its incising and the following uncontrolled brittle cracking caused by rotary movement of the rotor. Porous structure creation limits the phenomenon and emphasises the significance of cutting as the basic material segmentation manner. Pores created by introduction into the PS structure a blowing agent or a neutral gas moderate crack propagation while cutting and constitute a kind of its flexible phase. Chemically modified polystyrene segmentation is connected with the highest energy expenditure (Fig. 3), which indicates that in these cases the material disintegration takes place mainly through cutting.

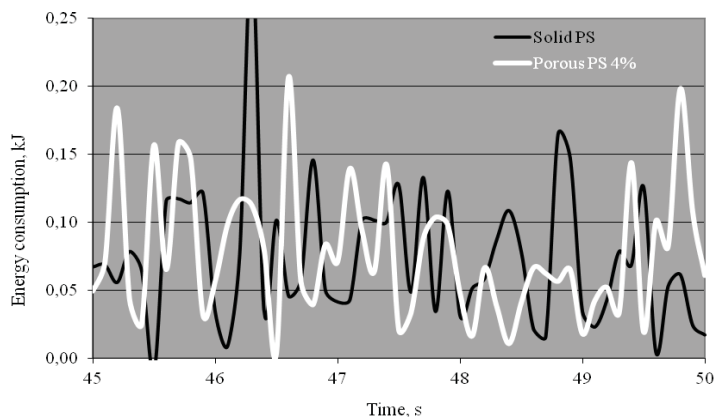


Fig. 3. The exemplary course of change of energy consumption (measurement at regular intervals - 0,1 s) required to disintegration polystyrene of different porosity degree

Obtaining a defined segmentation degree for solid PS is the most prolonged, and unitary energy expenditure for this material grinding is lower than for extruded PS with 4% of blowing agent in mass. This is the result of a high participation of gaseous phase in material, which constitutes the area of material unwholeness. The dominant participation of cutting in porous polystyrene disintegration is confirmed by the measurements of the temperature registered inside the mill chamber and in the area of the sieve. For all the cases considered in the research heat load is minor, and the temperature did not exceed 40°C.

The analysis of the obtained recycle disintegration shows the dominant participation of fraction of grain range of  $3,5 < x < 5$  mm, regardless the structure type (Fig. 4). This grain fraction participation constitutes about 35% of the whole mass of the obtained recycle. Fractions of  $5 < x < 6$  mm and  $6 < x < 7$  mm also have a great weight for the grain distribution. Together they constitute another 35% of the mass of the analysed recycle input regardless the polystyrene structure type. It can, therefore, be agreed that the sieve of  $\varnothing 9$  mm generates the greatest content of grains within the range of 3,5 to 7 mm, which, form the point of view of further processing, is a positive phenomenon.

It is also worth mentioning that the initial analysis of microscope pictures reveals that in case of porous polystyrene a set of grains with flat cross planes and straight edges was obtained (with clear marks of knife cutting), which shows the dominant significance of cutting in material division. Solid polystyrene recycle is characterised by similar shape. On the contrary, the difference in relation to porous material concerns the cutting surfaces which for recycle are less flat with elements of hollows and bulges. This shows a significant participation of percussive cracking in brittle polystyrene disintegration, which gives an additional confirmation of low energy consumption for solid PS. Initiated by cooperative cutting knives material cutting is, due to its hardness and brittleness, further propagated unprompted. The above described mechanism of polystyrene division finds its confirmation in the obtained recycle grain content.

Despite the use sieves of the hole diameter of 9 mm in the knife mill, about 50% of the mass is composed of grains of the average volume of 5 mm and less (Fig. 4).

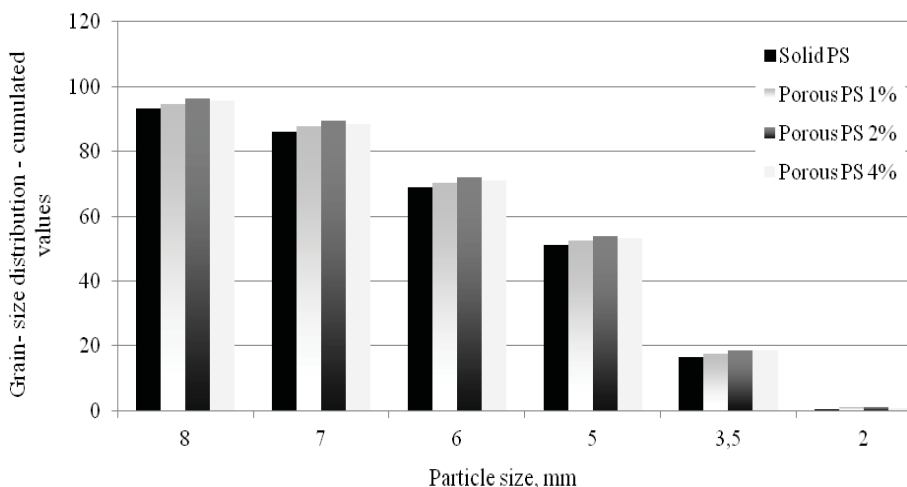


Fig. 4. Grain size distribution of the obtained PS recyclate

## 5. Conclusions

The presented research proves that the porous structure created in polystyrene significantly influences the material susceptibility to grinding. Together with the pore content growth in the PS structure, the material segmentation in a knife mill chamber takes place with the lower participation of impact cracking, mainly though cutting. Polystyrene modification through its pore-filling caused obtaining the material of a restricted susceptibility to impact cracking, whose segmentation to the grain degree allowing subsequent processing requires higher energy expenditures. Porous polystyrene grinding is from the point of view of efficiency and unitary energy consumption, far less effective. The employment of the same material disintegration conditions caused obtaining similar grinding degree. The dominant fractions, constituting more than 60% of the input mass, are a set of grains of much smaller dimensions than the ones used in the working chamber of the sieve (the hole diameter of  $\varnothing$  9mm).

## References

- [1] Bieliński, M., *Techniki porowania tworzyw termoplastycznych*, Akademia Techniczno-Rolnicza, Bydgoszcz 2004.
- [2] Sołtysiak, R., Bieliński, M., *Właściwości litych i porowatych płyt z PVC*, Inżynieria i Aparatura Chemiczna, SIMPress, 44 (36), pp. 74-75, Gliwice 2005.
- [3] Flizikowski, J., *Rozdrabnianie tworzyw sztucznych*, Akademia Techniczno-Rolnicza, Bydgoszcz 1998.
- [4] Sykutera, D., *Stanowisko badawcze i wstępne wyniki badań cięcia termoplastycznych tworzyw porowatych*, Przetwórstwo Tworzyw, IMPiB, 4 (136), pp. 214-217, Gliwice 2010.
- [5] Sykutera D., *Cięcie wolnoobrotowe porowatego PVC*, Inżynieria i Aparatura Chemiczna, SIMPress, 45 (37), pp.76-77, Gliwice 2006.
- [6] Sykutera, D., *Recykling mechaniczny porowatego polietylenu małej gęstości*, Przetwórstwo Tworzyw, IMPiB, 5 (143), pp. 382-384, Gliwice 2011.

- [7] Sykutera, D., *Stanowisko do cięcia i rozdrabniania porowatych tworzyw termoplastycznych*, Zeszyty Naukowe Politechniki Poznańskiej, 12, pp. 331-336, Poznań 2010.
- [8] Konieczka, R., Kałużny, W., Sykutera, D., *Drehschneiden im Prozess der Feinzerkleinerung von Gummi*, Kautschuk Gummi Kunststoffe, Hüthig Verlag, 9 (50), pp. 641-644, Heidelberg 1997.

Acknowledgments: The authors are grateful to Ministry of Science and Higher Education of Poland for financial support of this work (Project N° N508 442236)



## COMPUTER AIDED LABORATORY ACCREDITATION PROCESS - SERVICE TO THE CUSTOMER AS A REQUIREMENT OF ISO/IEC 17025 STANDARD – INITIAL DISCUSSION PAPER

Marek Szczutkowski

University of Technology and Life Sciences in Bydgoszcz  
ul. Prof. Kaliskiego 7 85-789 Bydgoszcz, Poland  
phone: +48 52 340 82 55, fax: +48 52 340 82 55  
e-mail: m.szczutkowski@utp.edu.pl

### *Abstract*

*The problem of quality of laboratory test results is essential in the context of their future application for example in machine design. Usually quality of test results means their reliability. To achieve it laboratories often tend to accredit their tests in national accreditation bodies in accordance with ISO/IEC 17025 standard. To fulfill the requirements means to introduce a lot of effort in technical and organizational areas of activity. In order to help and support such activities the attempt of elaboration of computer aided accreditation software is being developed. One of the key issues of the problem is to fulfill the mentioned requirements from the range of the clause 4.7 „Service to the Customer” but also from the point of view of an organization trying to achieve the highest level of the customer's satisfaction. The paper discusses the problem focusing on basic assumptions that need to be viewed. On the base of developed works and own experience suggestions for application are added.*

**Keywords:** quality, laboratory, accreditation, reliability of tests, service to the customer

### 1. Introduction

A laboratory is a place where tests are performed in order to gather data needed in various processes i.e. scientific, production, design ones. In such a case a matter of reliability of test results seems to be an essential issue. The laboratory has to prove its competency in performance of different test methods (the standard or own ones). In practice many problems may occur. They can be related among others with reliability of an applied testing method, order processing etc. Discussion on reliability leads to quality problems. In relation to laboratory processes there are doubts on quality of service [7, 8]. As a consequence of experience in the discussed field there were elaborated and issued international standards of ISO 9000 series. They are based on ideas and assumptions of total quality management (abbrev. TQM). The edited standards caused essential changes in approach to management processes. These standards show a producer can design, develop and present a quality management system. The goal of these standards is to define the base for such a system. The structure of mentioned standards is universal and can be applied in various conditions [6, 8].

In case of testing laboratories ISO 9000 standards can be applied as well. The next step to reach a customer's satisfaction in laboratory services is the implementation of requirements included in ISO/IEC 17025 standard [1]. Gaining an accreditation certificate in accordance with the standard confirms testing competencies of the laboratory. The standard widens requirements of ISO 9000 standards with technical competencies referring to essential activities of individual laboratories [5].

As it was mentioned above the problem of accreditation based on the consists of two parts: technical and management. While the second one is usually referred to well known ISO/IEC 9000 standard series and it is possible to find a lot of information on the issue so the first one has not been described sufficiently enough. As a result an author of the paper, supported by scientists working in the environment of strength and fatigue testing laboratories, decided to elaborate and develop software tools to implement, maintain and manage the quality system in accredited testing laboratories with a special reference to strength laboratories. The aim of works is to develop the methodology of implementation of quality system with accordance to ISO/IEC 17025:2005 standard on the base of propose software. Additionally, the aim of software is to face the most often problems connected usually with documentation, both traditional and electronic. Moreover the system will help in exchanging experience of laboratory specialists by communication with authors. Some developments of works can be found in various scientific papers i.e. [2] , [3] and [4].

What is more important in the context that modern generations communicate and work usually with usage of IT tools. While in the 1960s computers started to be implemented step by step in industry systems of files started to remove traditionally gathered and processed data. Since then database systems have started to become a standard tool [3, 4].

Service to the customer is an essential issue of most quality standards including ISO/IEC 17025. The aim of this paper is to present a role and basic assumptions for including the good customer service in the designed software in accordance with the standard [1].

## **2. Service to the customer as a requirement of ISO/17025 standard and an element of the designed software**

Designed software consists of 7 modules that are able to work independently. They can be a part of the management system (8th application – as in the algorithm) built in a different way what can increase the number of potential users. On the other hand the efficient working of individual modules can lead to implementation of all modules that support the system in the whole. System based on the proposed software can eliminate present problems, especially in the area of traditional and electronic documentation, facilitate the fulfilling of accreditation requirements, and enhance exchange of experience [2, 3].

Software, referring to requirements of ISO/IEC 17025:2005 standard, was divided into two groups:

- a) requirements referring to management system (documentation, internal audits, corrective and preventive actions, management system reviews),
- b) requirements referring to technical area (testing method, measurement database, personnel).

To facilitate the programming process (especially in the context of application of object-oriented programming) the above division was presented in fig. 1 [2, 3].

At the moment it is essential to compare the above described design with specific requirements of the standard [1] on the service to the customer. The clause 4.7 of the standard states:

*„4.7.1. The laboratory shall be willing to cooperate with customers or their representatives in clarifying the customer's request and in monitoring the laboratory's performance in relation to the work performed, provided that the laboratory ensures confidentiality to other customers.*

*NOTE 1. Such cooperation may include:*

- a) providing the customer or the customer's representative reasonable access to relevant areas of the laboratory for the witnessing of tests and/or calibrations performed for the customer;*
- b) preparation, packaging, and dispatch of test and/or calibration items needed by the customer for verification purposes.*

*NOTE 2. Customers value the maintenance of good communication, advice and guidance in technical matters, and opinions and interpretations based on results. Communication with the customer, especially in large assignments, should be maintained throughout the work. The*

laboratory should inform the customer of any delays or major deviations in the performance of the tests and/or calibrations.

4.7.2. The laboratory shall seek feedback, both positive and negative, from its customers. The feedback shall be used and analyzed to improve the management system, testing and calibration activities and customer service.

NOTE. Examples of the types of feedback include customer satisfaction surveys and review of test or calibration reports with customers.”

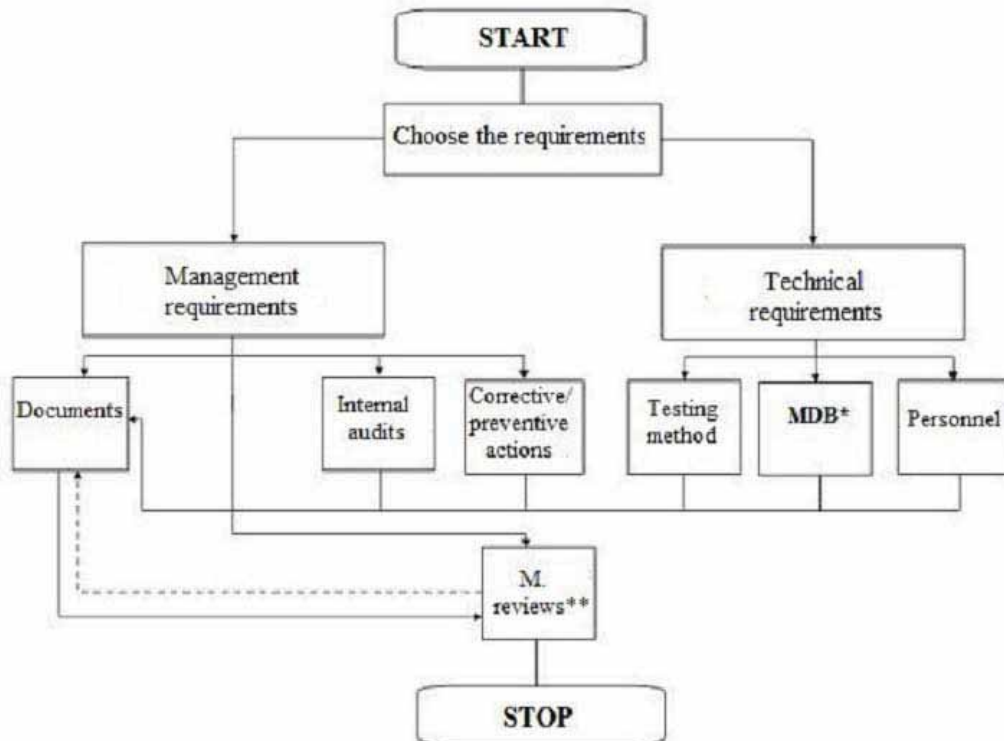


Fig. 1. Algorithm of computer aided accreditation software in testing laboratories, \*MDB – measurement database, \*\* M. reviews – management reviews [2, 3]

From the above it results that issues on the customer service are related with documents. But on the other hand, analysing fig. 1, it can be noticed that documents are connected with all technical requirements. So the question is what kind of assumptions should be considered in order to fulfill the requirements efficiently? How to fit service to the customer issues in the range of the designed software? Should it be a separate module or a part of one of the presented in fig. 1?

### 3. Basic assumptions for implementation of the customer service requirement

The first assumption is obviously connected with fulfillment of the above mentioned requirement. The standard [1] is the base for implementation of the quality management system in the laboratory and, as a next stage, gaining an accreditation certificate in accordance with the standard confirms testing competencies of the laboratory the propose software has to obey the requirements. But, from the different point of view, the customer service is a business process. Considering as a goal earning money, gathering funds for future investments most of laboratory managers base on their own experience building relationships with customers. From this point of

view an attempt to formulate assumptions, as input data for the customer service implementation as the element of the software, was undertaken. Following assumptions are suggested:

- a) computer aided service to the customer tool has to use present resources and facilities including the ones connected with hardware, software and knowledge of workers. Such an attitude will improve, accelerate the implementation as well as decrease associated costs also from the point of view of personnel trainings,
- b) computer aided service to the customer tool has to control the work of a servicing crew. In such a context the essential value should be connected with qualifications, education and personal skill of members of the servicing crew. computer aided service to the customer tool has to reflect such a situation so probably differences on mentioned features should be applied in various editions of the software focusing on relation software - user,
- c) computer aided service to the customer tool has to bring a result in possibility of customer's access to current information on the realized service. Such an attitude may result in increase of customer's confidence, trust and safety in the context of planning of own activities regarding the service and as a consequence increase of customer's satisfaction. It is trivial to state that today information is the most valuable good. Constant monitoring of test services can be another proof, for potential customer, that laboratory is a reliable testing unit and at the same time the customer can plan his/her activities in accordance with the stage of works,
- d) computer aided service to the customer tool has to enable the communication on the line customer – service provider (laboratory) not only in the aspect of deadlines but also technical details or organizational issues connected with the service process,
- e) computer aided service to the customer tool has to result in feedback that stands for the base of analysis and decision making processes on input data (related to hardware, software, personnel or global decisions in the context of the customer service) .

#### 4. Summary

The general idea of computer aided service to the customer is to fulfill the requirements of ISO/IEC 17025 standard and what is more to provide the customer service in a new, modernized form. Thanks to the form the customer receives the possibility of up-to-date service monitoring and new platform for communication with a service provider (laboratory) in more efficient way both in the time context as well as in the test technical context. Finally such approach may result in different innovations in the field of laboratory management. Implementing such a solution laboratories should consider different assumptions presented in the paper.

What is more the final goal of different activities (organizational, technical, promotional, scientific etc.) should result in efficiency increase and reliability of test results. Increase in confidence, trust and safety of current customers and gaining new clients may result in constant improvement of the laboratory.

#### References

- [1] ISO/IEC 17025:2005 - General requirements for the competence of testing and calibration laboratories.
- [2] Szczutkowski, M., *Computer aided laboratory accreditation process. Measurement database as a initial stage of software application*, Journal of POLISH CIMAC Vol. 6 No 3, 2011.
- [3] Szczutkowski M., *Narzędzia informatyczne wspomagające proces akredytacji laboratoriów wytrzymałościowych. Projekt bazy danych przyrządów pomiarowo – badawczych cz. 1 Etap wstępny projektu-podstawowe założenia*, Logistyka, Instytut Logistyki i Magazynowania, no. 6, 2010.
- [4] Szczutkowski, M., *Narzędzia informatyczne wspomagające proces akredytacji laboratoriów wytrzymałościowych. Projekt bazy danych przyrządów pomiarowo – badawczych cz. 2 Specyfika języka baz danych*, Logistyka, Instytut Logistyki i Magazynowania, no. 6, 2010.

- [5] Szczutkowski, M., *Walidacja metod badawczych w laboratorium akredytowanym. Część I. Podstawowe zagadnienia*, Inżynieria i Aparatura Chemiczna nr 2, 2009.
- [6] Szczutkowski, M.: *Zastosowanie zasad TQM w laboratoriach badawczych poddających się procesowi akredytacji*, X Międzynarodowa Konferencja „TQM Stymulatorem innowacyjności”, 2008.
- [7] Szczutkowski, M., Bromberek F., *Rola kierownika ds. jakości w uczelnianym laboratorium badawczym zarządzanym zgodnie z zasadami TQM*, XI Konferencja „Innowacyjność i jakość – wyznaczniki sukcesu”, 2010.
- [8] Szczutkowski M., Ligaj B., *Procedura szacowania niepewności badań trwałości zmęczeniowej - założenia i kluczowe elementy*, Logistyka 6/2010.





## ELABORATION OF THE WIND TURBINE CONSTANT DIAGNOSTIC SYSTEM AS A TESTING PROCEDURE IN AN ACCREDITED LABORATORY – THE PROCESS APPROACH TO WRITING THE DRAFT DOCUMENT

Marek Szczutkowski

University of Technology and Life Sciences in Bydgoszcz  
ul. Prof. Kaliskiego 7 85-789 Bydgoszcz, Poland  
phone: +48 52 340 82 55, fax: +48 52 340 82 55  
e-mail: m.szczutkowski@utp.edu.pl

### Abstract

*The paper deals with the problem of writing a test procedure as a document of an accredited testing laboratory in accordance with ISO/IEC 17025 standard. The test procedure is a key document presenting a test method of the laboratory while the test is not performed in accordance with a specific standard (i.e. standards on strength of materials and constructional elements). There is presented the process approach on the example of the wind turbine constant diagnostic system. Individual stages of works are presented as well as an example of modern methodology achievements in the range of testing methods on wind turbine diagnostics as an element of input data for the procedure. Reference materials are named and stated as basic sources to define criteria for evaluation of wind turbine conditions. The whole is summarized with general remarks on the process approach in reference to both organizational and technical aspect of the quality management system of the laboratory.*

**Keywords:** quality, laboratory, accreditation, testing methods, wind turbines.

### 1. Introduction

Renewable energy sources like wind energy are copiously available without any limitation. Wind turbines are used to tap the potential of wind energy, which is available in millions of MW. Reliability of wind turbine is critical to extract this maximum amount of energy from the wind [8]. Wind energy is undergoing expansion, and it is bound to grow to a commercial/consumer level in the decades to come. This growth has materialized in the form of large-scale wind farms, wind energy cooperatives, wind turbines owned by individual investors, and multinational exploration of remote sites and offshore locations. Despite the increasing rated capacity of wind turbines, operation and maintenance (O&M) costs remain high due to failures of wind turbine components such as gearboxes and blades. To make matters worse, in spite of several drawbacks associated with current/traditional maintenance practices, almost all industries are still following them. Thus, there is a great need to educate managers of such firms about the economic justification of performance monitoring in the wind industry, which is currently characterized by high maintenance costs [17].

Taking into consideration the above there are more and more companies that try to develop and offer new diagnostic services in the area of wind turbines. Usually, from the point of view of

competitiveness, there are at least several problems i.e. time issues, price, reliability of test results. In order to compete more efficiently and to reach a customer's satisfaction in laboratory services the implementation of requirements included in ISO/IEC 17025 standard [2] is an option for the testing service provider. Gaining an accreditation certificate in accordance with the standard confirms testing competencies of the laboratory. The standard widens requirements of ISO 9000 standards with technical competencies referring to essential activities of individual laboratories [10].

The aim of the paper is to present the process approach to writing the draft procedure on the wind turbine constant diagnostic system. As the requirement of ISO/IEC 17025 standard such a procedure can be a base, from the point of view of technical requirements, to create the quality management system and in the future to undergo the process of accreditation. As it was mentioned such a solution increases the competitiveness of the testing unit.

## **2. Testing method as a process**

The procedure is a document, in the range of the laboratory management system that describes in details the methodology of a test. In this case: wind turbine diagnostic system. If the test is performed in accordance with a standard there is no need of a special documentation describing the methodology. For instance if the laboratory deals with strength of the weld line in the metal layer and bonding between layers by use of a cone for multilayer M pipes in plastic piping systems its tests can be based on ISO/TR 18124:2006 standard [3] that specifies the method. However if the laboratory is able to reach goals set by the standard ; in a different way than it is described in the document [3] the procedure has to be developed and implemented.

Considering the topic of the wind turbine constant diagnostic system first of all, a goal for the procedure has to be set. As an assumed to create such a system that gives reliable test results minimizing time needed for essential operations. Minimization means to limit time for the direct work at the wind turbine. Time has to be limited to data gathering and data processing has to be performed at the laboratory of the service provider. Gaining the reliability of test results in the future is possible by elaboration of the own testing method in the for of procedure and undergoing the process of accreditation in order to confirm that laboratory fulfills the requirements of the standard [2]. Such an approach, apart from the mentioned competitiveness issues, results also as a organizational innovativeness source in the company that forces other technical activities influencing reliability of test results.

Another step, after actions described above, may be creation of the own computer support system for the defined testing process. The elaboration of a specific process and than its formalization as a testing procedure can be an input data to elaborate an algorithm of a special application software. The aim of the software would be to gather data at limited parameters – measurement is going to be performed only if a limit is crossed.

Moreover assuming that above mentioned issues the plan of works can be based on the scheme presented in fig. 1 [13]. The figure gives general approach and having in mind the aim of the paper the „processing” element should be completed with tests and materials and tools to fulfill the main goal defined in input data.

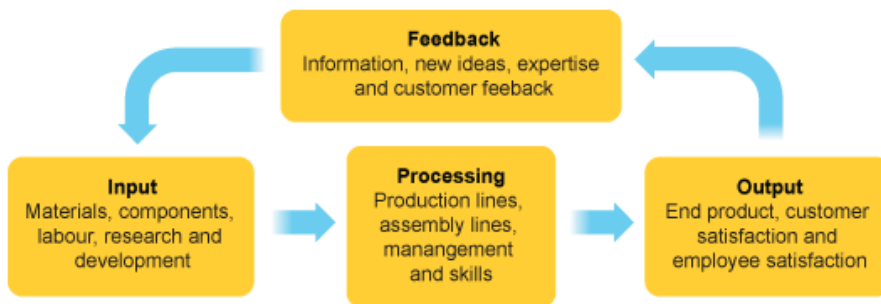


Fig. 1. Production/ service system with feed back [13]

In accordance to the above the following stages of works for the procedure writing were assumed:

- a) identification of input data for the process as the analysis of:
  - personnel qualifications,
  - needs of customers in the discussed area,
  - competitors in the market,
  - testing tools and methods in accordance with the modern achievements and requirements,*(Input data can be identified among others by literature review, gathering of data from the testing market, discussions with customers as well as the analysis of up-to-date experiences. The gathered information has to be elaborated and concluded before its transformation into the testing procedure.).*
- b) definition of precise requirements on tools and facilities (i.e. testing and measurement equipment) along with referring metrological requirements,
- c) design of the test system in the form of own testing procedure,
- d) summary connected with the cost analysis on the base of activities from a) to c),
- e) initial validation of test service/ procedure in cooperation with former customers that requires direct contacts and consultations,
- f) preparation of a report with an essential attachment in the form of the testing procedure.

### 3. Modern methodology achievements in the range of testing methods on wind turbine diagnostics as an element of input data for the procedure

In reference to the presented plan (stages of works) suitable technical and organizational assumptions have to be considered in the process of design of the testing procedure on the wind turbine diagnostic system. Obviously knowledge gathered from own experience, references, trainings or expert discussion is essential. As we cannot compare and classify experience, trainings or expert discussion one can say that the access to references nowadays is almost unlimited. In the era of Internet limitations may consider linguistic issues or the price of an individual file.

As it was mentioned there are various reference materials that can be useful in the process. Among different ones one can mention as interesting and worth reading such as [5, 6, 7, 9, 11, 12, 14, 15, 16, 17] The own analysis of reference materials enabled to define two base documents as well as two basic criteria for final works in the range of preparation of the testing procedure on the wind turbine diagnostic system. Base documents were recognized as following:

- a) VDI 3834 Part 1 - Measurement and evaluation of the mechanical vibration of wind energy turbines and their components - Onshore wind energy turbines with gears,
- b) ISO 10816-1:1995 - Mechanical vibration - Evaluation of machine vibration by measurements on non-rotating parts - Part 1: General guidelines.

VDI 3834 Part 1 gives practical advice on the measurement and evaluation of the mechanical vibrations of wind energy plants whereas ISO 10816 establishes the general conditions and procedures for the measurement and evaluation of vibration, using measurements made on the non-rotating parts of machines. The general evaluation criteria relate to both operational monitoring and acceptance testing and have been established primarily with regard to securing reliable long-term operation of the machine [1, 4].

The analysis of references led to define two basic criteria for evaluation:

a) machine component criterion – the wind turbine is defined by following components (fig. 2 presents the first criterion in accordance with [4]):

- gearbox,
- nacelle,
- tower,
- generator,

b) the values of the characteristics measured at these components:

- velocity,
- acceleration.

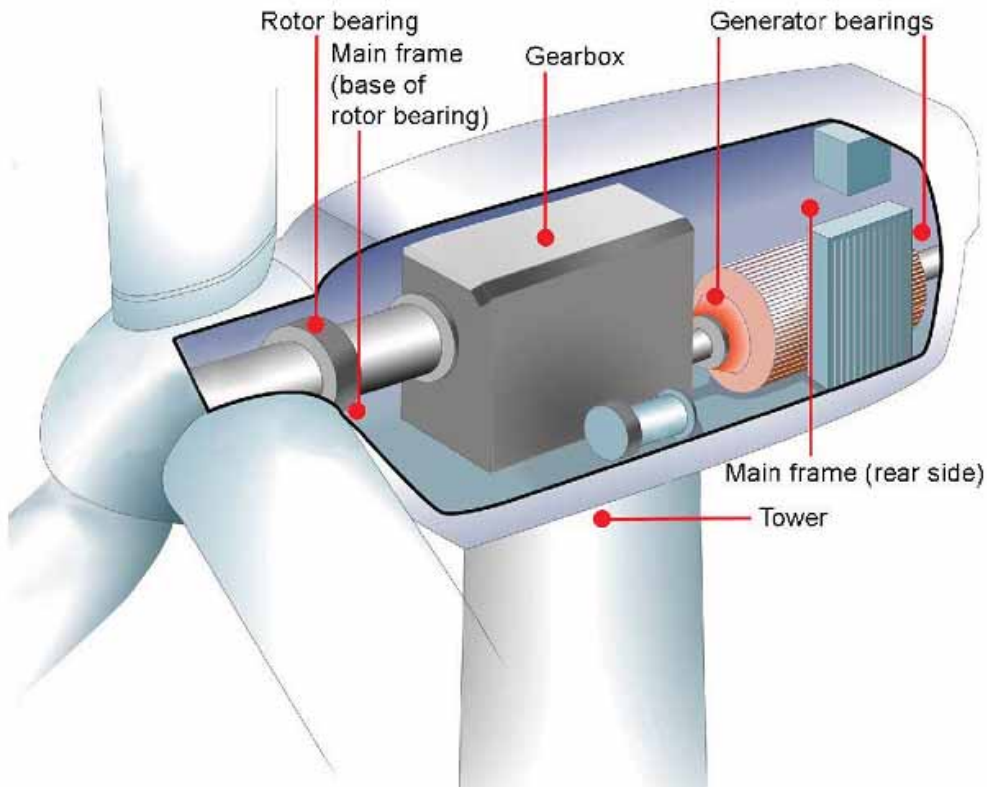


*Fig. 2 Components and measuring points to VDI 3834 part 1 [4, 14]*

#### 4. Summary

The goal of each company is to earn money as a result of its activity. Laboratories are units that offer unique services in comparison to other companies but economical laws and organizational problems are also their everyday reality. In order to improve their efficiency, develop management system, organizational skills they can implement the requirements of ISO/IEC 17025 standard. The tool is considered to be also efficient from the point of view of competitiveness.

Quality management systems generally base on the process approach. On this assumption in the paper there was presented the process approach to writing the draft testing procedure on the example of the wind turbine constant diagnostic system. Individual stages were discussed and followed by the example of modern methodology achievements in the range of testing methods on wind turbine diagnostics as an element of input data for the procedure.

Such a systematical approach enables to organize works more efficiently and reach reliability of test results in the process of elaboration of the testing procedure. Precise definition of input and output data is essential to design the correct transformation process. In such a case feedback information seems to be more clear and useful and in the range of corrective and preventive actions it is easier to define the sources of nonconformities.

#### References

- [1] ISO 10816-1:1995 - Mechanical vibration - Evaluation of machine vibration by measurements on non-rotating parts - Part 1: General guidelines.
- [2] ISO/IEC 17025 - General requirements for the competence of testing and calibration laboratories.
- [3] ISO/TR 18124:2006 - Plastics piping systems - Multilayer M (metal) pipes - Test method for strength of the weld line in the metal layer and bonding between layers by use of a cone
- [4] VDI 3834 Part 1 - Measurement and evaluation of the mechanical vibration of wind energy turbines and their components - Onshore wind energy turbines with gears.
- [5] Barszcz T., *Application of diagnostic algorithms for wind turbines*, Diagnostyka 2 (50), 2009.
- [6] Cotton, I., *Lightning protection for wind turbine blades and bearings*, Wind Energy, 2001.
- [7] European Commission / DG TREN, *Advanced maintenance and repair for offshore wind farms using fault prediction and condition monitoring techniques*, Final Report, NNE5/2001/710, FP5 Contract, 2005.
- [8] Hameed, Z., *Condition monitoring and fault detection of wind turbines and related algorithms: A review*, Renew Sustain Energy Rev, 2007.
- [9] Kusiak, A., Wenyan, L., *The prediction and diagnosis of wind turbine fault*, Renewable Energy 36, 201.
- [10] Szczutkowski, M., *Walidacja metod badawczych w laboratorium akredytowanym. Część I. Podstawowe zagadnienia*, Inżynieria i Aparatura Chemiczna nr 2, 2009.
- [11] Yan, Y., Osadciw, L.A., Benson, G., White, E., *Inverse data transformation for change detection in wind turbine diagnostics*, Proceedings of 22nd IEEE Canadian Conference on Electrical and Computer Engineering, Delta St. Johns, Newfoundland and Labrador, Canada, May 2009.
- [12] Ye, X., Veeramachaneni, K., Yan, Y., Osadciw L.A., *Unsupervised learning and fusion for failure detection in wind turbines*, Proceedings of 12th International Conference on Information Fusion, Seattle, Washington, USA, July 2009.
- [13] <http://www.bbc.co.uk>, 06/2012.
- [14] <http://www.mmf.de>, 06/2012.
- [15] <http://www.newagepublishers.com>, 09/2011.

- [16] <http://projekter.aau.dk>, 09/2011.
- [17] <http://www.windsystemsmag.com>, 09/2011.



## THE INFLUENCE OF ISOTHERMAL QUENCHING ON THE EFFECTS OF THERMOMECHANICAL TREATMENT OF SPHEROIDAL CAST IRON

Tedeusz Szykowny\*, Krzysztof Ciechacki

University of Technology and Life Sciences  
al. Prof. S. Kaliskiego 7, 85-789 Bydgoszcz, Poland  
tel.: +48 52 3408748, fax: +48 52 3408244  
\*e-mail: tadeusz.szykowny@utp.edu.pl

### Abstract

*Spheroidal cast iron was treated thermomechanically both in high as well as low temperature. The two temperatures we adopted for isothermal quenching were 370° and 300° C. Plastic deformation was obtained by rolling with 25% deformation. Testing was conducted on flat samples used for stretching with the thickness of 4mm. We determined the  $R_m$  tensile strength,  $R_{p0.2}$  proof stress,  $A$  elongation, and HRC hardness. A microstructure test (LM, SEM), and X-ray diffraction test were conducted. We found significant positive impact of thermomechanical treatment on the structural characteristics and properties of cast iron, particularly with upper ausferrite present.*

**Keywords:** spheroidal cast iron, thermomechanical treatment, structure, mechanical properties

### 1. Introduction

Merging thermal and mechanical treatments makes it possible to effectively increase strength properties of iron-carbon alloys. It is in fact the only treatment with the use of which it is possible to increase strength without detriment, and frequently even with an increase, to plasticity [1]. At present, interest in thermomechanical treatment of spheroidal cast iron is growing, which can be seen in the ever higher number of studies published on this topic [2-7,9].

Particularly interesting is thermomechanical treatment (OCP) of spheroidal cast iron which undergoes isothermal treatment to obtain the AADI cast iron (Ausforming Austempered Ductile Iron). The authors of [2] used rolling and isothermal quenching of spheroidal cast iron to obtain higher tensile strength, yield point and elongation as compared to the ADI cast iron (Austempered Ductile Iron).

In this study, we obtained AADI cast iron through low- or high-temperature thermomechanical treatment. We adopted two temperature values for isothermal quenching 300° or 370° C, with constant deformation value of 25%. Our objective was to obtain either lower (300° C) or upper (370° C) ausferrite structure from undercooled austenite with plastic deformation. We compared the properties of cast iron after thermomechanical treatment with the properties of cast iron having undergone only thermal treatment (OC).

## 2. Material, Schedule and Test Methods

In the study, we used spheroidal low-copper cast iron with the chemical content as seen in Table 1.

Table 1. Chemical content of cast iron, % of mass

| Element   | C    | Si   | Mn   | P    | S    | Cr   | Cu   | Mg   |
|-----------|------|------|------|------|------|------|------|------|
| % of mass | 3.76 | 3.07 | 0.35 | 0.07 | 0.02 | 0.04 | 0.48 | 0.06 |

The cast iron has been classified as grade EN-GJS-600-03. Its structure can be seen in Figure 1.

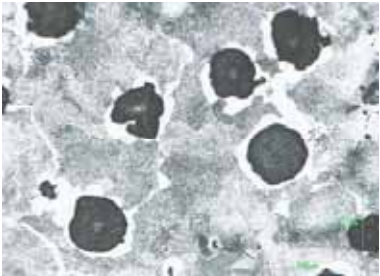


Figure 1. Cast iron microstructure in the as-cast condition, magnified 250x, times, nital edged

We cast YII samples in green-sand moulds. From the cuboid part of the wedge, we cut flat samples to be stretched, with the thickness of 4mm, measurement section width of 10mm, and measurement section length of 70mm. The samples were then treated as shown in Figure 2. The 25% cold work along the sample thickness was created through rolling on a rolling mill with plain-bodied rolls having the diameter of 95mm. Cast iron samples were austenitized in a chamber furnace, and quenched isothermally in a bath furnace with SO140 saltpetre.

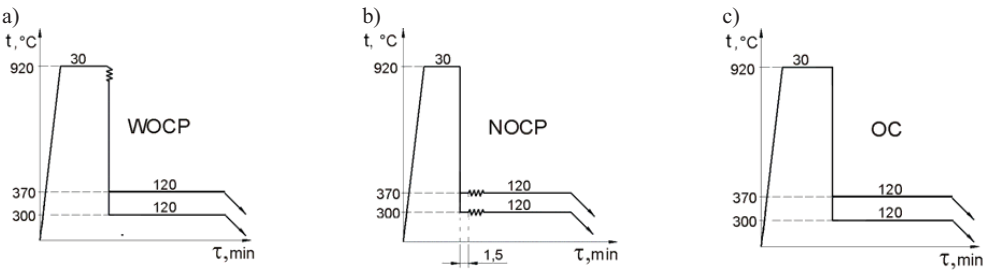


Figure 2. Spheroidal cast iron treatment diagram:  
a) high-temperature thermomechanical treatment (WOCP),  
b) low-temperature thermomechanical treatment (NOCP),  
c) isothermal heat treatment (OC)

The strength testing was conducted on an INSTRON 8501 machine. Using typical tensile tests (PN-EN ISO 6892-1:2010), we established the values of the  $R_{p0.2}$  yield point,  $R_m$  tensile strength, and A relative elongation. Microscopic examinations were conducted on microsections etched with 2%  $HNO_3$  solution. We used optical microscopy (NU2 microscope) or scanning microscopy (JSM 5600 microscopy).

X-ray diffraction testing was conducted on a DRON diffractometer. We used iron-filtered radiation from a cobalt anode lamp. Based on diffractograms, we determined the type and lattice parameters of phases present in a cast iron matrix. Austenite content was established by direct

comparison [10].

Carbon content in austenite was calculated based on the lattice parameter according to the relationship cited by Ogi K. et al. [8]:

$$C_{\gamma} = \frac{a_{\gamma} - 0,35621}{0,00441} \quad (1)$$

where:

$C_{\gamma}$  – carbon content in austenite, % of mass;

$a_{\gamma}$  – austenite lattice parameter, nm.

The value of the austenite lattice parameter was calculated from the following formula:

$$a = \frac{\lambda}{2 \sin \Theta} \sqrt{h^2 + k^2 + l^2} \quad (2)$$

where:

$\lambda$  –  $\text{Co}_{K\alpha 1,2}$  wave equal to 0.179021nm;

$\theta$  – diffraction angle, °;

$h, k, l$  – Miller plane indices.

The austenite lattice parameter was determined based on angular line location {111}, whereas the ferrite lattice parameter – based on angular line location in relation to the planes {110}.

### 3. Test Results and Their Analysis

The results of the static tensile and hardness tests are shown in Table 2. The tensile test results are the mean from three measurements, whereas the hardness test was conducted nine times on each sample. We set confidence interval for the mean values with  $1-\alpha = 0.95$ .

Table 2. Mechanical properties of cast iron depending on the type of treatment and isothermal quenching temperature

| Isothermal quenching temperature, $t$ , °C | Type of treatment | $R_{p0.2}$ , MPa | $R_m$ , MPa | A, %     | Hardness, HRC |
|--|-------------------|------------------|-------------|----------|---------------|
| 370  | WOCP              | 808 ±18          | 1112 ±26    | 5.7 ±0.3 | 38.7 ±0.6     |
|  | NOCP              | 1080 ±23         | 1252 ±19    | 2.5 ±0.2 | 43.1 ±1.1     |
|  | OC                | 828 ±28          | 1072 ±33    | 5.1 ±0.2 | 37.0 ±0.8     |
| 300  | WOCP              | 1001 ±29         | 1199 ±22    | 2.9 ±0.2 | 42.5 ±1.1     |
|  | NOCP              | -                | 893 ±38     | 0.4 ±0.3 | 48.9 ±1.6     |
|  | OC                | 752 ±32          | 1381 ±36    | 6.0 ±0.4 | 46.2 ±1.1     |

X-ray diffraction results are shown in Table 3.

Table 3. X-Ray diffraction results

| Isothermal quenching temperature, $t$ , °C | Type of treatment | Phase composition* | $a_{\gamma}$ <sup>1)</sup> nm | $C_{\gamma}$ <sup>2)</sup> % mas. | $v_{\gamma}$ <sup>3)</sup> % obj. | $a_{\alpha}$ <sup>4)</sup> nm |
|--|-------------------|--------------------|-------------------------------|-----------------------------------|-----------------------------------|-------------------------------|
| 370  | WOCP              | F+A+P              | 0.36217                       | 1.35                              | 38.1                              | 0.28590                       |
|  | NOCP              | F+A                | 0.36264                       | 1.46                              | 47.0                              | 0.28621                       |
|  | OC                | F+A                | 0.36264                       | 1.46                              | 30.1                              | 0.28515                       |
| 300  | WOCP              | F+A                | 0.36219                       | 1.36                              | 25.5                              | 0.28585                       |
|  | NOCP              | F+A+M              | 0.36287                       | 1.51                              | 30.1                              | 0.28607                       |
|  | OC                | F+A                | 0.36233                       | 1.39                              | 16.7                              | 0.28607                       |

\* F - ferrite, A – austenite, P – pearlite, M – martensite

<sup>1)</sup> austenite lattice parameter, <sup>2)</sup> carbon content in austenite, <sup>3)</sup> volumetric percentage of austenite, <sup>4)</sup> ferrite lattice parameter

The microstructure of cast iron quenched isothermally at 370°C is shown in Figure 3.

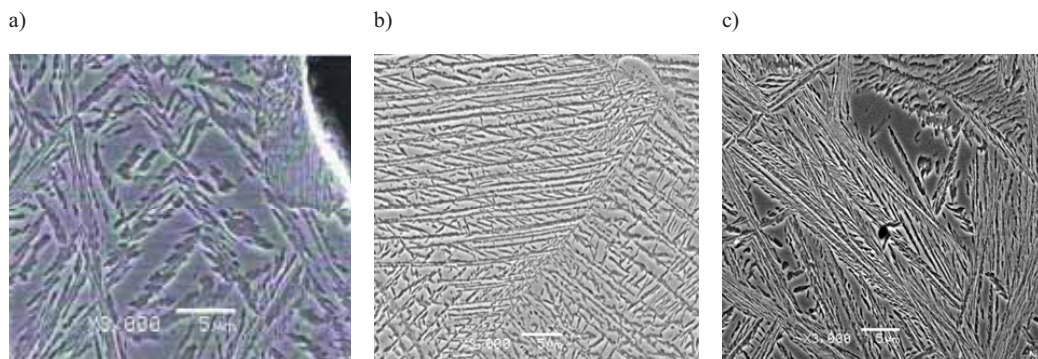


Figure 3. The microstructure of cast iron quenched isothermally at 370°C, magnified 3000x times, nital etched  
a) WOCP; b) NOCP; c) OC

The microstructure of cast iron quenched isothermally at 300°C is shown in Figure 4.

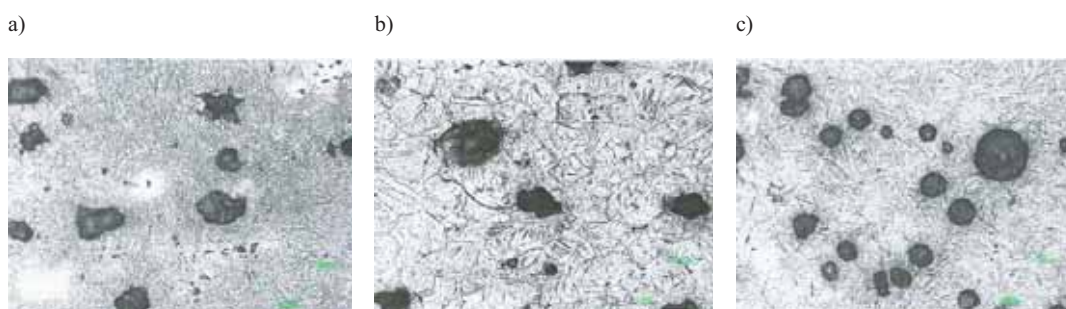


Figure 4. The microstructure of cast iron quenched isothermally at 300°C, magnified 250x times, nital etched  
a) WOCP; b) NOCP; c) OC

In the case of isothermal quenching at 370°C (upper ausferrite), any treatment (WOCP, NOCP, OC) increases strength two times as compared to cast iron in as-cast condition. High-temperature thermomechanical treatment causes slight increase in tensile strength and plasticity as compared to cast iron which is not treated mechanically (OC) (Table 2). The relatively small WOCP effect occurs due to the presence of some pearlite in the structure beside ausferrite (Figure 3a). Sole presence of upper ausferrite could not be achieved because of low hardening capability of cast iron. Hence, for WOCP, alloy cast iron should be used, for instance with copper or nickel content. Low-temperature thermomechanical treatment leads to the increase of strength indices ( $R_m = 1250\text{MPa}$ ,  $R_{p0.2} = 1080\text{MPa}$ ) as well as hardness (43HRC). Plasticity, however, is lowered. Relative elongation is 2.5%. NOCP treatment influences ausferrite morphology. Fibre orientation and the decrease of distance between ausferrite lines can be observed (Figure 3b). Example X-ray diffractograms of cast iron after low-temperature thermomechanical treatment (NOCP) are shown in Figure 5.

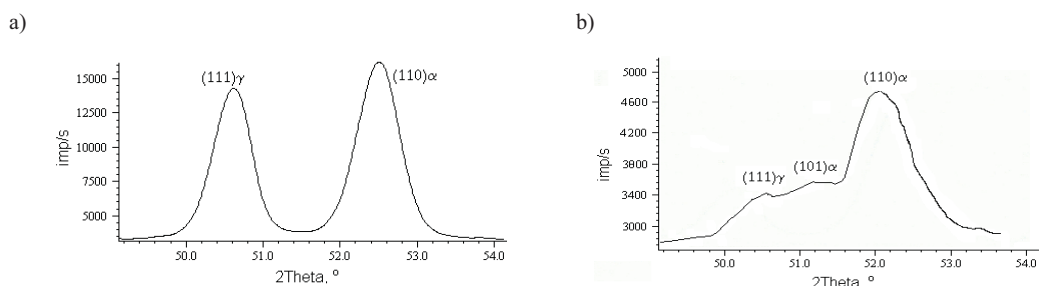


Figure 5. Cast iron diffractogramm after NOCP, quenched isothermally at: a) 370 °C, b) 300 °C

X-ray diffraction tests revealed that thermomechanical treatment increases austenite content as compared to cast iron undergoing only thermal treatment. Particularly high austenite content (47%) is present in cast iron undergoing NOCP.

With low-temperature thermomechanical treatment at 300°C, the objective will not be met (due to very low elongation and tensile strength). Obtained results can be explained by the presence of martensite in the structure (Figure 5b). Generally, it can be concluded that strength properties and hardness are higher in the case of quenching at 300°C, but plasticity is higher in the case of quenching at 370°C. Higher plasticity of cast iron at 370°C is related to higher content of austenite (Table 3) and ausferrite morphology (Figures 3 and 4).

#### 4. Conclusions

- High-temperature thermomechanical treatment with isothermal transformation at 370°C increases plasticity but lowers strength properties of cast iron as compared to 300°C;
- Low-temperature thermomechanical treatment with isothermal transformation at 370°C can be used to obtain grade EN-GJS-1200-2 of cast iron. NOCP at 300°C leads to martensite transformation in cast iron, which causes its premature brittle cracking;
- Favourable impact of thermomechanical treatment as compared to only thermal treatment occurs in isothermally quenched cast iron at 370°C;
- Introducing cold work during thermomechanical treatment results in increased content of stable high-carbon austenite, as compared to cast iron without any cold work.

#### References

- [1] **Przybyłowicz K.** (2008), Engineering iron alloys, Ed. Technical University of Kielce, Kielce
- [2] **Lakišev N.P., Ščerbedinski G.W.** (2001), Goračaja plastičeskaja deformacija vysokopročnogo čuguna, *MITOM*, nr 11, s. 16-17.
- [3] **Dettloff S.M. i inni** (2002), Ausforming austempered ductile iron. *International Scientific Conference, ADI – Foundry's Offer for Designers and Users of Castings, Foundry Research Institute, Kraków*, s II/1-8.
- [4] **Guzik E.** (2001), Cast processing operations. Selected topics, Archives of Foundry, Academy of Sciences, Katowice, Monograph, No. 1M.
- [5] **Chengchang J., Shigen Z.** (2006), Study of new type ductile iron for rolling: Composition design. *Materials Science and Engineering*, A419, pp. 318-325.
- [6] **Szykowny T., Giętka T.** (2006), Quenching and tempering of hot rolled ductile iron, Archives of Foundry, Academy of Sciences, Katowice, R.6, No. 19, pp. 349-354.

- [7] **Szykowny T., Ciechacki K.** (2006), Thermo-plastic ductile iron, Archives of Foundry, Academy of Sciences, Katowice, R.6, No. 19, pp. 341-348.
- [8] **Ogi K. i inni** (1989), Untersuchen einiger Aspekte des Austenitisierungsprozesses bei Gusseisen mit Kugelgraphit, *Giesserei-Praxis*, Nr 6, s. 73.
- [9] **Nofal A.A, Nasr El-din H., Ibrahim M.M** (2007), Thermomechanical treatment of austempered ductile iron, China Foundry, Vol. 4 No 4. S 304-309.
- [10] **Cullity B.D.** (1986), Fundamentals of X-ray diffraction. WNT, Warsaw.



## RENEWABLE FUELS - ADDITIONAL SOURCE OF HEAT ENERGY

Marek Szymczak

*University of Technology and Life Sciences in Bydgoszcz  
ul. Prof. S. Kaliskiego 7, 85-789 Bydgoszcz, Poland  
tel.: +48 52 340 82 58, fax: +48 52 340 84 62  
e-mail: marszym@utp.edu.pl*

### **Abstract**

*There is proposed a way of usage of dried sewage sediment with 90 % of dry mass as fuel to co-incineration with rape straw and next submitted to the process of gasification in order to increase the efficiency of the process. The purpose of putting into use that kind of fuel is to increase the possibility to obtain additional energy resources. The results of research on usage of fuel from sewage sediment and straw were presented.*

**Keywords:** biomass, dried sewage sediment, coburning/coincineration, gasifying, thermal process, heat

### **1. Introduction**

Signing by Poland Kyoto Protokol In 2002 introduces the duty of reduction of greenhouse gases and industrial dust emissions. Also EU supports these issues by introduction of Instruction 2001/77/WE on electric energy production generated in renewable energy sources. The regulation of Ministry of Economy, Work and Social Politics dated 30<sup>th</sup> May 2003 on particular duty of purchase of electric energy and heat from renewable energy sources and electric energy generated in the matching with heat generating what as a result gives the possibility of co-incineration of fuels.

All over the world the resources of biomass are estimated at the level of 280 EJ/year and are 6 times higher than the rate of their usage. And the increase of biomass production is connected with necessity of assignment of large areas of soil for energetic plants cultivation. World's biomass resources at present constitute from 9÷13% of energy requirements.

Statistical data show clear rising tendency as for the amount of communal and industry sediments for management. It is estimated that in 2015 the stream of mass will reach 720 Mg of dry mass/year. The management of sewage sediments has been limited to their disposal, composting, remanagement in agriculture as fertilizer or further processing with usage of thermal methods. Sewage sediment in waste water treatment plant undergoes fermentation process so as to use it for biogas production and burning it in gas generators.

The basic purpose of employed renewable fuel is assignment of parameters of gasifying of mass in the form of rape straw and dried sewage sediment of 90% of dry mass in various mass proportions and burning the obtained synthesis gas. The obtained research results may undergo comparison analysis with other types of biomass to estimate usability of used fuel for energetic purposes.

## 2. Sewage sediment

Drying of sewage sediments constitutes the basic condition enabling their potential management as fuel. Burning of dehydrated sediments after pressing, with moisture in the range of 75÷84% is virtually technologically impossible process and economically inefficient. Sediment with that high moisture can be disposed in landfills or, if it fulfils requirements, it is used as fertilizer in forestry and agriculture. It depends on possibilities of its management in the region where there is waste water treatment plant, on content of hazardous elements e.g. heavy metals and sale conditions.

Drying of sediment is extremely energy-consuming technological treatment. But heat for drying can be obtained by burning of biogas from sewage fermentation.

Treating part of sewage sediment as biomass and giving it thermal transformation it would allow to obtain extra energy. From sewage sediment which undergoes the process of evaporation we obtain organic fertilizer in the form of granulate of value 90% of dry mass.

Dried sewage sediment may be used again for co-burning as a mixture with wastes of wood, rape and rye straw, pine bark, willow *Salix viminalis*, and Pensylvanian mallow *Althea* and coal in various volume and mass ratio.

Heat of burning of sewage sediment is 17 MJ/kg for containing 70% of volatile substances. But for dried sewage sediment the burning value is about 14 MJ/kg. Dried sewage sediment is free from heavy metals but contains large amounts of ashes constituting about 35%.

From the definition of instruction 2001/77/WE dated 27th September 2001 results that term: biomass means susceptible for biological decay fractions of products, wastes and other agricultural industries wastes (together with vegetable and animal products), forestry and relative with it industries branches as well as fraction of industry and municipal wastes susceptible for biological decay.

Co-incineration of dried sewage sediment with biomass will allow to improve energetic rating and biomass in that form would be more attractive fuel. That mixture of biomass may be gasified what will increase cost-effectiveness and efficiency of burning. Dried sewage sediments consist of components which can be used for further management e.g. in the process of co-incineration with other materials.

## 3. Straw

The implementation of burning technology of unconventional renewable fuel which is rape straw will in practical application contribute to limitation of environment contamination with wastes and hazardous products of burning containing harmful nitrogen and sulfur compounds. So there is a necessity of research to increase knowledge about running of thermodynamic processes of rape straw burning and the use of the knowledge at the same time for improvement of equipment for incineration and techniques of raw material preparation.

Obvious is the fact that to obtain high efficiency of burning rape straw there is a need of pressure agglomeration of rape chaff called briquetting. The treatment, although energy-consuming, increases energetic attractiveness of this form of fuel as a result of increased density, reduced moisture, made distribution easier as well as storage and burning in conventional furnaces. The second premise resulting from the observations and experiences so far is the necessity to use boilers of special construction enabling the usage of pyrolysis of fuel charge. Thanks to fuel pyrolysis the energetic and ecological efficiency will increase as a result of temperature rise in the burning of fuel sphere and products of pyrolytic decomposition of briquettes from rape straw. The improvement of running of renewable fuels burning in the natural state may be achieved through pressure agglomeration called briquetting. The primary form of fuel undergoes the treatment improving its properties. The processed rape straw in the form of briquette is homogenous, has

stabilized heat, density and moisture parameters. Burning briquettes runs without disturbances in the determined conditions with the high thermal efficiency of thermic processes and conversion of chemical energy of the fuel for heat.

Agriculture production brings harvest in the form of straw in the amount of 25 mln tons/year but large amount is used as bedding, feed, or component of organic fertilizer used in animal production. Since the beginning of 1990s, particularly in north-western part of Poland, in the areas of ex-national farm production units(communistic cooperative farms) the surplus of straw has been rising and thus the potential of straw as fuel used in power engineering consisting now 195PJ, out of which 150 PJ is from cereal straw, and the rest of agricultural wastes consist rape straw and hey. If from the earlier mentioned 25 mln tons of straw, 50% could be used for energetic purposes(12,5 mln tons) it is possible to save about 5 mln tons of coal/year when thermal value of straw is supposed at the level of 16 MJ/kg. One should also take into consideration the profits connected with less contamination of environment.

Straws characterizes with neutral balance of carbon dioxide emission, much smaller is emission of sulfur dioxide, and emission f nitro gen oxides is AT the comparable level. Thermal value of straw depends on such factors as moisture content, kind of cereal, kind of soil and way of fertilizing. Maximal content of moisture should range from 18% to 22%. Total use of surplus of straw production may cover 4% of requirements for primary /original energy. Chemical energy of 1kg of straw with 15% of moisture constitutes 14,3 MJ what corresponds to chemical energy contained in 0,81 kg of combustible wood or 0,41 m<sup>3</sup> of high methane earth gas.

Thermal efficiency of biomass gasifying may be counted from:

$$\eta_z = \frac{v_{g\,pal} \cdot Q_{wg\,pal}}{Q_{wp}} \quad (1)$$

where:

$v_{g\,pal}$  - volume of combustible gas as the result of gasification 1 kg charge in  $\frac{m^3n}{kg}$ ,

$Q_{wg\,pal}$  - fuel value of combustible gas is  $4,6 \div 5,0 \frac{MJ}{m^3n}$ ,

$Q_{wp}$  - fuel value of fuel charge in  $\frac{kJ}{kg}$  .

Gas generated in gasifying chamber may be burnt in burning chamber and the emitting heat used for heating in air heat exchange or water or for water steam generation. Obtained gas after cleaning and cooling may be used as fuel for diesel engines.

Thermal conditions and the way of regulation of fuel pyrolysis decide about the amount of obtained decay products. Temperature regulation of processes in individual phases influences the speed of pyrolysis and composition of generated gas and process efficiency. Great influence for/on pyrolysis effects has the kind if biomass.

#### 4. Research on usage of fuel from sewage sediment and straw

Research of co-burning of rape straw with dried sewage sediment of 90% of dry mass were conducted for various percentage proportions of fuels fraction. Measures were conducted in air heater VIGAS-25N,where there was used double row heat exchanger of dimension 57x5 mm of 6 items in each row. The following percentage proportions of dried sewage sediment were taken: 20% and 40%. For research portions of fuel of 5 kg mass were taken co-incinerating percentage partitions for individual biomasses. For the suggested fuel proportions from biomass were assigned: burning heat, fuel value, contents of ashes, density, moisture, contents of volatile fractions. Measures of analysis of exhaust fumes were done. Measures results are presented in tables 1 to 3 and graphically on charts.

Table 1. Results of exhaust fumes analysis during burning of biomass and sewage sediment

| Parameter                     | Unit | Fuel       |                 |                            |                            |
|-------------------------------|------|------------|-----------------|----------------------------|----------------------------|
|                               |      | Rape straw | Sewage sediment | Straw 80% and sediment 20% | Straw 60% and sediment 40% |
| O <sub>2</sub>                | %    | 8,7        | 15,9            | 16,8                       | 15,1                       |
| CO                            | ppm  | 1654       | 1776            | 3725                       | 3509                       |
| NO                            | ppm  | 30         | 169             | 115                        | 232                        |
| NO <sub>2</sub>               | ppm  | 0,0        | 0,0             | 0,0                        | 0,0                        |
| NO <sub>x</sub>               | ppm  | 27         | 169             | 113                        | 230                        |
| SO <sub>2</sub>               | ppm  | 0,0        | 0,0             | 0,0                        | 0,0                        |
| Chimney losses                | %    | 15,3       | 19,1            | 25,9                       | 25,5                       |
| λ                             |      | 16,7       | 4,11            | 4,95                       | 3,55                       |
| CO <sub>2</sub>               | %    | 1,4        | 3,3             | 2,8                        | 3,9                        |
| H <sub>2</sub> S              | ppm  | 0,0        | 0,0             | 0,0                        | 0,0                        |
| H <sub>2</sub>                | ppm  | 2450       | 669             | 3633                       | 3638                       |
| Draught                       | mbar | 0,0        | 0,0             | 0,01                       | 0,0                        |
| E                             | %    | 77,6       | 80,9            | 74,1                       | 74,5                       |
| Air temp. for burning         | °C   | 16,9       | 24,5            | 17,9                       | 18,9                       |
| Temperature of combustion gas | °C   | 231,1      | 169,6           | 189,0                      | 241,6                      |

Boiler-room with boilers straw-fired with power of 1MW burns about 800 Mg of straw during one heating season as it is known rating of straw to coal is that for 1,5 kg of burnt straw we burn 1,0 kg of coal. Thus burning of 800Mg of straw replaces 533 Mg of coal. During burning of 1Mg of coal we generate about 2,05 Mg CO<sub>2</sub>. Replacement of coal with straw reduces emissions of CO<sub>2</sub> of 1.100 Mg per year.

Table 2. The amount of heat and energy obtained from gasifying of biomass for rape straw and dried sewage sediment of o content 9% of dry mass (listing for fuel of total mass 5kg )

| Kind of biomass  | Heat kJ  | Stream of heat kJ/h | Energy kWh |
|--|----------|---------------------|------------|
| Rape straw 100%  | 6943,710 | 1,5107              | 16,278     |
| Dried sewage sediment of value of 90% dry mass                 | 5257,090 | 0,4867              | 13,410     |
| Rape straw 80% fraction and dried sewage sediment 20% fraction | 2275,255 | 0,2632              | 13,541     |
| Rape straw 60% fraction and dried sewage sediment 40% fraction | 1910,555 | 0,2033              | 12,546     |

Table 3. Technical analysis for rape straw and dried sewage sediment of content 90% of dry mass depending on percentage content of fractions for individual fuels

| Kind of biomass  | Moisture content % | Ashes content % | Hydrogen content % | Volatile Parts content % | Burning heat kJ/kg | Combustible value kJ/kg |
|--|--------------------|-----------------|--------------------|--------------------------|--------------------|-------------------------|
| Rape straw   | 15,050             | 1,970           | 4,660              | 69,710                   | 15880              | 14495                   |
| Dried sewage sediment – 90% of dry mass                        | 10,90              | 32,80           | 3,127              | 53,290                   | 13350              | 12401                   |
| Rape straw 80% fraction and dried sewage sediment 20% fraction | 7,128              | 10,649          | 4,567              | 73,632                   | 14422              | 13251                   |
| Rape straw 60% fraction and dried sewage sediment 40% fraction | 6,506              | 16,540          | 4,275              | 68,854                   | 13656              | 12564                   |

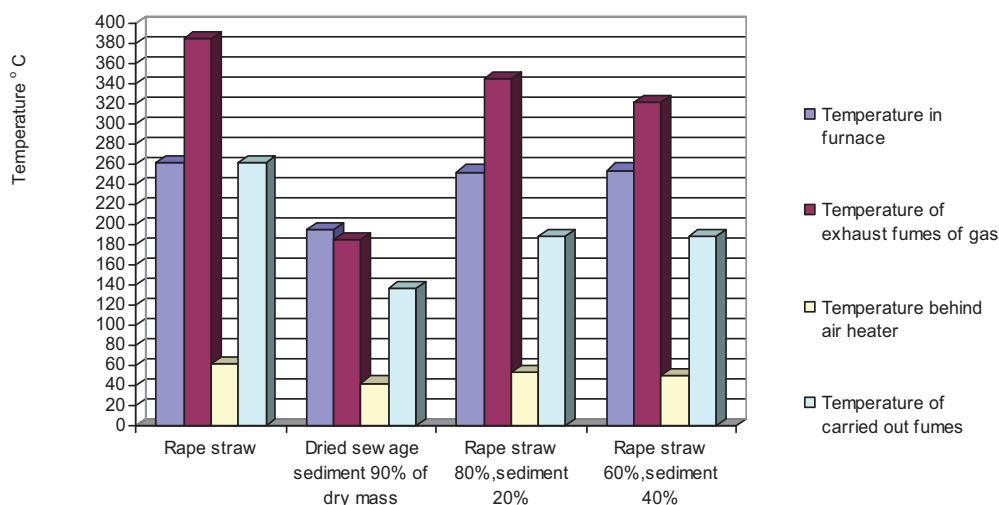


Chart 1. Temperature depending on percentage contents of biomass

## 5. Summary

The surplus of biomass and sewage sediment will force the search of new solutions so as to its proper management and usage. The instruction approved by EU saying about the fraction/partition of renewable energy in the general energy production, for Poland will extort/force activities connected with more efficient usage of energetic potential of straw as well as sewage sediment.

The presented research shows possibility to use ripe straw and dried sewage sediment for co-burning in the rate 20% to 40 %. With bigger rates proportions co-burning is not profitable because of low fuel quality.

The presented research show possibilities of rape straw usage and sewage sediment for co-incineration in the rating 20% to 40%. With bigger rating of co-burning is not profitable due to low combustible value.

Co-burning of both fuels is profitable assuming that moisture of rape straw is below 15% and dried sewage sediment is 10%. However one has to remember that the process of sediment drying till obtaining such parameters is energy-consuming one. Rape straw after pressure agglomeration is an ecological fuel of full value possible to use in heat engineering with the usage of dried sewage sediment with content 90% of dry mass.

## Literature

- [1] Chałamoński M., Łukasiewicz J., Szymczak M.: *Suszenie osadów ściekowych*, Instytut Techniki Budowlanej, Ośrodek Informacji, Miesięcznik INSTAL Nr. 1, s. 48-52, 2008r.
- [2] Grzybek A., P. Gradziuk, K. Kowalczyk: *Słoma energetyczne paliwo*, Wydawnictwo „Wies Jutra”, Warszawa 2003r.
- [3] Hejft R.: *Ciśnieniowa aglomeracja materiałów roślinnych*, Wydawnictwo Instytutu Technologii i Eksploatacji, Radom 2003r.
- [4] Kukliński M., Łukasiewicz J., Szymczak M.: *Optymalizacja bilansu cieplnego suszarni osadów ściekowych*. *Termodynamika w nauce i gospodarce* tom I s. 667-672.

XX Jubileuszowy Zjazd Termodynamików, Wrocław 02 - 06.09.2008r.  
ISBN 978-83-7493-406-0

- [5] Łukaszewicz J.: *Spalanie biopaliw*, IV Konferencja Naukowo-Techniczna, Krynica Zdrój 21-23 maj 2003r.
- [6] Szymczak M.: *Badania wskaźników energetycznych słomy rzepakowej*. Dwumiesięcznik Inżynieria i aparatura chemiczna, nr 1, s.119-121, XII Konferencja Żywnienie człowieka-inżynieria maszyn, Bydgoszcz 23 luty 2007r.
- [7] Szymczak M., Chalamoński M.: *Spalanie wysuszonego osadu ściekowego wymieszanego z korą sosnową*, miesięcznik Ciepłownictwo, Ogrzewnictwo, Wentylacja nr 2/2011, s. 58-61. Warszawa 2011r.
- [8] Szymczak M.: *Paliwa odnawialne w energetyce i ciepłownictwie*, Międzynarodowa Konferencja Procesów Energii ECO – EURO – ENERGIA, s. 237-245, 2-3 czerwca 2004r. Bydgoszcz.
- [9] Szymczak M., Łukasiewicz J.: *Paliwa odnawialne źródłem energii*. Miesięcznik INSTAL nr 7-8, s. 60-63, 2004r.



## INVESTIGATING THE SIZE EFFECT FOR THE SMALL-DIMENSION SPECIMENS MADE FROM THE EN AW-6063 ALUMINUM ALLOY

Tomasz Tomaszewski, Janusz Sempruch, Tomasz Piątkowski

*University of Technology and Life Sciences in Bydgoszcz  
ul. Kaliskiego 7, 85-796 Bydgoszcz, Poland  
tel.: +48 52 3408202, fax: +48 52 3408245  
e-mail: tomaszewski@utp.edu.pl*

### Abstract

*The paper concerns the size effect on fatigue life and fatigue strength. As for the mini specimens, smaller than the normative specimens, they show an increase in fatigue life with a decrease in the object cross-section area. Theoretically the calculational models assume a lack of sensitivity of the aluminum alloys to changes in the cross-section size, which is contrary to the experimental tests. The paper has been an attempt at determining the size effect for EN AW-6063 aluminum alloy mini specimens. Monotonic and fatigue tests were made. There were observed correlations of the results for the coefficient of material sensitivity to change in the cross-section. The results have made it possible to define the relationship of the ultimate tensile strength and fatigue strength for the specimens of various size.*

**Keywords:** size effect,  $\sigma_a$ - $N_f$  curve, high-cycle fatigue, mini specimen

### 1. Introduction

Fatigue characteristics defined with the use of specimens tested in laboratory conditions will be different than the characteristics for the real design object made from the same material, which is accounted for e.g. the size effect which describes the sensitivity of the material to the change in the area of the cross-section. Disregarding this effect often results in the occurrence of fatigue cracks much below the fatigue limit determined in laboratory conditions. Even though the size effect was experimentally tested for large and mini specimen sizes, frequently the implementation of that knowledge for specific conditions triggers many problems.

The paper concerns the size effect on fatigue strength for the specimens smaller than the normative ones. The specimens of the working cross-section from a few to a dozen or so square millimeters show various fatigue life values demonstrating an increase in the fatigue life for smaller cross-sections. The extent of the change in fatigue life is conditioned by the type of the material. The materials of heterogeneous structure or the so called ‘disordered’ ones show a greater sensitivity to the change in the measurements [1]. This information mostly refers to the steels for which the experimental tests results have been given in paper [9]. It is assumed that the size effect is characterized by coefficient [4]:

$$K_d = \frac{Z_d}{Z} \quad (1)$$

where:

- $Z_d$  – fatigue strength of specimen of any cross-section,
- $Z$  – fatigue strength of specimen of the same material, cross-section area  $20 \div 80 \text{ mm}^2$ .

Theoretical calculational models concerning the sensitivity of the material to the changes in the size of the cross-section define the value of coefficient  $K_d$  for aluminum alloy at level 1 [6]. The results of experimental tests are, in many cases, different than those assumed above.

As an example, Fig. 1 presents the relationship of the fatigue limit for  $10^7$  cycles for the specimens cross-section ( $3.2 \text{ mm} \div 48 \text{ mm}$ ). The experimental results reported concerned the tests made for 75S-T6 aluminum alloy. The specimens were tested in the rotary bending. The specimens were round in a shape of the hourglass [3]. The results reported identified the size effect where the higher the cross-section, the considerably lower the fatigue strength. According to those authors [4], as a result of a greater specimen volume there is a greater probability of the occurrence of inclusion initiated cracks.

There was observed an ambiguity of the calculational models and the testing results. For that reason there was experimentally verified the size effect for the specimens smaller (mini specimen) than the normative ones. It is justifiable to perform tests for mini specimens due to numerous advantages of tests involving mini specimens. One of them is the case when making a normative specimen is restricted by the measurements of the objects investigated. One of the solutions is the application of mini specimens [10]. The scope of interest of the specimens dimensions tested is given symbolically in Fig. 1.

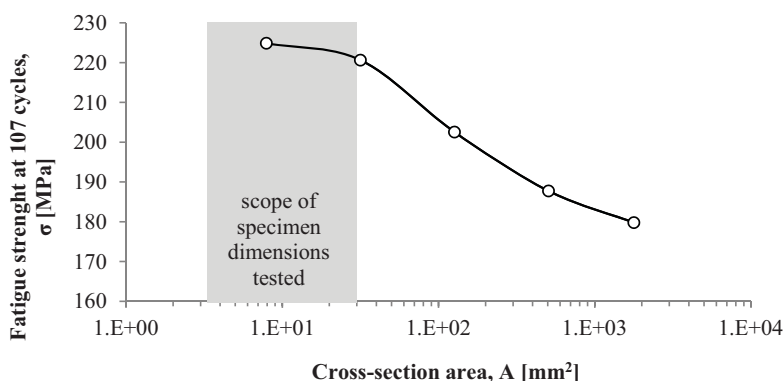


Fig. 1. Dependence of the fatigue limit for  $10^7$  cycles on the section area of the specimen made from the 75S-T6 aluminum alloy [3]

## 2. Methodology

The research methodology involves determining:

- the specimens material,
- material strength properties,
- mini and normative specimen geometry for fatigue testing,
- the scope of the stresses applied for high-cycle strength,
- the other fatigue testing conditions (frequency, cycle asymmetry coefficient, testing machine).

To determine the strength properties of the EN AW-6063 aluminum alloy investigated there was made a static tensile test according to [8]. Assuming that the strength properties (yield strength  $R_e$ , ultimate tensile strength  $R_m$ ) of aluminum alloys depend on the section area, the monotonic test was made for normative specimens (the working cross-section of  $28 \text{ mm}^2$ ) (Fig.

2a) and smaller specimens (the working cross-section of  $3.5 \text{ mm}^2$ ) (Fig 2b). The ratio of the cross-section of the normative specimen to the smaller specimen is 8. Compliant with numerous published research results, one can assume that the smaller specimen can be qualified as representing a group of small-cross-section specimens. The results are given in Table 1 and the strain-stress curve in Fig. 3.

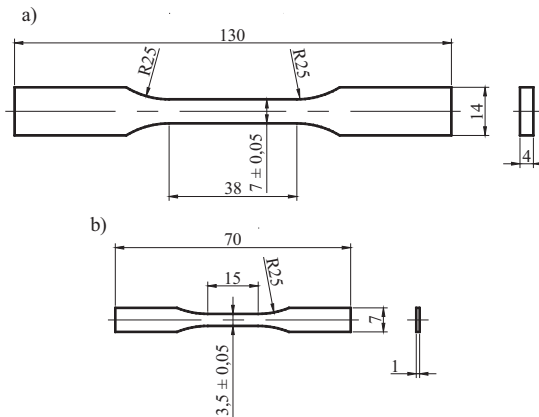


Fig. 2. Specimen geometry for monotonic tests: a) normative [8]; b) smaller

Tab. 1. Mechanical properties of the EN AW-6063 aluminum alloy

| Nr      | Normative specimen |                 |         |         | Smaller specimen |                 |         |         |
|---------|--------------------|-----------------|---------|---------|------------------|-----------------|---------|---------|
|         | $R_m$ , MPa        | $R_{e_s}$ , MPa | $A$ , % | $Z$ , % | $R_m$ , MPa      | $R_{e_s}$ , MPa | $A$ , % | $Z$ , % |
| 1       | 200                | 167             | 16,5    | 60,4    | 232              | 210             | 12,0    | 53,9    |
| 2       | 199                | 165             | 17,0    | 62,3    | 233              | 209             | 11,2    | 54,0    |
| 3       | 207                | 178             | 15,6    | 59,1    | 230              | 208             | 10,4    | 48,4    |
| 4       | 202                | 170             | 17,2    | 62,7    | 230              | 210             | 11,2    | 52,0    |
| 5       | 199                | 167             | 16,8    | 61,6    | 227              | 207             | 11,2    | 52,0    |
| Average | <b>200</b>         | <b>167</b>      | 16,6    | 61,2    | <b>230</b>       | <b>208</b>      | 10,8    | 53,0    |

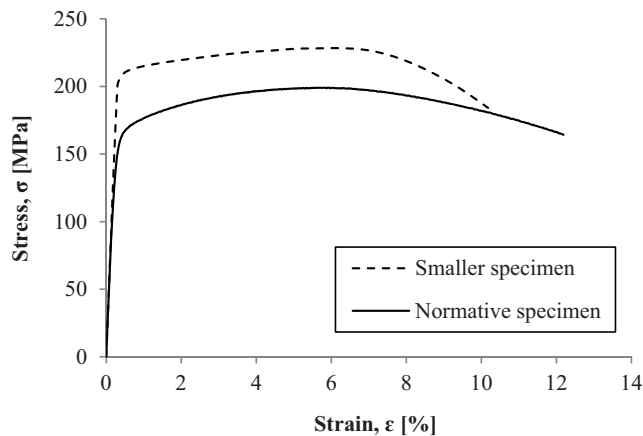


Fig. 3. Strain-stress curve for normative and smaller specimens

The results for monotonic tests demonstrated other values of strength properties. For normative specimens, the ultimate tensile strength was 15 % higher and the yield strength – 25 % higher than

for the smaller specimens. Parameters  $A$  (a 35 % decrease) and  $Z$  (a 13.4 % decrease) behave opposite.

High-cycle fatigue strength tests were made based on the normative specimen and the mini specimen (Fig. 4). There was eliminated the effect of the specimen shape on the results of experimental tests by applying the same theoretical stress concentration factor ( $\alpha_k$ ) equal 1.05.

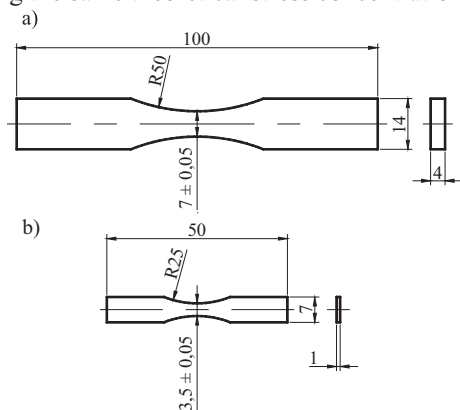


Fig. 4. Specimen geometry for fatigue tests: a) normative [7]; b) mini

The scope of the loads applied in fatigue testing for the aluminum alloy was much above the yield strength ( $R_e$ ). The material tested showed no stability of the cyclic properties. Tests were made into the strength properties of the cyclically pre-strained specimens. There was noted a 15 % increase in yield strength. The changes observed in the material properties are accounted for by cyclic hardening of the cyclically pre-strained specimens. The results have made it possible to reject the yield strength as the key criterion of high-cycle fatigue strength. A detailed report on testing and the results is covered in paper [10].

Fatigue testing was performed for high-cycle strength. To avoid specimens buckling, there was applied the cycle of the a change in load of cycle asymmetry coefficient  $R = 0.1$ . The tests were made at the frequency of the load change of 5 Hz. Fatigue and monotonic tests were performed using the Instron 8874 servo-hydraulic material testing machine (Fig. 5). The monotonic tests applied the extensometer of the measurement length of 25 mm.



Fig. 5. Servo-hydraulic material-testing machines, Instron 8874

### 3. Results

#### 3.1. Own testing results

Own fatigue tests were made based on the research methodology described. The macro crack has been assumed as the criterion of the end of fatigue testing. For the results received (the  $\sigma_a-N_f$  curve, Fig. 6, Table 2) with the use of the mini specimen, there was plotted a line of regression (slope  $m = 12.4$ ) of the coefficient of determination at the level of 0.93.

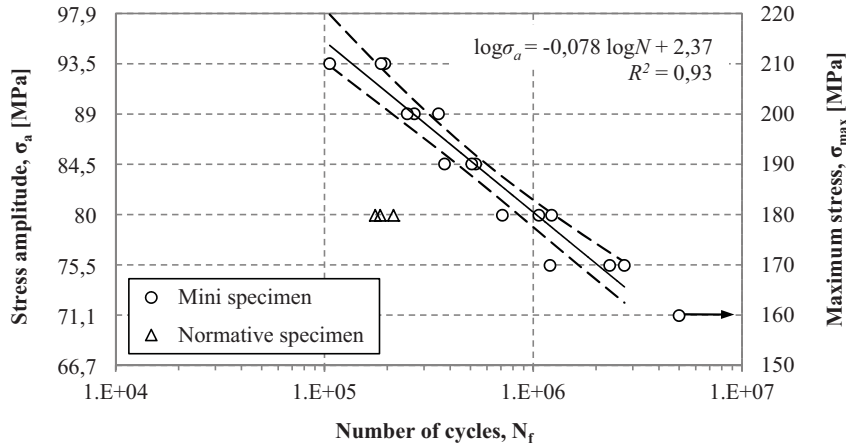


Fig. 6.  $\sigma_a-N_f$  curve for EN AW-6063 aluminum alloy

Tab. 2. Fatigue test results

| Specimen  | Maximum stress, $\sigma_{\max}$ [MPa] | Number of cycles, $N_f$ |           |
|-----------|---------------------------------------|-------------------------|-----------|
|           |                                       | For specimen            | Average   |
| Mini      | 210                                   | 105 970                 | 162 521   |
|           |                                       | 186 811                 |           |
|           |                                       | 194 782                 |           |
|           | 200                                   | 249 372                 | 290 347   |
|           |                                       | 269 602                 |           |
|           |                                       | 352 067                 |           |
|           | 190                                   | 376 419                 | 471 783   |
|           |                                       | 508 524                 |           |
|           |                                       | 530 407                 |           |
|           | 180                                   | 712 051                 | 1 001 094 |
|           |                                       | 1 065 530               |           |
|           |                                       | 1 225 700               |           |
|           | 170                                   | 1 205 043               | 2 088 888 |
|           |                                       | 2 327 384               |           |
|           |                                       | 2 734 238               |           |
|           | 160                                   | 5 000 000               | 5 000 000 |
| Normative | 190                                   | 214 033                 | 191 360   |
|           |                                       | 184 952                 |           |
|           |                                       | 175 094                 |           |

Fig. 7 presents the location of the macro crack against the geometrical center of the specimen (the ratio of the distance of fatigue fracture from the specimen center ( $a$ ) to the specimen width ( $b$ )). It demonstrates a random distribution. There was observed no effect of the geometry shape and other factors on the test results. The results which were considered credible were only those

when the specimen got destroyed in the distance not greater than 1.5 mm from the center. The specimens destroyed in the assumed crack range are given in Fig. 8.

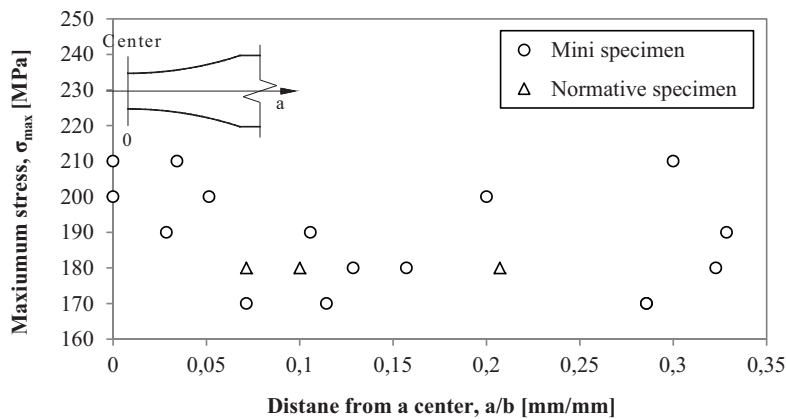


Fig. 7. Location of specimens crack for maximum stresses

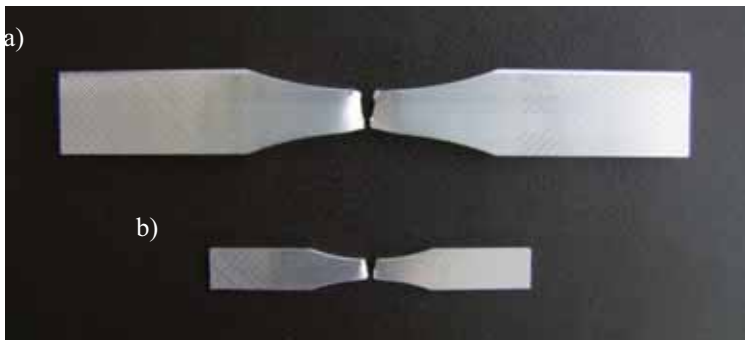


Fig. 8. Photograph of the crack location: a) normative specimen; b) mini specimen

### 3.2. Testing results reported in literature

The results of experimental tests for the EN AW-6063 aluminum alloy at state T7 for the high-cycle fatigue range have been described in detail in paper [5]. The tests involved determining the effect of material properties (the chemical composition, microstructure, thermal treatment) on material fatigue properties. The material used showed tensile strength at the level of 213 MPa and yield strength 186 MPa. Fig. 10 presents the  $\sigma_a-N_f$  curve for the results reported with the use of the normative specimen (Fig. 9) compliant with the ASTM E466-96 standard.

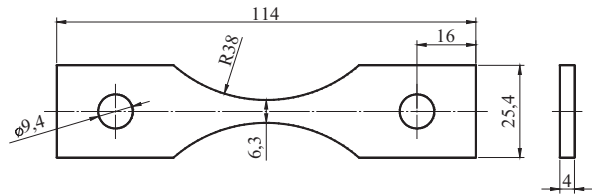


Fig. 9. Geometry of fatigue test specimen used in work [5]

The specimens were tested at the frequency in the range from 30 to 70 Hz. There was applied the sinusoidal cycle of cycle asymmetry coefficient  $R = 0.1$ . The tests parameters and results reported are comparable with those reported in own tests (3 samples at the level of stress amplitude of 80 MPa), and as such they were used for the purpose of the analysis of the results.

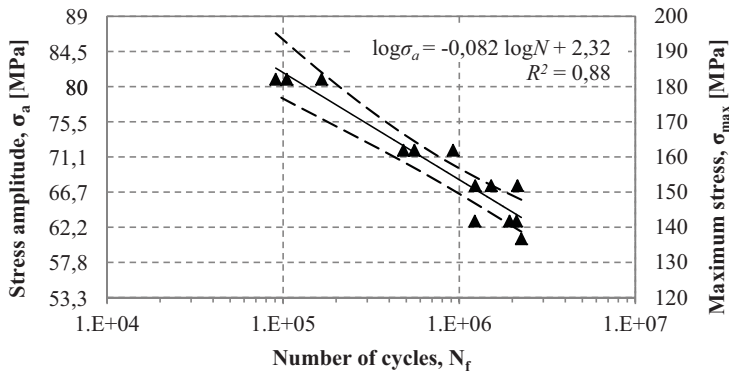


Fig. 10.  $\sigma_a$ - $N_f$  curve for EN AW-6063 aluminum alloy [5]

#### 4. Statistical analysis

The statistical analysis of the tests results involved the test of parallelism for the slope ( $a$ ) of the regression function ( $y = ax + b$ ) [2]. The aim was to verify the null hypothesis ( $H_0$ ) on the significance of the coefficients of linear regression recorded for the tests. The alternative hypothesis ( $H_1$ ) assumed various values of the slope of the line. The hypothesis were formulated as follows:  $H_0: a_1 = a_2$ ,  $H_1: a_1 \neq a_2$ .

There were received regression lines of the fatigue tests results (Fig. 11) for:

- normative specimen (according to source [5]):  $\log \sigma_a = -0.082 \log N + 2.32$
- mini specimen:  $\log \sigma_a = -0.078 \log N + 2.37$ .

The hypothesis was verified using the test of significance for two regression coefficients. The hypothesis was verified for the results received with the use of the mini specimen (own experiments) and the normative specimen (literature source [5]).

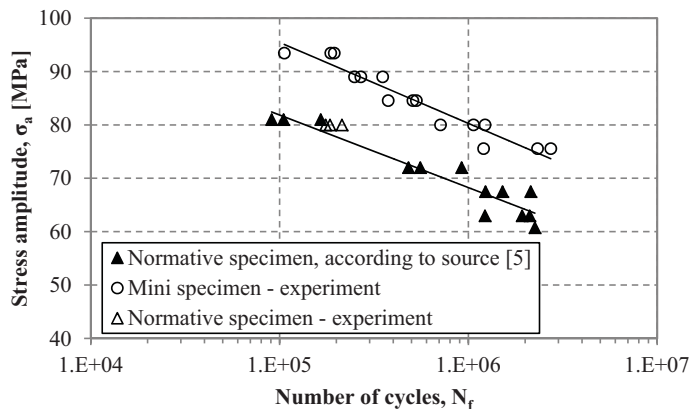


Fig. 11. Breakdown of the experimental tests results for the EN AW-6063 aluminum alloy

The value of test statistics  $t$  was determined for the degrees of freedom  $n_1 = 13$  (the normative specimen),  $n_2 = 15$  (the mini specimen). Critical value  $t_{lab}$  was read from  $t$  Student distribution for  $n_1 + n_2 - 4$  degrees of freedom of the two-tailed critical area. The test of parallelism was made at

the significance level of  $\alpha = 0.05$ . Inequality  $|t| < t_{tab}$  was received. There are no grounds for rejecting null hypothesis  $H_0$  of the equality of the slopes of regression lines for  $\sigma_a-N_f$  curves of the normative and mini specimens. The variable parameter is the absolute term ( $b$ ) of the equation of a straight line. For that reason the size effect can be described with the coefficient of the cross-section size  $K_d$  which, for the fatigue tests results reported was equal to 1.17.

## 5. Conclusions

There was investigated the size effect for the EN AW-6063 aluminum alloy within the scope of high-cycle fatigue. The experimental tests (monotonic, fatigue) results identified the material susceptibility to changes in the cross-section size for the specimens smaller (mini specimen) than the normative ones. The tensile strength/fatigue strength of mini specimens was higher than that of the normative specimens. Thanks to the statistical analysis made it was possible to verify the hypothesis of the parallelism of  $\sigma_a-N_f$  curves of the specimens geometry tested. The coefficient of cross-section size  $K_d$  for the values reported for monotonic specimens was determined (for tensile strength – 1.17) and fatigue tests (for fatigue strength – 1.15). The present tests suggest that the convergence of results makes it possible to refer coefficient  $K_d$  from monotonic tests directly to fatigue tests, which needs further verifying.

Defining the coefficient of the size effect for a material is an essential stage for referring the  $\sigma_a-N_f$  fatigue curve to the real object. Disregarding the effect of the cross-section size can be can trigger the occurrence of the fatigue fracture much below the characteristics determined for the normative specimens and the mini specimens.

## References

- [1] Carpinteri, A., Spagnoli, A., Vantadori, S., *Size effect in S-N curves: A fractal approach to finite-life fatigue strength*, International Journal of Fatigue 31, pp. 927-933, 2009.
- [2] Greń J., *Statystyka matematyczna. Modele i zadania*, Państwowe Wydawnictwo Naukowe, Poland, pp. 186-191, 1978.
- [3] Hyler W. S., Lewis R. A., Grover H. J., *Experimental investigation of notch-size effects on rotating-beam fatigue behaviour of 75S-T6 aluminum alloy*, National advisory committee for aeronautics, 1954.
- [4] Kocańda S., Szala J., *Podstawy obliczeń zmęczenia*, Państwowe Wydawnictwo Naukowe, Poland, pp. 101-103, 1997.
- [5] Luo A. A., Kubic R. C., Tartaglia J. M., *Microstructure and fatigue properties of hydroformed aluminum alloys 6063 and 5754*, Metallurgical and Materials Transactions A 34A, pp. 2549-2557, 2003.
- [6] Neimitz, A., Dzioba, I., Graba, M., Okrajni, J., *Ocena wytrzymałości, trwałości i bezpieczeństwa pracy elementów konstrukcyjnych zawierających defekty*, Wydawnictwo Politechniki Świętokrzyskiej, Poland, pp. 160-162, 2008.
- [7] PN-74/H-04327. Badanie metali na zmęczenie. Próba osiowego rozciągania – ściskania przy stałym cyklu obciążeń zewnętrznych.
- [8] PN-EN ISO 6892-1:2010. Metale - Próba rozciągania - Część 1: Metoda badania w temperaturze pokojowej.
- [9] Semppruch J., Tomaszewski T., *Application of mini specimens to high-cycle fatigue tests*, Journal of POLISH CIMAC, Vol. 6 No. 3, pp. 279-287, 2011.
- [10] Tomaszewski T., Semppruch J., *Determination of the fatigue properties of aluminum alloy using mini specimen*, Materials Science Forum, 2012.



## THE METASTABLE EUTECTIC GROWTH

**Małgorzata Trepczyńska-Lent**

*University of Technology and Life Sciences,  
Kaliskiego 7, 85-796 Bydgoszcz, Poland  
tel.: +48 52 3408719, fax: +48 52 3408245  
e-mail: [malgorzata.trepczynska-lent@utp.edu.pl](mailto:malgorzata.trepczynska-lent@utp.edu.pl)*

### **Abstract**

*The paper presents adaptation problem of metastable growth of eutectic. In the case of rapid solidification the ledeburite eutectic structure in Fe-C system is become. This cementite eutectic is one from the most commercial eutectic of quasi-regular eutectics group.*

**Keywords:** *eutectic, quasi-regular eutectic, cementite eutectic, ledeburite eutectic, kinetic, solidification,*

### **1. Introduction**

Normally in anomalous eutectics, the faceting of one of the phases leads to uncoupled growth and, as a result, a ragged (irregular) solid/liquid interface appears which produces an irregular (divorced) morphology as viewed in a transverse microsection. This is true not only when the volume fraction of the faceted phase is small, but also when it is large, i.e., 40% [1].

Growth of the austenite-iron carbide eutectic (ledeburite) (Fig.1) begins with the development of a cementite plate on which an austenite dendrite nucleates and grows. This destabilizes the  $\text{Fe}_3\text{C}$ , which then grows through the austenite. As a result, two types of eutectic structure develop: a lamellar eutectic with  $\text{Fe}_3\text{C}$  as a leading phase in the edgewise direction, and rod eutectic in the sidewise direction. Cooling rate significantly influences the morphology of the  $\gamma + \text{Fe}_3\text{C}$  eutectic [2].

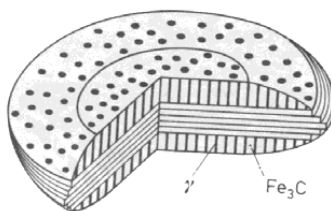


*Fig.1. Scheme of cementite eutectic grain in eutectic cast iron [3]*

Data on the spacing of the ledeburite ( $\text{Fe}+\text{Fe}_3\text{C}$ ) in pure Fe-C alloys has been extended to low solidification velocities. The data do not fit the standard theoretical model of  $\lambda^2V=\text{constant}$ , and it

is suggested that this result may be related to the faceted nature of the  $\text{Fe}_3\text{C}$  component of the ledeburite eutectic [4].

## 2. The ledeburite eutectic growth

Eutectic growth characterized by the cooperative growth of two solid phases from a liquid is an important pattern in crystal growth, and has been attracting much attention [5].

Eutectic alloys can grow into the lamellar - or rod - like regular structures or other anomalous structures. The exact morphology of a eutectic alloy depends on the crystal features of the products and their relative volumes [6].

Theoretical treatments of eutectic growth give relationships between undercooling  $\Delta T$ , lamellar spacing  $\lambda$ , and growth velocity  $V$  of the general form :

$$\Delta T = K_1 \lambda V + \frac{K_2}{\lambda} \quad (1)$$

where  $K_1$  and  $K_2$  are constants related to the material properties. Quasi-regular eutectics (like Fe- $\text{Fe}_3\text{C}$ ) are assumed to grow at the extreme, i.e. at maximum velocity or minimum undercooling. This leads to the well known relationships [7]:

$$\Delta T = 2\sqrt{K_1 + K_2} + \sqrt{V} = K_3 \sqrt{V} \quad (2)$$

$$\lambda = \sqrt{\frac{K_2}{K_1}} / \sqrt{V} = K_4 \sqrt{V} \quad (3)$$

Parameter, influencing the kind of eutectic received, is the fraction of the volume  $g_a$  occupied by one of eutectic phases. Quasi-regular eutectic solidification near the highest value of  $g_a$ , which is over 0,4. They are characterized by lamellar-fibrous morphology. The typical feature of quasi-regular eutectics, is much about equal volumetric contribution of both eutectic phases and the growth of one of the phases in the shape of the wall crystal [3].

The characteristic of this group is that although they are in the anomalous (faceted/nonfaceted) class almost regular micro-structures can be observed in these eutectics. In the quasi-regular eutectics the high degree of regularity may result from the fact that the faceted phase forms the matrix. Therefore, despite a high entropy of solution value, faceting may be prevented and the unpredicted appearance of almost regular microstructures can be explained [1].

The growth kinetics (Fig.2) of the faceted phase activates a defect mechanism for growth, which produces a very anisotropic growth behavior. The undercooling of grey (Fe-C) eutectic is much higher than the one for white (Fe- $\text{Fe}_3\text{C}$ ) eutectic. This is so for two reasons. The concentration difference between the two phases is much higher in Fe-C than in Fe- $\text{Fe}_3\text{C}$  (thus requiring a higher diffusion flux of carbon) [7].

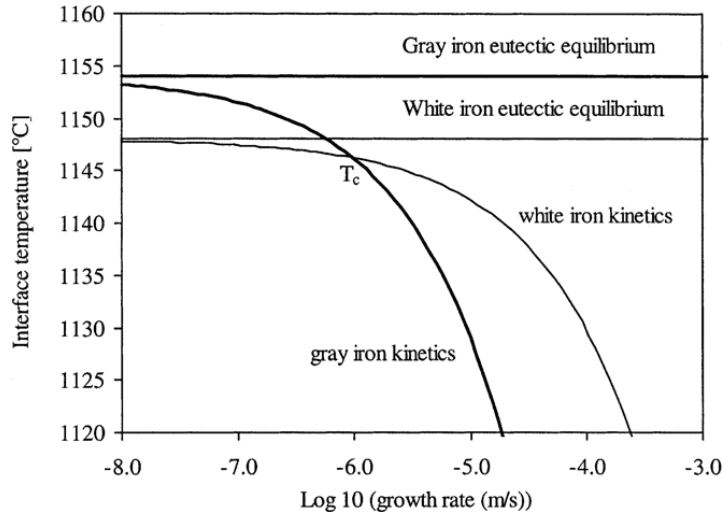


Fig. 2. Schematic of the growth kinetics of gray and white iron eutectics [8]

The unidirectional solidification conditions with an apparent temperature gradient along heat conduction direction also influence the growth of eutectic cementite. As for the eutectic growth, the structures are controlled by the ratio of the temperature gradient ( $G$ ) to the growth rate ( $R$ ). A relatively high  $G/R$  value results in a quasi-regular lamellar structure with edgewise growth and a smaller  $G/R$  value leads to a ledeburite structure with cooperation growth of austenite and  $\text{Fe}_3\text{C}$ . Therefore, the straight eutectic cementite in a strip-cast specimen can be attributed to the domination of the edgewise growth. And the triangular prisms comprising one carbon atom and six surrounding iron atoms are arranged along the C-axis parallel to the heat conduction direction. Consequently, the cementite of the strip-cast specimen has straight interfaces and a distinct texture close to the close packed  $[001]_c$  direction [9].

### 3. Nucleation metastable eutectic

The grain density data are as follows for the white eutectic:

$$N_w(\text{m}^{-2}) = 5.0 \times 10^5 + 1.0 \times 10^4 \dot{T} \quad (4)$$

$\dot{T}$  is the cooling rate [10].

The research indicated that total number of nucleation was given by  $N = A \times (\Delta T)^n$  where  $\Delta T$  is the undercooling with respect to the equilibrium temperature of the phase transformation,  $A$  and  $n$  are constants reflecting the inoculation treatment.

The real volume fractions of cementite ( $f_c$ ) eutectics can be described by:

$$f_c = \frac{f_{ce}}{f_{ge} + f_{ce}} \{1 - \exp[-(f_{ge} + f_{ce})]\} \quad (5)$$

where  $f_{ce}$  are the extended volume fractions of cementite eutectics, which, in turn, can be given by:

$$f_{ce} = \frac{4}{3} \pi N_c R_c^3 = \frac{4}{3} \pi N_c (u_c t)^3 = \frac{4}{3} \pi N_c [\mu_c (T_{mst} - T)^2 t]^3 \quad (6)$$

Equation (6) assume spherical geometry, where  $R_c$  are the mean radii of either the cementite cells;  $N_c$  is the numbers of cementite eutectic cells, per volume or cell densities; and  $t$  is the time [11].

The growth rate for cementite eutectic ( $u_c$ ) can be related to the degrees of undercooling through Eqs. (7), according to theoretical treatments on eutectic growth:

$$u_c = \mu_c \Delta T_c^2 \quad (7)$$

where

$$\Delta T_c = T_{mst} - T \quad (8)$$

In Eqs. (7, 8)  $\Delta T_c$  is the undercooling for cementite eutectic, and  $\mu_c$  are their respective growth coefficients; and  $T_{mst}$  are the metastable equilibrium temperatures of the cementite eutectics [11].

As shown in Fig. 3, the distribution pattern of the eutectic cementite changes from the network-like form to a discontinuous plate-like form with increasing carbon content. Research has also confirmed that the morphology of  $Fe_3C$  changes from ledeburitic to plate like as the undercooling is increased. Studies of directional solidification have indicated that the cooling rate as the austenite begins to crystallize into a columnar dendrite increases and the local solidification time of the austenite crystallization decreases with increasing carbon content, respectively. As mentioned, the cooling rate of the cast iron strips produced by using strip casting ranged within  $10^2$ - $10^3$  °C s<sup>-1</sup>. This high cooling rate accompanied with high carbon content could lead to high undercooling which enhances the formation of discontinuous plate-like eutectic. Moreover, the growth direction of plate-like cementite of high carbon specimens,  $[001]_c$ , also resulted from the edgewise growth along the heat conduction direction [9].

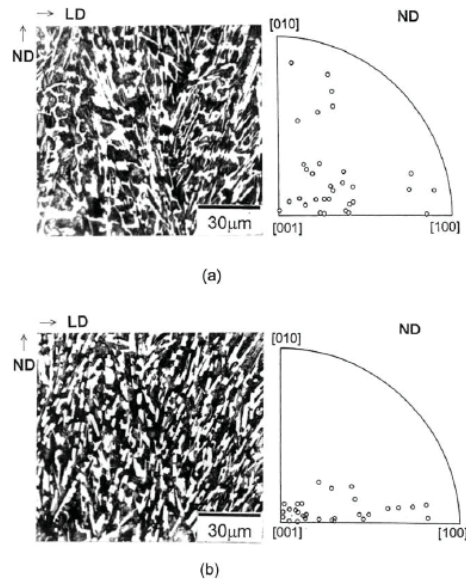


Fig. 3. The morphology and microtexture of the eutectic cementite in strips with different compositions: (a) 2,6C-4,0Si; (b) 3,5C-2,1Si [9]

#### 4. The microsegregation in white eutectic

It was proved that microsegregation of various elements had a significant effect on stable to metastable transition as well as the solid-state transformation or heat treatment. The microsegregation behavior is quite different among various elements, for example, silicon segregates negatively during stable while positively in metastable solidification; manganese segregates positively in both reactions, which makes the content of manganese in liquid increase during solidification. Therefore, stable and metastable eutectic equilibrium temperature must be calculated as a function of silicon and manganese concentration in the liquid.

At any time  $t$ , the distribution of the element  $X$  in liquid, white eutectics was approximately given by:

$$\langle X \rangle_{white}^t = K_{X,white} \langle X \rangle_{1...}^t \quad (9)$$

where  $\langle X \rangle_{white}^t$  are concentrations of  $X$  element in white eutectic at time  $t$ ,  $\langle X \rangle_{white}^t$  is partition coefficient of  $X$  element in liquid and white eutectic, and  $\langle X \rangle_{1...}^t$  is content of  $X$  element in liquid at time  $t$  [12].

The partition coefficients  $k_{Si,g}$  and  $k_{Si,w}$  are calculated using the following relationships:

$$k_{Si,g} = 1,70 - 0,31c_{Si} - 2,05c_{Si}^2 \quad (10)$$

$$k_{Si,w} = 0,88 - 0,05c_{Si} \quad (11)$$

where  $c_{Si}$  is the silicon concentration expressed in weight percent [8].

The eutectic temperatures white iron eutectics are obtained by:

$$T_w = 1147,2 - 6,93(c_{Si} + 2,5c_p) - 1,717(c_{Si} + 2,5c_p)^2 \quad (12)$$

Where  $c_p$  is the concentration of phosphorus, which is assumed to be constant [8].

As for the silicon effect, the primary action of silicon in controlling the morphology of white cast irons is to produce the rod eutectic form of ledeburite. In other words, the morphology of cementite changes from a plate-like eutectic for plane front growth to a rod eutectic for cellular and dendritic growth due to the effect of silicon. The reason for this is that the solubility in  $Fe_3C$ , which is known to be extremely low, results in a significant solute buildup in the liquid at the  $Fe_3C$  - liquid interface and this could give rise to the rod facet formation. This cooperative eutectic growth occurs at right angles to the primary  $Fe_3C$  plate, that is, the rod-like structure grows perpendicular to the plate like cementite, and will result in curved interfaces and a random growth direction [9].

#### 5. Discussion

Eutectic alloys can grow into the lamellar - or rod - like regular structures or other anomalous structures. The exact morphology of a eutectic alloy depends on the crystal features of the products and their relative volumes [13]. Evolution of solidification microstructures can be the strategic link between materials processing and materials behavior. The eutectic structure is the basis of most commercial casting alloys, and thus, the properties of these alloys strongly depend on the amount

and morphology of the eutectic phases, which, in turn, are affected by various variables, including cooling rate, modification, and faceted or nonfaceted nature of the constituent phases. In the quasi-regular eutectics the high degree of regularity may result from the fact that the faceted phase forms the matrix. Therefore, despite a high entropy of solution value, faceting may be prevented and the unpredicted appearance of almost regular microstructures can be explained.

## References

- [1] Savas M.A., Smith R.W., *Quasi-regular growth: a study of the solidification of some high volume-fraction faceted phase anomalous eutectics*, Journal of Crystal Growth 71, pp.66-74. 1985.
- [2] Nastac L., Stefanescu D.M., *Prediction of gray to white transition in cast iron by solidification modeling*, AFS Transactions pp. 329-337, 1995.
- [3] Fraś E., *Krystalizacja metali*, WNT, Warszawa, 2003.
- [4] Park J. S., Verhoeven J. D., *Directional solidification of white cast iron*, Metallurgical and Materials Transactions A, Vol. 27A, pp. 2328-2337, 1996.
- [5] Zhao S., Li J., L. Liu, Zhou Y., *Eutectic growth from cellular to dendritic form in the undercooled Ag-Cu eutectic alloy melt*. Journal of Crystal Growth 311, 2009.
- [6] Li J., Zhou Y., *Effect of interface kinetics on the eutectic growth*, Science in China ser. E. Engineering & Materials Science vol.48, no.4, 2005.
- [7] Magnin P., Kurz W., *Transition from grey to white and white to grey on Fe-C-X eutectic alloys*, Met. Res. Soc.Symp. Proc. Vol. 34, 1985.
- [8] Jacot A., Maijer D., Cockcroft S., *A two-dimensional model for the description of the columnar-to-equiaxed transition in competing gray and white iron eutectics and its application to calender rolls*, Metallurgical and Materials Transactions A, vol. 31a, August 2000.
- [9] Song J.M., Chen L.H., Lui T.S., *Examination on the growth textures of eutectic cementite of various morphologies*. Materials Science and Engineering A347, pp. 5-8, 2003.
- [10] Nastac L., Stefanescu D.M., *Modeling of stable to metastable structural transition in cast iron*, Advanced Materials Research vol. 4-5, 1997.
- [11] E Fraś, M.Górny, H.F López, *The transition from gray to white cast iron during solidification: Part I. Theoretical background*, Metallurgical and Materials Transactions A, vol. 36A, November 2005.
- [12] Magnin P., Kurz W., *Competitive growth of stable and metastable Fe-C-X eutectics. Part II. Mechanisms*, Metallurgical Transactions A, vol. 19A, August 1988.-5/09
- [13] Guzik E., *Model wzrostu eutektyki nieregularnej na przykładzie eutektyki grafitowej w stopach Fe-C*, Rozprawy monografie 15, Wydawnictwa AGH, Kraków 1994.



## GRAPHICAL ANALYSIS OF BUS LIFETIME

**Andrzej Wdzięczny**

*University of Technology and Life Science  
Faculty of Mechanical Engineering  
Kaliskiego av.7, 85-796 Bydgoszcz, Poland  
Email: [Andy@utp.edu.pl](mailto:Andy@utp.edu.pl)*

**Leszek Knopik**

*University of Technology and Life Science  
Faculty of Management Science  
Fordonska st. 424, 85-790 Bydgoszcz, Poland  
Email: [knopikl@utp.edu.pl](mailto:knopikl@utp.edu.pl)*

### Abstract

*The lifetime distribution is very important in reliability studies. The shape of lifetime distribution can vary considerably. It frequently cannot be approximated by simple distribution functions. The purpose of this paper is to introduce and describe graphical tools for lifetime data. This article is connected with problem of finding of lifetime distribution for a heterogeneous population of lifetime data. A heterogeneous population can be represented by a two component mixture. The numerical examples are given to illustrate two lifetime model. The parameter estimation is based on the maximum likelihood method. The methodology is illustrated by two real data set. The graphical illustration on lifetime distribution is presented.*

**Keywords:** *lifetime, mixture of distribution, Weibull distribution, exponential distribution, TTT-plots, reliability function, IFR, DFR.*

### 1. Introduction

The modeling and analysis of lifetimes is an important aspect of statistical work in a wide variety of scientific and technological fields. An important topic in the field of lifetime data analysis is to select the most appropriate lifetime distribution. This distribution describes the time to failure of a component, subsystem or system. The probability distribution of the lifetime of a technical object can be characterized by the failure rate function. The failure rate function is a basic concept in reliability theory and reliability practice. If lifetime distribution is absolutely continuous what very often can be assumed, the failure rate function uniquely determines the lifetime distributions. An important class of the lifetime distribution arises when the failure rate function is non-monotonic.

Occurrence of instantaneous or early failures in lifetime testing is observed in sets of failures of machines. This occurrence may be due to faulty constructions or inferior quality. Some failures result from natural damages of the machine while the other failures may be caused by inefficient repairs of previous failures resulting from incorrect organization of the repairs.

In the papers [8] and [14] the set of failures of a machine is divided into two subsets, namely into set of primary failures and the set secondary failures. This suggests that the population of lifetime is heterogeneous. The population of the time before failure can be described by using the statistical concept of mixture. This mixture, in particular case, has the unimodal failure rate function [9]. The purpose of this note is to bring attention to the use of graphical solution methods based on the total time on test TTT transform for detecting early failures. TTT-transform was introduced by Barlow and Campo [3] and further extended by Bergman and Klefsjo [4]. An application of TTT-plots in reliability theory is presented in paper [9]. Total time test (TTT) transformation plots are useful for analyzing non-negative data. The plots help choosing a mathematical model for the reliability data and provide the information about the failure rate function. In this study, graphical methods based on TTT-transform will be used to illustrate the variety of the failure rate shapes.

## 2. Basic definitions and ageing properties

Let  $F(t)$  be a lifetime distribution with finite mean  $ET$  and  $F(t) = 0$  for  $t < 0$ .  $T$  is random variable (lifetime) with distribution function  $F(t)$ , reliability function  $R(t) = 1 - F(t)$  and the failure rate function  $\lambda(t) = f(t) / R(t)$ .

### 2.1. Mixture

We consider a mixture of two lifetimes  $T_1, T_2$  with densities  $f_1(t), f_2(t)$ , reliability functions  $R_1(t), R_2(t)$ , failure rate function  $r_1(t), r_2(t)$  and weights  $p$  and  $q = 1 - p$ , where  $0 < p < 1$ . The mixed density is then written as

$$f(t) = f_1(t) + (1 - p) f_2(t)$$

and mixed reliability functions is

$$R(t) = p R_1(t) + (1 - p) R_2(t).$$

The failure rate function of the mixture can be written as the mixture [8]

$$r(t) = \omega(t) r_1(t) + (1 - \omega(t)) r_2(t),$$

where  $\omega(t) = p R_1(t) / R(t)$ .

### 2.2. TTT transformation

During another year, the fundamental concept was defined, studied and proven to be a useful tool. In the lifetime data analysis the total time test (TTT) is very useful rate function. The function:

$$H^{-1}(t) = \int_0^{F^{-1}(t)} R(u) du \quad \text{for } 0 \leq t \leq 1$$

is TTT transformation of  $F(t)$ . The mean of  $F(t)$  is given by

$$\mu = H^{-1}(1) = m(0).$$

The scale invariant transformation

$$H^{-1}(t)/\mu = \frac{1}{\mu} \int_0^{F^{-1}(t)} R(u) du$$

Different concepts are used not only for parametric modeling but also to define various nonparametric classes of lifetime distribution. The most well known of these are : IFR – increasing failure rate function and DFR – decreasing failure rate function.

### 2.3. Early and instantaneous failures

We consider a family of continuous distribution functions  $F(x; \Delta)$ , where  $\Delta$  is a set of parameters,  $F(0, \Delta) = 0$ . To accommodate a real life situation, where instantaneous failures are observed at the origin, the model  $F(x; \Delta)$  is modified to model  $G(x; \Delta, p)$  by using a mixture in the proportion  $1-p$  and  $p$  respectively of the singular random variable  $Z$  at zero and with random variable  $T$  with the distribution function  $F(x; \Delta)$ . Thus, the modified distribution function of lifetime is given as:

$$G(x; \Theta, p) = \begin{cases} 1-p & \text{for } x = 0 \\ 1-p + pF(x; \Theta) & \text{for } x > 0 \end{cases}$$

and the corresponding probability density function as:

$$f(x; \Theta, p) = \begin{cases} 1-p & \text{for } x = 0 \\ 1-p + pf(x; \Theta) & \text{for } x > 0 \end{cases}$$

The problem of statistical inference about  $(\Delta, p)$  has received considerable attention particularly when  $T$  is exponential. Some of the early references are: Aitchison [2], Kleyale and Dahiya [7], Jayade and Parasad [5], Muralidharan [10], [11],[12] Kale and Muralidharan [6] and the references contained therein. Muralidharan and Kale [6] considered the case where  $F$  is a two parameters gamma distribution with shape parameter  $\beta$  and scale parameter  $\alpha$ , and they obtained confidence interval for  $\delta = p\alpha\beta$  assuming  $\alpha$  as being known and unknown.

### 3. The lifetime model for bus engine

The analysis of  $n = 190$  data sets of lifetimes suggests that as the distribution time between two successive failures we can accept the distribution of mixture of two point distribution with exponential distribution. In our experiment the time between two successive failures was registered one time per day. Analysis of lifetime data shows that the number of recorded failures for  $t = 0$  and  $t = 1$  is considerably greater than for other time values. Firstly, in order to identify the shape of the life time distribution, we shall consider graphical methods based on Total Time on Test (TTT). Hence, we conclude that the statistical population is heterogeneous. This fact suggests that the distribution of lifetime may be the mixture of the two point distribution:

$$P\{X = 0\} = a, P\{X = 1\} = b, \text{ where } a + b = 1, a \geq 0, b \geq 0 \quad (1)$$

and the exponential distribution with the distribution function:

$$F_2(t) = 1 - \exp(-\lambda t) \quad \text{dla } x > 0 \quad (2)$$

This fact suggests that the distribution of lifetime may be the mixture of the two point distribution and the exponential distribution. The distribution function of the mixture has a form:

$$F(t) = p F_1(t) + (1-p) F_2(t) \quad (3)$$

The distribution function depends on parameters  $(a, b, \lambda, p)$ . These parameters are estimated by numerical maximum likelihood methods, thus obtaining:  $a = 0.792$ ,  $b = 0.208$ ,  $\lambda = 0.051$ ,  $p = 0.336$ .

The goodness fit test shows high consistence of both distributions. The value of the statistics  $\lambda$ -Kolmogorow's  $\lambda = 0.37$  it gives  $p\text{-value} = 0.75$ , whereas, the Person's  $\chi^2 = 23.13$  with  $p\text{-value} = 0.84$ .

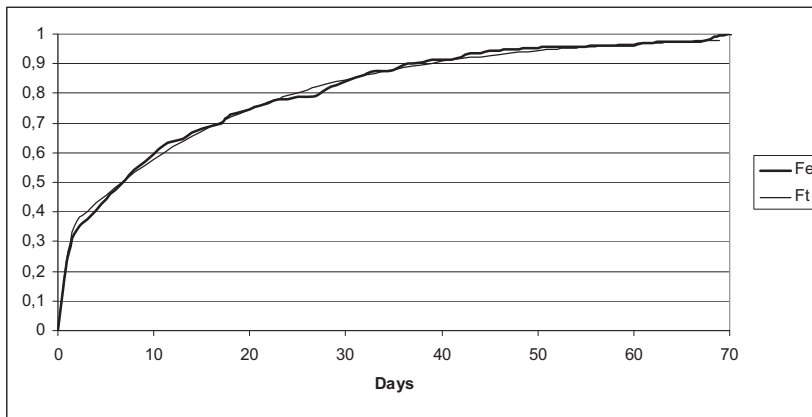


Fig.1. Empirical distribution and distribution of mixture

Fig.1 shows the charts of the empirical distribution functions and the mixture. Fig.2 demonstrates TTT-plots for the empirical distribution and the distribution after separation of the two-point distribution. The distribution after separation shows the good consistency with an exponential distribution.

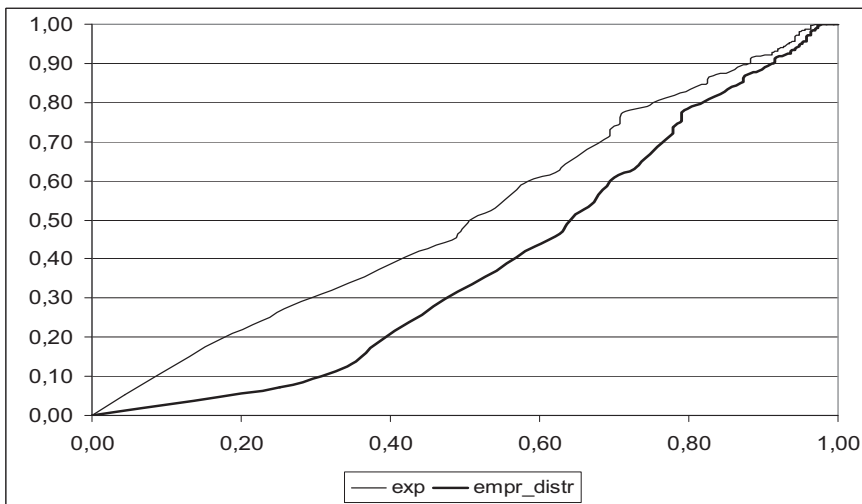


Fig. 2. TTT-plots for empirical distribution and the distribution after separation

#### 4. The model of time between failures of the bus electrical system

The analysis of  $n = 1576$  the lifetime between successive failures shows that the distribution of times until the failure is a mixture of an exponential distribution and Weibull distribution with the reliability function in the form:

$$R_2(t) = \exp(-c x^d), \text{ where } x > 0, c > 0, d > 0.$$

can be the model for this lifetime data.

The reliability function for distribution (4) has the form:

$$\lambda(t) = c d t^{d-1} \text{ dla } x > 0.$$

In this case the reliability function of mixture

$$R(t) = p \exp(-\lambda t) + (1-p) \exp(-c t^d) \text{ dla } x > 0$$

depends on four parameters ( $c, d, \lambda, p$ ).

These parameters are estimated by numerical maximum likelihood methods thus obtaining:

$c = 0.785, d = 0.487, \lambda = 0.0625, p = 0.627$ . Goodness of fit test of the empirical distribution with the distribution of the mixture gives for statistics  $\lambda$  – Kolmogorow's  $\lambda_k = 0.649$ , for  $p$  – value = 0.83. Goodness of fit test Pearson's  $\chi^2 = 74.45$  for  $p$  – value = 0.82. Both tests confirm good consistence of the empirical distribution and mixture distribution.

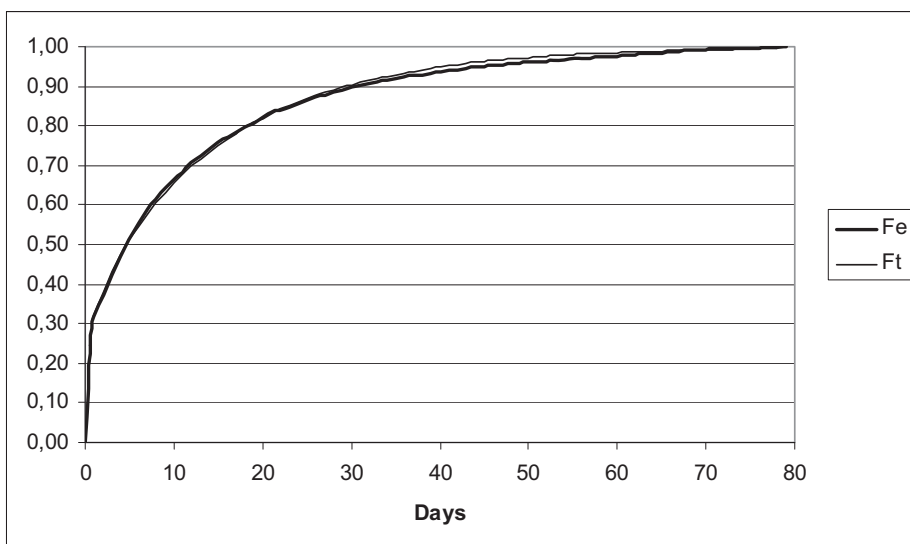


Fig.3 The empirical distribution and the distribution of mixture

Fig. 3 shows the plots of the empirical and mixture distributions and fig. 4 shows TTT-plots for both components of the mixture.

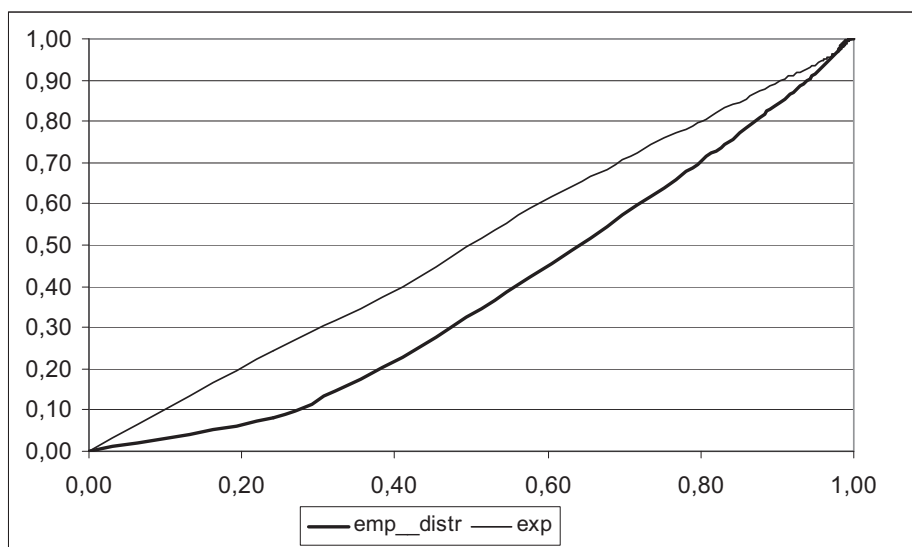


Fig. 4. TTT-plots of the empirical components of the mixture

## 5. Concluding remarks

In this paper, the lifetime distribution as a mixture of two known distributions, has been provided and discussed. It can be seen that the proposed model is a complete model for describing lifetime data of the bus subsystem. In the first example, a mixture of two points and exponential distribution as a lifetime of engine is considered. However, in the second example, Weibull mixture and an exponential distribution have been discussed as the electrical system's lifetime. It is proved that an empirical distribution and a mixture distribution fit each other.

## References

1. Aarset M.V., How to identify bathtub hazard rate. IEEE Transactions on Reliability, 1987, Vol. 36, pp. 106-108.
2. Aitchison I., On the distribution of a positive random variable having a discrete probability mass at origin, Journal of the American Statistical Associations, vol. 50, 1955, pp. 901-908.
3. Barlow R.E. and Campo R. Total time on test processes and applications to failure data analysis. In Barlow, Fussell Singpurwalla, editors. Reliability and Fault Tree Analysis, SIAM 1975. pp. 235-272.
4. Bergman B. and Klefsjo B., A graphical method applicable to age replacement problems, IEEE Transactions on Reliability, 1982, Vol. 31, pp. 478-481.
5. Jayade V. P. and Parasad M. S., Estimations of parameters of mixed failure time distribution. Communications Statistics, Theory and Method, vol19, 1996, pp. 4667-4677.
6. Kale B. K. and Muralidharan K., Optimal estimating equations in mixture distributions accommodating instantaneous or early failures, Journal Indian Statistical Associations, vol. 38, 2000, pp.317-329.
7. Kleyale R.M. and Dahiya R.L., Estimation of parameters of mixed failure time distribution from censored data, Communications Statistics, Theory and Method, vol.4, 1975, pp. 873-882.
8. Knopik L., Mixture of distributions as a lifetime distribution of a technical object, Scientific Problems of Machines Operation and Maintenance, 2010, vol.45, 2 (165), pp. 53-60.

9. Kunitz H. and Pamme H., Graphical tools life time data analysis. Statistical Papers, Vol. 32, 1991, pp. 85-113.
10. Muralidharan K., Test for mixing proportion in mixture of a degenerate and exponential distributions, Journal Indian Statistical Associations, vol.37,1999, pp.105-119.
11. Muralidharan K., The UMVUE and Bayes estimate of reliability of mixed failure time distribution, Communications Statistics, Simulation Computer, vol. 29, No 2, 2000, pp.603-158.
12. Muralidharan K., Modified gamma distribution with singularity at zero, Communications Statistics, Simulation Computer, vol. 31, No1,2002, pp.143-158.
13. Muralidharan K. and Lathika P., Analysis of instantaneous and early failures in Weibull distribution, Metrika vol. 64, 2006, pp.305-316.
14. Wdzięczny A. Woropay M. and Muślewski Ł., Division and investigation of damages to technical object and their influence on the reliability of operation and maintenance systems Scientific Problems of Machines Operation and Maintenance, 2008, vol.44, 2(154), 2008, pp. 31-43.





## EVALUATION OF THE EFFECTIVENESS OF REPAIRS CARRIED OUT OF CENTRES OF THE ROAD TRANSPORT

Andrzej Wdzięczny

University of Technology and Life Sciences in Bydgoszcz  
Al. Prof. S. Kaliskiego 7, 85-789 Bydgoszcz  
tel.: +48 52 3408217,  
email: andy@utp.edu.pl

### Abstract

*The transport systems and especially the means of transport are the sources of life and health hazard and the natural environment pollution. Exploitation process influence on the elements of the technical objects and decrease the values of the important features of them. This is the mechanism of the damage process. Wear factors could be divided into two groups. One of them are the factors results from the bed operation of the object operators and the second group consists of the factors results from the environment interaction. The damages are the events which are very important from the reliability point of view because are the reason of the partly or full disability. In the paper the damage is defined as the exceeding the acceptable thresholds of the technical object important features.*

*Keywords: transport, system, damage,*

### 1. Introduction

Based on the analysed references in question as well as on the results of our own research it has been found that the damages to the means of transport, being utilised within the transport systems, are a result of interaction of various forcing factors. These factors may be divided into:

- working factors – affecting a machine due to realization of the working process by the machine (depend on the machine performance),
- external factors – describing influence of the environment on the machine (do not depend on the machine performance),
- antropotechnic factors – affecting the machine due to conscious or un conscious men's actions (e.g. men's faults made during the process of utilisation and maintenance).

Because of the nature of the forcing factors affecting a technical object, they may be divided into the fundamental classes:

- which depend on the machine performance (they affect the machine only when the working process is being performed by the machine),
- which do not depend on the machine performance (they affect the machine also when the machine does work).

Some number of the damages result from the natural wear of the machine elements, while some other damages may be caused by ineffective repair of the damage occurred previously. Subsequently so called secondary damages appear within a short time interval. They result from incorrect organization of the repairs, poor training level of the repair team workers, constraints related to the before and after repair diagnostic activities, etc.

In the framework of the operation and maintenance investigations carried out within a real system of operation and maintenance of the means of transport, the time intervals occurring between the consecutive damages to the elements of the means of transport and the moments they appear were analysed.

When analysing statistically the moments the damages to the means of transport occur, a difference between the theoretical distribution and empiric one of the time interval values occurring between these moments (Fig.1) was observed. The significant difference between the theoretical distribution and the empiric one occurring at the beginning of the interval  $(0, t_p)$ , from the moment  $p$  declines to zero. However inside the interval  $(t_p, \infty)$  the theoretical function is consistent with the empiric distribution. This discrepancy results from the secondary damages caused by improper quality of the repairs of the damaged elements that occurs in the interval  $(0, t_p)$ . The investigations prove that the moments of the secondary damages are included inside the interval from 0 to 7 days (Fig. 1).

The analysis of the empiric data (the length of the time intervals between the damages) indicates that it is reasonable to describe the probability distribution of the correct work times with the reliability function  $R(x)$  formulated as follows:

$$R(x) = pe^{-\lambda x} + (1-p)R_w(t), \quad (1)$$

It is a combination of the exponential distribution  $pe^{-\lambda x}$  (with unknown value of the parameters  $(p\lambda)$ ) and the reliability function  $R_w(t)$ . The estimation of the distribution parameters  $(p\lambda)$  with the reliability function described with the dependence (1) is a complex problem.

Assuming that for unknown distribution (times of correct work) focused on the limited time interval  $(0, t_p)$  it is possible to estimate the values of the parameters  $p$  and  $\lambda$ , then for high values of  $t$  it may be assumed that:  $R(t) \approx p \cdot \exp(-\lambda t)$ . In that case using the methods of the linear regression (in the semi-logarithmic system) the values of the parameters  $p$  and  $\lambda$  may be evaluated for different random tests cut off from the bottom. For each such a approximation a regression standard fault is calculated –  $S(i)$ , where  $i$  stands for the index of the day from which the data are analysed. The analysis of the changes  $S(i)$  depending on the value of  $i$  indicates that there is a minimum  $s(i)$  for various  $i$ , most frequently for  $i = 5, 6, 7, \dots, 12$ .

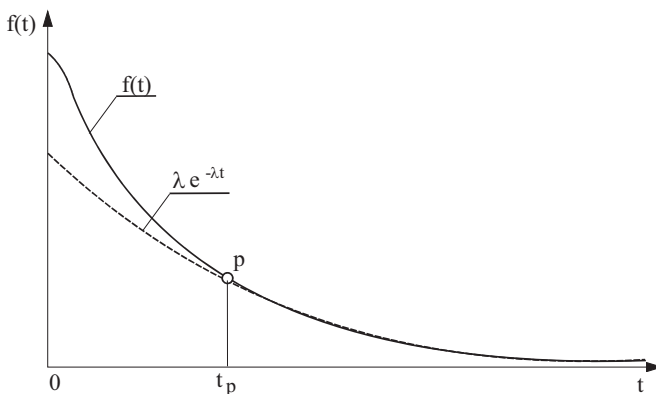


Fig. 1. Changes of the value of the exponential function and the real function at the time  $t$  [1,4]

The changes of the real function may be described by a combination of the probability distribution with density  $g(t)$  and exponential distribution. Let  $\tau_i(k)$ , where  $i = 0, 1, 2, \dots, \tau_0(k) = 0$ ,  $k = 0, 1, 2, \dots, n$  stand for the stream (moments) of the damages of the  $k$ -th technical object.

The difference  $\tau_{i+1}(k) - \tau_i(k)$  for  $i = 0, 1, 2, \dots$ , stands for the length of the time interval between  $i+1$ -st and  $i$ -th damage of the  $k$ -th technical object.  $Y_i(n)$  denotes superposition  $n$  – of the damage streams. Let  $X_i(n) = Y_i(n) - Y_{i-1}(n)$ , where  $i = 0, 1, 2, \dots, Y_0 = 0$

It is assumed that the distribution of the random variable  $X_i(n)$  does not depend on  $i$ . According to the theorem of Grigelionis it is known that with  $n \rightarrow \infty$  the random variable  $X(n)$  has exponential distribution.

It is assumed that the probability density of the random variable  $T$  is formulated as follows:

$$f(t) = \alpha \cdot g(t) + (1 - \alpha)e^{-\lambda t} \quad \text{for } f(t) \geq 0, \quad (2)$$

It is a combination of the probability distribution with the density  $g(t)$  and the exponential distribution with the density given with the formula (3):

$$g_1(t) = \lambda \cdot e^{-\lambda t}, \quad (3)$$

The estimation of the parameter  $\alpha$  and  $\lambda$  of the density (2) is based on the assumption that the density  $g(t)$  takes the values above zero, and that they are relatively low and included within the range from  $\langle t_p, \infty \rangle$ .

The analysis of the results of the operation and maintenance investigations regarding the moments the damages occur prove that the set of the damages may be divided into subsets of the *primary* and *secondary* damages.

It results from the fact that the consecutive moments of the damages to the same subsystems are gathered sequentially after a single damage occurred.

The figure 2 shows an exemplary damage stream of a chosen subsystem of a mean of transport.

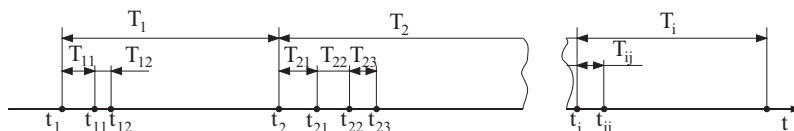


Fig. 2. Time intervals between the primary and secondary damages  $t_i$  – the moments the primary damages occur,

$t_{ij}$  – the moments the secondary damages occur,

$T_i$  – the time intervals between the moments the primary damages occur,

$T_{ij}$  – the time intervals between the moments the secondary damages occur.

As it is shown in the figure 2, the first of the damages which occurred at the moments  $t_i$ , cause the sequences of the subsequent damages to the same subsystem within short time intervals. These damages are called *primary*. Whereas the next of them, with the finite number of repetitions, occurring at the moments  $t_{ij}$ , are called *secondary*. Based on the analysis of the investigation results it has been found that the reason for the secondary damages is, in general, improper quality of the repairs of the primary damages to the subsystem elements. Reduction of the conditional probability of the occurrence of a secondary damage may be an initial point for reducing the damage intensity. It may be achieved by eliminating the damages occurring due to unreasonable realization of the repair process.

As it is shown in the figure 2 the faulty repairs represent one of the most important reasons for the occurred damages to the vehicle subsystems. Comparison of the significant reasons for the damages to the means of transport are shown in the figure 3.

The analysis of the operation and maintenance investigation results prove that reduction of the number of the secondary damages is an essential problem, the solution of which makes it possible to have an influence on the operation reliability level of the means of transport.

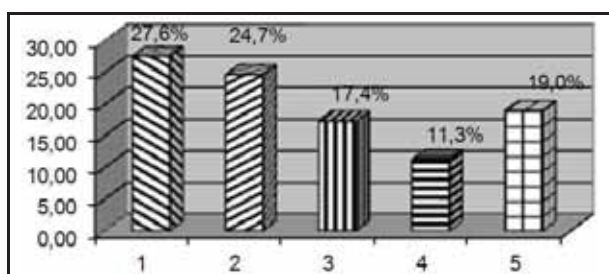


Fig. 3. Occurrence frequency of the reasons for the damages to the elements of the means of transport  
1-faulty repairs, 2-faulty utilisation, 3-influence of the environment, 4-damages to the co-working elements, 5-others.

## 2. Purpose of the paper

The purpose of this paper is to evaluate the influence of the means of transport on the operation reliability level of a transport system.

## 3. Object of the investigations

The objects of the investigations are damages to the subsystems of the means of transport being operated and maintained within a chosen transport system. Whereas the subject of the investigation is the influence of these damages on the operation reliability level of the transport system.

A detailed example of a transport system is one of the road transport systems – an urban transport, covering the bus transport system. Despite a series of advantages such as: punctuality, frequency, regularity, reliability, accessibility, directness, comfort, movement speed, transport fare, safety, no need to use a traction or railway subgrades, being characteristic for an urban bus transport system when compared it to the trolley-bus or tramway transport system, it is also characterised by some disadvantages, and namely: it is a source of various road dangers to the health and life of the people, technical objects and the natural environment.

The investigations performed within a bus urban transport system referred to the damages to the subsystems of the means of transport and to the moments they occurred. They were carried out by a passive experiment method under real operation and maintenance conditions. A random set consisting of 28 means of transport utilised in the real operation and maintenance conditions was selected for the investigation purposes. The results of the investigations cover five-year long period of the operation and maintenance of the means of transport.

## 4. Damage classification methodology

The classification of the damages to the means of transport was done for their respective subsystems. That was why the object under investigations was decomposed to its subsystems. Symbols denoting the subsystems of the mean of transport were determined at the decomposition stage, as presented in the Table 1.

So called significant subsystems, that means such systems whose damage effects occurred within the time interval under investigation affect the operation reliability of the means of transport to the highest extent were selected in order to analyse the damage stream.

Table 1. Set of the subsystems of the decomposed mean of transport

| Subsystem Code | Subsystem Name |
|----------------|----------------|
|----------------|----------------|

|    |                              |
|----|------------------------------|
| SI | - Engine                     |
| PN | - Drive transmission         |
| UJ | - Wheels and steering system |
| IE | - Electric system            |
| HA | - Braking system             |
| NA | - Bodywork                   |
| UK | - Steering system            |
| SP | - Compressed air feed system |
| ZA | - Suspension system          |
| IN | - Others                     |

In order to classify the damages as primary and secondary ones the following criteria were adopted:

- a) **essential criterion** – the average distance in kilometres travelled between the consecutive damages of the  $j$ -the subsystem depending on:

$L_u$  – stands for the summarized number of the damages to the bus under investigation,

$L_{u1}$  – stands for the number of the damages to the electric system IE,

$L_{u2}$  – stands for the number of the damages to the bodywork NA,

$L_{u3}$  – stands for the number of the damages to the drive transmission system PN,

$L_{u4}$  – stands for the number of the damages to the engine SI,

$L_{u5}$  – stands for the number of the damages to the braking system HA,

$P_c$  – stands for the total distance travelled by the bus during the investigation time [km],

$L_{srj}$  – average distance travelled between two consecutive damages of the investigated  $j$ -th subsystem [km], described with the following dependence (4):

$$L_{srj} = \frac{P_c}{L_{uj}}, \quad j = 1, 2, 3, 4, 5, \quad (4)$$

$s_j'$  – standard deviation [km], described with the dependence (5):

$$s_j' = \pm \sqrt{\frac{\sum_{i=1}^n (L_{ij} - L_{srj})^2}{n-1}}, \quad (5)$$

where:

$L_{ij}$  – the distance travelled between the consecutive repairs [km] of the  $j$ -the subsystem,

$n$  – number of the measurements that is the number of runs between the consecutive repairs of the  $j$ -th subsystem.

$s_j$  – standard deviation including the t-Student's index depending on the number of the measurements  $n$  and the confidence coefficient  $1-\alpha$ , has been described with the dependence (6):

$$s_j = f_{1-\alpha} s_j', \quad j = 1, 2, 3, 4, 5 \quad (6)$$

The closer the confidence coefficient is to 1, the more extensive coefficient range is achieved. The confidence coefficient adopted in the paper is  $1-\alpha = 0.95$ . It is the most frequent value of this coefficient used in the statistical research. Along with the increase of its value the standard deviation  $s$  goes up $j$ :

- previous damage to the  $j$ -the subsystem was a primary one  $L_{upj}$  on condition that the following dependence was fulfilled (7):

$$L_{upj} = L_{ij} \geq L_{srj} - s_j, \quad j=1, 2, 3, 4, 5 \quad (7)$$

- previous damage to the  $j$ -the subsystem was secondary  $L_{uwj}$  on condition that the following dependence was fulfilled (8):

$$L_{uwj} = L_{ij} < L_{srj} - s_j, \quad j=1, 2, 3, 4, 5 \quad (8)$$

where:

$L_{srj} - s_j$  – the value describing the threshold between the primary and secondary damages [km]

- b) auxiliary criterion – critical time  $s_{kr}$  determined on the basis of the average time of correct operation between the consecutive damages to the subsystem.

Basing on the analysis of the operation and maintenance investigation results it was assumed that the time intervals of the correct operation between the consecutive damages to a bus subsystem may be expressed by means of an exponential distribution. While the condition of the critical time  $t_{kr}$  (9) [1,2,3,4].

$$t_{kr} = -\frac{1}{\hat{a}} \ln \alpha \quad (9)$$

where:

$\alpha$  - significance level,

$\hat{a} = \frac{1}{\bar{t}}$  - parameter estimator with the moment method,

$\bar{t}$  - average value of the time interval of the correct operation between the damages to the subsystem.

In order to set the value of the efficiency factor of the performed repairs the following descriptions and dependences were adopted.

$N(t)$  – summarized number of the repairs of the mean of transport under investigation up to the moment  $t$ , described with the dependence (10):

$$N(t) = \sum_j N_j(t), j = 1, 2, \dots, m \quad (10)$$

$N_j(t)$  – number of the repairs of the  $j$ -th subsystem up to the moment  $t$ , described with the dependence (11):

$$N_j(t) = N_j^S(t) + N_j^N(t), j = 1, 2, \dots, m \quad (11)$$

where:

$N_j^S(t)$  – number of effective repairs of the  $j$ -th subsystem up to the moment  $t$

$N_j^N(t)$  – number of ineffective repairs of the  $j$ -th subsystem up to the moment  $t$

The values  $N_j^S(t)$  and  $N_j^N(t)$  were determined on the basis of the following dependence:

$L_{srj}(t)$  – average travelled distance between the repairs of the  $j$ -th subsystem, described with the dependence (12):

$$L_{srj}(t) = \frac{L_{1j}(t) + L_{2j}(t) + \dots + L_{nj}(t)}{N_j(t)} = \frac{1}{N_j(t)} \sum_{i=1}^n L_{ij}(t) \quad (12)$$

for  $i = 1, 2, \dots, n, j = 1, 2, \dots, m$

where:

$L_{ij}(t)$  – the travelled distance between the consecutive repairs of the  $j$ -th subsystem up to the moment  $t$ ,

$N_j(t)$  – number of the repairs of the  $j$ -th subsystem up to the moment  $t$ .

The value of the *efficiency factor* of the performed repairs of the  $j$ -th subsystem of the investigation object is described with the dependence (13):

$$WS_j = \frac{N_j(t) - N_j^N(t)}{N_j(t)} = \frac{N_j^S(t)}{N_j(t)}, j = 1, 2, \dots, m \quad (13)$$

The value of this factor may be expressed as follows:

$$WS_j = \frac{N_j^s}{N_j} * 100[\%], \quad j = 1, 2, 3, 4, 5 \quad (14)$$

Based on the analysis of the values of the travelled distance and the time intervals between the damages to the subsystems of a mean of transport, a criterion to classify the damages as primary and secondary ones was adopted according to the dependence (7), (8) and (9). Having classified the damages, the essential statistical parameters such as: numbers of the primary damages ( $L_{up}$ ), numbers of the secondary damages ( $L_{uw}$ ), etc. were determined.

## 6. Investigation results

Table 2 presents selected investigation results regarding the number of the repairs of the selected bus subsystems, which are characterised by the highest numbers of the damages occurred when performing the operation and maintenance investigations.

Table 2. Comparison of the number of repairs of the selected bus subsystems under investigation

| Number of bus       | Subsystem code | Number of repairs | Number of effective repairs | Number of ineffective repairs | Repair efficiency factor expressed in % |
|---------------------|----------------|-------------------|-----------------------------|-------------------------------|---|
| <b>Ikarus IK260</b> |                |                   |                             |                               |   |
| 1                   | IE             | 147               | 48                          | 99                            | 32,65                                   |
|                     | PN             | 126               | 45                          | 81                            | 35,71                                   |
|                     | NA             | 86                | 26                          | 60                            | 30,23                                   |
|                     | SI             | 66                | 20                          | 46                            | 30,30                                   |
|                     | HA             | 55                | 20                          | 35                            | 36,36                                   |
| 2                   | IE             | 186               | 66                          | 120                           | 35,48                                   |
|                     | PN             | 141               | 42                          | 99                            | 29,79                                   |
|                     | NA             | 99                | 31                          | 68                            | 31,31                                   |
|                     | SI             | 62                | 28                          | 34                            | <b>45,16</b>                            |
|                     | HA             | 76                | 24                          | 52                            | 31,58                                   |
| 3                   | IE             | 108               | 29                          | 79                            | 26,85                                   |
|                     | PN             | 84                | 26                          | 58                            | 30,95                                   |
|                     | NA             | 78                | 22                          | 56                            | 28,21                                   |
|                     | SI             | 49                | 19                          | 30                            | 38,78                                   |
|                     | HA             | 115               | 44                          | 71                            | 38,26                                   |
| 4                   | IE             | 53                | 16                          | 37                            | 30,19                                   |
|                     | PN             | 29                | 12                          | 17                            | <b>41,38</b>                            |
|                     | NA             | 61                | 25                          | 36                            | <b>40,98</b>                            |
|                     | SI             | 43                | 14                          | 29                            | 32,56                                   |
|                     | HA             | 64                | 22                          | 42                            | 34,38                                   |
| 5                   | IE             | 61                | 23                          | 38                            | 37,70                                   |
|                     | PN             | 81                | 26                          | 55                            | 32,10                                   |
|                     | NA             | 38                | 12                          | 26                            | 31,58                                   |
|                     | SI             | 45                | 13                          | 32                            | 28,89                                   |
|                     | HA             | 56                | 17                          | 39                            | 30,36                                   |
| 6                   | IE             | 230               | 70                          | 160                           | 30,43                                   |
|                     | PN             | 237               | 90                          | 147                           | <b>37,97</b>                            |
|                     | NA             | 158               | 50                          | 108                           | 31,65                                   |
|                     | SI             | 86                | 26                          | 60                            | 30,23                                   |
|                     | HA             | 189               | 65                          | 124                           | 34,39                                   |
| 7                   | IE             | 99                | 36                          | 63                            | 36,36                                   |
|                     | PN             | 51                | 20                          | 31                            | 39,22                                   |
|                     | NA             | 64                | 20                          | 44                            | 31,25                                   |
|                     | SI             | 38                | 13                          | 25                            | 34,21                                   |
|                     | HA             | 42                | 14                          | 28                            | 33,33                                   |

## 7. Analysis of the investigation result and conclusions

As it results from the data stated in the table 4 the maximal percentage of the secondary damages in the total number of the damages is equal to 74%. Such a high percentage causes

significant reduction of the operation reliability of the means of transport resulting from impossibility to perform the tasks. It makes the decision maker of the transport system use so called substitutive buses in order to follow the scheduled runs, what in turn is related to extra expenditures to accomplish the tasks.

The results of the operation and maintenance investigation prove that the realization of the actions aimed at reduction of the number of the secondary damages is reasonable and that they are to be considered as the essential actions to increase the operation reliability level of a transport system.

From the analysed source information it results that the secondary damages to the bus subsystem elements are to be eliminated inside the service and repair process. It may be accomplished by:

- correct diagnostic activities performed before and after repairs,
- using correct spare parts,
- using adequate repair measures,
- observing scheduled times to carry out surveys and replacements,
- correct assembly and disassembly,
- introducing technical control over the repairs performed,
- increasing the employee's qualifications,
- appropriate employee's motivation,
- providing the repair stands with the technological and repairing tools,

After completing the investigations in a repair department it was found that it was necessary to introduce identification of the person repairing the damaged subsystem. Having introduced these changes, a significant reduction of the number of the secondary damages was noticed.

It is reasonable to carry out further operation and maintenance investigations regarding the identification of the reasons for the secondary damages and the evaluation of their significance in terms of the possibility to undertake reasonable actions aimed at increasing the operation reliability of a transport system.

## References

- [1] Fisz M. *Rachunek prawdopodobieństwa i statystyka matematyczna*. PWN, Warszawa 1969
- [2] Woropay M., Wdzięczny A. *Analysis and evaluation of risk in a transport system*. Warszawa – Naęczów 2006. Journal Of KONES. European Science Society of Powertrain and Transport Publication, vol. 13 no. 2.
- [3] Woropay M., Wdzięczny A. *Analysis and evaluation of the influence of the bus braking subsystem damages on origination of damagers in a sociotechnical system*. Kraków 2006. Journal of KONBiN. the 4<sup>th</sup> International Conference on Safety and Reliability KONBiN, vol.1.
- [4] Woropay M., Migawa K., Szumiński H., Wdzięczny A. *Analiza skuteczności realizowanych napraw podzespołów autobusów eksploatowanych w systemie komunikacji miejskiej*. Warszawa 2004, Materiały konferencyjne, Międzynarodowa Konferencja Naukowa – Transport XXI Wieku.



## ZIRCONIUM DIOXIDE AS A BIOMATERIAL; THE MICROSTRUCTURE

Mateusz Wirwicki, Tomasz Topoliński,

University of Technology and Life Sciences in Bydgoszcz  
ul. Kaliskiego 7, 85-796 Bydgoszcz, Poland  
tel.: +48 52 3408497, fax: +48 52 3408245  
e-mail: [wirwicki@utp.edu.pl](mailto:wirwicki@utp.edu.pl)

### Abstract

*Zirconium dioxide is a material which, over the recent years, has been attracting support among dental technicians and dentists, thanks to its chemical composition and mechanical properties, it can replace non-anaesthetic foundations or metal crowns. Additionally zirconium dioxide is a material which is easy to work in. Zirconium dioxide is a polymorphic material demonstrating three phases: monocyclic, cubic and tetragonal. Additionally during the crack propagation the material shows the reinforcing transformation; the replacement of the phase and increasing the volume of the molecules, which inhibits the microcracks in the material. Thanks to such potential, zirconium dioxide has acquired a very high recognition in stomatology and orthodontics. Interestingly, the factor which has a considerable impact on the fatigue life and strength of zirconium dioxide is an adequate treatment and tool operation temperature; the slightest undesired effect can trigger the accumulation of stresses and thus decrease the material strength. A lower mechanical strength can be also due to other conditions, e.g. varied nutrition habits in the patient and the frequency of oral cavity hygiene practises.*

*Keywords: zirconium dioxide, microstructure, biomaterial, structure reinforcement*

### 1. Introduction

Zirconium dioxide is a ceramic material the dentists have been getting convinced about since the 1990s. Porcelain as a supplement of tooth losses was improved in 1956 when it was baked over the metal core [19]. This technique provided an adequate strength, however, it was not so much aesthetic. Since then attempts have been made to enrich the chemical composition of porcelain to such extent that the tooth restoration is possible only by using porcelain without metal elements. In the early days of dental prosthodontics one could differentiate between the following materials helping the elimination of tooth losses: feldspathic porcelain, mica-reinforced ceramic, leucite-reinforced ceramic, lithium-disilicate ceramic, aluminium trioxide ceramic, zirconium-dioxide-reinforced ceramic [22,23]. It turns out that leucite, lithium-disilicate and aluminium ceramic shows very low strength while applying the multi-section structures. A search has been launched to find the ceramic material of high mechanical strength which would allow for producing dental arches, fixed dental restorations. Such material has been used for a long time already, however in other fields of human life it is zirconium [24,25]. Yet another advantage, despite a high mechanical strength, is an easy treatment also possible using CNC tools, thanks to which the application of zirconium as early as in the 1990s, it was possible to develop a technology which would facilitate the formation of restorations adjusted to the conditions in the patient's oral cavity [14].

### 2. Microstructure of zirconium dioxide

The most frequent zirconium porcelain used in workshops and dental surgeries is zirconium dioxide 96%  $\text{ZrO}_2$  of which mixes with 4%  $\text{Y}_2\text{O}_3$  [7,17]. The zirconium dioxide crystal grains themselves are  $0.2 \div 1 \text{ }\mu\text{m}$  in size [5,7,21]. Zirconium dioxide is a polymorphic material which can occur in three forms: monoclinic (commonly referred to as slanted), cubic and tetragonal. Depending on the temperature of the environment, the material occurs in one of the following forms: at room temperature it will occur in a monoclinic – monoclinic form. Heating the material to  $1170^\circ\text{C}$ , one can note a tetragonal phase and above  $2370^\circ\text{C}$  – the cubic one. From the perspective of biomechanics, it is the tetragonal phase which is the best form of the arrangement of the molecules [8,9,10]. Thanks to such additions as yttrium, magnesium and cerium, it is possible to reach that phase at room temperature. Adding 8% of magnesium oxide triggers changes in the volume of the phase during zirconium dioxide cooling. Adding  $2 \div 3\%$  stops the withdrawal of zirconium dioxide from the tetragonal phase to the cubic phase [6]. During the zirconium dioxide structure crack propagation it changes its phase from the tetragonal one into the monoclinic phase, which triggers the transformation of the molecules; hence the structure reinforcement. Such phenomenon can be referred to as the reinforcing transformation. During that process there is observed a  $3 \div 5\%$  increase in the volume of the zirconium dioxide molecules, thus decreasing the destruction energy and, in turn, decreasing the crack propagation (Fig. 1) [4,3,1]. The process decreases the dispersion of microcracks in the structure.

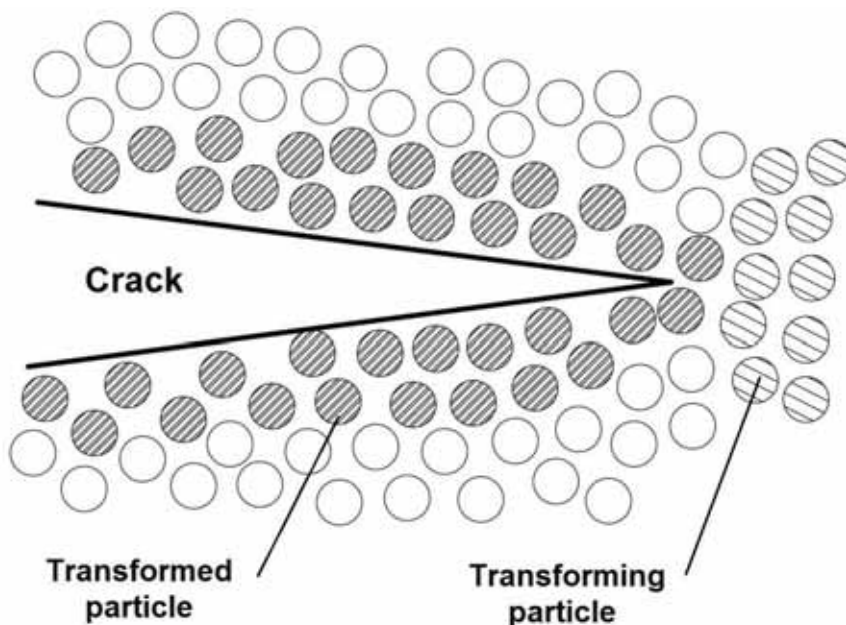


*Fig. 1. Diagram of the crack propagation with a change in the phase from tetragonal to monoclinic [2].*

Zirconium dioxide with supplementary ingredients, stabilizing the structure, has been highly recognized in such areas as dental braces; the grips correcting the tooth position in the oral cavity, endodontics as hinges, dowels supporting the tooth, single teeth and fixed dentures [11,12]. Analysing the strength, one must note that preparing the material itself, the zirconium dioxide, bonded with another supplementing element, plays a very big role. The dental labs preparing the surfaces use fine cutters the operation of which does not disturb the arrangement of the material structure molecules, namely an increase in strength. Operating coarse cutters triggers considerable defects in the material structure and thus high stresses. Similarly during operation one shall

consider the effect of temperature which plays an essential role in the structural changes and even triggers reverse transformation [13,16].

### 3. Summary

Over the recent years one can note a growing interest in the material such as zirconium dioxide. Thanks to various chemical bonds, yttrium, magnesium and cerium, it is possible to adjust the microstructure to the required application in orthodontics or endodontics of the oral cavity. Zirconium demonstrates high mechanical strength and easy treatment. Thanks to special CNC devices and the CAD/CAM software, the dental technicians can make dental crowns and arch bridges. A special process of ceramic burning taking even up to 11 hours at the temperature of 1400°C and the accompanying contraction reaching  $18 \div 25\%$  point to a high material life [13, 15]. The only problem has been, so far, a low number of studies which would determine whether the material ages, under which conditions it ages and what affects that process. It can be due to other material work conditions in the oral cavity, various nutrition habits in the patient as well as the frequency of the oral cavity hygiene practises. An interesting phenomenon which occurs in the zirconium dioxide material during the crack propagation is its self-strengthening, the so called self-repair potential [20]. Material ions go through various phases and increase their volume even up to 5%, thanks to which the material microcrack propagation decreases. The strength is also affected by the material preparation process itself as well as its treatment. The application of the adequate tools; fine cutters which, while at work, do not trigger a considerable temperature increase, will not result in a change in the material phase and, as a result, high stress concentrations [25].

### References

- [1] Bitter K., Meyer-Luckel H., Priehn K., Martus P., Kielbassa A.M., *Bond strengths of resin cements to fiber – reinforced composite posts*. Am J Dent 19, pp.138–42, 2006.
- [2] Butler E.P., *Transformation toughened zirconia ceramics*. Mat Sci Tech 1 pp.417 – 32,1985.
- [3] Chevalier J., *What future for zirconia as a biomaterial?* Biomater., 27, pp. 539-546,2006.
- [4] Conrad H. J., Seong W. J., Pesun I. J., *Current ceramic materials and systems with clinical recommendations: A systematic review*. J. Prosthet. Dent., 98,pp. 389-404, 2007.
- [5] Della Bona A., Kelly J.R., *The clinical success of all-ceramic restorations*. J Am Dent Assoc 139, pp. 8–13, 2008.
- [6] Denry I., Kelly J.R., *State of the art of zirconia for dental applications*. Dent Mater 24, pp. 299–307, 2008.
- [7] Dejak B., Kacprzak M., Suliborski B., Śmielak B. *Struktura i niektóre właściwości ceramiek dentystycznych stosowanych w uzupełnieniach pełnoceramicznych w świetle literatury*. Protet. Stomatol., LVI 6, pp. 471-477, 2006.
- [8] Garvie R. C., Hannink R. H., Pascoe R. T., *Ceramic steel?* Nature 258, pp. 703-704, 1975.
- [9] Garvie R.C., Nicholson P.S., *Structure and thermodynamical properties of partially stabilized zirconia in the CaO – ZrO<sub>2</sub> system*. J Amer Ceram Soc 55, pp.152 -7, 1972..
- [10] Gupta T.K., Bechtold J.H., Kuznickie R.C., Cado L.H., Rossing B.R., *Stabilization of tetragonal phase in polycrystalline zirconia*. J Mater Sci 13, pp.1464,1978.
- [11] Kelly J. R., Denry I.: *Stabilized zirconia as a structural ceramic: An overview*. Dent. Mater., 24,pp. 289-298,2008.
- [12] Lasek K., Okoński P., Mierzwińska – Nastalska E., *Tlenek cyrkonu – właściwości fizyczne i zastosowanie kliniczne*. Protet. Stomatol., LIX 6, pp. 415 – 422, 2009.
- [13] Nakamura K., Kanno T., Milleding P., Ortengren U., *Zirconia as a dental implant abutment material: a systematic review*. Int J Prosthodont. 23,pp. 299-309, 2010.

- [14] Rieth P.H., Reed J.S., Naumann A.W., *Fabrication and flexural strength of ultra-fine grained yttria-stabilised zirconia*. Bull Am Ceram Soc 55, pp. 717, 1976.
- [15] Ruff O., Ebert F., Stephen E., *Contributions to the ceramics of highly refractory materials: II. System zirconia-lime*. Z Anorg Allg Chem 180, pp. 215–24.
- [16] Subbarao E.C., *Zirconia – an overview*. In: Heuer AH, Hobbs LW, editors. *Advances in ceramics, vol. 3. Science and Technology of Zirconia*. Elsevier ,pp. 1 - 24 Amsterdam 1981.
- [17] Sundh A., Molin M., Sjörgen G., *Fracture resistance of yttrium oxide partially stabilized zirconia all-ceramic bridges after veneering and mechanical fatigue testing*. Dent. Mater., 21,pp. 476-482,2005.
- [18] Szczyrek P., *Historia zastosowania ceramiki w stomatologii*. Protet. Stomatol., LIII 2,pp. 112-114, 2003.
- [19] Theunissen, Bouma J.S., Winnbust A.J.A., Burggraaf A.J., *Mechanical properties of ultra-fine grained zirconia ceramics*. J Mater Sci 27, pp.:4429 – 38,1992.
- [20] Trzebiatowski W.: *Chemia nieorganiczna*, Wyd. PWN, Warszawa 1969,
- [21] Sahafi A., Peutzfeldt A., Asmussen E., Gotfredsen K., *Bond strength of resin cement to dentin and to surface-treated posts of titanium alloy, glass fiber, and zirconia*. J Adhes Dent 5,pp.153–62, 2003.
- [22] Sahafi A., Peutzfeldt A., Asmussen E., Gotfredsen K., *Retention and failure morphology of prefabricated posts*. Int J Prosthodont;17, pp. 307–12, 2004.
- [23] Sahafi A., Peutzfeldt A., Asmussen E., Gotfredsen K., *Effect of surface treatment of prefabricated posts on bonding of resin cement*. Oper Dent 29, pp.60–8, 2004.
- [24] Perdigao J., Geraldini S., Lee I.K., *Push-out strengths of tooth-colored posts bonded with different adhesive systems*. Am J Dent;17, pp. 422–6, 2004.
- [25] Xible A.A., De Jesus Tavaréz R., de Araujo C.R.P., Bonachela W.C., *Effect of silica coating and silanization on flexural and composite-resin bond strengths of zirconia posts: an in vitro study*. J Prosthet Dent 95, pp. 224–9, 2006.



## DAMPING BUILDING VIBRATIONS EXCITED BY SURFACE WAVE PROPAGATING IN THE GROUND

Janusz Zachwieja, Irena Gołębiewska

*University of Technology and Life Sciences*

*Department of Applied Mechanics, Faculty of Mechanical Engineering*

*Department of Building Construction, Faculty of Civil and Environmental Engineering*

*ul. S. Kaliskiego 5, 85-796 Bydgoszcz*

### **Abstract**

*This paper presents anticipated results of reducing vibrations of a laboratory building by separating its foundation from the ground. In order to carry out a numerical analysis, the building and the foundation soil were modelled with the use of Multibody System Dynamics (MSD). In a real system, vibrations of walls and floors are caused by propagation of waves in the ground. Such waves are excited by cyclic impact of operating crushing elements of a roller-bowl mill located in the vicinity of the building. Energy carried by the waves is so high that they cause vibrations of the building when the waves encounter an obstacle in the form of the foundation. The vibrations have the velocity of several millimetres per second. This phenomenon has an adverse effect as far as the strength of elements made of brittle materials such as concrete and bricks is concerned, and it becomes critical when high-sensitivity measuring instruments are located in the rooms. Then, vibrations may cause incorrect readings of such instruments and damage of the elements, mainly electronic ones. In order to determine the extent of vibrations propagated from the mill to the laboratory building foundation, measurements of vibration parameters were carried out and amplitude-frequency responses of the investigated objects were obtained. The results of a simulation revealed that an expansion gap having a calculated effective height would allow reducing the level of vibrations in the building as well as in laboratory stations located inside.*

**Key words:** *proper vibrations, minimisation of vibrations, resonance frequency values, propagation of disturbances in the ground, seismic and para-seismic actions*

### **1. Introduction**

Civil structures are exposed to various types of dynamic loads among which seismic and para-seismic actions can be recognized. Seismic excitations occur due to earthquakes, whereas para-seismic excitations are caused by human activity such as vibrations of machines supported on own foundations, shooting in quarries, driving sheet piling, rail and road traffic, etc. Dynamic impact which is transferred by the ground to civil structures causes vibrations in them. Machines which are percussive in operation are usually located within a safe distance from buildings. However, it should be remembered that percussive-borne vibrations can propagate as disturbance in the soil medium over significantly long distances depending on the type of the base, depth of groundwater, above- and underground infrastructure, etc. [3]. As the distance from the source of vibrations increases, amplitudes of ground vibrations decrease, because the density of conveyed energy decreases, vibrations are damped and the energy is dissipated at the borders of ground layers [1]. Vibrations have an adverse impact on the strength of structures as well as the durability of elements of machines located inside. Therefore, actions are taken to devise the most effective methods of minimising vibrations for every case of such excitations [5, 7]. Three main types of methods for protection against vibrations such as passive, semi active and active ones can be

distinguished [2]. Methods which involve direct interference with the source by eliminating the cause of vibrations lead to the best results. As an example, rotor balancing is a much simpler and effective solution than an attempt of limiting vibration levels by applying vibration insulation. A particularly important task from the viewpoint of engineering is to lower the level of vibrations in large structures and foundations of machines when the vibrations are caused by excitations which are resonant in nature [6]. In such cases, prior to corrective actions, there should be a numerical analysis so that results of applied solutions intended for minimisation of the level of vibrations can be anticipated [4].

This paper presents the concept of reducing the level of vibrations in a laboratory building caused by excitations from the system of a roller-bowl mill. The investigated object is located about 200 m away from the source of such vibrations. Surface waves which propagate in the ground in the form of shocks carry such a high amount of energy that vibrations having high amplitudes occur in the building due to the waves which reach the foundation, even though the source is located far away. The problem is quite serious as vibrating walls and floor make the laboratory tables and measuring instruments vibrate.

## 2. Measured parameters of vibrations in the structures

Measurements and analysis of vibration parameters were carried out *in situ* and aimed at determining the mechanism of how vibrations propagate from the ground to the laboratory building. The investigated structure is a two-storey building made of bricks. It was supported on strip footings and has a basement. The operating mill which is the source of vibrations is supported on reinforced-concrete foundations having dimensions of 10 m x 10 m x 3 m and is supported on Franki piles having the length of 12 m. The laboratory building is located about 200 m away from the milling station (the mill). A diagram of the roller-bowl mill in operation is presented in Fig. 1.

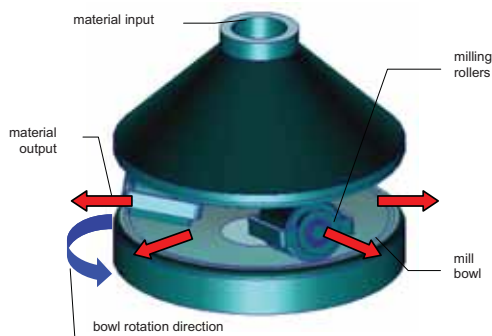


Fig. 1. A schematic view of the bowl with rollers as the element of the mill which excites vibrations

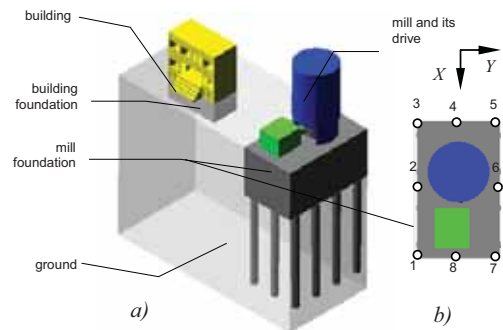


Fig. 2. A schematic view of the location of the mill with reference to the building (a) and location of measuring points at the foundation (b)

The material to be ground is fed from the top, and then it falls onto the bowl where it is ground down by three rollers moving on the bowl. The milling is removed by a system of fans, and then it is fed to separators so as to separate various grain sizes. The mill belongs to the group of machines which are percussive in operation. During the milling process rotation of the rollers is forced by the bowl rotating around the axis of the mill. The rollers can also move vertically. By falling onto the bowl the roller hits it and a quite significant amount of energy is transferred to the mill.

Measuring sensors were placed along the edge of the foundation of the mill (Fig. 2b) and at the bowl (Fig. 3a). Fig. 3 shows typical amplitude-frequency responses of vibration velocities of the mill bowl in the reduction gear axis (horizontally and vertically). Velocity amplitudes of bowl

vibrations are considerable and equal to 3 to 4 mm·s<sup>-1</sup>. The maximum RMS values measured in the axis of the reduction gear of the bowl driving system reached the value as high as 8.42 mm·s<sup>-1</sup>. Instantaneous values reached even the level of 28 mm·s<sup>-1</sup>. Frequency of vibration components in the measured band ranged from 3.5 to 11.5 Hz.

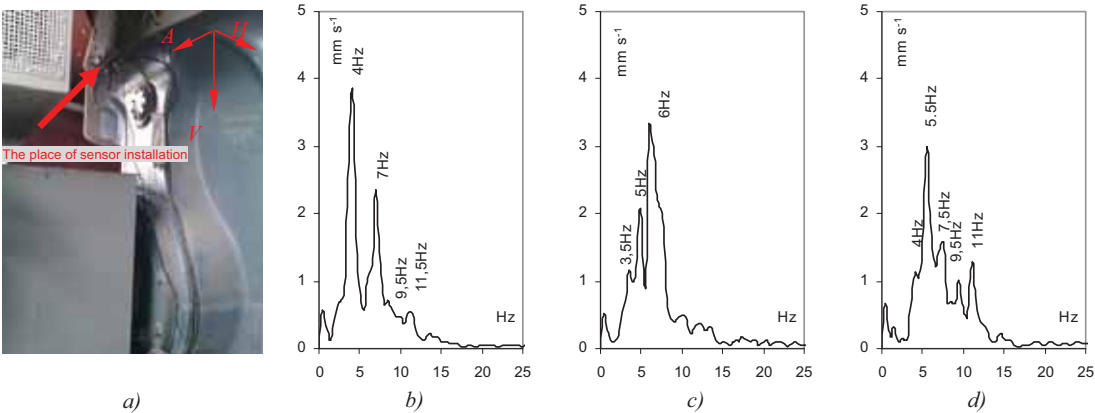


Fig. 3. Location of the measurement spot at the bowl a), an amplitude-frequency response of vibration velocity b) in the axis of the reduction gear, c) horizontally, d) vertically

Figs. 4 and 5 show amplitude-frequency responses of vibration acceleration values of the mill foundation in Y-axis, at point 1 and 3 respectively.

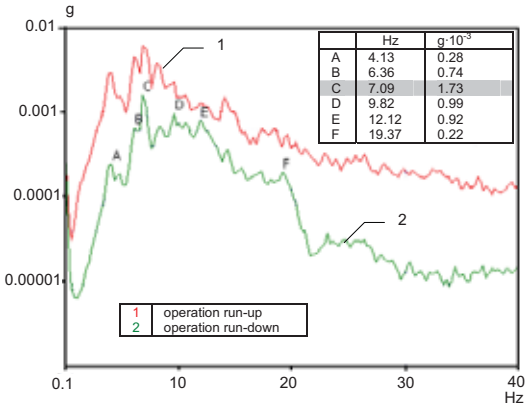


Fig. 4. An amplitude-frequency response of the vibration acceleration value of the mill foundation at point (1) in Y-axis

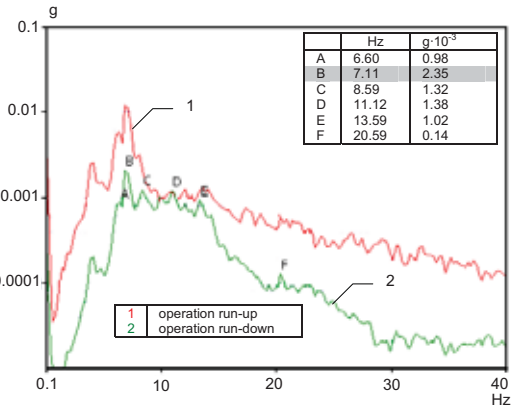


Fig. 5. An amplitude-frequency response of the vibration acceleration value of the mill foundation at point (3) in Y-axis

The responses were obtained on the basis of vibration acceleration values of the mill foundation in the function of time during mill operation run-up and run-down periods. By analysing the measurement results it can be observed that the area of foundation vibrations carrying lots of energy applies for the frequency ranging from 4 to 12 Hz. The recorded parameters of vibrations of the mill foundation prove that there are good conditions for applying insulation with the damping effect of 20 dB.

The maximum values of acceleration amplitudes for the mill foundation in Z-axis (vertical) correspond to higher frequency values than the maximum acceleration amplitudes of vibrations in

the horizontal plane. For the frequency of ~13 Hz the value is 2.57 mg ( $0.025 \text{ m}\cdot\text{s}^{-2}$ ) (Fig. 6). The same effect can be observed in case of vibrations of the mill bowl.

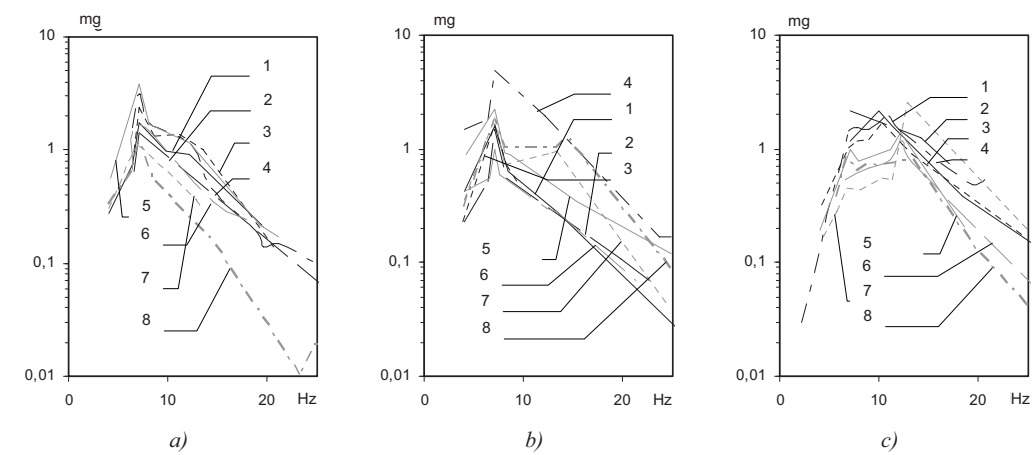


Fig. 6. Amplitude-frequency responses of vibration acceleration values of the mill foundation in a) X-axis, b) Y-axis, c) Z-axis

Changes of selected parameters of vibrations along time in the laboratory building were recorded as well. The sensors were placed in several places such as the laboratory on the working top of the table (point #1) and on the floor (point #2) (Fig. 7).

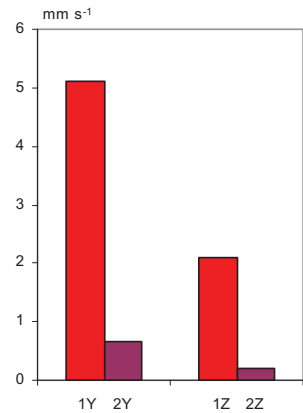
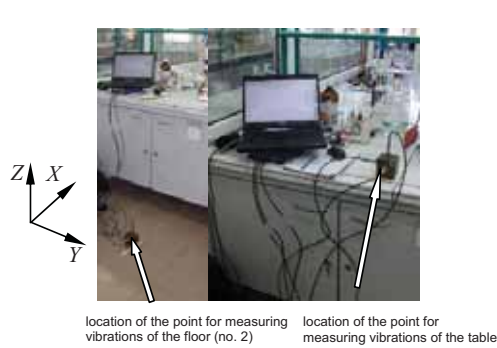


Fig. 7. A view of points for measuring vibrations of the table

Fig. 8. Values of vibration velocity amplitudes at point 1 and 2 at the frequency of 7 Hz

Fig. 8 shows examples of vibration velocity amplitudes in the measuring points 1 (table) and 2 (floor) at 7 Hz, whereas Fig. 9 shows an amplitude-frequency response of a table vibration acceleration value in Y-axis.

By analysing the measurement results it can be observed that the value of table vibration velocity is higher in both horizontal and vertical plane when compared with vibrations of the floor. Resonant vibration can be observed in Y-axis.

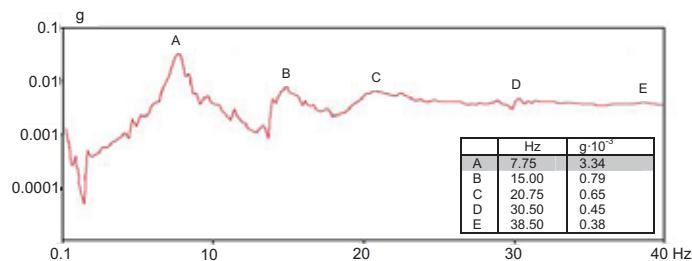


Fig. 9. An amplitude-frequency response of the vibration acceleration value of the table in Y-axis

The amplitude of floor vibration velocity in the horizontal plane is almost 8 times higher than the corresponding amplitude of table vibration velocity in the vertical plane (Figs. 10 and 11).

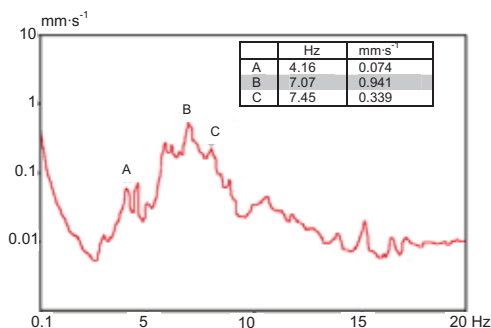


Fig. 10. An amplitude-frequency response of vibration velocity on the floor in Y-axis

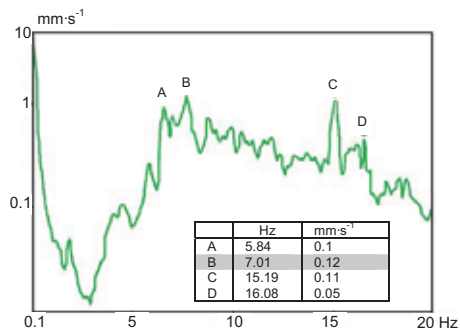


Fig. 11. An amplitude-frequency response of vibration velocity on the floor in Z-axis

### 3. Calculation model and numerical analysis

*Multibody System Dynamics (MSD)* was used for the purpose of a numerical analysis of vibrations propagating through the ground to the foundation of the building and the response of the system to the applied excitations with implemented damping insulation. The laboratory table where instruments are placed, as well as elements of the building such as the floor, walls, foundations and the ground, are modelled as rigid bodies (Fig. 12). Between the floor and the table there is a contact reaction. The contact between the foundation and the ground was modelled as an elastic-damping coupling for which parameters were selected in such a manner that proper vibration frequencies of the model would correspond approximately to the values obtained from the experiments.

Dynamic rigidity coefficients of the ground were determined by means of Savinov method in accordance to a standard. The coefficients depend on the type of ground, foundation pressure on the base as well the shape and dimensions of the foundation. For the purpose of calculations the following six discrete values of base rigidity coefficients  $k_x = k_y = k_z = 10^6 \text{ N/mm}$  and  $k_{\phi x} = k_{\phi y} = k_{\phi z} = 10^8 \text{ N mm}$  were assumed. The analysis was carried out in the range of linear elasticity.

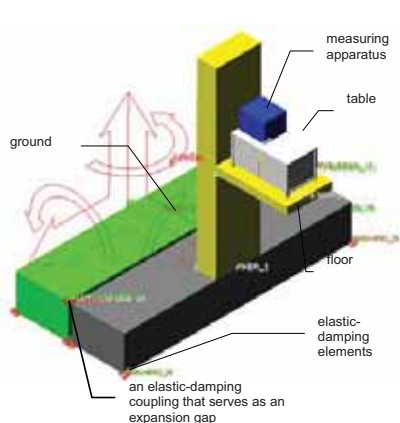


Fig. 12. The model applied in the numerical analysis

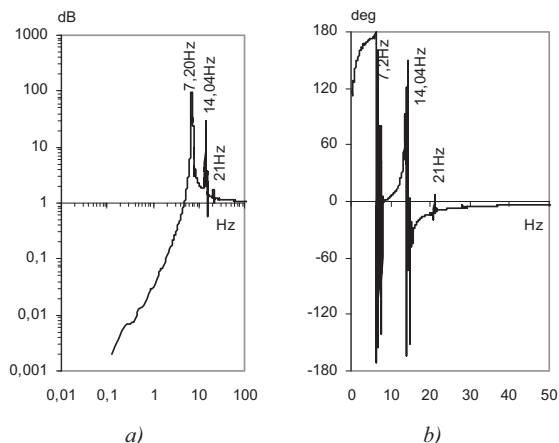


Fig. 13. An amplitude-frequency response of vibration velocity of the table in Y-axis for the assumed model

For a kinematic excitation assumed in the numerical analysis, determined at the foundation level, the horizontal component of ground vibration acceleration excited by the operating mill was assumed. Fig. 14 presents the first three forms of proper vibrations of the laboratory building. Deformation of the rigid body, here the building, at the frequency of 7.8 Hz corresponds to torsional vibrations.

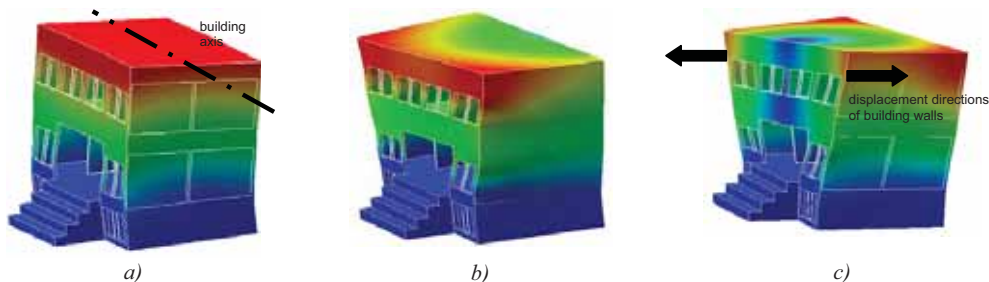


Fig. 14. Forms of building proper vibrations at the following frequencies: a) 4.1 Hz, b) 5.2 Hz and c) 7.8 Hz

The first three forms of proper vibrations of the ‘table – floor – wall – foundation – ground’ system are presented in Fig. 15. The first form of proper vibrations of the system being analysed corresponds to torsional vibrations around Y-axis, whereas the second one reflects the displacement along Y-axis. At the frequency of 18.8 Hz, the table vibrates in Z-axis and rotates simultaneously around X-axis.

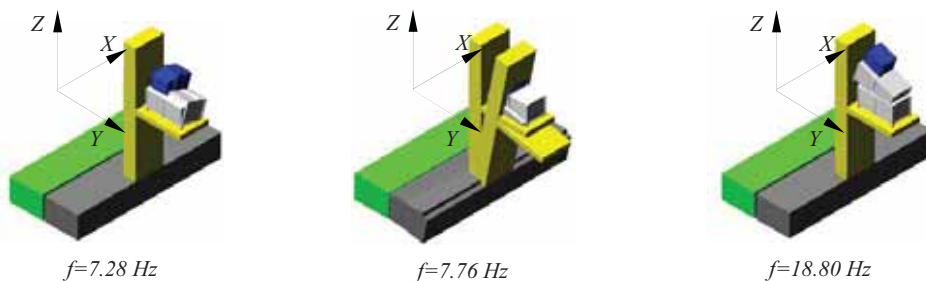


Fig. 15. Forms corresponding to the first three frequency values of proper vibrations of the investigated system

Fig. 16 presents amplitude-frequency responses of floor vibration velocity in Y-axis and Z-axis respectively. Calculated floor vibration velocity amplitudes at  $\sim 7$  Hz in Y-axis and in Z-axis have the respective values:  $0.53 \text{ mm}\cdot\text{s}^{-1}$  and  $0.044 \text{ mm}\cdot\text{s}^{-1}$  (Fig. 16). The values are lower than the measured values which were determined to be  $0.65 \text{ mm}\cdot\text{s}^{-1}$  (Y-axis) and  $0.2 \text{ mm}\cdot\text{s}^{-1}$  (Z-axis).

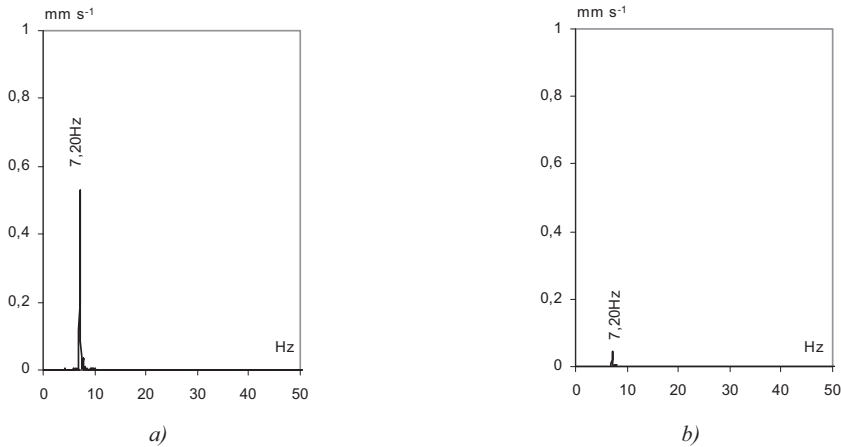


Fig. 16. An amplitude-frequency response of vibration velocity on the floor in a) Y-axis and b) Z-axis

The results obtained from the numerical analysis of table vibrations confirm that the table displaces with reference to the floor both horizontally and vertically. Vibration velocity of the table in Y-axis is much higher than in case of vibration velocity of the floor (Fig. 17).

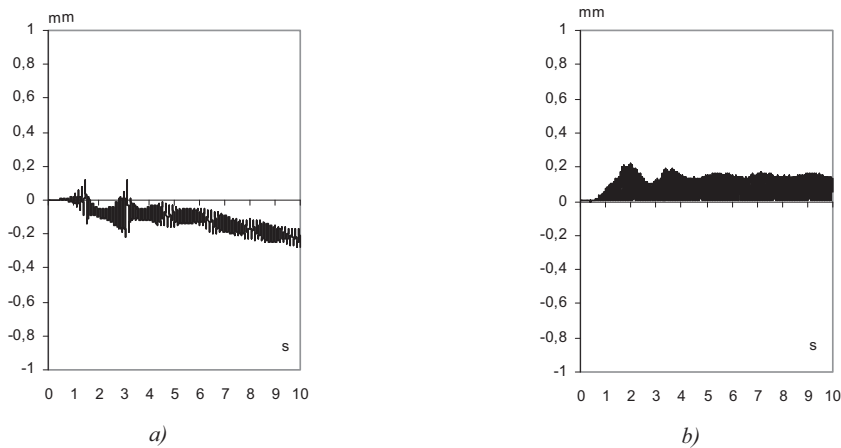


Fig. 17. Table displacement along the floor in a) Y-axis b) Z-axis in the function of time.

The vibrations are resonant in nature which is implied by the shape of spectrum containing ultraharmonic components of excitation frequency being  $3\times$  and  $5\times$  (Fig. 18). The values of table vibration velocity amplitudes obtained from the calculations at 7.20 Hz in Y and Z axes are as follows:  $6.7 \text{ mm}\cdot\text{s}^{-1}$  and  $1.26 \text{ mm}\cdot\text{s}^{-1}$ . In comparison, the values obtained from the measurements of table vibration velocity have the following values respectively:  $5.1 \text{ mm}\cdot\text{s}^{-1}$  and  $2.1 \text{ mm}\cdot\text{s}^{-1}$ .

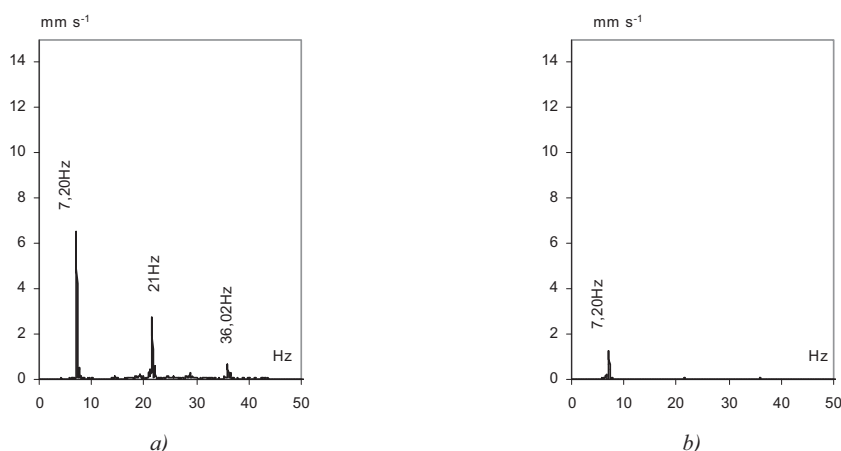


Fig. 18. An amplitude-frequency response of vibration velocity of the table in a) Y-axis and b) Z-axis

In order to damp the propagation of disturbances in the ground, excited by the operating mill, an expansion gap was simulated in the model within the foundation-ground plane. Fig. 19 presents the anticipated effect of reducing table vibrations in Y and Z axes when an expansion gap having the depth of 0.9 of the foundation block height is applied.

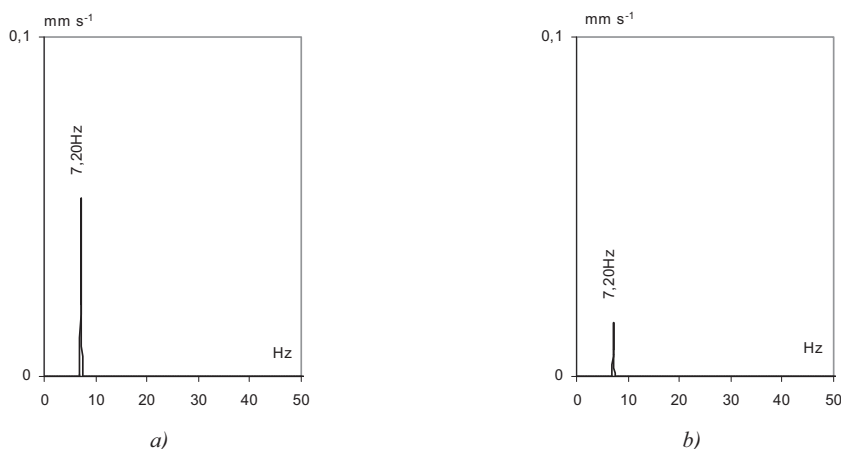


Fig. 19. An amplitude-frequency response of vibration velocity of the table in a) Y-axis and b) Z-axis once an expansion gap at the building foundation has been applied

Once the separation gap has been added to the calculation model for the ‘table – floor – wall – foundation – ground’ system, a significant reduction of table vibration velocity amplitude was obtained. The value decreased from  $6.7 \text{ mm}\cdot\text{s}^{-1}$  to  $0.05 \text{ mm}\cdot\text{s}^{-1}$  in Y-axis, and from  $1.26 \text{ mm}\cdot\text{s}^{-1}$  to  $0.02 \text{ mm}\cdot\text{s}^{-1}$  in Z-axis at the excitation frequency of 7.2 Hz.

#### 4. Conclusions

The main objective of this paper was to analyse the possibility of damping vibrations in a laboratory building where measuring equipment requiring high accuracy of indications is located. Experiments carried out for the object in a real scale confirmed that there were high-amplitude vibrations in the laboratory tables, and standard values were significantly exceeded. In

order to anticipate how effective damping of the level of building vibrations would be, conditions assuming no contact between the ground and the foundation at some level were taken into consideration in the numerical analysis. As results from the analysis of the problem, application of an expansion gap considerably reduces vibrations in the laboratory building.

## References

- [1] Auld B. A., Acoustic Waves and Field in Solids, Vol. I and II, New York: Wiley, 1973.
- [2] Gołębiowska I., Sakiewicz W., Minimalizacja drgań fundamentu z maszyną, Inżynieria and Aparatura Chemiczna, 3, pp. 30-31, 2006.
- [3] Kawecki J., Diagnostyka dynamiczna konstrukcji zagłębionych w gruncie, XX Ogólnopolska Konferencja Warsztatów Pracy Projektanta Konstrukcji, Wisła - Ustroń, 2005.
- [4] Zachwieja J., Numerical modelling of vibrations of machine foundations with percussive characteristics of work, Developments in Machinery Design and Control, 5, pp. 83-96, 2007.
- [5] Zachwieja J., The role of vibroisolators in damping an radial fan's vibrations, Diagnostyka, 44, pp. 113-118, 2007.
- [6] Zachwieja J., Gołębiowska I., Efektywność wybranych metod ochrony przeciwdrganiowej konstrukcji wsporczej separatorów, Budownictwo Ogólne, Wydawnictwa Uczelniane UTP, pp. 119-126, 2009.
- [7] Zachwieja J., Peszyński K., Vibroisolators application for damping vibrations in industrial fans, Engineering Mechanics, National Conference with International Participation, SVRATKA, Czech Republic, pp. 1390-1401, 2008.





## CONSTITUTING OF COMPOSITE MATERIALS FROM RECYCLED PLASTICS SHOWING NOISE-SUPPRESSING PROPERTIES

**Joachim Zimniak**

*University of Technology and Life Sciences,  
Faculty of Mechanical Engineering  
ul. Kaliskiego 7, 85-789 Bydgoszcz, Poland  
e-mail: zimniak@utp.edu.pl*

**Bogusław Królikowski**

*Institute for Engineering of Polymer Materials and Dyes  
ul. M. Curie-Skłodowskiej 55, 87-100 Toruń, Poland*

### **Abstract**

*The characteristic feature of contemporary civilization is generation of excessive noise level into the environment. To avoid this problem several solutions are proposed and applied, natural and artificial ones. The paper presents the conditions of constituting polymer composites consisting of recycled polymers and rubber (also particle size distribution of the components) for which the best noise suppression may be obtained.*

**Keywords:** composite materials, acoustic screens, noise suppression

### **1. Introduction, objective of the work**

Many scientific and research centers and industrial institutes are looking for the convenient constructional and technological solutions which allow to minimize the harmful influence of noise, especially at the source of its arising. Figures 1 and 2 show the example of main sources of noise generation in everyday life.



*Fig. 1 Noise generation when contacting: tire - road surface [5]*



*Fig. 2 Noise generation by movement of rail vehicles [5]*

To avoid this arduous problem different solutions are applied, i.e. natural (like green areas along the communication routes) as well as artificial ones being an effect of research and experience in this matter thoroughly presented in professional literature [2, 4, 11]. There are also indirect solutions joining both solutions. The great expectations are connected with so called noise-suppressing shields (screens) for highway engineering. Certain materials are usually used for this purpose like aluminum plates/mineral wool, or concrete/wood. More and more often polymer materials are used, especially polymer composites. The properties assigning such composites for this application are, first of all: inflammability and impact resistance [6, 8].

Application of polymer composites for manufacturing of noise-damping elements has another advantage, i.e. pro-ecological activity. At present, when the problem of huge mass of post-consumer plastics wastes is of ever growing importance, the waste management focuses on material recycling. Polymer composites are the best example of materials, which may be produced relatively easy, at low cost, using secondary plastics and elastomers [3, 10, 12, 13] (fig. 3).

More and more RD&A tasks are undertaken in connection with application of acoustic screens made of plastics including composites, the functional properties of which may be constituted in wide range.

From the scientific and useful point of view the most important is searching for the determined constructive-technological conditions connected with constituting polymer materials and composites of special properties as well as determination of processability of those composites for practical application [6, 8, 10, 12]. One has admitted a thesis that there are determined constructive-technological conditions of constituting polymer materials and composites for which the most advantageous properties may exist and that there are the modes of realization of those assumptions (e.g. special conditions of size-reduction, mixing components and pressure compacting), the choice of which will decide about quality of products made themof.

Basing on literature analysis as well as long-lasting cooperation with scientific centers the admitted operations are [3-10]:

- size-reduction of starting materials, especially repeatability of grain fraction, assessment of shape and surface of elementary grains,
- processes of mixing starting materials (in solid state) in grainy form) and assessment of mixing degree of starting materials,
- processing operations used for preparing composites (extrusion, injection moulding, high pressure compacting).

In table 1 (column I) the unit processes have been listed that have significant influence on functional properties of the composites. It turns out from the table 1 that condition of efficient development of wanted solution is closer cognition of listed constituent processes which, in qualitative way, could determine the influence of selected constructional and technological factors (column III) concerning sort, dimensions of the material to be size-reduced and mixed, susceptibility to pressure compacting, and to injection moulding, described by the functions of the tested object and their influence on physical parameters determining effectiveness of a constituent process (shown in column II as a measure).

Polymer composites are prepared by mixing polymer matrix with minor phase. The matrix usually is thermoplastic polymer as a single or mixture of polymers. Minor phase usually is, except of size-reduced rubber, other material like glass fiber, fillers a.s.o. To get the composite the components must be subjected to operations, the basic of which are size-reduction, mixing and processing. The size-reduction is a constituent process which enables the proper grain size distribution of the components, mixing is responsible for preparing the composite as a polymer mixture of proper component proportions.

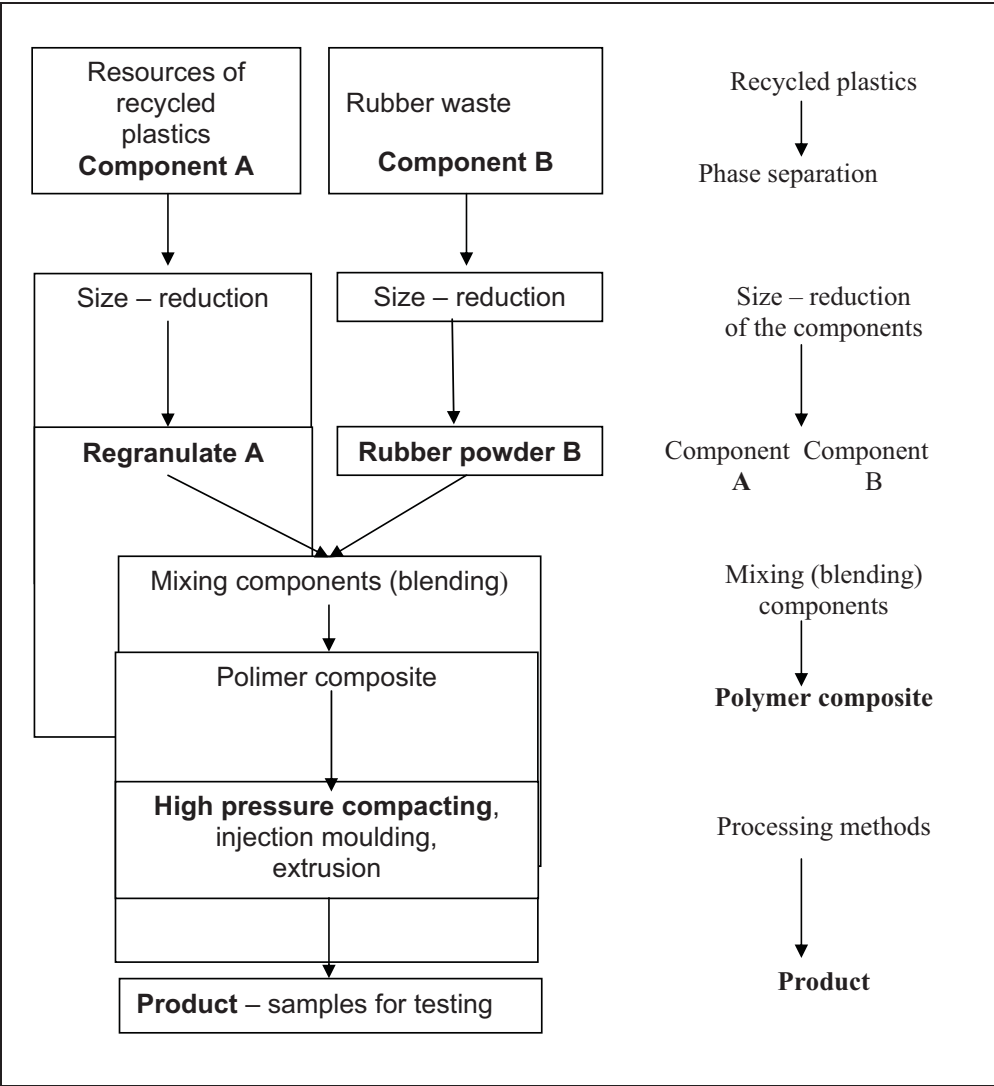


Fig.3. Block scheme of constituting composite materials made of recycled plastics [14]

Table 1. List of constituent processes influencing functional properties of composite [4, 13, 14]

| Name of the constituent processes   |     | Parameter determining the effectiveness of the constituent process                                     | Constructional and technological factors significant for constituent process |
|---|-----|--|--|
| I   |     | II   | III  |
| <b>A</b> Size – reduction process   | OBI | Torque: $M_o$<br>Cutting force: $F_c$  | $M_o, F_c = f(a_1, a_2, \dots, a_n)$   |
| <b>B</b> Mixing process   | OBI | Power $N$ , time $t_m$ , stopień zmieszania $M_m$  | $N, t_m, M_m = f(b_1, b_2, \dots, b_n)$                                      |
| <b>C</b> Processing: (injection moulding, high pressure compacting operations and others) | OBI | Temperature, pressure $p_p$ , time $t_p$ of pressing, injection moulding                               | $p_p, t_p = f(c_1, c_2, \dots, c_n)$   |
| <b>D</b> Verification of the research tasks   | OBI | Strength parameters e.g. tensile strength $R_m$ , degree of mixing $M_m$ , acoustic screens $\Delta L$ | $R_m, M_m, \Delta L = f(V_1, \varphi_1, V_n, \varphi_n)$                     |
| <b>N</b> Others   | OBN | .....  | $\Psi, \Phi = f(x_1, x_2, \dots, x_n)$                                       |

The general objective of the work is presentation of the concept enabling determining the conditions of constituting composites in technological process to obtain products made of them of required acoustic properties. The detailed research objectives are:

- influence of mass fraction of rubber powder in polymer matrix,
- influence of grain size of the rubber powder in composite,
- number of effective layers in the sample on noise-suppressing properties of selected composites.

## 2. Research program – realization of the tests

To determine the grain size and mass fraction of the filler on noise-suppressing acoustic vibrations the samples have been prepared using recycled PP and rubber powder type SBR. The mixtures have been prepared in the framework of the other research task [7,12]. The share of components, grain size distribution of the SBR rubber powder and components, have been gathered in table 2.

## 3. Test stand

The experimental was realized in two phases:

- pressure compacting plates made of composite using special compacting mould (fig. 4) for basic tests (table 2),
- testing of noise-suppressing ability – scheme of the test stand shown on fig. 5.

Tab.2. List of composites used for testing [7,14]

| Denotation of the composite | Grain size distribution of the rubber powder type SBR, mm | Content of the rubber powder SBR in composite, wt.% |
|-----------------------------|---|---|
| K <sub>0</sub>              | -   | -   |
| K <sub>1</sub>              | 0,8   | 30  |
| K <sub>2</sub>              | 0,8   | 40  |
| K <sub>3</sub>              | 0,8   | 50  |
| K <sub>4</sub>              | 1,2   | 30  |
| K <sub>5</sub>              | 1,2   | 40  |
| K <sub>6</sub>              | 1,2   | 50  |
| K <sub>7</sub>              | 1,6   | 30  |
| K <sub>8</sub>              | 1,6   | 40  |
| K <sub>9</sub>              | 1,6   | 50  |
| K <sub>10</sub>             | 2,0   | 30  |
| K <sub>11</sub>             | 2,0   | 40  |
| K <sub>12</sub>             | 2,0   | 50  |

The composites K<sub>1</sub> to K<sub>12</sub> listed in table 2 have been presented after growing grain size in the composite. K<sub>0</sub> sample is a reference sample made of pure recycled PP for further tests and comparisons.



Fig. 4. The view of the compacting mould for composite plates [15]

The plates of dimension 210x180x6 mm from which test samples of dimension 75x75 mm for further testing are made.

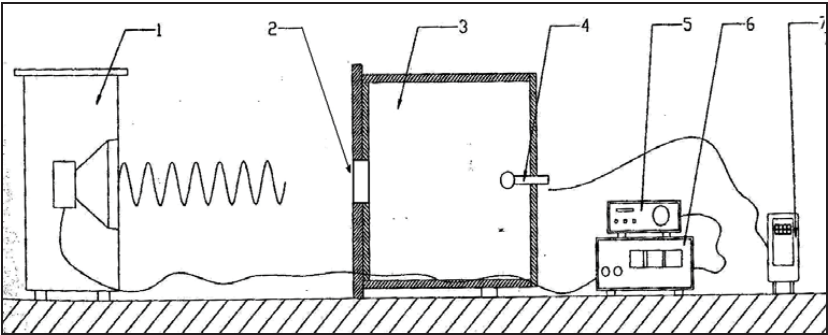


Fig. 5. Scheme of the test stand for determining the noise-suppressing ability of acoustic vibrations: 1 – loud speaker, 2 – sample of the composite, 3 – measuring chamber, 4 – microphone, 5 – frequency generator, 6 – amplifier, 7 – vibration damping meter [15]

For testing purposes following composite samples were used as: single-, double-, triple-, and quadruple – layered piles subjected to tests using frequency bands ranging from 63Hz to 4kHz to get the acoustic spectra for dominating frequencies 63, 125, 250, 500, 1000, 2000, 4000Hz [7,14, 15]. In the first stage the referencing spectrum for test equipment has been determined. It has been denoted as  $Leg_w$  and next the spectra for samples have been determined and denoted as  $Leg_z$ . The result of damping ability (denoted as  $\Delta L$ ), i.e. difference concerning two values:  $Leg_w - Leg_z$ . The smaller  $\Delta L$  value, the better damping capacity of acoustic vibrations [10, 15].

#### 4. Test results

The results of testing influence of layers’ multiplicity of samples, grain size distribution and rubber powder content in the composite on damping ability has been gathered in figs. 6 – 8.

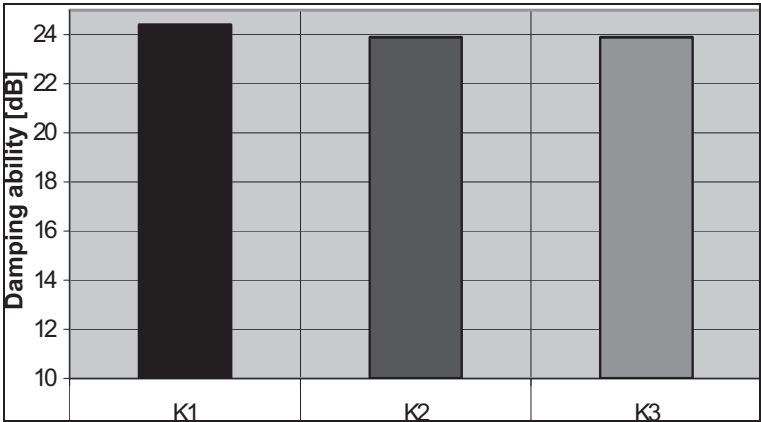


Fig. 6: Influence of layers’ multiplicity of samples on damping capacity of acoustic vibrations (X axis – number of layers, Y axis – damping ability  $\Delta L$  in dB)

The results show that comparing  $\Delta L$  values there is no considerable influence of rubber powder content in the composite and layers’ multiplicity of samples on damping ability. However,

grain size distribution ranging from 0,8 to 2,0 mm have considerable influence on damping ability. The most advantageous may be observed for composite denoted as K<sub>12</sub> after table 2, i.e. for grain size 2,0 mm.

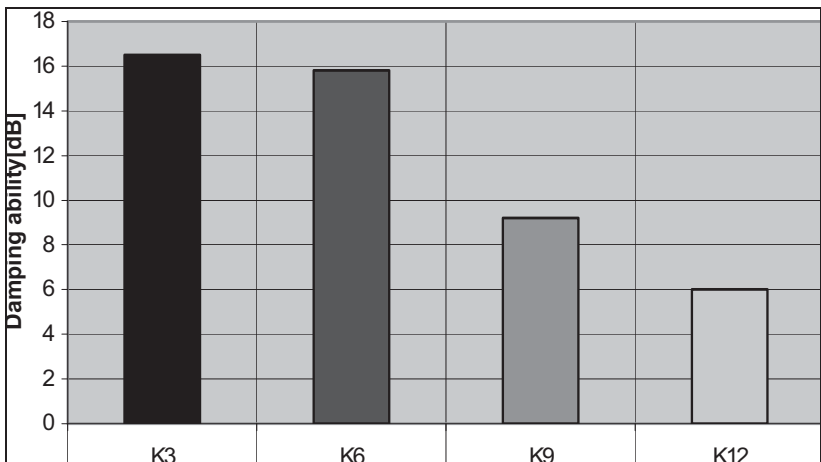


Fig. 7: Influence of rubber powder content in the composite on damping capacity of acoustic vibrations (X axis – rubber powder content in wt.%, Y axis – damping ability  $\Delta L$  in dB)

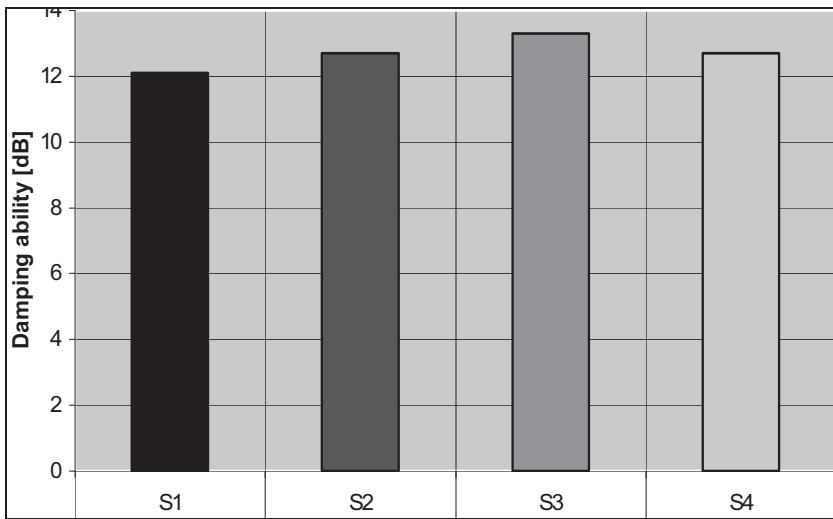


Fig. 8: Influence of grain size distribution of rubber powder on damping capacity of acoustic vibrations (X axis – grain size distribution, Y axis – damping ability  $\Delta L$  in dB)

### 5. Summary

Within the framework of the article an attempt of verification of thesis has been undertaken that there exist a determined grain size distribution of components and their mass shares for which the product of most advantageous damping noise capacity may be obtained. From the results of the tests it can be seen that the range of constituting acoustic properties of the composites is relatively wide. Preliminary lab tests showed that the most important factor is grainy component as a minor phase, especially its grain size (grain size distribution). The results may be helpful in constructing

the acoustic shields. Program of further research should concern application of other materials for minor phase of different grain size distribution compared to those applied in this work.

## References

- [1] Boss J., *Mieszanie materiałów ziarnistych*, PWN, Warszawa 1987.
- [2] Brandrup J., *Die Wiederverwertung von Kunststoffen*, Carl Hanser Verlag München - Wien 1997.
- [3] Flizikowski J., *Rozdrabnianie tworzyw sztucznych*. Wydawnictwa Uczelniane ATR, Bydgoszcz 1998.
- [4] Hannes M., Zimniak J., *Analiza konstytuowania właściwości użytkowych polimerowych tworzyw kompozytowych*, Zeszyty Naukowe nr 233 – Mechanika 50, ATR w Bydgoszczy 2001.
- [5] <http://www.techbud.com.pl/ekrany-danete-cs-typ-3.htm>
- [6] Jurkowska B., Jurkowski B., *Mieszanie kompozycji polimerowych*, Wydawnictwo Politechniki Poznańskiej, Poznań 1991.
- [7] Konieczka R., *Grundlagen der mechanischen Rezirkulations- Prozesse von PE-LD Folien*, Wydawnictwa Uczelniane ATR, Bydgoszcz 1996.
- [8] Królikowski B., Zimniak J., *Prasowanie płytowe wysokociśnieniowe kompozytów z tworzyw wtórnych*, III Środkowo-Europejska Konferencja „Recykling Materiałów Polimerowych, Nauka-Przemysł”, Krynica 2004.
- [9] Obraz J., *Ultradźwięki w technice pomiarowej*, Wydawnictwa Naukowo-Techniczne, Warszawa 1983.
- [10] Piotrowski J.: *Prasowanie ciśnieniowe tworzyw polimerowych kompozytowych*, Praca dyplomowa ATR Bydgoszcz 2004r. (Promotor: dr hab. inż. J. Zimniak).
- [11] Sikora R., *Przetwórstwo tworzyw wielkocząsteczkowych*, Wydawnictwa Edukacyjne, Warszawa 1993.
- [12] Zimniak J., Śliwa W., *Tworzywa polimerowe o specjalnych właściwościach akustycznych*, Zeszyty Naukowe Nr 216- Mechanik (43)-1998, ATR Bydgoszcz.
- [13] Zimniak J., *Procesy jednostkowe a konstytuowanie właściwości użytkowych kompozytów polimerowych*, Polska Akademia Nauk, Komitet Budowy Maszyn, Sekcja Podstaw Technologii. Zeszyt nr 77, pod redakcją Huberta Latosia, ATR Bydgoszcz, 2006.
- [14] Zimniak J., *Constitution of useful property of composite*, Journal of polish CIMAC. No. 2, Vol. 4 Gdańsk University of Technology, Section of Transport Technical Means of Transports, Committee of Polish Academy of Science, Gdańsk, 2009.
- [15] Zimniak J., Królikowski B., *Polymer composites of special acoustic properties*, TECHNOMER'09, ETP19, Chemnitz 2009.

## Acknowledgments:

This research work was supported by Polish Ministry of Education and Science (**Project No. 6170/B/T02/2011/40**)



## SELECTED PROBLEMS OF TEMPERATURE CONTROL IN INJECTION MOULDS

**Joachim Zimniak, Bartosz Sadowski**

*University of Technology and Life Sciences,  
Faculty of Mechanical Engineering  
ul. Kaliskiego 7, 85-789 Bydgoszcz, Poland  
e-mail: zimniak@utp.edu.pl*

### **Abstract**

*This paper contains the analysis and summary of the best solutions of temperature control of injection moulds put into production in recent years. It is also an attempt to design further, more advanced methods of temperature control, which may find wider application in future.*

**Keywords:** injection moulds, temperature tempering procedures, temperature control

### **1. Introduction**

In recent years there has been a marked development of methods and techniques of injection mould thermostating procedures. This development is related to the ever-increasing requirements in regards to the moulded pieces of the injection moulding process itself. Very strict quality requirements are now characteristic of the modern production processes of synthetic materials – for example in regards to the technical moulded pieces, the requirements specify the accurateness of the shapes, lack of deformation and manufacturing within narrow ranges of tolerance. The injection moulds used by the food, cosmetics and home appliances sectors need to fulfil stringent requirements in regards to their visual side – there can be no shrinkage sink marks, the mouldings need to have a regular shape, their colour needs to be the same, the lights need to be regularly reflected or refracted and the injection process cannot be prolonged. In order to achieve the above mentioned goals, correct planning of the injection mould thermostating procedures needs to be in place, with the use of all available modern techniques. This work describes some chosen modern methods and techniques of thermostating, which are often required as part of the injection moulding process, in order to ensure high quality and efficiency of the synthetic material manufacturing

### **2. Technological problems occurring during the thermostating processes of smaller moulded elements**

It is not easy to achieve appropriate cooling of small mould cores within an injection mould. The small size of such a metal mould core causes it to warm up very quickly, over the allowed mould temperature values. At the same time its size prevents the use the traditional methods of

material removal processing, like drilling, milling or hollowing, in order to drill holes or cooling channels in the surface of the mould core. If the moulded pieces have not been properly cooled, they often contain faults, such as shrinkage sink marks, deformations, knock-outs which come out into the moulded pieces or even fracturing, as well as an extended production cycle. The solutions which were available until now were either based on the process of hollowing of the cooling channels in the elements of the mould, which were adjacent to the over-heating area or carried out using the heat transfer rods – additional interconnecting elements which transfer the heat from the over-heating areas to the cooler ones. At present, the modern laser incremental techniques allow the cooling channels to have a very complicated geometry and a very small size [3, 4, 6, 7, 9]. Thanks to that, the conformal cooling channels can be designed to be carried out in areas which are inaccessible to other methods of machining, and the shape of the cooling channel can now relate to often complicated mould shapes. Figures 1a and 1b compare the cooling channels made using the traditional methods and the conformal channels carried out using the laser incremental techniques. The colour cross-sections made using the injection mould simulation techniques show a much more advantageous temperature layout in regards to the second mould core.

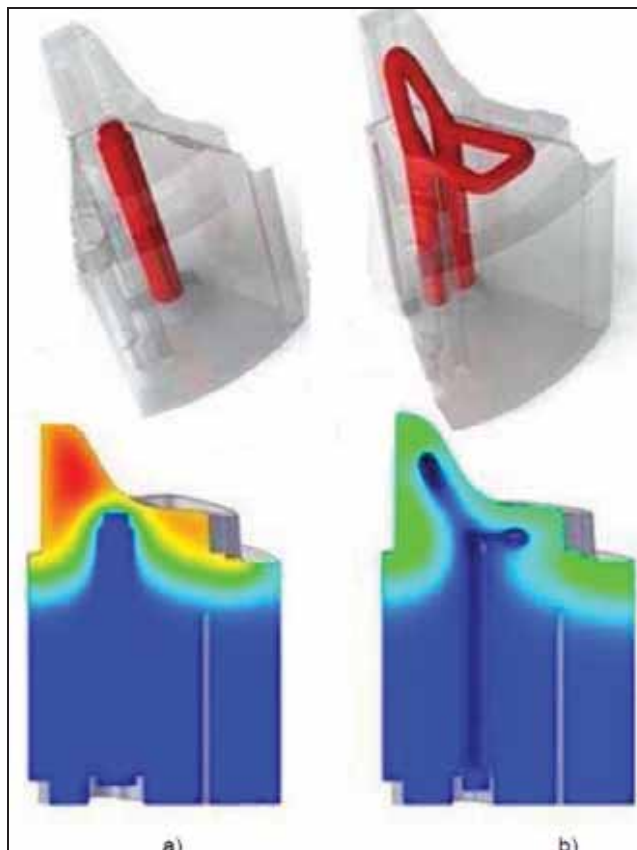


*Fig.1. Shape of the cooling channel: a - traditionally drilled, b - produced by laser incremental techniques [1]*

The cooling channels which are shaped to their advantage receive the heat from the cooling moulded piece also in a better and more uniform way. As a result, any deformations and other moulding sizing mistakes can be expected to be less frequent, the moulds are easier to fill and the production cycle is shortened. Fig. 2 and 3 show a mould cavity where the cooling surfaces have

the shape of a honeycomb. Such a layout of channels, where they run strictly along the moulding surface, ensures the best and the most regular heat transforming from the moulded pieces. The cavity manufacturer JB Ventures BV confirms that their aim was the reduction in warpage and cycle time [5].

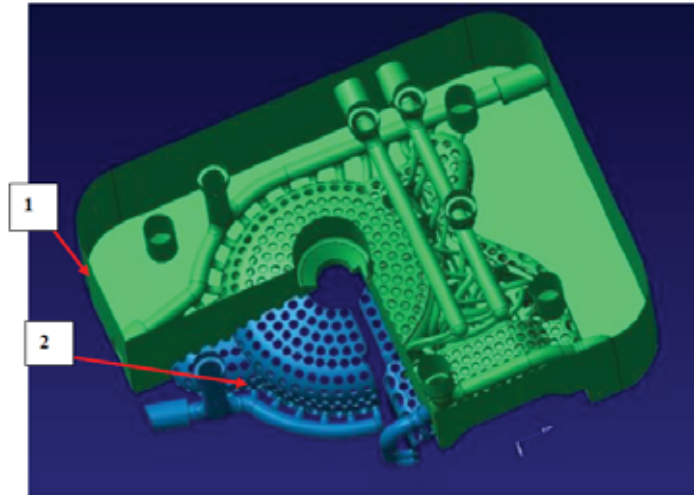


*Fig.2 Mould cavity CAD model (1) with honeycomb shaped surface cooling (2) [3]*



*Fig.3 Front of the cavity insert in which the honeycomb shaped cooling was made [3]*

When using the method of direct injection into a cavity with a hot nozzle, it often happens that there is a significant increase in temperature around the injection point – which in turns causes thickening or fullering of the material which is too hot and comes in the form of a string when the moulded piece is ejected from the mould, it also results in an extended cooling period.

At present the manufacturers of hot runner systems often suggest the use of an additional cooling bush, which includes the hot runner tip and aims to guarantee a direct cooling of the injection point. This area is, however, not very big and poses quite significant problems when using the traditional techniques to carry out the cooling channels. The laser incremental techniques also come to the rescue in such cases, as they allow to carry out more complicated cooling

channels which are much smaller. Figure 4 shows cooling bushes with conformal channels which include the hot runners manufactured by DME. As it can be seen, the channels are located near the injection point and they regularly adhere to the over-heated areas of the moulded pieces.

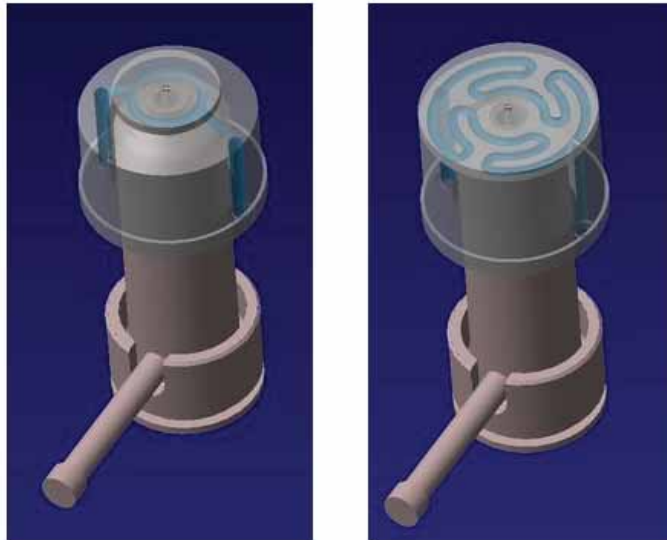


*Fig. 4. Cooling bushes with conformal channels manufactured by laser incremental techniques [6]*

Recently it can be seen that there is a marked development of the materials which are used to make mould cavities for injection moulds, which are characterised by significantly higher thermal conductivity values and larger endurance to the forces present during the injection of the material. The materials which were up to now known to have high thermal conductivity values, such as beryllium bronze, had lower compression strength and lower resistance to the forces present during the injection of the material. As a result, these materials cannot be used in many instances. At present, the materials designed by the Mecobond firm are coming into use (fig. 5) – steel cavities with a copper core and HTCS-130 steels which are quick to conduct heat (fig. 6) - thermal conductivity of these types of steel is between 48-58 W/m K, depending on the operating temperature.

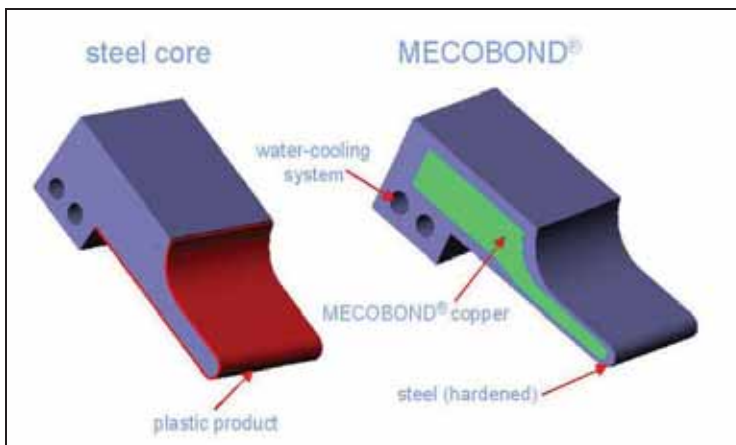


*Fig. 5. Mould inserts containing copper core by Mecobond [2]*

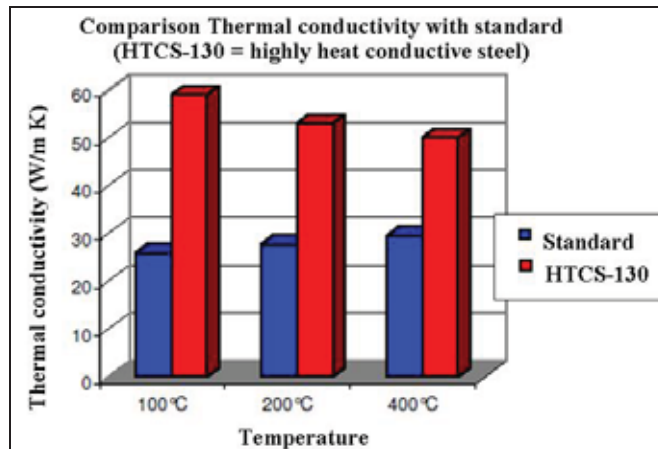


Fig. 6. Comparison of thermal conductivity of HTCS-130 steel with special thermal properties and the standard tool steels [2]

As it is commonly known, the injection process has a cyclic nature, where at a certain point the material is heated to the injection temperature, and after the moulded piece is given its respective shape, it is followed by a cooling process, when the temperature is lowered to one allowing for the material to be ejected from the moulded piece. Therefore, it is desired to use a pulse cooling system (fig. 7) [2, 5, 8].

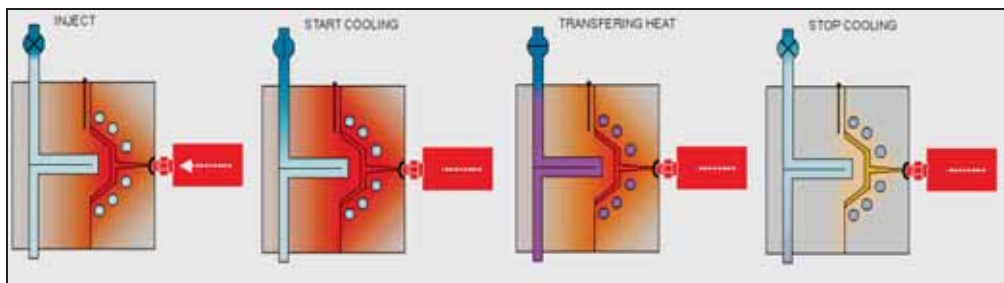


Fig. 7. Diagram of the pulse cooling system in the injection mould during the operation of an injection moulding machine [2, 5]

Such a thermostating procedure allows for an intensive cooling period when the material is freezing in the mould and allows the cooling to stop during the injection, the extruder material feeding and while the mould is being closed, which means that the core does not get unnecessary cool when the material is filling the mould.

The areas which have become too cool, especially if the moulded pieces are larger and thin-walled, might mean that the material is slower to flow, can signify that the gates and cold runners can freeze too early and can prevent the cores of the moulds from becoming full and the details caused by the holding pressure may not be completed. It applies mostly to the moulded pieces where the walls are thin – approx. 0.6 – 1.5 mm and the material quickly loses its heat and freezes before the final points are reached [5, 9].

In such cases, using pulse cooling systems for the moulds will allow the core to maintain a higher temperature during the injection itself and will enable to carry out an intensive cooling process to go ahead when the moulded piece is being cooled down. Using pulse cooling systems also allows the total manufacture process of a moulding to be shortened by about 10-30%

depending on the type of the material.

#### 4 Conclusion

Most up-to-date injection mould thermostating procedures are aiming to secure a more uniform way of heat removal from the whole volume of the moulded piece. In many instances it is now possible to design cooling channel shapes in areas which are prohibitive to the traditional machining methods. As a result of this, the products are of much higher quality – they are more accurate when it comes to size, the deflections and sink marks are avoided.

The modern methods of injection mould thermostating procedures also allow for the details in thin-walled moulds to be achieved and make the production processes shorter – which is caused by the variation of the temperatures of the cooling liquid during the injection cycle – the mould is being intensively cooled down before the moulded piece is ejected from the core and it is cooled down less intensively during the injection itself, so as not to slow down the flow of the hot material.

Using the modern techniques of injection moulding can be financially viable and can also relate to the product quality. In many cases using one of the above described methods becomes a necessity when the ever-growing requirements are taken into account – in regards to the accuracy of the moulded pieces size, the shortening of the production cycles and in relation to the amount of the material being used to manufacture thin-walled products.

#### References

- [1] Abbot, R., Combs, R., Kazmer, D., *Elimination of Process Constraints in Plastic Injection Molding*, International Polymer Processing, Vol.13 Issue 3, 2003, s. 249-255.
- [2] Cha, S., Lai, F.S.: *Analytical study of thin-wall injection moulding: Filling and cooling analysis*, Conference Proceedings Annual Technical Conference – ANTEC'96, 1996.
- [3] Dimla, D.E., Camilotto, M., Miani F., *Design and optimisation of conformal cooling channels in injection moulding tools*, Journal of Materials Processing Technology 164–165 (2005), s. 1294–1300.
- [4] Ferreira, J.C., Mateus, A., *Studies of rapid soft tooling with conformal cooling channels for plastic injection moulding*. J. Mat. Proc. Technol. 2/2003, (142), s. 508–516.
- [5] <http://www.lasercusing.nl>
- [6] Oczkoś, K.E., *Rozwój kształtowania przyrostowego wyrobów*. Mechanik, 2/2007 (80), s. 65 ÷ 73.
- [7] Saifullah A.B.M., Masood S.H.: *Cycle Time Reduction in Injection Molding with Conformal Cooling Channels*, Conference Proceedings of the International Conference on Mechanical Engineering, 2007 s. 29- 31.
- [8] Xu, X., Sachs, E., Allen, S., *The Design of Conformal Cooling Channels in Injection Molding Tooling*, Polymer Engineering & Science, Vol. 41, Issue 7, pp 1265-1279, 2007.
- [9] Shia-Chung, C., Pham-Son, M., Sheng, H., Yan-Chen, C., *Improve Cooling Effect of Injection Molding by Pulse-Cooling Method*, Conference Proceedings Annual Technical Conference – ANTEC'09, 2009.

#### Acknowledgments:

This research work was supported by Polish Ministry of Education and Science (**Project No. 6170/B/T02/2011/40**)